Dissertation zur Erlangung des Doktorgrades
der Fakultät für Chemie und Pharmazie
der Ludwig-Maximilians-Universität München

Highly Reactive Pyridinamide Anions in Lewis Base Catalysis

Veronika Maria Burger
aus
Landshut, Deutschland

2024

Erklärung

Diese Dissertation wurde im Sinne von § 7 der Promotionsordnung vom 28. November 2011 von Herrn Prof. Dr. Hendrik Zipse betreut.

Eidesstattliche Versicherung

Diese Dissertation wurde eigenständig und ohne unerlaubte Hilfe erarbeitet.

München, 24.10.2024

……

Veronika Burger

Dissertation eingereicht am: 25.10.2024

1. Gutachter: Prof. Dr. Hendrik Zipse

2. Gutachterin: Prof Dr. Ruth M. Gschwind

Mündliche Prüfung am: 05.12.2024

Acknowledgement

This dissertation has been quite a journey, on which many wonderful people accompanied me. To all of you, thank you very much for being a part of this.

First, I would like to thank Prof. Hendrik Zipse for offering me this opportunity by welcoming me into his group. He allowed me to shape my research project as I saw fit and still offered advice when needed.

Prof. Ruth Gschwind, I thank for being my "Zweitgutachter" and for joining in on countless (zoom) discussions about ion pairs, conductivity models, DOSY curves and more. She always brought a fresh perspective and a lot of enthusiasm to these discussions.

Also, I would like to extend my thanks to Dr. Armin Ofial. Also, for participating in the countless (zoom) discussions about ion pairs and their nucleophilicity measurements, and for offering his advice and expertise. He kindly allowed me to use his groups equipment for numerous measurements.

Maximilian Franta, I thank for his collaboration and the many hours he spent measuring DOSY NMRs for this project.

These four people will be fondly remembered by me as "ion pair team". Without them a large part of this thesis would not have been possible.

I would also like to thank the analytical department of the Ludwig-Maximilians-Universität, Dr. Peter Mayer for determining crystal structures and all other employees who have supported me in my work.

Furthermore, I would like to thank my colleagues for the daily collaboration in the lab. Dr. Harish Jangra, Dr. Julian Helberg, Dr. Benjamin Pölloth, Dr. Stefanie Mayer, Dr. Salavat Ashirbaev and Dr. Fabian Zott welcomed me into the group and always offered help and advice when needed. Harish and Fabian always knew how to fix any computational issue, and with Benjamin and Steffi I often discussed the joy of organocatalysis. Also, I want to thank my current colleagues Caroline Carter, for our regular discussions about chemistry and life in general, Jan Brossette for his help with any computational questions I have had, Kuangjie Liu for his help on several occasions and Marc Krähling, who will continue the project of pyridinamide ion pairs. Additional thanks to Steffi, Caroline, and Marc for proofreading parts of this work.

Special thanks to my friends who helped me recharge when work got demanding. Game nights with Alex, Kathi, Tobi, and Stefan were always full of laughter and fun. Meet-ups with Carina and Kim always helped me find my balance again. Lunch dates with Kyra were always a welcome change on a workday.

Last, but not least I want to thank my loved ones who made my doctorate possible in the first place: my parents, my brother, my grandmothers and grandfathers, my aunts, uncles, and cousins. Thank you for your affection and your support. One of you gave me the most memorable push of all: "Why don't you just finish it so you can be done with it!" And sometimes that is all you need to hear.

The biggest thank you goes to Stefan who helped me through all the ups and downs during my dissertation in the last five years. He always encouraged and had an open ear for all my troubles. Thank you for being there for me.

List of Publications in this work

Parts of this thesis have been published as follows:

1. V. Burger, M. Franta, A. R. Ofial, R. M. Gschwind, H. Zipse, "Highly Nucleophilic Pyridinamide Anions in Apolar Organic Solvents due to Asymmetric Ion Pair Association", *manuscript accepted*.

2. V. Burger, M. Franta, A. C. O'Donoghue, A. R. Ofial, R. M. Gschwind, H. Zipse, "Pyridinamide Ion Pairs - Design Principles for Super-Nucleophiles in Apolar Solution", *manuscript in revision*.

Other Publications

H. A. El-Sayed, V. M. Burger, M. Miller, K. Wagenbauer, M. Wagenhofer, H. A. Gasteiger, "Ionic Conductivity Measurements – A Powerful Tool for Monitoring Polyol Reduction Reactions", *Langmuir*, **2017**, 33 (47), pp 13615-13624.

List of RTG Retreats

04/2021	Kick-off meeting (Chair).
10/2021	Annual retreat in Tutzing.
11/2021	RTG graduate only retreat, LMU Munich (Chair).
05/2022	Annual retreat in Kloster Weltenburg (Presentation).
07/2022	Annual retreat in Tutzing.
12/2022	RTG graduate only retreat, St. Englmar (Poster).
03/2023	Annual retreat in TaLa Landshut (Presentation).
03/2024	Annual retreat in Burg Wernfels.
06/2024	Report retreat in Tutzing.

List of Conferences

09/2024	ORCHEM 2024 in Regensburg (Poster).

Table of Content

Summary

This thesis was conducted as part of the research training group “Ion Pair Effects in Molecular Reactivity”. The RTG 2620 focuses on exploring the reactivity, structure, and mechanisms of ion pairs in chemical reactions, aiming to bridge the gap between experiment and theory. Within the framework of my thesis, this led to a comprehensive study of pyridinamide ion pairs in apolar solvents. As a result, a toolbox of various methods was used, allowing conclusions to be drawn about their association state and reactivity in apolar solvents.

Chapter 2: Highly Nucleophilic Pyridinamide Anions in Apolar Organic Solvents due to Asymmetric Ion Association[1]

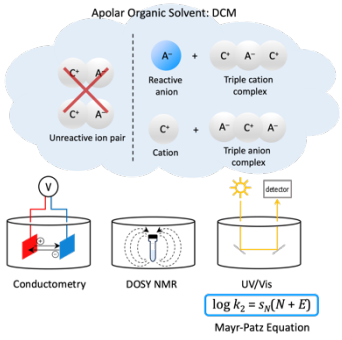

Pyridinamide phosphonium ion pairs were studied in dichloromethane using a combination of conductivity measurements, diffusion-ordered (DOSY) NMR, and kinetic measurements utilizing a refined ionic strength-controlled benzhydrylium ion methodology. This approach offered specific insights into the ion concentrations, their association state and nucleophilicity of the involved anion. It was revealed that pyridinamide tetraphenylphosphonium salts aggregate asymmetrically in dichloromethane solution, forming cationic and anionic sandwich-type complexes along with their corresponding counterion. The nucleophilicity of free pyridinamide ions exceeds that of the neutral reference nucleophile 9-azajulolidine (TCAP) by up to two orders of magnitude. We propose that asymmetric association in organic solvents of low polarity might offer a pathway to enhance the reactivity of anionic nucleophiles.

Chapter 3: Pyridinamide Ion Pairs – Design Principles for Super-Nucleophiles in Apolar Organic Solvents[2]

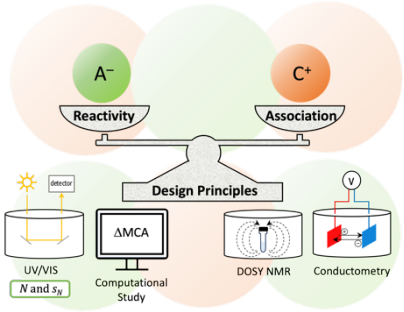

The developed comprehensive analytical protocol, combining conductivity, diffusion-ordered NMR, and photometric kinetic measurements, was used to characterize a library of pyridinamide ion pairs in organic solvents of low polarity. The results indicate a strong influence of cation size on association patterns, with larger cations favoring cationic triple ion sandwich complexes, which leave the free and highly nucleophilic anions as reactive species. Kinetic studies using the ionic strength-controlled benzhydrylium ion method demonstrate that pyridinamide anions exhibit a significantly enhanced nucleophilicity compared to established organocatalysts, particularly in low polarity solvents. With the gained insights the design of next generation pyridinamide ion pairs can be optimized to modulate the catalytic activity by controlling the asymmetric association. The Brønsted basicity of pyridinamide salts was quantified via the determination of their pK_a values in water and water/organic solvent mixtures and their Lewis basicity was quantified through quantum chemically calculated cation affinity data. Furthermore, the catalytic activity of pyridinamide ion pairs was tested in the reaction of isocyanates with alcohols.

[1] Submitted to *Journal of the American Chemical Society*, Manuscript *accepted* with DOI: 10.1021/jacs.4c14825.
[2] Submitted to *Journal of Organic Chemistry* with Manuscript ID jo-2024-02668y, *in revision*.

Chapter 4: Application of Ion Pair Catalysts in Acylation Reactions

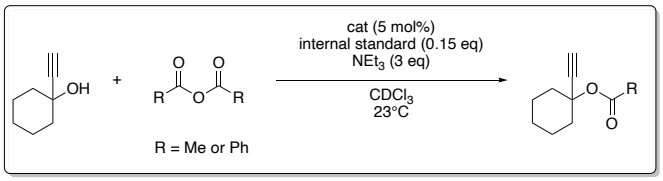

Pyridinamide ion pairs represent a promising class of organocatalysts that have demonstrated their catalytic potential in addition reactions such as the urethane synthesis and the *aza*-Morita-Baylis Hillman reaction. This study examined their catalytic activity in acylation reactions, using the acylation of 1-ethinylcyclohexanol as a benchmark reaction. The acylation with acetic anhydride was studied, with neutral organocatalysts dimethylamino pyridine (DMAP) and TCAP serving as references. The effective reaction rates k_{eff} (M^{-1} s^{-1}) showed that the most active pyridinamide ion pair catalyst exhibited about half the catalytic activity of TCAP. However, the previously most active pyridinamide ion pair catalyst only displayed moderate activity in this benchmark reaction. The observed deviation in catalytic activity led to an investigation of potential protonation-induced deactivation, which was ruled out by testing various auxiliary bases. To identify the cause of this moderate activity, further studies are required. Solvent effects were examined, showing that the choice of solvent significantly influences the catalytic activity of both pyridinamide catalysts and neutral organocatalysts, with the effect being more pronounced for pyridinamide salts. In a second benchmark reaction, four selected pyridinamide ion pair catalysts were employed in the acylation of 1-ethinylcyclohexanol with benzoic anhydride. The observed effective reaction rates k_{eff} (M^{-1} s^{-1}) were lower than those observed in the benchmark reaction with acetic anhydride. Nevertheless, the gap in catalytic efficiency between TCAP and the most active pyridinamide ion pair catalyst was reduced by half in these reaction conditions. These findings suggests that pyridinamide ion pairs could be effective in reactions that produce acidic byproducts. However, to fully optimize their catalytic potential in acylation reaction, further studies have to be conducted.

Chapter 5: Reactivity Enhancement of Chiral Lewis Catalysts through Ion Pair Formation

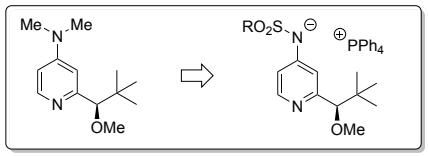

In the fifth chapter, we shift our focus to the synthesis of chiral pyridinamide derivatives. As already demonstrated, utilizing an anionic pyridine moiety can significantly increase the catalytic potential of the resulting organocatalyst. We intended to further explore this approach by selecting a known neutral chiral organocatalyst with high selectivity but poor reactivity, using its scaffold as a reference for the synthesis of a chiral pyridinamide. Vedejs' chiral organocatalyst, DMAP with a chiral substituent at the C2 position, was chosen as reference for this study. The original synthesis began with DMAP and involved a protection step, followed by metalation at the C2-position with lithium tetramethylpiperidine (LiTMP) and subsequent acylation with pivaloyl chloride. This was followed by an enantioselective reduction using a borane complex, yielding a chiral alcohol, which was then methylated using potassium hydride and methyl iodide to form the desired catalyst. The goal of this study was to synthesize a chiral pyridinamide ion pair catalyst based on the scaffold of Vedejs' chiral DMAP catalyst. Multiple attempts were made using starting materials such as 4-aminopyridine and 2-bromopyridine derivatives. Despite obtaining promising intermediates, several challenges were encountered in isolating the desired product. Various synthetic modifications were explored, including lithium-bromide exchange and subsequent acylation or nitrile addition, though without success. Further studies are needed to establish a synthetic route. Additionally, quantum chemical calculations were conducted to assess the Lewis basicity and stereoinductive potential of future chiral pyridinamide salts.

General Comments and Conventions

As part of this thesis is already submitted or prepared for publication, my contributions to multi-author publications are explicitly mentioned at the beginning of every chapter. The contributions from other authors are omitted from the experimental part. The main project of my dissertation is partitioned into two parts: Chapter 2 focuses on the development of the methodology and Chapter 3 on the insight gained from applying said methodology. This leads to unavoidable changes in the numbering when moving from Chapter 2 to Chapter 3. The following substrates will be consecutively numbered throughout starting in Chapter 2: 4-dimehtylaminopyridine (DMAP, **1**), 9-azajulolidine (TCAP, **2**) and pyridinamide salts **3a** and **4a** (see Chart 0.1). In Chapter 3 additional pyridinamide salts will be numbered consecutively.

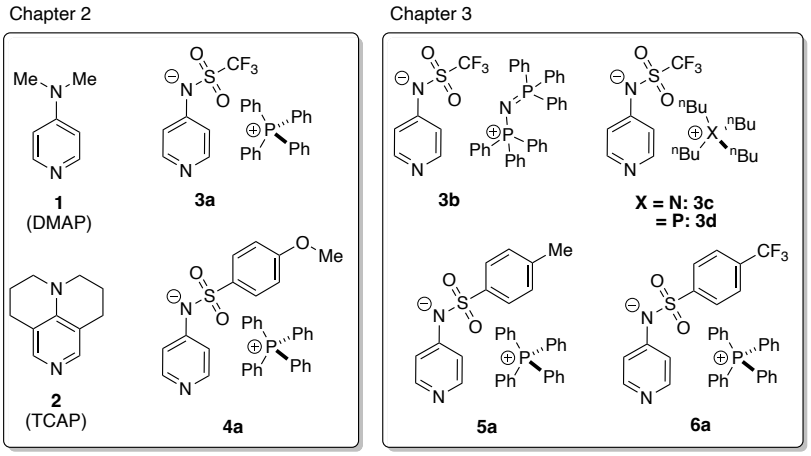

Chart 0.1. Structures of neutral organocatalysts DMAP (**1**) and TCAP (**2**), and pyridinamide ion pair catalysts **3a-d**, **4-6a**.

Since Chapter 2 only includes the pyridinamide ion pair **3a** and **4a**, consequently, the numbers of other reoccurring compounds will change when moving forward to Chapter 3, where more pyridinamide ion pairs will be discussed. To mitigate confusion, the concerned compounds with their respective number per chapter and any potential changes regarding the numbering in between chapters are listed below in Table 0.1.

Table 0.1. Compounds with their respective numbering in Chapter 2 and Chapter 3.

Compound	Numbering in Chapter 2	Numbering in Chapter 3
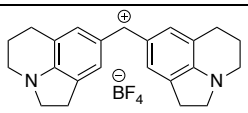 $(lil)_2CH^+BF_4^-$	**5a**	**8a**
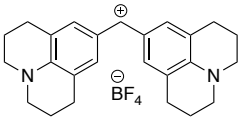 $(jul)_2CH^+BF_4^-$	**5b**	**8b**
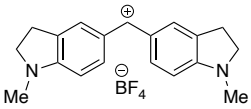 $(ind)_2CH^+BF_4^-$	**5c**	**8c**
PPh_4BF_4	**6**	**7a**

Starting with Chapter 3 all compounds will be numbered consecutively.

Chapter 1. Introduction

1.1 Organocatalysis

Organocatalysis refers to the acceleration of chemical reactions using small organic molecules as catalysts. These molecules typically contain elements such as carbon, nitrogen, sulfur, or phosphorus.[1] The term "organocatalysis" was first introduced by MacMillian in 2000, even though, the concept itself has been known since the 19th century, when Liebig catalyzed the reaction of cyanide and water to form oxamide by using acetaldehyde as the catalyst.[2,3] Despite its early origins, systematic research about organocatalysis has only gained significant momentum over the past two decades, establishing it as a widely studied and impactful area in organic chemistry.[3,4] As shown in Figure 1.1, organocatalysis can be classified based on the type of catalyst used for the transformation.

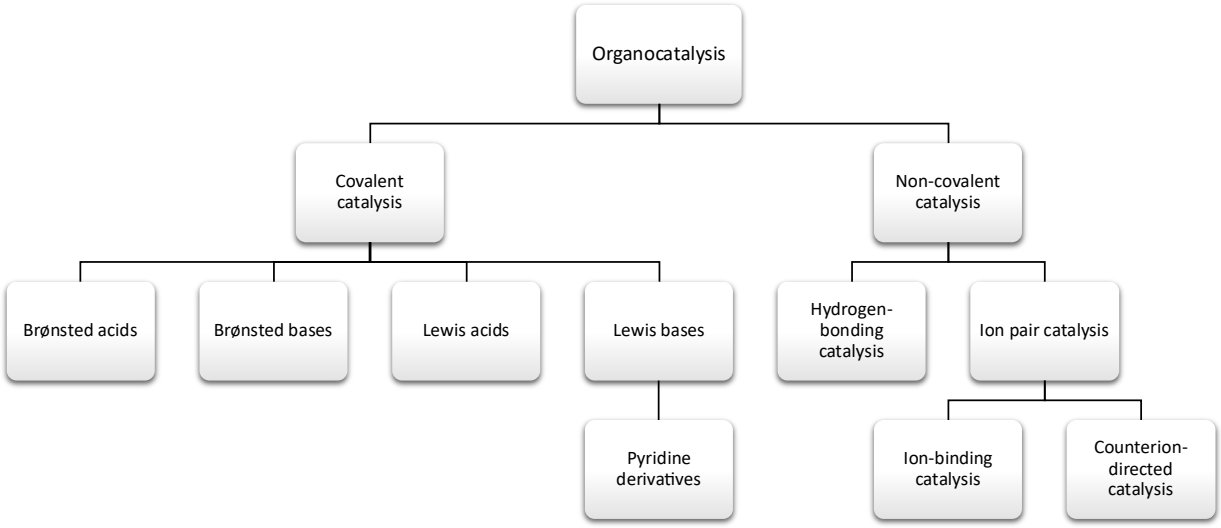

Figure 1.1. Classification for areas in organocatalysis based on the type of catalyst.

Broadly, organocatalysis can be partitioned into the two major branches covalent and non-covalent catalysis. While covalent catalysts form a bond with the substrate, non-covalent catalysts use non-covalent interactions (NCIs), such as hydrogen-bonding, ion binding, halogen bonding, and/or dispersion interactions to coordinate with the substrate.[5] The classification of these catalysts often depends on the degree of the inherent directionality in the interaction between the catalyst and the substrate (see Figure 1.2).

For instance, covalent iminium-based catalysis[6,7] relies heavily on strong, directional interactions, and has been proven highly effective for enantioselective carbonyl activations. Conversely, catalysts that interact through hydrogen-bond donors, such as organic-based Lewis acids and Brønsted acids[8,9], show weaker and less directional interactions. Ion pairing interactions are even less inherently directional, but represent a powerful strategy for enantioselective transformations when charged intermediates are involved, even though finding the right catalyst design is challenging.[10,11]

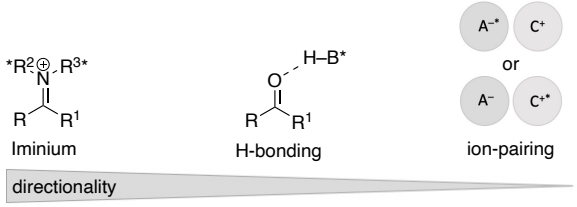

Figure 1.2. Trend of increasing inherent directionality in catalyst-substrate interactions for non-covalent asymmetric catalysis systems with B*H = chiral hydrogen bond donor; A^- = anion; C^+ = cation, * = chiral ion).[11]

In terms of covalent organocatalysts, four distinct categories can be defined based on their role within the catalytic cycle: Brønsted acid or base catalysis, where the catalyst donates or accepts a proton, and Lewis base or acid catalysis, where the catalyst donates or accepts electron pairs.[12,13] This work focuses on nitrogen-based Lewis base catalysts, which are widely applied in various synthetic processes.

1.1.1 Lewis Base Catalysis

Denmark[14] defined Lewis base catalysis as a "process by which an electron-pair donor increases the rate of a given chemical reaction by interacting with an acceptor atom in one of the reagents or substrates. The binding event may enhance either the electrophilic or nucleophilic character of the bound species." Jensen[14,15] proposed that all Lewis acid-base interactions could be classified in terms of the interacting orbitals. The most commonly recognized form of Lewis base catalysis is represented by *n*-π^* interactions which occur between the nonbonding electron pair *n* of the Lewis base and the antibonding π^* acceptor orbital, which are contained in carbonyls, alkenes or other unsaturated functional groups. In the field of Lewis basic organocatalysts nitrogen-based catalysts are the most common ones, followed by phosphanes and sulfides. The use of nitrogen-based nucleophilic catalysts can be traced back to 1898, when Einhorn and Hollandt[16] demonstrated that pyridine facilitated acylation reactions of alcohols and phenols. This discovery provided the foundation for further advancements in this field. The development of 4-dimethylaminopyridine (DMAP) by Litvinenko and Kirichenko[17] in 1967, and independently by Steglich and Höfle[18] in 1969, marked a significant milestone. DMAP has since been a widely used catalyst for accelerating group transfer reactions such as acylations,[19–22] alkylations,[23] and silylations.[24,25] Since then, continuous efforts have been undertaken to develop more catalytically active Lewis base catalysts. Progress was made by introducing a better electron donating group such as pyrrolidine, yielding of 4-pyrrolidinopyridine (PPY)[20,21] in 1970. A significant advance was achieved by conformational fixation of the dialkylamino group in DMAP, leading to the development of tricyclic 9-azajulodine (TCAP)[26] in 2003. The increased catalytic potential is attributed to stronger *n*-π^* interactions between the nitrogen lone pair and the acylated intermediate, further improved by the increased positive inductive effect of the alkyl substituent towards the pyridine ring. Therefore, TCAP surpasses DMAP by a factor of approx. six in catalytic benchmark reactions due to the enhanced stabilization of the cationic acylated pyridinium intermediate.

Building on the success of the TCAP moiety, researchers have explored various structural modifications to further improve the catalytic efficiency of DMAP-based organocatalysts as it can be seen in Chart 1.1. For example, guanidinyl substituents have been introduced as electron-donating group in pyridine-based catalysts of type **A**.[27] Bicyclic and tricyclic systems of type **B** have been generated through the incorporation of multiple amin-donor groups.[28,29] Other variation included the introduction of alkyl groups and additional nitrogen atoms into the ring system, resulting in catalysts such as 3,4-diaminopyridine of type **C** and 3,4,5-triaminopyridine derivatives (**D**).[28,30] Based on computational studies using methyl and acetyl cation affinity values as predictive tools by the Zipse group,[29] Lewis base catalysts of type **B** and **C** were expected to be more catalytically active than TCAP. However, this computational prediction was not confirmed experimentally.

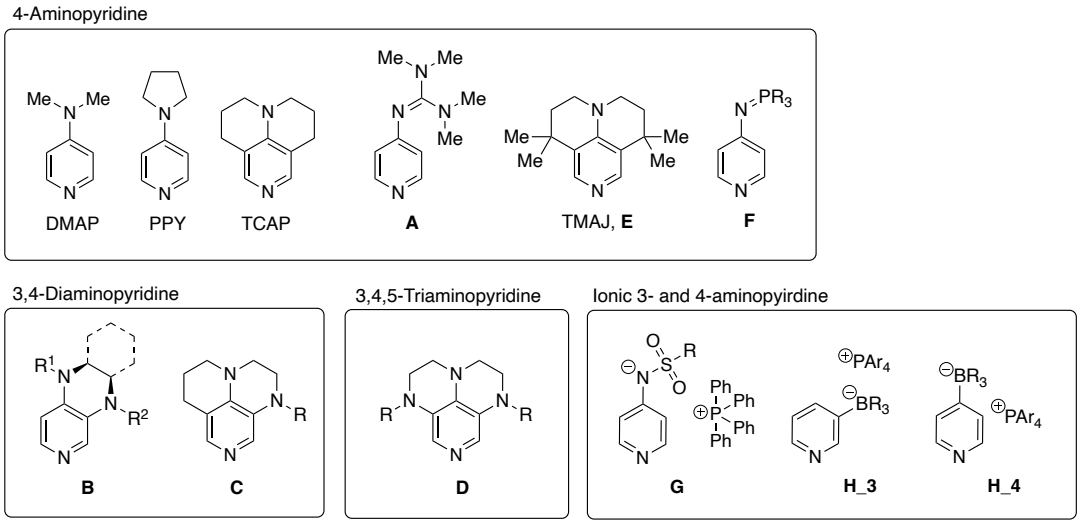

Chart 1.1: Pyridine-based Lewis based catalysts.

Thus, while all these new catalysts are more reactive than DMAP, the catalytic activity of TCAP has not yet significantly surpassed. In 2020, the Namba group synthesized 1,1,7,7-tetramethyl-9-azajulolidine (TMAJ, **E**),[31] a derivative of TCAP, which exhibited 1.5 times the catalytic activity of TCAP in a benchmark acylation reaction, which is in agreement with quantum chemical studies conducted by Zipse *et al*.[32] Shortly thereafter, Dyker *et al*. introduced 4-iminophosphorano pyridines (**F**), a new class of neutral organocatalysts, in which the most reactive derivative outperformed TCAP by a factor of two in acylation reactions.[33] As it can be seen in Chart 1.1, the pyridine ring has been systematically substituted with various types of donor substituents to generate a Lewis base organocatalyst with enhanced catalytic potential.

Recently, Helberg and Zipse[34] introduced a long-overlooked approach to increase the electron density of the pyridine ring by using stabilized 4-pyridinylamide anions. The developed pyridinamide ion pair (**G**) proved to be more catalytically active than TCAP by a factor of three in urethane reactions and by a factor of 15 in an inherently slow *aza*-Morita-Baylis Hillman reaction. For the first time in years a Lewis base catalyst displayed a catalytic potential significantly higher than TCAP. In 2023, Kass *et al.*[35] followed a similar approach by introducing 3-pyridinyl (**H_3**) and 4-pyridinyl (**H_4**) borate salts, which exhibit catalytic activity comparable to the most active pyridinamide ion pair catalyst in urethane reactions.

Though we will discuss *pyridinamide ion pair catalysts* in this thesis, based on their role in the catalytic cycle and their theorized type of connection with the substrate, they would be classified as Lewis base catalysts. Nevertheless, we wanted to give a short conceptual survey of what the field of *ion pair catalysis* entails.

1.1.2 Ion Pair Catalysis

Non-covalent organocatalysis has become a fundamental area of research in modern organic chemistry and can be divided into two key areas: hydrogen-bonding catalysis[36,37] and ion pair catalysis.[11,37,38] Hydrogen-bonding catalysis involves the activation of neutral electrophiles by neutral catalysts, whereas ion pair catalysis is characterized by the interaction of charged species. Since almost all organic reactions proceed via at least one charged intermediate, ion pair catalysis is a versatile tool for controlling both reactivity and selectivity. The concept of utilizing non-covalent interactions has been long established, especially in the field of phase-transfer catalysis (PTC), which emerged in the 1960s with the use of quaternary ammonium and phosphonium salts to mediate reactions between reagents in two immiscible phases.[39–41] While PTC is a well-known form of non-covalent organocatalysis, ion pair catalysis has

emerged as a distinct area, focusing on interactions between charged species within the same phase, thus extending the scope of classical PTC.[11,41] The design of catalysts that exploit non-covalent interactions, particularly ion pairing, presents unique opportunities for achieving selectivity in chemical transformations. As a result, ion pair catalysts have found widespread application in asymmetric catalysis.[42]

In ion pair catalysis, two key approaches have been identified: ion-binding catalysis[11,43] and counterion-directed catalysis[44] (see Figure 1.3). These approaches are further subdivided into anionic and cationic strategies, based on the charge of the interacting species. Counterion-directed catalysis typically involves a chiral charged catalyst directing the reaction through ion-pair interactions, whereas ion-binding catalysis employs a neutral catalyst that binds non-covalently to a charged species, forming a supramolecular complex.

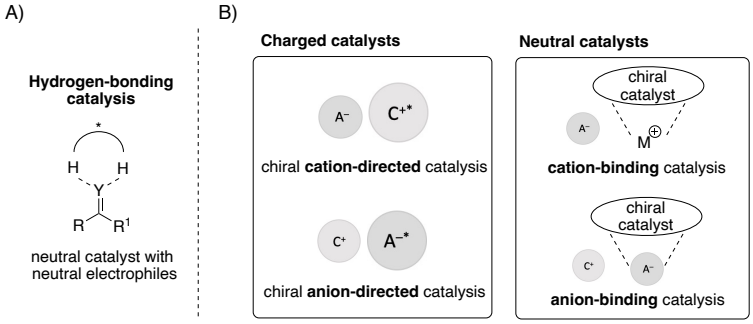

Figure 1.3. A) General activation mode of hydrogen-bonding catalysis. B) Types of asymmetric ion pairing catalysis.

Note that the concepts of ion-binding catalysis and counterion-directed catalysis differ significantly from one another. In counterion-directed catalysis, a charged (chiral) catalyst is used to direct the reaction via ion pairing interaction, whereas in ion-binding catalysis a neutral catalyst binds non-covalently to a charged species, resulting in a supramolecular complex. In recent year, ion pair catalysis has been further developed and novel approaches to design selective ion pair catalysts have been considered.[45–47] With ongoing research, the concept of ion pairing is also combined with other types of catalysis such as photochemical[48] or transition metal catalysis[49] which opens the new pathways to highly stereoselective organic transformations.

Understanding the challenges of designing selective asymmetric ion pair catalysts requires an appreciation of the underlying physical principles of ion pairs. The concept of ion pairs as distinct chemical entities was introduced in 1926 by Bjerrum.[50,51] An ion pair consists of two oppositely charged ions, a cation and an anion, that are associated with each other due to electrostatic interactions, but are not covalently bonded. The strength of an ionic interaction is dictated by Coulomb's law[50,51] (eq. 1.1), in which the interaction energy E is a function of the distance between the two charges q_1 and q_2, and is inversely related to the distance r between the ions and the relative permittivity ε of the surrounding medium.[11,43] Anslyn and Dougherty[52] further clarified that ion pairs form when the electrostatic attraction between ions exceeds the thermal energy required to separate them via Brownian motion. This interaction is described by the Bjerrum length λ_B, which defines the distance between the two charged species q_1 and q_2, at which electrostatic forces dominate over thermal energy as described in eq. 1.2 with ε_r being the relative permittivity of the medium, ε_0 being the vacuum permittivity, k_B being the Boltzmann constant, and T being the absolute temperature. With eq. 1.2, the distance where electrostatic interactions matter in catalysis can be calculated. Therefore, solvation effects play an important role in ion pair catalysis.

$$E = \frac{q_1 q_2}{4\pi\varepsilon\varepsilon_0 r} \tag{1.1}$$

$$\lambda_B = \frac{q_1 q_2}{4\pi\varepsilon\varepsilon_0 r} \times \frac{1}{k_B T} \tag{1.2}$$

Ion pairs can be classified into three different types based on the degree of solvation as depicted in Figure 1.4.[53,54] In solvents with lower permittivity, *contact ion pairs* with a common solvation shell and no solvent molecules between the anion and cation, are energetically favored, whereas *solvent-shared ions*, where the ions are separated by a shared solvation shell, and *solvent-separated ion pairs*, where each ion has its own solvation shell, are predominant in solvents with higher permittivity.[53,55,56]

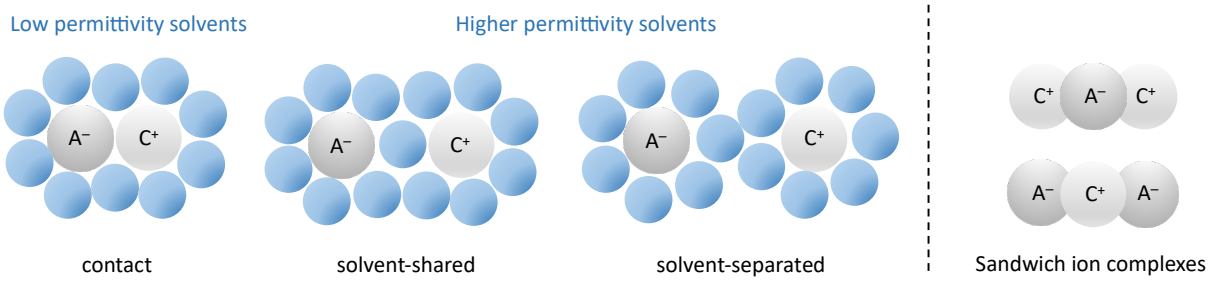

Figure 1.4. Types of ion pairs based on the degree of solvation and potentially higher aggregates.[53]

In solvents of low permittivity, ion association can proceed beyond ion pairing to form triple ions or higher aggregates.[53,54] The formation of triple ions, in this work also referred to as sandwich ions (Chapter 2 and 3), was first introduced by Fuoss and Kraus.[57] The concept has been adopted by other researchers who studied the conductivity of electrolytes in non-aqueous solutions. Nevertheless, the evidence for triple ions formed through purely electrostatic forces is ambiguous. However, several theoretical arguments are favorable, as are our findings, which are discussed in Chapter 2 and 3 of this work.[54]

1.2 Aim of this thesis

This introductory chapter provides an overview of the steps taken in the development pyridine-based Lewis base organocatalysts with enhanced catalytic activity. The most recent advancement was achieved by utilizing pyridinamide anions in combination with cations carrying aromatic substituents in organic transformation reactions. The initially conducted studies already demonstrated their enhanced catalytic potential in addition reactions such as the urethane synthesis and the *aza*-Morita-Baylis Hillman reaction.[34] However, working with ionic substrates requires a new methodical approach and a distinct toolbox of techniques than those previously employed in our studies of neutral Lewis base catalysts.[58,59] Classical methods such as ^{1}H-NMR spectroscopy, gas chromatography (GC) or high-performance liquid chromatography (HPLC) are insufficient for gaining the desired insights into the unique behavior of pyridinamide ion pairs in solution.

The primary objective of this study is to identify the association pattern of pyridinamide salts in organic solvents of low polarity and how the association state influences their reactivity. To achieve this goal, a combination of conductivity, diffusion-ordered NMR and photometric kinetic measurements is employed. Conductivity data and DOSY NMR combined are utilized to assess the association pattern. Association constants are determined based on the conductivity data alone, utilizing numerical simulations. Kinetic measurements utilizing a refined ionic strength-controlled benzhydrylium ion methodology quantify the reactivity of pyridinamide salts in terms of the nucleophilicity of the involved anion. By studying a library of pyridinamide salts according to this methodology, we seek to identify key

properties that will allow us to design the reactivity of future pyridinamide catalysts. Furthermore, we aim to investigate the scope of reaction types suitable for utilizing ionic pyridinamide catalysts. Finally, the synthesis of chiral pyridinamide anions is attempted.

1.3 References

[1] D. W. C. MacMillan, *Nature* **2008**, *455*, 304–308.

[2] J. F. von Liebig, *Annalen der Chemie und Pharmacie*, G.C. Wittstein, Leipzig, **1861**.

[3] K. A. Ahrendt, C. J. Borths, D. W. C. MacMillan, *J. Am. Chem. Soc.* **2000**, *122*, 4243–4244.

[4] P. I. Dalko, L. Moisan, *Angew. Chem. Int. Ed.* **2004**, *43*, 5138–5175.

[5] P. Hobza, K. Müller-Dethlefs, *Non-Covalent Interactions: Theory and Experiment*, Royal Society of Chemistry, Cambridge, **2010**.

[6] Y. Huang, A. M. Walji, C. H. Larsen, D. W. C. MacMillan, *J. Am. Chem. Soc.* **2005**, *127*, 15051–15053.

[7] A. Erkkilä, I. Majander, P. M. Pihko, *Chem. Rev.* **2007**, *107*, 5416–5470.

[8] P. R. Schreiner, *Chem. Soc. Rev.* **2003**, *32*, 289–296.

[9] P. M. Pihko, *Hydrogen Bonding in Organic Synthesis*, Wiley VCH, Weinheim, **2009**.

[10] S. Beckendorf, S. Asmus, O. G. Mancheño, *ChemCatChem* **2012**, *4*, 926–936.

[11] K. Brak, E. N. Jacobsen, *Angew. Chem. Int. Ed.* **2013**, *52*, 534–561.

[12] B. List, *Chem. Rev.* **2007**, *107*, 5413–5415.

[13] E. Vedejs, S. E. Denmark, *Lewis Base Catalysis in Organic Synthesis, 3 Vol. Set*, Wiley-VCH, Weinheim, **2016**.

[14] S. E. Denmark, G. L. Beutner, *Angew. Chem. Int. Ed.* **2008**, *47*, 1560–1638.

[15] W. B. Jensen, *Chem. Rev.* **1978**, *78*, 1–22.

[16] A. Einhorn, F. Hollandt, M. von Alfred Einhorn, *Justus Liebigs Ann. Chem.,* **1898**, *301*, 95–115.

[17] L. M. Litvinenko, A. I. Kirichenko, *Dokl. Akad. Nauk SSSR Ser. Khim.,* **1967**, *176*, 97–100.

[18] W. Steglich, G. Höfle, *Angew. Chem. Int. Ed.* **1969**, *8*, 981–981.

[19] W. Steglich, G. Höfle, *Tetrahedron Lett.* **1970**, *11*, 4727–4730.

[20] A. Hassner, V. Alexanian, *Tetrahedron Lett.* **1978**, *19*, 4475–4478.

[21] G. Höfle, W. Steglich, H. Vorbrüggen, *Angew. Chem. Int. Ed.* **1978**, *17*, 569–583.

[22] B. Neises, W. Steglich, *Angew. Chem. Int. Ed.* **1978**, *17*, 522–524.

[23] S. K. Chaudhary, O. Hernandez, *Tetrahedron Lett.* **1979**, *20*, 95–98.

[24] S. K. Chaudhary, O. Hernandez, *Tetrahedron Lett.* **1979**, *20*, 99–102.

[25] P. Patschinski, C. Zhang, H. Zipse, *J. Org. Chem.* **2014**, *79*, 8348–8357.

[26] M. R. Heinrich, H. S. Klisa, H. Mayr, W. Steglich, H. Zipse, *Angew. Chem. Int. Ed.* **2003**, *42*, 4826–4828.

[27] A. Hassner, L. R. Krepski, V. Alexanian, *Tetrahedron* **1978**, *34*, 2069–2076.

[28] S. Singh, G. Das, O. V. Singh, H. Han, *Org. Lett.* **2007**, *9*, 401–404.

[29] I. Held, S. Xu, H. Zipse, *Synthesis* **2007**, *2007*, 1185–1196.

[30] R. Tandon, T. Unzner, T. A. Nigst, N. De Rycke, P. Mayer, B. Wendt, O. R. P. David, H. Zipse, *Chem. Eur. J.* **2013**, *19*, 6435–6442.

[31] T. Tsutsumi, A. Saitoh, T. Kasai, M. Chu, S. Karanjit, A. Nakayama, K. Namba, *Tetrahedron Lett.* **2020**, *61*, 152047.

[32] I. Held, A. Villinger, H. Zipse, *Synthesis* **2005**, 1425–1430.

[33] N. A. Richard, G. D. Charlton, C. A. Dyker, *Org. Biomol. Chem.* **2021**, *19*, 9167–9171.

[34] J. Helberg, T. Ampßler, H. Zipse, *J. Org. Chem.* **2020**, *85*, 5390–5402.

[35] S. H. Dempsey, A. Lovstedt, S. R. Kass, *J. Org. Chem.* **2023**, *88*, 10525–10538.

[36] M. S. Taylor, E. N. Jacobsen, *Angew. Chem. Int. Ed.* **2006**, *45*, 1520–1543.

[37] E. Matador, R. Fernández, J. M. Lassaletta, L. Dell'Amico, in *Asymmetric Organocatalysis: New Strategies, Catalysts, and Opportunities*, (Eds.: L. Albrecht, A. Albrecht, L. Dell'Amico), Wiley-VCH, Weinheim, **2023**, pp.121–149.

[38] D. Qian, J. Sun, *Chem. Eur. J.* **2019**, *25*, 3740–3751.

[39] C. M. Starks, *J. Am. Chem. Soc.* **1971**, *93*, 195–199.

[40] S. Shirakawa, K. Maruoka, *Angew. Chem. Int. Ed.* **2013**, *52*, 4312–4348.

[41] J. Otevrel, M. Waser, in *Asymmetric Organocatalysis: New Strategies, Catalysts, and Opportunities*, (Eds.: L. Albrecht, A. Albrecht, L. Dell'Amico), Wiley-VCH, Weinheim, **2023**, pp. 71–120.

[42] M. Waser, J. Novacek, K. Gratzer, in *Cooperative Catalysis: Designing Efficient Catalysts for Synthesis* (Ed.: R. Peters), Wiley-VCH, Weinheim, **2015**, pp. 197–226.

[43] F. Dressler, P. R. Schreiner, in *Anion-Binding Catalysis* (Ed.: O. G. Mancheño), Wiley-VCH, Weinheim, **2022**, pp. 1–77.
[44] M. Mahlau, B. List, *Angew. Chem. Int. Ed.* **2013**, *52*, 518–533.
[45] J. E. Gillespie, A. Fanourakis, R. J. Phipps, *J. Am. Chem. Soc.* **2022**, *144*, 18195–18211.
[46] A. J. Neel, M. J. Hilton, M. S. Sigman, F. D. Toste, *Nature* **2017**, *543*, 637–646.
[47] K. Ohmatsu, *Bull. Chem. Soc. Jpn.* **2023**, *96*, 1169–1178.
[48] T. E. Schirmer, B. König, *J. Am. Chem. Soc.* **2022**, *144*, 19207–19218.
[49] Z. Zhang, V. Smal, P. Retailleau, A. Voituriez, G. Frison, A. Marinetti, X. Guinchard, *J. Am. Chem. Soc.* **2020**, *142*, 3797–3805.
[50] K. D. Bjerrum, *Videsk. Selesk. Math.-Fys Medd.,* **1926**.
[51] M. Szwarc, *Acc. Chem. Res.* **1969**, *2*, 87–96.
[52] E. V. Anslyn, D. A. Dougherty, *Modern Physical Organic Chemistry*, University Science Books, **2006**.
[53] Y. Marcus, G. Hefter, *Chem. Rev.* **2006**, *106*, 4585–4621.
[54] Y. Marcus, *Ions in Solution and Their Solvation*, Wiley-VCH, Weinheim, **2015**.
[55] E. Grunwald, *Anal. Chem.* **1954**, *26*, 1696–1701.
[56] S. Winstein, E. Clippinger, A. H. Fainberg, G. C. Robinson, *J. Am. Chem. Soc.* **1954**, *76*, 2597–2598.
[57] R. M. Fuoss, C. A. Kraus, *J. Am. Chem. Soc.* **1933**, *55*, 2387–2399.
[58] B. Pölloth, M. P. Sibi, H. Zipse, *Angew. Chem. Int. Ed.* **2021**, *60*, 774–778.
[59] S. Mayr, H. Zipse, *Eur. J. Org. Chem.* **2022**, *2022*, e202101521.

Chapter 2. Highly Nucleophilic Pyridinamide Anions in Apolar Organic Solvents due to Asymmetric Ion Pair Association

Veronika Burger, Maximilian Franta, Armin R. Ofial*, Ruth M. Gschwind* and Hendrik Zipse*

J. Am. Chem. Soc., **2024**, *accepted* (DOI: 10.1021/jacs.4c14825).

Autor contributions: Veronika Burger (V.B.) and Hendrik Zipse (H.Z.) conceived the study. All experimental studies were performed by V.B. with exception of DOSY NMR measurements, which were performed by Maximilian Franta (M.F.). The manuscript was jointly written by V.B., Ruth M. Gschwind (R.M.G.), Armin R. Ofial (A.R.O.) and H.Z. The supporting information was prepared by V.B. and M.F.

Additional information: The here displayed supporting information is an altered and shorted version of the submitted SI. The DOSY results are used for the explanation of findings, but no technical details are discussed in this thesis. These can be found in the original file. For comparison of this thesis and the original SI file, the numbering includes the original item number as shown below.

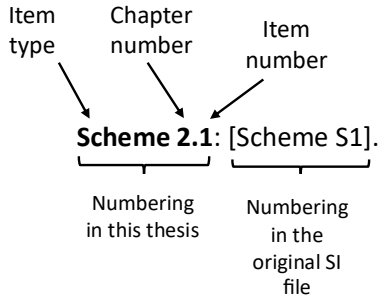

Highly Nucleophilic Pyridinamide Anions in Apolar Organic Solvents due to Asymmetric Ion Pair Association

Veronika Burger[a], Maximilian Franta[b], Armin R. Ofial*[a], Ruth M. Gschwind*[b] and Hendrik Zipse*[a]

[a]Department of Chemistry, Ludwig-Maximilians-Universität München, Butenandtstr. 5-13, 81377 München, Germany; [b]Institute for Organic Chemistry, University Regensburg, Universitätsstr. 31, 93053 Regensburg, Germany

KEYWORDS: conductivity, DOSY, asymmetric association, nucleophilicity, kinetics.

ABSTRACT: Free ions in organic solvents of low polarity would be valuable tools for the activation of low reactivity substrates. However, the formation of unreactive ion pairs at concentrations relevant for synthesis has prevented the success of this concept so far. On the example of highly nucleophilic pyridinamide phosphonium salts in dichloromethane we show that asymmetric aggregation offers a solution to this general problem. A combination of conductivity, diffusion-ordered NMR (DOSY), and kinetic measurements utilizing a refined ionic strength-controlled benzhydrylium ion methodology enables uniqueinsight about the number of ions with their aggregation/association state and nucleophilicity of the involved anions. This approach reveals that pyridinamide tetraphenylphosphonium salts aggregate in dichloromethane solution asymmetrically to sandwich-type cations and anions together with their free counterions. The nucleophilicity of free pyridinamide ions exceeds that of the neutral reference nucleophile 9-azajulolidine (TCAP) by up to two orders of magnitude. Based on these results we suggest that asymmetric aggregation in organic solvents of low polarity might be a general pathway to boost the reactivity of anionic nucleophiles.

INTRODUCTION

Lewis basic pyridines, such as 4-(dimethylamino)pyridine (DMAP, **1**)[1] or the more reactive 9-azajulolidine (TCAP, **2**),[2] are frequently used catalysts for group transfer reactions such as acylations,[3-6] esterifications,[4,6] alkylations,[7] and silylations (Chart 1).[8,9] The nucleophilicity of these catalysts, together with other donor-substituted pyridines, has been quantified using Mayr's benzhydrylium ion method.[10–13] Even higher nucleophilicities and possibly also higher catalytic activities in Lewis base-mediated reactions may be expected for anionic Lewis bases. Given that anionic reagents unavoidably require a counter-cation, such salts tend to form ion pairs when dissolved in organic solvents of low polarity, such as dichloromethane.[14,15] This ion clustering has beneficially been used in ion pair catalysis,[16-18] which extends from classical cationic phase-transfer (PT) catalysis[19] to applications in asymmetric synthesis.[16,20-22] Recently, the Zipse group introduced Lewis basic pyridinamide ion pair catalysts, which outperformed TCAP and other neutral organocatalysts in selected catalytic benchmark reactions.[23,24]

Chart 1. Structures of neutral organocatalysts DMAP (1) and TCAP (2), and of pyridinamide ion pair catalyst 3a and 4a.

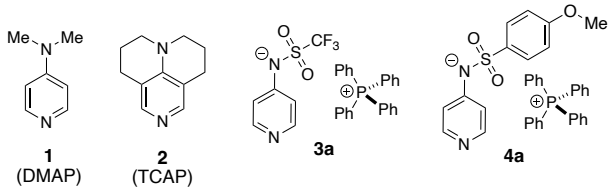

The pyridinamide phosphonium salts (such as **3a** and **4a** in Chart 1) investigated so far show the general usefulness of the concept of anionic nucleophilic organocatalysis, whose development tails that of neutral systems.[25-27]

In order to minimize ion pairing effects, most kinetic studies aiming at the quantification of the reactivity of anionic nucleophiles have been performed in highly polar solvents (water, DMSO, etc.), often in combination with crown ether additives to further reduce the interactions between metal counter-ions and the reacting anion.[28] In solvents of low polarity, the intrinsic nucleophilicity of a free anion should be far higher than in more polar media. However, the reactivity of anions is attenuated by ion pair formation, which also gives rise to non-linear effects and, thus, complicates systematic kinetic studies in organic solvents of low polarity (dichloromethane (DCM), THF, toluene etc.) commonly employed in organocatalysis.

In order to elucidate the underlying principles responsible for the experimentally observed high nucleophilicity of the anions in salts such as **3a** and **4a**, we report here a combination of conductivity measurements, diffusion-ordered NMR (DOSY) measurements at very low concentrations, and photometric kinetic measurements by utilizing an ionic strength-controlled benzhydrylium methodology. This combination of physicochemical methods is expected to be generally applicable to ion pair chemistry and catalysis and may help to uncover the full potential of this field.

RESULTS AND DISCUSSION

Conductivity. Conductivity measurements have frequently been employed to quantify ion pairing effects.[29-32] This method was therefore applied to determine the association of the cationic and anionic components of phosphonium salt **3a** selected here as a reference system in DCM and acetonitrile (MeCN). In both solvents **3a** is expected to be more reactive towards electrophiles than DMAP (**1**). Conductivity measurements were

performed for concentrations ranging from 0.02 mM to 1.0 mM as this appears to represent the onset of ion pair formation from free ions. At low electrolyte concentrations and for the case of non-interacting ions the experimentally determined conductivity κ depends on the specific molar conductivity Λ_m and the ion concentration [A] as expressed in Equation (1).

$$\kappa = \Lambda_m[A] \quad (1)$$

In the polar aprotic solvent MeCN the ions of **3a** are well stabilized and exist mainly as free ions as indicated by a nearly perfect linear increase of conductivity with [**3a**] (see SI, Figure S1). In the less polar solvent DCM the situation is more complex and two different domains can be seen in Figure 1B: (a) At low **3a** concentrations (region I, blue background, [**3a**] < 0.04 mM) the conductivity κ correlates linearly with [**3a**], and (b) a non-linear part II at higher concentrations of **3a** (see Figure 1B beige background). While linear region I is assumed to represent the behavior of free anions (**3**) and cations (**a**), three ion association models were tested for non-linear region II. The first corresponds to the formation of ion pair **3a** (purple box in Figure 1A), while the second model involves formation of "sandwich cation" **a3a** together with free anion **3** (grey box in Figure 1A), and the third model considers formation of an analogous sandwich anion **3a3** (blue box in Figure 1A). The latter model was originally proposed to account for the properties of tetraalkyl ammonium salts in apolar solution,[33] and subsequently employed for a variety of systems in organic solvents.[34-37] In order to compare both models on equal footing, the respective equilibrium constants K_{IP} and K_{CAC} are defined relative to two equivalents each of free cation **a** and free anion **3**.

The 1:1 ion pair model retains the specific molar conductivity Λ_m derived from the linear region I and adds the effects of reducing the number of conducting species through formation of overall neutral (and thus inactive) ion pairs **3a**. Fitting this model to the observed conductivities up to an overall concentration of 1.0 mM yields ion pair formation constant $K_{IP} = 6.86 \times 10^5$ M^{-2} with good accuracy. The second model involves formation of sandwich cation **a3a** together with one equivalent of free anion **3** (grey box in Figure 1A), again combined with the specific molar conductivity Λ_m value obtained from linear region I. This model fits the observed conductivity values in the region up to 1.0 mM with sandwich association constant $K_{CAC} = 6.38 \times 10^6$ M^{-2} with equally good accuracy. This is also true for the third model involving formation of sandwich anion **3a3** (blue box in Figure 1A), for which the optimized association constant is $K_{ACA} = 6.38 \times 10^6$ M^{-2}, numerically identical with K_{CAC}. The measured conductivity values together with the model predictions are depicted in Figure 1B (grey line for the **a3a** sandwich model, blue line for the **3a3** sandwich model, and purple dotted line for the 1:1 ion pair), which illustrates that all models fit the experimental conductivity curve equally well as indicated by largely similar RMSE values of RMSE(K_{CAC}) = 0.17, RMSE(K_{ACA}) = 0.17, and RMSE(K_{IP}) = 0.30, respectively.

DOSY NMR. Since conductivity measurements alone cannot provide direct information on the size of the contributing ions, DOSY-NMR measurements of **3a** were performed in DCM-d_2 for concentrations ranging from 0.005 mM to 1.0 mM (see Figure 1C and SI, Chapter 4 for detailed information). To enable DOSY measurements at these low concentrations, a 600 MHz spectrometer with a helium cryo probe and measurement times up to 16 h per sample were employed. The DOSY results were compared to calculated volumes of anion **3** (215 Å^3), cation **a** (362 Å^3), and contact ion pair **3a** (570 Å^3), which are based on the van der Waals cavities employed in the SMD continuum solvation model at the SMD(DCM)/B3LYP-D3/6-31+G(d) level of theory and indicated through the horizontal dashed lines in Figure 1C. At [**3a**] = 0.005 mM as the lowest concentration accessible for DOSY measurements we determined volumes of 367 Å^3 for cation **a** and 192 Å^3 for anion **3**, both of which agree closely with the SMD-derived volumes for cation **a** and anion **3**. At any concentration of **3a** > 0.005 mM considerably larger cation and anion volumes were observed already in region I (for full data see SI, Chapter 4). In the 1:1 association model shown in the purple box in Figure 1A, the volumes of both species are expected to converge to the SMD-derived value of 570 Å^3 for the 1:1 ion pair **3a**. Instead, we persistently detected substantially different effective volumes for cation **a** and anion **3** also at higher concentrations (region II), and also note that the DOSY-derived volume for cation **a** exceeds that calculated for the 1:1 ion pair **3a**.

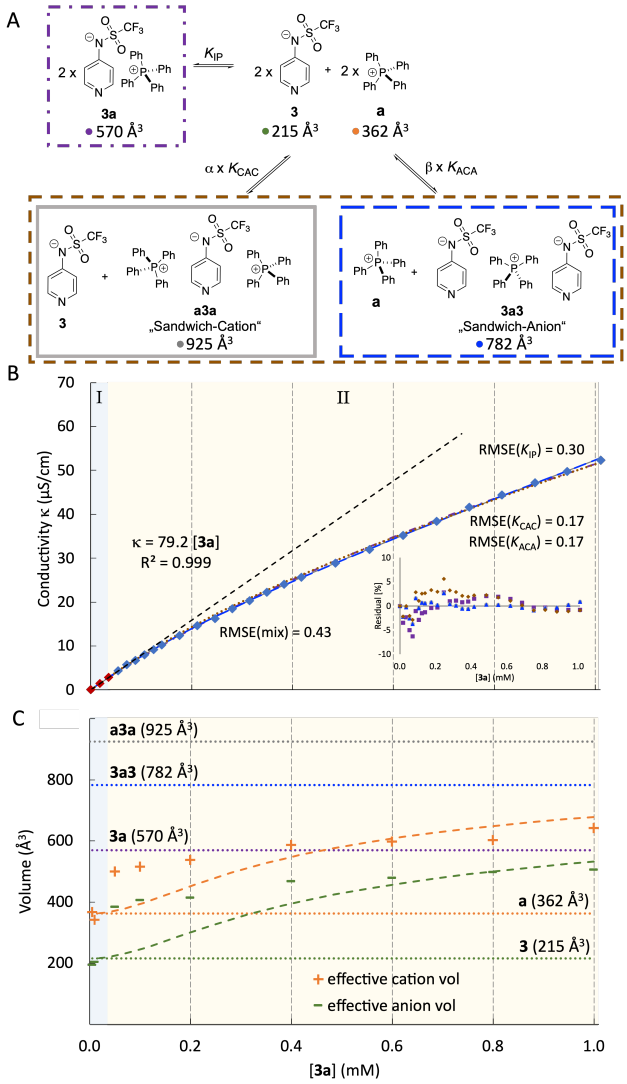

Figure 1. (A) 1:1 ion pair **3a**, sandwich cation **a3a**, and sandwich anion **3a3** as potential association models for anion **3** and cation **a** together with SMD-derived molecular volumes; (B) conductivity profile for **3a** in DCM fits to the calculated conductivity data for the 1:1 association model (purple dotted/dashed line), and the two sandwich association models (grey and blue line); (C) DOSY-derived ion volumes [Å^3] compared to SMD-derived volumes (dashed horizontal lines) for single anion **3**, single cation **a**, ion pair **3a**, cation sandwich **a3a**, and anion sandwich **3a3**.

This latter observation can be rationalized with the sandwich ion models, where the DOSY-derived cation volume is expected to approach that of the **a3a** sandwich cation of 925 Å^3. Combining the SMD-derived molecular volumes of ions with the equilibrium constants obtained from conductivity measurements allows us to predict concentration-dependent effective cation and anion volumes. These are shown in Figure 1C as a green line for anion and an orange line for cation volumes. Comparing experimentally derived with theoretically predicted volumes shows these to coincide quite well between 0.4 mM and 1.0 mM for the cation sandwich model.[38] In contrast, the 1:1 model predicts volumes for both ions which are significantly lower than the experimental values (by more than 200 Å^3 for the cation and >100 Å^3 for the anion, see SI). This is also true for the **3a3** anion sandwich model that predicts larger anion than cation volumes not consistent with the DOSY experiments. The agreement between experimentally determined DOSY volumes and model predictions can be further improved by combining the two sandwich models considered here. This requires optimization of the two scaling factors α and β shown in Figure 1A such that the agreement with the conductivity data and the DOSY volumes is optimized. Best agreement for ion pair **3a** is found for α = 0.44 and β = 0.21, which implies that 50% of the anion **3** is free while the other 50% is stored in the two sandwich complexes at I = 1.0 mM. In contrast, for ion pair **4a** the DOSY experiments show inverted relative ion volumes with larger values for anion **4** (see SI, Chapter 4). This is reflected by the mixing coefficients for ion pair **4a** amounting to α = 0.12 and β = 0.61. This implies that 34% of anion **4** is free and 66% is hidden in the two sandwich complexes. The performance of these "mixed sandwich" models is quite satisfactory in concentration region II, but less so in region I with its rapid increase of ion volumes with salt concentration. It is an intriguing aspect of the formation of sandwich cation **a3a** that it generates one equivalent of free anion **3** as the counterion. The concentration of free anion **3** will quite obviously impact the efficiency of pyridinamide-anion based catalytic systems, where free anion **3** is expected to account for most of the observed activity.

Kinetics. To characterize the nucleophilic reactivity of ion pairs **3a** and **4a** in an organic solvent of low polarity, such as DCM, we refined Mayr's well-known benzhydrylium ion method by implementing an ionic strength-control. This enabled the characterization of free anionic nucleophiles for the first time in DCM. Mayr's methodology has repeatedly demonstrated its utility to describe the reactivity of a wide range of carbon-, nitrogen, oxygen-, sulfur-, and phosphor-based nucleophiles in different solvents,[39] including DMAP (**1**) and TCAP (**2**).[10,11,39] In short, the benzhydrylium ion method involves the photometric monitoring of the reactions of colored benzhydrylium salts, such as **5a**–**5c** (Table 1) whose electrophilic reactivities are characterized by the solvent-independent parameters E, with nucleophiles used in excess concentration to achieve kinetics under pseudo-first order conditions. The first-order rate constants k_{obs} (s^{-1}) can then be obtained by fitting a mono-exponential decay function to the decreasing absorption of **5** during the reaction with **3**. The conductivity measurements (see SI, Figure S1) had shown that **3a** and **4a** fully dissociate into anions and cations when dissolved in MeCN. Accordingly, a linear increase of pseudo-first order rate constants k_{obs} with nucleophile concentrations [**3**] (or [**3a**]) was observed in the kinetics of reactions of **3a** with **5** [Equation (2)].

$$k_{obs} = k_2[\mathbf{3}] \quad (2)$$

$$\log k_2 = s_N(N + E) \quad (3)$$

Equation (2) thus yields the second-order rate constants k_2 (M^{-1} s^{-1}) for the reactions of **3** with **5a**-**5c** in acetonitrile (Table 1). The rate constants k_2 for **3** are approx. three times larger than those for analogous reactions of **5** with DMAP (**1**) and quite similar to those for reactions with TCAP (**2**). Analyzing the kinetic data with the Mayr-Patz Equation (3) yields the nucleophilicity N = 16.38 (s_N = 0.60) of **3** in MeCN. Following exactly the same approach for ion pair **4a** yields N(**4a**) = 17.28 (s_N = 0.65), in excellent agreement with the results obtained for these two systems in selected catalytic transformations.[23]

Table 1. Second-order rate constants k_2 for the reactions of DMAP (1), TCAP (2), and pyridinamide salts 3a and 4a with reference electrophiles 5a, 5b, and 5c in MeCN (at 20 °C) analyzed by equation (3) to give the nucleophile-specific reactivity parameters N (and s_N).

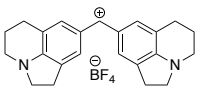

(lil)$_2$CH$^+$ (**5a**)
E = -10.04

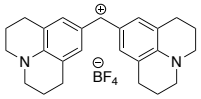

(jul)$_2$CH$^+$ (**5b**)
E = -9.45

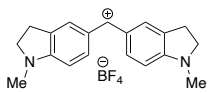

(ind)$_2$CH$^+$ (**5c**)
E = -8.76

Cat	k_2 [M^{-1} s^{-1}]			N (s_N)
	5a	**5b**	**5c**	
1[a]	2.11 × 10^3	5.30 × 10^3	1.29 × 10^4	15.51 (0.62)[e]
2[b]	6.30 × 10^3	–	4.17 × 10^4	15.60 (0.68)[e]
3[c]	7.16 × 10^3	1.53 × 10^4	4.13 × 10^4	16.38 (0.60)
4[d]	5.11 × 10^4	1.36 × 10^5	3.47 × 10^5	17.28 (0.65)

[a] Second-order rate constants k_2 from ref. [10]. [b] Second-order rate constants k_2 from ref. [11]. [c] Assuming that [**3**] = [**3a**]$_0$. [d] Assuming that [**4**] = [**4a**]$_0$. [e] Additional k_2 values from refs. [10,11] were used to determine N (and s_N).

The kinetics of reactions of **3a** with the reference electrophiles **5** in DCM solution, however, showed a more complex dependence of k_{obs} on [**3a**] in the concentration range from 0.01 to 1.0 mM (red and blue diamonds in Figure 2). In analogy to the conductivity measurements, an initial region I with linear k_{obs} vs. [**3a**]$_0$ relation was observed (Figure 2, blue background, experimental values marked in red). At higher [**3a**] values this is followed by non-linear region II (blue diamonds on beige background in Figure 2), where the observed rate constants deviate negatively from the linear correlation extrapolated from region I. The degree of deviation reflects the fraction of anion **3** captured in the (presumably) unreactive sandwich cation **a3a** and the (presumably) less reactive sandwich anion **3a3**.

Analysis of the kinetic data in region I (0.01 – 0.03 mM) is straightforward as conductivity measurements in combination with the sandwich association models indicate almost complete (> 97%) dissociation into separate ions **3** and **a**, that is [**3**] = [**3a**]$_0$. Application of eq. (2) then yields k_2(**5a**) = 1.84 × 10^6 M^{-1} s^{-1} as indicated by the dashed line in Figure 2.

In synthetic applications, the concentration of ion pair catalysts is usually 1.0 mM or higher, which is far into the non-linear region II. Increasing ion concentrations may impact the reaction rates not only through shifting the association equilibrium towards a higher fraction of ionic aggregates, but also through non-specific polarity effects. To assess the influence of the high salt concentration on the solvent polarity, we determined Reichardt's E_T(30) values in DCM solutions with increasing concentrations of pyridinamide salt **3a** and additive $Ph_4P^+BF_4^-$ (**6**). As shown in Figure 2 this additive combines the common unreactive ions in the reaction mixture, that is, the BF_4^- of the benzhydrylium salts and the unreactive Ph_4P^+ countercation of the pyridinamide salts. We observed insignificant

changes of the $E_T(30)$ values even at total salt concentrations of up to 6.0 mM (see SI).

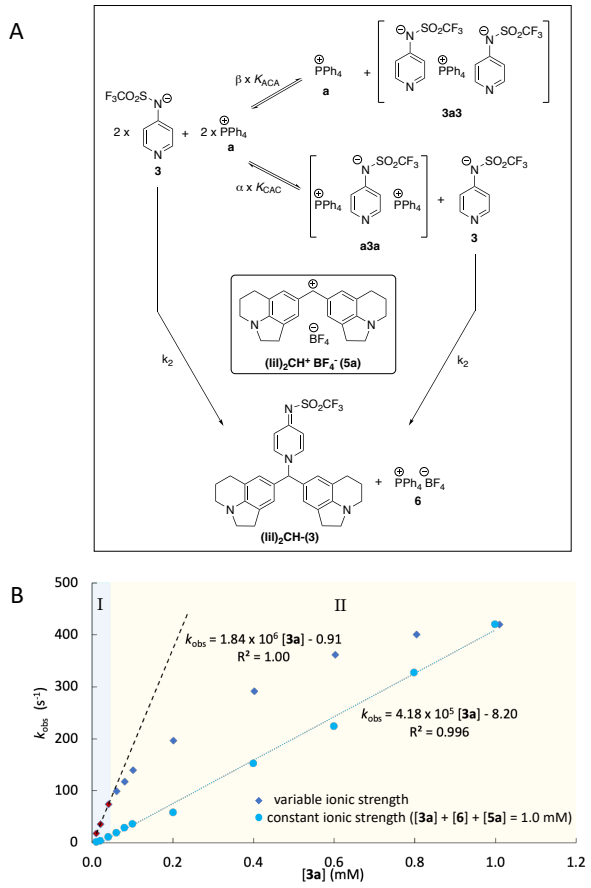

Figure 2. (A) Benzhydrylium ion reaction applied for the quantification of nucleophilicity of **3**. (B) Correlation of k_{obs} for the reaction of **5a** with **3a** for salt concentrations [**3a**] from 0.01 – 1.0 mM in DCM at 20°C (blue diamonds), and in the presence of additive PPh_4BF_4 (**6**) (turquoise dots).

We conclude, therefore, that addition of **6** to a reaction mixture of **3a** and **5a-c** does not change the overall polarity of the solvent system and only affects the position of the ion pairing equilibrium shown in Figure 2, where higher concentrations of Ph_4P^+ (= **a**) give rise to an increase of [**a3a**]. To further investigate the effect of the $Ph_4P^+BF_4^-$ (**6**) additive, the ion volumes of selected **3a** + **6** mixtures were determined by DOSY measurements. The DOSY experiments show that the volumes of the cation and anion determined for **3a** + **6** mixtures at an ionic strength of I = 1.0 mM are in the same region as the volumes obtained for a pure **3a** solution at [**3a**] = 1.0 mM (for details see SI).[40] The kinetics of the reaction of **3a** + **5a** was subsequently studied at constant ionic strength (I) of I = 1.0 mM as this represents the highest concentration of **3a** in this study. At [**3a**] < 1.0 mM, the ionic strength of the DCM solution was adjusted by addition of **6** such that in each kinetic measurement the condition [**3a**] + [**6**] + [**5a**] = 1.0 mM is fulfilled. By maintaining I = 1.0 mM, the rate constants k_{obs} for **3a** + **5a** reactions in DCM correlated linearly with [**3a**] in the entire concentration range from 0.01 to 1.0 mM (turquoise points in Figure 2). When we account for the fact that variable fractions of anion **3** are caught in unreactive sandwich cation **a3a** (and to a smaller extend also in anion sandwich **3a3**), and also consider the effect of additive **6** on [Ph_4P^+], we obtain k_2(**5a**) = 5.42 × 10^5 M^{-1} s^{-1} for the reaction of **3** with **5a**, which is by a factor of 3.5 lower than k_2 obtained in the low-concentration region (Table 2). Analogous kinetic measurements at I = 1.0 mM were performed for reactions of **3a** with the more reactive benzhydryl salts **5b** and **5c** (Table 2).

Table 2. Second-order rate constants k_2 of the reactions of DMAP (1), TCAP (2), and pyridinamide salt 3a with the reference electrophiles 5a, 5b, and 5c in DCM (at 20 °C).

Cat	k_2 [M^{-1} s^{-1}]		
	5a	**5b**	**5c**
1[a]	6.45 × 10^3	9.84 × 10^3	4.96 × 10^4
2[b]	1.42 × 10^4	3.11 × 10^4	1.28 × 10^5
3[c]	1.82 × 10^6 (LC)	4.23 × 10^6 (LC)	1.98 × 10^7 (LC)
3[d]	5.42 × 10^5 (mix)	1.25 × 10^6 (mix)	4.64 × 10^6 (mix)
4[e]	1.69 × 10^6 (mix)	4.19 × 10^6 (mix)	1.15 × 10^7 (mix)

[a] Second-order rate constants k_2 from ref. [10a]. [b] This work, see Supporting Information for details of the kinetic experiments. [c] Determined at [**3**] < 0.03 mM, that is, in the low concentration (LC) region I (Figure 2), by assuming [**3**] = [**3a**]$_0$. [d] Determined over a concentration range [**3a**] = 0.1 to 0.3 mM at constant ionic strength I = 1.0 mM (kept by addition of salt **6**) by assuming a mixed sandwich association model (see SI for details). [e] Determined over a concentration range [**4a**] = 0.04 to 0.1 mM at constant ionic strength I = 1.0 mM (kept by addition of salt **6**) by assuming a mixed sandwich association model

In DCM as the solvent, we note a moderate increase in the bimolecular rate constants k_2 when going from DMAP (**1**) to TCAP (**2**), but a significantly larger increase of the k_2 values for **3a** (Table 2). The k_2 values for reaction of **3a** with **5a-5c** in DCM in the low concentration (LC) region I (as defined in Figure 2) exceed those for **2** by approx. two orders of magnitude. Analyzing the LC kinetic data by the Mayr-Patz equation (3) gives N = 17.78 (s_N = 0.81) for **3a**. Rate constants k_2 for reactions of **3** with all three benzhydryl cations **5a-5c** decrease slightly (by a factor of 3.5-4.5) under conditions of constant ion strength (I = 1.0 mM). The resulting N-parameter for **3** is, however, hardly changed at N = 17.88 (s_N = 0.73). Following the same mode of analysis for **4a** under reactions conditions where I = 1.0 mM, we find that anion **4** exceeds the nucleophilicity of **3** by a factor of 3.0±0.5 in its reaction with benzhydryl cations **5a-5c**, which is also reflected in the respective nucleophilicity parameter of N(**4**) = 19.63 (s_N = 0.65).

These measurements thus establish **3a** and **4a** as potent and highly nucleophilic pyridine derivatives in solvents of low polarity (Figure 3). That **4a** is more nucleophilic than **3a** is in full agreement with the results for selected organocatalytic transformations performed in $CDCl_3$ as the solvent.[23] The combined methodology developed here thus allows for a quantitative assessment of catalyst nucleophilicity at synthetically relevant concentrations.

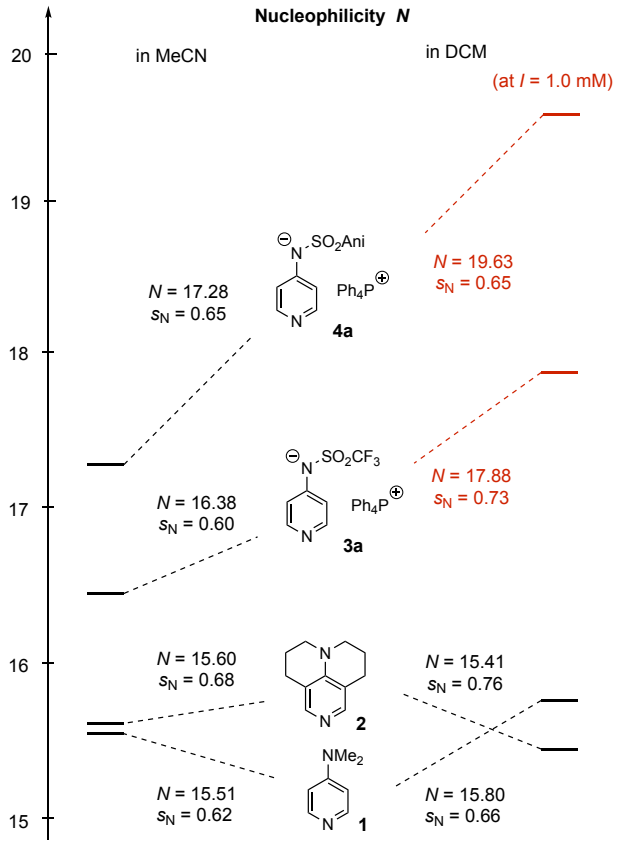

Figure 3. Mayr nucleophilicities N (and s_N) of DMAP (**1**), TCAP (**2**), and the pyridinamide anions **3** and **4** (Ani = *p*-methoxyphenyl) in MeCN and DCM.

CONCLUSION

Pyridinamide ion pairs **3a** and **4a** exceed the nucleophilic reactivity of the highly reactive neutral Lewis base TCAP (**2**) by up to two orders of magnitude in DCM. Employing a combination of conductivity and DOSY measurements, we have deciphered an asymmetric association behavior of both pyridinamide ion pairs in the low polarity solvent DCM, which includes both cationic and anionic sandwich complexes but not the commonly assumed and unreactive 1:1 ion pair. Without the combination of conductivity and DOSY measurements this result could not have been achieved since conductivity alone does not give insight into the type of charged species that are being measured. The reactivity of the super-nucleophilic anions **3** and **4** was quantified with the newly developed ionic strength-controlled benzhydrylium ion method, which facilitates the comparison of **3a** and **4a** with neutral nucleophilic catalysts, such as DMAP or TCAP. In DCM, we were able to evaluate kinetic data not only at low ion pair concentrations, but also at synthetically relevant higher concentrations by keeping the ionic strength constant throughout the measurement to prevent the interference of ion association. The direct comparison of k_2 values for reactions with cationic reference electrophiles reveals reactivity values of pyridinamide anions **3** and **4** (at high concentration) that are 39 and 90 times higher than that of TCAP (**2**). The superior reactivity of pyridinamide anions **3** and **4** has recently been observed in catalytic reactions with isocyanates and Michael acceptors as electrophiles[23,24] This indicates that the higher nucleophilicity of **3** and **4** in comparison to neutral nucleophilic catalysts might be comparably effective for reactions with neutral electrophiles in low polarity media (alkanes, THF, Et_2O). The asymmetric ion association described here, opens the general avenue for employing highly reactive free anions to activate so far inaccessible substrates in catalytic transformations.

ASSOCIATED CONTENT

Supporting Information

The Supporting Information is available free of charge on the ACS Publications website. It contains additional experimental and computational details as well as analysis procedures and methods, including step by step descriptions. (PDF)

Accession Codes

CCDC accession codes 2310788 - 2310789 contain the supplementary crystallographic data for this paper. These data can be obtained free of charge via www.ccdc.cam.ac.uk/ data_request/cif, or by emailing data_request@ccdc.cam.ac.uk, or by contacting the Cambridge Crystallographic Data Centre, 12 Union Road, Cambridge CB2 1EZ, UK; fax: +44 1223 336033.

AUTHOR INFORMATION

Corresponding Author

Hendrik Zipse – *Department of Chemistry, Ludwig-Maximilians-Universität München, Butenandtstr. 5-13, 81377 München, Germany; orcid.org/0000-0002-0534-3585; E-mail: zipse@cup.uni-muenchen.de*

Armin R. Ofial – *Department of Chemistry, Ludwig-Maximilians-Universität München, Butenandtstr. 5-13, 81377 München, Germany; orcid.org/0000-0002-9600-2793; E-mail: ofial@lmu.de*

Ruth M. Gschwind – *Institute for Organic Chemistry, University Regensburg, Universitätsstr. 31, 93053 Regensburg, Germany; orcid.org/0000-0003-3052-0077; Email: ruth.gschwind@ur.de*

Author

Veronika Burger – *Department of Chemistry, Ludwig-Maximilians-Universität München, Butenandtstr. 5-13, 81377 München, Germany; orcid.org/0009-0003-5482-9025*

Maximilian Franta – *Institute for Organic Chemistry, University Regensburg, Universitätsstr. 31, 93053 Regensburg, Germany: orcid.org/0009-0006-4861-9808*

Author Contributions

The manuscript was written through contributions of all authors. / All authors have given approval to the final version of the manuscript.

Funding Sources

This work was funded by the Deutsche Forschungsgemeinschaft (DFG, German Research Foundation) – 426795949 through the Research Training Group (RTG) 2620 “Ion Pair Effects in Molecular Reactivity”.

ACKNOWLEDGMENT

This work was funded by the Deutsche Forschungsgemeinschaft (DFG, German Research Foundation) – 426795949 through the Research Training Group (RTG) 2620 “Ion Pair Effects in Molecular Reactivity”. The authors are thankful to Dr. Robert J. Mayer (LMU) for help with the conductivity measurements, Nathalie Hampel (LMU) for the synthesis of **5a-5c,** Dr. Fabian Zott (LMU) for help with kinetics simulations, and Christian Scholtes (Regensburg) for providing a python script for the DOSY evaluation.

REFERENCES

(1) (a) Litvinenko, L. M.; Kirichenko. A. I. Basicity and Stereospecificity in Nucleophile Catalysis by Tertiary Amines. *Dokl. Akad. Nauk SSSR Ser. Khim.* **1967**, *176*, 97–100.; (b) Steglich, W.; Höfle, G. N,N-Dimethyl-4-pyridinamine, a Very Effective Acylation Catalyst. *Angew. Chem. Int. Ed. English* **1969**, *8* (12), 981–981. DOI: 10.1002/anie.196909811.

(2) Heinrich, M. R.; Klisa, H. S.; Mayr, H.; Steglich, W.; Zipse, H. Enhancing the Catalytic Activity of 4-(Dialkylamino)Pyridines by Conformational Fixation. *Angew. Chem. Int. Ed.* **2003**, *42* (39), 4826–4828. DOI: 10.1002/anie.200352289.

(3) Steglich, W.; Höfle, G. ÜBER EINE EINFACHE DARSTELLUNG VON ACYL-OXAZOLINONEN-(5) AUS 5-ACYLOXY-OXAEOLEN II. MITTEILUNG UBER HYPERNUCLEOPHILE ACYLIERUNGKATALYSATOREN. *Tetrahedron Lett.* **1970**, No. 54, 4727–4730.

(4) Hassner, A.; Alexanian, V. DIRECT ROOM TEMPERATURE ESTERIFICATION OF CARBOXYLIC ACIDS. *Tetrahedron Lett.* **1978**, No. 46, 4475–4478.

(5) Höfle, G.; Steglich, W.; Vorbrüggen, H. 4-Dialkylaminopyridines as Highly Active Acylation Catalysts. *Angew. Chem. Int. Engl.* **1978**, *17*, 569–583.

(6) Neises, B.; Steglich, W. Simple Method for the Esterification of Carboxylic Acids. *Angew. Chem. Int. Ed. English* **1978**, *17* (7), 522–524. DOI: 10.1002/anie.197805221.

(7) Chaudhary, S. K.; Hernandez, O. A Simplified Procedure for the Preparation of Triphenylmethylethers. *Tetrahedron Lett.* **1979**, *20* (2), 95–98. DOI: 10.1016/S0040-4039(01)85892-5.

(8) Patschinski, P.; Zhang, C.; Zipse, H. The Lewis Base-Catalyzed Silylation of Alcohols-a Mechanistic Analysis. *J. Org. Chem.* **2014**, *79* (17), 8348–8357. DOI: 10.1021/jo5016568.

(9) Chaudhary, S. K.; Hernandez, O. 4-Dimethylaminopyridine: An Efficient and Selective Catalyst for the Silylation of Alcohols. *Tetrahedron Lett.* **1979**, *20* (2), 99–102. DOI: 10.1016/S0040-4039(01)85893-7.

(10) For the nucleophilic reactivity of DMAP in MeCN, see: (a) Brotzel, F.; Kempf, B.; Singer, T.; Zipse, H.; Mayr, H. Nucleophilicities and Carbon Basicities of Pyridines. *Chem. Eur. J.* **2007**, *13* (1), 336–345. DOI: 10.1002/chem.200600941; (b) for supplementary kinetic data and revised N (and s_N) parameters for DMAP (**1**), see: Nigst, T. A.; Ammer, J.; Mayr, H. Photogeneration of Benzhydryl Cations by Near-UV Laser Flash Photolysis of Pyridinium Salts. *J. Phys. Chem. A* **2012**, *116* (33), 8494–8499. DOI: 10.1021/jp3049247.

(11) Tandon, R.; Unzner, T.; Nigst, T. A.; De Rycke, N.; Mayer, P.; Wendt, B.; David, O. R. P.; Zipse, H. Annelated Pyridines as Highly Nucleophilic and Lewis Basic Catalysts for Acylation Reactions. *Chem. Eur. J.* **2013**, *19* (20), 6435–6442. DOI: 10.1002/chem.201204452.

(12) Mayr, H. Reactivity scales for quantifying polar organic reactivity: the benzhydrylium methodology. *Tetrahedron* **2015**, *71*, 5095–5111.

(13) Lakhdar, S. in *Lewis Base Catalysis in Organic Synthesis*, First Ed. (Eds.: E. Vedejs, S. E. Denmark), Wiley-VCH, Weinheim, 2016, Chapt. 4, pp. 85-116.

(14) Marcus, Y.; Hefter, G. Ion Pairing. *Chem. Rev.* **2006**, *106* (11), 4585–4621. DOI: 10.1021/cr040087x.

(15) Reichardt, C. *Solvents and Solvent Effects in Organic Chemistry* (3rd ed.), VCH, Weinheim, **2003**, Chapt. 5.5.5.

(16) Brak, K.; Jacobsen, E. N. Asymmetric Ion-Pairing Catalysis. *Angew. Chem. Int. Ed.* **2013**, *52* (2), 534–561. DOI: 10.1002/anie.201205449.

(17) (a) Waser, M.; Novacek, J.; Gratzer, K. "Cooperative Catalysis Involving Chiral Ion Pair Catalysts" in *Cooperative Catalysis*, R. Peters (Ed.), Wiley-VCH Weinheim (Germany), **2015**, Chapter 7, pp. 197-226 DOI: 10.1002/9783527681020.ch7; (b) Otevrel J.; Waser M. "Asymmetric Phase-Transfer Catalysis – From Classical Application to New Concepts" in *Asymmetric Organocatalysis: New Strategies, Catalysts, and Opportunities,* Ł. Albrecht, A. Albrecht, L. Dell'Amico (Eds.), Wiley-VCH, **2023**, Chapter 3, pp. 71-120.

(18) Ye, X.; Tan, C. H. Enantioselective Transition Metal Catalysis Directed by Chiral Cations. *Chem. Sci.* **2021**, *12* (2), 533–539. DOI: 10.1039/d0sc05734g.

(19) Shirakawa, S.; Maruoka, K. Recent Developments in Asymmetric Phase-Transfer Reactions. *Angew. Chem. Int. Ed.* **2013**, *52* (16), 4312–4348. DOI: 10.1002/anie.201206835.

(20) Merten, C.; Pollok, C. H.; Liao, S.; List, B. Stereochemical Communication within a Chiral Ion Pair Catalyst. *Angew. Chem. Int. Ed.* **2015**, *54* (30), 8841–8845. DOI: 10.1002/anie.201501271.

(21) Mahlau, M.; List, B. Asymmetric Counteranion-Directed Catalysis: Concept, Definition, and Applications. *Angew. Chem. Int. Ed.* **2013**, *52* (2), 518–533. DOI: 10.1002/anie.201205343.

(22) Phipps, R. J.; Hamilton, G. L.; Toste, F. D. The Progression of Chiral Anions from Concepts to Applications in Asymmetric Catalysis. *Nat. Chem.* **2012**, *4* (8), 603–614. DOI: 10.1038/nchem.1405.

(23) Helberg, J.; Ampßler, T.; Zipse, H. Pyridinyl Amide Ion Pairs as Lewis Base Organocatalysts. *J. Org. Chem* **2020**, *85*, 5390–5402.

(24) Dempsey, S. H.; Lovstedt, A.; Kass, S. R. Electrostatically Enhanced 3- and 4-Pyridyl Borate Salt Nucleophiles and Bases. *J. Org. Chem.* **2023**, *88* (15), 10525–10538. DOI: 10.1021/acs.joc.3c00523.

(25) Dale, H. J. A.; Hodges, G. R.; Lloyd-Jones, G. C. Kinetics and Mechanism of Azole N−π*-Catalyzed Amine Acylation. *J. Am. Chem. Soc.* **2023**, *145* (32), 18126–18140. DOI: 10.1021/jacs.3c06258.

(26) Yang, X.; Birman, V. B. Acyl Transfer Catalysis with 1,2,4-Triazole Anion. *Org. Lett.* **2009**, *11* (7), 1499–1502. DOI: 10.1021/ol900098q.

(27) Mai, B. K.; Koenigs, R. M.; Nguyen, T. V.; Lyons, D. J. M.; Empel, C.; Pace, D. P.; Dinh, A. H. Tropolonate Salts as Acyl-Transfer Catalysts under Thermal and Photochemical Conditions: Reaction Scope and Mechanistic Insights. *ACS Catal.* **2020**, *10* (21), 12596–12606. DOI: 10.1021/acscatal.0c03702.

(28) Liotta, C. L.; Harris, H. P. The Chemistry of "Naked" Anions. I. Reactions of the 18-Crown-6 Complex of Potassium Fluoride with Organic Substrates in Aprotic Organic Solvents1. *J. Am. Chem. Soc.* **1974**, *96*, 2250–2252.

(29) Coury, L. Conductance Measurements Part 1 : Theory. *Current* **1999**, *3* (2), 91–96.

(30) Mizuhata, M. Electrical Conductivity Measurement of Electrolyte Solution†,††. *Electrochemistry* **2022**, *90* (10), 1–12. DOI: 10.5796/electrochemistry.22-66111.

(31) Martínez, L. Measuring the Conductivity of Very Dilute Electrolyte Solutions, Drop by Drop. *Quim. Nova* **2018**, *41* (7), 814–817. DOI: 10.21577/0100-4042.20170216.

(32) Schneider, R.; Mayr, H.; Plesch, P. H. Ionisation and Dissociation of Diarylmethyl Chlorides in BCl_3/CH_2Cl_2 Solution: Spectroscopic Evidence for Carbenium Ion Pairs. *Ber. Bunsenges. Phys. Chem.* **1987**, *91*, 1369–1374

(33) The triple ion sandwich model has first been proposed in: Fuoss, R. M.; Kraus, C. A. Properties of Electrolytic Solutions. IV. The Conductance Minimum and the Formation of Triple Ions Due to the Action of Coulomb Forces. *J. Am. Chem. Soc.* **1933**, *55*, 2387-2399. DOI: 10.1093/nq/s6-V.129.467d.

(34) Jiang, J.; Dennis, K. P. N. G. A Decade Journey in the Chemistry of Sandwich-Type Tetrapyrrolato-Rare Earth Complexes. *Acc. Chem. Res.* **2009**, *42* (1), 79–88. DOI: 10.1021/ar800097s.

(35) Hojo, M.; Moriyama, H. Conductance in Isodielectric Mixed Solvents Containing Triple Ions. *J. Solution Chem.* **1996**, *25* (7), 681–694. DOI: 10.1007/BF00972682.

(36) Hojo, M.; Ueda, T.; Inoue, T.; Ike, M.; Kobayashi, M.; Nakai, H. UV - Visible and ^{1}H or ^{13}C NMR Spectroscopic Studies on the Specific Interaction between Lithium Ions and the Anion from Tropolone or 4-Isopropyltropolone (Hinokitiol) and on the Formation of Protonated Tropolones in Acetonitrile or Other Solvents. *J. Phys. Chem. B* **2007**, *111* (7), 1759–1768. DOI: 10.1021/jp066756n.

(37) Zhu, F.; Zhang, W.; Liu, H.; Wang, X.; Zhou, Y.; Fang, C.; Zhang, Y. Micro–Raman and Density Functional Theory Analyses of Ion Pairs in Concentrated Sodium Tetrahydroxyborate Droplets. *Spectrochim. Acta - Part A Mol. Biomol. Spectrosc.* **2020**, *224* (3), 117308. DOI: 10.1016/j.saa.2019.117308.

(38) Note: At concentrations lower than 0.4 mM the experimental values of ion volumes deviate considerably from the theoretical curve. This shows that the equilibrium between free ions and sandwich ion cannot be described by a simple model. However, the concentration limits of DOSY prevent further refinements.

(39) A database of published reactivity parameters E, N, and s_N is freely accessible at https://www.cup.lmu.de/oc/mayr/reaktionsdaten-bank2/ (accessed on 10/09/2024).

(40) Note: For **4a**, where the anionic sandwich **4a4** dominates, the DOSY measurements show that addition of additive **6** (**a**-BF_4) eventually leads to an inversion of the sandwich ion populations towards the cationic **a4a** (see SI, Chapter 4).

2.1 Supplementary Data

2.1.1 General Information

All reagents were purchased from Sigma Aldrich, TCI, or Acros and used without further purification unless otherwise noted. Solvents were obtained from Acros Organics, Sigma Aldrich, or Merck and purified by simple distillation in a rotary evaporator, unless otherwise specified.

All air- and moisture-sensitive reactions were performed under a nitrogen atmosphere and the glassware and magnetic stirrers were dried in a dry oven at 110 °C overnight.

CH_2Cl_2 for nucleophilicity measurements was stirred over concentrated H_2SO_4 for two weeks before extraction with water (1 x 1.0 L), $NaHCO_3$ (1 x 1.0 L), and again water (1 x 1.0 L). CaH_2 was added as a drying agent, and the solvent was freshly distilled over CaH_2 prior to use.

Melting points were acquired using Büchi Melting Point M-560 devices and are uncorrected.

Nuclear magnetic resonance (NMR) spectra were recorded on a Bruker 400 MHz or INOVA 400 and 600 MHz machines. The following abbreviations were used in the analysis of NMR spectra: s = singlet, d = doublet, t = triplet, q = quartet, m = multiplet, br s = broad singlet. NMR signals were assigned based on 2D spectra (COSY, HSQC, HMBC, NOESY) experiment analysis. Chemical shifts are given in ppm. The internal reference was set to the residual solvent signals (CD_2Cl_2, $CDCl_3$, DMSO-d_6). The ^{13}C NMR spectra (101 or 151 MHz) were recorded under broadband proton-decoupling. ^{19}F NMR spectra were referenced using the solvent signal.[1] The spectra were imported and processed in the program MestreNova (version 14.1.1).

Infrared (IR) spectra were measured on a Perkin Elmer Spectrum BX-59343 instrument with a Smith Detection DuraSamplIR II Diamond ATR sensor for liquids or neat for solids. Intensities are described as vs = very strong, m = medium, w = weak, br = broad.

High-resolution mass spectra (HRMS) were recorded on a Thermo Finnigan LTQ FT Ultra Fourier Transform Ion Cyclotron Resonance mass spectrometer with electrospray ionization (ESI) for sample ionization. For EI (70 eV) measurements a Thermo Finnigan of the MAT 95 type with a direct exposure probe (DEP) was used.

Crystal structures were recorded using an Oxford Diffraction XCalibur with Sapphire CCD-detector and a molybdenum-K_α-source ($\lambda = 0.71073$) with a concentric circle kappa-device. The structures were resolved using the program SHELXS or SIR97 and refined with SHELXS.

2.1.2 Additional Figures and Correlations

Details on data evaluation of conductivity data can be found in Chapter 2.1.4.

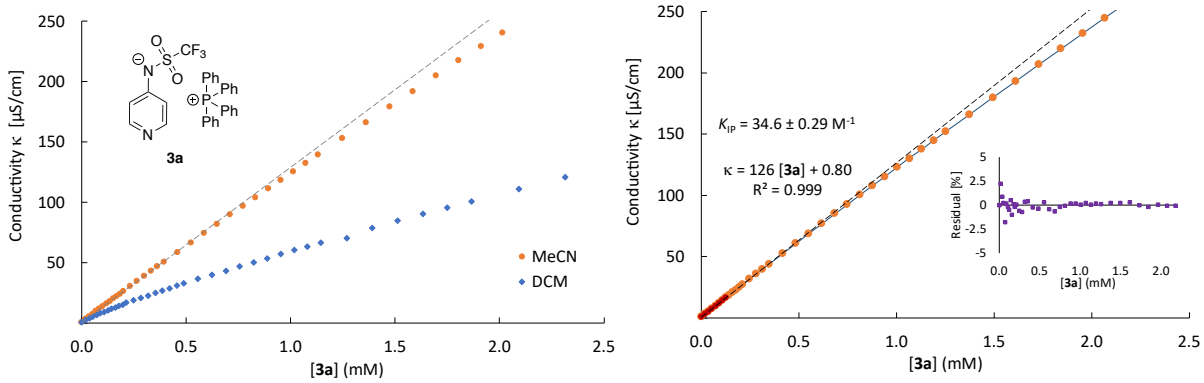

Figure 2.1: [Figure S1]. Left: conductivity of **3a** in MeCN (orange points) and in DCM (blue points) at 20 °C with extrapolated conductivity profile of fully dissociated salt (dotted grey line); right: conductivity of **3a** in MeCN (orange points) and fit (black line) of the experimental data according to the 1:1 association model at 20 °C with extrapolated conductivity profile of fully dissociated salt (dotted grey line). Conductivity measurements were performed for concentrations ranging from 0.02 – 2.5 mM but only values in the range 0.02 to 1.0 mM are interpreted as 1.0 mM appears to represent the threshold onset of ion pair formation from the free ions.

The data displayed in Figure 2.1 in the manuscript can be found in Table 2.1

Table 2.1: [Table S1]. List of measured conductivity values (without solvent background conductivity of 0.8 µS cm^{-1}), DOSY measurement results (given as the hydrodynamic volume) and kinetic results for ion pair **3a** in DCM.

Conductivity		DOSY NMR			Wide Range[b]	
[3a] (mM)	κ (µS/cm)	[3a] (mM)	Vol Anion (Å^3)	Vol Cation (Å^3)	[3a] (mM)	k_{obs} (s^{-1})
0.00	0.00	–	–	–	–	–
–	–	0.005	193	367	–	–
–	–	0.01	203	342	0.01	18.0
0.02	1.44	–	–	–	0.02	36.4
0.04	2.72	–	–	–	0.04	74.1
0.05	4.32	0.05	383	500	0.06	99.2
0.07	5.76	–	–	–	0.08	118
0.09	6.80	0.10	405	515	0.10	140
0.11	8.00	–	–	–	–	–
0.12	9.12	–	–	–	–	–
0.14	10.2	–	–	–	–	–
0.18	12.4	–	–	–	–	–
0.21	14.6	0.20	413	537	0.20	197
0.25	16.2	–	–	–	–	–
0.28	18.4	–	–	–	–	–
0.31	20.3	–	–	–	–	–
0.35	22.2	–	–	–	–	–
0.38	24.0	–	–	–	–	–
0.42	25.6	0.40	466	587	0.40	292
0.48	28.8	–	–	–	–	–
0.55	32.0	–	–	–	–	–
0.62	35.2	0.60	477	598	0.60	362
0.68	38.4	–	–	–	–	–
0.75	41.6	–	–	–	–	–
0.82	44.3	0.80	497	603	0.80	400
0.88	47.2	–	–	–	–	–
0.94	49.8	–	–	–	–	–
1.01	52.3	1.00	505[a]	642[a]	1.01	420

[a] averaged value based on data from ref [2]; [b] "wide range" is the description of kinetic measurements performed according to the Mayr's benzhydrylium method over a concentration range from *c* = 0.01 – 1.0 mM.

2.1.3 Synthesis of Compounds

1,1,1-Trifluoro-*N*-(pyridin-4(1*H*)-ylidene)methanesulfonamide (PA_**3**)_

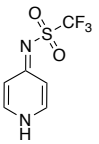
PA_**3**

4-Aminopyridine (2.37 g, 25.2 mmol, 1.0 eq) was dissolved in dry pyridine (30.0 mL) under nitrogen atmosphere. Triethylamine (8.00 mL, 57.4 mmol, 2.3 eq) was added and stirred for 10 min. The reaction mixture was cooled to 0 °C and trifluoromethanesulfonyl chloride (5.00 g, 29.7 mmol, 1.2 eq) was added. After stirring for 10 min at 0 °C, the mixture was refluxed for 3.5 h under nitrogen atmosphere before the solvent was removed. The crude product was suspended in H_2O, refluxed for 20 min and filtered while hot. This process was repeated with acetone and methyl-*tert*-butyl ether (MTBE), yielding pyridinamide **3** (3.55 g, 15.7 mmol, 62%) as a light brown solid.

^{1}H NMR (400 MHz, DMSO-d_6): δ [ppm] = 13.60 (s, 1H), 8.28 (d, *J* = 7.3 Hz, 2H), 7.27 (d, *J* = 7.3 Hz, 2H).

^{13}C NMR (101 MHz, DMSO-d_6): δ [ppm] = 163.7, 140.2, 120.7 (q, *J* = 325.6 Hz), 116.9.

^{19}F NMR (377 MHz, DMSO-d_6): δ [ppm] = -77.69.

HRMS (ESI): calc. for $C_6H_5F_3N_2O_2S^+$ [M^+]: 226.0018, found 226.0019.

4-Methoxy-*N*-(pyridin-4(1*H*)-ylidene)benzenesulfonamide (PA_**4**)

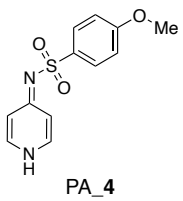
PA_**4**

4-Aminopyridine (2.03 g, 21.6 mmol, 1.0 eq) and NEt_3 (8.50 mL, 61.0 mmol, 2.8 eq) were dissolved in pyridine (22.0 mL). The mixture was cooled to 0 °C and 4-methoxybenzenesulfonyl chloride (5.35 g, 25.9 mmol, 1.2 eq) was added and stirred for 20 min. The reaction mixture was refluxed for 3 h before being cooled down to rt. The solvent was removed, and the resulting precipitate was repeatedly refluxed in H_2O, acetone, and MTBE. The final product was dried *in vacuo*. Pyridinamide **4** (4.78 g, 18.1 mmol, 84%) was obtained as an off-white solid.

^{1}H NMR (400 MHz, DMSO-d_6): δ [ppm] = 12.1 (s, 1H), 8.04 (d, *J* = 6.5 Hz, 2H), 7.74 (d, *J* = 8.9 Hz, 1H), 7.03 (d, *J* = 8.9 Hz, 1H), 6.95 – 6.89 (m, 2H), 3.79 (s, 3H).

^{13}C NMR (101 MHz, DMSO-d_6): δ [ppm] = 161.7, 151.1, 141.7, 134.4, 128.3, 114.1, 113.8, 55.5.

HRMS (ESI): calc. for $C_{12}H_{12}N_2O_3S^+$ [M^+]: 264.0563, found 264.0567.

Tetraphenylphosphonium pyridin-4-yl((trifluoromethyl)sulfonyl)amide (**3a**)

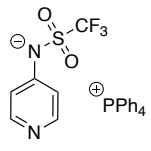
3a

Pyridinamide **3** (402 mg, 1.78 mmol, 1.0 eq) was added to a solution of NaOH (78.2 mg, 1.96 mmol, 1.1 eq) in H_2O (5.0 mL). Tetraphenyl bromide (746 mg, 1.78 mmol, 1.0 eq) was added, and the reaction mixture was stirred at rt. for 1 h. DCM (5.0 mL) was added, and the two phases were separated. The aqueous phase was extracted with DCM (3 x 15 mL). The collected organic phase was dried over $MgSO_4$, filtered and the solvent was evaporated. The crude product was crystallized from DCM overlayered with toluene. Pyridinamide ion pair **3a** (787 mg, 1.39 mmol, 78%) was obtained in form of colorless needles.

^{1}H NMR (400 MHz $CDCl_3$): δ [ppm] = 8.05 – 8.00 (m, 2H), 7.88 – 7.81 (m, 4H), 7.71 (td, *J* = 7.9, 3.6 Hz, 4H), 7.55 (ddd, *J* = 13.0, 8.4, 1.3 Hz, 4H), 7.02 – 6.97 (m, 2H).

^{13}C NMR (101 MHz, $CDCl_3$): δ [ppm] = 156.1, 149.5, 135.9 (d, *J* = 3.1 Hz), 134.5 (d, *J* = 10.3 Hz), 130.9 (d, *J* = 12.9 Hz), 122.2 (q, *J* = 328.6 Hz), 118.0 (d, *J* = 6.4 Hz), 117.1.

^{19}F NMR (377 MHz, $CDCl_3$): δ [ppm] = -76.8.

^{31}P NMR (162 MHz, $CDCl_3$): δ [ppm] = 23.19.

IR (ATR): ν (cm^{-1}) = 3060 (br), 1588 (m), 1484 (w), 1438 (m), 1317 (s), 1288 (s), 1198 (vs), 1155 (s), 1108 (m), 1000 (m), 832 (w), 723 (m).

Elemental Analysis: $C_{30}H_{24}F_3N_2O_2PS$ (564.56 g/mol): calc. (%) C, 63.82; H, 4.29; N, 4.96; S, 5.68; Found (%): C, 63.79; H, 4.32; N, 5.00; S, 5.45.

HRMS (ESI): calc. for $C_6H_4F_3N_2O_2S^-$ [A^-]: 224.9951; found 224.9948; calc. for $C_{24}H_{20}P^+$ [C^+]: 339.1297; found: 339.1289.

m. p: 183-185 °C.

Tetraphenylphosphonium ((4-methoxyphenyl)sulfonyl)(pyridin-4-yl)amide (**4a**)

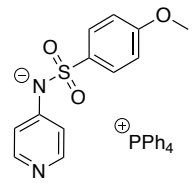

4a

Pyridinamide **4** (501 mg, 1.90 mmol, 1.0 eq) was added to a solution of NaOH (78.9 mg, 1.97 mmol, 1.1 eq) in H_2O (5.0 mL). Tetraphenylphosphonium bromide (795 mg, 1.90 mmol, 1.0 eq) was dissolved in DCM and added dropwise over 30 min through a dropping funnel. The reaction mixture was stirred at rt. for 2 h. More DCM (5.0 mL) was added, and the two phases were separated. The aqueous phase was extracted with DCM (3 x 25 mL). The collected organic phase was dried over $MgSO_4$, filtered and the solvent was evaporated. The crude product was crystallized from DCM overlayered with toluene and heptane (0.5 mL) while stored in the fridge. Ion Pair **4a** (782 mg, 1.30 mmol, 69%) was obtained in form of colorless crystals.

^{1}H NMR (600 MHz, $CDCl_3$): δ [ppm] = 7.90 – 7.79 (m, 1H), 7.77 – 7.69 (m, 1H), 7.61 – 7.53 (m, 1H), 6.79 – 6.72 (m, 4H), 3.74 (s, 3H).

^{13}C NMR (151 MHz, $CDCl_3$): δ [ppm] = 160.5, 157.9, 148.8, 138.8, 135.9 (d, *J* = 3.1 Hz), 134.5 (d, *J* = 10.3 Hz), 130.9 (d, *J* = 12.9 Hz), 128.7, 117.5 (d, *J* = 89.5 Hz), 116.3, 113.2, 55.4.

^{31}P NMR (162 MHz, $CDCl_3$): δ [ppm] = 23.03.

Elemental Analysis: $C_{36}H_{31}N_2O_3PS$ (602.69 g/mol): calc. (%) C, 71.74; H, 5.18; N, 4.65; S, 5.32; Found (%): C, 71.35; H, 5.24; N, 4.62; S, 5.77.

Tetraphenylphosphonium tetrafluoroborate (**6**)

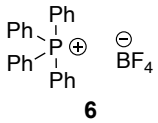

6

Tetraphenylphosphonium bromide (1.05 g, 2.50 mmol, 1.0 eq) was dissolved in water and sodium tetrafluoroborate (276 mg, 2.50 mmol, 1.0 eq) was added in portions. The resulting cloudy suspension was stirred for 2 h at rt. DCM (10 mL) was added, and the two phases were separated. The aqueous phase was extracted with DCM (3 x 20 mL). The collected organic phase was dried over $MgSO_4$, filtered and the solvent was evaporated. The crude product was dissolved in DCM and precipitated by adding toluene. Product **6** (940 mg, 2.21 mmol, 88%) was obtained as colorless needles.

^{1}H NMR (400 MHz CD_2Cl_2): δ [ppm] = 7.98 – 7.87 (m, 4 H), 7.81 – 7.72 (m, 8 H), 7.66 – 7.56 (m, 8 H).

^{13}C NMR (101 MHz, CD_2Cl_2): δ [ppm] = 36.2 (d, *J* = 3.3 Hz), 134.8 (d, *J* = 10.4 Hz), 131.0 (d, *J* = 13.0 Hz).

^{19}F NMR (377 MHz, CD_2Cl_2): δ [ppm] = -153.43.

^{31}P NMR (162 MHz, CD_2Cl_2): δ [ppm] = 23.12.

IR (ATR): ν (cm^{-1}) = 1586 (w), 1436 (m), 1108 (m), 1052 (s), 750 (w), 689 (s).

Elemental Analysis: $C_{24}H_{20}BF_4P$ (426.20 g/mol): calc. (%) C, 67.64; H, 4.73; Found (%): C, 67.58; H, 4.62.

HRMS (ESI): calc. for BF_4^- [A^-]: 87.0035; found: 87.0034; calc. for $C_{24}H_{20}P^+$ [C^+]: 339.1297; found: 339.1292.

m. p: 350-352 °C.

2.1.4 Conductometric Measurements

2.1.4.1 Sample Preparation and Data Acquirement

For the measurement, an 0.02 M solution of the respective catalyst is prepared in a 10 mL volumetric flask and is given portion-wise to the pure solvent in a measuring cell at 20 °C. Conductivity measurements were done using a WTW conductometer with a Pt electrode LTA 1/NS in MeCN and DCM. Calibration was done as described in ref. [3]. Temperature control (20.0 ± 0.1 °C) was achieved by using a circulating bath cryostat. The conductivity is measured in volts (V) and depicted in "ME-REDLab Data Acquisition V1.1", developed by Dr. B. Kempf 2010, where the conductivity is plotted against time. After adding a portion of salt stock solution, one must wait until the conductivity value reaches a stable plateau (min 30 sec up to 100 sec) from which the average conductivity value is read off. In Excel this value (V) is then converted into (μS cm^{-1}) by multiplying it with the cell parameter of the used electrode (z = 160). The cell parameter was obtained by calibrating the conductometric set up with aqueous KCl solutions (0.007 M, 0.0145 M, and 0.0375 M; commercial conductivity standard solutions purchased from Alfa Aesar) referring to the conductivity of 1273 μS/cm for an 0.01 M solution of aq. KCl at 20 °C.[4]

2.1.4.2. Data Analysis – 1:1 Association Model

The conductivity of a substance is defined as its ability to conduct electricity and depends on the number of charge carriers in solution. Therefore, it can be expressed as a molar quantity where κ is the measured conductivity, Λ_m is the molar conductivity and c is the measured concentration of electrolyte.

$$\kappa = \Lambda_m c \tag{2.1}$$

Analysis of the conductivity profile shown in Figure S2 can most easily be approached assuming the formation of a 1:1 ion pair system with concentration [IP] from diffusively free anions A and cations C. For this situation the association constant K_{IP} is given by eq. 2.2.

$$K_{IP} = \frac{[IP]}{[A][C]} \tag{2.2}$$

The combination of eq. 2.2 with eq. 2.3 for the ion pair concentration yields eq. 2.4, which relates the concentration of free ions [A] to the total salt concentration $[IP]_{tot}$ and the association constant K_{IP}.

$$[IP] = [IP]_{tot} - [A] \tag{2.3}$$

$$[A] = [C] = \frac{-1 + \sqrt{1 + 4K_{IP}[IP]_{tot}}}{2K_{IP}} \tag{2.4}$$

The experimentally determined conductivity κ depends on the specific molar conductivity Λ_m and the ion concentration [A] as expressed in eq. 2.5, whose combination with eq. 2.4 the combination of which then yields eq. 2.6.

$$\kappa = \Lambda_m[A] \tag{2.5}$$

$$\kappa = \Lambda_m \times \left\{\frac{-1 + \sqrt{1 + 4K_{IP}[IP]_{tot}}}{2K_{IP}}\right\} + BG \tag{2.6}$$

The value for the specific molar conductivity Λ_m for the combined ions of salt **3a** is derived from the extrapolated linear regression line of the red-marked conductivity values (first three points). The background conductivity (BG) included here is the conductivity of the used solvent (BG = 0.80 μS cm^{-1}).

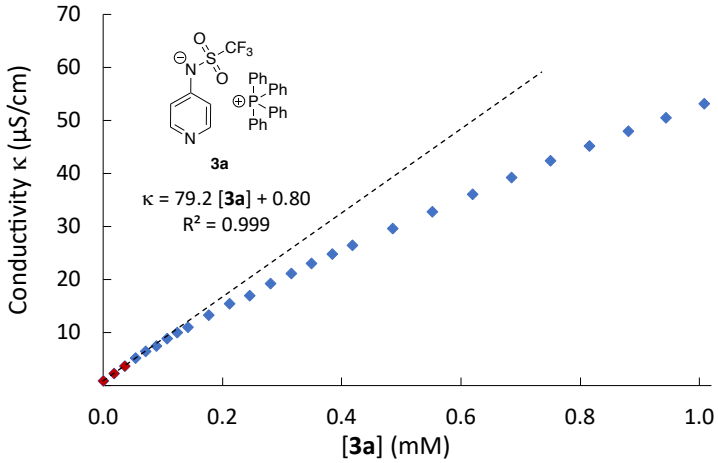

Figure 2.2: [Figure S2]. Concentration-dependent conductivity profile for catalyst **3a** in DCM with Λ_m = 79.2 S cm^2 mol^{-1} and solvent background BG = 0.8 µS cm^{-1}at 20 °C.

Eq. 2.6 was used in the fitting program "ProFit7" (version 7.0.18) to obtain the ion pairing constant K_{IP} from the conductivity profiles measured in DCM and MeCN. The specific molar conductivity Λ_m was extrapolated using the first three data points in DCM and the first eight data points in MeCN. The results are collected in Table 2.2.

Table 2.2: [Table S2]. Association constants K_{IP} of ion catalyst **3a** in MeCN and DCM according to eq. 2.6 at 20 °C.

	K_{IP} (M^{-1})	
	MeCN	**DCM**
Ion Pair	[45.6][a]	[40.7][a]
3a	34.6 ± 0.3	828 ± 8.27

[a] $E_T(30)$ [kcal mol^{-1}] solvent polarity parameters taken from Reichardt[5].

In a second approach the complex pathway simulation program, COPASI[6], was used to numerically analyze the obtained conductivity data. After starting COPASI, a biochemical model was chosen and the association of a single anion **A** reacting with a single cation **C** into the ion pair **IP** was added as reaction (see Scheme 2.1).

$$A + C \rightleftharpoons[K_{IP}] IP$$

Scheme 2.1: [Scheme S1]. Equation for numerical simulations of 1:1 ion association for salt **3a.**

The reaction was set to be reversible, which is also indicated by the equal sign "=" in the reaction equation. In the "Symbol Definition" section the starting compound (A + C) is listed with rate constant k_1 as well as the product (IP) with rate constant k_2, defining the ion pairing constant as $k_1/k_2 = K_{IP}$.

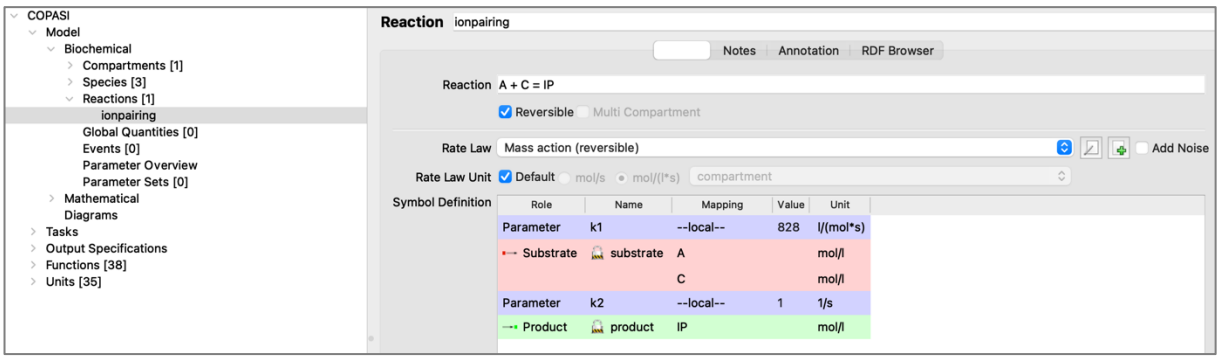

To find the ion pairing constant K_{IP} (M^{-1}) that best fits our experimental data in the section "Reactions" the reaction constant k_2 was set to be 1, while the rate constant k_1 was changed until the best fit between the simulated and experimental conductivity curve was found.

In the section “Species” the individual concentration for all compounds was added. This would be zero for the 1:1 ion pair **IP** and the first measured total salt concentration of the anion **A** and for the cation **C** (in this example 1.78 x 10^{-5} M).

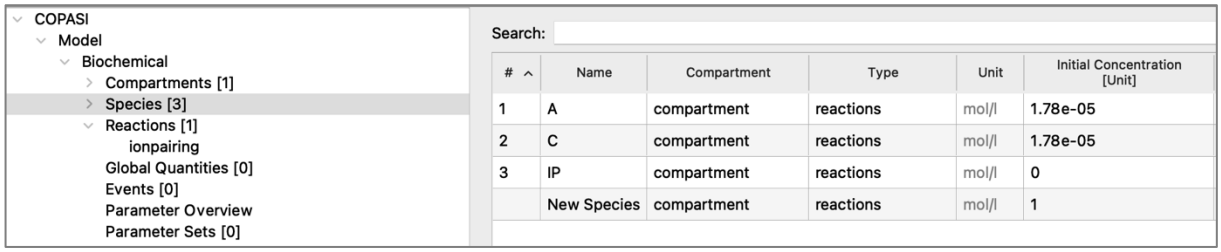

Next, we moved on to the "Tasks" menu and selected the "Steady-State" option there. Clicking the "Run" button at the bottom of the window, COPASI ran through a steady state analysis and then reports the results as follows:

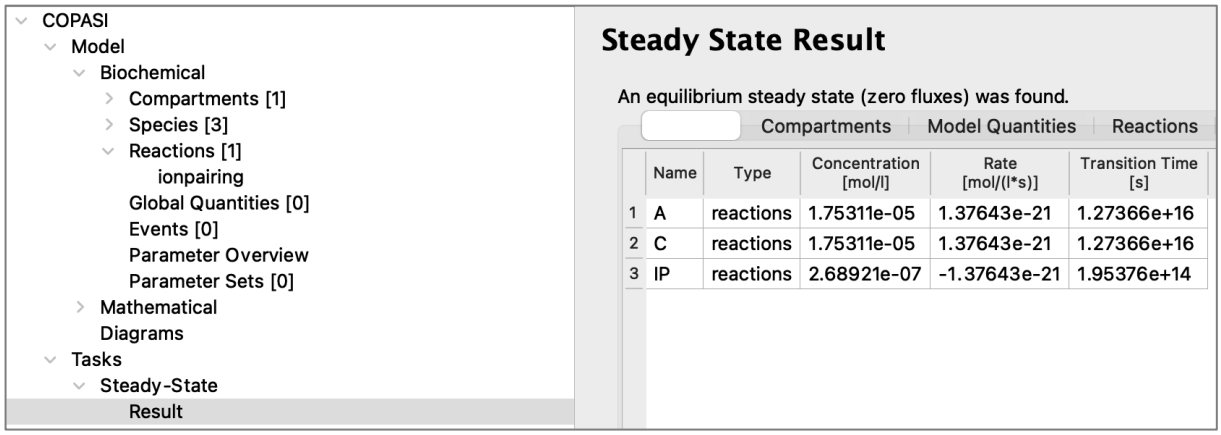

The obtained values for [**A**], [**C**], and [**IP**] were copied into an Excel analysis sheet, that contains all relevant data. The obtained concentrations for those three species were then converted into conductivity values according to eq. 2.5. Therefore, the solvent conductivity background of 0.8 µS cm^{-1} was subtracted from the measured conductivity values. The molar conductivity Λ_m can be divided into the limited molar conductivity λ_i of each single ionic species *i* in solution according to eq. 2.7.

$$\Lambda_m = \lambda_A + \lambda_C \tag{2.7}$$

Since the concentration of both ionic species **A** and **C** is always identical in this association model, the individual conductivity contributions are not of critical importance. For now, we assumed that the single anion **A** and the single cation **C** contribute equally to the total molar conductivity Λ_m, that was extracted from region I of the conductivity profile. The 1:1 ion pair **IP** was assigned zero contribution to the molar conductivity Λ_m. The conductivity value of each species is summed up and the final value is compared to the experimental value. This step is repeated until the simulated and experimental conductivity value are close to identical.

This procedure can be tremendously sped up by the use of a Phyton script that automatically performs the “steady state” function for any given numbers of concentrations.[7] The “root mean square error” (RMSE) is kept as a control measure and k_1 is optimized until the minimum RMSE for the chosen concentration range is found (which, in some cases, includes up to 5 decimal places). With the assistance of the Python script, we can examine all measured conductivity values right from the start to find the association constant K_{IP}.

The 1:1 association model is the simplest model that can be applied and is usually the first model that is tested for the analysis of the association of a newly designed salt.

By comparing the solutions for the association constant K_{IP} found with the integrated method and the numerical simulations performed with COPASI no difference could be observed (see Figure 2.3).

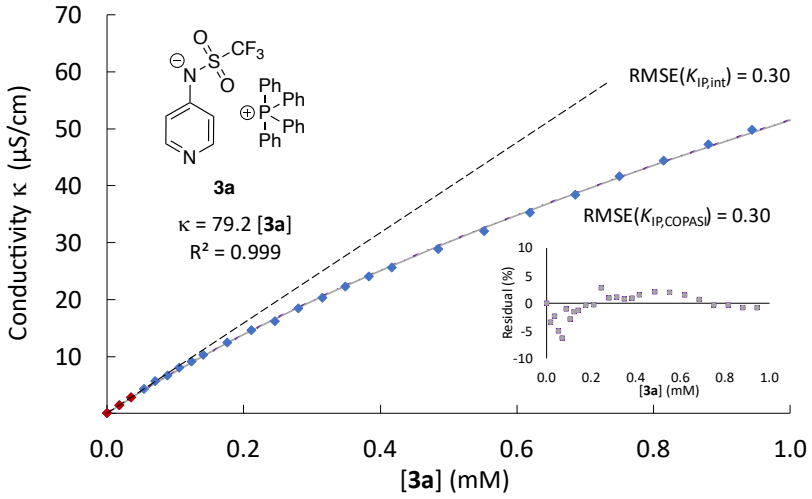

Figure 2.3: [Figure S3]. Comparing results of integrated method (purple dotted-dashed line) and numerical simulation according to 1:1 ion association model (grey line) for conductivity data of salt **3a.**

The RMSE values do not differentiate as well as the percentage residual between the experimental data and simulated conductivity values. Therefore, we conclude that the two methods can be used interchangeably for the determination of the ion association constant K_{IP}.

2.1.4.3 Double Ion Pair Association Model

DOSY measurements revealed a deviation from the previously assumed 1:1 association model. Instead, we presume an aggregate formation where two cations with one anion form a triple cation ion complex, leaving one anion free. Here, four charged ions associate into two charged species. To compare this "sandwich" association type with the classical 1:1 model on equal footing, the existing model was modified to involve four ions combining into two separate charge-neutral ion pairs (see Scheme 2.2).

$$2 * A + 2 * C \overset{K_{IP}}{\rightleftharpoons} 2 * IP$$

Scheme 2.2: [Scheme S2]. Equation for numerical simulations of double 1:1 ion association for salt **3a**.

The above detailed procedure was followed to determine and optimize the ion pairing constant K_{IP} (M^{-2}). The final result was found to be $K_{IP} = 6.86 \times 10^5$ M^{-2} for pyridinamide ion pair **3a** in DCM.

2.1.4.4 Sandwich Association Model

With DOSY measurements, it was determined that instead of the previously assumed simple 1:1 association of anion and cation, a "sandwich cation" aggregate form first. This new insight necessitates a reconsideration of the previously applied association model. Since a mathematical description of this new association model has not yet been achieved, the software COPASI was utilized for the numerical analysis of this newly derived model. The association of two single anions **A** and cations **C** into the sandwich cation **CAC** and one free **A** (see Scheme 2.3) was numerically simulated using COPASI.

$$2 * A + 2 * C \overset{K_{CAC}}{\rightleftharpoons} A + CAC$$

Scheme 2.3: [Scheme S3]. Equation for numerical simulations of newly derived cationic sandwich association model for salt **3a.**

The reaction was selected to be reversible. The sandwich association constant is defined as $k_1/k_2 = K_{CAC}$ with to $k_2 = 1$ being a fixed value.

2.1.4.4.1 Model 1

The procedure to find the best fitting sandwich association constant K_{CAC} is identical to the one described for the 1:1 association model. However, when converting the obtained concentration of each species, anion **A**, cation **C**, and sandwich-cation **CAC**, into conductivity values, the contribution of each species towards the molar conductivity is critical. Through literature search, we found the limited molar ionic conductivity λ_{NBu4} of tetrabutylammonium cation (NBu_4^+, **b**) to be 45.5 S cm^2 mol^{-1},[8] which is also part of our pyridinamide ion pair library in combination with anion **3**, giving pyridinamide ion pair **3b** (see Scheme S4).

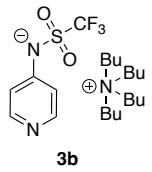

3b

Scheme 2.4: [Scheme S4]. Structure of pyridinamide ion pair **3b.**

By recording the conductivity profile **3b** in DCM, its molar conductivity was identified to be 57.9 S cm^2 mol^{-1} (see Figure 2.4, red-marked initial three points for extrapolation of Λ_m).

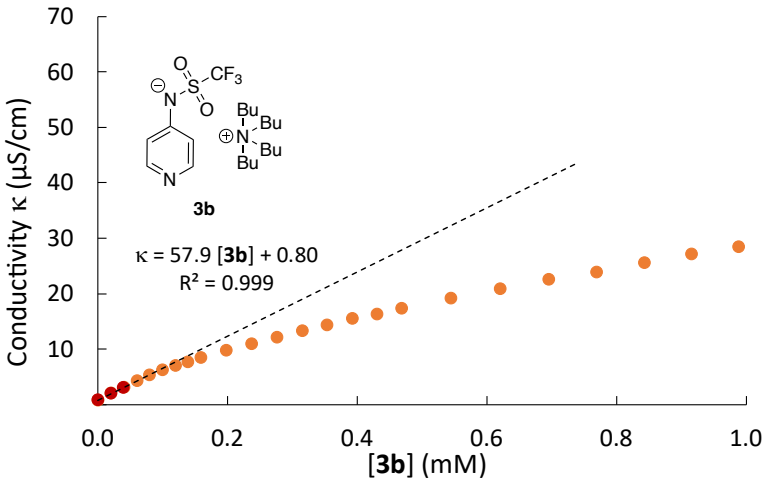

Figure 2.4: [Figure S4]. Concentration-dependent conductivity profile for catalyst **3b** in DCM with Λ_m = 57.9 S cm^2 mol^{-1} without solvent background at 20 °C.

By subtracting the limited molar ionic conductivity λ_{NBu4} of NBu_4^+ form the molar conductivity Λ_m of salt **3b**, the limited molar ionic conductivity λ_{an3} of anion **3** is determined to be λ_{an3} = 11.4 S cm^2 mol^{-1}. Since the molar conductivity of salt **3a** is 79.2 S cm^2 mol^{-1} in DCM, it can be concluded that the limited molar ionic conductivity of cation **a** is λ_{PPh4} = 67.8 S cm^2 mol^{-1}. This translates to a contribution of 14% for the anion **A** and 86% for the cation **C** towards the total molar conductivity Λ_m of salt **3a**. Next, it is necessary to evaluate the contribution of the sandwich cation to the overall molar conductivity Λ_m of 79.2 S cm^2 mol^1.

According to literature, it is common to assume a specific quotient for the limited molar conductivity of the sandwich-cation (λ_{CAC}/Λ_m). Most often the quotient is assumed to be 1/3[9–11], 2/3[12], or $(1/3)^{(1/3)}$ = 0.693[13,14]. The quotient λ_{CAC}/Λ_m = (1/3) was used for different salts, like lithium and tributylammonium thiocyanates[10] or 1-ethyl-3-methylimidazolium tetrafluoroborate and 1-butyl-3-

methylimidazolium tetrafluoro borate[11], in various solvents. The quotient $\lambda_{CAC}/\Lambda_m = (1/3)^{(1/3)}$ was mainly used to describe the fluoroalkanoates and triethylamine chlorides in polar solvents as MeCN. Meanwhile, the quotient $\lambda_{CAC}/\Lambda_m = 2/3$ has been used for the analysis of tetraphenyl boron salts in THF, which is another spheric ion in an nonpolar solvent.[12] Therefore, it serves as the best reference for our system **3a**. So, for the future analysis of equilibria with sandwich cation formations in DCM, the quotient $\lambda_{CAC}/\Lambda_m = \delta_{CAC} = 2/3$ will be used. Here, we introduce δ_i as *scaling factor* for the conversion of Λ_m into the respective λ_i. The final result for the sandwich association constant with 14% anion contribution, 86% cation contribution and 2/3 sandwich cation contribution would be $K_{CAC} = 2.62 \times 10^6$ M^{-2} for pyridinamide ion pair **3a** in DCM with an RMSE = 0.62 (see Table 2.3).

Table 2.3: [Table S3]. Association constant K_{CAC} for pyridinamide ion pair **3a** according to model 1 with the respective limited molar ionic conductivities λ_i.

λ_A (S cm² mol⁻¹)	λ_C (S cm² mol⁻¹)	λ_{CAC} (S cm² mol⁻¹)	K_{CAC} (M^{-2})	RMSE
0.14 x Λ_m	0.86 x Λ_m	(2/3) x Λ_m	2.62×10^6	0.62

2.1.4.4.2 Model 2

a) Cationic Sandwich Association (Model 2a)

The recent DOSY result, however, made us question if conventional conductivity measurements are able to measure solutions of high enough dilution to guarantee fully dissociated ions. Therefore, we decided on a second approach toward the determination of the sandwich association constant based on the conductivity measurements, where the ratio between the anion and cation contribution to the molar conductivity Λ_m is treated as a second variable parameter. Since the model always starts from fully dissociated ions the sum of the scaling factors $\delta_A + \delta_C$ cannot exceed 1. The contribution of the sandwich cation was still set to be $2/3\Lambda_m$. Different ratios for δ_A/δ_C were tested and the full analysis to find K_{CAC} was done. Then the RMSE value for this sandwich association constant was compared (see Table 2.4).

Table 2.4: [Table S4]. List of optimization steps for limited molar ionic conductivities λ_i with the corresponding association constants K_{CAC} for pyridinamide ion pair **3a** according to model 1.

λ_A (S cm² mol⁻¹)	λ_C (S cm² mol⁻¹)	λ_{CAC} (S cm² mol⁻¹)	K_{CAC} (M^{-2})	RMSE
0.14 x Λ_m	0.86 x Λ_m	(2/3) x Λ_m	2.62×10^6	0.620
0.30 x Λ_m	0.70 x Λ_m		$4.0 \times 10^6 – 5.0 \times 10^6$	<0.35
0.33 x Λ_m	0.67 x Λ_m		5.20×10^6	0.210
0.35 x Λ_m	0.65 x Λ_m		5.70×10^6	0.183
0.36 x Λ_m	0.64 x Λ_m		5.97×10^6	0.175
0.37 x Λ_m	0.63 x Λ_m		6.27×10^6	0.173
0.38 x Λ_m	0.62 x Λ_m		6.57×10^6	0.176
0.40 x Λ_m	0.60 x Λ_m		7.31×10^6	0.200

The best fit was found for $K_{CAC} = 6.27 \times 10^6$ M^{-2} with a RMSE = 0.17, which is the final result for the sandwich association constant of pyridinamide ion pair **3a**.

Both equilibrium constants were used to determine the percentage speciation (see Table 2.5 and 2.6).

Table 2.5: [Table S5]. Speciation of pyridinamide ion pair **3a** in 1:1 model in DCM with $K_{IP} = 6.86 \times 10^5$ M^{-2} and their percentage.

[3a] / (M)	[A] / (M)	[C] / (M)	[IP] / (M)	[A]%	[C]%	[IP]%
0.00	0.00	0.00	0.00	–	–	–
1.78×10^{-5}	1.75×10^{-5}	1.75×10^{-5}	2.55×10^{-7}	0.99	0.99	0.01
3.55×10^{-5}	3.45×10^{-5}	3.45×10^{-5}	9.87×10^{-7}	0.97	0.97	0.03
5.40×10^{-5}	5.18×10^{-5}	5.18×10^{-5}	2.22×10^{-6}	0.96	0.96	0.04
7.09×10^{-5}	6.72×10^{-5}	6.72×10^{-5}	3.74×10^{-6}	0.95	0.95	0.05

8.86×10^{-5}	8.29×10^{-5}	8.29×10^{-5}	5.69×10^{-6}	0.94	0.94	0.06
1.06×10^{-4}	9.80×10^{-5}	9.80×10^{-5}	7.96×10^{-6}	0.92	0.92	0.08
1.24×10^{-4}	1.13×10^{-4}	1.13×10^{-4}	1.06×10^{-5}	0.91	0.91	0.09
1.41×10^{-4}	1.28×10^{-4}	1.28×10^{-4}	1.35×10^{-5}	0.90	0.90	0.10
1.76×10^{-4}	1.56×10^{-4}	1.56×10^{-4}	2.01×10^{-5}	0.89	0.89	0.11
2.11×10^{-4}	1.83×10^{-4}	1.83×10^{-4}	2.78×10^{-5}	0.87	0.87	0.13
2.46×10^{-4}	2.10×10^{-4}	2.10×10^{-4}	3.64×10^{-5}	0.85	0.85	0.15
2.80×10^{-4}	2.34×10^{-4}	2.34×10^{-4}	4.55×10^{-5}	0.84	0.84	0.16
3.15×10^{-4}	2.59×10^{-4}	2.59×10^{-4}	5.57×10^{-5}	0.82	0.82	0.18
3.49×10^{-4}	2.83×10^{-4}	2.83×10^{-4}	6.62×10^{-5}	0.81	0.81	0.19
3.83×10^{-4}	3.06×10^{-4}	3.06×10^{-4}	7.74×10^{-5}	0.80	0.80	0.20
4.17×10^{-4}	3.28×10^{-4}	3.28×10^{-4}	8.91×10^{-5}	0.79	0.79	0.21
4.85×10^{-4}	3.71×10^{-4}	3.71×10^{-4}	1.14×10^{-4}	0.76	0.76	0.24
5.52×10^{-4}	4.12×10^{-4}	4.12×10^{-4}	1.40×10^{-4}	0.75	0.75	0.25
6.19×10^{-4}	4.51×10^{-4}	4.51×10^{-4}	1.68×10^{-4}	0.73	0.73	0.27
6.85×10^{-4}	4.88×10^{-4}	4.88×10^{-4}	1.97×10^{-4}	0.71	0.71	0.29
7.50×10^{-4}	5.23×10^{-4}	5.23×10^{-4}	2.27×10^{-4}	0.70	0.70	0.30
8.15×10^{-4}	5.58×10^{-4}	5.58×10^{-4}	2.57×10^{-4}	0.68	0.68	0.32
8.80×10^{-4}	5.91×10^{-4}	5.91×10^{-4}	2.89×10^{-4}	0.67	0.67	0.33
9.44×10^{-4}	6.23×10^{-4}	6.23×10^{-4}	3.21×10^{-4}	0.66	0.66	0.34
1.01×10^{-3}	6.55×10^{-4}	6.55×10^{-4}	3.55×10^{-4}	0.65	0.65	0.35

Table 2.6: [Table S6]. Speciation of pyridinamide ion pair **3a** in sandwich association model in DCM with $K_{CAC} = 6.27 \times 10^{6}$ M^{-2} and their percentage.

[3a] / (M)	**[A] / (M)**	**[C] / (M)**	**[CAC] / (M)**	**[A]%**	**[C]%**	**[CAC]%**
0.00	0.00	0.00	0.00	–	–	–
1.78×10^{-5}	1.78×10^{-5}	1.77×10^{-5}	3.50×10^{-8}	1.00	1.00	0.00
3.55×10^{-5}	3.52×10^{-5}	3.50×10^{-5}	2.70×10^{-7}	0.99	0.98	0.01
5.40×10^{-5}	5.31×10^{-5}	5.22×10^{-5}	9.07×10^{-7}	0.98	0.97	0.02
7.09×10^{-5}	6.90×10^{-5}	6.70×10^{-5}	1.94×10^{-7}	0.97	0.95	0.03
8.86×10^{-5}	8.51×10^{-5}	8.15×10^{-5}	3.54×10^{-6}	0.96	0.92	0.04
1.06×10^{-4}	1.00×10^{-4}	9.47×10^{-5}	5.64×10^{-6}	0.95	0.89	0.05
1.24×10^{-4}	1.16×10^{-4}	1.07×10^{-4}	8.35×10^{-6}	0.93	0.87	0.07
1.41×10^{-4}	1.30×10^{-4}	1.18×10^{-4}	1.14×10^{-5}	0.92	0.84	0.08
1.76×10^{-4}	1.57×10^{-4}	1.38×10^{-4}	1.88×10^{-5}	0.89	0.79	0.11
2.11×10^{-4}	1.83×10^{-4}	1.55×10^{-4}	2.78×10^{-5}	0.87	0.74	0.13
2.46×10^{-4}	2.08×10^{-4}	1.70×10^{-4}	3.79×10^{-5}	0.85	0.69	0.15
2.80×10^{-4}	2.31×10^{-4}	1.83×10^{-4}	4.85×10^{-5}	0.83	0.65	0.17
3.15×10^{-4}	2.55×10^{-4}	1.94×10^{-4}	6.03×10^{-5}	0.81	0.62	0.19
3.49×10^{-4}	2.77×10^{-4}	2.04×10^{-4}	7.24×10^{-5}	0.79	0.59	0.21
3.83×10^{-4}	2.98×10^{-4}	2.13×10^{-4}	8.49×10^{-5}	0.78	0.56	0.22
4.17×10^{-4}	3.19×10^{-4}	2.21×10^{-4}	9.79×10^{-5}	0.77	0.53	0.23
4.85×10^{-4}	3.60×10^{-4}	2.35×10^{-4}	1.25×10^{-4}	0.74	0.48	0.26
5.52×10^{-4}	3.99×10^{-4}	2.47×10^{-4}	1.53×10^{-4}	0.72	0.45	0.28
6.19×10^{-4}	4.38×10^{-4}	2.57×10^{-4}	1.81×10^{-4}	0.71	0.41	0.29
6.85×10^{-4}	4.75×10^{-4}	2.65×10^{-4}	2.10×10^{-4}	0.69	0.39	0.31
7.50×10^{-4}	5.11×10^{-4}	2.73×10^{-4}	2.39×10^{-4}	0.68	0.36	0.32
8.15×10^{-4}	5.47×10^{-4}	2.79×10^{-4}	2.68×10^{-4}	0.67	0.34	0.33
8.80×10^{-4}	5.83×10^{-4}	2.85×10^{-4}	2.97×10^{-4}	0.66	0.32	0.34
9.44×10^{-4}	6.17×10^{-4}	2.91×10^{-4}	3.27×10^{-4}	0.65	0.31	0.35
1.01×10^{-3}	6.53×10^{-4}	2.95×10^{-4}	3.57×10^{-4}	0.65	0.30	0.35

In both association models the anion and cation are mainly dissociated at low concentrations. While in the 1:1 model the concentration of anion and cation are always identical, in the sandwich association the concentration of free cation [C] is faster declining than the concentration of free anion [A] due to the formation of the sandwich cation. In both association model the concentration of free anion [A] is 65% and available to react as nucleophilic catalyst in solution.

The ion pair **4a** and additive **6** were analyzed the same way as pyridinamide salt **3a** with the two-parameter approach (model 2) for the sandwich association constant K_{CAC}. The results can be found in Table 2.7.

Table 2.7: [Table S7]. Association constants K_{IP} and K_{CAC} according to the respective biochemical models of ion catalysts **3a**, **4a**, and additive **6** at 20 °C in DCM.

Ion Pair	K_{IP} (M^{-2})	K_{CAC} (M^{-2})
3a	6.86×10^5	6.27×10^6
4a	8.79×10^5	6.71×10^6
6	1.01×10^6	7.28×10^6

b) Anion Sandwich Association (Model 2b)

Aside from the previously discussed cationic sandwich association, the contrasting anionic sandwich association leading to a free cation **C** and a sandwich anion **ACA**, which consists of two anions **A** and one central cation **C**, is equally thinkable. For the analysis of this association type, we applied the same numerical model as discussed earlier using COPASI (see Scheme 2.5).

$$2 * A + 2 * C \rightleftharpoons[K_{ACA}] C + ACA$$

Scheme 2.5: [Scheme S5]. Equation for numerical simulations of anionic sandwich association model for salt **3a.**

The anion sandwich association constant is defined as $k_1/k_2 = K_{ACA}$ with to $k_2 = 1$ being a fixed value. The contribution of the sandwich anion was also set to be $2/3*\Lambda_m$. Different ratios for $\lambda_A + \lambda_C$ were tested, and numerical simulation were performed until the best association constant K_{ACA} was found. The RMSE value for the anion sandwich association constant K_{ACA} was used as a quality control measure.

Following the above-described guideline for model 2 resulted in exactly the same anion sandwich association constant as the cationic sandwich association with $K_{ACA} = K_{CAC} = 6.27 \times 10^6\ M^{-2}$. This was to be expected since the individual ionic conductivity contributions λ_i towards the overall molar conductivity Λ_m are treated as variables here, while the sandwich ion contribution λ_i is fixed to be $2/3*\Lambda_m$. Therefore, the molar ionic conductivity contributions interchanged by moving from the cationic sandwich association to the anionic sandwich association (see Table 2.8).

Table 2.8: [Table S8]. Association constants K_{CAC} and K_{ACA} for pyridinamide ion pair **3a** according to model 2 with the respective limited molar ionic conductivities λ_i.

Sandwich Type	λ_A (S cm² mol⁻¹)	λ_C (S cm² mol⁻¹)	$\lambda_{i=CAC,ACA}$ (S cm² mol⁻¹)	K (M^{-2})	RMSE
Cationic	$0.37 \times \Lambda_m$	$0.63 \times \Lambda_m$	$(2/3) \times \Lambda_m$	6.27×10^6	0.17
Anionic	$0.63 \times \Lambda_m$	$0.37 \times \Lambda_m$	$(2/3) \times \Lambda_m$	6.27×10^6	0.17

To conclude, based on the conductivity data, we cannot determine with certainty which type of sandwich ion association is favored.

2.1.4.4.3 Model 3

a) Cation Sandwich Association (Model 3a)

Further development of the conductivity model led to the following changes. We specifically focused on how we determine the contribution made towards the molar specific conductivity Λ_m by each of the charged species. Fuoss *et al*. stated that the limited molar ionic conductivity λ of each ion is proportional to their volume.[15,16] Therefore, we applied this approach by using the calculated cavity volumes of each anion, cation, and ion pair to calculate the percentage share of the anion volume ***A*** and cation volume ***C*** (see eq. 2.8), which will then be used as scaling factors δ_i to convert Λ_m into the respective λ_i.

$$\delta_A = \frac{\mathrm{vol(A)}}{\mathrm{vol(IP)}} \tag{2.8a}$$

$$\delta_C = \frac{\mathrm{vol(C)}}{\mathrm{vol(IP)}} \tag{2.8b}$$

Here, the calculated volumes of anion **3** (215 Å^3), cation **a** (362 Å^3),and contact ion pair **3a** (570 Å^3), which are based on the van der Waals cavities employed in the SMD continuum solvation model at the SMD(DCM)/B3LYP-D3/6-31+G(d) level of theory are used (see Table 2.16). Since there is no known way to determine the limited molar ionic conductivity λ_{CAC} for the cation sandwich in DCM, we decided to treat it as another variable instead of assigning a set value to it. This refined approach gives us the following results for the cationic sandwich association (see Table 2.9). All scaling factors δ_i are limited to two decimals, when used in the excel sheet to transform concentration into conductivity values.

Table 2.9: [Table S9]. Association constant K_{CAC} for salt **3a**, **4a**, and **6** according to model 3a with the respective limited molar ionic conductivities λ_i and the scaling factors δ_i.

Ion Pair	Λ_m (S cm² mol^{-1})	λ_A (S cm² mol^{-1})	λ_C (S cm² mol^{-1})	$\delta_A/\delta_C/\delta_{CAC}$	K_{CAC} (M^{-2})	RMSE
3a	79.2	29.3	49.9	37/63/67	6.38 x 10^6	0.17
4a	73.6	32.4	41.2	44/56/54	6.50 x 10^6	0.12
6	95.2	15.2	80.0	16/84/80	7.05 x 10^6	0.16

Comparing the results from model 2 with model 3 show only small deviations between the obtained sandwich association constants K_{CAC}.

b) Anion Sandwich Association (Model 3b)

The analysis of the conductivity data according to model 3 for the anion sandwich association gives the same value for the anionic sandwich association constant K_{ACA} as for the cationic sandwich association with $K_{ACA} = K_{CAC} = 6.38 \times 10^6$ M^{-2} for ion pair **3a** and $K_{ACA} = K_{CAC} = 6.50 \times 10^6$ M^{-2} for ion pair **4a**. The results are summarized in Table 2.10.

Table 2.10: [Table S10]. Association constant K_{ACA} for salt **3a** and **4a** according to model 3b with the respective limited molar ionic conductivities λ_i and the scaling factors δ_i.

Ion Pair	Λ_m (S cm² mol^{-1})	λ_A (S cm² mol^{-1})	λ_C (S cm² mol^{-1})	$\delta_A/\delta_C/\delta_{ACA}$	K_{ACA} (M^{-2})	RMSE
3a	79.2	29.3	49.9	37/63/41	6.38 x 10^6	0.17
4a	73.6	32.4	41.2	44/56/42	6.50 x 10^6	0.12

Thus, both sandwich association types are not distinguishable based on conductivity data alone. Therefore, we need to look at the DOSY measurements to gain an understanding of which association type is a better fit for each respective ion pair.

2.1.4.5 Mixed Sandwich Association (Model 4)

So far, we have separately analyzed the conductivity data for both cationic and anionic sandwich association. However, the comparison between the simulated DOSY volumes based on the numerical simulation of conductivity data for both association types and the experimentally determined DOSY volumes revealed significant deviations (see Figure 2.5).

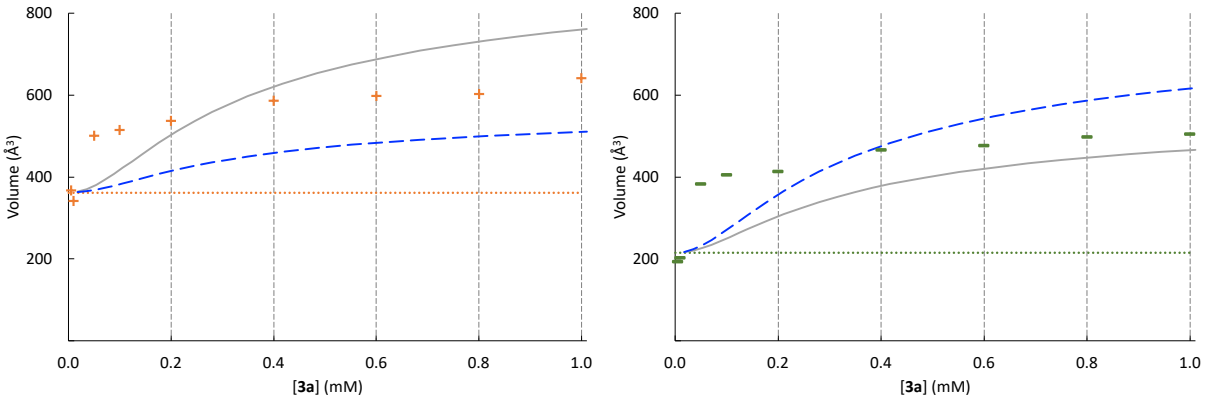

Figure 2.5: [Figure S5]. Concentration-dependent volumes of cations **a** (orange "+" symbols) and anions **3** (green "–" symbols) of salt **3a** in CD_2Cl_2 as calculated from DOSY experiments (with data from ref [2]) with the respective free ion volumes (dotted line; cation in orange; anion in green), the simulated trend for the cationic (grey line) and anionic (blue dashed line) sandwich model.

To minimize this deviation, we extended our earlier described conductivity model 3. Since the resulting association constant was identical for both the cationic and anionic sandwich associations under model 3, the idea was to combine both sandwich association types into one model, which we will refer to as the *mixed association model* moving forward.

$$2 * A + 2 * C \overset{K_{CAC}}{\rightleftharpoons} A + CAC$$

$$2 * A + 2 * C \overset{K_{ACA}}{\rightleftharpoons} C + ACA$$

Scheme 2.6: [Scheme S6]. Cation sandwich association and anion sandwich association model for pyridinamide ion pair **3a.**

To find the right balance between the cation sandwich association and the anion sandwich association each association constant was assigned a *scaling factor*, which would be multiplied with the respective sandwich association constant whereas, where α would be a fixed value decreasing from 1.0 in steps of 0.1 (see eq. 2.9)

$$K_{CAC} \times \alpha \qquad (2.9a)$$

$$K_{ACA} \times \beta \qquad (2.9b)$$

For each step the best β value with the smallest RMSE for the conductivity data was determined by employing numerical simulations. The optimization of the scaling factor was limited to two relevant decimals.

Table 2.11: [Table S11]. List of association constants based on the optimized scaling factors α and β with the calculated anion and cation volumes (Å³) and the respective percentual residual between the reference ion volume and calculated ion volume for pyridinamide ion pair **3a**.

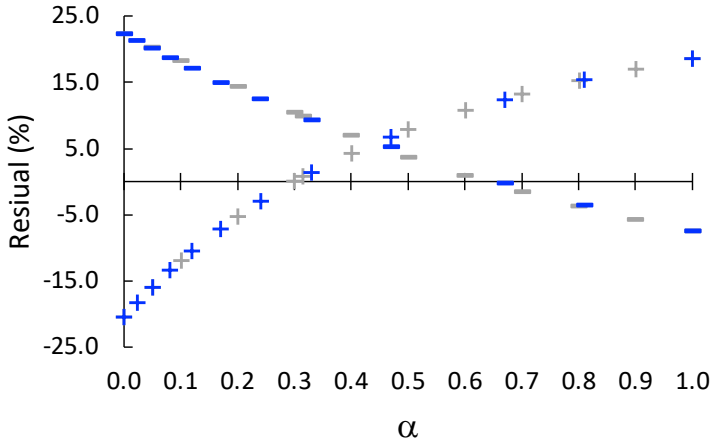

K_{CAC} (M^{-2})	K_{ACA} (M^{-2})	α	β	RMSE	V_{an} (Å³)	V_{cat} (Å³)	Residual (%) Anion	Residual (%) Cation
Reference					505	642		
6.38×10^6	0.00	1.00	0.00	0.17	467	761	-7.51	18.64
5.74×10^6	1.47×10^5	0.90	0.023	0.18	476	751	-5.72	17.05
5.10×10^6	3.19×10^5	0.80	0.05	0.22	486	739	-3.73	15.23
4.47×10^6	5.17×10^5	0.70	0.081	0.28	497	726	-1.60	13.18
3.83×10^6	7.66×10^5	0.60	0.12	0.34	509	711	0.84	10.74
3.19×10^6	1.08×10^6	0.50	0.17	0.4	523	692	3.58	7.84
2.55×10^6	1.53×10^6	0.40	0.24	0.45	540	669	6.94	4.30
2.01×10^6	2.01×10^6	0.315	0.315	0.46	554	647	9.84	0.75
1.91×10^6	2.11×10^6	0.30	0.33	0.46	557	642	10.38	0.03
1.28×10^6	3.00×10^6	0.20	0.47	0.42	577	608	14.38	-5.24
6.38×10^5	4.27×10^6	0.10	0.67	0.3	597	565	18.26	-11.93
3.19×10^5	5.17×10^6	0.05	0.81	0.22	607	540	20.24	-15.91
0.00	6.38×10^6	0.00	1.00	0.17	617	511	22.28	-20.38
1.47×10^5	5.74×10^6	0.023	0.90	0.18	612	524	21.26	-18.28
3.19×10^5	5.10×10^6	0.05	0.80	0.22	606	540	20.07	-15.93
5.17×10^5	4.47×10^6	0.081	0.70	0.28	599	556	18.68	-13.39
7.66×10^5	3.83×10^6	0.12	0.60	0.34	591	575	17.01	-10.44
1.08×10^6	3.19×10^6	0.17	0.50	0.4	580	596	14.98	-7.08
1.53×10^6	2.55×10^6	0.24	0.40	0.45	568	623	12.49	-2.97
2.11×10^6	1.91×10^6	0.33	0.30	0.46	552	651	9.29	1.46
3.00×10^6	1.28×10^6	0.47	0.20	0.42	531	685	5.25	6.71
4.27×10^6	6.38×10^5	0.67	0.10	0.3	503	721	-0.26	12.32
5.17×10^6	3.19×10^5	0.81	0.05	0.22	486	740	-3.65	15.37

This routine was repeated with β as the fixed factor and α as the factor to be optimized, ensuring compliance between both approaches, as shown in Figure 2.6.

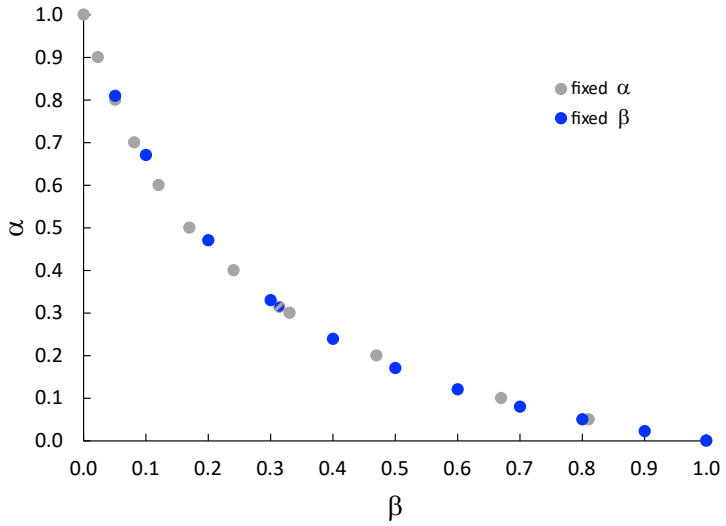

Figure 2.6: [Figure S6]. Graphical representation of the ratio of the optimized scaling factors α and β with α being the fixed value for the optimization of β (grey dots) and in reverse β being the fixed value for the optimization of α (blue dots) for pyridinamide ion pair **3a**.

The two data sets are almost identical with small deviations especially in the outer regions where one factor is significantly larger than the other. Therefore, the performance of each optimization step based on both scaling factors α and β is crucial since each chosen fix point offers a unique point of view onto the ideal sandwich association mixture. The zenith is found at α = β = 0.315 with K_{CAC} = K_{ACA} = 2.01 x 10^6 M^{-2}.

The next step involved incorporating experimental DOSY data by using the experimental DOSY volumes of ion pair **3a** as a reference value (with V_{an} = 505 Å^3 and V_{cat} = 642 Å^3). Numerical simulations provided concentrations used to calculate simulated DOSY volumes (see eq. 2.10).

$$\mathrm{vol_{cat}} = \frac{[\mathrm{C}]}{[\mathrm{IP}]_{\mathrm{tot}}} \times 362 + \left(\frac{2 \times [\mathrm{CAC}]}{[\mathrm{IP}]_{\mathrm{tot}}}\right) \times 925 + \left(\frac{[\mathrm{ACA}]}{[\mathrm{IP}]_{\mathrm{tot}}}\right) \times 782 \qquad (2.10a)$$

$$\mathrm{vol_{an}} = \frac{[\mathrm{A}]}{[\mathrm{IP}]_{\mathrm{tot}}} \times 215 + \left(\frac{[\mathrm{CAC}]}{[\mathrm{IP}]_{\mathrm{tot}}}\right) \times 925 + \left(\frac{2 \times [\mathrm{ACA}]}{[\mathrm{IP}]_{\mathrm{tot}}}\right) \times 782 \qquad (2.10b)$$

Subsequently, the percentual residual between experimental and simulated ion volumes determined the optimal mix of cationic and anionic sandwich association, showing that α = β = 0.44/0.21 for ion pair **3a** was optimal (see Table 2.12). The previous optimization steps of α and β indicates in what region further optimization steps need to be taken e.g. for ion pair **3a** additional optimization was done starting from α/β = 0.47/0.20.

Table 2.12: [Table S12]. List of association constants based on the optimized scaling factors α and β with the calculated anion and cation volumes (Å³) and the respective percentual residual between the reference ion volume and calculated ion volume with focus on the area around the smallest percentual residue for both ion volumes for **3a**.

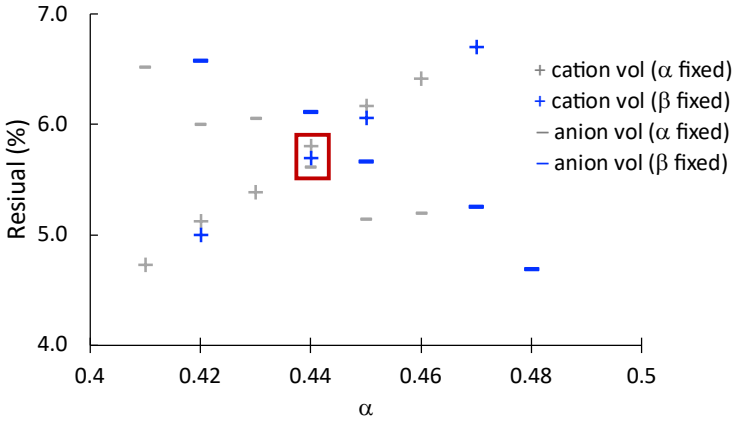

K_{CAC} (M^{-2})	K_{ACA} (M^{-2})	α	β	RMSE	V_{an} (Å³)	V_{cat} (Å³)	Residual (%) Anion	Residual (%) Cation
Reference					505	642		
2.93 x 10^6	1.28 x 10^6	0.46	0.20	0.42	531	683	5.20	6.42
2.87 x 10^6	1.28 x 10^6	0.45	0.20	0.43	531	681	5.15	6.17
2.81 x 10^6	1.34 x 10^6	**0.44**	**0.21**	0.43	533	679	**5.61**	**5.80**
2.74 x 10^6	1.40 x 10^6	0.43	0.22	0.44	535	676	6.06	5.39
2.68 x 10^6	1.40 x 10^6	0.42	0.22	0.44	535	675	6.01	5.12
2.62 x 10^6	1.47 x 10^6	0.41	0.23	0.44	538	672	6.52	4.73
3.06 x 10^6	1.21 x 10^6	0.48	0.19	0.41	528	687	4.68	7.08
3.00 x 10^6	1.28 x 10^6	0.47	0.20	0.42	531	685	5.25	6.71
2.87 x 10^6	1.34 x 10^6	0.45	0.21	0.43	533	681	5.66	6.06
2.81 x 10^6	1.40 x 10^6	**0.44**	**0.22**	0.43	536	678	**6.11**	**5.70**
2.68 x 10^6	1.47 x 10^6	0.42	0.23	0.44	538	674	6.57	5.00

Comparing the simulated DOSY data based on Model 3 for the cationic and anionic sandwich association with the newly introduced mixed model demonstrated a significant improved overlap with experimental data than any other association model (see Figure 2.7).

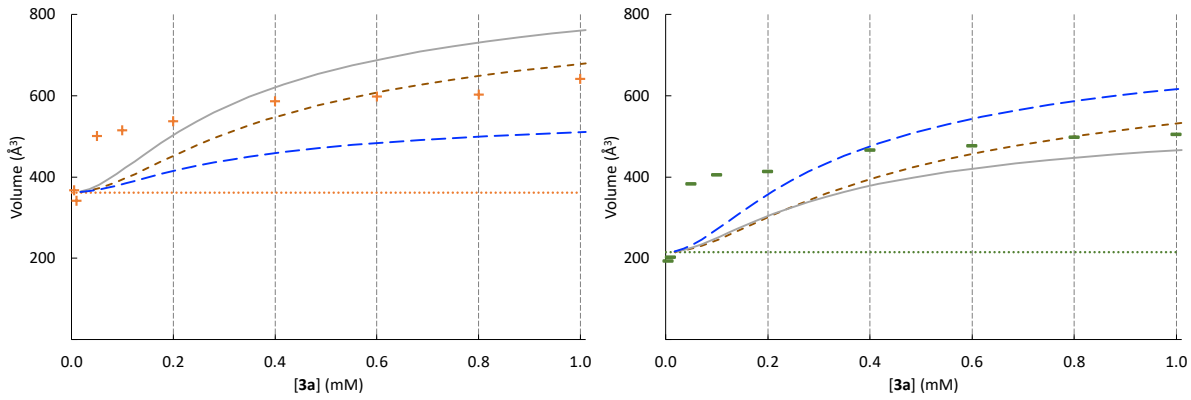

Figure 2.7: [Figure S7]. Concentration-dependent volumes of cation **a** (orange "+" symbols) and anion **3** (green "–" symbols) of salt **3a** in CD_2Cl_2 as calculated from DOSY experiments (with data from ref [2]) with the respective free ion volumes (dotted line; cation in orange; anion in green), the simulated trends for the cationic (grey line) and anionic (blue dashed line) sandwich model, and the mixed sandwich association model (brown short-dashed line).

This procedure was repeated for pyridinamide ion pair **4a**. The results of the mixed model analysis are summarized in Table 2.13.

Table 2.13: [Table S13]. Specific molar conductivity Λ_m, the scaling factors δ_i and association constants K_{CAC} and K_{ACA} with their respective scaling factor α and β for pyridinamide ion pair **3a** and **4a**.

Ion Pair	Λ_m (S cm^2 mol^{-1})	δ_A /δ_C /δ_{CAC}//δ_{ACA}	α x K_{CAC} (M^{-2})	β x K_{ACA} (M^{-2})	α/β (%)	RMSE
3a	79.2	37/63/67/41	2.81 x 10^6	1.34 x 10^6	44/21	0.43
4a	73.6	44/56/54/42	7.80 x 10^5	3.97 x 10^6	12/61	0.35

The resulting association constants of the mixed model analysis for pyridinamide ion pair **3a** and **4a** were used to determine the percentage speciation (see Table 2.14 and Table 2.15).

Table 2.14: [Table S14]. Speciation of pyridinamide ion pair **3a** in model 4 with α x K_{CAC} = 2.81 x 10^6 M^{-2} and β x K_{ACA} = 1.34 x 10^6 M^{-2} (α/β = 0.44/0.21), and the percentage of each involved charged species.

[3a]	[A] (M)	[C] (M)	[CAC] (M)	[ACA] (M)	[A]%	[C]%	[CAC]%	[ACA]%
0.00	0.00	0.00	0.00	0.00	–	–	–	–
1.78 x 10^{-5}	1.78 x 10^{-5}	1.78 x 10^{-5}	1.58 x 10^{-8}	7.51 x 10^{-9}	1.00	1.00	0.00	0.00
3.55 x 10^{-5}	3.53 x 10^{-5}	3.52 x 10^{-5}	1.23 x 10^{-7}	5.86 x 10^{-8}	0.99	0.99	0.00	0.00
5.40 x 10^{-5}	5.32 x 10^{-5}	5.30 x 10^{-5}	4.19 x 10^{-7}	2.01 x 10^{-7}	0.98	0.98	0.01	0.00
7.09 x 10^{-5}	6.91 x 10^{-5}	6.86 x 10^{-5}	9.15 x 10^{-7}	4.39 x 10^{-7}	0.97	0.97	0.01	0.01
8.86 x 10^{-5}	8.53 x 10^{-5}	8.44 x 10^{-5}	1.71 x 10^{-6}	8.22 x 10^{-7}	0.96	0.95	0.02	0.01
1.06 x 10^{-4}	1.01 x 10^{-4}	9.91 x 10^{-5}	2.77 x 10^{-6}	1.34 x 10^{-6}	0.95	0.93	0.03	0.01
1.24 x 10^{-4}	1.16 x 10^{-4}	1.14 x 10^{-4}	4.19 x 10^{-6}	2.04 x 10^{-6}	0.93	0.92	0.03	0.02
1.41 x 10^{-4}	1.29 x 10^{-4}	1.27 x 10^{-4}	5.82 x 10^{-6}	2.84 x 10^{-6}	0.92	0.90	0.04	0.02
1.76 x 10^{-4}	1.56 x 10^{-4}	1.51 x 10^{-4}	1.00 x 10^{-5}	4.93 x 10^{-6}	0.89	0.86	0.06	0.03
2.11 x 10^{-4}	1.81 x 10^{-4}	1.73 x 10^{-4}	1.52 x 10^{-5}	7.57 x 10^{-6}	0.86	0.82	0.07	0.04
2.46 x 10^{-4}	2.03 x 10^{-4}	1.93 x 10^{-4}	2.12 x 10^{-5}	1.07 x 10^{-5}	0.83	0.78	0.09	0.04
2.80 x 10^{-4}	2.24 x 10^{-4}	2.10 x 10^{-4}	2.78 x 10^{-5}	1.41 x 10^{-5}	0.80	0.75	0.10	0.05
3.15 x 10^{-4}	2.44 x 10^{-4}	2.27 x 10^{-4}	3.52 x 10^{-5}	1.80 x 10^{-5}	0.77	0.72	0.11	0.06
3.49 x 10^{-4}	2.62 x 10^{-4}	2.41 x 10^{-4}	4.28 x 10^{-5}	2.22 x 10^{-5}	0.75	0.69	0.12	0.06
3.83 x 10^{-4}	2.79 x 10^{-4}	2.55 x 10^{-4}	5.09 x 10^{-5}	2.66 x 10^{-5}	0.73	0.67	0.13	0.07
4.17 x 10^{-4}	2.95 x 10^{-4}	2.67 x 10^{-4}	5.93 x 10^{-5}	3.12 x 10^{-5}	0.71	0.64	0.14	0.07
4.85 x 10^{-4}	3.26 x 10^{-4}	2.90 x 10^{-4}	7.69 x 10^{-5}	4.12 x 10^{-5}	0.67	0.60	0.16	0.08
5.52 x 10^{-4}	3.53 x 10^{-4}	3.10 x 10^{-4}	9.52 x 10^{-5}	5.18 x 10^{-5}	0.64	0.56	0.17	0.09
6.19 x 10^{-4}	3.79 x 10^{-4}	3.28 x 10^{-4}	1.14 x 10^{-4}	6.30 x 10^{-5}	0.61	0.53	0.18	0.10
6.85 x 10^{-4}	4.02 x 10^{-4}	3.44 x 10^{-4}	1.33 x 10^{-4}	7.46 x 10^{-5}	0.59	0.50	0.19	0.11
7.50 x 10^{-4}	4.24 x 10^{-4}	3.58 x 10^{-4}	1.53 x 10^{-4}	8.64 x 10^{-5}	0.57	0.48	0.20	0.12
8.15 x 10^{-4}	4.45 x 10^{-4}	3.71 x 10^{-4}	1.73 x 10^{-4}	9.86 x 10^{-5}	0.55	0.46	0.21	0.12
8.80 x 10^{-4}	4.65 x 10^{-4}	3.84 x 10^{-4}	1.92 x 10^{-4}	1.11 x 10^{-4}	0.53	0.44	0.22	0.13
9.44 x 10^{-4}	4.84 x 10^{-4}	3.95 x 10^{-4}	2.12 x 10^{-4}	1.24 x 10^{-4}	0.51	0.42	0.22	0.13
1.01 x 10^{-3}	5.02 x 10^{-4}	4.06 x 10^{-4}	2.33 x 10^{-4}	1.37 x 10^{-4}	0.50	0.40	0.23	0.14

Table 2.15: [Table S15]. Speciation of pyridinamide ion pair **4a** in model 4 with α x K_{CAC} = 7.80 x 10^5 M^{-2} and β x K_{ACA} = 3.97 x 10^6 M^{-2} (α/β = 0.12/0.61), and the percentage of each involved charged species.

[4a] (M)	[A] (M)	[C] (M)	[CAC] (M)	[ACA] (M)	[A]%	[C]%	[CAC]%	[ACA]%
0.00	0.00	0.00	0.00	0.00	–	–	–	–
1.96 x 10^{-5}	1.95 x 10^{-5}	1.96 x 10^{-5}	5.83 x 10^{-9}	2.96 x 10^{-8}	1.00	1.00	0.00	0.00
3.91 x 10^{-5}	3.86 x 10^{-5}	3.88 x 10^{-5}	4.53 x 10^{-8}	2.29 x 10^{-7}	0.99	0.99	0.00	0.01
5.86 x 10^{-5}	5.70 x 10^{-5}	5.76 x 10^{-5}	1.47 x 10^{-7}	7.42 x 10^{-7}	0.97	0.98	0.00	0.01
7.81 x 10^{-5}	7.44 x 10^{-5}	7.58 x 10^{-5}	3.33 x 10^{-7}	1.67 x 10^{-6}	0.95	0.97	0.00	0.02
9.75 x 10^{-5}	9.08 x 10^{-5}	9.32 x 10^{-5}	6.15 x 10^{-7}	3.05 x 10^{-6}	0.93	0.96	0.01	0.03
1.17 x 10^{-4}	1.06 x 10^{-4}	1.10 x 10^{-4}	1.00 x 10^{-6}	4.92 x 10^{-6}	0.91	0.94	0.01	0.04
1.36 x 10^{-4}	1.20 x 10^{-4}	1.26 x 10^{-4}	1.48 x 10^{-6}	7.21 x 10^{-6}	0.88	0.93	0.01	0.05
1.56 x 10^{-4}	1.34 x 10^{-4}	1.42 x 10^{-4}	2.10 x 10^{-6}	1.01 x 10^{-5}	0.86	0.91	0.01	0.06
1.76 x 10^{-4}	1.46 x 10^{-4}	1.57 x 10^{-4}	2.82 x 10^{-6}	1.34 x 10^{-5}	0.83	0.89	0.02	0.08
1.94 x 10^{-4}	1.57 x 10^{-4}	1.70 x 10^{-4}	3.55 x 10^{-6}	1.67 x 10^{-5}	0.81	0.88	0.02	0.09
2.13 x 10^{-4}	1.68 x 10^{-4}	1.84 x 10^{-4}	4.41 x 10^{-6}	2.05 x 10^{-5}	0.79	0.86	0.02	0.10

2.32×10^{-4}	1.77×10^{-4}	1.97×10^{-4}	5.36×10^{-6}	2.46×10^{-5}	0.76	0.85	0.02	0.11
2.71×10^{-4}	1.96×10^{-4}	2.22×10^{-4}	7.54×10^{-6}	3.38×10^{-5}	0.72	0.82	0.03	0.12
3.09×10^{-4}	2.12×10^{-4}	2.45×10^{-4}	9.95×10^{-6}	4.37×10^{-5}	0.69	0.79	0.03	0.14
3.47×10^{-4}	2.26×10^{-4}	2.68×10^{-4}	1.26×10^{-5}	5.42×10^{-5}	0.65	0.77	0.04	0.16
3.84×10^{-4}	2.38×10^{-4}	2.88×10^{-4}	1.54×10^{-5}	6.50×10^{-5}	0.62	0.75	0.04	0.17
4.22×10^{-4}	2.50×10^{-4}	3.08×10^{-4}	1.85×10^{-5}	7.66×10^{-5}	0.59	0.73	0.04	0.18
4.59×10^{-4}	2.61×10^{-4}	3.27×10^{-4}	2.18×10^{-5}	8.83×10^{-5}	0.57	0.71	0.05	0.19
4.97×10^{-4}	2.71×10^{-4}	3.46×10^{-4}	2.53×10^{-5}	1.01×10^{-4}	0.54	0.70	0.05	0.20
5.34×10^{-4}	2.80×10^{-4}	3.64×10^{-4}	2.88×10^{-5}	1.13×10^{-4}	0.52	0.68	0.05	0.21
5.71×10^{-4}	2.88×10^{-4}	3.81×10^{-4}	3.25×10^{-5}	1.25×10^{-4}	0.50	0.67	0.06	0.22
6.08×10^{-4}	2.96×10^{-4}	3.97×10^{-4}	3.64×10^{-5}	1.38×10^{-4}	0.49	0.65	0.06	0.23
6.81×10^{-4}	3.10×10^{-4}	4.29×10^{-4}	4.44×10^{-5}	1.63×10^{-4}	0.45	0.63	0.07	0.24
7.54×10^{-4}	3.22×10^{-4}	4.59×10^{-4}	5.29×10^{-5}	1.89×10^{-4}	0.43	0.61	0.07	0.25
8.26×10^{-4}	3.34×10^{-4}	4.87×10^{-4}	6.18×10^{-5}	2.15×10^{-4}	0.40	0.59	0.07	0.26
8.98×10^{-4}	3.44×10^{-4}	5.14×10^{-4}	7.10×10^{-5}	2.42×10^{-4}	0.38	0.57	0.08	0.27
9.69×10^{-4}	3.53×10^{-4}	5.40×10^{-4}	8.05×10^{-5}	2.68×10^{-4}	0.36	0.56	0.08	0.28
1.04×10^{-3}	3.62×10^{-4}	5.66×10^{-4}	9.03×10^{-5}	2.94×10^{-4}	0.35	0.54	0.09	0.28

For both pyridinamide ion pair mainly dissociated anion and cation were shown at low concentrations.

At 1.0 mM salt concentration, the association of pyridinamide ion pair **3a** still showed 50% of free anion in solution which acted as reactive nucleophile. Meanwhile, pyridinamide ion pair **4a** only has 35% free anion at 1.0 mM since here the anionic sandwich association is more pronounced. This, however, was no concern in the nucleophilicity measurement since DOSY NMR tests revealed a shift in ion volumes for mixtures of **4a** with additive **6** (for details see Chapter 2.1.5).

2.1.4.6 Workflow summary

The above detailed workflow for the determination of ion pairing constant K_{IP} and sandwich association constant K_{CAC}/K_{ACA}, and the composition of mixed model for pyridinamide ion pairs based on conductivity measurements in DCM, can be summarized in the following steps:

Determination of Ion Pairing constant K_{IP} for salt **3a**

a) Measure conductivity for **3a**.
b) Determine the molar conductivity Λ_m by linear extrapolation of the first three data points.
c) Use eq. 2.6 or the respective biochemical model (for details see Scheme 2.1 or 2.2) concentrations for all compound involved in the model, copy the concentrations into Excel to convert them into conductivity values by assigning both ion 50% contribution towards Λ_m.
d) Compare sum of theoretical conductivity with experimental values (without solvent background conductivity).
e) Use the RMSE value as a quality control measure.
f) Adjust k_1 in $K_{CAC} = k_1/k_2$ until the minimum RMSE is found, to obtain K_{IP}.

Determination of cationic and anionic sandwich association constant K_{CAC} or K_{ACA} for salt **3a** (Model 3)

g) Measure conductivity for **3a**.
h) Determine the molar conductivity Λ_m by linear extrapolation of the first three data points.
i) Set the limited molar ionic conductivity for the anion λ_A and cation λ_C to the calculated values of the scaling factor δ_i based on eq. 2.8. The sum of $\delta_A+\delta_C$ cannot exceed 1.
j) Treat $\delta_{CAC} = \lambda_{CAC}/\Lambda_m$(**3a**) as a second variable. Select at starting value e.g. $\delta_{CAC} = 0.67$ and start the optimization process for K_{CAC}.
k) Use the respective sandwich association model (Model 3) to obtain concentrations for all species involved, copy them into Excel to convert them into conductivity values using eq. 2.5.

l) Compare sum of theoretical conductivity with experimental values (without solvent background conductivity).
m) Use the RMSE values as a quality control measure.
n) Adjust k_1 in $K_{CAC} = k_1/k_2$ until minimum RMSE is found, to obtain the final K_{CAC}.
o) Adjust the limited molar ionic conductivity for the sandwich ion λ_{CAC} to find the percentual distribution that fits the conductivity data the best. For each new percentual distribution, repeat step k) – n) until the global minimum RMSE is found.

For analysis of the additive **6** follow these steps:

p) Measure conductivity for **6**.
q) Follow step i) – o) as described above to obtain K_{CAC} for additive **6**.

Determination of composition of cationic and anionic sandwich association for salt **3a** (Model 4)

After determination of the cationic sandwich association constant K_{CAC} and the anionic sandwich association K_{ACA} the mix of both association types that fits the experimental data best is ascertained.

r) Assign each association constant a *scaling factor*: K_{CAC} x α and K_{ACA} x β.
s) Set α to a fixed value starting at 1.0 and going down in steps of 0.1. Optimize β to achieve the smallest RMSE value for the conductivity data using numerical simulations. Limit each factor to two relevant decimals.
t) Repeat step s) vice versa for factor β.
u) Determine the composition of cationic and anionic sandwich association in reference to the measured DOSY volume at 1.0 mM by calculating the percentual residual between experimental and simulated ion volumes.
v) Take further optimization steps until finding the α/β ratio with the smallest percentual residual for both cation and anion volume.

2.1.4.7 Data of Conductivity Measurements in MeCN

Raw data of concentration dependent conductivity profile of **3a** in MeCN at 20 °C

[**3a**]/M	Conductivity κ (µS/cm)
0.00	0.80
1.77 x 10^{-5}	2.96
3.54 x 10^{-5}	5.20
5.30 x 10^{-5}	7.44
7.06 x 10^{-5}	9.84
8.82 x 10^{-5}	11.8
1.06 x 10^{-4}	14.1
1.23 x 10^{-4}	16.3
1.41 x 10^{-4}	18.3
1.58 x 10^{-4}	20.8
1.75 x 10^{-4}	22.7
1.93 x 10^{-4}	25.0
2.10 x 10^{-4}	27.0
2.45 x 10^{-4}	31.5
2.79 x 10^{-4}	35.8
3.13 x 10^{-4}	39.7
3.47 x 10^{-4}	43.8
4.15 x 10^{-4}	52.5
4.83 x 10^{-4}	60.8
5.50 x 10^{-4}	68.5
6.16 x 10^{-4}	77.0
6.82 x 10^{-4}	85.2
7.47 x 10^{-4}	92.6
8.12 x 10^{-4}	100
8.76 x 10^{-4}	108
9.40 x 10^{-4}	115
1.00 x 10^{-3}	123
1.07 x 10^{-3}	130
1.13 x 10^{-3}	138
1.19 x 10^{-3}	145
1.25 x 10^{-3}	152
1.37 x 10^{-3}	166
1.49 x 10^{-3}	180
1.61 x 10^{-3}	193
1.73 x 10^{-3}	207
1.84 x 10^{-3}	220
1.96 x 10^{-3}	232
2.07 x 10^{-3}	245
2.18 x 10^{-3}	257

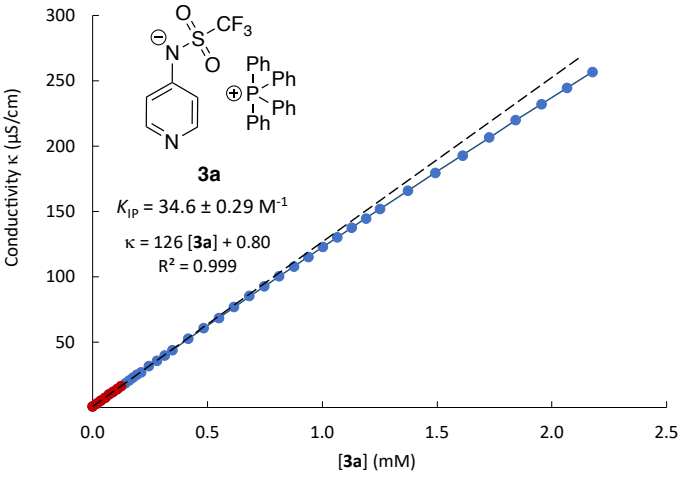

Raw data of concentration dependent conductivity data of **4a** in MeCN at 20 °C

[**4a**]/M	Conductivity κ (µS/cm)
0.00	0.80
1.85 x 10^{-5}	2.88
3.86 x 10^{-5}	5.04
5.78 x 10^{-5}	7.12
7.70 x 10^{-5}	9.28
9.62 x 10^{-5}	11.4
1.15 x 10^{-4}	13.6
1.34 x 10^{-4}	15.6
1.53 x 10^{-4}	17.5
1.72 x 10^{-4}	19.7
1.91 x 10^{-4}	21.8
2.10 x 10^{-4}	23.7
2.29 x 10^{-4}	25.8
2.67 x 10^{-4}	29.9
3.04 x 10^{-4}	33.9
3.42 x 10^{-4}	37.9
3.79 x 10^{-4}	42.2
4.53 x 10^{-4}	49.6
5.27 x 10^{-4}	57.1
5.99 x 10^{-4}	65.0
6.72 x 10^{-4}	72.6
7.44 x 10^{-4}	80.0
8.15 x 10^{-4}	87.4
8.85 x 10^{-4}	94.6
9.56 x 10^{-4}	102
1.03 x 10^{-3}	109
1.09 x 10^{-3}	116
1.23 x 10^{-3}	129
1.37 x 10^{-3}	143
1.50 x 10^{-3}	156
1.63 x 10^{-3}	168
1.76 x 10^{-3}	181
1.88 x 10^{-3}	193
2.01 x 10^{-3}	205
2.13 x 10^{-3}	217
2.25 x 10^{-3}	229
2.37 x 10^{-3}	240
2.49 x 10^{-3}	251
2.61 x 10^{-3}	262
2.72 x 10^{-3}	273
2.84 x 10^{-3}	283
2.95 x 10^{-3}	294

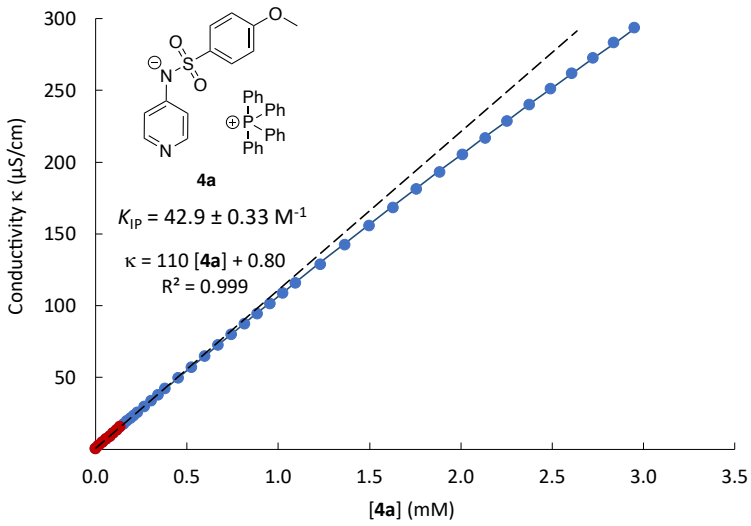

Raw data of concentration dependent conductivity profile of **6** in MeCN at 20 °C

[**6**]/M	Conductivity κ (µS/cm)
0.00	0.8
1.98×10^{-5}	3.5
3.96×10^{-5}	7.0
5.93×10^{-5}	9.8
7.90×10^{-5}	13.9
9.86×10^{-5}	17.0
1.18×10^{-4}	20.3
1.38×10^{-4}	23.6
1.57×10^{-4}	26.7
1.77×10^{-4}	29.8
1.96×10^{-4}	33.0
2.16×10^{-4}	36.0
2.35×10^{-4}	39.3
2.74×10^{-4}	45.4
3.12×10^{-4}	51.5
3.50×10^{-4}	57.8
3.89×10^{-4}	63.8
4.65×10^{-4}	76.0
5.40×10^{-4}	87.2
6.15×10^{-4}	98.8
6.89×10^{-4}	111
7.62×10^{-4}	122
8.35×10^{-4}	133
9.08×10^{-4}	144
9.80×10^{-4}	155
1.05×10^{-3}	166
1.12×10^{-3}	176
1.19×10^{-3}	184
1.26×10^{-3}	196
1.33×10^{-3}	207
1.40×10^{-3}	217
1.54×10^{-3}	237
1.67×10^{-3}	257
1.80×10^{-3}	275

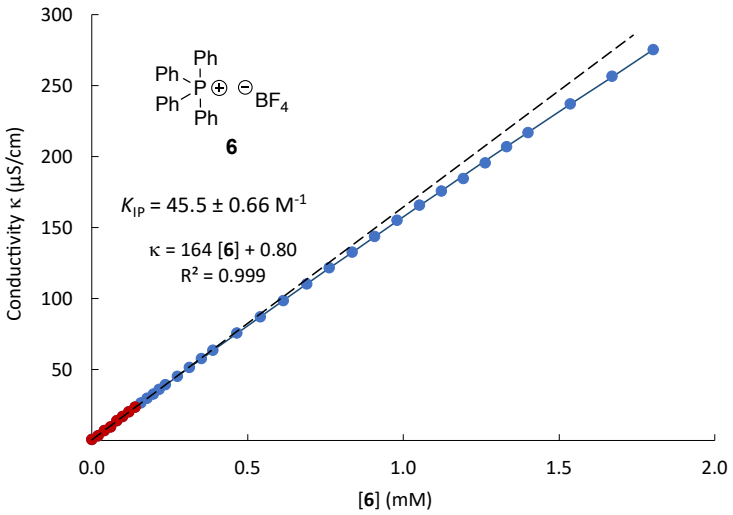

2.1.4.8 Data of Conductivity Measurements in DCM

Raw data of concentration dependent conductivity profile of **3a** in DCM at 20 °C

[**3a**]/M	Conductivity κ (µS/cm)
0.00	0.80
1.78×10^{-5}	2.24
3.55×10^{-5}	3.60
5.40×10^{-5}	5.12
7.09×10^{-5}	6.48
8.86×10^{-5}	7.44
1.06×10^{-4}	8.80
1.24×10^{-4}	9.92
1.41×10^{-4}	11.0
1.76×10^{-4}	13.2
2.11×10^{-4}	15.4
2.46×10^{-4}	17.0
2.80×10^{-4}	19.2
3.15×10^{-4}	21.1
3.49×10^{-4}	23.0
3.83×10^{-4}	24.8
4.17×10^{-4}	26.4
4.85×10^{-4}	29.6
5.52×10^{-4}	32.8
6.19×10^{-4}	36.0
6.85×10^{-4}	39.2
7.50×10^{-4}	42.4
8.15×10^{-4}	45.1
8.80×10^{-4}	48.0
9.44×10^{-4}	50.6
1.01×10^{-3}	53.1

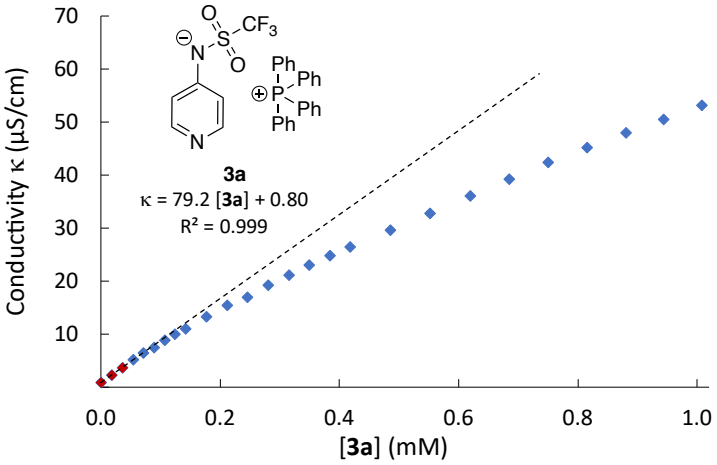

Raw data of concentration dependent conductivity profile of **3b** in DCM at 20 °C

[**3b**]/M	Conductivity κ (µS/cm)
0.00	0.80
2.00×10^{-5}	2.00
3.99×10^{-5}	3.09
5.98×10^{-5}	4.24
7.97×10^{-5}	5.28
9.95×10^{-5}	6.24
1.19×10^{-4}	6.96
1.39×10^{-4}	7.68
1.59×10^{-4}	8.40
1.98×10^{-4}	9.76
2.37×10^{-4}	10.9
2.76×10^{-4}	12.1
3.15×10^{-4}	13.3
3.54×10^{-4}	14.3
3.92×10^{-4}	15.4
4.30×10^{-4}	16.3
4.69×10^{-4}	17.4

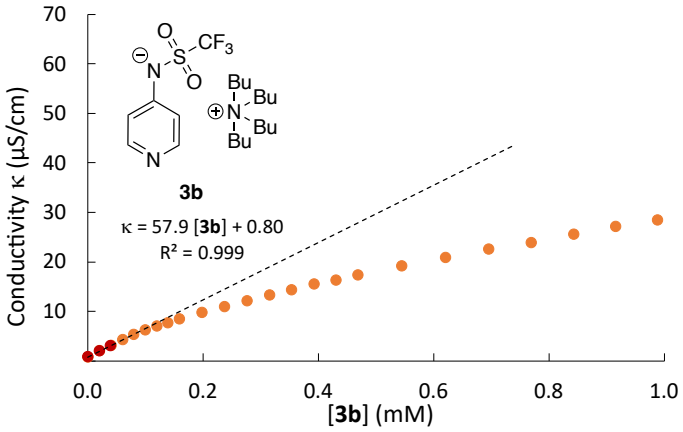

5.45 x 10^{-4}	19.1
6.20 x 10^{-4}	20.8
6.95 x 10^{-4}	22.6
7.69 x 10^{-4}	23.9
8.43 x 10^{-4}	25.5
9.16 x 10^{-4}	27.1
9.88 x 10^{-4}	28.5
1.06 x 10^{-3}	29.8

Raw data of concentration dependent conductivity profile of **4a** in DCM at 20 °C

[**4a**]/M	Conductivity **κ** (μS/cm)
0.00	0.80
1.96 x 10^{-5}	2.24
3.91 x 10^{-5}	3.68
5.86 x 10^{-5}	5.04
7.81 x 10^{-5}	6.40
9.75 x 10^{-5}	7.52
1.17 x 10^{-4}	8.96
1.36 x 10^{-4}	9.92
1.56 x 10^{-4}	11.0
1.76 x 10^{-4}	12.2
1.94 x 10^{-4}	13.1
2.13 x 10^{-4}	14.2
2.32 x 10^{-4}	15.3
2.71 x 10^{-4}	17.0
3.09 x 10^{-4}	19.0
3.47 x 10^{-4}	20.8
3.84 x 10^{-4}	22.6
4.22 x 10^{-4}	24.2
4.59 x 10^{-4}	25.9
4.97 x 10^{-4}	27.5
5.34 x 10^{-4}	29.2
5.71 x 10^{-4}	30.7
6.08 x 10^{-4}	32.5
6.81 x 10^{-4}	35.4
7.54 x 10^{-4}	38.2
8.26 x 10^{-4}	41.1
8.98 x 10^{-4}	43.7
9.69 x 10^{-4}	46.6
1.04 x 10^{-3}	49.1

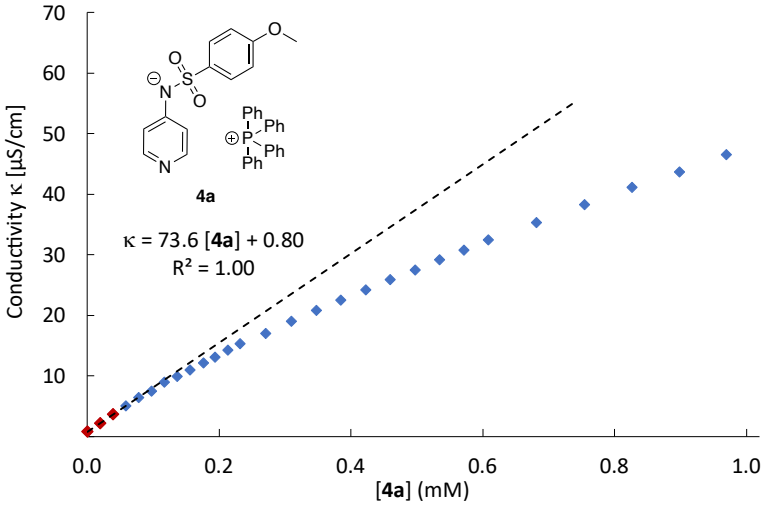

Raw data of concentration dependent conductivity profile of **6** in DCM at 20 °C

[6]/M	Conductivity κ (µS/cm)
0.00	0.80
1.93×10^{-5}	2.64
3.86×10^{-5}	4.48
5.79×10^{-5}	6.24
7.71×10^{-5}	7.84
9.63×10^{-5}	9.36
1.15×10^{-4}	10.6
1.35×10^{-4}	12.3
1.54×10^{-4}	13.8
1.92×10^{-4}	16.4
2.30×10^{-4}	19.0
2.67×10^{-4}	21.4
3.05×10^{-4}	23.9
3.42×10^{-4}	26.1
3.80×10^{-4}	28.4
4.17×10^{-4}	30.5
4.54×10^{-4}	32.6
5.27×10^{-4}	36.6
6.00×10^{-4}	40.6
6.73×10^{-4}	44.1
7.45×10^{-4}	47.9
8.16×10^{-4}	51.4
8.87×10^{-4}	55.0
9.57×10^{-4}	58.2
1.03×10^{-3}	61.7

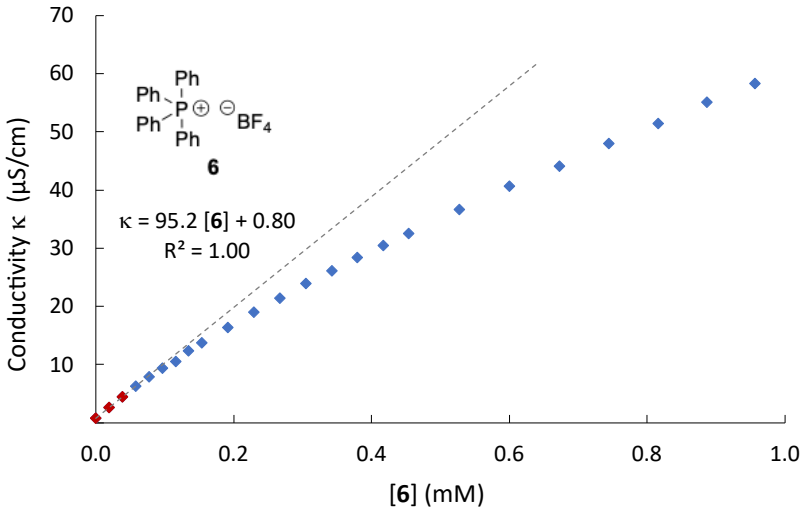

2.1.5 DOSY NMR Measurements

2.1.5.1 Cationic Sandwich Model

The DOSY volumes of compound **3a** were plotted against the salt concentration [**3a**] for both anion **3** and cation **a** (see Figure 2.8). At the lowest concentration ([**3a**] = 0.005 mM and 0.01 mM), volumes that closely matched the calculated values for the free ions (cation **a**: 362 Å^3 and anion **3**: 215 Å^3, see Table 2.16) were observed. In the 1:1 association model, as the concentration increased, the volumes of both ions were expected to rise and gradually converge, until they became identical at higher concentrations. Hereby, the anion volume would need to increase more rapidly than the cation volume to achieve this convergence, as expected for a 1:1 aggregation.

However, despite an increase in the volumes for both the anion **3** and cation **a** at concentrations higher than 0.01 mM, a significant offset between the cation **a** and the anion **3** volume was observed. The volume of cation **a** increased more than that of anion **3,** leading to a growing offset between the two volumes, contrary to the expected behavior in a 1:1 association, where the volumes of anion and cation should converge and approach 570 Å^3 for the monomeric ion pair **3a**. Additionally, in the concentration range of 0.4-1.0 mM, the cation volume plateaued at a value significantly exceeding the calculated monomeric ion pair volume of **3a** (642 Å^3 vs. 570 Å^3). These observations suggest the involvement of an additional species.

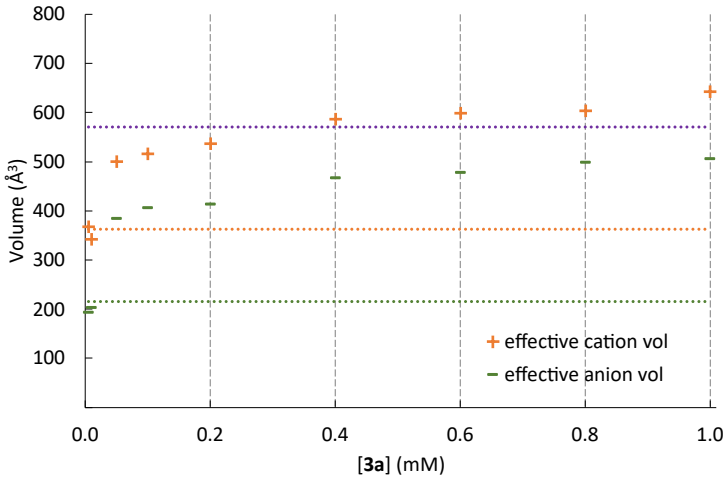

Figure 2.8: [Figure S9]. Concentration-dependent volumes of cation **a** (orange "+" symbols) and anion **3** (green "–" symbols) of salt **3a** in CD_2Cl_2 as calculated from DOSY experiments (with data from ref [2]) with the respective calculated free ion volumes (dotted line; cation **a** in orange; anion **3** in green), and the calculated volumes of the 1:1 ion pair **3a** (purple dotted line).

To account for this deviation, a "sandwich association" model was proposed, in which two cations **a** and one anion **3** form a "sandwich-cation" complex **a3a** with a calculated volume of 925 Å^3 (see Table 2.16), along with an additional free anion **3** (calculated volume of 215 Å^3). This model explains the increasing offset between the volumes of cation **a** and anion **3** during the ion association, as the free anion reduces the average DOSY anion volume. The higher cation volumes (642 Å^3) observed at increasing concentrations can be attributed to the formation of sandwich-cations that are included in the average DOSY cation volume.

The theoretical volumes for the free ions, the 1:1 monomeric ion pair **3a**, and the sandwich model were calculated based on the van der Waals cavity used in the SMD solvation model at the B3LYP-D3/6-31+G(d) level of theory (see Table 2.16).

Table 2.16: [Table S19]. Calculated volumes of all proposed species based on the van der Waals cavity used in the SMD solvation model at the B3LYP-D3/6-31+G(d) level of theory.

Species	Volume (Å³)
Anion **3**	215
Anion **4**	285
Cation **a**	362
1:1 ion pair **3a**	570
Cation sandwich **a3a**	925
Anion sandwich **3a3**	782
1:1 ion pair **4a**	641
Cation sandwich **a4a**	995
Anion sandwich **4a4**	920

The volumes of the free anion **3** and free cation **a** at a given overall salt concentration were calculated according to eq. 2.11 with the aid of numerical simulation based on the conductivity data (see 1.1.4).

$$\mathrm{vol_{cat}} = \frac{[\mathrm{C}]}{[\mathrm{IP}]_{\mathrm{tot}}} \times 362 + \left(\frac{2 \times [\mathrm{CAC}]}{[\mathrm{IP}]_{\mathrm{tot}}}\right) \times 925 \qquad (2.11a)$$

$$\mathrm{vol_{an}} = \frac{[\mathrm{A}]}{[\mathrm{IP}]_{\mathrm{tot}}} \times 215 + \left(\frac{[\mathrm{CAC}]}{[\mathrm{IP}]_{\mathrm{tot}}}\right) \times 925 \qquad (2.11b)$$

Based on the calculated populations of the respective free ion, the theoretical DOSY volumes were simulated (see Figure 2.9).

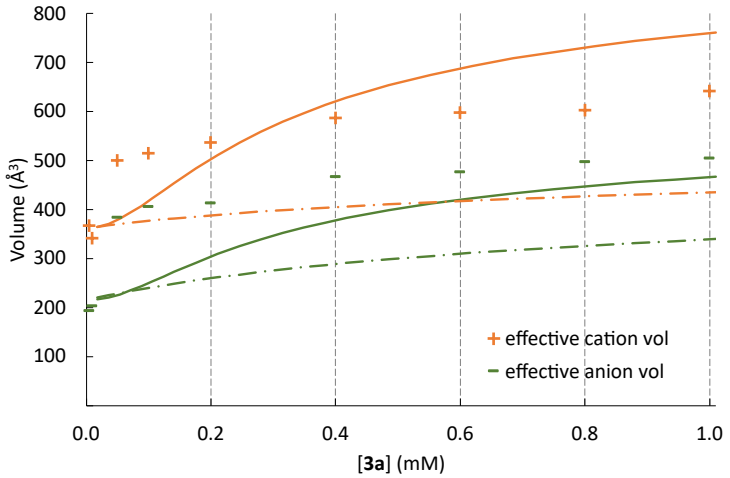

Figure 2.9: [Figure S10]. Concentration-dependent volumes of cation **a** (orange "+" symbols) and anion **3** (green "–" symbols) of salt **3a** in CD_2Cl_2 as calculated from DOSY experiments (with data from ref [2]) with the simulated trends for the cationic sandwich association model (orange line for cation **a**, green line for anion **3**), and the 1:1 ion association model (orange dotted-dashed line for cation **a**, green dotted-dashed line for anion **3**).

For both ions, the calculated trend for the 1:1 ion aggregation model led to far lower volumes than observed by the DOSY measurements, with discrepancies of up to 250 Å³ (see Figure 2.9). By involving the sandwich cation, the calculated curves fit far better to the observed trends in volume (see Figure 2.10). Therefore, the volumes cannot be explained by a single 1:1 aggregation, but other species such as the sandwich cation **a3a** have to be considered.

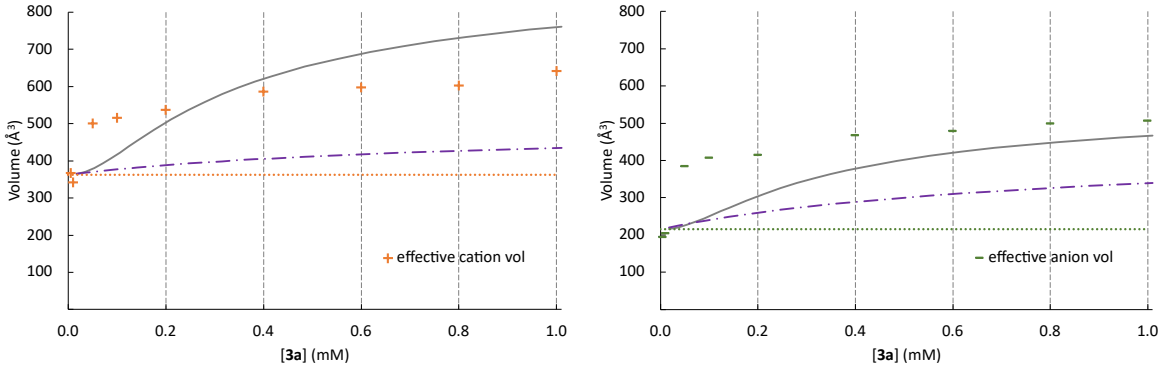

Figure 2.10: [Figure S11 + S12]. Concentration-dependent volumes of cations **a** (orange "+" symbols) and anions **3** (green "–" symbols) of salt **3a** in CD_2Cl_2 as calculated from DOSY experiments (with data from ref [2]) with the respective free ion volumes (dotted line; cation in orange; anion in green), the simulated trend for the 1:1 ion association model (purple dotted-dashed line), and cationic sandwich model (grey line).

2.1.5.2 Anionic Sandwich Model

When plotting the DOSY volumes for salt **4a** against the salt concentration [**4a**], a different trend is observed, indicating the presence of an additional species. Unlike **3a**, the volume of anion **4** showed a significantly greater increase than the volume of cation **a** with increasing concentration, and eventually surpassed the cation volume. At 0.005 mM, the determined volumes for anion **4** (296 Å^3) and cation **a** (403 Å^3) are close to the calculated volumes of the free ions (anion: 285 Å^{3}and cation: 360 Å^3, see Table 2.16). As the concentration increases, both volumes rose, but the anion volume increased more rapidly than the cation volume. This led to a crossover at 0.05 mM, where their volumes were nearly identical, before the volume of anion **4** (765 Å^3) exceeded that of cation **a** (682 Å^3). Both the anion and cation volumes exceeded the calculated volume of the monomeric ion pair **4a** (641 Å^3), suggesting that the formation of a 1:1 ion pair or a sandwich-cation was unlikely. Instead, these trends point towards the formation of another type of aggregate.

Considering the formation of the sandwich-cation for **3a**, a similar aggregate in form of a sandwich-anion was proposed for **4a** involving two anions **4** and one cation **a** in the sandwich-anion complex **4a4**, leaving a free cation **a**. This anionic sandwich association model explains the observed increase in anion volume and the crossing point, as well as the cation volumes that were higher than the calculated volumes of the monomeric ion pair **4a**, since the DOSY volumes display the average volumes of all cationic species in solution.

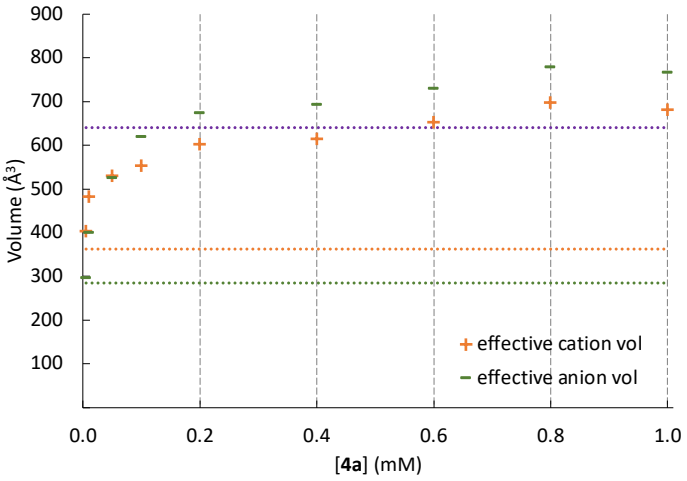

Figure 2.11: [Figure S15]. Concentration-dependent volumes of cation **a** (orange "+" symbols) and anion **4** (green "–" symbols) of salt **4a** in CD_2Cl_2 as calculated from DOSY experiments (with data from ref [2]) with the respective calculated free ion volumes (dotted line; cation **a** in orange; anion **4** in green), and the calculated volumes of the 1:1 ion pair **4a** (purple dotted line).

Additional experiments with a fixed cation concentration at 1.0 mM were performed. Three different ion pair **4a** concentrations (0.2 mM, 0.5 mM, 0.8 mM) were measured, using additive **6** to maintain the overall ionic strength *I* at *I* = 1.0 mM (for data see SI of ref [2]). The anionic sandwich association model dictates that the anion volume should decrease with increasing proportion of additive **6** since the formation of the sandwich-anion is less likely to occur with increasing cation concentration. And indeed, the anion volume decreased significantly (from 780 Å^3 to 576 Å^3) as the additive portion increased. Meanwhile, the cation volume remained relatively stable (680 Å^3 to 698 Å^3), leading to another crossing point where the cation volume exceeded that of the anion (see Figure 2.12). These findings further support the anionic sandwich association model for ion pair **4a**.

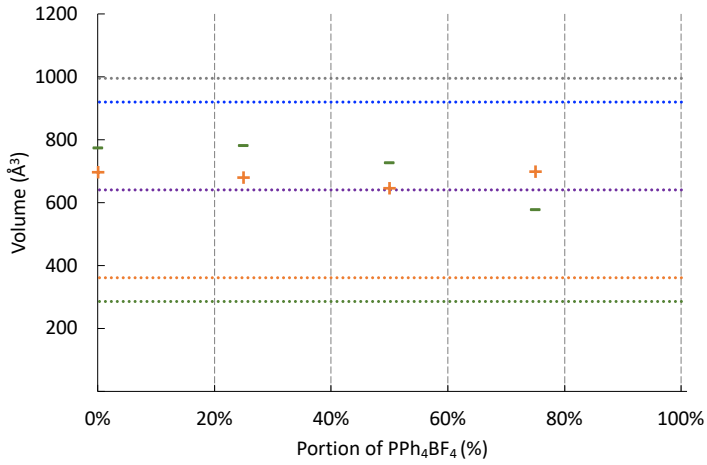

Figure 2.12: [Figure S16]. Concentration-dependent volumes of cation **a** (orange "+" symbols) and anion **4** (green "–" symbols) of **4a**/additive **6** mixtures with increasing amounts of **6** at *I* = 1.0 mM in CD_2Cl_2 as calculated from DOSY experiments (with data from ref [2]) with the respective calculated free ion volumes (dotted line; cation **a** in orange; anion **4** in green), and the calculated volumes of the 1:1 ion pair **4a** (purple dotted line), the sandwich cation **a4a** (grey dotted line), and the sandwich anion **4a4**(blue dotted line).

Furthermore, numerical simulations comparing the cationic sandwich association, the anionic sandwich association, the 1:1 ion association, and the mixed sandwich association were conducted and compared to the DOSY data (see Figures 1.11 and Figure 1.12). For ion pair **4a**, the anionic sandwich association model and the mixed association model provided the best fit to the experimental data, whereas the cationic sandwich association model and the 1:1 ion association model showed significantly larger deviations. This further supports the presence of the sandwich anion **4a4** in solution. To conclude, the

mixed sandwich association model, where both types of sandwich complexes coexist, with the anionic sandwich association being the predominate association pattern, provided the best fit between simulation and experimental data.

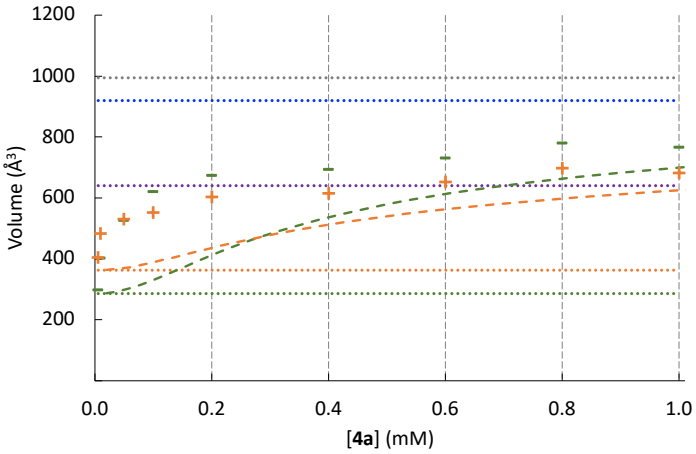

Figure 2.13: [Figure S17]. Concentration-dependent volumes of cation **a** (orange "+" symbols) and anion **4** (green "–" symbols) of salt **4a** in CD_2Cl_2 as calculated from DOSY experiments (with data from ref [2]) with the respective calculated free ion volumes (dotted line; cation **a** in orange; anion **4** in green), and the calculated volumes of the 1:1 ion pair **4a** (purple dotted line), the sandwich cation **a4a** (grey dotted line), the sandwich anion **4a4**(blue dotted line), and the simulated trend for the mixed sandwich association model (short-dashed line).

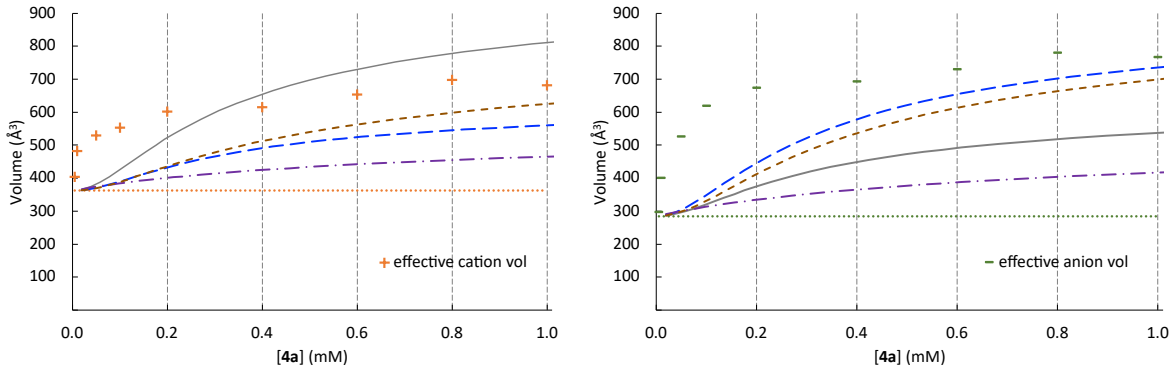

Figure 2.14: [Figure S18 + S19]. Concentration-dependent volumes of cation **a** (orange "+" symbols) and anion **4** (green "–" symbols) of salt **4a** in CD_2Cl_2 as calculated from DOSY experiments (with data from ref [2]) with the respective free ion volumes (dotted line; cation in orange; anion in green), the simulated trends for the 1:1 ion association model (purple dotted-dashed line), the cationic (grey line) and anionic (blue dashed line) sandwich association model, and the mixed sandwich association model (brown short-dashed line).

2.1.6 Characterization of Additive PPh_4BF_4 (**6**)

The "wide range" measurement for **3a** were performed with the total ion concentration in solution being kept constant by the addition of an additive, that remained structurally as close as possible to catalyst **3a**. Therefore, tetraphenylphosphonium tetrafluoroborate (PPh_4BF_4, **6**) was synthesized by salt metathesis from tetraphenylphosphonium bromide with sodium tetrafluoroborate in water. After extraction with DCM, the final product was obtained by precipitation from DCM with toluene with 88% yield.

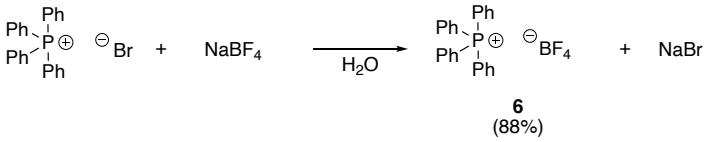

6
(88%)

Scheme 2.7: [Scheme S7]. Synthesis of tetraphenylphosphonium tetrafluoroborate PPh_4BF_4 (**6**).

Additive **6** was examined with conductivity measurements in MeCN and DCM. The results are shown in Figure 2.15. In both solvents, additive **6** showed a slightly higher conductivity than ion pair catalyst **3a**.

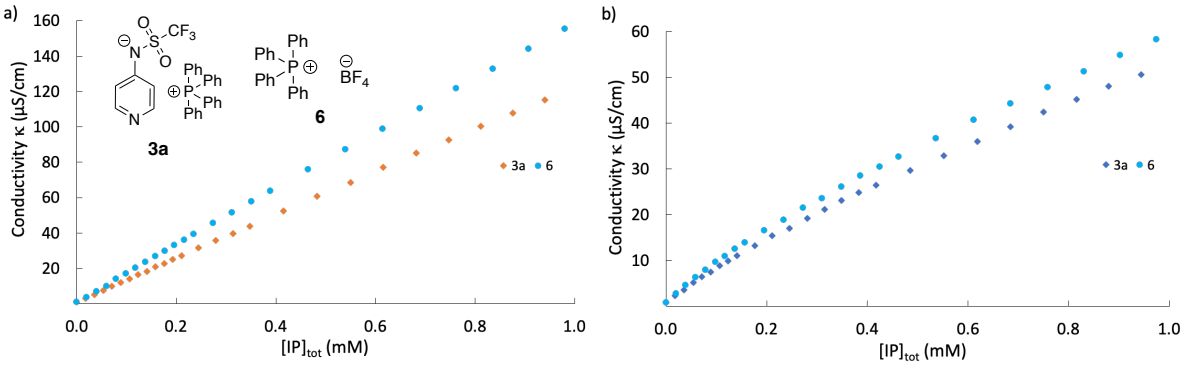

Figure 2.15: [Figure S21]. a) Concentration-dependent conductivity profile for additive **6** and catalyst **3a** in MeCN at 20 °C, b) Concentration-dependent conductivity profile for additive **6** and catalyst **3a** in DCM at 20 °C.

The conductivity profile of **6** was used to determine the respective association constants *K* (Table 2.17) which were obtained by employing eq. 2.6, the double ion pairing model as well as the sandwich association model 3a (see Chapter 2.1.4.4). For the determination of the sandwich association constant K_{CAC}, it was crucial to assess the contribution of the single ion towards the molar conductivity Λ_m, gained by linear extrapolation of the initial three data points.

Table 2.17: [Table S21]. Association constants K_{IP} in different solvents according to eq. 2.6, double K_{IP}, and K_{CAC} according to model 3a of pyridinamide ion pairs **3a**, **4a** and additive **6** and at 20 °C.

	K_{IP} (M^{-1})		K_{IP} (M^{-2})	K_{CAC} (M^{-2})
Ion Pair	**MeCN**	**DCM**	**DCM**	**DCM**
	[45.6][a]	[40.7][a]	[40.7][a]	[40.7][a]
3a	34.6	828	6.86×10^5	6.38×10^6
4a	42.9	938	8.79×10^5	6.50×10^6
6	45.6	1004	1.01×10^6	7.05×10^6

[a] $E_T(30)$ [kcal mol^{-1}] solvent polarity parameters taken from Reichardt[5].

Next, additive **6** was employed in the wide range measurement of **3a** in DCM. Except for the addition of **6** as a second stock solution, the method was remained unchanged. In a first step, the overall ionic concentration *I* was set to be 1.0 mM for all eleven data point of this measurement (Figure S9, turquoise diamonds). Now, instead of the previously measured non-linear correlation between $[IP]_{tot}$ and k_{obs}, a linear correlation was observed.

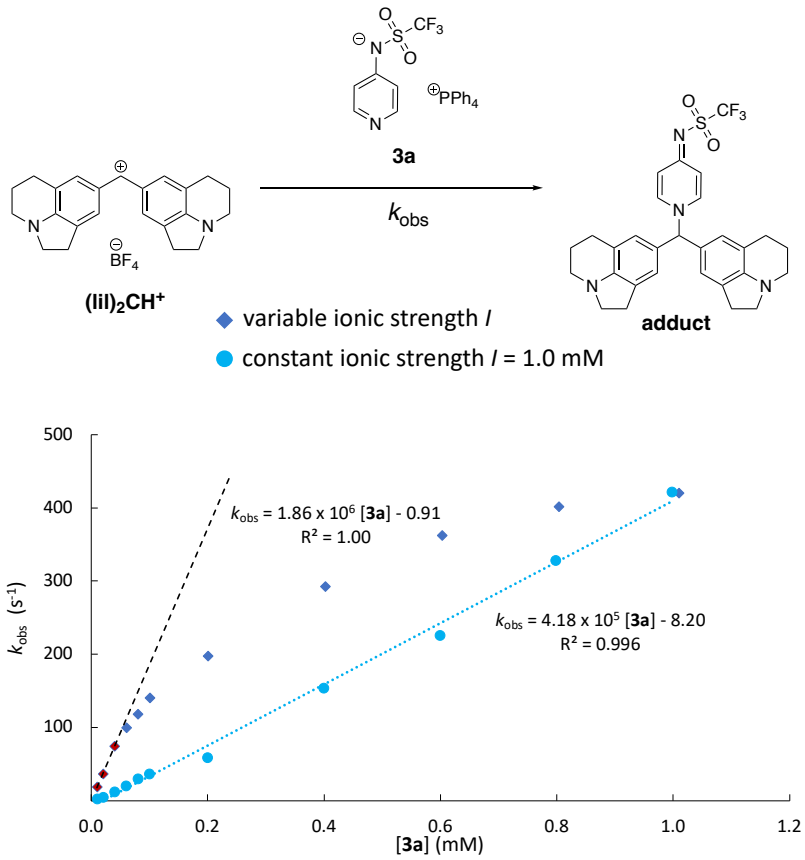

Figure 2.16: [Figure S22]. Plot of k_{obs} vs. concentration of catalysts [**3a**] over a concentration range from 0.01–1.0 mM in DCM at 20°C (blue diamonds), and with the additive PPh_4BF_4 (**6**) with a total ionic strength I = 1.0 mM (turquoise points).

There are two ways to interpret this data: A) The association equilibrium of **3a** was pushed to the product side by the addition of additive **6** while the solvent polarity remains unchanged. B) The solvent polarity was changed by the addition of additive **6**, indicating that the second-order reaction rate k_2 and the association constant K_{IP} are depending on the concentration of salt **6**. Which one of the assumptions holds true, was checked with DOSY measurements as well as $E_T(30)$ value measurements of DCM at different salt concentrations.

First, the solvent polarity was determined by using the Reichardt's dye betaine $E_T(30)$. The $E_T(30)$ dye was dissolved in dry DCM and mixed with stock solutions of the respective salt. The UV/Vis spectrum was measured. The $E_T(30)$ values of the mixture were calculated according to eq. 2.12 in which h is the Planck's constant, c is the speed of light, and N_A is the Avogadro's constant.

$$E_T = \frac{hcN_A}{\lambda_{max}} = \frac{28951}{\lambda_{max}} \qquad (2.12)$$

A gradual increase in the $E_T(30)$ values was observed for DCM with increasing concentrations of **3a** and **6**, respectively. The results are listed in Table 2.18.

Table 2.18: [Table S22]. Structure of Betaine $E_T(30)$ with a list of measured λ_{max} of Betaine respective with ion pair **3a** and additive **6** in DCM.

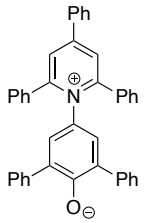

Betaine $E_T(30)$

Salt (mM)	λ_{max} (nm) with 3a	$E_T(30)$ (kcal mol^{-1})	λ_{max} (nm) with 6	$E_T(30)$ (kcal mol^{-1})
0.1	698	41.0	698	41.0
0.5	698	41.0	698	41.0
1.0	697	41.0	700	40.9
2.0	696	41.1	700	40.9
3.0	698	41.1	699	40.9
4.0	694	41.2	694	41.2
5.0	694	41.2	–	–
6.0	696	41.1	–	–

As a second measure, DOSY measurements were utilized to determine the association state at an overall salt concentration of 1.0 mM with an increasing portion of ion pair **3a** in solution (Table 2.19).

Table 2.19: [Table S13]. Viscosity corrected hydrodynamic radii r_H and resulting volumes of ion pair **3a** while fixing the overall ion concentrations at 1.0 mM. PPh_4BF_4 was chosen as additive (Add) to keep the ion concentration at 1.0 mM. The ratio of 3a/Add is given in percentage. TMS was used as viscosity reference for the experimental self-diffusion coefficients D_i to allow for a comparison of hydrodynamic radii r_H and resulting volumes V_A. SW = 22 Hz, O1P = 10.0 ppm, gradient strength 5-95% linear. Samples were measured at room temperature.

	[3a] (mM)	Radius (Å)	Volume (Å^3)
Cation	1.0	5.51	642[a]
Anion	1.0	5.15	505[a]
Cation	0.2	5.32	631
	0.5	5.44	673
	0.8	5.39	656
Anion	0.2	4.98	519
	0.5	5.03	528
	0.8	5.03	535

[a] averaged value based on data from ref [2]**.**

To summarize, the measured volumes of the anion at an overall salt concentration of 1.0 mM were located in the same region as the anion volume of pure **3a** at 1.0 mM. By keeping a constant salt concentration throughout the measurement through the addition of additive **6**, the association of the respective pyridinamide ion pair can be “frozen” at a certain association state.

2.1.7 Nucleophilicity Data

The rates of the reactions of ion pair catalysts **3a** and **4a** as well as of **TCAP** with the reference electrophiles were measured photometrically on a stopped-flow spectrophotometer. The temperature was controlled with a circulating bath cryostat. The reactions were carried out under pseudo-first-order conditions (ion pair = nucleophile, excess compound) and monitored at the absorption maximum of benzhydrylium ion in the respective solvent as described previously by the H. Mayr group.[17] First-order rate constants k_{obs} (s^{-1}) were derived by fitting the absorbance decay according to the mono-exponential function $A_t = A_0 \exp(-k_{obs}\, t) + C$ (see Figure 2.17).

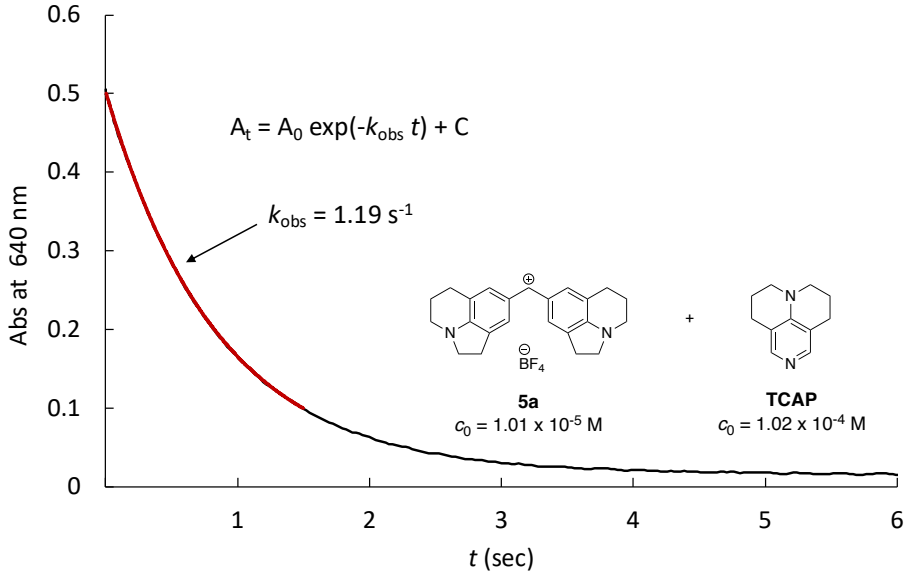

Figure 2.17: [Figure S23]. Absorbance decay of benzhydrylium salt **5a** reacting with the nucleophile TCAP (**2**) in DCM at 20°C, fitted by a mono-exponential decay function resulting in k_{obs} = 1.19 s^{-1}.

Second-order rate constants k_2 (L mol^{-1} s^{-1}) were obtained from the slope of the linear plots of k_{obs} (s^{-1}) vs [Nu] since $k_{obs} = k_2$[Nu]. The subsequent characterization is based on the Mayr-Patz eq. (2.13) where the second-order rate constants (log $k_2^{20\,°C}$) for the reaction of the nucleophile with the electrophile is expressed as a function of the nucleophilicity parameter *N*, the nucleophile-associated sensitivity parameter s_N, and the electrophilicity parameter *E*. Both, *N* and s_N parameter are solvent dependent.[17–19]

$$\log k_2^{20\,°C} = s_N(N + E) \qquad (2.13)$$

2.1.7.1 Mayr's benzhydrylium method – Results in MeCN and DCM at *c* = 0.01-0.03 mM

Mayr's benzhydrylium method is applicable for dissociated ion pairs, therefore, the data gathered in MeCN can be easily analyzed according to the standard procedure. Measurements done in DCM require more consideration for the analysis since ion association affects the measurements. Salt **3a** will be used as reference system to discuss any new model and data analysis procedures. To circumvent the effects of association, initial measurements in DCM were done between 0.01 – 0.03 mM where salt **3a** is assumed to be fully dissociated into the free anion **3** and cation **a**, with anion **3** being the only nucleophilic species in solution. The total amount of the fully dissociated **3a** in solution is annotated as $[\mathbf{3}]_{tot}$, meaning that the weighed amount of **3a** = amount of free anion **3** in solution. Kinetic data obtained using Mayr's benzhydrylium method are summarized in Table 2.20.

Table 2.20: [Table S24]. Second-order rate constants for the reactions of **3a** with $(lil)_2CHBF_4$ (**5a**), $(jul)_2CHBF_4$ (**5b**), and $(ind)_2CHBF_4$ (**5c**) determined in the concentration range $[\mathbf{3}]_{tot}$ = 0.01 – 0.03 mM in DCM (blue diamonds) and MeCN (orange dots) at 20 °C and the corresponding *N*- and s_N-parameters.

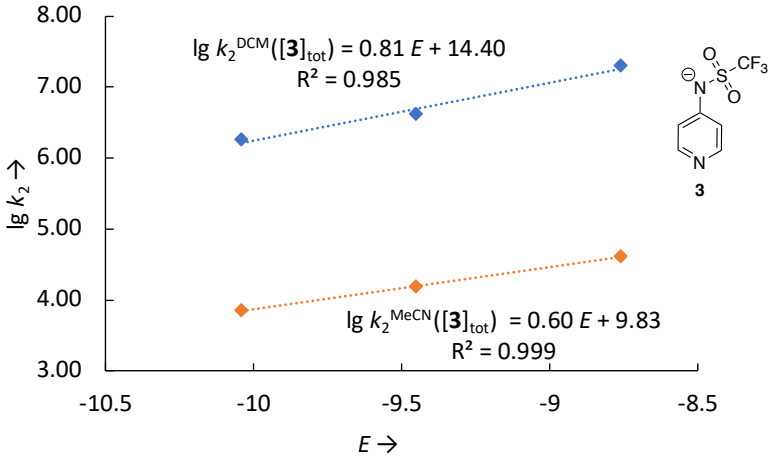

Solvent	Nucleophile	k_2 (M^{-1} s^{-1})			N/s_N
		5a	5b	5c	
MeCN	$[\mathbf{3}]_{tot}$	7.16 x 10^3	1.53 x 10^4	4.13 x 10^4	16.38/0.60
DCM	$[\mathbf{3}]_{tot}$	1.82 x 10^6	4.23 x 10^6	1.98 x 10^7	17.75/0.81

In MeCN, the correlation between k_{obs} for **3** + **5** reactions and the total concentration of **3a** in solution are linear (see Table 2.20). This is due to the sufficient polarity of MeCN to dissociate salts into the corresponding free anions and cations. However, this stabilizing influence also results in a considerably lower nucleophilicity of **3** when compared to its measurement in DCM. In DCM, the nucleophilic anion **3** experiences less solvation, rendering it more readily available to react with electrophiles **5**. Consequently, the second-order rate constant k_2 for **3** + **5** reactions are approx. three orders of magnitude higher in DCM than in MeCN.

This analysis was made under the assumption that **3a** is mainly, if not fully, dissociated in DCM at concentrations below 0.03 mM. A way to check this assumption is using numerical simulations according to the cationic sandwich association model (see Chapter 2.1.4.4) to determine how much free anion **3** was present in solution. We know the total salt concentration of **3a** at each data point, so this concentration was given as the initial concentration of the anion and cation concentration in COPASI. In the section "reaction", the rate constant k_1 was set to the value of the cationic sandwich association constant K_{CAC}, while the rate constant k_2 was fixed to 1. Then, the function "Steady State" was used to get the concentration for each species at the given concentration. This process was repeated for each salt concentration of **3a**. Now the first-order rate constant k_{obs} were plotted against the anion concentration [**3**] to get the second-order rate constant k_2 for the nucleophilic anion **3** in solution. This led to the results listed in Table 2.21.

Table 2.21: [Table S25]. Second-order rate constants for the reactions of **3a** in the full dissociation model (where [**3**] = [**3a**]$_{tot}$, blue diamonds) and the sandwich association model (purple dots) with benzhydrylium electrophile salts (lil)$_2$CHBF$_4$ (**5a**), (jul)$_2$CHBF$_4$ (**5b**), and (ind)$_2$CHBF$_4$ (**5c**) between 0.01 – 0.03 mM in DCM at 20 °C and the corresponding *N*- and s_N-parameters.

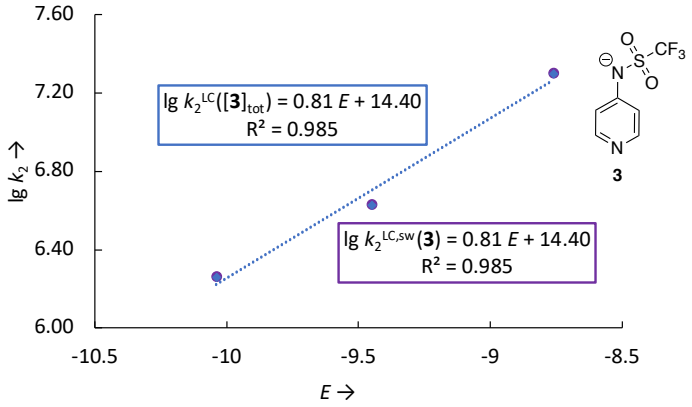

Conditions	Superscript	Nucleophile	k_2 (M^{-1} s^{-1})			N/s_N
			5a	5b	5c	
I = 0.01-0.03 mM	LC	[**3**]$_{tot}$	1.84 x 10^6[a]	4.23 x 10^6	1.98 x 10^7	17.78/0.81
Sandwich model	LC,sw	[**3**]	1.84 x 10^6	4.28 x 10^6	2.00 x 10^7	17.78/0.81

[a] the reaction of **3a** with **5a** was measured twice, resulting in k_2^{LC} = 1.82 x 10^6 M^{-1} s^{-1} (*I* = 0.01-0.03 mM) and k_2^{LC} = 1.86 x 10^6 M^{-1} s^{-1} (*I* = 0.01-0.04 mM, initial three data points of wide range measurement) giving an average k_2^{LC} = 1.84 x 10^6 M^{-1} s^{-1}.

At low salt concentrations, where [**3a**] = 0.01 – 0.03 mM in DCM (superscript LC), the second-order rate constant k_2^{LC} were obtained by assuming that the total salt concentration [**3**]$_{tot}$ = the free anion concentration [**3**]. Additionally, second-order rate constant $k_2^{LC,sw}$ were determined by using the free anion concentration [**3**] obtained with numerical simulations. The resulting rate constant k_2^{LC} and $k_2^{LC,sw}$ revealed only minor differences and identical *N* and s_N parameters. We conclude that at low concentrations salt **3a** is mainly dissociated, and the assumption of [**3**] = [**3a**]$_{tot}$ is valid.

By applying the cationic sandwich model (model 3a) to the kinetic data of the wide range measurement performed in DCM over a wider concentration range (0.01 – 1.0 mM), the concentration of free anion **3** was determined and plotted against the pseudo-first order rate constant k_{obs}. The resulting correlation between k_{obs} and anion **3** concentration was expected to be linear and following the black dashed trendline (see Figure 2.18).

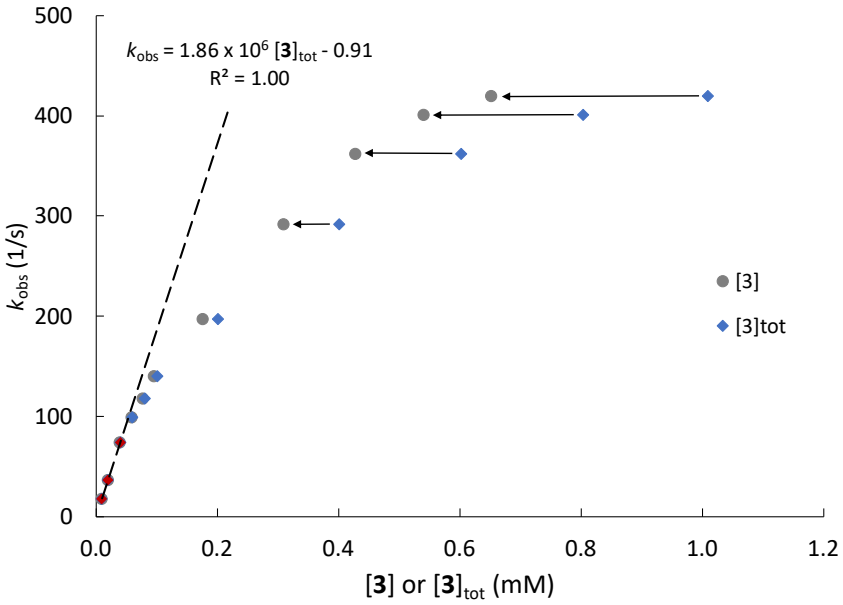

Figure 2.18: [Figure S24]. Plot of k_{obs} vs. concentration of catalysts **3a** over a concentration range from 0.01–1.0 mM in DCM at 20°C (blue diamonds), and vs. concentration of anion **3** over a concentration range from 0.01–1.0 mM in DCM at 20°C (grey dots).

Instead, the result was a steeper, but still non-linear correlation indicating that the association of **3a** is not the only process that influences the kinetic measurements. Assuming that the change in overall ionic strength when going from 0.01 mM to 1.0 mM salt concentrations might be responsible for this non-linear behavior, rate measurements were repeated in the presence of $PPh_4^+BF_4^-$ (**6**). The additive was added to maintain a constant ionic strength of 1.0 mM over all pyridinamide salt concentrations. The choice of salt **6** combined cation **a** of **3a** with the tetrafluoro borate anion (BF_4^-), which is the counter-anion of the benzhydrylium electrophile salts. Addition of **6** increased the concentration of phosphonium cation **a** and, thus the concentration of sandwich cation **a3a**, resulting in a linear correlation of the first-order rate constant k_{obs} and the nucleophile concentration (see Figure 2.19, turquoise points).

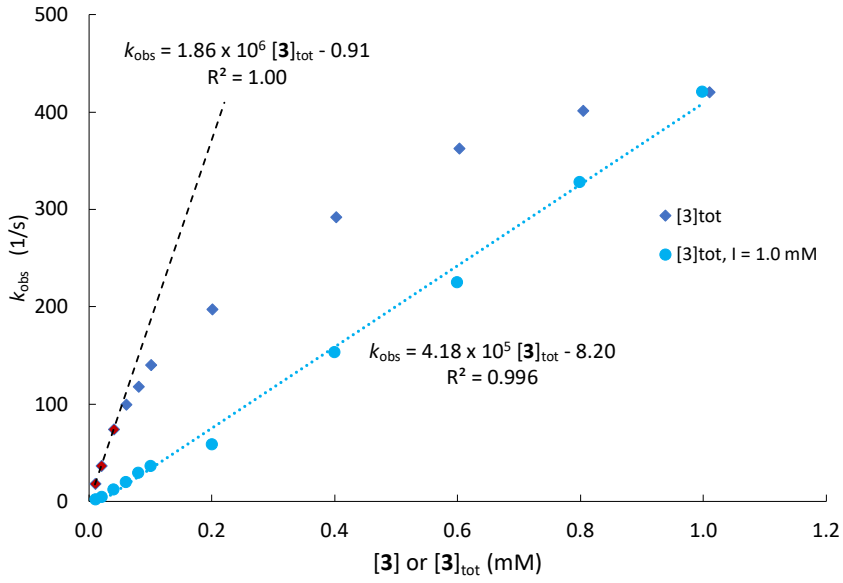

Figure 2.19: [Figure S25]. Plot of k_{obs} vs. concentration of catalysts **3a** over a concentration range from 0.01–1.0 mM in DCM at 20°C (blue diamonds), and with additive PPh_4BF_4 (**6**) with a $[IP]_{tot}$ = 1.0 mM (turquoise points).

2.1.7.2 Cationic Sandwich Association Extension

The measurements performed with the addition of additive **6** can be analyzed in multiple ways. The first way would be to assume that the amount of weighted salt **3a** equals the amount of nucleophile in solution. Here, we would simply use the standard Mayr's benzhydrylium method to obtain the second-order rate constant k_2 and subsequently gain the N parameter and s_N parameter (see Table 2.22).

From the combination of conductivity and DOSY measurements, we know that the salt **3a** associates into triple ionic adducts, so-called sandwich cations. Therefore, the weighted amount of salt **3a** is most likely not equivalent to the concentration of the reactive nucleophile in solution. We assume here, that the sandwich complex does not react as a nucleophile, but rather only the free anion **3**.

Again, we use the earlier established association model 3a for the cationic sandwich association with $K_{CAC} = k_1/k_2 = 6.38 \times 10^6\ M^{-2}$. Except now, we have to add one more reaction to the biochemical model for the sandwich association of **3a** in COPASI to incorporate the influence of additive **6** in the numerical simulations. The additive can either associate according to the 1:1 model or according to the sandwich model (see eq. 2.14)

$$2 * C + 2 * B \overset{K_{IP}(add)}{\rightleftharpoons} 2 * CB \qquad (2.14a)$$

$$2 * C + 2 * B \overset{K_{CAC}(add)}{\rightleftharpoons} B + CBC \qquad (2.14b)$$

Depending on the chosen association type, either eq. 2.14a or eq. 2.14b was added to the biochemical model as "additive association" with **C** = PPh_4^+, **B** = BF_4^-, and **CD** = PPh_4BF_4 (**6**) or the sandwich adduct **CBC** = $PPh_4BF_4PPh_4$.

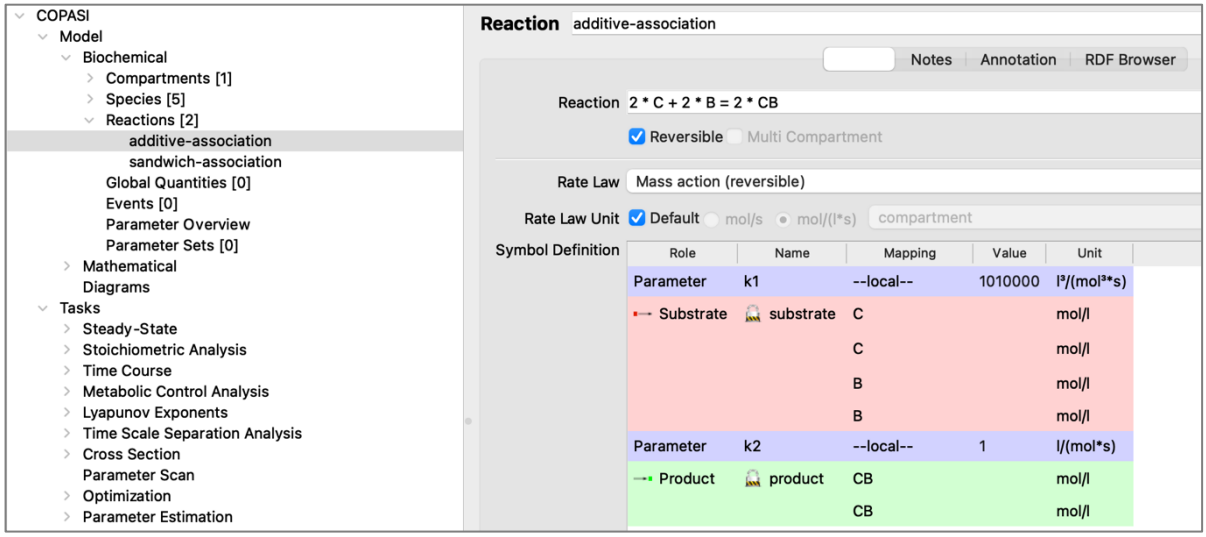

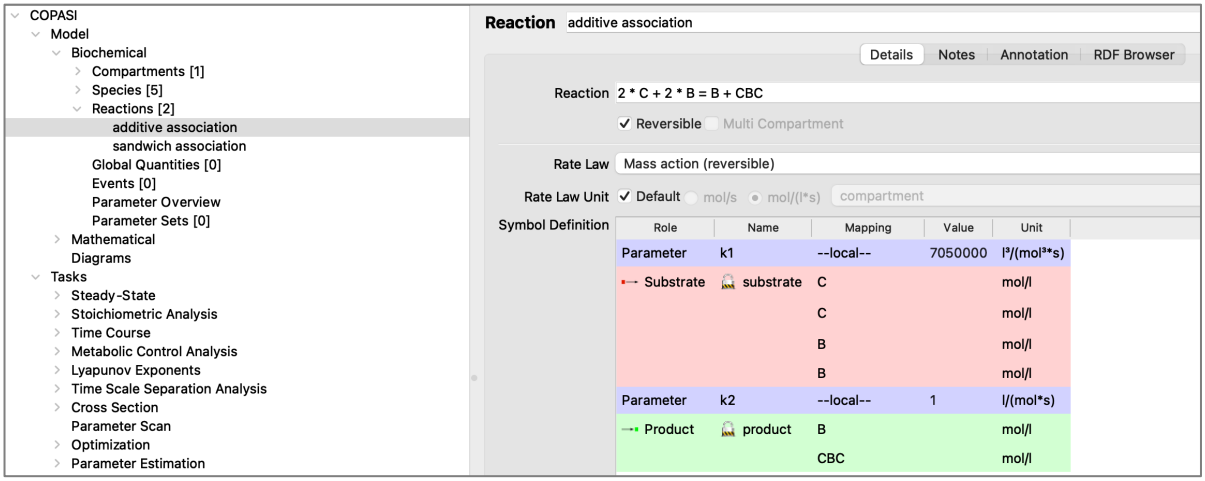

The additive association constant was determined using the same procedure as for the sandwich association constant K_{CAC} of compound **3a** and was defined as either K_{IP}(**6**) = k_1/k_2 = 1.01 x 10^6 M^{-2} or K_{CAC}(**6**) = k_1/k_2 = 7.05 x 10^6 M^{-2}.

Next, in the section "Species" the individual concentration for all compounds were added. As a starting point for this model, we assume that both salts are completely dissociated. Therefore, [**A**] = concentration of salt **3a**, [**C**] = concentration of salt **3a** + concentration of additive **6**, and [**B**] = concentration of additive **6** + concentration of the respective benzhydrylium salt **6**.

The function "Steady State" was used to obtain the concentrations for each species for the given association constants. This process was repeated for each salt concentration of **3a**. Subsequently, the concentration of the single anion **3** can be plotted against k_{obs} to get the second-order rate constant k_2 for the reactive nucleophilic anion **3** in solution. All three resulting sets of reaction rates k_{obs} are depicted in Figure 2.20.

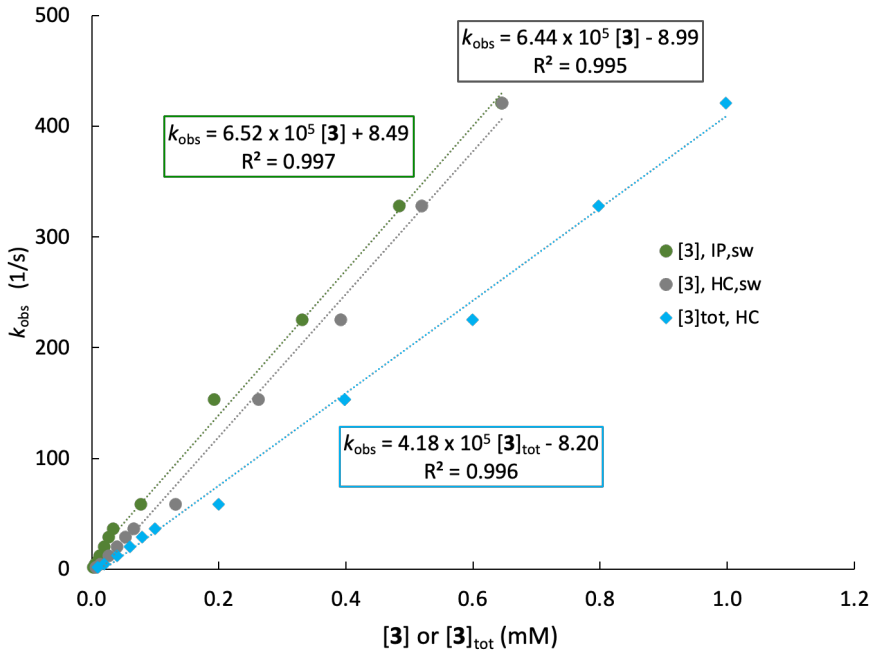

Figure 2.20: [Figure S26]. Plot of k_{obs} vs. concentration of catalysts **3a** with additive **6** (turquoise diamonds), concentration of anion [**3**] obtained with model "HC,IP" (green dots) and concentration of anion [**3**] obtained with model "HC,sw" (grey dots) over a concentration range from 0.01–1.0 mM in DCM at 20°C with constant ionic strength *I* = 1.0 mM.

To distinguish the second-order rate constants k_2 obtained with all model variations, the following superscripts were introduced: "LC" = [**3**]$_{tot}$ with *I* = variable (blue); "LC,sw" = [**3**] with *I* = variable (purple);

"HC" = $[\mathbf{3}]_{tot}$ with I = 1.0 mM (turquoise); "HC,IP" = [**3**] with I = 1.0 mM (green); "HC,sw" = [**3**] with I = 1.0 mM (grey, see Table 2.22).

Table 2.22: [Table S26]. Second-order rate constants obtained with all five possible analysis methods for salt **3a** with benzhydrylium electrophiles salts $(lil)_2CHBF_4$ (**5a**), $(jul)_2CHBF_4$ (**5b**), and $(ind)_2CHBF_4$ (**5c**) between 0.01 – 0.03 mM in DCM at 20 °C and the corresponding N- and s_N-parameters.

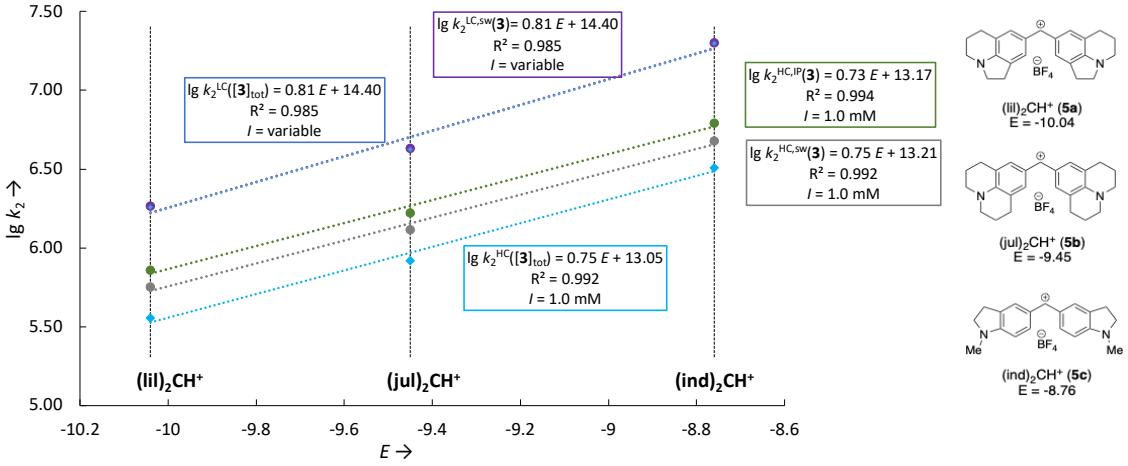

Conditions	Superscript	Nucleophile	k_2 (M^{-1} s^{-1})			N/s_N
			5a	5b	5c	
I = 0.01-0.03 mM	LC	$[\mathbf{3}]_{tot}$	1.84 x 10^6[a]	4.23 x 10^6	1.98 x 10^7	17.78/0.81
Sandwich model	LC,sw	**3**	1.84 x 10^6	4.28 x 10^6	2.00 x 10^7	17.78/0.81
I = 1.0 mM	HC	$[\mathbf{3}]_{tot}$	3.58 x 10^5	8.28 x 10^5	3.23 x 10^6	17.40/0.75
6 –> 1:1 association	HC,IP	**3**	7.23 x 10^5	1.67 x 10^6	7.17 x 10^6	18.04/0.73
6 –> sw associaton	HC,sw	**3**	5.43 x 10^5	1.25 x 10^6	4.87 x 10^6	17.61/0.75

[a] the reaction of **3a** with **5a** was measured twice, resulting in k_2^{LC} = 1.82 x 10^6 M^{-1} s^{-1} (I = 0.01-0.03 mM) and k_2^{LC} = 1.86 x 10^6 M^{-1} s^{-1} (I = 0.01-0.04 mM, initial three data points of wide range measurement) giving an average k_2^{LC} = 1.84 x 10^6 M^{-1} s^{-1}.

To summarize, at low concentrations between 0.01 – 0.03 mM while the ionic strength I in solution is variable, the second-order rates k_2^{LC} and $k_2^{LC,sw}$ are almost identical, which results in identical N and s_N parameters. With the addition of additive **6**, the main issue for the determination of the nucleophilicity of anion **3** at higher concentrations being the ongoing association of **3a** was circumvented. Depending on the chosen model for the subsequent analysis, the resulting second-order rate constants k_2 differ from one another. So was $k_2^{HC,IP}$ 1.3 times faster than $k_2^{HC,sw}$, while both were 2.0 and 1.5 times faster than k_2^{HC}, respectively. Overall, the nucleophile-specific sensitivity s_N fell within a narrow window (0.81 vs. 0.73), implying that the relative reactivity of anion **3** was not significantly influenced by the addition of additive **6**.

2.1.7.3 Mixed Sandwich Association Extension

Previously, we applied the cationic sandwich model (model 3a) to determine the concentration of free nucleophilic anion **3** in kinetic measurements performed in DCM at higher concentrations, expecting a linear correlation between k_{obs} and [**3**] (grey dots, see Figure 2.21). Instead, a steeper but still non-linear correlation was observed. By applying the mixed sandwich association model (model 4) to the same kinetic data, the resulting correlation between k_{obs} and [**3**] was still non-linear, but closer to the ideal theoretical correlation than the correlation based on model 3a (brown dots, see Figure 2.21).

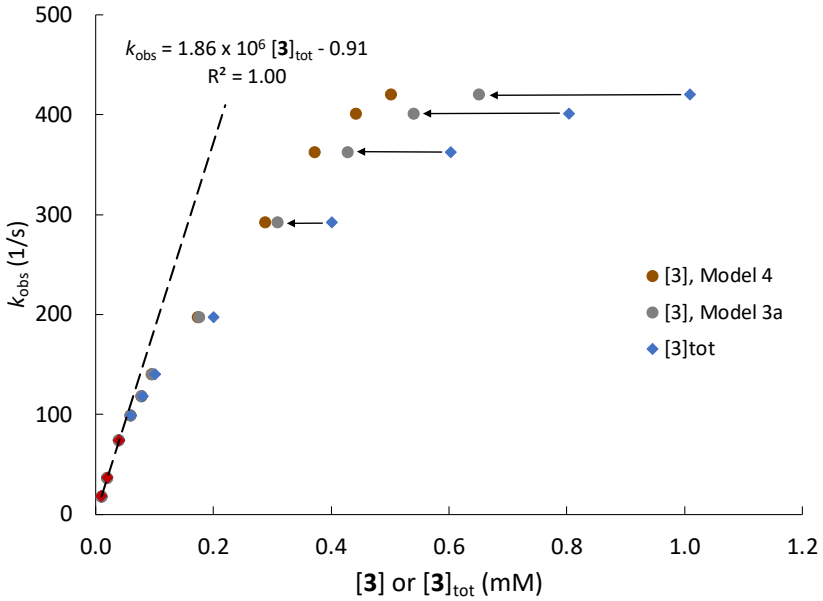

Figure 2.21: [Figure S27]. Plot of k_{obs} vs. concentration of catalysts 3a over a concentration range from 0.01–1.0 mM in DCM at 20°C (blue diamonds), vs. concentration of anion 3 over a concentration range from 0.01–1.0 mM in DCM at 20°C based on the sandwich association model 3a (grey dots), and vs. concentration of anion 3 over a concentration range from 0.01–1.0 mM in DCM at 20°C based on the mixed sandwich association model 4 (brown dots).

The mixed model came closer to the theoretical ideal case of the predicted linear correlation between k_{obs} and [**3**], indicating a step forward in the development of a comprehensive association model for pyridinamide ion pairs as **3a**.

Next, the mixed sandwich association model (model 4) was used to analyze the ionic strength-controlled kinetic data. Therefore, model 4 was extended by adding eq. 2.14b to account for the additive association whilst taking both cationic and anionic sandwich association into account in analyzing the nucleophilicity data (see Scheme 2.8). Moving forward, it was assumed that additive **6** associates in according to the cationic sandwich association model.

$$2 * A + 2 * C \overset{\alpha \times K_{CAC}}{\rightleftharpoons} A + CAC$$

$$2 * A + 2 * C \overset{\beta \times K_{ACA}}{\rightleftharpoons} C + ACA$$

$$2 * C + 2 * B \overset{K_{CAC}(add)}{\rightleftharpoons} B + CBC$$

Scheme 2.8: [Scheme S8]. Mixed model with additive association extension for the analysis of nucleophilicity data.

For numerical simulations, the same procedure was followed as described earlier for the cationic sandwich association extension. For ion pair **3a**, the following association constants K_{CAC}(**3a**) = k_1/k_2 = 2.81 x 10^6 M^{-2}, and K_{ACA}(**3a**) = k_1/k_2 = 1.34 x 10^6 M^{-2}, were applied with K_{CAC}(**6**) = 7.05 x 10^6 M^{-2} still being the same value as before for measurements done with constant ionic strength I = 1.0 mM.

Numerical simulation according to the mixed sandwich association extension gave the concentration of the free anion **3** as well as the concentration of the sandwich anion **3a3**, which could potentially act as another nucleophile. To discuss the different options, we look at the correlation between k_{obs} and the respective nucleophile concentration (see Figure 2.22).

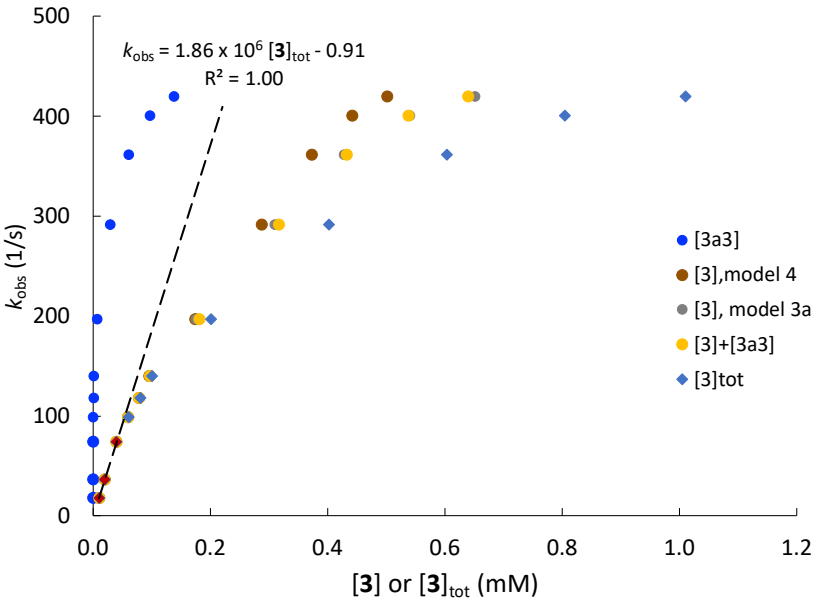

Figure 2.22: [Figure S28]. Plot of k_{obs} vs. concentration of catalysts **3a** over a concentration range from 0.01–1.0 mM in DCM at 20°C (blue diamonds), k_{obs} vs. anion [**3**] over a concentration range from 0.01–1.0 mM in DCM at 20°C based on the sandwich association model 3a (grey dots), k_{obs} vs. anion [**3**] + anion sandwich [**3a3**] over a concentration range from 0.01–1.0 mM in DCM at 20°C based on the mixed sandwich association model 4 (yellow dots), k_{obs} vs. anion [**3**] over a concentration range from 0.01–1.0 mM in DCM at 20°C based on the mixed sandwich association model 4 (brown dots), and k_{obs} vs. anion sandwich [**3a3**] over a concentration range from 0.01–1.0 mM in DCM at 20°C based on the mixed sandwich association model 4 (blue dots).

The anionic sandwich complex **3a3** is unlikely to be the more reactive nucleophile due to its reduced reactivity caused by complexation. Simultaneously, its concentration was far too low to plausible be the main reacting nucleophile. In the best-case scenario both the free anion **3** and the anion sandwich **3a3** react equally as nucleophiles (yellow correlation). This would give a correlation that is virtually overlapping with the correlation obtained with numerical simulation according to the cationic sandwich association model 3a (grey dots). As already established, the correlation for k_{obs} vs. [**3**] obtained by applying the mixed sandwich association model 4 (brown dots) was closest to the predicted ideal linear correlation. Moving forward, we will focus on two possible nucleophiles in solution being either the free anion [**3**] or the combination of [**3**] + [**3a3**].

Looking at the second-order rate constant obtained by plotting k_{obs} against [**3**] based on model 3a or model 4 and k_{obs} against [**3**] + [**3a3**], it can be determined that the deviations are clearly visible, but all are in a reasonable window (see Figure 2.23).

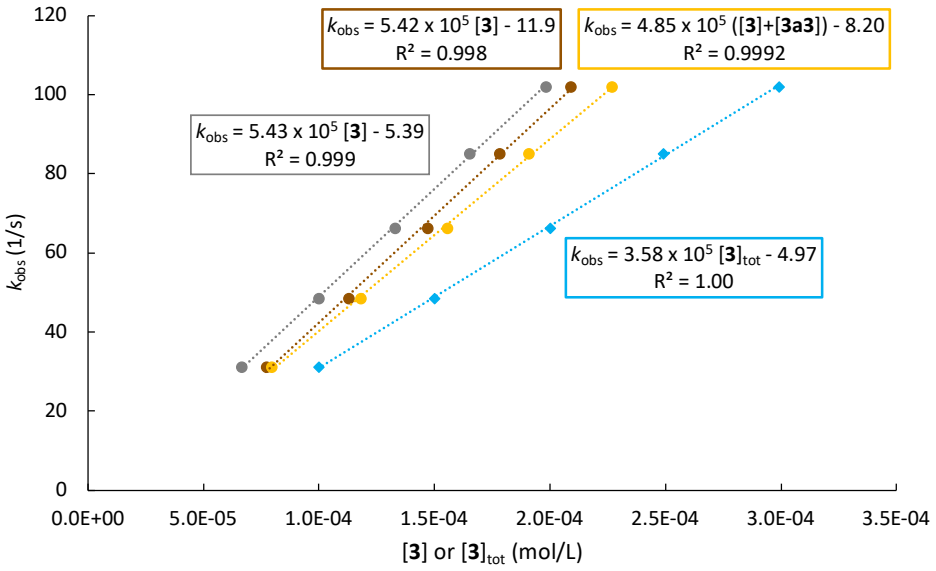

Figure 2.23: [Figure S29]. Plot of k_{obs} vs. concentration of catalysts **3a** with additive **6** (turquoise diamonds), concentration of anion [**3**]+[**3a3**] obtained with model 4 ("HC,mix", yellow dots), concentration of anion [**3**] obtained with model 4 ("HC,mix", brown dots), and concentration of anion [**3**] obtained with model ("HC,sw", grey dots) over a concentration range from 0.01–1.0 mM in DCM at 20°C with constant ionic strength I = 1.0 mM.

The new superscript "HC,mix" = [**3**]$_{tot}$ with I = 1.0 mM (brown) was introduced to distinguish the second-order rate constants k_2 and the resulting N- and s_N-parameters based on the derived mixed sandwich association extension. While the differences in the second-order rate constant are still noticeable, the resulting N- and s_N-parameter are almost overlapping. Therefore, while the analysis of the kinetic data with due regard to the effects of ion association is relevant to obtain a reliable second-order rate constant, for practicability, it is within a justifiable window of deviation to use the overall ion pair concentration [**3**]$_{tot}$ and follow the established Mayr method for the data evaluation of the ionic strength-controlled measurements. In Table 2.23, all second-order rate constants k_2 and the resulting N- and s_N-parameter are summarized for all seven executed ways of evaluation for pyridinamide ion pair **3a**.

Table 2.23: [Table S27]. Second-order rate constants obtained with all seven possible analysis methods for salt **3a** with benzhydrylium electrophiles salts (lil)$_2$CHBF$_4$ (**5a**), (jul)$_2$CHBF$_4$ (**5b**), and (ind)$_2$CHBF$_4$ (**5c**) between 0.01 – 0.03 mM in DCM at 20 °C and the corresponding N- and s_N-parameters.

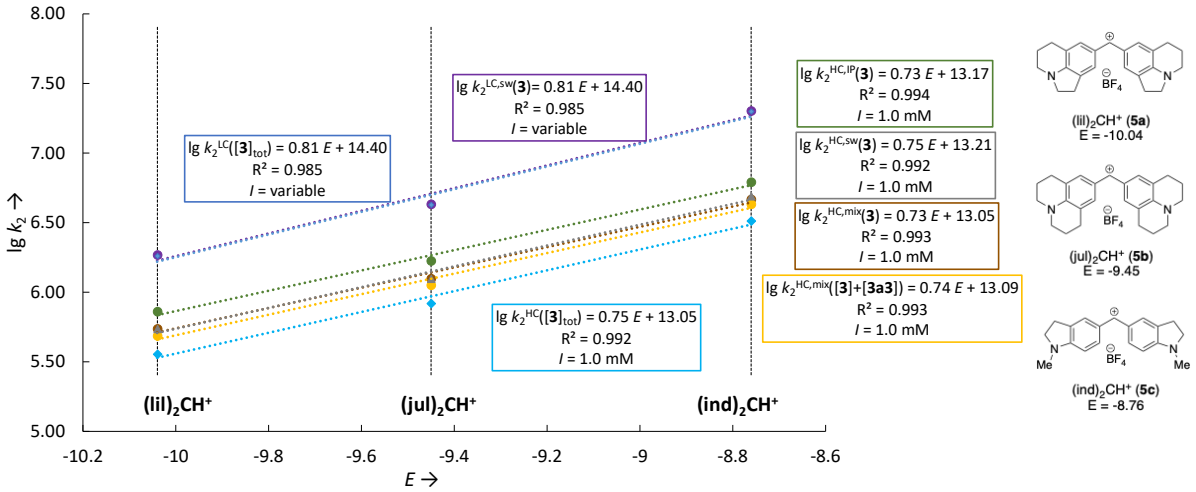

Conditions	Superscript	Nucleophile	k_2 (M^{-1} s^{-1})			N/s_N
			5a	5b	5c	
I = 0.01-0.03 mM	LC	[**3**]$_{tot}$	1.84 x 10^6[a]	4.23 x 10^6	1.98 x 10^7	17.78/0.81
Sandwich model	LC,sw	**3**	1.84 x 10^6	4.28 x 10^6	2.00 x 10^7	17.78/0.81

I = 1.0 mM	HC	**[3]$_{tot}$**	3.58 x 10^5	8.28 x 10^5	3.23 x 10^6	17.40/0.75
6 –> 1:1 association	HC,IP	**3**	7.23 x 10^5	1.67 x 10^6	7.17 x 10^6	18.04/0.73
6 –> sw associaton	HC,sw	**3**	5.43 x 10^5	1.25 x 10^6	4.87 x 10^6	17.61/0.75
6 –> sw associaton	HC,mix	**[3]+[3a3]**	4.85 x 10^5	1.12 x 10^6	4.26 x 10^6	17.69/0.74
6 –> sw associaton	HC,mix	**3**	5.42 x 10^5	1.25 x 10^6	4.64 x 10^6	17.88/0.73

[a] the reaction of **3a** with **5a** was measured twice, resulting in k_2^{LC} = 1.82 x 10^6 M^{-1} s^{-1} (*I* = 0.01-0.03 mM) and k_2^{LC} = 1.86 x 10^6 M^{-1} s^{-1} (*I* = 0.01-0.04 mM, initial three data points of wide range measurement) giving an average k_2^{LC} = 1.84 x 10^6 M^{-1} s^{-1}.

In future applications of the mixed sandwich association model, the free anion **3** is treated as the only active nucleophile in solution. The sandwich anion will not be considered in the analysis.

2.1.7.4 Nucleophilicity Measurement Data

2.1.7.4.1 Nucleophilicity of TCAP in DCM at 20 °C

Reaction of **TCAP** with $(lil)_2CH^+BF_4^-$ (stopped-flow, λ = 640 nm)

$[(lil)_2CH^+BF_4^-]$ (mol L^{-1})	**[TCAP] (mol L^{-1})**	**k_{obs} (s^{-1})**
1.01 x 10^{-5}	1.02 x 10^{-4}	1.19
	1.53 x 10^{-4}	1.92
	2.04 x 10^{-4}	2.62
	2.55 x 10^{-4}	3.32
	3.06 x 10^{-4}	4.10

k_2 = 1.42 x 10^4 L mol^{-1} s^{-1}

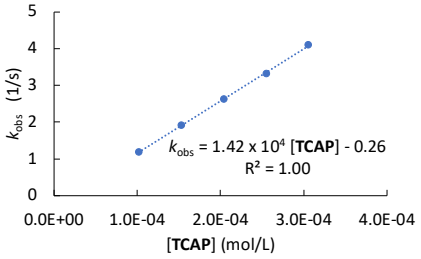

Reaction of **TCAP** with $(jul)_2CH^+BF_4^-$ (stopped-flow, λ = 643 nm)

$[(jul)_2CH^+BF_4^-]$ (mol L^{-1})	**[TCAP] (mol L^{-1})**	**k_{obs} (s^{-1})**
9.85 x 10^{-6}	1.02 x 10^{-4}	2.71
	1.53 x 10^{-4}	4.41
	2.04 x 10^{-4}	6.04
	2.55 x 10^{-4}	7.39
	3.06 x 10^{-4}	9.15

k_2 = 3.11 x 10^4 L mol^{-1} s^{-1}

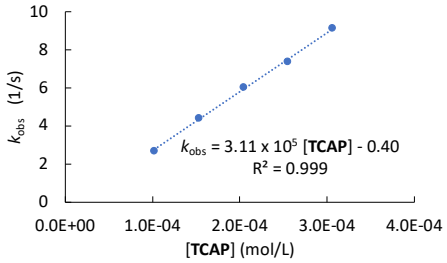

Reaction of **TCAP** with $(ind)_2CH^+BF_4^-$ (stopped-flow, λ = 626 nm)

$[(ind)_2CH^+BF_4^-]$ (mol L^{-1})	**[TCAP] (M^{-1})**	**k_{obs} (s^{-1})**
9.90 x 10^{-6}	1.02 x 10^{-4}	11.4
	1.53 x 10^{-4}	18.9
	2.04 x 10^{-4}	25.2
	2.55 x 10^{-4}	31.8
	3.06 x 10^{-4}	37.1

k_2 = 1.28 x 10^5 L mol^{-1} s^{-1}

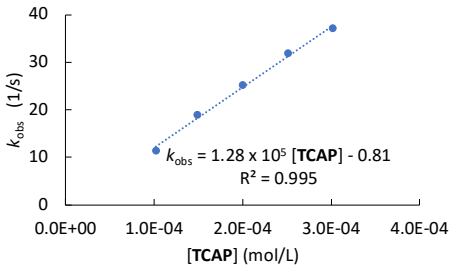

Reaction of **TCAP** with $(pyr)_2CH^+BF_4^-$ (stopped-flow, λ = 620 nm)

$[(pyr)_2CH^+BF_4^-]$ (mol L^{-1})	[TCAP] (mol L^{-1})	k_{obs} (s^{-1})
1.01 x 10^{-5}	1.02 x 10^{-4}	61.9
	1.53 x 10^{-4}	102
	2.04 x 10^{-4}	137
	2.55 x 10^{-4}	178
	3.06 x 10^{-4}	210

k_2 = 7.41 x 10^5 L mol^{-1} s^{-1}

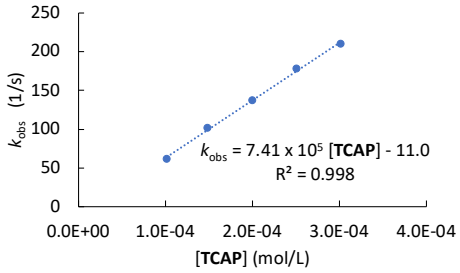

Reaction of **TCAP** with $(dma)_2CH^+BF_4^-$ (stopped-flow, λ = 613 nm)

$[(dma)_2CH^+BF_4^-]$ (mol L^{-1})	[TCAP] (mol L^{-1})	k_{obs} (s^{-1})
9.90 x 10^{-6}	1.02 x 10^{-4}	197
	1.53 x 10^{-4}	323
	2.04 x 10^{-4}	461
	2.55 x 10^{-4}	576
	3.06 x 10^{-4}	719

k_2 = 2.58 x 10^6 L mol^{-1} s^{-1}

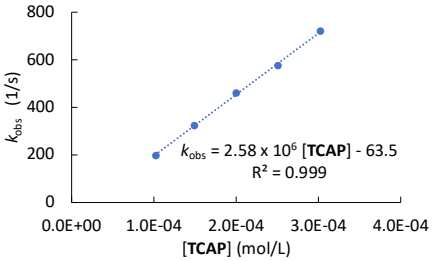

Determination of *N* and s_N parameter for **TCAP** in DCM

Electrophile	*E*	k_2 (M^{-1} s^{-1})
Lil	-10.04	1.42 x 10^4
Jul	-9.45	3.11 x 10^4
Ind	-8.76	1.28 x 10^5
Pyr	-7.69	7.41 x 10^5
Dma	-7.02	2.58 x 10^6

***N* = 15.41** **s_N = 0.76**

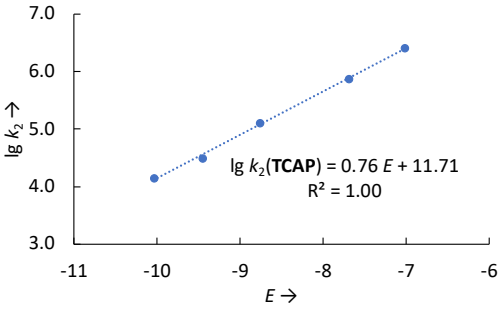

2.1.7.4.2 Nucleophilicity of 3a in MeCN at 20 °C

Reaction of **3a** with $(lil)_2CH^+BF_4^-$ (stopped-flow, λ = 632 nm)

[5a] (mol L^{-1})	[3a] (mol L^{-1})	k_{obs} (s^{-1})
1.11 x 10^{-6}	1.00 x 10^{-5}	0.34
	1.50 x 10^{-5}	0.38
	2.00 x 10^{-5}	0.41
	2.51 x 10^{-5}	0.45
	3.01 x 10^{-5}	–

k_2 = 7.16 x 10^3 L mol^{-1} s^{-1}

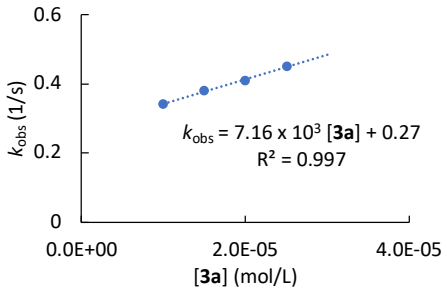

Reaction of **3a** with $(jul)_2CH^+BF_4^-$ (stopped-flow, λ = 635 nm)

[5b] (mol L^{-1})	[3a] (mol L^{-1})	k_{obs} (s^{-1})
1.00 x 10^{-6}	1.00 x 10^{-5}	–
	1.50 x 10^{-5}	0.86
	2.00 x 10^{-5}	0.92
	2.51 x 10^{-5}	1.00
	3.01 x 10^{-5}	1.09

k_2 = 1.53 x 10^4 L mol^{-1} s^{-1}

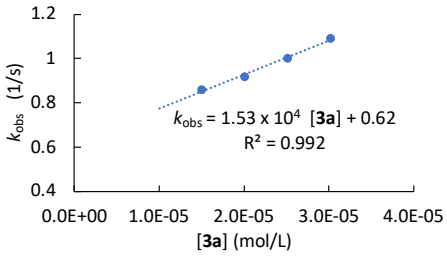

Reaction of **3a** with $(ind)_2CH^+BF_4^-$ (stopped-flow, λ = 616 nm)

[5c] (mol L^{-1})	[3a] (mol L^{-1})	k_{obs} (s^{-1})
9.27 x 10^{-7}	1.00 x 10^{-5}	–
	1.50 x 10^{-5}	0.86
	2.00 x 10^{-5}	1.08
	2.51 x 10^{-5}	1.30
	3.01 x 10^{-5}	1.48

k_2 = 4.13 x 10^4 L mol^{-1} s^{-1}

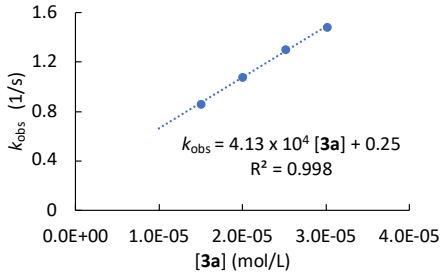

Determination of *N* and s_N parameter for **3a** in MeCN

Electrophile	*E*	k_2 (M^{-1} s^{-1})
5a	-10.04	7.16 x 10^3
5b	-9.45	1.53 x 10^4
5c	-8.76	4.13 x 10^4

N = 16.38 **s_N = 0.60**

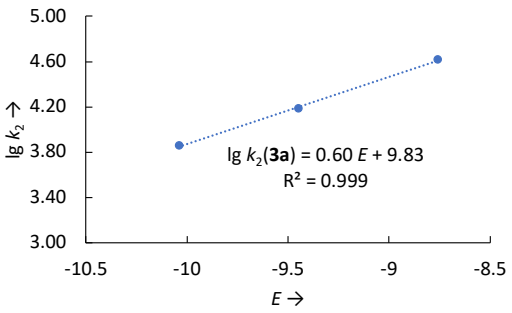

2.1.7.4.3 Nucleophilicity of 4a in MeCN at 20 °C

Reaction of **4a** with $(lil)_2CH^+BF_4^-$ (stopped-flow, λ = 632 nm)

[5a] (mol L^{-1})	[4a] (mol L^{-1})	k_{obs} (s^{-1})
9.69 x 10^{-7}	9.89 x 10^{-6}	0.33
	1.53 x 10^{-5}	0.73
	1.98 x 10^{-5}	0.97
	2.52 x 10^{-5}	1.12
	2.97 x 10^{-5}	1.40

k_2 = 5.11 x 10^4 L mol^{-1} s^{-1}

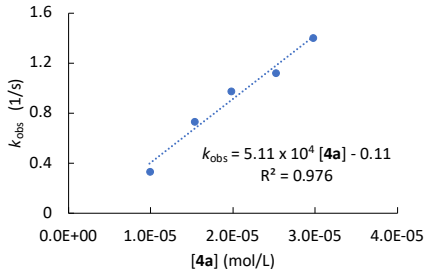

Reaction of **4a** with $(jul)_2CH^+BF_4^-$ (stopped-flow, λ = 635 nm)

[5b] (mol L^{-1})	[4a] (mol L^{-1})	k_{obs} (s^{-1})
9.89 x 10^{-7}	9.89 x 10^{-6}	0.58
	1.53 x 10^{-5}	1.49
	1.98 x 10^{-5}	2.09
	2.52 x 10^{-5}	–
	2.97 x 10^{-5}	3.32

k_2 = 1.36 x 10^5 L mol^{-1} s^{-1}

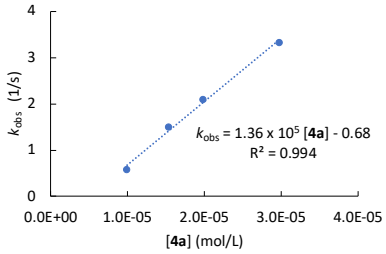

Reaction of **4a** with $(ind)_2CH^+BF_4^-$ (stopped-flow, λ = 616 nm)

[5c] (mol L^{-1})	[4a] (mol L^{-1})	k_{obs} (s^{-1})
1.06 x 10^{-6}	9.89 x 10^{-6}	1.81
	1.53 x 10^{-5}	3.59
	1.98 x 10^{-5}	5.16
	2.52 x 10^{-5}	–
	2.97 x 10^{-5}	8.66

k_2 = 3.47 x 10^5 L mol^{-1} s^{-1}

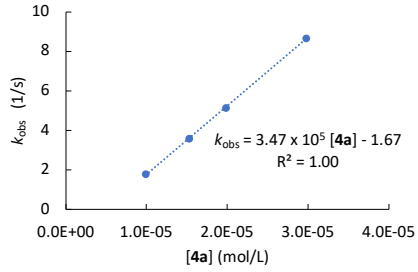

Determination of *N* and s_N parameter for **4a** in MeCN

Electrophile	*E*	k_2 (M^{-1} s^{-1})
5a	-10.04	5.11 x 10^4
5b	-9.45	1.36 x 10^5
5c	-8.76	3.47 x 10^5

***N* = 17.28** **s_N = 0.65**

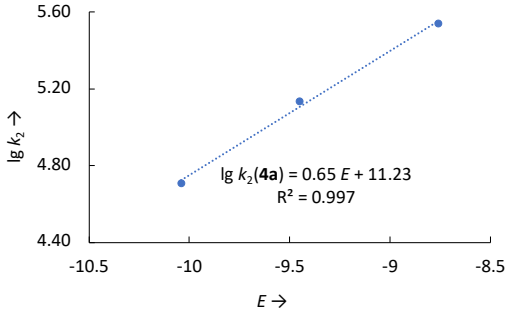

2.1.7.4.4 Nucleophilicity of 3a in DCM at 20 °C (*c* = 0.01 – 0.03 mM)

Equilibrium constants for numerical simulation: K_{CAC} = 6.38 x 10^6 M^{-2} for **3a**. Reaction of salt **3a** with $(lil)_2CH^+BF_4^-$ (stopped-flow, λ = 640 nm)

[5a] (mol L^{-1})	$[3]_{tot}$ (mol L^{-1})	[3] (mol L^{-1})	k_{obs} (s^{-1})
8.63 x 10^{-7}	9.98 x 10^{-6}	9.97 x 10^{-6}	22.2
	1.50 x 10^{-5}	1.50 x 10^{-5}	34.1
	2.00 x 10^{-5}	2.00 x 10^{-5}	43.7
	2.50 x 10^{-5}	2.49 x 10^{-5}	52.2
	2.99 x 10^{-5}	2.97 x 10^{-5}	58.6

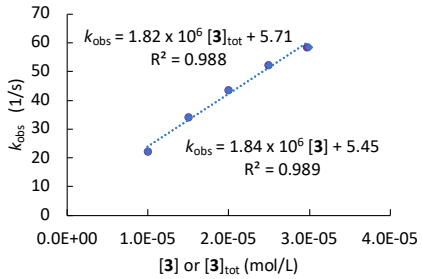

k_2^{LC} = 1.82 x 10^6 L mol^{-1} s^{-1} for $[3]_{tot}$ **$k_2^{LC,sw}$ = 1.84 x 10^6 L mol^{-1} s^{-1}** for [**3**]

Reaction of **3a** with $(jul)_2CH^+BF_4^-$ (stopped-flow, λ = 643 nm)

[5b] (mol L^{-1})	$[3]_{tot}$ (mol L^{-1})	[3] (mol L^{-1})	k_{obs} (s^{-1})
8.82 x 10^{-7}	9.95 x 10^{-6}	9.94 x 10^{-6}	33.2
	1.49 x 10^{-5}	1.49 x 10^{-5}	63.3
	1.99 x 10^{-5}	1.99 x 10^{-5}	84.2
	2.49 x 10^{-5}	2.48 x 10^{-5}	102
	2.98 x 10^{-5}	2.96 x 10^{-5}	119

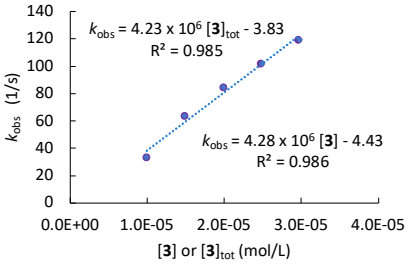

k_2^{LC} = 4.23 x 10^6 L mol^{-1} s^{-1} for $[3]_{tot}$ **$k_2^{LC,sw}$ = 4.28 x 10^6 L mol^{-1} s^{-1}** for [**3**]

Reaction of **3a** with $(ind)_2CH^+BF_4^-$ (stopped-flow, λ = 626 nm)

[5c] (mol L^{-1})	$[3]_{tot}$ (mol L^{-1})	[3] (mol L^{-1})	k_{obs} (s^{-1})
9.87 x 10^{-7}	9.95 x 10^{-6}	9.94 x 10^{-6}	110
	1.49 x 10^{-5}	1.49 x 10^{-5}	222
	1.99 x 10^{-5}	1.99 x 10^{-5}	338
	2.49 x 10^{-5}	2.48 x 10^{-5}	426
	2.98 x 10^{-5}	2.96 x 10^{-5}	501

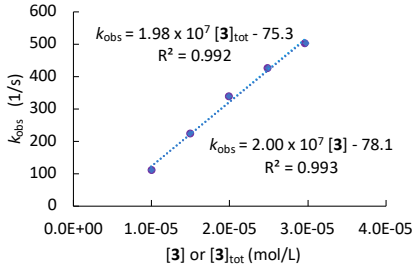

k_2^{LC} = 1.98 x 10^7 L mol^{-1} s^{-1} for $[3]_{tot}$ **$k_2^{LC,sw}$ = 2.00 x 10^7 L mol^{-1} s^{-1}** for [**3**]

Determination of *N* and s_N parameter for **3a** in DCM

Electrophile	*E*	k_2^{LC} (M^{-1} s^{-1}) for $[3]_{tot}$	$k_2^{LC,sw}$ (M^{-1} s^{-1}) for [**3**]
5a	-10.04	1.82 x 10^6	1.84 x 10^6
5b	-9.45	4.23 x 10^6	4.28 x 10^6
5c	-8.76	1.98 x 10^7	2.00 x 10^7

N = 17.78 **s_N = 0.81** for $[3]_{tot}$

N = 17.78 **s_N = 0.81** for [**3**]

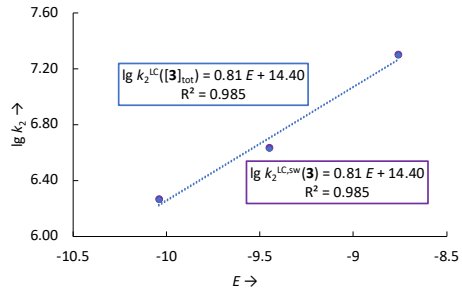

2.1.7.4.5 Nucleophilicity of 3a in DCM at *I* = 1.0 mM at 20 °C (1:1 model for additive 6)

Equilibrium constants for numerical simulation: K_{CAC} = 6.38 x 10^6 M^{-2} for **3a**, K_{IP} = 1.01 x 10^7 M^{-2} for **6**.

Reaction of **3a + 6** with $(lil)_2CH^+BF_4^-$ (stopped-flow, λ = 640 nm)

[5a] (mol L^{-1})	$[3]_{tot}$ (mol L^{-1})	[3] (mol L^{-1})	[6] (mol L^{-1})	k_{obs} (s^{-1})
9.27 x 10^{-6}	9.98 x 10^{-5}	3.47 x 10^{-5}	8.91 x 10^{-4}	31.1
	1.50 x 10^{-4}	5.63 x 10^{-5}	8.34 x 10^{-4}	48.5
	2.00 x 10^{-4}	8.68 x 10^{-5}	7.87 x 10^{-4}	66.2
	2.49 x 10^{-4}	1.05 x 10^{-4}	7.41 x 10^{-4}	85.0
	2.99 x 10^{-4}	1.33 x 10^{-4}	6.94 x 10^{-4}	102

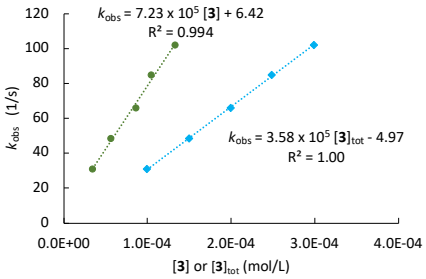

k_2^{HC} = 3.58 x 10^5 L mol^{-1} s^{-1} for [**3a**] **$k_2^{HC,IP}$ = 7.23 x 10^5 L mol^{-1} s^{-1}** for [**3**]

Reaction of **3a + 6** with $(jul)_2CH^+BF_4^-$ (stopped-flow, λ = 643 nm)

[5b] (mol L^{-1})	$[3]_{tot}$ (mol L^{-1})	[3] (mol L^{-1})	[6] (mol L^{-1})	k_{obs} (s^{-1})
9.40 x 10^{-6}	9.98 x 10^{-5}	3.47 x 10^{-5}	8.91 x 10^{-4}	62.1
	1.50 x 10^{-4}	5.63 x 10^{-5}	8.34 x 10^{-4}	101
	2.00 x 10^{-4}	8.68 x 10^{-5}	7.87 x 10^{-4}	141
	2.49 x 10^{-4}	1.05 x 10^{-4}	7.41 x 10^{-4}	183
	2.99 x 10^{-4}	1.33 x 10^{-4}	6.94 x 10^{-4}	227

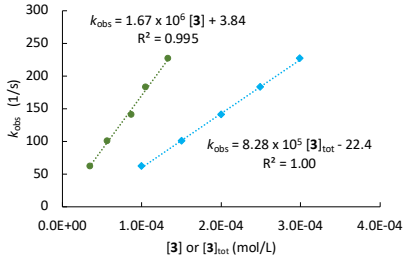

k_2^{HC} = 8.28 x 10^5 L mol^{-1} s^{-1} for [**3a**] **$k_2^{HC,IP}$ = 1.67 x 10^6 L mol^{-1} s^{-1}** for [**3**]

Reaction of **3a + 6** with $(ind)_2CH^+BF_4^-$ (stopped-flow, λ = 626 nm)

[5c] (mol L^{-1})	$[3]_{tot}$ (mol L^{-1})	[3] (mol L^{-1})	[6] (mol L^{-1})	k_{obs} (s^{-1})
9.99 x 10^{-6}	9.98 x 10^{-5}	3.47 x 10^{-5}	8.91 x 10^{-4}	244
	1.50 x 10^{-4}	5.63 x 10^{-5}	8.34 x 10^{-4}	400
	2.00 x 10^{-4}	8.68 x 10^{-5}	7.87 x 10^{-4}	568
	2.49 x 10^{-4}	1.05 x 10^{-4}	7.41 x 10^{-4}	
	2.99 x 10^{-4}	1.33 x 10^{-4}	6.94 x 10^{-4}	

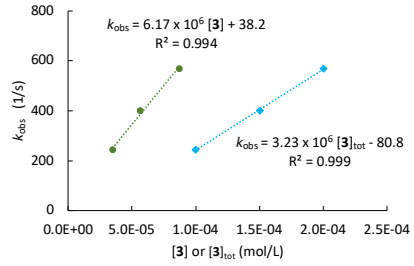

k_2^{HC} = 3.23 x 10^6 L mol^{-1} s^{-1} for [**3a**] **$k_2^{HC,IP}$ = 7.17 x 10^6 L mol^{-1} s^{-1}** for [**3**]

Determination of *N* and s_N parameter for **3a** in DCM at constant ionic strength of 1.0 mM

Electrophile	*E*	k_2^{HC} (M^{-1} s^{-1}) for $[3]_{tot}$	$k_2^{HC,IP}$ (M^{-1} s^{-1}) for [3]
5a	-10.04	3.58 x 10^5	7.23 x 10^5
5b	-9.45	8.28 x 10^5	1.67 x 10^6
5c	-8.76	3.23 x 10^6	7.17 x 10^6

N = 17.40 **s_N = 0.75** for $[3]_{tot}$

N = 18.04 **s_N = 0.73** for [**3**]

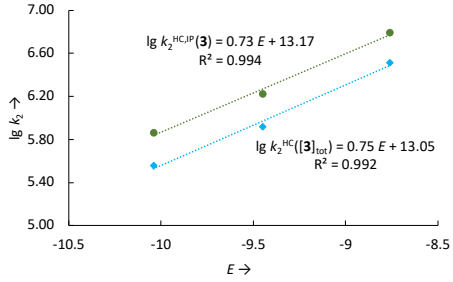

2.1.7.4.6 Nucleophilicity of 3a in DCM at *I* = 1.0 mM at 20 °C (cationic sandwich model for additive 6)

Equilibrium constants for numerical simulation: K_{CAC} = 6.38 x 10^6 M^{-2} for **3a**, K_{CAC} = 7.05 x 10^6 M^{-2} for **6**.

Reaction of **3a + 6** with $(lil)_2CH^+BF_4^-$ (stopped-flow, λ = 640 nm)

[5a] (mol L^{-1})	$[3]_{tot}$ (mol L^{-1})	[3] (mol L^{-1})	[6] (mol L^{-1})	k_{obs} (s^{-1})
9.27 x 10^{-6}	9.98 x 10^{-5}	6.65 x 10^{-5}	8.91 x 10^{-4}	31.1
	1.50 x 10^{-4}	9.98 x 10^{-5}	8.34 x 10^{-4}	48.5
	2.00 x 10^{-4}	1.33 x 10^{-4}	7.87 x 10^{-4}	66.2
	2.49 x 10^{-4}	1.65 x 10^{-4}	7.41 x 10^{-4}	85.0
	2.99 x 10^{-4}	1.98 x 10^{-4}	6.94 x 10^{-4}	102

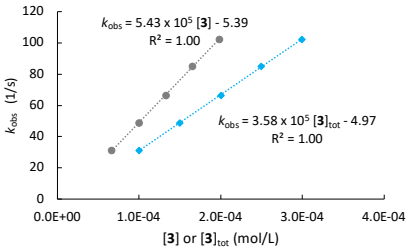

k_2^{HC} = 3.58 x 10^5 L mol^{-1} s^{-1} for $[3]_{tot}$ **$k_2^{HC,sw}$ = 5.43 x 10^5 L mol^{-1} s^{-1}** for [3]

Reaction of **3a + 6** with $(jul)_2CH^+BF_4^-$ (stopped-flow, λ = 643 nm)

[5b] (mol L^{-1})	$[3]_{tot}$ (mol L^{-1})	[3] (mol L^{-1})	[6] (mol L^{-1})	k_{obs} (s^{-1})
9.40 x 10^{-6}	9.98 x 10^{-5}	6.65 x 10^{-5}	8.91 x 10^{-4}	62.1
	1.50 x 10^{-4}	9.98 x 10^{-5}	8.34 x 10^{-4}	101
	2.00 x 10^{-4}	1.33 x 10^{-4}	7.87 x 10^{-4}	141
	2.49 x 10^{-4}	1.65 x 10^{-4}	7.41 x 10^{-4}	183
	2.99 x 10^{-4}	1.98 x 10^{-4}	6.94 x 10^{-4}	227

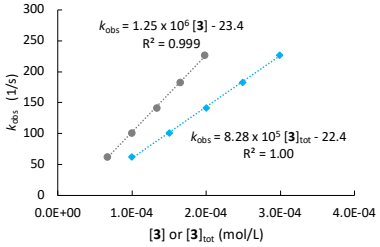

k_2^{HC} = 8.28 x 10^5 L mol^{-1} s^{-1} for $[3]_{tot}$ **$k_2^{HC,sw}$ = 1.25 x 10^6 L mol^{-1} s^{-1}** for [3]

Reaction of **3a + 6** with $(ind)_2CH^+BF_4^-$ (stopped-flow, λ = 626 nm)

[5c] (mol L^{-1})	$[3]_{tot}$ (mol L^{-1})	[3] (mol L^{-1})	[6] (mol L^{-1})	k_{obs} (s^{-1})
9.99 x 10^{-6}	9.98 x 10^{-5}	6.65 x 10^{-5}	8.91 x 10^{-4}	244
	1.50 x 10^{-4}	9.98 x 10^{-5}	8.34 x 10^{-4}	400
	2.00 x 10^{-4}	1.33 x 10^{-4}	7.87 x 10^{-4}	568
	2.49 x 10^{-4}	1.65 x 10^{-4}	7.41 x 10^{-4}	
	2.99 x 10^{-4}	1.98 x 10^{-4}	6.94 x 10^{-4}	

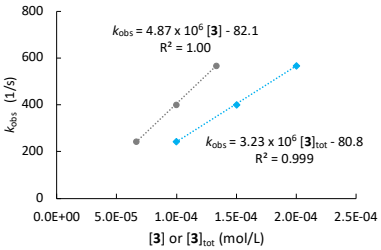

k_2^{HC} = 3.23 x 10^6 L mol^{-1} s^{-1} for $[3]_{tot}$ **$k_2^{HC,sw}$ = 4.87 x 10^6 L mol^{-1} s^{-1}** for [3]

Determination of *N* and s_N parameter for **3a** in DCM at constant ionic strength of 1.0 mM

Electrophile	*E*	k_2^{HC} (M^{-1} s^{-1}) for $[3]_{tot}$	$k_2^{HC,sw}$ (M^{-1} s^{-1}) for [3]
5a	-10.04	3.58 x 10^5	5.43 x 10^5
5b	-9.45	8.28 x 10^5	1.25 x 10^6
5c	-8.76	3.23 x 10^6	4.87 x 10^6

N = 17.40 **s_N = 0.75** for $[3]_{tot}$

N = 17.61 **s_N = 0.75** for [3]

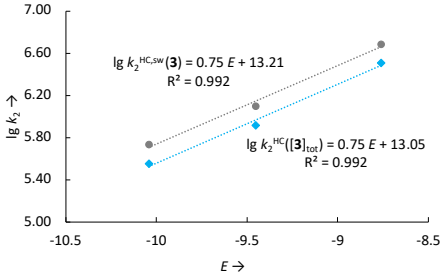

2.1.7.4.7 Nucleophilicity of 3a in DCM at *I* = 1.0 mM at 20 °C (mixed sandwich model extension)

Equilibrium constants for numerical simulation: α x K_{CAC} = 2.81 x 10^6 M^{-2} and β x K_{ACA} = 1.34 x 10^6 M^{-2} for **3a** (α/β = 0.44/0.21), K_{CAC} = 7.05 x 10^6 M^{-2} for **6**. Reaction of **3a + 6** with $(lil)_2CH^+BF_4^-$ (stopped-flow, λ = 640 nm)

[5a] (mol L^{-1})	$[3]_{tot}$ (mol L^{-1})	[3] (mol L^{-1})	[6] (mol L^{-1})	k_{obs} (s^{-1})
9.27 x 10^{-6}	9.98 x 10^{-5}	7.72 x 10^{-5}	8.91 x 10^{-4}	31.1
	1.50 x 10^{-4}	1.13 x 10^{-4}	8.34 x 10^{-4}	48.5
	2.00 x 10^{-4}	1.47 x 10^{-4}	7.87 x 10^{-4}	66.2
	2.49 x 10^{-4}	1.78 x 10^{-4}	7.41 x 10^{-4}	85.0
	2.99 x 10^{-4}	2.09 x 10^{-4}	6.94 x 10^{-4}	102

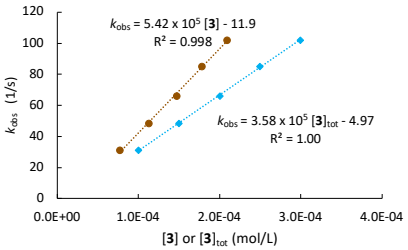

k_2^{HC} = 3.58 x 10^5 L mol^{-1} s^{-1} for $[3]_{tot}$ **$k_2^{HC,mix}$ = 5.42 x 10^5 L mol^{-1} s^{-1}** for [3]

Reaction of **3a + 6** with $(jul)_2CH^+BF_4^-$ (stopped-flow, λ = 643 nm)

[5b] (mol L^{-1})	$[3]_{tot}$ (mol L^{-1})	[3] (mol L^{-1})	[6] (mol L^{-1})	k_{obs} (s^{-1})
9.40 x 10^{-6}	9.98 x 10^{-5}	7.72 x 10^{-5}	8.91 x 10^{-4}	62.1
	1.50 x 10^{-4}	1.13 x 10^{-4}	8.34 x 10^{-4}	101
	2.00 x 10^{-4}	1.47 x 10^{-4}	7.87 x 10^{-4}	141
	2.49 x 10^{-4}	1.78 x 10^{-4}	7.41 x 10^{-4}	183
	2.99 x 10^{-4}	2.09 x 10^{-4}	6.94 x 10^{-4}	227

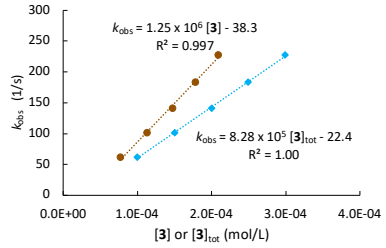

k_2^{HC} = 8.28 x 10^5 L mol^{-1} s^{-1} for $[3]_{tot}$ **$k_2^{HC,mix}$ = 1.25 x 10^6 L mol^{-1} s^{-1}** for [3]

Reaction of **3a + 6** with $(ind)_2CH^+BF_4^-$ (stopped-flow, λ = 626 nm)

[5c] (mol L^{-1})	$[3]_{tot}$ (mol L^{-1})	[3] (mol L^{-1})	[6] (mol L^{-1})	k_{obs} (s^{-1})
9.99 x 10^{-6}	9.98 x 10^{-5}	7.72 x 10^{-5}	8.91 x 10^{-4}	244
	1.50 x 10^{-4}	1.13 x 10^{-4}	8.34 x 10^{-4}	400
	2.00 x 10^{-4}	1.47 x 10^{-4}	7.87 x 10^{-4}	568
	2.49 x 10^{-4}	1.78 x 10^{-4}	7.41 x 10^{-4}	
	2.99 x 10^{-4}	2.09 x 10^{-4}	6.94 x 10^{-4}	

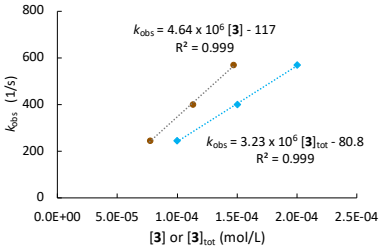

k_2^{HC} = 3.23 x 10^6 L mol^{-1} s^{-1} for $[3]_{tot}$ **$k_2^{HC,mix}$ = 4.64 x 10^6 L mol^{-1} s^{-1}** for [3]

Determination of *N* and s_N parameter for **3a** in DCM at constant ionic strength of 1.0 mM

Electrophile	*E*	k_2^{HC} (M^{-1} s^{-1}) for $[3]_{tot}$	$k_2^{HC,mix}$ (M^{-1} s^{-1}) for [3]
5a	-10.04	3.58 x 10^5	5.42 x 10^5
5b	-9.45	8.28 x 10^5	1.25 x 10^6
5c	-8.76	3.23 x 10^6	4.64 x 10^6

N = 17.40 **s_N = 0.75** for $[3]_{tot}$

N = 17.88 **s_N = 0.73** for [3]

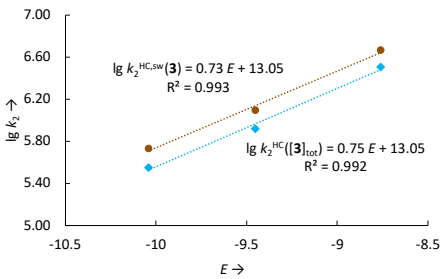

2.1.7.4.8 Nucleophilicity of 4a in DCM at *l* = 1.0 mM at 20 °C (cationic sandwich model for additive 6)

Equilibrium constants for numerical simulation: K_{CAC} = 6.50 x 10^6 M^{-2} for **4a**, K_{CAC} = 7.05 x 10^6 M^{-2} for **6**.

Reaction of **4a + 6** with $(lil)_2CH^+BF_4^-$ (stopped-flow, λ = 640 nm)

[5a] (mol L^{-1})	$[4]_{tot}$ (mol L^{-1})	[4] (mol L^{-1})	[6] (mol L^{-1})	k_{obs} (s^{-1})
4.21 x 10^{-6}	3.96 x 10^{-5}	2.62 x 10^{-5}	9.54 x 10^{-4}	29.0
	5.93 x 10^{-5}	3.91 x 10^{-5}	9.41 x 10^{-4}	51.6
	7.91 x 10^{-5}	5.22 x 10^{-5}	9.14 x 10^{-4}	76.6
	9.89 x 10^{-5}	6.52 x 10^{-5}	9.00 x 10^{-4}	99.3
	1.19 x 10^{-4}	7.82 x 10^{-5}	8.87 x 10^{-4}	127

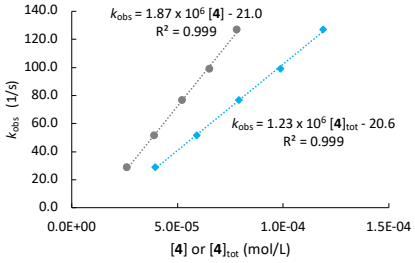

k_2^{HC} = 1.23 x 10^6 L mol^{-1} s^{-1} for $[4]_{tot}$ **$k_2^{HC,sw}$ = 1.87 x 10^6 L mol^{-1} s^{-1}** for [4]

Reaction of **4a + 6** with $(jul)_2CH^+BF_4^-$ (stopped-flow, λ = 643 nm)

[5b] (mol L^{-1})	$[4]_{tot}$ (mol L^{-1})	[4] (mol L^{-1})	[6] (mol L^{-1})	k_{obs} (s^{-1})
4.06 x 10^{-6}	3.96 x 10^{-5}	2.62 x 10^{-5}	9.54 x 10^{-4}	59.0
	5.93 x 10^{-5}	3.91 x 10^{-5}	9.41 x 10^{-4}	119
	7.91 x 10^{-5}	5.22 x 10^{-5}	9.14 x 10^{-4}	188
	9.89 x 10^{-5}	6.52 x 10^{-5}	9.00 x 10^{-4}	235
	1.19 x 10^{-4}	7.82 x 10^{-5}	8.87 x 10^{-4}	303

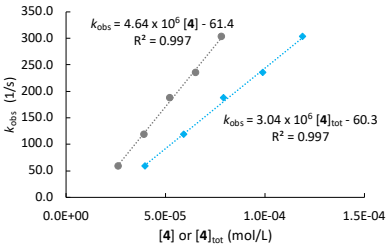

k_2^{HC} = 3.04 x 10^6 L mol^{-1} s^{-1} for $[4]_{tot}$ **$k_2^{HC,sw}$ = 4.64 x 10^6 L mol^{-1} s^{-1}** for [4]

Reaction of **4a + 6** with $(ind)_2CH^+BF_4^-$ (stopped-flow, λ = 626 nm)

[5c] (mol L^{-1})	$[4]_{tot}$ (mol L^{-1})	[4] (mol L^{-1})	[6] (mol L^{-1})	k_{obs} (s^{-1})
4.14 x 10^{-6}	3.96 x 10^{-5}	2.62 x 10^{-5}	9.54 x 10^{-4}	188
	5.93 x 10^{-5}	3.91 x 10^{-5}	9.41 x 10^{-4}	378
	7.91 x 10^{-5}	5.22 x 10^{-5}	9.14 x 10^{-4}	588
	9.89 x 10^{-5}	6.52 x 10^{-5}	9.00 x 10^{-4}	
	1.19 x 10^{-4}	7.82 x 10^{-5}	8.87 x 10^{-4}	846

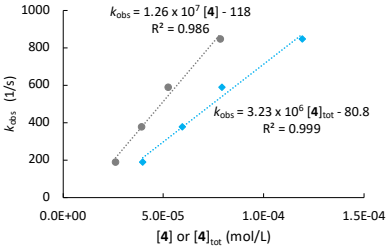

k_2^{HC} = 8.27 x 10^6 L mol^{-1} s^{-1} for $[4]_{tot}$ **$k_2^{HC,sw}$ = 1.26 x 10^7 L mol^{-1} s^{-1}** for [4]

Determination of *N* and s_N parameter for **4a** in DCM at constant ionic strength of 1.0 mM

Electrophile	*E*	k_2^{HC} (M^{-1} s^{-1}) for $[4]_{tot}$	$k_2^{HC,sw}$ (M^{-1} s^{-1}) for [4]
5a	-10.04	1.23 x 10^6	1.87 x 10^6
5b	-9.45	3.04 x 10^6	4.64 x 10^6
5c	-8.76	8.27 x 10^6	1.26 x 10^7

N = 19.35 **s_N = 0.65** for $[4]_{tot}$

N = 19.66 **s_N = 0.65** for [4]

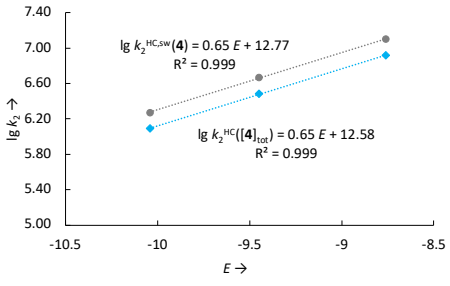

2.1.7.4.9 Nucleophilicity of 4a in DCM at *I* = 1.0 mM at 20 °C (mixed sandwich model extension)

Equilibrium constants for numerical simulation: α x K_{CAC} = 7.80 x 10^5 M^{-2} and β x K_{ACA} = 3.97 x 10^6 M^{-2} for **4a** (α/β = 0.12/0.61), K_{CAC} = 7.05 x 10^6 M^{-2} for **6**. Reaction of **4a + 6** with $(lil)_2CH^+BF_4^-$ (stopped-flow, λ = 640 nm)

[5a] (mol L^{-1})	$[4]_{tot}$ (mol L^{-1})	[4] (mol L^{-1})	[6] (mol L^{-1})	k_{obs} (s^{-1})
4.21 x 10^{-6}	3.96 x 10^{-5}	3.47 x 10^{-5}	9.54 x 10^{-4}	29.0
	5.93 x 10^{-5}	5.02 x 10^{-5}	9.41 x 10^{-4}	51.6
	7.91 x 10^{-5}	6.50 x 10^{-5}	9.14 x 10^{-4}	76.6
	9.89 x 10^{-5}	7.90 x 10^{-5}	9.00 x 10^{-4}	99.3
	1.19 x 10^{-4}	9.23 x 10^{-5}	8.87 x 10^{-4}	127

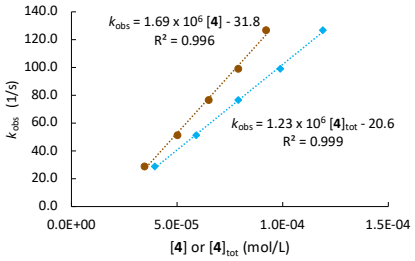

k_2^{HC} = 1.23 x 10^6 L mol^{-1} s^{-1} for $[4]_{tot}$ **$k_2^{HC,mix}$ = 1.69 x 10^6 L mol^{-1} s^{-1}** for [4]

Reaction of **4a + 6** with $(jul)_2CH^+BF_4^-$ (stopped-flow, λ = 643 nm)

[5b] (mol L^{-1})	$[4]_{tot}$ (mol L^{-1})	[4] (mol L^{-1})	[6] (mol L^{-1})	k_{obs} (s^{-1})
4.06 x 10^{-6}	3.96 x 10^{-5}	3.47 x 10^{-5}	9.54 x 10^{-4}	59.0
	5.93 x 10^{-5}	5.02 x 10^{-5}	9.41 x 10^{-4}	119
	7.91 x 10^{-5}	6.50 x 10^{-5}	9.14 x 10^{-4}	188
	9.89 x 10^{-5}	7.90 x 10^{-5}	9.00 x 10^{-4}	235
	1.19 x 10^{-4}	9.23 x 10^{-5}	8.87 x 10^{-4}	303

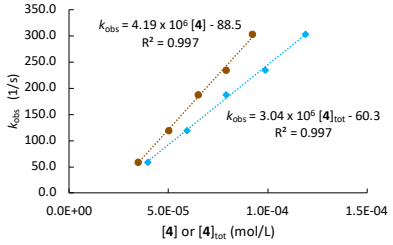

k_2^{HC} = 3.04 x 10^6 L mol^{-1} s^{-1} for $[4]_{tot}$ **$k_2^{HC,mix}$ = 4.19 x 10^6 L mol^{-1} s^{-1}** for [4]

Reaction of **4a + 6** with $(ind)_2CH^+BF_4^-$ (stopped-flow, λ = 626 nm)

[5c] (mol L^{-1})	$[4]_{tot}$ (mol L^{-1})	[4] (mol L^{-1})	[6] (mol L^{-1})	k_{obs} (s^{-1})
4.14 x 10^{-6}	3.96 x 10^{-5}	3.47 x 10^{-5}	9.54 x 10^{-4}	188
	5.93 x 10^{-5}	5.02 x 10^{-5}	9.41 x 10^{-4}	378
	7.91 x 10^{-5}	6.50 x 10^{-5}	9.14 x 10^{-4}	588
	9.89 x 10^{-5}	7.90 x 10^{-5}	9.00 x 10^{-4}	
	1.19 x 10^{-4}	9.23 x 10^{-5}	8.87 x 10^{-4}	846

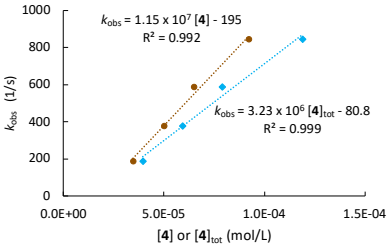

k_2^{HC} = 8.27 x 10^6 L mol^{-1} s^{-1} for $[4]_{tot}$ **$k_2^{HC,mix}$ = 1.15 x 10^7 L mol^{-1} s^{-1}** for [4]

Determination of *N* and s_N parameter for **4a** in DCM at constant ionic strength of 1.0 mM

Electrophile	*E*	k_2^{HC} (M^{-1} s^{-1}) for $[4]_{tot}$	$k_2^{HC,mix}$ (M^{-1} s^{-1}) for [4]
5a	-10.04	1.23 x 10^6	1.69 x 10^6
5b	-9.45	3.04 x 10^6	4.19 x 10^6
5c	-8.76	8.27 x 10^6	1.15 x 10^7

N = 19.35 **s_N = 0.65** for $[4]_{tot}$

N = 19.63 **s_N = 0.65** for [4]

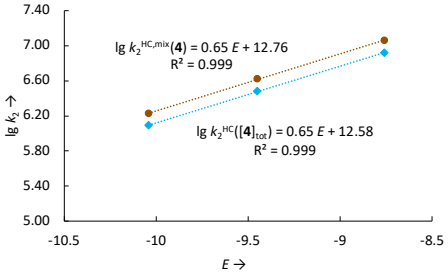

2.1.7.5 Kinetic Data of wide range measurements

The herein called wide range measurements employ the same principle as the benzhydrylium kinetics except for covering a much larger concentration range (1 x 10^{-5} to 4 x 10^{-3} M). The aim of these measurement was to illustrate the influence of ion pair association on the first-order reaction rate k_{obs} (s^{1}) with increasing concentration. The hereby potentially obtained second order rate constants k_2 (M^{-1} s^{-1}) are not included in the *N* and s_N parameter determination. The benzhydrylium salt $(lil)_2CH^+BF_4^-$ (**5a**) was used as electrophile at λ = 640 nm.

2.1.7.5.1 Wide range data at 20 °C

Reaction of **3a** with $(lil)_2CH^+BF_4^-$ in MeCN (stopped-flow, λ = 632 nm).

[5a] (mol L^{-1})	[3a] (mol L^{-1})	k_{obs} (s^{-1})
1.05 x 10^{-6}	1.02 x 10^{-5}	0.36
	2.04 x 10^{-5}	0.40
	4.07 x 10^{-5}	0.55
	6.11 x 10^{-5}	0.72
	8.15 x 10^{-5}	0.83
	1.02 x 10^{-4}	0.97
	2.04 x 10^{-4}	1.51
	4.07 x 10^{-4}	2.48
	5.91 x 10^{-4}	3.46
	7.94 x 10^{-4}	4.20
	9.98 x 10^{-4}	5.34
	2.00 x 10^{-3}	10.6
	4.07 x 10^{-3}	22.6

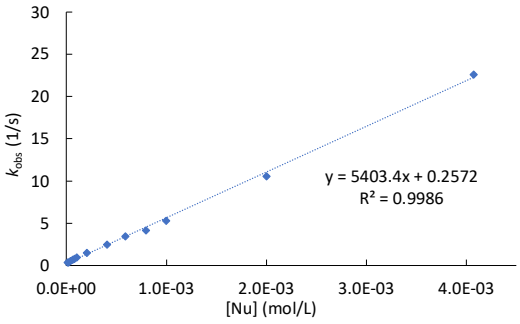

Reaction of **3a** with $(lil)_2CH^+BF_4^-$ in DCM (stopped-flow, λ = 640 nm), equilibrium constants for numerical simulation: K_{CAC} = 6.38 x 10^6 M^{-2} for **3a** (cationic sandwich model 3a).

[5a] (mol L^{-1})	[3a] (mol L^{-1})	[3] (mol L^{-1})	k_{obs} (s^{-1})
9.62 x 10^{-7}	1.01 x 10^{-5}	1.01 x 10^{-5}	18.0
	2.01 x 10^{-5}	2.01 x 10^{-5}	36.4
	4.02 x 10^{-5}	3.98 x 10^{-5}	74.1
	6.03 x 10^{-5}	5.90 x 10^{-5}	99.2
	8.04 x 10^{-5}	7.76 x 10^{-5}	118
	1.01 x 10^{-4}	9.59 x 10^{-5}	140
	2.01 x 10^{-4}	1.76 x 10^{-4}	197
	4.02 x 10^{-4}	3.09 x 10^{-4}	292
	6.03 x 10^{-4}	4.28 x 10^{-4}	362
	8.04 x 10^{-4}	5.40 x 10^{-4}	401
	1.01 x 10^{-3}	6.52 x 10^{-4}	420

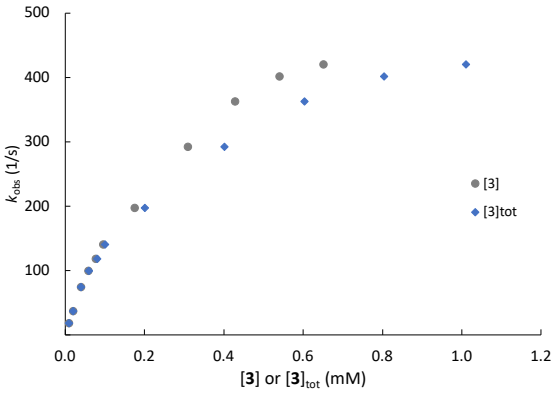

Reaction of **3a** with $(lil)_2CH^+BF_4^-$ in DCM (stopped-flow, λ = 640 nm), equilibrium constants for numerical simulation: α x K_{CAC} = 2.81 x 10^6 M^{-2} and β x K_{ACA} = 1.34 x 10^6 M^{-2} for **3a** (α/β = 0.44/0.21) (mixed sandwich association model 4).

[5a] (mol L^{-1})	[3a] (mol L^{-1})	[3] (mol L^{-1})	[3a3] (mol L^{-1})	k_{obs} (s^{-1})
9.62 x 10^{-7}	1.01 x 10^{-5}	1.01 x 10^{-5}	1.38 x 10^{-9}	18.0
	2.01 x 10^{-5}	2.01 x 10^{-5}	1.08 x 10^{-8}	36.4
	4.02 x 10^{-5}	3.99 x 10^{-5}	8.46 x 10^{-8}	74.1
	6.03 x 10^{-5}	5.92 x 10^{-5}	2.76 x 10^{-7}	99.2
	8.04 x 10^{-5}	7.78 x 10^{-5}	6.27 x 10^{-7}	118
	1.01 x 10^{-4}	9.62 x 10^{-5}	1.18 x 10^{-6}	140
	2.01 x 10^{-4}	1.74 x 10^{-4}	6.76 x 10^{-6}	197
	4.02 x 10^{-4}	2.88 x 10^{-4}	2.91 x 10^{-5}	292
	6.03 x 10^{-4}	3.73 x 10^{-4}	6.03 x 10^{-5}	362
	8.04 x 10^{-4}	4.42 x 10^{-4}	9.65 x 10^{-5}	401
	1.01 x 10^{-3}	5.02 x 10^{-4}	1.37 x 10^{-4}	420

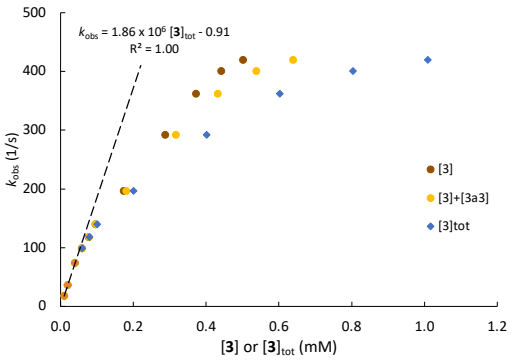

Reaction of **4a** with $(lil)_2CH^+BF_4^-$ in DCM (stopped-flow, λ = 640 nm), equilibrium constants for numerical simulation: K_{CAC} = 6.50 x 10^6 M^{-2} for **4a** (cationic sandwich model 3a).

[5a] (mol L^{-1})	[4a] (mol L^{-1})	[4] (mol L^{-1})	k_{obs} (s^{-1})
9.99 x 10^{-7}	1.01 x 10^{-5}	1.01 x 10^{-5}	50.6
	2.02 x 10^{-5}	2.02 x 10^{-5}	156
	4.05 x 10^{-5}	4.01 x 10^{-5}	291
	6.07 x 10^{-5}	5.94 x 10^{-5}	522
	8.09 x 10^{-5}	7.80 x 10^{-5}	587
	1.01 x 10^{-4}	9.59 x 10^{-5}	–

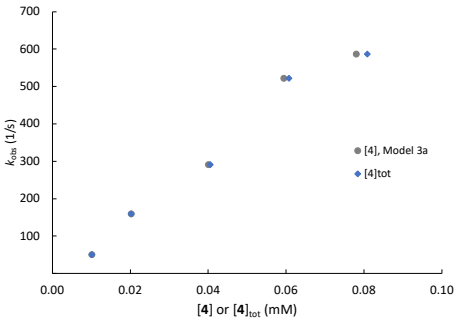

Reaction of **4a** with $(lil)_2CH^+BF_4^-$ in DCM (stopped-flow, λ = 640 nm), equilibrium constants for numerical simulation: α x K_{CAC} = 7.80 x 10^5 M^{-2} and β x K_{ACA} = 3.97 x 10^6 M^{-2} for **4a** (α/β = 0.12/0.61) (mixed sandwich association model 4).

[5a] (mol L^{-1})	[4a] (mol L^{-1})	[4] (mol L^{-1})	[4a4] (mol L^{-1})	k_{obs} (s^{-1})
9.99 x 10^{-7}	1.01 x 10^{-5}	1.01 x 10^{-5}	4.08 x 10^{-9}	50.6
	2.02 x 10^{-5}	2.02 x 10^{-5}	3.24 x 10^{-8}	156
	4.05 x 10^{-5}	4.01 x 10^{-5}	2.54 x 10^{-7}	291
	6.07 x 10^{-5}	5.94 x 10^{-5}	8.20 x 10^{-7}	522
	8.09 x 10^{-5}	7.80 x 10^{-5}	1.84 x 10^{-6}	587
	1.01 x 10^{-4}	9.59 x 10^{-5}	3.35 x 10^{-6}	–

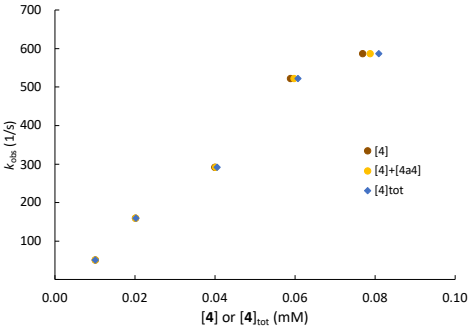

2.1.7.5.2 Wide range data of 3a at *I* = 1.0 mM at 20 °C (1:1 model for additive 6)

Reaction of **3a + 6** with $(lil)_2CH^+BF_4^-$ in DCM (stopped-flow, λ = 640 nm), equilibrium constants for numerical simulation: K_{CAC} = 6.38 x 10^6 M^{-2} for **3a**, K_{IP} = 1.01 x 10^7 M^{-2} for **6**.

[5a] (mol L^{-1})	[3a] (mol L^{-1})	[3] (mol L^{-1})	[6] (mol L^{-1})	k_{obs} (s^{-1})
1.18 x 10^{-6}	9.98 x 10^{-6}	2.98 x 10^{-6}	9.83 x 10^{-4}	1.91
	2.00 x 10^{-5}	6.05 x 10^{-6}	9.83 x 10^{-4}	4.34
	3.99 x 10^{-5}	1.25 x 10^{-5}	9.63 x 10^{-3}	12.0
	5.99 x 10^{-5}	1.93 x 10^{-5}	9.43 x 10^{-4}	20.1
	7.98 x 10^{-5}	2.66 x 10^{-5}	9.24 x 10^{-4}	29.2
	9.98 x 10^{-5}	3.43 x 10^{-5}	9.04 x 10^{-4}	36.5
	2.00 x 10^{-4}	7.77 x 10^{-5}	8.06 x 10^{-4}	58.6
	3.99 x 10^{-4}	1.93 x 10^{-4}	5.99 x 10^{-4}	153
	5.99 x 10^{-4}	3.31 x 10^{-4}	4.03 x 10^{-4}	225
	7.98 x 10^{-4}	4.84 x 10^{-4}	1.97 x 10^{-4}	328
	9.98 x 10^{-4}	6.45 x 10^{-4}	–	421

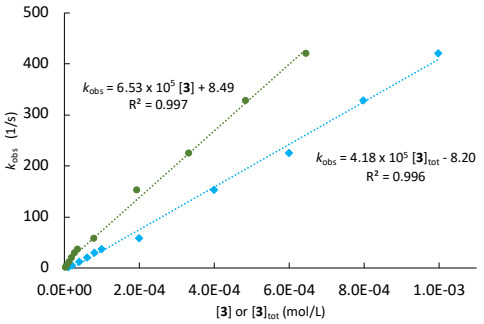

2.1.7.5.3 Wide range data of 3a at *I* = 1.0 mM at 20 °C (cationic sandwich model for additive 6)

Reaction of **3a + 6** with $(lil)_2CH^+BF_4^-$ in DCM (stopped-flow, λ = 640 nm), equilibrium constants for numerical simulation: K_{CAC} = 6.38 x 10^6 M^{-2} for **3a**, K_{CAC} = 7.05 x 10^6 M^{-2} for **6**.

[5a] (mol L^{-1})	[3a] (mol L^{-1})	[3] (mol L^{-1})	[6] (mol L^{-1})	k_{obs} (s^{-1})
1.18 x 10^{-6}	9.98 x 10^{-6}	6.63 x 10^{-6}	9.83 x 10^{-4}	1.91
	2.00 x 10^{-5}	1.33 x 10^{-5}	9.83 x 10^{-4}	4.34
	3.99 x 10^{-5}	2.65 x 10^{-5}	9.63 x 10^{-3}	12.0
	5.99 x 10^{-5}	3.98 x 10^{-5}	9.43 x 10^{-4}	20.1
	7.98 x 10^{-5}	5.30 x 10^{-5}	9.24 x 10^{-4}	29.2
	9.98 x 10^{-5}	6.62 x 10^{-5}	9.04 x 10^{-4}	36.5
	2.00 x 10^{-4}	1.32 x 10^{-4}	8.06 x 10^{-4}	58.6
	3.99 x 10^{-4}	2.62 x 10^{-4}	5.99 x 10^{-4}	153
	5.99 x 10^{-4}	3.92 x 10^{-4}	4.03 x 10^{-4}	225
	7.98 x 10^{-4}	5.19 x 10^{-4}	1.97 x 10^{-4}	328
	9.98 x 10^{-4}	6.46 x 10^{-4}	–	421

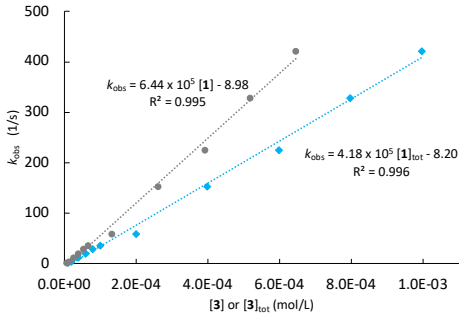

Reaction of **4a + 6** with $(lil)_2CH^+BF_4^-$ in DCM (stopped-flow, λ = 640 nm), equilibrium constants for numerical simulation: K_{CAC} = 6.50 x 10^6 M^{-2} for **4a**, K_{CAC} = 7.05 x 10^6 M^{-2} for **6**.

[5a] (mol L^{-1})	[4a] (mol L^{-1})	[4] (mol L^{-1})	[6] (mol L^{-1})	k_{obs} (s^{-1})
1.15 x 10^{-6}	9.93 x 10^{-6}	6.55 x 10^{-6}	9.90 x 10^{-4}	
	1.99 x 10^{-5}	1.31 x 10^{-5}	9.79 x 10^{-4}	1.09
	3.97 x 10^{-5}	2.62 x 10^{-5}	9.56 x 10^{-3}	27.1
	5.96 x 10^{-5}	3.93 x 10^{-5}	9.45 x 10^{-4}	48.7
	7.94 x 10^{-5}	5.23 x 10^{-5}	9.23 x 10^{-4}	63.4
	9.93 x 10^{-5}	6.54 x 10^{-5}	9.00 x 10^{-4}	100
	1.99 x 10^{-4}	1.31 x 10^{-4}	7.99 x 10^{-4}	306

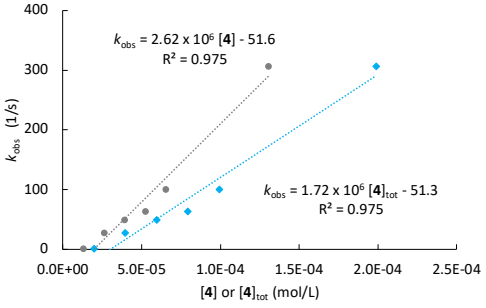

2.1.7.5.4 Wide range data of 3a at *I* = 1.0 mM at 20 °C (mixed sandwich model extension)

Reaction of **3a + 6** with $(lil)_2CH^+BF_4^-$ in DCM (stopped-flow, λ = 640 nm), equilibrium constants for numerical simulation: α x K_{CAC} = 2.81 x 10^6 M^{-2} and β x K_{ACA} = 1.34 x 10^6 M^{-2} for **3a** (α/β = 0.44/0.21), K_{CAC} = 7.05 x 10^6 M^{-2} for **6**.

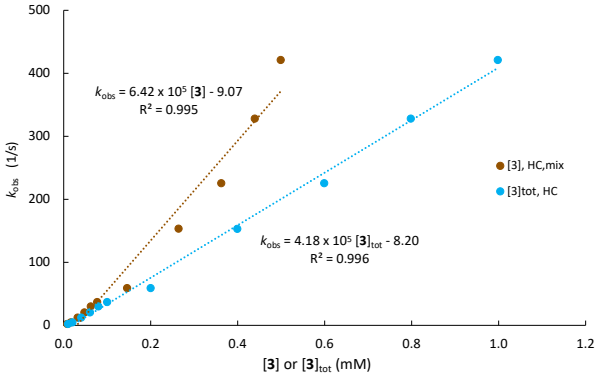

[5a] (mol L^{-1})	[3a] (mol L^{-1})	[3] (mol L^{-1})	[3a3] (mol L^{-1})	[6] (mol L^{-1})	k_{obs} (s^{-1})
1.18 x 10^{-6}	9.98 x 10^{-6}	8.12 x 10^{-6}	2.49 x 10^{-8}	9.83 x 10^{-4}	1.91
	2.00 x 10^{-5}	1.62 x 10^{-5}	9.91 x 10^{-8}	9.83 x 10^{-4}	4.34
	3.99 x 10^{-5}	3.19 x 10^{-5}	3.87 x 10^{-7}	9.63 x 10^{-3}	12.0
	5.99 x 10^{-5}	4.73 x 10^{-5}	8.58 x 10^{-7}	9.43 x 10^{-4}	20.1
	7.98 x 10^{-5}	6.23 x 10^{-5}	1.50 x 10^{-6}	9.24 x 10^{-4}	29.2
	9.98 x 10^{-5}	7.71 x 10^{-5}	2.30 x 10^{-6}	9.04 x 10^{-4}	36.5
	2.00 x 10^{-4}	1.46 x 10^{-4}	8.57 x 10^{-6}	8.06 x 10^{-4}	58.6
	3.99 x 10^{-4}	2.64 x 10^{-4}	2.98 x 10^{-5}	5.99 x 10^{-4}	153
	5.99 x 10^{-4}	3.62 x 10^{-4}	5.97 x 10^{-5}	4.03 x 10^{-4}	225
	7.98 x 10^{-4}	4.39 x 10^{-4}	9.54 x 10^{-5}	1.97 x 10^{-4}	328
	9.98 x 10^{-4}	4.99 x 10^{-4}	1.35 x 10^{-4}	–	421

Reaction of **4a + 6** with $(lil)_2CH^+BF_4^-$ in DCM (stopped-flow, λ = 640 nm), equilibrium constants for numerical simulation: α x K_{CAC} = 7.80 x 10^5 M^{-2} and β x K_{ACA} = 3.97 x 10^6 M^{-2} for **4a** (/β = 0.12/0.61), K_{CAC} = 7.05 x 10^6 M^{-2} for **6**.

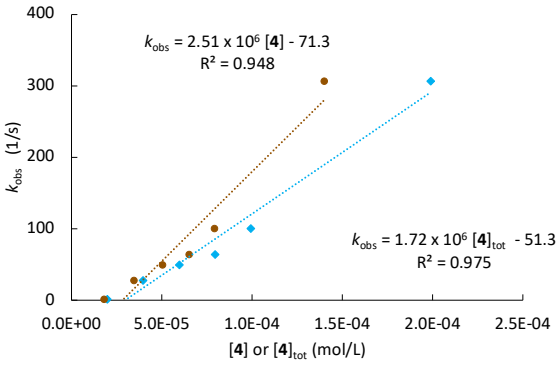

[5a] (mol L^{-1})	[4a] (mol L^{-1})	[4] (mol L^{-1})	[4a4] (mol L^{-1})	[6] (mol L^{-1})	k_{obs} (s^{-1})
1.15 x 10^{-6}	9.93 x 10^{-6}	9.17 x 10^{-6}	9.45 x 10^{-8}	9.90 x 10^{-4}	
	1.99 x 10^{-5}	1.80 x 10^{-5}	3.67 x 10^{-7}	9.79 x 10^{-4}	1.09
	3.97 x 10^{-5}	3.47 x 10^{-5}	1.37 x 10^{-6}	9.56 x 10^{-3}	27.1
	5.96 x 10^{-5}	5.05 x 10^{-5}	2.92 x 10^{-6}	9.45 x 10^{-4}	48.7
	7.94 x 10^{-5}	6.52 x 10^{-5}	4.93 x 10^{-6}	9.23 x 10^{-4}	63.4
	9.93 x 10^{-5}	7.92 x 10^{-5}	7.35 x 10^{-6}	9.00 x 10^{-4}	100
	1.99 x 10^{-4}	1.40 x 10^{-4}	2.41 x 10^{-5}	7.99 x 10^{-4}	306

2.1.8 Crystallographic Data

Tetraphenylphosphonium pyridin-4-yl((trifluoromethyl)sulfonyl)amide (**3a**)

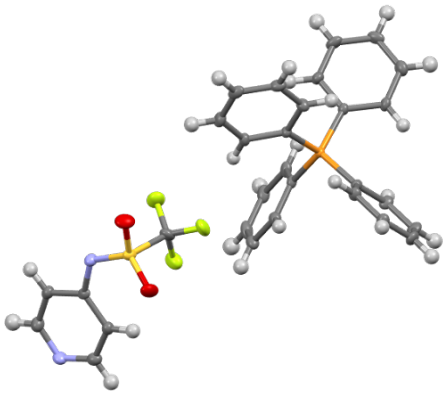

Table 2.24: [Table S28]. Crystallographic details for ion pair catalyst **3a**.

net formula	$C_{30}H_{24}F_3N_2O_2PS$
M_r/g mol^{-1}	564.54
crystal size/mm	0.100 × 0.050 × 0.040
T/K	102.(2)
radiation	MoKα
diffractometer	'Bruker D8 Venture TXS'
crystal system	orthorhombic
space group	'P n a 21'
a/Å	20.5906(10)
b/Å	34.3669(14)
c/Å	14.7169(6)
α/°	90
β/°	90
γ/°	90
V/Å^3	10414.2(8)
Z	16
calc. density/g cm^{-3}	1.440
μ/mm^{-1}	0.240
absorption correction	Multi-Scan
transmission factor range	0.97–0.99
refls. measured	183497
R_{int}	0.0575
mean σ(I)/I	0.0349
θ range	2.306–27.103
observed refls.	20396
x, y (weighting scheme)	0.0737, 5.0008
hydrogen refinement	constr
Flack parameter	−0.024(15)
refls in refinement	22927
parameters	1405
restraints	1
$R(F_{obs})$	0.0458
$R_w(F^2)$	0.1260
S	1.040
shift/error$_{max}$	0.001
max electron density/e Å^{-3}	0.894
min electron density/e Å^{-3}	−0.324

Tetraphenylphosphonium tetrafluoroborate (**6**)

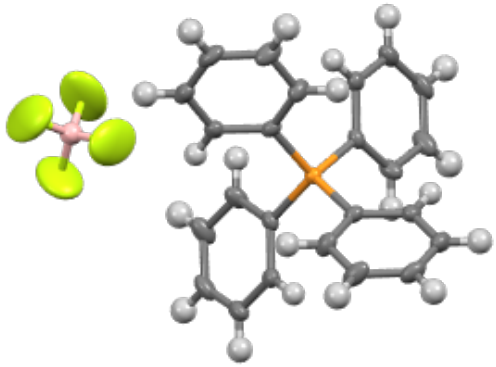

Table 2.25: [Table S29]. Crystallographic details for tetraphenylphosphonium tetrafluoroborate (**6**).

net formula	$C_{24}H_{20}BF_4P$
M_r/g mol^{-1}	426.18
crystal size/mm	0.100 × 0.080 × 0.060
T/K	173.(2)
radiation	MoKα
diffractometer	'Bruker D8 Venture TXS'
crystal system	tetragonal
space group	'I -4'
a/Å	12.0191(4)
b/Å	12.0191(4)
c/Å	6.8981(3)
α/°	90
β/°	90
γ/°	90
V/Å^3	996.49(8)
Z	2
calc. density/g cm^{-3}	1.420
μ/mm^{-1}	0.183
absorption correction	Multi-Scan
transmission factor range	0.97–0.99
refls. measured	8833
R_{int}	0.0318
mean σ(*I*)/*I*	0.0179
θ range	3.390–27.094
observed refls.	1070
x, y (weighting scheme)	0.0470, 0.7488
hydrogen refinement	constr
Flack parameter	−0.04(3)
refls in refinement	1098
parameters	73
restraints	0
$R(F_{obs})$	0.0345
$R_w(F^2)$	0.0919
S	1.106
shift/error$_{max}$	0.001
max electron density/e Å^{-3}	0.432
min electron density/e Å^{-3}	−0.189

The X-ray crystal structure of compound **6** is consistent with previously reported X-ray crystal data by Chen *et al*.[20]

2.1.9 NMR Spectra of Newly Synthesized Compounds

Tetraphenylphosphonium pyridin-4-yl((trifluoromethyl)sulfonyl)amide (**3a**)

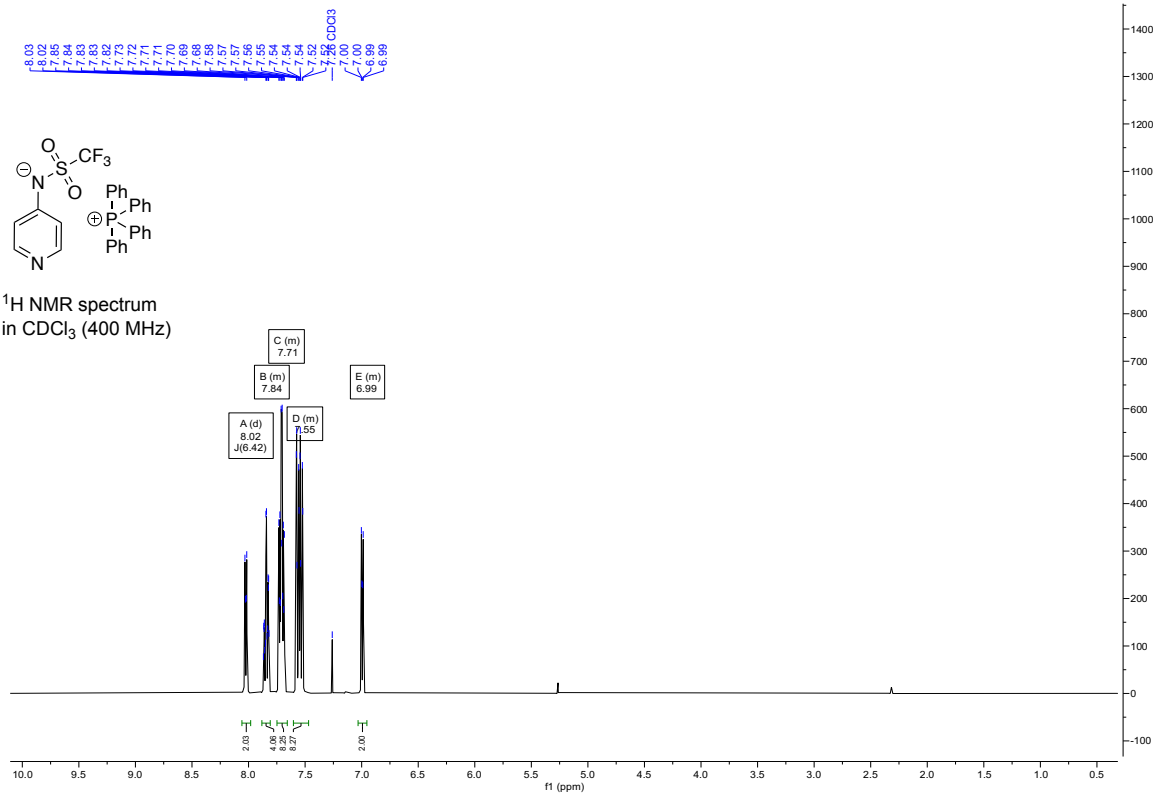

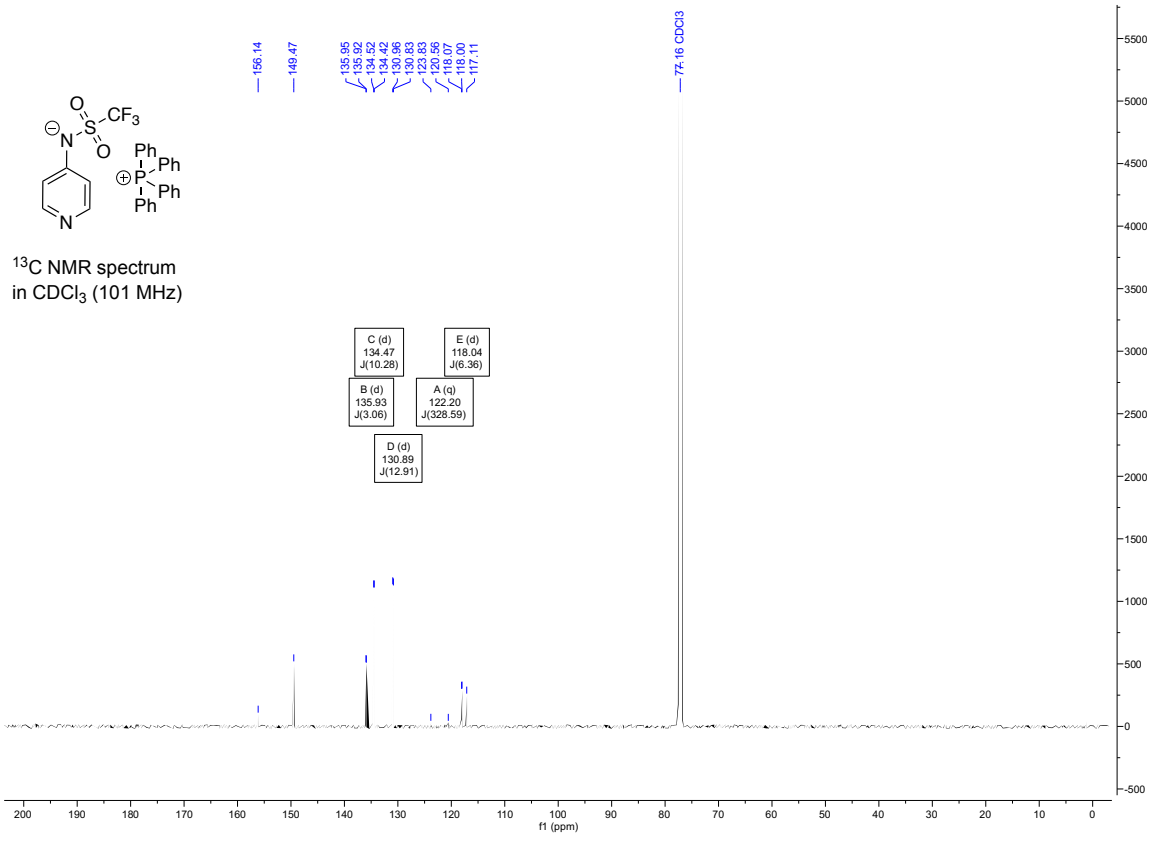

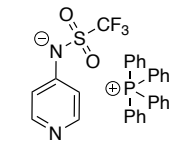

^{19}F NMR spectrum
in $CDCl_3$ (377 MHz)

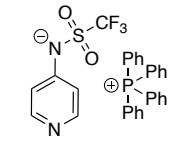

^{31}P NMR spectrum
in $CDCl_3$ (162 MHz)

Tetraphenylphosphonium tetrafluoroborate (**6**)

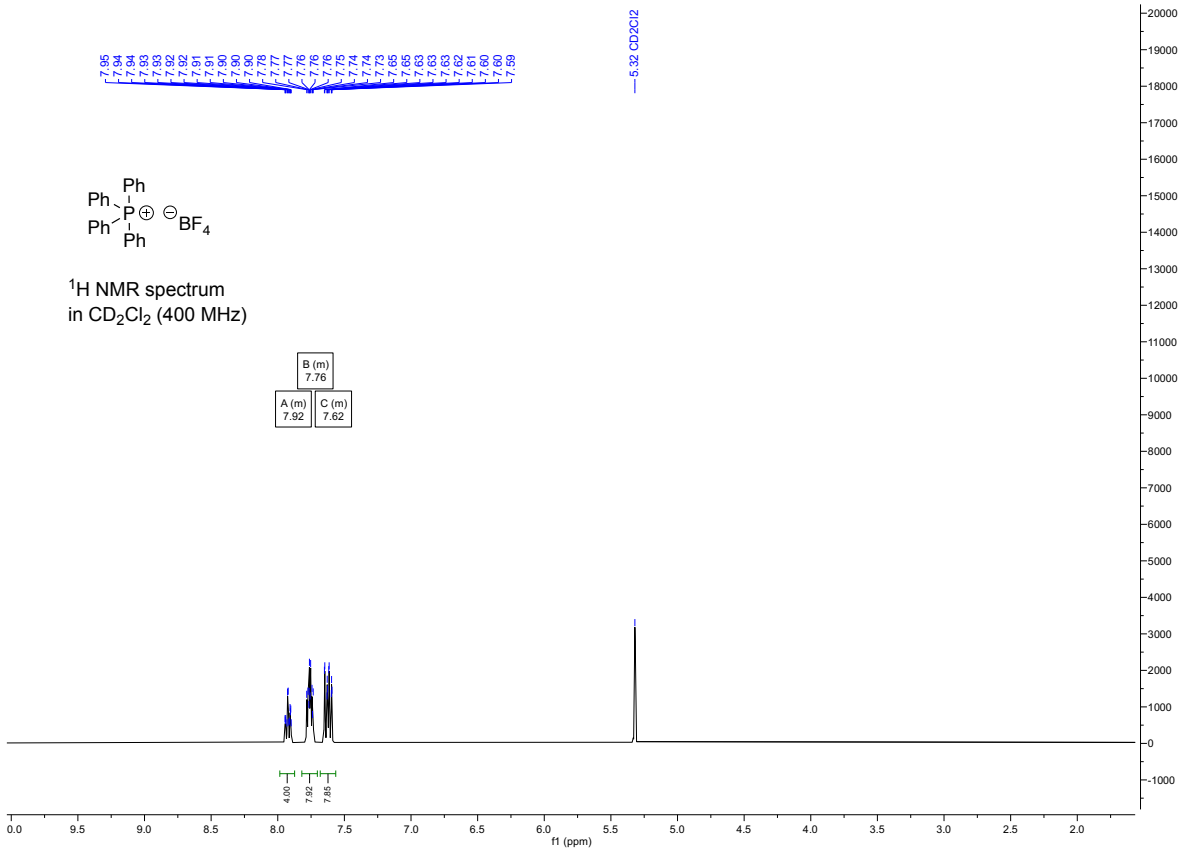

^{1}H NMR spectrum
in CD_2Cl_2 (400 MHz)

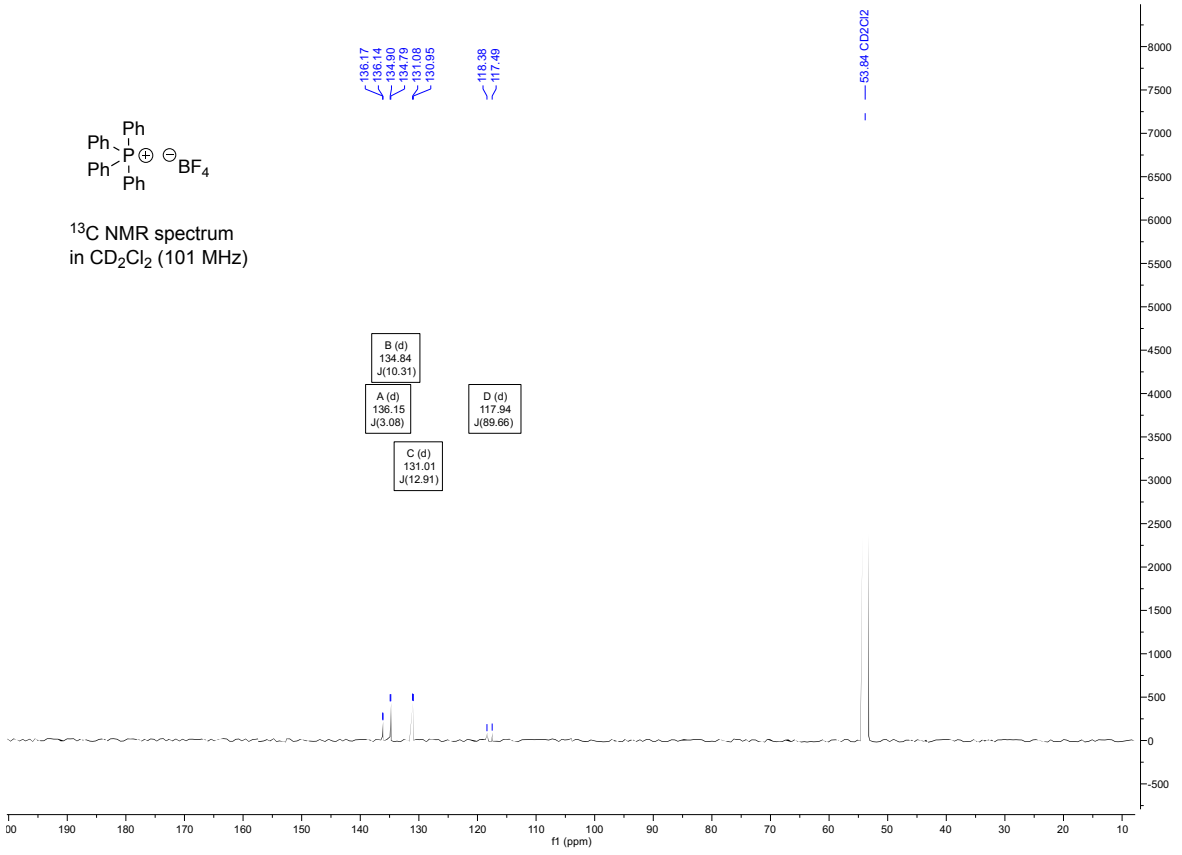

^{13}C NMR spectrum
in CD_2Cl_2 (101 MHz)

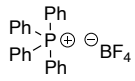

^{19}F NMR spectrum
in CD_2Cl_2 (377 MHz)

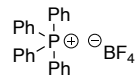

^{31}P NMR spectrum
in CD_2Cl_2 (162 MHz)

2.1.10 Computational Study

2.1.10.1. General information

All substrate structures were optimized with the B3LYP-D3 hybrid functional[21–23] with the 6-31+G(d) basis set.[24] Solvent effects for dichloromethane and acetonitrile have been calculated with the SMD continuum solvation model.[25] This combination has worked well in previous studies of charge-separated intermediates.[26–29] Frequency and single point calculations were performed at the same level of theory. Thermochemical correction to 198.15 K has been applied to all found minima from unscaled vibrational frequencies obtained at the same level of theory. To lessen the impact of low-lying frequencies of large systems on entropy and enthalpy in an unpredictable manner, a free-rotor approximation for entropy as proposed by Grimme[30] and a quasi-harmonic treatment with a cutoff value of 100 cm^{-1} using Goodvibes[31] was applied. Free energies in solution have been corrected to the reference state of 1.0 mol L^{-1} at 298.15 K by adding 7.925 kJ mol^{-1} to the free energies ($G_{298,qh,corr}$). All reported calculations were done with Gaussian 16, Revision A.03[32] and B.01[33].

The conformational search was performed with Maestro[34]. For ion pair systems, a set of 150 starting points was obtained by using the stochastic kick procedure invented by Saunders[35] and further developed by Sakic[36]. At a time, a set of 50 starting points was generated by a combination of the best and the second-best conformer of the prior separately optimized anion and cation. The last 50 starting points were obtained from the combination of the best anion conformer with the third best cation conformer. The following kick settings were used: Distance parameter: 3 Å, Minimal Distance 1.5 Å, Number of Fragments: 1, Number of Files: 50.

Starting points for the conformers of the ion pair systems were obtained from Julian Helberg. Conformers for the new systems with tetraphenyl phosphonium as cation (**3a**) were obtained by manual modification of the corresponding triphenyl methyl phosphonium containing systems, initially calculated by Helberg[37], whereby the methyl group was replaced by a phenyl group.

Starting points for the conformers of the sandwich cation and sandwich anion were obtained by sorting the optimized structures of the respective ion pair according to the total energy. The best six conformers were chosen and in combination with the best cation **a** conformer the stochastic kick procedure invented by Saunders[35] and further developed by Sakic[36] was applied to generate 60 new substrate structures in total. The following kick settings were used: Distance parameter: 3 Å, Minimal Distance 1.5 Å, Number of Fragments: 1, Number of Files: 10.

The goal in calculating the respective sandwich conformers was to obtain the volumes based on the van der Waals cavities employed in the SMD continuum solvation model at the SMD(DCM)/B3LYP-D3/6-31+G(d) level of theory for the calculation of the volumes of ions based on the simulated concentrations in each respective conductivity model to compare the DOSY results with the results of the numerical simulations. Due to the heavy nature of the calculated systems (between 81 – 119 atoms) the less costly r^2SCAN-3c developed by Grimme[38] with Orca 5.0.3[39] was used for pre-optimizations, followed by single point calculations at the SMD(DCM)/B3LYP-D3/6-31+G(d) level of theory with Gaussian 16, Revision C.01[40].

2.1.10.2 System **3a** – computational information

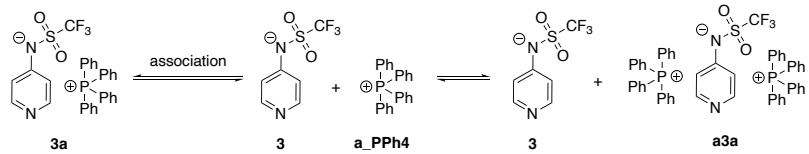

Figure 2.24: [Figure S30]. Ion pair formation of **3a** and the single ions**.**

The Boltzmann-averaged free reaction energy of the ion pairing of **3a** amounts to $\Delta G_{qh,298,corr}$ = +1.6 kJ mol^{-1} in DCM solution. Focusing only on the best conformers of the reactants and product the free reaction energy of the ion pairing of **3a** changes to $\Delta G_{qh,298,corr}$ = +1.1 kJ mol^{-1} in DCM solution. This result is mainly due to solvation effects since the gas phase free energy of the ion pairing amounts to $\Delta G_{qh,298}$ = -218.5 kJ mol^{-1}. In addition, we note that the contribution of the D3-dispersion correction amounts to ΔE_{disp} = -57.7 kJ mol^{-1} for the free energy in the DCM solution and in the gas phase. The blue marked cells show the Boltzmann-averaged values.

According to $\Delta G_{qh,298,corr}$ = -RT ln*K* and assuming R = 8.314 J K^{-1} mol^{-1} and T = 298.15 K, the respective equilibrium constant amounts to *K*(**3a**, DCM) = 0.63 for the best conformer of **3a** and to *K*(**3a**, DCM) = 0.52 for the Boltzmann-averaged free reaction energy. In this case the equilibrium constant K corresponds to the concentration of the reactants and products in the following way: K = [**3a**]/[**3**] [**a_PPh4**] = [**3a**]/[**3**]^2.

Table 2.26: [Table S30]. Energies for all systems shown in Figure 2.24.

System	E_{tot} SMD(DCM)/ B3LYP-D3/ 6-31+G(d)	H_{298} SMD(DCM)/ B3LYP-D3/ 6-31+G(d)	$G_{qh,298}$ SMD(DCM)/ B3LYP-D3/ 6-31+G(d)	$G_{qh,298,corr}$ SMD(DCM)/ B3LYP-D3/ 6-31+G(d)	Cavity Volume (Å^3)	Relative Population Parameter based on $G_{qh,298}$
3						
an3_001	**-1188.8384606**	**-1188.7186926**	**-1188.769809**	**-1188.766790**	**215**	0.91
an3_002	-1188.8357192	-1188.7160622	-1188.7673382	-1188.7643197	214	0.09
			-1188.7693051	**-1188.7662866**	**215**	
a_PPh4						
PPh4_003a	-1267.9099858	**-1267.5207058**	**-1267.5885298**	**-1267.5855113**	**360**	0.46
PPh4_001	-1267.9100736	-1267.5203936	-1267.5881566	-1267.5851381	364	0.31
PPh4_002f	**-1267.9100864**	-1267.5202704	-1267.5878314	-1267.5848129	362	0.22
			-1267.5882580	**-1267.5852395**	**362**	
a3a						
sw_a3a_010	**-3724.703838**	**-3723.800207**	**-3723.937041**	**-3723.934022**	**923**	0.53

sw_a3a_005	-3724.703051	-3723.799441	-3723.936260	-3723.933242	924	0.23
sw_a3a_org_015	-3724.702257	-3723.798129	-3723.933960	-3723.930942	928	0.02
sw_a3a_025a	-3724.701993	-3723.797917	-3723.934093	-3723.931075	930	0.02
sw_a3a_org_014	-3724.701889	-3723.798305	-3723.934938	-3723.931919	927	0.06
sw_a3a_024	-3724.701649	-3723.797640	-3723.934056	-3723.931037	929	0.02
sw_a3a_org_040	-3724.701627	-3723.797598	-3723.933697	-3723.930679	927	0.02
sw_a3a_014a	-3724.701442	-3723.798070	-3723.935298	-3723.932279	928	0.08
sw_a3a_org_012	-3724.700803	-3723.796599	-3723.933000	-3723.929982	927	0.01
sw_a3a_org_026a	-3724.699820	-3723.796143	-3723.932959	-3723.929941	924	0.01
sw_a3a_org_010	-3724.699491	-3723.795677	-3723.930122	-3723.927104	929	0.00
sw_a3a_021a	-3724.699216	-3723.795440	-3723.931151	-3723.928132	927	0.00
sw_a3a_016	-3724.698871	-3723.795018	-3723.931547	-3723.928529	930	0.00
sw_a3a_001	-3724.698495	-3723.794062	-3723.930329	-3723.927311	928	0.00
sw_a3a_org_027	-3724.697508	-3723.793778	-3723.930638	-3723.927619	928	0.00
sw_a3a_org_009a	-3724.697404	-3723.793943	-3723.931035	-3723.928016	925	0.00
sw_a3a_011	-3724.696265	-3723.793325	-3723.928885	-3723.925866	928	0.00
sw_a3a_007	-3724.696019	-3723.793061	-3723.930496	-3723.927478	928	0.00
sw_a3a_org_016	-3724.696018	-3723.792326	-3723.929178	-3723.926160	930	0.00
			-3723.936250	**-3723.933231**	**925**	
3a[b]						
cat3a_008	-2456.770628	**-2456.259420**	**-2456.354582**	**-2456.351563**	**570**	0.09
cat3a_002	-2456.770669	-2456.259399	-2456.354514	-2456.351496	571	0.08
cat3a_018	**-2456.770818**	-2456.259384	-2456.354496	-2456.351478	570	0.08
cat3a_029	-2456.770644	-2456.259350	-2456.354385	-2456.351367	571	0.07
cat3a_033	-2456.770628	-2456.259315	-2456.354345	-2456.351327	571	0.07
cat3a_036	-2456.770661	-2456.259254	-2456.354273	-2456.351255	570	0.06
cat3a_023	-2456.770337	-2456.258979	-2456.354117	-2456.351099	571	0.05
cat3a_003p	-2456.770003	-2456.258866	-2456.354031	-2456.351012	571	0.05
cat3a_003m	-2456.770027	-2456.258808	-2456.353985	-2456.350967	570	0.05
cat3a_035	-2456.769988	-2456.258756	-2456.353923	-2456.350905	570	0.04
cat3a_013	-2456.769688	-2456.258611	-2456.353788	-2456.350770	570	0.04
cat3a_010	-2456.769703	-2456.258506	-2456.353635	-2456.350617	570	0.03
cat3a_016	-2456.769943	-2456.258424	-2456.353559	-2456.350540	571	0.03
cat3a_005	-2456.769461	-2456.258282	-2456.353405	-2456.350387	566	0.02
cat3a_004a	-2456.769364	-2456.258138	-2456.353293	-2456.350275	570	0.02
cat3a_021a	-2456.769198	-2456.258025	-2456.353238	-2456.350219	571	0.03
cat3a_026b	-2456.770013	-2456.258268	-2456.353138	-2456.350119	572	0.02
cat3a_038	-2456.769095	-2456.257968	-2456.353103	-2456.350084	569	0.02
cat3a_027a	-2456.769251	-2456.257914	-2456.353035	-2456.350016	572	0.02

cat3a_006	-2456.769635	-2456.258078	-2456.352947	-2456.349928	569	0.02
all			**-2456.353922**	**-2456.350904**	**570**	
ΔE	-58.47	-52.57	+9.06	+1.14		
all			+9.56	+1.63		

Table 2.27: [Table S31]. Energies of the best conformer for all systems shown in Figure 2.24.at different levels of theory.

System	E_{tot}[a] B3LYP-D3/ 6-31+G(d)	$G_{qh,298}$[a] B3LYP-D3/ 6-31+G(d)	E_{tot}[a] B3LYP/ 6-31+G(d)	$G_{qh,298}$[a] B3LYP/ 6-31+G(d)	E_{tot}[a] SMD(DCM)/ B3LYP/ 6-31+G(d)	$G_{qh,298,corr}$[a] SMD(DCM)/ B3LYP/ 6-31+G(d)
3						
an3_001	**-1188.770301**	**-1188.701344**	**-1188.753230**	**-1188.684273**	**-1188.821390**	**-1188.7494140**
a_PPh4						
PPh4_003a	**-1267.828115**	**-1267.506659**	**-1267.778739**	**-1267.457283**	**-1267.860609**	**-1267.5361348**
a3a						
sw_a3a_010	**-3724.586374**	**-3723.819577**	**-3724.415638**	**-3723.648841**	**-3724.533101**	**-3723.7632859**
cat3a						
cat3a_008	**-2456.707283**	**-2456.291237**	**-2456.618859**	**-2456.202813**	**-2456.682204**	**-2456.2631398**
ΔE(3a, 3, a)	-285.83	-218.53	-228.13	-160.83	-0.54	+58.83

[a] using geometries optimized at SMD(DCM)/B3LYP-D3/6-31+G(d) level.

Table 2.28: [Table S32]. Charge of system **3a** and selected structural data of the best conformer and the crystal structure of system **3a**.

System	Charge SMD(DCM)/ B3LYP-D3/ 6-31+G(d)	Charge B3LYP-D3/ 6-31+G(d)	D_1 (pm) N_{py} - H_{cat}	D_2 (pm) N_{amid} - H_{cat}	D_3 (pm) O_{anion} - H_{cation}
3					
an3_001	-1.0000	-1.0000			
a_PPh4					

PPh4_003a	+1.0000	+1.0000			
cat3a					
cat3a_008	-0.9932 (Anion) +0.9932 (Cation)	-0.9445 (Anion) +0.9445 (Cation)	268.43 (α-H)	332.43 (β-H)	242.49 (α-H)

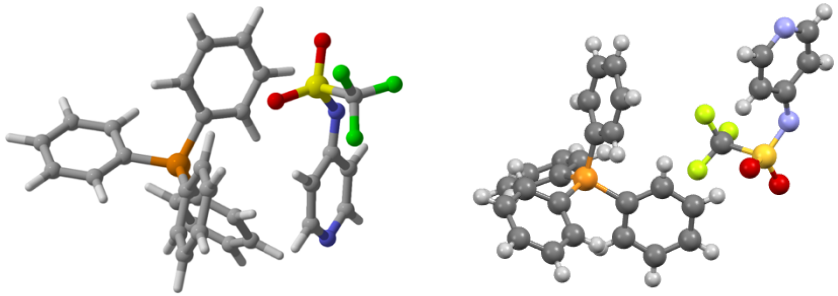

Figure 2.25: [Figure S31]. left: energetically best conformer of ion pair **3a** (SMD(DCM)/ B3LYP-D3/6-31+G(d) level of theory). Right: crystal structure of one ion pair **3a**.

Table 2.29: [Table S33]. Molecular volume (in Å^3) of cation PPh_4^+ cation (**a**) calculated with different theoretical approaches[d].

System	SMD(DCM)/ B3LYP-D3/ 6-31+G(d) (SMD volume)[a]	SMD(DCM)/ M06-2X/ cc-pVDZ (SMD volume)[a]	SMD(DCM)/ M06-2X/ cc-pVDZ (SMD volume)[b]	SMD(DCM)/ B3LYP-D3/ 6-31+G(d) (MC volume)[a]	M06-2X/ cc-pVDZ (MC volume)[a]	M06-2X/ cc-pVDZ (MC volume)[c]
Gaussian 16, Rev. C.02						
PPh4_002f	**362.0**	362.0	360.5	440.3 (2974.9 Bohr^3)	406.5 (2746.7 Bohr^3)	444.5 (3003.1 Bohr^3)
ORCA Rev. 5.0.2						
PPh4_002f			356.2 (2406.9 Bohr^3)			

[a] using geometries optimized at SMD(DCM)/B3LYP-D3/6-31+G(d) level. [b] using geometries optimized at SMD(DCM)/M06-2X/cc-pVDZ level. [c] using geometries optimized at M06-2X/cc-pVDZ level. [d] A conversion factor of vol(Å^3) = 0.148 vol(Bohr^3) has been used.

Table 2.30: [Table S34]. Molecular volume (in Å^3) of pyridinamide anion **3** calculated with different theoretical approaches[c].

System	SMD(DCM)/ B3LYP-D3/ 6-31+G(d) (SMD volume)[a]	SMD(DCM)/ M06-2X/ cc-pVDZ (SMD volume)[a]	SMD(DCM)/ M06-2X/ cc-pVDZ (SMD volume)[b]	SMD(DCM)/ B3LYP-D3/ 6-31+G(d) (MC volume)[a]	M06-2X/ cc-pVDZ (MC volume)[a]	M06-2X/ cc-pVDZ (MC volume)
Gaussian 16, Rev. C.02						
an1_001 an1_003 an1_004 an1_005	**214.6**	214.6	212.7			
an1_002	214.2					
ORCA Rev. 5.0.2						
an1_006			211.8 (Å^3) (1431.3 Bohr^3)			

[a] using geometries optimized at SMD(DCM)/B3LYP-D3/6-31+G(d) level. [b] using geometries optimized at SMD(DCM)/M06-2X/cc-pVDZ level. [c] A conversion factor of vol(Å^3) = 0.148 vol(Bohr^3) has been used.

2.1.10.3 System **4a** – computational information

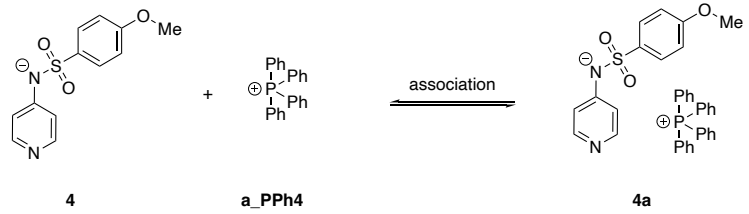

Figure 2.26: [Figure S32]. Ion pair formation of **4a** and the single ions.

The Boltzmann-averaged free reaction energy of the ion pairing of **4a** amounts to $\Delta G_{qh,298,corr}$ = -4.3 kJ mol^{-1} in DCM solution. Focusing only on the best conformers of the reactants and product the free reaction energy of the ion pairing of **4a** changes to $\Delta G_{qh,298,corr}$ = -6.7 kJ mol^{-1} in DCM solution. This result is mainly due to solvation effects since the gas phase free energy of the ion pairing amounts to $\Delta G_{qh,298}$ = -227.3 kJ mol^{-1}. In addition, we note that the contribution of the D3-

dispersion correction amounts to ΔE_{disp} = +136.6 kJ mol^{-1} for the free energy in the DCM solution and in the gas phase. The blue marked cells show the Boltzmann-averaged values.

According to $\Delta G_{qh,298,corr}$ = -RT lnK and assuming R = 8.314 J K^{-1} mol^{-1} and T = 298.15 K, the respective equilibrium constant amounts to *K*(**4a**, DCM) = +15.0 for the best conformer of **4a** and to *K*(**4a**, DCM) = +5.6 for the Boltzmann-averaged free reaction energy. In this case the equilibrium constant K corresponds to the concentration of the reactants and products in the following way: K = [**4a**]/[**4**] [**a_PPh4**] = [**4a**]/[**4**]^2.

Table 2.31: [Table S35]. Energies for all systems shown in Figure 2.26.

System	E_{tot} SMD(DCM)/ B3LYP-D3/ 6-31+G(d)	H_{298} SMD(DCM)/ B3LYP-D3/ 6-31+G(d)	$G_{qh,298}$ SMD(DCM)/ B3LYP-D3/ 6-31+G(d)	$G_{qh,298,corr}$ SMD(DCM)/ B3LYP-D3/ 6-31+G(d)	Cavity Volume (Å^3)	Relative Population Parameter based on $G_{qh,298}$
4						
an4_003	**-1197.397984**	**-1197.165232**	**-1197.223213**	**-1197.220195**	**285**	0.50
an4_002	-1197.397861	-1197.165102	-1197.223086	-1197.220068	285	0.44
an4_001	-1197.395672	-1197.163018	-1197.221274	-1197.218256	285	0.06
			-1197.223034	**-1197.220015**	**285**	
a_PPh4						
PPh4_003a	-1267.9099858	**-1267.5207058**	**-1267.5885298**	**-1267.5855113**	**360**	0.46
PPh4_001	-1267.9100736	-1267.5203936	-1267.5881566	-1267.5851381	364	0.31
PPh4_002f	**-1267.9100864**	-1267.5202704	-1267.5878314	-1267.5848129	362	0.22
			-1267.588258	**-1267.585239**	**362**	
cat4a[b]						
cat4a_050_dcm	**-2465.334938**	**-2464.710187**	**-2464.811281**	**-2464.808262**	**642**	0.21
cat4a_030_dcm	-2465.334896	-2464.710055	-2464.811095	-2464.808077	642	0.17
cat4a_025_dcm	-2465.333350	-2464.708548	-2464.809594	-2464.806575	646	0.03
cat4a_037_dcm	-2465.333341	-2464.708434	-2464.809435	-2464.806416	640	0.03
cat4a_108_dcm	-2465.333336	-2464.708800	-2464.810174	-2464.807155	642	0.06
cat4a_026_dcm	-2465.333194	-2464.708774	-2464.810286	-2464.807268	640	0.07
cat4a_055_dcm	-2465.332897	-2464.708336	-2464.809530	-2464.806512	640	0.03
cat4a_047_dcm	-2465.332521	-2464.708173	-2464.809641	-2464.806623	643	0.04
cat4a_018_dcm	-2465.332388	-2464.708158	-2464.809636	-2464.806617	641	0.04
cat4a_105_dcm	-2465.332334	-2464.708102	-2464.809786	-2464.806767	642	0.04
cat4a_100p_dcm	-2465.332005	-2464.707868	-2464.809694	-2464.806676	641	0.04
cat4a_032_dcm	-2465.331988	-2464.707080	-2464.808050	-2464.805031	638	0.01
cat4a_063_dcm	-2465.331873	-2464.707386	-2464.808686	-2464.805668	637	0.01

cat4a_042_dcm	-2465.331767	-2464.707018	-2464.808010	-2464.804991	636	0.01
cat4a_002_dcm	-2465.331657	-2464.707287	-2464.808608	-2464.805589	636	0.01
cat4a_089_dcm	-2465.331606	-2464.708112	-2464.808197	-2464.805178	640	0.01
cat4a_054_dcm	-2465.331512	-2464.707211	-2464.808728	-2464.805709	638	0.01
cat4a_004_dcm	-2465.331365	-2464.706715	-2464.807939	-2464.804921	636	0.01
cat4a_024_dcm	-2465.331340	-2464.706870	-2464.808260	-2464.805242	640	0.01
cat4a_051_dcm	-2465.331046	-2464.706547	-2464.807769	-2464.804751	641	0.01
all			**-2464.809896**	**-2464.806877**	**641**	
ΔE	-70.80	-63.67	+1.21	-6.71	-299.34	-227.32
all			+3.67	-4.26		

[a] using geometries optimized at SMD(DCM)/B3LYP-D3/6-31+G(d) level. [b] best 20 conformers according to E_{tot} at SMD(DCM)/B3LYP-D3/6-31+G(d) level of theory.

Table 2.32: [Table S36]. Energies of the best conformer for all systems shown in Figure 2.26 at different levels of theory.

System	E_{tot}[a] B3LYP-D3/ 6-31+G(d)	$G_{qh,298}$[a] B3LYP-D3/ 6-31+G(d)	E_{tot}[a] B3LYP/ 6-31+G(d)	$G_{qh,298}$[a] B3LYP/ 6-31+G(d)	E_{tot}[a] SMD(DCM)/ B3LYP/ 6-31+G(d)	$G_{qh,298,corr}$[a] SMD(DCM)/ B3LYP/ 6-31+G(d)
4						
an4_003	**-1197.312402**	**-1197.137631**	**-1197.368222**	**-1197.193451**	**-1197.282640**	**-1197.104850**
a_PPh4						
PPh4_003a	**-1267.828115**	**-1267.506659**	**-1267.778739**	**-1267.457283**	**-1267.860609**	**-1267.5361348**
cat4a						
cat4a_050	**-2465.254530**	**-2464.730873**	**-2465.141852**	**-2464.618195**	**-2465.222260**	**-2464.6955847**
ΔE(4a, 4, a)	-299.34	-227.32	+13.41	+85.43	-207.44	-143.35

[a] using geometries optimized at SMD(DCM)/B3LYP-D3/6-31+G(d) level.

Table 2.33: [Table S37]. Charge of system **4a** and selected structural data of the best conformer and the crystal structure of system **4a**.

System	Charge SMD(DCM)/ B3LYP-D3/ 6-31+G(d)	Charge B3LYP-D3/ 6-31+G(d)	D_1 (pm) N_{py} - H_{cat}	D_2 (pm) N_{amid} - H_{cat}	D_3 (pm) O_{anion} - H_{cation}
4					
an4_003	-1.0000	-1.0000			
a_PPh4					
PPh4_003a	+1.0000	+1.0000			
4a					
cat4a_050	-0.7949 (Anion) +0.7949 (Cation)	-0.6926 (Anion) +0.6926 (Cation)	292.50 (α-H)	270.23 (α-H)	280.83 (β-H)

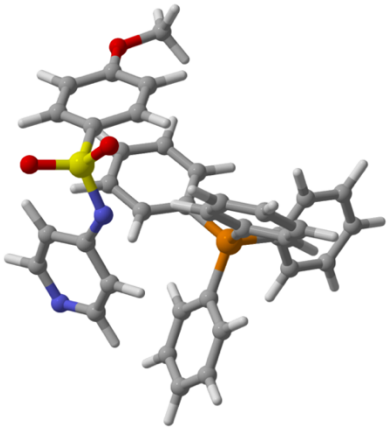

Figure 2.27: [Figure S33]. Structure of conformer cat**4a**_050 calculated at SMD(DCM)/ B3LYP-D3/6-31+G(d) level of theory.

2.1.10.4 System PPh_4BF_4 (**6**) – computational information

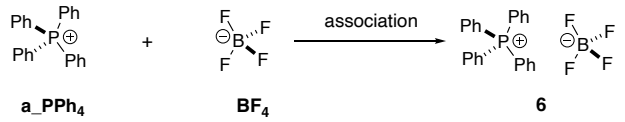

Figure 2.28: [Figure S34]. Ion Pair Formation of salt **6** and the single ions.

The Boltzmann-averaged free reaction energy of the ion pairing of **6** amounts to $\Delta G_{qh,298,corr}$ = +11.1 kJ mol^{-1} in DCM solution. Focusing only on the best conformers of the reactants and product the free reaction energy of the ion pairing of **6** changes to $\Delta G_{qh,298,corr}$ = +10.6 kJ mol^{-1} in DCM solution. The blue marked cells show the Boltzmann-averaged values.

According to $\Delta G_{qh,298,corr}$ = -RT ln*K* and assuming R = 8.314 J K^{-1} mol^{-1} and T = 298.15 K, the respective equilibrium constant amounts to *K*(**6**, DCM) = 0.014 for the best conformer of **6** and to *K*(**6**, DCM) = 0.011 for the Boltzmann-averaged free reaction energy. In this case the equilibrium constant *K* corresponds to the concentration of the reactants and products in the following way: *K* = [**6**]/[**BF_4**] [**a_PPh4**] = [**6**]/[**BF_4**]^2.

Table 2.34: [Table S38]. Energies for all systems shown in Figure 2.28.

System	E_{tot} SMD(DCM)/ B3LYP-D3/ 6-31+G(d)	H_{298} SMD(DCM)/ B3LYP-D3/ 6-31+G(d)	$G_{qh,298}$ SMD(DCM)/ B3LYP-D3/ 6-31+G(d)	$G_{qh,298,corr}$ SMD(DCM)/ B3LYP-D3/ 6-31+G(d)	Cavity Volume (Å^3)	Relative Population Parameter based on $G_{qh,298}$
BF_4						
borate_001_dcm	**-424.6525330**	**-424.6336440**	**-424.6644660**	**-424.6614475**	**69.7**	1.00
			-424.6644660	**-424.6614475**	**69.7**	
a_PPh4						
PPh4_003a	-1267.9099858	**-1267.5207058**	-**1267.5885298**	**-1267.5855113**	**360**	0.46
PPh4_001	-1267.9100736	-1267.5203936	-1267.5881566	-1267.5851381	364	0.31
PPh4_002f	**-1267.9100864**	-1267.5202704	-1267.5878314	-1267.5848129	362	0.22
			-1267.5882580	**-1267.5852395**	**362**	
6[a]						
add6_034_dcm	**-1692.5752397**	**-1692.1650487**	**-1692.2459257**	**-1692.2429072**	**430**	0.06
add6_146_dcm	-1692.5752471	-1692.1650451	-1692.2459061	-1692.2428876	430	0.05
add6_012_dcm	-1692.5752413	-1692.1650293	-1692.2459003	-1692.2428818	430	0.05
add6_089_dcm	-1692.5752306	-1692.1649816	-1692.2458436	-1692.2428251	430	0.05
add6_140_dcm	-1692.5752321	-1692.1649631	-1692.2458121	-1692.2427936	430	0.05
add6_006_dcm	-1692.5752514	-1692.1649734	-1692.2458104	-1692.2427919	430	0.05

add6_134_dcm	-1692.5750318	-1692.1648098	-1692.2457278	-1692.2427093	429	0.05
add6_042_dcm	-1692.5752256	-1692.1648236	-1692.2456156	-1692.2425971	430	0.04
add6_126_dcm	-1692.5750552	-1692.1646782	-1692.2455882	-1692.2425697	430	0.04
add6_051_dcm	-1692.5751517	-1692.1647177	-1692.2455337	-1692.2425152	430	0.04
add6_059_dcm	-1692.5750835	-1692.1646505	-1692.2455245	-1692.2425060	429	0.04
add6_145_dcm	-1692.5749650	-1692.1646460	-1692.2455130	-1692.2424945	430	0.04
add6_055_dcm	-1692.5749721	-1692.1646461	-1692.2455101	-1692.2424916	429	0.04
add6_056_dcm	-1692.5750124	-1692.1646304	-1692.2454694	-1692.2424509	430	0.03
add6_111_dcm	-1692.5749883	-1692.1646063	-1692.2454543	-1692.2424358	430	0.03
add6_133_dcm	-1692.5748036	-1692.1645456	-1692.2453376	-1692.2423191	430	0.03
add6_076_dcm	-1692.5746177	-1692.1644227	-1692.2453177	-1692.2422992	430	0.03
add6_136_dcm	-1692.5748232	-1692.1644452	-1692.2452622	-1692.2422437	430	0.03
add6_114_dcm	-1692.5747759	-1692.1643989	-1692.2452389	-1692.2422204	429	0.03
add6_116_dcm	-1692.5745338	-1692.1642658	-1692.2451478	-1692.2421293	429	0.02
all			**-1692.2454665**	**-1692.2424480**	**430**	
ΔE	-33.2	-28.1	+18.6	+10.6		
all			**+19.1**	**+11.1**		

[a] best 20 conformers according to $G_{qh,298}$ at SMD(DCM)/B3LYP-D3/6-31+G(d) level of theory.

2.1.10.5 Sandwich systems – computational information

Table 2.35: [Table S39]. Energies for all sandwich systems of ion pair **3a** optimized with SMD(DCM)/r²SCAN-3c level of theory with subsequent single point calculations at SMD(DCM)/B3LYP-D3/6-31+G(d).

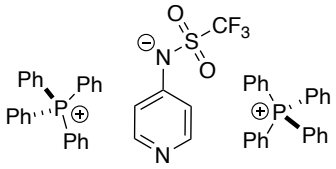

a3a

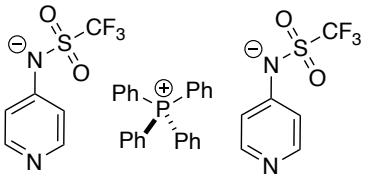

3a3

System	E_{tot} SMD(DCM)/ B3LYP-D3/6-31+G(d)	Cavity Volume (Å³)	Relative Population Parameter based on E_{298}	System	E_{tot} SMD(DCM)/ B3LYP-D3/6-31+G(d)	Cavity Volume (Å³)	Relative Population Parameter based on E_{298}
sw_a3a_new_033b_dcm_sp	**-3724.7011753**	**925**	**0.39**	asw_3a3_058b_dcm_sp	**-3645.6244701**	**781**	**0.23**
sw_a3a_new_030a_dcm_sp	-3724.7008822	923	0.28	asw_3a3_011a_dcm_sp	-3645.6233739	780	0.07
sw_a3a_new_005na_dcm_sp	-3724.6995552	925	0.07	asw_3a3_044a_dcm_sp	-3645.6233403	781	0.07
sw_a3a_new_039a_dcm_sp	-3724.6993743	926	0.06	asw_3a3_032a_dcm_sp	-3645.6231043	783	0.05
sw_a3a_new_015b_dcm_sp	-3724.6989764	926	0.04	asw_3a3_053a_dcm_sp	-3645.6231020	783	0.05
sw_a3a_new_042a_dcm_sp	-3724.6989336	927	0.04	asw_3a3_006_dcm_sp	-3645.6230698	781	0.05
sw_a3a_new_010b_dcm_sp	-3724.6985369	927	0.02	asw_3a3_047a_dcm_sp	-3645.6230374	782	0.05
sw_a3a_new_045c_dcm_sp	-3724.6984005	926	0.02	asw_3a3_039b_dcm_sp	-3645.6229589	782	0.05
sw_a3a_new_014_dcm_sp	-3724.6980441	926	0.01	asw_3a3_045b_dcm_sp	-3645.6228896	780	0.04
sw_a3a_new_047a_dcm_sp	-3724.6976338	926	0.01	asw_3a3_049a_dcm_sp	-3645.6228146	783	0.04
sw_a3a_new_018a_dcm_sp	-3724.6975821	926	0.01	asw_3a3_048b_dcm_sp	-3645.6227627	784	0.04
sw_a3a_new_038a_dcm_sp	-3724.6975740	927	0.01	asw_3a3_057b_dcm_sp	-3645.6226849	781	0.03
sw_a3a_new_020a_dcm_sp	-3724.6971852	926	0.01	asw_3a3_050_dcm_sp	-3645.6223597	781	0.02
sw_a3a_new_004a_dcm_sp	-3724.6970783	926	0.01	asw_3a3_059b_dcm_sp	-3645.6223396	782	0.02
sw_a3a_new_003_dcm_sp	-3724.6968941	928	0.00	asw_3a3_022a_dcm_sp	-3645.6220941	781	0.02
sw_a3a_new_052b_dcm_sp	-3724.6967130	925	0.00	asw_3a3_037_dcm_sp	-3645.6219701	785	0.02
sw_a3a_new_013b_dcm_sp	-3724.6964818	925	0.00	asw_3a3_008a_dcm_sp	-3645.6217232	783	0.01
sw_a3a_new_029a_dcm_sp	-3724.6964377	925	0.00	asw_3a3_051b_dcm_sp	-3645.6217229	785	0.01
sw_a3a_new_040a_dcm_sp	-3724.6963431	924	0.00	asw_3a3_033_dcm_sp	-3645.6216873	780	0.01
sw_a3a_new_055b_dcm_sp	-3724.6963343	928	0.00	asw_3a3_004a_dcm_sp	-3645.6216535	780	0.01
	-3724.7002363	**925**			**-3645.6230836**	**782**	

Table 2.36: [Table S40]. Energies for all sandwich systems of ion pair **4a** optimized with SMD(DCM)/r²SCAN-3c level of theory with subsequent single point calculations at SMD(DCM)/B3LYP-D3/6-31+G(d).

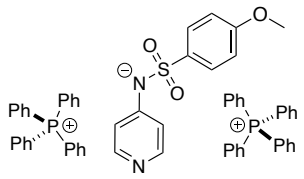 **a4a**				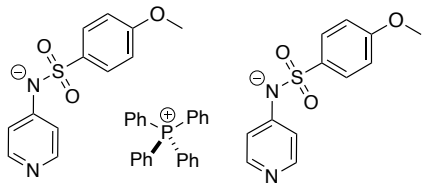 **4a4**			
System	**E_{tot} SMD(DCM)/ B3LYP-D3/6-31+G(d)**	**Cavity Volume (Å³)**	**Relative Population Parameter based on E_{298}**	**System**	**E_{tot} SMD(DCM)/ B3LYP-D3/6-31+G(d)**	**Cavity Volume (Å³)**	**Relative Population Parameter based on E_{298}**
sw_a4a_018_dcm_sp	**-3733.2653541**	**993**	**0.39**	asw_4a4_005a_dcm_sp	**-3662.7548378**	**921**	**0.53**
sw_a4a_049a_dcm_sp	-3733.2653444	995	0.39	asw_4a4_016_dcm_sp	-3662.7535339	921	0.13
sw_a4a_004b_dcm_sp	-3733.2635672	998	0.06	asw_4a4_011a_dcm_sp	-3662.7534663	920	0.12
sw_a4a_040b_dcm_sp	-3733.2629560	999	0.03	asw_4a4_015a_dcm_sp	-3662.7532492	920	0.10
sw_a4a_022_dcm_sp	-3733.2629292	997	0.03	asw_4a4_006_dcm_sp	-3662.7526111	915	0.05
sw_a4a_017a_dcm_sp	-3733.2628530	997	0.03	asw_4a4_031a_dcm_sp	-3662.7516599	923	0.02
sw_a4a_005a_dcm_sp	-3733.2626049	998	0.02	asw_4a4_024a_dcm_sp	-3662.7515888	923	0.02
sw_a4a_011a_dcm_sp	-3733.2619594	998	0.01	asw_4a4_059n_dcm_sp	-3662.7514401	922	0.01
sw_a4a_008a_dcm_sp	-3733.2613398	998	0.01	asw_4a4_001_dcm_sp	-3662.7495052	924	0.00
sw_a4a_028a_dcm_sp	-3733.2612325	995	0.01	asw_4a4_034_dcm_sp	-3662.7493973	923	0.00
sw_a4a_007_dcm_sp	-3733.2611335	999	0.00	asw_4a4_021a_dcm_sp	-3662.7488765	923	0.00
sw_a4a_039a_dcm_sp	-3733.2608890	999	0.00	asw_4a4_002_dcm_sp	-3662.7486765	922	0.00
sw_a4a_016_dcm_sp	-3733.2606781	998	0.00	asw_4a4_014_dcm_sp	-3662.7485596	922	0.00
sw_a4a_047a_dcm_sp	-3733.2603097	994	0.00	asw_4a4_023a_dcm_sp	-3662.7485027	920	0.00
sw_a4a_038b_dcm_sp	-3733.2602851	997	0.00	asw_4a4_042b_dcm_sp	-3662.7484625	918	0.00
sw_a4a_044_dcm_sp	-3733.2601809	994	0.00	asw_4a4_035a_dcm_sp	-3662.7480696	923	0.00
sw_a4a_037a_dcm_sp	-3733.2601341	995	0.00	asw_4a4_050a_dcm_sp	-3662.7480102	915	0.00
sw_a4a_013a_dcm_sp	-3733.2597333	998	0.00	asw_4a4_057n_dcm_sp	-3662.7479483	923	0.00
sw_a4a_023b_dcm_sp	-3733.2595989	996	0.00	asw_4a4_019b_dcm_sp	-3662.7477695	921	0.00
sw_a4a_015a_dcm_sp	-3733.2593335	998	0.00	asw_4a4_028b_dcm_sp	-3662.7477203	922	0.00
	-3733.2647588	**995**			**-3662.7539922**	**920**	

2.2 Supplementary References

[1] R. K. Harris, E. D. Becker, S. M. C. de Menezes, R. Goodfellow, P. Granger, *Pure Appl. Chem.* **2001**, *73*, 1795–1818.

[2] V. Burger, M. Franta, A. R. Ofial, R. M. Gschwind, H. Zipse, *J. Am. Chem. Soc.* **2024**, *accepted*.

[3] R. J. Mayer, A. R. Ofial, H. Mayr, C. Y. Legault, *J. Am. Chem. Soc.* **2020**, *142*, 5221–5233.

[4] Y. C. Wu, W. F. Koch, K. W. Pratt, *J. Res. Natl. Inst. Stand. Technol.* **1991**, *96*, 191–201.

[5] C. Reichardt, T. Welton, *Solvents and Solvent Effects in Organic Chemistry: Fourth Edition*, Wiley-VCH, Weinheim, **2011**.

[6] S. Hoops, S. Sahle, R. Gauges, C. Lee, J. Pahle, N. Simus, M. Singhal, L. Xu, P. Mendes, U. Kummer, *Bioinformatics* **2006**, *22*, 3067–3074.

[7] F. Zott, *GitHub repository*, "fabianzott/steadystate_analysis", **2023**, available at https://github.com/fabianzott/steadystate_analysis.

[8] N. G. Tsierkezos, A. I. Philippopoulos, *Fluid Phase Equilibria* **2009**, *277*, 20–28.

[9] R. M. Fuoss, C. A. Kraus, *J. Amercian Chem. Soc.* **1933**, *55*, 2387–2399.

[10] M. Hojo, Y. Miyauchi, A. Tanio, Y. Lmai, *J. Chem. Soc. Faraday Trans.* **1991**, *87*, 3847–3852.

[11] A. Boruń, A. Bald, *Int. J. Electrochem. Sci.* **2016**, *11*, 7714–7725.

[12] S. Boileau, P. Hemery, *Electrochimica Acta* **1976**, *21*, 647–655.

[13] Y. Miyauchi, M. Hojo, Hironori Moriyama, H. Moriyama, Y. Imai, *J. Chem. Soc. Faraday Trans.* **1992**, *88*, 3175–3182.

[14] M. Hojo, H. Moriyama, *J. Solut. Chem.* **1996**, *25*, 681–694.

[15] A. M. Brown, R. M. Fuoss, *J. Am. Chem. Soc.* **1960**, *64*, 1341–1342.

[16] R. M. Fuoss, E. Hirsch, *J. Am. Chem. Soc.* **1960**, *82*, 1013–1017.

[17] H. Mayr, T. Bug, M. F. Gotta, N. Hering, B. Irrgang, B. Janker, B. Kempf, R. Loos, A. R. Ofial, G. Remennikov, H. Schimmel, *J. Am. Chem. Soc.* **2001**, *123*, 9500–9512.

[18] F. Brotzel, B. Kempf, T. Singer, H. Zipse, H. Mayr, *Chem. Eur. J.* **2007**, *13*, 336–345.

[19] N. De Rycke, G. Berionni, F. Couty, H. Mayr, R. Goumont, O. R. P. David, *Org. Lett.* **2011**, *13*, 530–533.

[20] G. Chen, S. Guo, H. Feng, Z. Qian, *J. Mater. Chem. C* **2019**, *7*, 14535–14542.

[21] A. D. Becke, *J. Chem. Phys.* **1993**, *98*, 1372–1377.

[22] S. Grimme, *J. Chem. Phys.* **2006**, *124*, DOI 10.1063/1.2148954.

[23] C. Lee, W. Yang, R. G. Parr, *Phys. Rev. B* **1988**, *37*, 785–789.

[24] G. W. Spitznagel, T. Clark, J. Chandrasekhar, P. V. R. Schleyer, *J. Comput. Chem.* **1982**, *3*, 363–371.

[25] A. V. Marenich, C. J. Cramer, D. G. Truhlar, *J. Phys. Chem. B* **2009**, *113*, 6378–6396.

[26] M. Marin-Luna, P. Patschinski, H. Zipse, *Chem. Eur. J.* **2018**, *24*, 15052–15058.

[27] M. Marin-Luna, B. Pölloth, F. Zott, H. Zipse, *Chem. Sci.* **2018**, *9*, 6509–6515.

[28] B. Pölloth, M. P. Sibi, H. Zipse, *Angew. Chem. Int. Ed.* **2021**, *60*, 774–778.

[29] S. Mayr, M. Marin-Luna, H. Zipse, *J. Org. Chem.* **2021**, *86*, 3456–3489.

[30] S. Grimme, *Chem. Eur. J.* **2012**, *18*, 9955–9964.

[31] G. Luchini, J. V. Alegre-Requena, I. Funes-Ardoiz, R. S. Paton, *F1000Research* **2020**, *9*, 1–14.

[32] Gaussian 16, Revision A.03, M. J. Frisch, G. W. Trucks, H. B. Schlegel, G. E. Scuseria, M. A. Robb, J. R. Cheeseman, G. Scalmani, V. Barone, G. A. Petersson, H. Nakatsuji, X. Li, M. Caricato, A. V. Marenich, J. Bloino, B. G. Janesko, R. Gomperts, B. Mennucci, H. P. Hratchian, J. V. Ortiz, A. F. Izmaylov, J. L. Sonnenberg, D. Williams-Young, F. Ding, F. Lipparini, F. Egidi, J. Goings, B. Peng, A. Petrone, T. Henderson, D. Ranasinghe, V. G. Zakrzewski, J. Gao, N. Rega, G. Zheng, W. Liang, M. Hada, M. Ehara, K. Toyota, R. Fukuda, J. Hasegawa, M. Ishida, T. Nakajima, Y. Honda, O. Kitao, H. Nakai, T. Vreven, K. Throssell, J. A. Jr. Montgomery, J. E. Peralta, F. Ogliaro, M. J. Bearpark, J. J. Heyd, E. N. Brothers, K. N. Kudin, V. N. Staroverov, T. A. Keith, R. Kobayashi, J. Normand, K. Raghavachari, A. P. Rendell, J. C. Burant, S. S. Iyengar, J. Tomasi, M. Cossi, J. M. Millam, M. Klene, C. Adamo, R. Cammi, J. W. Ochterski, R. L. Martin, K. Morokuma, O. Farkas, J. B. Foresman, D. J. Fox, **2016**, p Gaussian, Inc, Wallingford CT.

[33] Gaussian 16, Revision B.01, M. J. Frisch, G. W. Trucks, H. B. Schlegel, G. E. Scuseria, M. A. Robb, J. R. Cheeseman, G. Scalmani, V. Barone, G. A. Petersson, H. Nakatsuji, X. Li, M. Caricato, A. V. Marenich, J.

Bloino, B. G. Janesko, R. Gomperts, B. Mennucci, H. P. Hratchian, J. V. Ortiz, A. F. Izmaylov, J. L. Sonnenberg, D. Williams-Young, F. Ding, F. Lipparini, F. Egidi, J. Goings, B. Peng, A. Petrone, T. Henderson, D. Ranasinghe, V. G. Zakrzewski, J. Gao, N. Rega, G. Zheng, W. Liang, M. Hada, M. Ehara, K. Toyota, R. Fukuda, J. Hasegawa, M. Ishida, T. Nakajima, Y. Honda, O. Kitao, H. Nakai, T. Vreven, K. Throssell, J. A. Jr. Montgomery, J. E. Peralta, F. Ogliaro, M. J. Bearpark, J. J. Heyd, E. N. Brothers, K. N. Kudin, V. N. Staroverov, T. A. Keith, R. Kobayashi, J. Normand, K. Raghavachari, A. P. Rendell, J. C. Burant, S. S. Iyengar, J. Tomasi, M. Cossi, J. M. Millam, M. Klene, C. Adamo, R. Cammi, J. W. Ochterski, R. L. Martin, K. Morokuma, O. Farkas, J. B. Foresman, D. J. Fox, **2016**, p Gaussian, Inc, Wallingford CT.

[34] Maestro, rev 12.2.012. Schrödinger, New York, **2019**.

[35] M. Saunders, *J. Comput. Chem.* **2004**, *25*, 621–626.

[36] D. Šakić, M. Hanževački, D. M. Smith, V. Vrček, *Org. Biomol. Chem.* **2015**, *13*, 11740–11752.

[37] J. Helberg, T. Ampßler, H. Zipse, *J. Org. Chem.* **2020**, *85*, 5390–5402.

[38] S. Grimme, A. Hansen, S. Ehlert, J. M. Mewes, *J. Chem. Phys.* **2021**, *154*, DOI 10.1063/5.0040021.

[39] F. Neese, *WIREs Comput. Mol. Sci.* **2022**, *12*, e1606.

[40] Gaussian 16, Revision C.01, M. J. Frisch, G. W. Trucks, H. B. Schlegel, G. E. Scuseria, M. A. Robb, J. R. Cheeseman, G. Scalmani, V. Barone, G. A. Petersson, H. Nakatsuji, X. Li, M. Caricato, A. V. Marenich, J. Bloino, B. G. Janesko, R. Gomperts, B. Mennucci, H. P. Hratchian, J. V. Ortiz, A. F. Izmaylov, J. L. Sonnenberg, D. Williams-Young, F. Ding, F. Lipparini, F. Egidi, J. Goings, B. Peng, A. Petrone, T. Henderson, D. Ranasinghe, V. G. Zakrzewski, J. Gao, N. Rega, G. Zheng, W. Liang, M. Hada, M. Ehara, K. Toyota, R. Fukuda, J. Hasegawa, M. Ishida, T. Nakajima, Y. Honda, O. Kitao, H. Nakai, T. Vreven, K. Throssell, J. A. Jr. Montgomery, J. E. Peralta, F. Ogliaro, M. J. Bearpark, J. J. Heyd, E. N. Brothers, K. N. Kudin, V. N. Staroverov, T. A. Keith, R. Kobayashi, J. Normand, K. Raghavachari, A. P. Rendell, J. C. Burant, S. S. Iyengar, J. Tomasi, M. Cossi, J. M. Millam, M. Klene, C. Adamo, R. Cammi, J. W. Ochterski, R. L. Martin, K. Morokuma, O. Farkas, J. B. Foresman, D. J. Fox, **2016**, p Gaussian, Inc, Wallingford CT.

Chapter 3. Pyridinamide Ion Pairs – Design Principles for Super-Nucleophiles in Apolar Organic Solvents

Veronika Burger, Maximilian Franta, AnnMarie C. O'Donoghue*, Armin R. Ofial*, Ruth M. Gschwind* and Hendrik Zipse*

J. Org. Chem., **2024**, *in revision* (Manuscript ID jo-2024-02668y).

Autor contributions: Veronika Burger (V.B.) and Hendrik Zipse (H.Z.) conceived the study. All experimental studies were performed by V.B. with exception of DOSY NMR measurements, which were performed by Maximilian Franta (M.F.). AnnMarie C. O'Donoghue (A.C.O) supervised the design and execution of pK_a measurements, which were performed at Durham University. The manuscript was jointly written by V.B., Ruth M. Gschwind (R.M.G.), Armin R. Ofial (A.R.O.) and H.Z. The supporting information was prepared by V.B. and M.F.

Additional information: The here displayed supporting information is an altered and shorted version of the submitted SI. The DOSY results are used for the explanation of findings, but no technical details are discussed in this thesis. These can be found in the original file. For comparison of this thesis and the original SI file, the numbering includes the original item number as shown below.

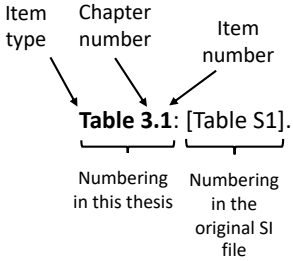

Pyridinamide Ion Pairs – Design Principles for Super-Nucleophiles in Apolar Organic Solvents

Veronika Burger[a], Maximilian Franta[b], AnnMarie C. O'Donoghue*[c] Armin R. Ofial*[a], Ruth M. Gschwind*[b] and Hendrik Zipse[*a]

[a]Department of Chemistry, Ludwig-Maximilians Universität München, Butenandtstr. 5-13, 81377 München, Germany; [b]Institute for Organic Chemistry, University Regensburg, Universitätsstr. 31, 93053 Regensburg, Germany; [c]Department of Chemistry, Durham University, South Road, Durham DH1 3LE, United Kingdom.

KEYWORDS: conductivity, DOSY, asymmetric association, catalyst design, nucleophilicity, kinetics, catalysis

ABSTRACT: A comprehensive analytical protocol combining conductivity, diffusion-ordered NMR (DOSY), and photometric kinetic measurements is employed to analyze the nucleophilic reactivity of pyridinamide ion pairs in low polarity organic solvents. The association patterns of these systems are found to strongly depend on cation size, with larger cations favoring the formation of cationic triple ion sandwich complexes together with free and highly nucleophilic anions. Kinetic studies using the ionic strength-controlled benzhydrylium method demonstrate that pyridinamide ions exhibit significantly higher nucleophilicities as compared to established organocatalysts, particularly in low polarity solvents. Nucleophilicities are furthermore found to correlate well with Brønsted basicities measured in water and with Lewis basicities calculated in dichloromethane. Taken together these findings provide quantitative guidelines for the future design of highly active Lewis base catalysts.

INTRODUCTION

In the field of organic synthesis, ion pair catalysis has emerged as a powerful tool that leverages the interaction between charged species to enhance catalytic activity and selectivity to facilitate various chemical transformations.[1–4] Its application extends from classical phase-transfer (PT) catalysis[5] to asymmetric synthesis.[6–9] Recent studies have shown that ion pair catalysis offers unique opportunities for selectivity control and overcomes challenges where conventional methods may fall short.[10,11] Pyridinamide ion pairs have recently been introduced as a new class of Lewis base catalysts capable of outperforming established structurally related neutral organocatalysts such as 4-(dimethylamino)pyridine (DMAP, **1**)[12,13] and the more reactive 9-azajulolidine (TCAP, **2**)[14] in selected benchmark reactions.[15,16] In contrast to neutral pyridine-based catalysts **1** and **2**, the actual state of the ion pair catalysts shown in Chart 1 depends on a variety of factors such as the solvent polarity, the choice of additives, and the concentration regime used in catalytic processes. For pyridinamide phosphonium salts, such as **3a** and **4a** (Chart 1), we have recently outlined a protocol for quantifying their concentration-dependent speciation and the nucleophilicity of the free anion component towards reference electrophiles of known reactivity in organic solvents of low polarity such as dichloromethane (DCM).[17] Most kinetic studies aiming to quantify the reactivity of anionic nucleophiles rely on highly polar solvents such as water, DMSO, acetonitrile (MeCN), often in combination with additives such as crown ethers to reduce interactions between the cationic counter-ion and the reacting anion.[18] The intrinsic nucleophilicity of a free anion is, however, expected to be higher in organic solvents of low polarity (DCM, THF, toluene) commonly used in organocatalytic transformations. Ion pairs tend to associate in apolar media in a concentration-dependent manner causing non-linear effects and, thus, complicate systematic kinetic studies.

Chart 1. Structures of neutral organocatalysts DMAP (1), TCAP (2), and the pyridinamide ion pair library.

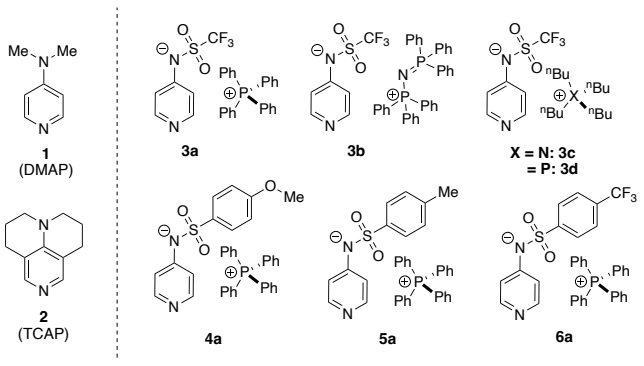

Our recently introduced analytical protocol combines conductivity measurements, diffusion-ordered NMR spectroscopy (DOSY) measurements, and photometric kinetic measurements utilizing an ionic strength-controlled benzhydrylium ion methodology and enables us to uniquely link insights into the concentration of ions with their association state and nucleophilicity. For **3a** as a reference system, the results from conductivity and DOSY experiments can best be rationalized by assuming the concentration-dependent formation of the "sandwich"-type cations (**a3a**) and anions (**3a3**) shown in Figure 1, with little interference of the respective 1:1 ion pair (**3a**). Key properties obtained from DOSY experiments in DCM are the

concentration-dependent "effective" cation and anion volumes, whose combination with conductivity data then yields the equilibrium constants for all three aggregates **3a**, **a3a**, and **3a3** shown in Figure 1.

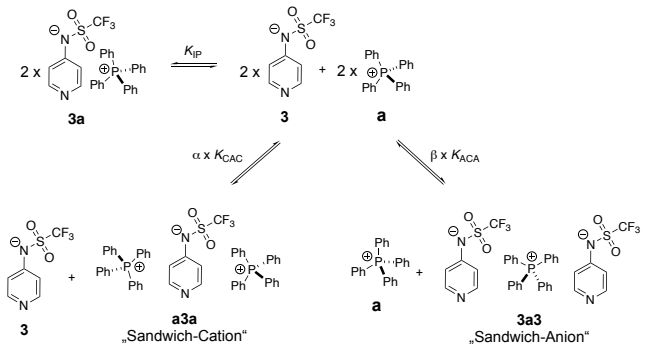

Figure 1. Association types of anion **3** and cation **a** leading to either the 1:1 ion pair **3a**, the sandwich cation **a3a**, or the sandwich anion **3a3** with their respective association constants K_{IP}, K_{CAC}, and K_{ACA}.

While it is, in principle, possible to fit concentration-dependent conductivity and DOSY profiles to only one of the equilibria shown in Figure 1, the best possible fit is obtained when assuming simultaneous formation of both sandwich ion species **a3a** and **3a3**. In practical terms this requires optimization of the mixing parameters α (contribution of sandwich cation **a3a**) and β (contribution of sandwich anion **3a3**) shown in Figure 1. In the following we will refer to this model as the "mixed sandwich ion model" (see SI). The accurate description of concentration profiles for all species was then combined with the ionic strength-controlled benzhydrylium method to determine the nucleophilicity of free pyridinamide anions in DCM and MeCN. Based on the results obtained for pyridinamide ion pairs **3a-d** and **4-6a** we aim to extract key design principles for the synthesis of highly reactive pyridinamide ion pair systems.

RESULTS AND DISCUSSION

Conductivity. Conductivity measurements were performed in DCM for salt concentrations ranging from 0.02 – 1.0 mM. At low electrolyte concentrations and for the case of non-interacting ions, the experimentally determined conductivity κ depends on the specific molar conductivity Λ_m and the ion concentration [IP] as expressed in equation (1).

$$\kappa = \Lambda_m[IP] \quad (1)$$

The conductivity curves for ion pairs composed of anion **3** and cations **a-d** shown in Figure 2A appear to fall into two separate groups. The first of these includes cation **a** (PPh_4^+) and **b** ($PPh_3NPPh_3^+$) carrying aromatic substituents and displays systematically higher conductivities as compared to the second group with cation **c** (NBu_4^+) and **d** (PBu_4^+) carrying unbranched aliphatic side chains. For simplicity, we will focus our discussion on the cationic sandwich association constants K_{CAC}. Pyridinamide ion pair **3b** shows the weakest degree of association of all ion pairs in DCM with K_{CAC}(**3b**) = 4.65 x 10^6 M^{-2}, closely followed by **3a** with K_{CAC}(**3a**) = 6.38 x 10^6 M^{-2}. In contrast, ion pairs **3c** and **3d** show systematically higher values with K_{CAC}(**3c**) = 1.01 x 10^7 M^{-2}, and K_{CAC}(**3d**) = 1.07 x 10^7 M^{-2}, respectively, indicating a higher degree of aggregation in DCM.

Variation of the anion substitution pattern leads, in contrast, to only minor variations in the association behavior as is easily seen from the similar conductivity curves displayed in Figure 2B. In quantitative terms this is reflected in the respective association constants of K_{CAC}(**4a**) = 6.50 x 10^6 M^{-2}, K_{CAC}(**5a**) = 5.15 x 10^6 M^{-2}, and K_{CAC}(**6a**) = 6.75 x 10^6 M^{-2}, all of which are in close proximity to one another and quite similar to that of **3a**. The conductivity measurements thus clearly document that the lowest degree of aggregation (and thus the highest concentration of free ions) will be obtained with the two phosphonium ions **a** and **b** carrying aromatic substituents.

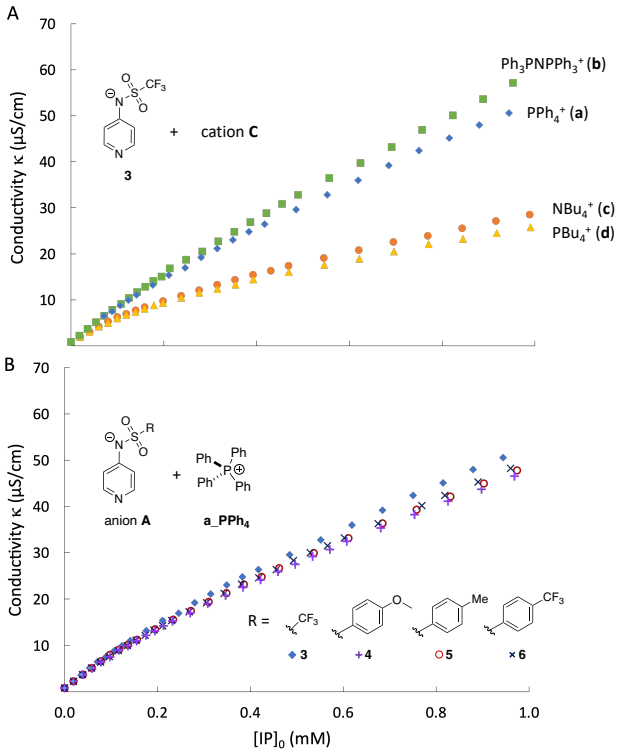

Figure 2. A) Conductivity profiles for **3a**, **3b**, **3c**, and **3d** measured in DCM at 20 °C, B) Conductivity profiles for **3a**, **4a**, **5a**, and **6a** measured in DCM at 20 °C.

DOSY NMR. Since conductivity data alone cannot determine which sandwich association type predominates for a given pyridinamide ion pair, DOSY NMR measurements were performed in DCM-d_2 for concentrations ranging from 0.005 mM to 1.0 mM (see SI, Chapter 4). DOSY measurements at these low concentrations require a 600 MHz spectrometer with a helium cryo probe and measurement times up to 16 h per sample. The DOSY results were compared to calculated volumes of ions and associated complexes of the respective pyridinamide ion pair which are based on the van der Waals cavities employed in the SMD continuum solvation model at the SMD(DCM)/B3LYP-D3/6-31+G(d) level of theory. Recent DOSY measurements of pyridinamide ion pair **3a** and **4a** revealed a prevailing cationic sandwich association for **3a**, and a mainly anionic sandwich association for **4a**.[17] Thereby, the cationic sandwich association is indicated by a higher increase of the hydrodynamic cation volume in comparison to the hydrodynamic anion volume, while the anionic sandwich association displays a distinct crossing point of both ionic volumes when the anion volume surpasses the cation volume of the respective salt in the DOSY measurement. Thus, additional DOSY measurements for the remaining pyridinamide ion pairs were performed to reveal trends in the association behavior.

The concentration dependent DOSY plots of ion pair **3b**, **3c**, and **3d** display a similar curve with cation volumes larger than expected as shown for **3a**. Here the effective cation volume increases more strongly with increasing concentration than the anion volume which is most easily rationalized with predominant formation of cationic sandwich complexes of "**a3a**"-type (see SI for details). In contrast, for ion pairs **4a**, **5a**, and **6a** a crossing point of anion and cation volumes is observed where the anion volume exceeds the cation volume, which is typical for the anionic sandwich complexes of "**a4a**"-type.

Combined analysis of the conductivity and DOSY NMR data points to a predominance of cation sandwich formation for **3a-d** and a predominance of anion sandwich formation for pyridinamide ion pairs **4-6a**. This is quantitatively reflected in the scaling factors α and β collected in Table 1. For ion pair **3b** and **3d** all experimental observables can be rationalized with excellent accuracy with the cation sandwich model alone, that is, α/β = 100/0.

Table 1. List of pyridinamide ion pairs with their optimized scale factors α and β and the association constants K_{CAC} and K_{ACA} in the mixed sandwich ion model.

IP	α/β	α x K_{CAC} [M^{-2}]	β x K_{ACA} [M^{-2}]	RMSE
3a	44/21	2.81 x 10^6	1.34 x 10^6	0.43
3b	100/0	4.65 x 10^6	0.00	0.11
3c	33/23	3.33 x 10^6	2.32 x 10^6	0.61
3d	100/0	1.07 x 10^7	0.00	0.10
4a	12/61	7.80 x 10^5	3.97 x 10^6	0.35
5a	11/67	5.67 x 10^5	3.45 x 10^6	0.29
6a	16/52	1.08 x 10^6	3.51 x 10^6	0.38

In summary, the conductivity data demonstrates the association pattern is more influenced by the choice of cation than anion, whilst the DOSY data reveals a switch from cation sandwich to anion sandwich association when moving from small anion **3** (215 $Å^3$) to larger anions such as **4** (285 $Å^3$), **5** (266 $Å^3$), or **6** (295 $Å^3$) when using **a** (362 $Å^3$) as the cation component. The size difference between the chosen anion and cation components as listed in Table 2 thus appears to represent a controlling factor for the speciation of ion pairs in organic solvents of low polarity. For the first two entries **3a** and **3b** combining aryl phosphonium cations **a** and **b** with the comparatively small anion **3** we find a predominance of cationic sandwich association. For the combinations of larger anions **4** - **6** with phosphonium cation **a** the volume difference is significantly smaller (< 100 $Å^3$) and all experiments point to a mixture of cation and anion sandwich association.

Table 2. Analysis of volume difference between anions and cations in pyridinamide ion pairs with aryl substituted cations a and b.

IP	Cation volume ($Å^3$)	Anion volume ($Å^3$)	Volume difference[a]
3a	362	215	147
3b	559	215	344
4a	362	285	77.0
5a	362	266	96.0
6a	362	295	67.0

[a] Volume difference = cation volume - anion volume.

While the difference between anion and cation volume may not be the only factor that determines the association pattern of pyridinamide ion pairs in organic solvents of low polarity, it is a feature that can be adjusted in a straightforward manner to shift the association equilibria towards the formation of cationic sandwich aggregates (accompanied by an increase of the free anion concentration in solution).

Kinetics. To characterize the nucleophilic reactivity of pyridinamide ion pairs we used the established Mayr benzhydrylium ion method suitable for the quantification of the reactivity of carbon-, nitrogen-, oxygen-, sulfur-, and phosphorous-based nucleophiles in different solvents,[19,20] including DMAP (**1**) and TCAP (**2**).[21–23] In order to separate the effects of increasing nucleophile concentration from those of increasing solution ionic strength, we employ the ionic strength-controlled methodology described earlier by adding the non-nucleophilic salts **7a-d** composed of BF_4^- and the respective cation components (see Chart 2) to the reaction mixture to keep the ionic strength (*I*) constant at *I* = 1.0 mM as the upper concentration limit chosen in conductivity, DOSY, and kinetics measurements.

Chart 2. Structures of non-nucleophilic additives 7a-d employed in ionic-strength controlled benzhydrylium measurements.

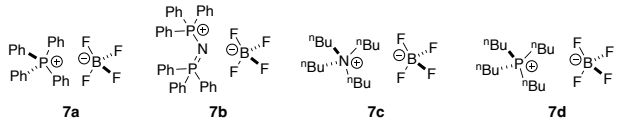

The benzhydrylium ion method involves the photometric monitoring of the reactions of colored benzhydrylium salts, such as **8a**–**8c** (Table 3) whose electrophilic reactivities are characterized by the solvent-independent parameters *E*, with nucleophiles used in excess concentration to achieve kinetics under pseudo-first order conditions. The first-order rate constants k_{obs} (s^{-1}) can then be obtained by fitting a mono-exponential decay function to the decreasing absorption of **8** during the reaction with the nucleophile which is assumed to be the anion of the respective ion pair. In MeCN, pyridinamide ion pairs fully dissociate into anion and cation as shown by conductivity measurements. Accordingly, a linear increase of pseudo-first order rate constants k_{obs} with nucleophile concentrations [**A**] (= anion concentration or total salt concentration) was observed in the kinetics of reactions of pyridinamide ion pairs with **8** [equation (2)].

$$k_{obs} = k_2[\mathbf{A}] \quad (2)$$

$$\log k_2 = s_N(N + E) \quad (3)$$

Equation (2) thus yields the second-order rate constants k_2 (M^{-1} s^{-1}) for the reactions of pyridinamide ion pair **3a-d**,**4-6a** with **8a-8c** in acetonitrile (Table 3). All measured ion pairs containing anion **3** display largely similar bimolecular rate constant k_2, the spread of individual values amounting to ±10%. From all pyridinamide anions studied here, anion **3** is the least reactive species, but still reacts about three times faster with electrophiles **8** than DMAP (**1**) and similarly fast as TCAP (**2**). The highest rate constant k_2 was measured for anion **4** with an electron donating aryl substituent (4-MeO), which is approx. eight times larger than those for analogous reactions of **8** with TCAP (**2**) and closely followed by the rate constants k_2 for anion **5** and anion **6**. The nucleophilicity parameter for pyridinamide ion pairs in MeCN were obtained by analyzing the kinetic data

according to the Mayr-Patz Equation (3). They range between $N = 16.38$ ($s_N = 0.60$) for anion **3** to $N = 17.28$ ($s_N = 0.65$) for anion **4** with the only outlier being $N = 19.51$ for anion **6** due to its relatively low nucleophile-specific sensitivity parameter $s_N = 0.46$. This makes direct comparison of N values less convenient than the inspection of the second-order rate constants, which amount to $k_2 = 2.92 \times 10^4\ M^{-1}\ s^{-1}$ for anion **6** and $k_2 = 3.45 \times 10^4\ M^{-1}\ s^{-1}$ for anion **5** in reactions with **8a**.

Table 3. Second-order rate constants k_2 for the reactions of DMAP (1), TCAP (2), and pyridinamide salts 3a-d, 4a, 5a, and 6a with reference electrophiles 8a, 8b, and 8c in MeCN (at 20 °C) analyzed by equation (3) to give the nucleophile-specific reactivity parameters N and s_N.

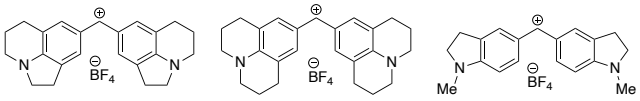

(lil)$_2$CH$^+$ (**8a**) E = -10.04 | (jul)$_2$CH$^+$ (**8b**) E = -9.45 | (ind)$_2$CH$^+$ (**8c**) E = -8.76

IP	k_2 [$M^{-1}\ s^{-1}$]			N (s_N)
	8a	8b	8c	
1[a]	2.11×10^3	5.30×10^3	1.29×10^4	15.51 (0.62)[d]
2[b]	6.30×10^3	–	4.17×10^4	15.60 (0.68)[d]
3a[c]	7.16×10^3	1.53×10^4	4.13×10^4	16.38 (0.60)
3b	8.37×10^3	1.37×10^4	4.74×10^4	16.68 (0.59)
3c	8.45×10^3	1.37×10^4	4.79×10^4	16.68 (0.59)
3d	8.79×10^3	1.63×10^4	5.03×10^4	16.48 (0.60)
4a[c]	5.11×10^4	1.36×10^5	3.47×10^5	17.28 (0.65)
5a	3.45×10^4	9.36×10^4	2.30×10^5	17.19 (0.64)
6a	2.92×10^4	5.95×10^4	1.16×10^5	19.51 (0.47)

[a] Second-order rate constants k_2 from ref. 21,22. [b] Second-order rate constants k_2 from ref 23. [c] Second-order rate constants k_2 from ref. 17. [d] Additional k_2 values from ref. 21–23 were used to determine N (and s_N).

Reactions of pyridinamide ion pairs **3a-d**,**4-6a** with electrophiles **8** in DCM are more complex and require a slightly different approach to gain reliable reactivity parameters (for details see ref 17). We recently developed the ionic strength-controlled method where a non-nucleophilic and structurally related additive salt **7** is added to fulfill the condition of [**IP**]$_0$ + [**7**] + [**8**] = 1.0 mM in each kinetic measurement. This resulted in a linear correlation for k_{obs} for **IP** + **8** reactions in DCM in a concentration range from 0.01 – 1.0 mM. Numerical analysis of all kinetic data accounts for the fact that variable fractions of the nucleophilic pyridinamide anions **3-6** are caught in unreactive cationic sandwich complexes CAC and/or in less reactive anionic sandwich complexes ACA (see Figure 3). The rate constants k_2 collected in Table 4 for the reaction of pyridinamide ion pairs **3a-d**,**4-6a** with benzhydrylium ions **8a - 8c** thus reflect the reaction rates of the free anion component at $I = 1.0$ mM. In DCM as the solvent, the bimolecular rate constant k_2 increases moderately when moving from DMAP (**1**) to TCAP (**2**). Meanwhile, we observe a significantly larger increase for pyridinamide ion pairs, which exceed those for **2** by at least one order of magnitude und the respective k_2 values obtained in MeCN by approx. two orders of magnitude.

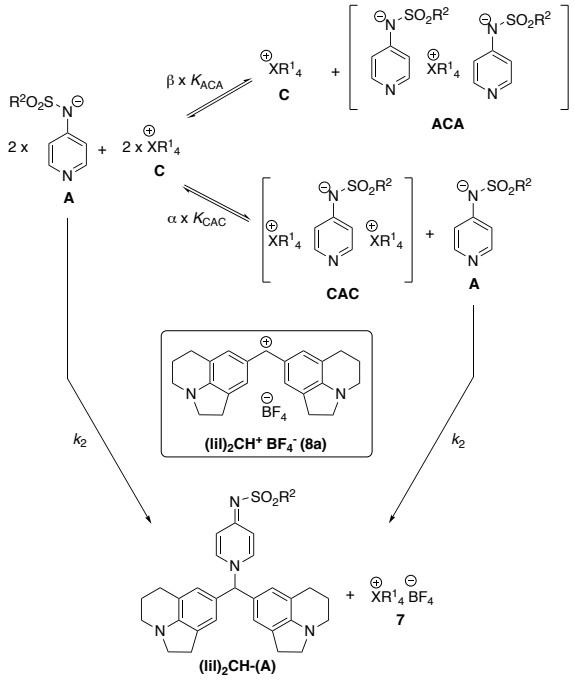

Figure 3. Benzhydrylium ion reaction employed for the quantification of nucleophilicities of anion **A**.

Table 4. Second-order rate constants k_2 of the reactions of DMAP (1), TCAP (2), and pyridinamide salts with the reference electrophiles 8a, 8b, and 8c in DCM (at 20 °C).

IP	k_2 [$M^{-1}\ s^{-1}$]		
	8a	8b	8c
1[a]	6.45×10^3	9.84×10^3	4.96×10^4
2[b]	1.42×10^4	3.11×10^4	1.28×10^5
3a[b]	5.42×10^5	1.25×10^6	4.64×10^6
3b[c]	4.92×10^5	1.30×10^6	4.51×10^6
3c	3.38×10^5	8.32×10^5	3.17×10^6
3d[c]	3.57×10^5	9.06×10^5	3.45×10^6
4a[b]	1.69×10^6	4.19×10^6	1.15×10^7
5a	1.79×10^6	3.99×10^6	1.23×10^7
6a	1.14×10^6	3.08×10^6	9.48×10^6

[a] Second-order rate constants k_2 from ref. 21. [b] Second-order rate constants k_2 from ref. 17. [c] cationic sandwich association model for analysis.

Following the same mode of analysis as in Burger *et al.*[17] for our library of pyridinamide ion pairs, we find the four measured rate constants k_2 for anion **3** to be again largely similar for the systems **3a** - **3d**, the spread of individual values now being somewhat larger at ±23% as compared to acetonitrile. Closer inspection shows the bimolecular rate constants for anion **3** in ion pairs **3a** and **3b** to be quite similar, as are the rate constants for ion pairs **3c** and **3d**. As already found in MeCN, the anion reactivity order in DCM is anion **3** < anion **6** < anion **5** ≈ anion **4**. These measurements establish pyridinamide ion pairs as potent and exceedingly nucleophilic pyridine derivatives in solvents of low polarity (Figure 4). Pyridinamide ion pair **4a** displays the highest nucleophilicity, which is in full agreement with the results for selected benchmark reactions performed in $CDCl_3$ as solvent.[15,16] The pyridinamide ion pairs studied here are thus significantly more reactive in DCM as the reaction medium as compared to cyclic guanidines such as 1,5,7-

triazabicyclo[4.4.0]dec-5-ene (TBD) identified in earlier studies as the most reactive N-nucleophiles with N/s_N = 16.16/0.75.[34]

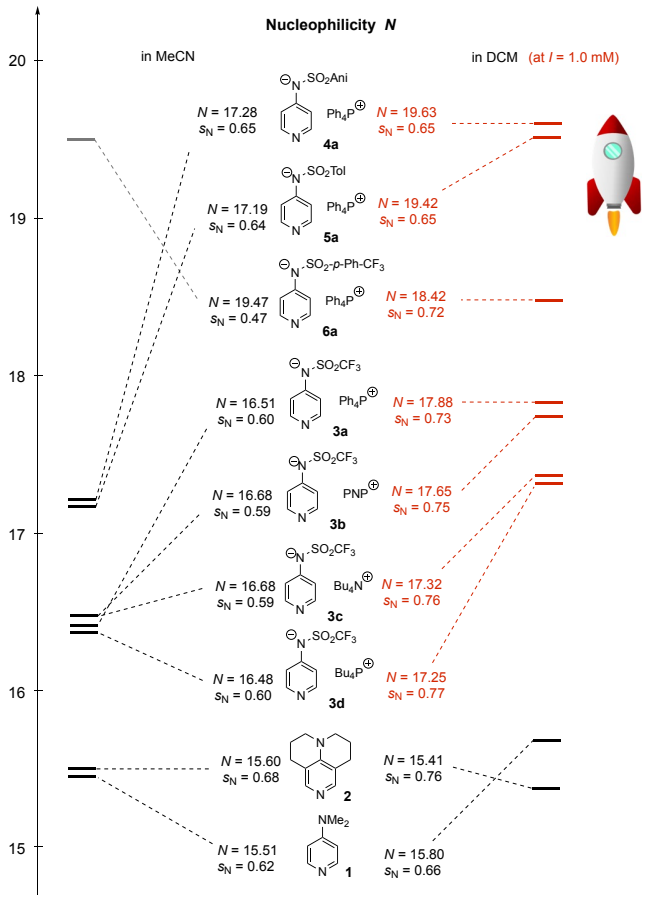

Figure 4. Mayr nucleophilicity parameter N (and s_N) of DMAP (**1**), TCAP (**2**), and pyridinamide ion pairs in MeCN and DCM, where all nucleophilicities for ion pairs were obtained by applying the mixed sandwich ion model (**3b** and **3d** obtained with CAC model extension).

Testing for catalytic efficiency. The reaction of *n*-butanol (**10**) with *p*-tolyl isocyanate (**9**) to urethane **11** was used as a primary benchmark reaction in earlier studies.[15] The procedure established by Helberg *et al.*[15] was followed to determine the effective rate constants k_{eff} for the newly synthesized pyridinamide ion pairs. The role of Lewis base catalysts in this reaction may involve both, the initial Lewis base addition to the isocyanate, or the Lewis base complexation of reactant alcohols.[24-27]

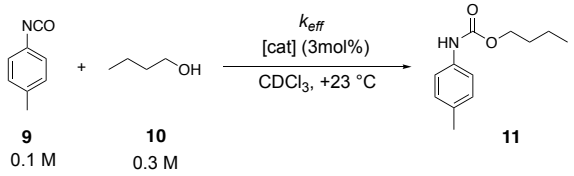

Scheme 1. Reaction of *n*-butanol (10) with *p*-tolyl isocyanate (9) employed as catalytic benchmark reaction.

Reaction progress was quantified by ^{1}H NMR spectroscopy via integration of well-separated signals. Effective rate constants were obtained by numerical simulations of the turnover curves based on an effective second-order mechanism as described in Helberg *et al.*[15] TCAP (**2**) is the most reactive neutral organocatalyst and, as expected based on the nucleophilicity measurements, pyridinamide salt **4a** catalyzes the urethane reaction three times faster than TCAP (**2**), followed by salt **5a** and **6a** on the scale of effective rate constants k_{eff} (Figure 5). As previous kinetic measurements indicated, **3c** is the least catalytically active ion pair catalyst and close to DMAP (**1**).

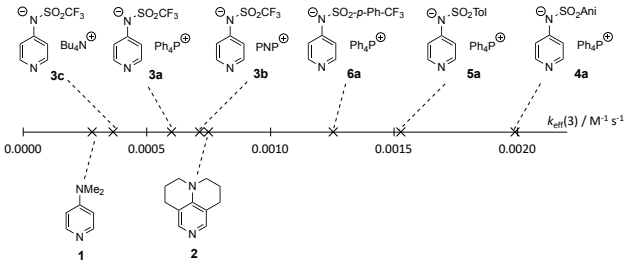

Figure 5. Effective rate constants k_{eff} for the benchmark reaction shown in Scheme 1 with 3.0 mol% of catalyst. Data for **1**, **2**, **3c**, and **4a** were taken from ref. 15.

The effective rate constants k_{eff} obtained in the catalytic benchmark reaction for pyridinamide salts correlate linearly with the rate constants k_2 determined for the reaction with benzhydryl cation **8a** as shown in the double logarithmic plot in Figure 6. The good fidelity of this correlation implies that neither the change in solvent from DCM to $CDCl_3$ nor the change in concentration regime is of major importance for the systems studied here. The reactivity parameters obtained from the ionic-strength-controlled benzhydrylium method can, either in form of the individual k_2 values or in their condensed form as N/s_N parameters, thus be expected to be highly useful in the development and analysis of Lewis-base mediated catalytic reactions involving pyridinamide ion pair catalysts.

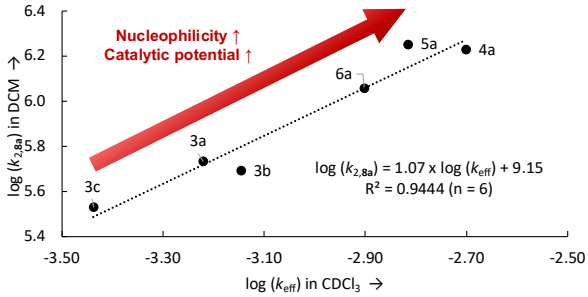

Figure 6. Correlation of log k_{eff} vs. log k_2(**8a**) for pyridinamide ion pair catalysts.

pK_a Values. In order to test whether the reactivities of pyridinamide anions **3** - **6** towards electrophiles correlate with their Brønsted basicities, their pK_a values were determined in three water/co-solvent mixtures using a spectrophotometric titration method at 25 °C (Table 5, for details see SI). The ionic strength was controlled with KCl in the buffer solution and set to I = 0.3 M. Starting from the neutral pyridine sulfonamide (**PA**), a first pK_a value (referred to as pK_{a1}) can be determined for protonation at the sulfonamide nitrogen atom, while the second pK_a value (referred to as pK_{a2}) describes deprotonation towards anions **3-6**. That neutral sulfonamides **PA** have a preference for the imino tautomeric form shown in Table 5 is supported by X-ray crystal structures of these systems.[15] The assignment of tautomeric form **PA_H** is only tentative and rests on X-ray crystal structures of complexes of **PA** with protic solvents. The UV/Vis absorbance of the substrate is measured across the full p*H*

range. For pK_{a2}, the pH-absorbance plot is fitted to equation 4, where A_{obs} is the observed absorbance, A_{max} is the maximum absorbance of the neutral compound, A_{min} is the minimum absorbance (at which the substrate is fully deprotonated), pH is that of the used buffer, and K_a is the acid dissociation constant for the substrate.

$$A_{obs} = \frac{10^{-pH} \times A_{max} + K_a \times A_{min}}{10^{-pH} + K_a} \quad (4)$$

The pK_a of the pyridinamide compounds was determine in aqueous solutions, H_2O/MeCN mixtures (volume ratio = 1:1), and H_2O/DMSO mixtures (volume ratio = 1:1). The pK_a of DMAP was chosen as a reference and is in agreement with literature values.[28] To exclude a potential interference of the countercation when using pyridinamide salts instead of neutral sulfonamide for the pK_a determination, pyridinamide ion pair **5a** was measured under the same conditions (see SI, Chapter 6).

Table 5. List of measured pK_a values for pyridinamides (PA) in selected aqueous solvent mixtures at 25 °C.

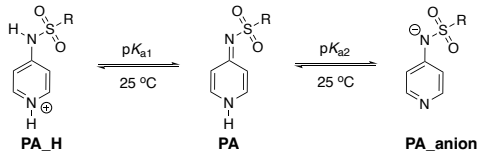

PA	pK_{a1}	pK_{a2}	solvent
1	9.85	–	H_2O + 2.5% MeCN
3	–	7.62[a]	H_2O + 2.5% MeCN
4	3.57[a]	8.85[a]	H_2O + 2.5% MeCN
5	3.44[a]	8.83[a]	H_2O + 2.5% MeCN
6	2.69[a]	8.65[a]	H_2O + 2.5% MeCN
1	8.73[a,b]	–	H_2O/MeCN = 1:1
IP_3a	–	7.31[a,b]	H_2O/MeCN = 1:1
IP_4a	3.46[a,b]	8.70[a,b]	H_2O/MeCN = 1:1
IP_5a	3.32[a,b]	8.67[a,b]	H_2O/MeCN = 1:1
IP_6a	2.45[a,b]	8.35[a,b]	H_2O/MeCN = 1:1
3	7.46[c]	–	H_2O/DMSO = 1:1
4	n.d	8.97[c]	H_2O/DMSO = 1:1
5	n.d	8.92[c]	H_2O/DMSO = 1:1
6	n.d	8.57[c]	H_2O/DMSO = 1:1

[a] averaged pK_a values over two measurement series. [b] conversion factor -0.257 for 50% MeCN[29] content applied on pH of the baseline. [c] single measurement series of observed pK_a with 50% DMSO content.

The observed pK_a values of sulfonamides were similar in all employed solvent mixtures with sulfonamide **4** being the most basic one in all cases. The overall basicity trend **3** < **6** < **5** < **4** also remains the same when switching solvents. Contrary to the sulfonamides, the pK_a value of DMAP responds strongly to changes in solvent: moving from almost pure water to the 1:1 water/MeCN mixture lowers the pK_a value from +9.85 to +8.73. Correlating the measured pK_a values of the sulfonamides in the 1:1 H_2O/MeCN solvent mixture with the logarithmic rate constant for reactions of pyridinamide ion pairs with electrophile **8a** in MeCN shows a good correlation. This correlation, however, is not universal as adding DMAP (**1**) to the dataset shows (Fig. 7).

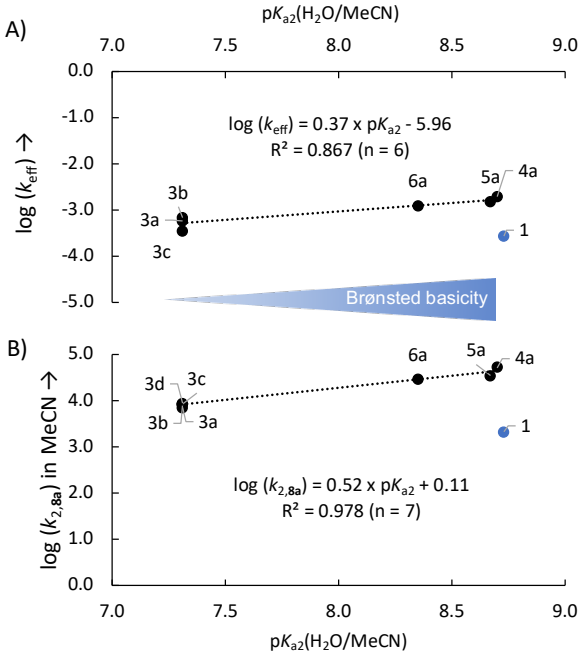

Figure 7. A) Correlation of log(k_{eff}) vs. pK_{a2} values in H_2O/MeCN = 1:1 for pyridinamide ion pairs **3a-c,4-6a** and pK_{a1} of DMAP (**1**). B) Correlation of log($k_{2,8a}$) in MeCN vs. pK_{a2} values in H_2O/MeCN = 1:1 for pyridinamide ion pair **3a-d,4-6a** and pK_{a1} of DMAP (**1**). The results for DMAP were excluded from the correlation in both cases.

Computational studies. To quantify the Lewis basicity of pyridinamide ion pairs, methyl cation affinities (MCA) have been calculated at the SMD(DCM)/B3LYP-D3/6-31+G(d) level of theory. This type of relative affinity value has previously been shown to correlate well with experimentally determined rate constants.[15,30,31] In agreement with those studies, pyridine was chosen as reference base for the group transfer reaction shown in eq. 5 and the relative Lewis basicity towards Me^+ (ΔMCA) was calculated as the free reaction energy at 298.15 K.

(5)

The resulting ΔMCA values are plotted against the experimentally obtained effective rate constant k_{eff} for the synthesis of urethane **11** with a catalyst load of 3.0 mol% in Figure 8, which shows a strong correlation between those two parameters. The relative Lewis basicity parameter ΔMCA displays the same general trend observed for the nucleophilicity, pK_a values and in the effective rate constant k_{eff} in the urethane benchmark reaction. In all measurements the most basic pyridinamide ion pair **4a** achieves the highest value. It should be added that higher catalyst basicity may[32] or may not[33] translate into higher reaction rates of catalytic transformations with pyridine-derived Lewis bases.

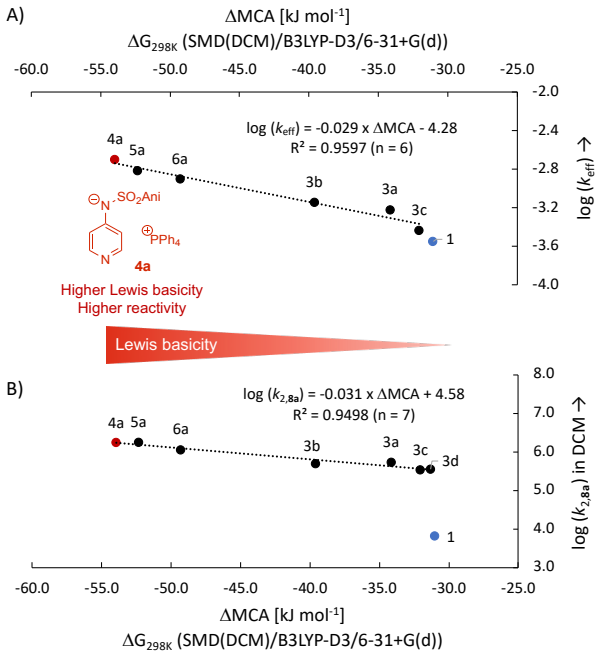

Figure 8. A) Correlation of effective rate constant log(k_{eff}) for urethane synthesis (3.0 mol% catalyst loading) with Lewis basicity parameter ΔMCA, and B) correlation of bimolecular rate constant log($k_{2,\mathbf{8a}}$) with Lewis basicity parameter ΔMCA calculated at the SMD(DCM)/B3LYP-D3/6-31+G(d) level of theory. The results for DMAP were excluded from the correlation in both cases.

CONCLUSION

By employing a combination of conductivity, DOSY NMR, and kinetic measurements for a focused library of pyridinamide ion pairs, we were able to elucidate the complex asymmetric association behavior of these ions and its impact on their catalytic performance. Key insights include the strong dependence of the association pattern on the size and structure of the cation, which significantly influences the balance between cationic and anionic sandwich association. The association constants of ion pair **3a-d** derived from conductivity data revealed a lower degree of association in ion pairs with larger aryl substituted cation, which also correlates with their catalytic activity. DOSY NMR results further support this theory and show a predominant cationic sandwich association in smaller anion – larger cation volume pairs, which is essential for maintaining a higher concentration of free nucleophilic anions in solution.

Kinetic studies using the ionic strength-controlled benzhydrylium method confirmed a superior nucleophilicity of pyridinamide anions in DCM compared to neutral organocatalysts such as TCAP (**2**). Comparing the bimolecular rate constants k_2 for reactions with cationic reference electrophiles reveal the most nucleophilic pyridinamide compound being anion **4** with a 90 times higher rate constant than TCAP (**2**). This is also reflected in the determined reaction rate of urethane benchmark reaction, where **4a** catalyzes the reaction seven times more effectively than TCAP (**2**). Kinetic data for the single step nucleophilicity measurements as well as the multi-step catalytic benchmark experiments correlate well with the Brønsted and Lewis basicities of the respective ion pair systems. These latter quantities thus represent, together with the volume parameters obtained from SMD-type calculations, valuable guidelines for the future design of highly reaction ion pair systems.

ASSOCIATED CONTENT

Supporting Information

The Supporting Information is available free of charge on the ACS Publications website and includes additional experimental and computational details, analysis procedures and methods, including step by step descriptions. (PDF)

Accession Codes

CCDC accession codes 2310788 - 2310789 and 2386693 - 2386697 contain the supplementary crystallographic data for this paper. These data can be obtained free of charge via www.ccdc.cam.ac.uk/data_request/cif, or by emailing data_request@ccdc.cam.ac.uk, or by contacting the Cambridge Crystallographic Data Centre, 12 Union Road, Cambridge CB2 1EZ, UK; fax: +44 1223 336033.

AUTHOR INFORMATION

Corresponding Author

Hendrik Zipse – *Department of Chemistry, Ludwig-Maximilians Universität München, Butenandtstr. 5-13, 81377 München, Germany; orcid.org/0000-0002-0534-3585; E-mail: zipse@cup.uni-muenchen.de*

Armin R. Ofial – *Department of Chemistry, Ludwig-Maximilians Universität München, Butenandtstr. 5-13, 81377 München, Germany; orcid.org/0000-0002-9600-2793; E-mail: ofial@lmu.de*

Ruth M. Gschwind – *Institute for Organic Chemistry, University Regensburg, Universitätsstr. 31, 93053 Regensburg, Germany; orcid.org/0000-0003-3052-0077; Email: ruth.gschwind@ur.de*

AnnMarie C. O'Donoghue – *Department of Chemistry, Durham University, South Road, Durham DH1 3LE, United; orcid.org/0000-0001-8652-8225; Email: annmarie.odonoghue@durham.ac.uk*

Author

Veronika Burger – *Department of Chemistry, Ludwig-Maximilians Universität München, Butenandtstr. 5-13, 81377 München, Germany; orcid.org/0009-0003-5482-9025*

Maximilian Franta – *Institute for Organic Chemistry, University Regensburg, Universitätsstr. 31, 93053 Regensburg, Germany: orcid.org/0009-0006-4861-9808*

Author Contributions

The manuscript was written through contributions of all authors. / All authors have given approval to the final version of the manuscript.

Funding Sources

This work was funded by the Deutsche Forschungsgemeinschaft (DFG, German Research Foundation) – 426795949 through the Research Training Group (RTG) 2620 "Ion Pair Effects in Molecular Reactivity".

ACKNOWLEDGMENT

The authors are thankful to Nathalie Hampel for the synthesis of **8a-8c**, Dr. Fabian Zott (LMU) for help with kinetics simulations, and Christian Scholtes (Regensburg) for providing a python script for the DOSY evaluation.

ABBREVIATIONS

DCM, dichloromethane; DMAP, 4-dimethylaminopyridine; DMSO, dimethylsulfoxide; DOSY, diffusion-ordered NMR spectroscopy; IP, ion pair; MCA, methyl cation affinity; MeCN, acetonitrile; PA, pyridinamide; TCAP, 9-azajulolidine.

REFERENCES

(1) Yang, Z.; Xu, C.; Zhou, X.; Cheong, C. B.; Kee, C. W.; Tan, C. H. A Chiral Pentanidium and Pyridinyl-Sulphonamide Ion Pair as an Enantioselective Organocatalyst for Steglich Rearrangement. *Chem. Sci.* **2023**, *14* (45), 13184–13190. https://doi.org/10.1039/d3sc04397e.

(2) Yang, X.; Birman, V. B. Acyl Transfer Catalysis with 1,2,4-Triazole Anion. *Org. Lett.* **2009**, *11* (7), 1499–1502. https://doi.org/10.1021/ol900098q.

(3) Lyons, D. J. M.; Empel, C.; Pace, D. P.; Dinh, A. H.; Mai, B. K.; Koenigs, R. M.; Nguyen, T. V. Tropolonate Salts as Acyl-Transfer Catalysts under Thermal and Photochemical Conditions: Reaction Scope and Mechanistic Insights. *ACS Catal.* **2020**, *10* (21), 12596–12606. https://doi.org/10.1021/acscatal.0c03702.

(4) Dale, H. J. A.; Hodges, G. R.; Lloyd-Jones, G. C. Kinetics and Mechanism of Azole N−π*-Catalyzed Amine Acylation. *J. Am. Chem. Soc.* **2023**, *145* (32), 18126–18140. https://doi.org/10.1021/jacs.3c06258.

(5) Shirakawa, S.; Maruoka, K. Recent Developments in Asymmetric Phase-Transfer Reactions. *Angew. Chem. Int. Ed.* **2013**, *52* (16), 4312–4348. https://doi.org/10.1002/anie.201206835.

(6) Brak, K.; Jacobsen, E. N. Asymmetric Ion-Pairing Catalysis. *Angew. Chem. Int. Ed.* **2013**, *52* (2), 534–561. https://doi.org/10.1002/anie.201205449.

(7) Merten, C.; Pollok, C. H.; Liao, S.; List, B. Stereochemical Communication within a Chiral Ion Pair Catalyst. *Angew. Chem. Int. Ed.* **2015**, *54* (30), 8841–8845. https://doi.org/10.1002/anie.201501271.

(8) Mahlau, M.; List, B. Asymmetric Counteranion-Directed Catalysis: Concept, Definition, and Applications. *Angew. Chem. Int. Ed.* **2013**, *52* (2), 518–533. https://doi.org/10.1002/anie.201205343.

(9) Phipps, R. J.; Hamilton, G. L.; Toste, F. D. The Progression of Chiral Anions from Concepts to Applications in Asymmetric Catalysis. *Nat. Chem.* **2012**, *4*, 603–614. https://doi.org/10.1038/nchem.1405.

(10) Gillespie, J. E.; Fanourakis, A.; Fanourakis, A.; Phipps, R. J.; Phipps, R. J. Strategies That Utilize Ion Pairing Interactions to Exert Selectivity Control in the Functionalization of C–H Bonds. *J. Am. Chem. Soc.* **2022**. https://doi.org/10.1021/jacs.2c08752.

(11) Iribarren, I.; Mates-Torres, E.; Trujillo, C. Revisiting Ion-Pair Interactions in Phase Transfer Catalysis: From Ionic Compounds to Real Catalyst Systems. *Dalton Trans.* **2023**. https://doi.org/10.1039/d3dt03978a.

(12) Litvinenko, L. M.; Kirichenko, A. I. Basicity and Stereospecificity in Nucleophile Catalysis by Tertiary Amines. *Dokl Akad Nauk SSSR Ser Khim* **1967**, *176*, 97–100.

(13) Steglich, W.; Höfle, G. N,N-Dimethyl-4-pyridinamine, a Very Effective Acylation Catalyst. *Angew. Chem. Int. Ed.* **1969**, *8* (12), 981–981. https://doi.org/10.1002/anie.196909811.

(14) Heinrich, M. R.; Klisa, H. S.; Mayr, H.; Steglich, W.; Zipse, H. Enhancing the Catalytic Activity of 4-(Dialkylamino)Pyridines by Conformational Fixation. *Angew. Chem. Int. Ed.* **2003**, *42* (39), 4826–4828. https://doi.org/10.1002/anie.200352289.

(15) Helberg, J.; Ampßler, T.; Zipse, H. Pyridinyl Amide Ion Pairs as Lewis Base Organocatalysts. *J. Org. Chem.* **2020**, *85* (8), 5390–5402. https://doi.org/10.1021/acs.joc.0c00114.

(16) Dempsey, S. H.; Lovstedt, A.; Kass, S. R. Electrostatically Enhanced 3- and 4-Pyridyl Borate Salt Nucleophiles and Bases. *J. Org. Chem.* **2023**, *88* (15), 10525–10538. https://doi.org/10.1021/acs.joc.3c00523.

(17) Burger, V.; Franta, M.; Ofial, A. R.; Gschwind, R. M.; Zipse, H. Highly Nucleophilic Pyridinamide Anions in Apolar Organic Solvents Due to Asymmetric Ion Pair Association. *J. Am. Chem. Soc.* **2024**, accepted.

(18) Liotta, C. L.; Harris, H. P. The Chemistry of "Naked" Anions. I. Reactions of the 18-Crown-6 Complex of Potassium Fluoride with Organic Substrates in Aprotic Organic Solvents. *J. Am. Chem. Soc.* **1974**, *96* (7), 2250–2252. https://doi.org/10.1021/ja00814a044.

(19) A database of published reactivity parameters E, N, and sN is freely accessible at. https://www.cup.lmu.de/oc/mayr/reaktionsdatenbank2/.

(20) Mayr, H. Reactivity Scales for Quantifying Polar Organic Reactivity: The Benzhydrylium Methodology. *Tetrahedron* **2015**, *71* (32), 5095–51111. https://doi.org/10.1016/j.tet.2015.05.055.

(21) Brotzel, F.; Kempf, B.; Singer, T.; Zipse, H.; Mayr, H. Nucleophilicities and Carbon Basicities of Pyridines. *Chem. Eur. J.* **2007**, *13* (1), 336–345. https://doi.org/10.1002/chem.200600941.

(22) Nigst, T. A.; Ammer, J.; Mayr, H. Photogeneration of Benzhydryl Cations by Near-UV Laser Flash Photolysis of Pyridinium Salts. *J. Phys. Chem. A* **2012**, *116* (33), 8494–8499. https://doi.org/10.1021/jp3049247.

(23) Tandon, R.; Unzner, T.; Nigst, T. A.; De Rycke, N.; Mayer, P.; Wendt, B.; David, O. R. P.; Zipse, H. Annelated Pyridines as Highly Nucleophilic and Lewis Basic Catalysts for Acylation Reactions. *Chem. Eur. J.* **2013**, *19* (20), 6435–6442. https://doi.org/10.1002/chem.201204452.

(24) Helberg, J.; OE, Y.; Zipse, H. Mechanistic Analysis and Characterization of Intermediates in the Phosphane-Catalyzed Oligomerization of Isocyanates. *Chem. Eur. J.* **2018**, *24,* 14387–14391. https://doi.org/10.1002/chem.201804016.

(25) Bacaloglu, R.; Cotarca, L.; Marcu, N.; Tölgiy, S. Reactions of Aryl lsocyanates with Alcohols in the Presence of Tertiary Amines. *J. Prakt. Chem.* **1988**, *330*, 530–540.

(26) Alsarraf, J.; Ammar, Y. A.; Robert, F.; Cloutet, E.; Cramail, H.; Landais, Y. Cyclic Guanidines as Efficient Organocatalysts for the Synthesis of Polyurethanes. *Macromolecules* **2012**, *45*, 2249–2256. https://doi.org/10.1021/ma2026258.

(27) Sardon, H.; Pascual, A.; Mecerreyes, D.; Taton, D.; Cramail, H.; Hedrick, J. L. Synthesis of Polyurethanes Using Organocatalysis: A Perspective. *Macromolecules* **2015**, *48*, 3153–3165. https://doi.org/10.1021/acs.macromol.5b00384.

(28) Sooväli, L.; Rodima, T.; Kaljurand, I.; Kütt, A.; Koppel, I. A.; Leito, I. Basicity of Some P1 Phosphazenes in Water and in Aqueous Surfactant Solution. *Org. Biomol. Chem.* **2006**, *4* (11), 2100–2105. https://doi.org/10.1039/B602797K.

(29) Gagliardi, L. G.; Castells, C. B.; Ràfols, C.; Rosés, M.; Bosch, E. δ Conversion Parameter between pH Scales in Acetonitrile/Water Mixtures at Various Compositions and Temperatures. *Anal. Chem.* **2007**, *79* (8), 3180–3187. https://doi.org/10.1021/ac062372h.

(30) Marin-Luna, M.; Patschinski, P.; Zipse, H. Substituent Effects in the Silylation of Secondary Alcohols: A Mechanistic Study. *Chem. Eur. J.* **2018**, *24* (56), 15052–15058. https://doi.org/10.1002/chem.201803014.

(31) Mayr, S.; Marin-Luna, M.; Zipse, H. Size-Driven Inversion of Selectivity in Esterification Reactions: Secondary Beat Primary Alcohols. *J. Org. Chem.* **2021**, *86* (4), 3456–3489. https://doi.org/10.1021/acs.joc.0c02848.

(32) Richard, N. A.; Charlton, G. D.; Dyker, C. A. Enhancing catalytic activity of pyridines via para-iminophosphorano substituents. *Org. Biomol. Chem.* **2021**, *19*, 9167–9171. https://doi.org/10.1039/d1ob01630j.

(33) Kluga, R.; Kinens, A.; Suna, E. Chiral 4-MeO-Pyridine (MOPY) Catalyst for Enantioselective Cyclopropanation: Attenuation of Lewis Basicity Leads to Improved Catalytic Efficiency. *Chem. Eur. J.* **2024**, *30*, e202301136. https://doi.org/10.1002/chem.202301136.

(34) Maji, B.; Stephenson, D. S.; Mayr, H. Guanidines: Highly Nucleophilic Organocatalysts. *ChemCatChem* **2012**, *4*, 993 - 999.

3.1 Supplementary Data

3.1.1 General Information

All reagents were purchased from Sigma Aldrich, TCI, or Acros and used without further purification unless otherwise noted. Solvents were obtained from Acros Organics, Sigma Aldrich, or Merck and purified by simple distillation in a rotary evaporator, unless otherwise specified.

All air- and moisture-sensitive reactions were performed under a nitrogen atmosphere and the glassware and magnetic stirrers were dried in a dry oven at 110 °C overnight.

CH_2Cl_2 for nucleophilicity measurements was stirred over concentrated H_2SO_4 for two weeks before extraction with water (1 x 1.0 L), $NaHCO_3$ (1 x 1.0 L), and again water (1 x 1.0 L). CaH_2 was added as a drying agent, and the solvent was freshly distilled over CaH_2 prior to use.

Melting points were acquired using Büchi Melting Point M-560 devices and are uncorrected.

Nuclear magnetic resonance (NMR) spectra were recorded on a Bruker 400 MHz or INOVA 400 and 600 MHz machine. The following abbreviations were used in the analysis of NMR spectra: s = singlet, d = doublet, t = triplet, q = quartet, m = multiplet, br s = broad singlet. NMR signals were assigned based on 2D spectra (COSY, HSQC, HMBC) analysis. Chemical shifts are given in ppm. The internal reference was set to the residual solvent signals (CD_2Cl_2, $CDCl_3$, DMSO-d_6). The ^{13}C NMR spectra (101 or 151 MHz) were recorded under broadband proton-decoupling. ^{19}F NMR spectra were referenced using the solvent signal.[1] The spectra were imported and processed in the program MestreNova (version 14.1.1).

Infrared (IR) spectra were measured on a Perkin Elmer Spectrum BX-59343 instrument with a Smith Detection DuraSamplIR II Diamond ATR sensor for liquids or neat for solids. Intensities are described as vs = very strong, m = medium, w = weak, br = broad.

High-resolution mass spectra (HRMS) were recorded on a Thermo Finnigan LTQ FT Ultra Fourier Transform Ion Cyclotron Resonance mass spectrometer with electrospray ionization (ESI) for sample ionization. For EI (70 eV) measurements a Thermo Finnigan of the MAT 95 type with a direct exposure probe (DEP) was used.

Crystal structures were recorded using an Oxford Diffraction XCalibur with Sapphire CCD-detector and a molybdenum-K_α-source ($\lambda = 0.71073$) with a concentric circle kappa-device. The structures were resolved using the program SHELXS or SIR97 and refined with SHELXS.

3.1.2 Additional Figures and Correlations

Conductivity profiles in MeCN for all pyridinamide ion pairs are depicted in Figure 3.1.

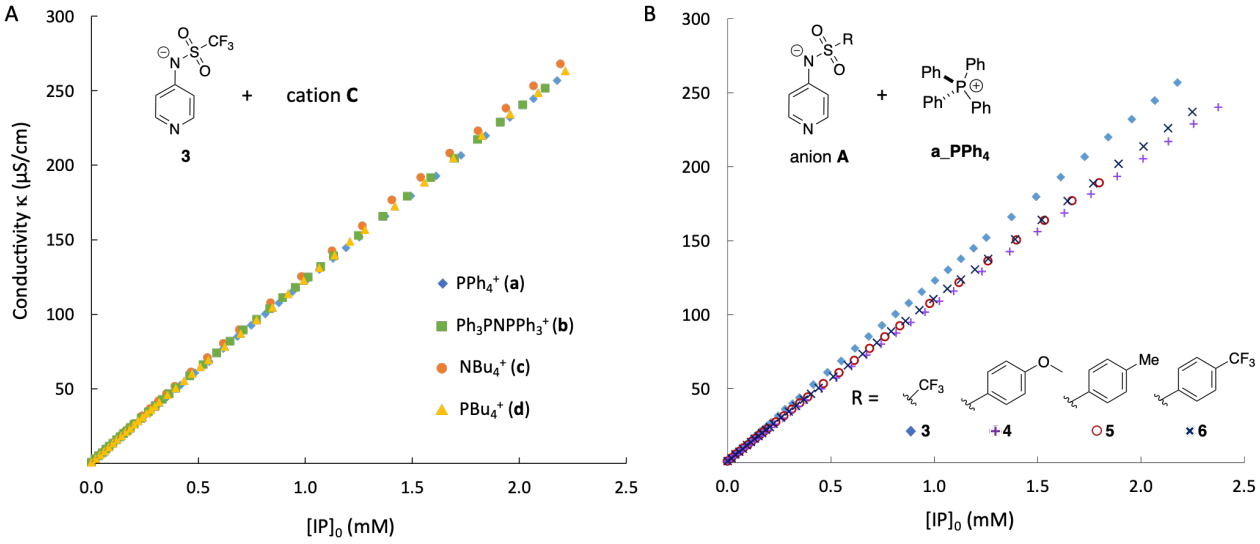

Figure 3.1: [Figure S1]. A) Conductivity profiles for **3a-d** measured in MeCN at 20 °C, B) Conductivity profiles for **3-6a** measured in MeCN at 20 °C.

The association constant K_{IP} for the association in MeCN was determined according to the simple 1:1 ion association model described in Zipse *et al*.[2] The resulting association constants K_{IP} (M^{-1}) are summarized in Table 3.1.

Table 3.1: [Table S1]. Association constants K_{IP} (M^{-1}) of pyridinamide ion catalysts **3a-d,4-6a** at 20 °C in MeCN.

System	Λ_m (S cm² mol^{-1})	K_{IP} (M^{-1})
3a	126	34.6 ± 0.29
3b	130	50.6 ± 0.50
3c	133	44.0 ± 0.63
3d	129	44.0 ± 0.34
4a	110	42.9 ± 0.33
5a	113	44.5 ± 0.80
6a	115	49.3 ± 0.55

Additional correlations were performed for pK_a values with the respective effective rate constants of the urethane benchmark reaction. Both experimental values correlate strongly with each other in Figure 3.2, however, adding the results of DMAP to the data set demonstrated that this is not a universal correlation for pyridine-based compounds.

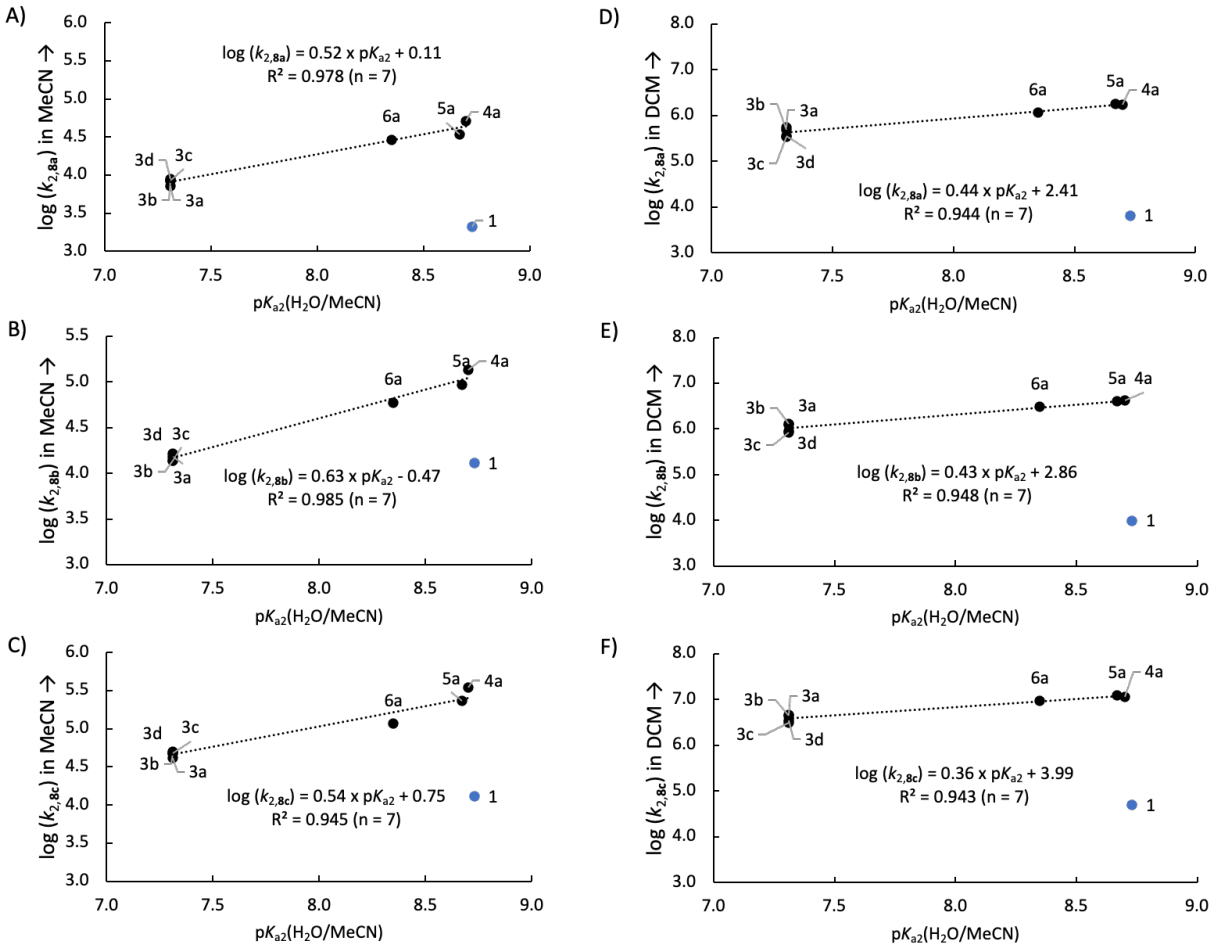

Figure 3.2: [Figure S2]. Correlation of A) log ($k_{2,8a}$) in MeCN**,** B) log ($k_{2,8b}$) in MeCN, C) log ($k_{2,8c}$) in MeCN, D) log ($k_{2,8a}$) in DCM, E) log ($k_{2,8b}$) in DCM, and F) log ($k_{2,8c}$) in DCM with pK_a values measured in H$_2$O/MeCN = 1:1 for pyridinamide salts **3-6a**.

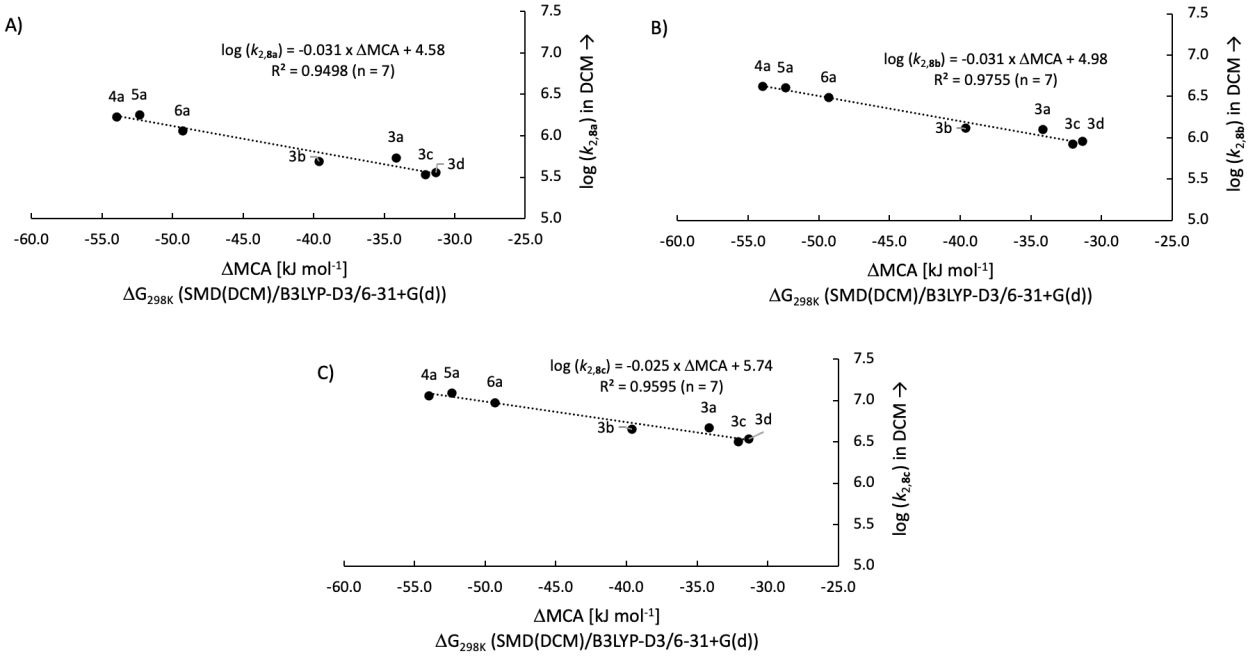

Figure 3.3: [Figure S3]. Correlation of A) bimolecular rate constant log ($k_{2,8a}$), B) bimolecular rate constant log ($k_{2,8b}$), C) bimolecular rate constant log ($k_{2,8c}$) with Lewis basicity parameter ΔMCA calculated at the SMD(DCM)/B3LYP-D3/6-31+G(d) level of theory.

In Table 3.2 and Table 3.3 below the most important results of the conductivity data analysis is summarized to enable a quick and easy overview over the specific molar conductivities Λ_m (S cm^2 mol^{-1}), the limited molar ion conductivities λ_i (S cm^2 mol^{-1}) of all charged species, their scaling factors δ_i and the resulting association constant of all applied model (see Chapter 2.1.4 and 3.1.4 for details).

Table 3.2: [Table S2]. List of specific molar conductivities Λ_m (S cm^2 mol^{-1}) with the corresponding limited molar ionic conductivities λ_i (S cm^2 mol^{-1}) with their scaling factor δ_i of all charged species and the resulting ion association constant K_{IP} (M^{-2}), the cationic and anionic sandwich association constants K_{CAC} and K_{ACA} (M^{-2}) with the respective RMSE values for all pyridinamide ion pairs.

Ion Pair	Λ_m (S cm^2 mol^{-1})	λ_A (S cm^2 mol^{-1})	λ_C (S cm^2 mol^{-1})	λ_{CAC} (S cm^2 mol^{-1})	λ_{ACA} (S cm^2 mol^{-1})	δ_A /δ_C /δ_{CAC}//δ_{ACA}	K_{IP} (M^{-2}) (RMSE)	K_{CAC} (M^{-2}) (RMSE)	K_{ACA} (M^{-2}) (RMSE)
3d	56.0	22.4	33.6	8.40	–	40/60/15/–	7.35 x 10^6 (0.33)	1.07 x 10^7 (0.09)	–
3c	57.9	23.7	34.2	12.7	2.32	41/59/22/4	5.00 x 10^6 (0.26)	1.01 x 10^7 (0.10)	1.01 x 10^7 (0.10)
3b	80.3	22.4	57.8	73.1	37.8	28/72/91/47	2.96 x 10^5 (0.32)	4.65 x 10^6 (0.11)	4.65 x 10^6 (0.11)
3a	79.2	29.3	49.9	53.1	32.5	37/63/67/41	6.86 x 10^5 (0.30)	6.38 x 10^6 (0.17)	6.38 x 10^6 (0.17)
5a	73.2	30.7	42.5	41.7	30.0	42/58/57/41	6.92 x 10^5 (0.23)	5.15 x 10^6 (0.13)	5.15 x 10^6 (0.13)
4a	73.6	32.4	41.2	39.7	30.9	44/56/54/42	8.79 x 10^5 (0.27)	6.50 x 10^6 (0.12)	6.50 x 10^6 (0.12)
6a	74.2	33.4	40.8	44.5	37.1	45/55/60/50	6.89 x 10^5 (0.32)	6.75 x 10^6 (0.12)	6.75 x 10^6 (0.12)
7a	95.2	15.2	80.0	76.2	–	16/84/80/–	1.01 x 10^6 (0.33)	7.05 x 10^6 (0.16)	–
7b	91.3	10.0	81.3	90.4	–	11/89/99/–	3.98 x 10^5 (0.47)	4.61 x 10^6 (0.24)	–
7c	68.2	12.3	55.9	23.2	–	18/82/34/–	2.49 x 10^7 (0.22)	3.51 x 10^7 (0.15)	–
7d	59.9	10.8	49.1	18.0	–	18/82/30/–	3.04 x 10^7 (0.21)	3.46 x 10^7 (0.12)	–

Table 3.3: [Table S3]. List of cationic and anionic sandwich association constants K_{CAC} and K_{ACA} (M^{-2}) with the respective RMSE values as result of the separated models and the mixed sandwich association model with their scaling factors α and β as well as the reference DOSY ion volumes and the calculated ion volumes with their percentual residual at c = 1.0 mM for all ion pairs.

Ion Pair	K_{CAC} (M^{-2}) (RMSE)	K_{ACA} (M^{-2}) (RMSE)	α/β	α x K_{CAC} (M^{-2})	β x K_{ACA} (M^{-2})	RMSE	V_{an} (Å^3)	V_{cat} (Å^3)	Residual (%) Anion	Residual (%) Cation
DOSY ref(3c)							**571**	**660**		
3c	1.01 x 10^7 (0.10)	1.01 x 10^7 (0.10)	33/23	3.33 x 10^6	2.32 x 10^6	0.61	535	619	-6.21	-6.23
DOSY ref(3b)							**473**	**944**		
3b	4.65 x 10^6 (0.11)	4.65 x 10^6 (0.11)	100/0	4.65 x 10^6	0.00	0.11	590	1076	+24.7	+14.0
DOSY ref(3a)							**505**	**642**		
3a	6.38 x 10^6 (0.17)	6.38 x 10^6 (0.17)	44/21	2.81 x 10^6	1.34 x 10^6	0.43	533	679	+5.61	+5.80
DOSY ref(5a)							**727**	**652**		
5a	5.15 x 10^6 (0.13)	5.15 x 10^6 (0.13)	11/67	5.67 x 10^5	3.45 x 10^6	0.29	670	601	-7.90	-7.79
DOSY ref(4a)							**765**	**682**		
4a	6.50 x 10^6 (0.12)	6.50 x 10^6 (0.12)	12/61	7.80 x 10^5	3.97 x 10^6	0.35	706	630	-7.79	-7.67
DOSY ref(6a)							**772**	**714**		
6a	6.75 x 10^6 (0.12)	6.75 x 10^6 (0.12)	16/52	1.08 x 10^6	3.51 x 10^6	0.38	711	657	-7.90	-7.93

3.1.3 Synthesis of Compounds

In this supporting information the data for the following ion pair (see Chart 3.1) will be discussed. Pyridinamide ion pair **3a** will be used as reference system. Synthetic procedures for compounds PA_**3**, PA_**4**, ion pair **3a**, **4a**, and additive **6** (in this chapter **7a**) can be found in Chapter 2.1

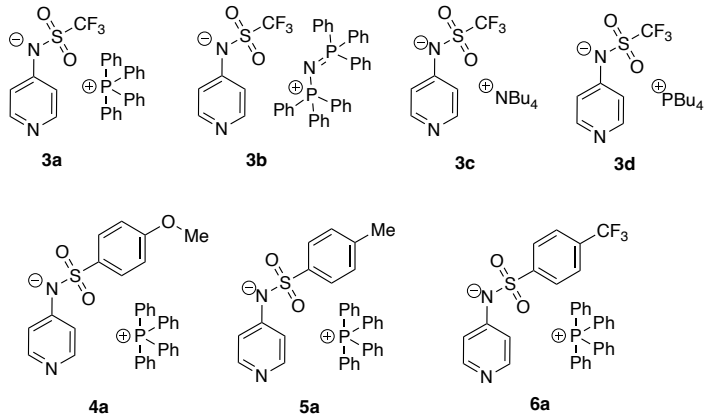

Chart 3.1: [Chart S1]. Pyridinamide ion pair library.

3.1.3.1 Synthesis of Neutral Pyridinamides

4-Methyl-*N*-(pyridin-4(1*H*)-ylidene)benzenesulfonamide (PA_**5**)

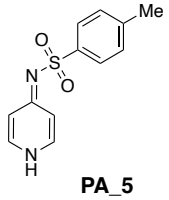
PA_5

Following a modified procedure of Helberg and Zipse,[3] 4-aminopyridine (2.00 g, 1.0 eq, 21.3 mmol) was dissolved in pyridine (22.0 mL). Triethylamine (8.00 mL, 57.4 mmol, 2.3 eq) was added and the mixture was stirred for 10 min. After cooling to 0 °C, 4-methylbenzenesulfonyl chloride (4.86 g, 1.2 eq, 25.5 mmol) was added and the mixture was stirred at 0 °C for 30 min. Subsequently, the reaction mixture was refluxed for 3 h before being cooled down to rt. The solvent was evaporated, and the crude product was suspended in H_2O, refluxed for 20 min and filtered while hot. This process was repeated with ethanol and MTBE, yielding pyridinamide **5** (4.78 g, 19.59 mmol, 91%) as an off-white solid.

^{1}H NMR (400 MHz, DMSO-d_6): δ [ppm] = 12.3 (s, 1H), 8.01 (d, J = 6.7 Hz, 2H), 7.71 – 7.65 (m, 2H), 7.30 (d, J = 8.0 Hz, 2H), 6.95 – 6.86 (m, 2H), 2.33 (s, 2H).

^{13}C NMR (101 MHz, DMSO-d_6): δ [ppm] = 141.6, 140.2, 129.3, 126.2, 114.1, 20.9.

HRMS (ESI): calc. for $C_{12}H_{12}N_2O_2S^+$ [M^+]: 248.0614, found: 248.0614.

The spectroscopic data is consistent with the literature.[3]

N-(pyridin-4(1*H*)-ylidene)-4-(trifluoromethyl)benzenesulfonamide (PA_**6**)

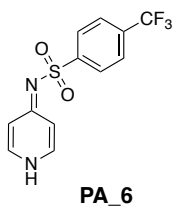
PA_6

4-Aminopyridine (1.00 g, 10.6 mmol, 1.0 eq) was dissolved in dry pyridine (12.0 mL) under nitrogen atmosphere. Triethylamine (3.30 mL, 23.4 mmol, 2.2 eq) was added and the reaction mixture was stirred for 10 min before being cooled down to 0 °C. 4-Trifluoromethylbenzenesulfonyl chloride (2.86 g, 11.7 mmol, 1.1 eq) was added and the mixture was stirred for 20 min before being refluxed for 2.5 h. The solvent was evaporated, and the crude product was suspended in H_2O, refluxed for 20 min and filtered while hot. This process was repeated with ethanol and MTBE, yielding pyridinamide **6** (2.64 g, 8.73 mmol, 82%) as an off-white solid.

^{1}H NMR (400 MHz, DMSO-d_6): δ [ppm] = 12.8 (s, 1H), 8.00 (dd, *J* = 7.6, 5.4 Hz, 4H), 7.87 (d, *J* = 8.2 Hz, 2H), 6.94 (d, *J* = 7.3 Hz, 2H).

^{13}C NMR (101 MHz, DMSO-d_6): δ [ppm] = 162.5, 147.8, 139.2, 131.0 (q, *J* = 32.1 Hz), 126.9, 125.9 (q, *J* = 3.8 Hz), 123.7 (q, *J* = 272.6 Hz), 114.9.

^{19}F NMR (377 MHz, $CDCl_3$): δ [ppm] = -61.4

IR (ATR): ν (cm^{-1}) = 3049 (w), 2660 (w), 1635 (m), 1617 (m), 1477 (s). 1330 (s), 1194 (m), 1140 (vs), 1086 (s), 950 (s), 834 (s), 766 (m), 706 (m).

HRMS (ESI): calc. for $C_{12}H_9F_3N_2O_2S^+$ [M^+]: 302.0331, found 302.0335.

m. p: 298-301 °C

3.1.3.2 Synthesis of Pyridinamide Ion Pairs

Triphenyl ((triphenyl-λ5-phosphaneylidene)amino) phosphonium pyridin-4-yl (trifluoromethyl) sulfonyl) amide (**3b**)

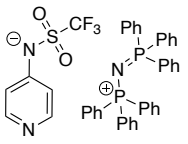

3b

Pyridinamide **3** (349 mg, 1.55 mol, 1.0 eq) was added to a solution of NaOH (67.0 mg, 1.70 mmol, 1.1 eq) in H_2O (5.00 mL). Bis-(triphenylphosphoranyliden)-ammonium chloride (886 mg, 1.55 mmol, 1.0 eq) was added, and the reaction mixture was stirred at rt. overnight. DCM (5.00 mL) was added, and the two phases were separated. The aqueous phase was extracted with DCM (3 x 15 mL). The collected organic phase was dried over $MgSO_4$, filtered and the solvent was evaporated. The crude product was crystallized from DCM overlayered with toluene in a 250 mL flask closed with a septum with one inserted needle, cooled to -40 °C (CO_2/MeCN) and left in the cooling bath overnight. Ion Pair **3b** (952 mg, 1.25 mmol, 81%) was obtained in form of colorless crystals.

^{1}H NMR (400 MHz, $CDCl_3$): δ [ppm] = 8.10 (d, *J* = 6.6 Hz, 2H), 7.63 (td, *J* = 5.7, 2.6 Hz, 6H), 7.49 – 7.38 (m, 24H), 7.12 (d, *J* = 6.5 Hz, 2H).

^{13}C NMR (101 MHz, $CDCl_3$): δ [ppm] = 156.3, 149.4, 134.08 – 133.82 (m), 132.41 – 131.92 (m), 129.99 – 129.37 (m), 127.1 (dd, *J* = 107.9, 1.9 Hz), 122.3 (q, *J* = 328.7 Hz), 118.1.

^{19}F NMR (376 MHz, $CDCl_3$): δ [ppm] = -76.8.

^{31}P NMR (162 MHz, $CDCl_3$): δ [ppm] = 21.03.

IR (ATR): ν (cm^{-1}) = 3058 (br), 1588 (m), 1438 (m), 1319 (s), 1288 (vs), 1198 (s), 1155 (s), 1115 (s), 999 (m), 832 (w), 723 (s), 692 (m).

Elemental Analysis: $C_{42}H_{34}F_3N_3O_2P_2S$ (763.76 g/mol): calc. (%) C, 66.05; H, 4.49; N, 5.50; S, 4.20; Found (%): C, 65.84; H, 4.56; N, 5.43; S, 4.21.

HRMS (ESI): calc. for $C_6H_4F_3N_2O_2S^-$ [A^-]: 224.9951; found 224.9952; calc. for $C_{36}H_{30}NP_2^+$ [C^+]: 538.1848; found: 538.1849.

m. p: 139-140 °C

Tetrabutylammonium pyridin-4-yl((trifluoromethyl)sulfonyl)amide (**3c**)

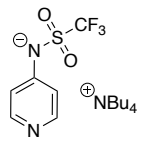

3c

Following a modified procedure of Helberg and Zipse,[3] pyridinamide **3** (400 mg, 1.77 mmol, 1.0 eq) was added to a solution of NaOH (76.3 mg, 1.91 mmol, 1.0 eq) in H_2O (6.00 mL). Tetrabutylammonium bromide (570 mg, 1.77 mmol, 1.0 eq) was added portion-wise. The resulting reaction mixture was stirred at rt. overnight. DCM (6 mL) was added, and the two phases were separated. The aqueous phase was extracted with DCM (3 x 15 mL) and the collected organic phase was dried over $MgSO_4$, filtered, and concentrated *in situ*. The crude product was crystallized from DCM overlayered with toluene and heptane. Pyridinamide ion pair **3c** (710 mg, 1.52 mmol, 86%) were obtained in form of off-white crystals.

^{1}H NMR (600 MHz, $CDCl_3$): δ [ppm] = 8.16 (d, *J* = 6.4 Hz, 2H), 7.04 (d, *J* = 6.4 Hz, 2H), 3.16 – 3.08 (m, 8H), 1.58 – 1.51 (m, 8H), 1.36 (h, *J* = 7.3 Hz, 8H), 0.95 (t, *J* = 7.4 Hz, 12H).

^{13}C NMR (151 MHz, $CDCl_3$): δ [ppm] = 155.8, 149.6, 122.1 (q, *J* = 328.2 Hz), 118.1 58.8, 24.0, 19.7, 13.7.

^{19}F NMR (377 MHz, $CDCl_3$): δ [ppm] = -76.8.

EA: $C_{22}H_{40}F_3N_3O_2S$ (467.64 g/mol): calc. (%): C, 56.51; H, 8.62; N, 8.99; S, 6.86; Found (%): C, 56.34; H, 8.45; N, 9.00; S, 6.63.

The spectroscopic data is consistent with the literature.[3]

Tetrabutylphosphonium pyridin-4-yl((trifluoromethyl)sulfonyl)amide (**3d**)[3]

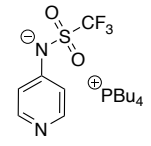

3d

Pyridinamide **3** (402 mg, 1.78 mmol, 1.0 eq) was suspended in tetrabutylphosphonium hydroxide (1.25 mL, 40% in H_2O, 1.78 mmol, 1.0 eq) and H_2O (5.00 mL) was added. The reaction mixture was stirred at rt. for 2 h. DCM (5.00 mL) was added, and the two phases were separated. The aqueous phase was extracted with DCM (3 x 15 mL). The collected organic phase was dried over $MgSO_4$, filtered and the solvent was evaporated. The crude product was crystallized from DCM overlayered with toluene, *iso*-hexane (1.00 mL), and heptane (2.50 mL). The mixture was stored in the fridge overnight. Ion Pair **3d** (718 mg, 1.48 mmol, 88%) was obtained in form of off-white crystals.

^{1}H NMR (600 MHz, $CDCl_3$): δ [ppm] = 8.17 (d, *J* = 6.4 Hz, 2H), 7.04 (d, *J* = 6.5 Hz, 2H), 2.18 – 2.08 (m, 8H), 1.49 – 1.43 (m, 16H), 0.96 – 0.90 (m, 12H).

^{13}C NMR (151 MHz, , $CDCl_3$): δ [ppm] = 155.6, 149.7, 122.1 (q, *J* = 328.1 Hz), 118.1, 23.9 (d, *J* = 15.3 Hz), 23.7 (d, *J* = 4.8 Hz), 18.7 (d, *J* = 47.5 Hz), 13.4.

^{19}F NMR (376 MHz, $CDCl_3$): δ [ppm] = -76.84.

^{31}P NMR (162 MHz, $CDCl_3$): δ [ppm] = 32.98.

Elemental Analysis: $C_{22}H_{40}F_3N_2O_2PS$ (484.60 g/mol): calc. (%) C, 54.53; H, 8.32; N, 5.78; S, 6.62; Found (%): C, 54.41; H, 8.41; N, 5.67; S, 6.89.

The spectroscopic data is consistent with the literature.[3]

Tetraphenylphosphonium pyridin-4-yl(tosyl)amide (**5a**)

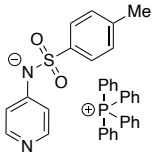

5a

Pyridinamide **5** (449 mg, 1.81 mmol, 1.0 eq) was added to a solution of NaOH (74.3 mg, 1.86 mmol, 1.1 eq) in H_2O (5.00 mL). Tetraphenylphosphonium bromide (746 mg, 1.78 mmol, 1.0 eq) was dissolved in DCM and added dropwise over 10 min through a dropping funnel. The reaction mixture was stirred at rt. for 2 h. DCM (5.00 mL) was added, and the two phases were separated. The aqueous phase was extracted with DCM (3 x 15 mL). The collected organic phase was dried over $MgSO_4$, filtered and the solvent was evaporated. The crude product was crystallized from DCM overlayered with toluene while stored in the fridge. Ion Pair **5a** (905 mg, 1.54 mmol, 85%) was obtained in form of colorless crystals.

^{1}H NMR (400 MHz, $CDCl_3$): δ [ppm] = 7.90 – 7.80 (m, 8H), 7.75 (td, *J* = 7.8, 3.6 Hz, 8H), 7.64 – 7.54 (m, 8H), 7.08 (d, *J* = 7.8 Hz, 2H), 6.76 – 6.72 (m, 2H), 2.28 (s, 3H)

^{13}C NMR (101 MHz, $CDCl_3$): δ [ppm] = 157.9, 148.6, 143.4, 139.5, 135.91 (d, J = 3.0 Hz), 134.48 (d, J = 10.3 Hz), 130.91 (d, J = 12.9 Hz), 128.7, 126.9, 117.5 (d, *J* = 89.6 Hz), 116.2, 21.4.

^{31}P NMR (162 MHz, $CDCl_3$): δ [ppm] = 23.08.

IR (ATR): ν (cm^{-1}) = 3958 (br), 2177 (br), 1586 (m), 1483 (m), 1437 (m), 1314 (m), 1246 (m), 1127 (s), 1107 (s), 1083 (s), 990 (m), 816 (w), 722 (vs), 689 (s).

Elemental Analysis: $C_{36}H_{31}N_2O_2PS$ (586.69 g/mol): calc. (%) C, 73.70; H, 5.33; N, 4.77; S, 5.46; Found (%): C, 73.02; H, 5.45; N, 4.59; S, 5.66.

HRMS (ESI): calc. for $C_{12}H_{11}N_2O_2S^-$ [A^-]: 247.0547; found 247.0547; calc. for $C_{24}H_{20}P^+$ [C^+]: 339.1297; found: 339.1297.

m. p: 160-165 °C

Tetraphenylphosphonium pyridin-4-yl((4-(trifluoromethyl)phenyl)sulfonyl)amide (**6a**)

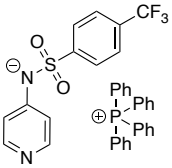

6a

Pyridinamide **6** (299 mg, 0.99 mmol, 1.0 eq) was added to a solution of NaOH (40.0 mg, 1.00 mmol, 1.1 eq) in H_2O (5.00 mL). Tetraphenylphosphonium bromide (415 mg, 0.99 mmol, 1.0 eq) was added and the reaction mixture was stirred at rt. overnight. DCM (5.00 mL) was added, and the two phases were separated. The aqueous phase was extracted with DCM (3 x 10 mL). The collected organic phase was dried over $MgSO_4$, filtered and the solvent was evaporated. The crude product was crystallized from DCM overlayered with toluene and heptane (0.50 mL) while stored in the fridge. The obtained crystals were dissolved in little DCM and the solvent was removed *in vacuum*, yielding a colorless foam that was dried under N_2 for two days. Ion Pair **6a** (537 mg, 0.84 mmol, 85%) was obtained as a colorless solid.

^{1}H NMR (400 MHz, $CDCl_3$): δ [ppm] = 8.06 – 8.01 (m, 1H), 7.92 – 7.83 (m, 3H), 7.73 (td, *J* = 7.9, 3.6 Hz, 4H), 7.61 – 7.49 (m, 5H), 6.81 (d, *J* = 5.5 Hz, 1H).

^{13}C NMR (101 MHz, $CDCl_3$): δ [ppm] = 157.5, 150.3, 148.9,8 135.95 (d, *J* = 3.1 Hz), 134.45 (d, *J* = 10.3 Hz), 130.9 (d, *J* = 12.9 Hz), 127.3, 125.15 (q, *J* = 3.8 Hz), 124.1 (*virt*. q, *J* = 272.3 Hz, *C*F_3), 117.55 (d, *J* = 89.5 Hz), 166.4.

^{31}P NMR (162 MHz, $CDCl_3$): δ [ppm] = 23.09.

^{19}F NMR (376 MHz, $CDCl_3$): δ [ppm] = -62.61.

IR (ATR): ν (cm^{-1}) = 3060 (bs), 1587 (m), 1483 (m), 1438 (m), 1322 (vs), 1253 (w), 1128 (s), 1108 (s), 1060 (m), 992 (m), 970 (w), 757 (w), 723 (m), 690 (m).

Elemental Analysis: $C_{36}H_{28}F_3N_2O_2PS$ (640.66 g/mol): calc. (%) C, 67.49; H, 4.41; N, 4.37; S, 5.00; Found (%): C, 64.34; H, 4.43; N, 4.09; S, 4.74.

HRMS (ESI): calc. for $C_{12}H_8F_3N_2O_2S^-$ [A^-]: 301.0264; found 301.0264; calc. for $C_{24}H_{20}P^+$ [C^+]: 339.1297; found: 339.1297.

m. p: 75-78 °C

3.1.3.3 Synthesis of Additives

Triphenyl((triphenyl-λ5-phosphaneylidene)amino)phosphonium tetrafluoroborate (**7b**)

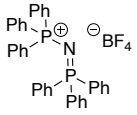

7b

Bis-(triphenylphosphoranyliden)-ammonium chloride (804 mg, 1.50 mmol, 1.0 eq) was suspended in H_2O and sodium tetrafluoroborate (154 mg, 1.40 mmol, 1.0 eq) was added in portions. The resulting cloudy suspension was stirred for 2 h at rt. DCM (10.0 mL) was added, and the two phases were separated. The aqueous phase was extracted with DCM (3 x 20 mL). The collected organic phase was dried over $MgSO_4$, filtered and the solvent was evaporated. The crude product was dissolved in DCM and the solvent was removed *in vacuum* until dryness. Product **7b** (804 mg, 1.29 mmol, 92%) was obtained as colorless platelet.

^{1}H NMR (400 MHz CD_2Cl_2): δ [ppm] = 7.69 – 7.61 (m, 6 H), 7.54 – 7.39 (m, 24 H).

^{13}C NMR (101 MHz, CD_2Cl_2): δ [ppm] = 134.1 (t, *J* = 1.1 Hz), 132.8 – 132.4 (m), 130.1 – 129.6 (m), 127.4 (dd, *J* = 108.0, 2.0 Hz).

^{19}F NMR (377 MHz, CD_2Cl_2): δ [ppm] = -153.59.

^{31}P NMR (162 MHz, CD_2Cl_2): δ [ppm] = 21.06

IR (ATR): ν (cm^{-1}) = 3058 (w), 1588 (w), 1482 (m), 1437 (m), 1263 (m), 1184 (w), 1113 (m), 1052 (s), 995 (m), 955 (w), 798 (w), 761 (w), 747 (m), 723 (s), 691 (s).

Elemental Analysis: $C_{36}H_{30}BF_4NP_2$ (625.39 g/mol): calc. (%) C, 69.14; H, 4.84; N, 2.24; Found (%): C, 65.07; H, 4.77; N, 1.96.

HRMS (ESI): calc. for BF_4^- [A^-]: 87.0035; found: 87.0034; calc. for $C_{36}H_{30}NP_2^+$ [C^+]: 538.1848; found: 538.1835.

m. p: 350-352 °C.

Tetrabutylammonium tetrafluoroborate (**7c**)

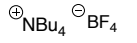

7c

Tetrabutylammonium tetrafluoroborate was purchased from Sigma Aldrich (99% purity) and used without further purification after analysis.

^{1}H NMR (400 MHz CD_2Cl_2): δ [ppm] = 3.24 – 3.06 (m, 8 H), 1.70 – 1.52 (m, 8 H), 1.41 (h, *J* = 7.3 Hz, 8 H), 1.00 (t, *J* = 7.3 Hz, 12 H).

^{13}C NMR (101 MHz, CD_2Cl_2): δ [ppm] = 59.0, 24.1, 20.0, 13.7.

^{19}F NMR (376 MHz, CD_2Cl_2): δ [ppm] = -151.98

Elemental Analysis: $C_{16}H_{36}BF_4N$ (329.28 g/mol): calc. (%) C, 58.36; H, 11.02; N, 4.25; Found (%): C, 58.41; H, 10.81; N, 4.20.

HRMS (ESI): calc. for BF_4^- [A^-]: 87.0035; found: 87.0034; calc. for $C_{16}H_{36}N^+$ [C^+]: 242.2842; found: 242.2842.

Tetrabutylphosphonium tetrafluoroborate (**7d**)

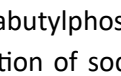

7d

Tetrabutylphosphonium hydroxide (1.91 g, 40% in H_2O, 1.77 mmol, 1.0 eq) was added to a solution of sodium tetrafluoroborate (303 mg, 2.77 mmol, 1.0 eq) in H_2O (10.0 mL). The resulting cloudy suspension was stirred for 2 h at rt. DCM (10.0 mL) was added, and the two phases were separated. The aqueous phase was extracted with DCM (3 x 20 mL). The collected organic phase was dried over $MgSO_4$, filtered and the solvent was evaporated. The crude product was dissolved in DCM and the solvent evaporated until dryness. Product **7d** (958 mg, 1.45 mmol, 52%) was further dried *in vacuum*, resulting in a colorless solid.

^{1}H NMR (400 MHz CD_2Cl_2): δ [ppm] = 2.22 – 2.01 (m, 8 H), 1.60 – 1.43 (m, 16 H), 1.05 – 0.92 (m, 12 H).

^{13}C NMR (101 MHz, CD_2Cl_2): δ [ppm] = 24.3 (d, *J* = 15.4 Hz), 23.8 (d, *J* = 4.8 Hz), 18.9 (d, *J* = 47.7 Hz), 13.5.

^{19}F NMR (376 MHz, CD_2Cl_2): δ [ppm] = -151.65

^{31}P NMR (162 MHz, CD_2Cl_2): δ [ppm] = 33.10

IR (ATR): ν (cm^{-1}) = 2960 (m), 2934 (m), 2874 (w), 1467 (w), 1417 (w), 1382 (w), 1284 (w), 1234 (w), 1096 (m), 1049 (s), 1036 (s), 906 (w), 831 (w), 719 (w).

Elemental Analysis: $C_{16}H_{36}BF_4P$ (346.24 g/mol): calc. (%) C, 55.50; H, 10.48; Found (%): C, 55.58; H, 10.54.

HRMS (ESI): calc. for BF_4^- [A^-]: 87.0035; found: 87.0034; calc. for $C_{16}H_{36}P^+$ [C^+]: 259.2549; found: 259.2548.

m. p: 95-96 °C

3.1.4 Conductometric Measurements

For the measurement, a 0.02 M stock solution of the respective catalyst was prepared in a 10 mL volumetric flask and was given portion-wise to the pure solvent in a measuring cell at 20 °C. Conductivity measurements were performed using a WTW conductometer with a Pt electrode LTA 1/NS in MeCN and DCM. Calibration was done as described in ref. [4]. Temperature control (20.0 ± 0.1 °C) was achieved by using a circulating bath cryostat. The conductivity was measured in volts (V) and depicted in "ME-REDLab Data Acquisition V1.1", developed by Dr. B. Kempf 2010, where the conductivity was plotted against time. After adding a portion of salt stock solution, one must wait until the conductivity value reaches a stable plateau (min 30 sec up to 100 sec) from which the average conductivity value is read off. In Excel this value (V) was converted into (µS cm^{-1}) by multiplying it with the cell parameter of the used electrode (z = 160). The cell parameter was obtained by calibrating the conductometric set up with aqueous KCl solutions (0.007 M, 0.0145 M, and 0.0375 M; commercial conductivity standard solutions purchased from Alfa Aesar) referring to the conductivity of 1273 µS cm^{-1} for an 0.01 M solution of aq. KCl at 20 °C.[5]

3.1.4.2 Conductivity Data Analysis

The conductivity of a substance is defined as its ability to conduct electricity and depends on the number of charge carrier in solution. Therefore, it can be expressed as a molar quantity where κ is the measured conductivity, Λ_m is the molar conductivity and *c* is the measured concentration of electrolyte.

$$\kappa = \Lambda_m c \tag{3.1}$$

The experimentally determined conductivity κ depends on the specific molar conductivity Λ_m of the measured salt and the ion concentration [X] as expressed in eq. 3.2.

$$\kappa = \Lambda_m [X] \tag{3.2}$$

The molar conductivity Λ_m consists of the sum of all limited molar ionic conductivities λ_i of all ionic species *i* in solution according to eq. 3.3.

$$\Lambda_m = \sum \lambda_i \tag{3.3}$$

The value for the specific molar conductivity Λ_m for the combined ions is derived from the extrapolated linear regression line of the red marked conductivity values (first three data points) assuming that the respective measured salt is fully dissociated in this concentration area (see Figure 3.4). Therefore, the specific molar conductivity Λ_m can be divided into the limited molar ionic conductivity of the cation λ_{cat} and of the anion λ_{an}. The limited molar ionic conductivities are determined by applying Fuoss' theory that the limited molar conductivity λ of each ion is proportional to their volume.[6,7] By using the calculated volumes of each anion, cation, and ion pair based on the Van der Waals cavities employed in the SMD continuum solvation model at the SMD(DCM)/B3LYP-D3/6-31+G(d) level of theory the scaling factor δ_i for the conversion of Λ_m into λ_i of the respective anion **A** and cation **C** was obtained (see eq. 3.4).

$$\delta_A = \frac{\mathrm{vol(A)}}{\mathrm{vol(IP)}} \tag{3.4a}$$

$$\delta_C = \frac{\mathrm{vol(C)}}{\mathrm{vol(IP)}} \tag{3.4b}$$

The background conductivity (BG) included here is the conductivity of the used solvent (BG = 0.8 µS cm^{-1}).

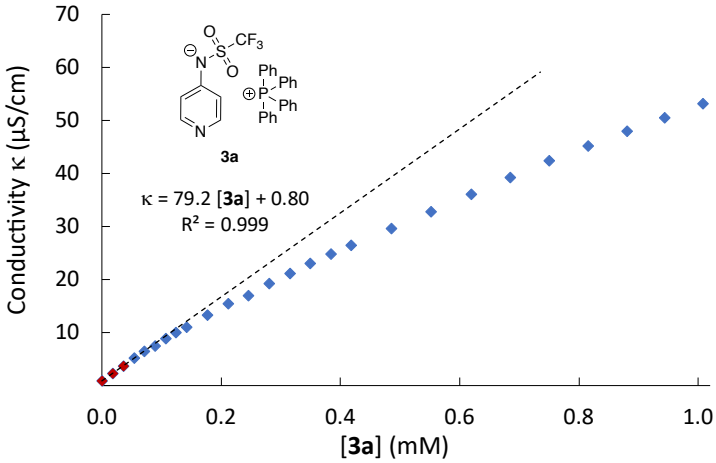

Figure 3.4: [Figure S4]. Concentration-dependent conductivity profile for catalyst **3a** in DCM with Λ_m = 79.2 S cm^2 mol^{-1} and solvent background BG = 0.80 µS cm^{-1}at 20 °C.

Determination of the respective association constants were achieved by numerical simulation utilizing the complex pathway simulation program, COPASI[8], for the analysis of the conductivity data.

Therefore, a biochemical model was opened, and the to be investigated association type was described as a reaction. The reaction was set to be reversible, which is also indicated by the equal sign "=" in the reaction equation. In the "Symbol Definition" section the starting compounds are listed with rate constant k_1 as well as the product with rate constant k_2, defining the association constant as $k_1/k_2 = K$.

For the optimization of the association constant K the reaction constant k_2 was set to be 1, while the rate constant k_1 was changed until the best fit between the simulated and experimental conductivity curve was found. The "root-mean-square-error" RMSE was used as a quality control measure.

In the section "Species" the individual concentration for all compounds were added. This was zero for the product(s) and the total salt concentration for both educts (e.g. for anion **A** and for cation **C**).

Next, in the section "Tasks" menu the "Steady-State" option was selected. By clicking the "Run" button at the bottom of the window, COPASI ran through a steady state analysis and then reported the concentration of each species of the biochemical model.

The obtained concentrations were then transferred to an excel sheet where the concentrations were converted into conductivity values according to eq. 3.5 with λ_i being the limited molar ionic conductivity of a charged species, δ_i the scaling factor of a charged species for the conversion of the specific molar conductivity Λ_m into the respective λ_i, and $[X]_i$ being the concentration of this respective charged species. The scaling factor $\delta_i = \lambda_i/\Lambda_m$ was introduced to simplify the conversion process in excel.

$$\kappa = \sum \lambda_i \times [X]_i \tag{3.5a}$$

$$\kappa = \sum \delta_i \times \Lambda_m \times [X]_i \tag{3.5b}$$

These simulated conductivity values were then compared to the experimental data. The conductivity background of the solvents was subtracted from the data points giving the conductivity of the pure salt and the RMSE was calculated as a quality control measure. The rate constant k_1 was optimized until the minimum of the RMSE was found.

This procedure was semi-automated by using a phyton script that automatically performs the "steady state" function for a given numbers of concentrations.[9] The following association types were analyzed by employing numerical simulations.

3.1.4.3 Model I – Double 1:1 Ion Pair Association

The 1:1 association model included two anions **A** and two cation **C** combining into two charge-neutral non-conducting ion pairs **IP** is described in Scheme 3.1.

$$2 * A + 2 * C \rightleftharpoons[K_{IP}] 2 * IP$$

Scheme 3.1: [Scheme S1]. Equation for numerical simulations of double 1:1 ion association for pyridinamide ion pairs.

The 1:1 ion pair association constant was defined as $k_1/k_2 = K_{IP}$ with $k_2 = 1$ being a fixed value. The limited molar ionic conductivities for the anion and cation were calculated according to eq. 3.4, while it was assumed that the neutral ion pair does not contribute towards the overall conductivity (λ_{IP} = 0.0 S cm^2 mol^{-1}). The results of this model for all ion pairs systems are summarized below in Table 3.4.

Table 3.4: [Table S4]. Double ion association constants K_{IP} (M^{-2}) with the specific molar conductivities Λ_m (S cm^2 mol^{-1}) and limited ionic conductivities λ_i (S cm^2 mol^{-1}) and the scaling factor δ_i for pyridinamide ion pairs.

Ion Pair	Λ_m (S cm^2 mol^{-1})	δ_A	δ_C	λ_A (S cm^2 mol^{-1})	λ_C (S cm^2 mol^{-1})	K_{IP} (M^{-2})	RMSE
3d	56.0	0.40	0.60	22.4	33.6	7.35 x 10^6	0.329
3c	57.9	0.41	0.59	23.7	34.2	5.00 x 10^6	0.261
3b	80.3	0.28	0.72	22.4	57.8	2.96 x 10^5	0.318
3a	79.2	0.37	0.63	29.3	49.9	6.86 x 10^5	0.304
5a	73.2	0.42	0.58	30.7	42.5	6.92 x 10^5	0.228
4a	73.6	0.44	0.56	32.4	41.2	8.79 x 10^5	0.274
6a	74.2	0.45	0.55	33.4	40.8	6.89 x 10^5	0.320

While this model fit the conductivity data reasonably well, it did not concur with the DOSY NMR data. Instead of observing a convergence of the diffusion coefficients D_i (m^2 s^{-1}) and hence the corresponding ion volumes, the measurements showed a clear deviation between both ions. The resulting DOSY volumes for exemplary **3a** were plotted against the used concentrations for both cation and anion (see Figure 3.5, with data from ref. [2]) and compared to simulated ion volumes calculated according to eq. 3.6 and based on the concentration obtained by numerical simulation of the 1:1 ion pair association model I.

$$\mathrm{vol_{cat}} = \left(\frac{[\mathrm{C}]}{[\mathrm{IP}]_{\mathrm{tot}}}\right) \times 362 + \left(\frac{[\mathrm{IP}]}{[\mathrm{IP}]_{\mathrm{tot}}}\right) \times 570 \qquad (3.6a)$$

$$\mathrm{vol_{an}} = \left(\frac{[\mathrm{A}]}{[\mathrm{IP}]_{\mathrm{tot}}}\right) \times 215 + \left(\frac{[\mathrm{IP}]}{[\mathrm{IP}]_{\mathrm{tot}}}\right) \times 570 \qquad (3.6b)$$

For the lowest concentrations the measured volumes were close to the calculated ones for the free ions (anion: 215 Å^3 and cation: 362 Å^3). For concentrations higher than 0.01 mM, a clear increase of the volumes for the anion **3** and the cation **a** was observed with a large off-set between the anion and cation volumes. If the association follows a 1:1 ion pair association the volumes of anion and cation should converge and approach 570 Å^3 for a monomeric ion pair **3a**. Instead with increasing salt concentration the volume of the cation even exceeded the calculated volume for the 1:1 monomeric ion pair **3a** (641 Å^3 versus 570 Å^3 at 1.0 mM). On the other hand, the simulated volume of the cation based on the concentrations of the conductivity evaluation lay far below the calculated volume the 1:1 monomeric ion pair **3a** (435 Å^3 versus 570 Å^3 at 1.0 mM).

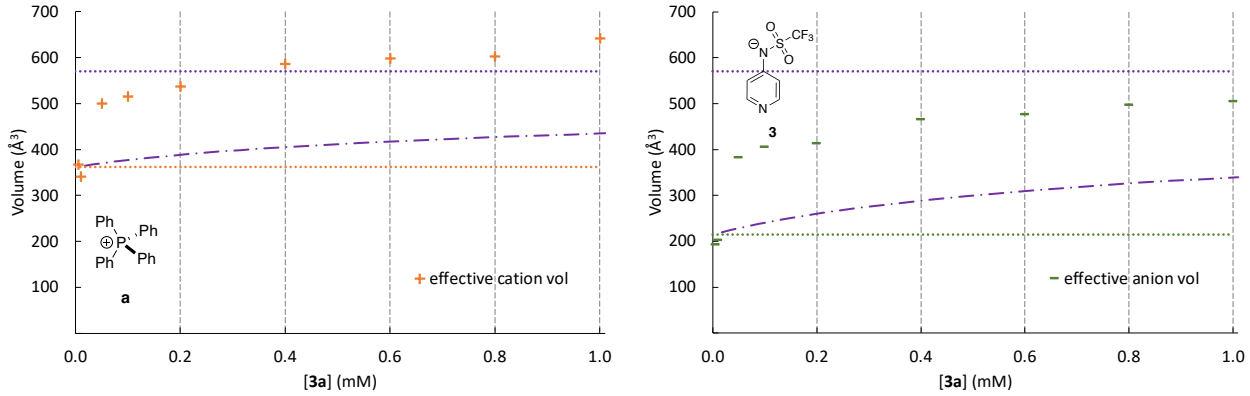

Figure 3.5: [Figure S5]. Concentration-dependent volumes of cations **a** (orange "+" symbols) and anions **3** (green "–" symbols) of salt **3a** in CD_2Cl_2 as calculated from DOSY experiments (with data from ref. [2]) with the respective free ion volumes (dotted line; cation in orange; anion in green) and the calculated trend for 1:1 ion association for each ion volume (purple dotted line).

All these observations suggested the involvement of an additional charged species.

3.1.4.4 Model IIa – Cationic Sandwich Association

Based on the finding of DOSY NMR measurements further association types were investigated. One was a cationic sandwich association consisting of four ions, two anions **A** and two cations **C** associating into a formally positive charged sandwich complex **CAC** which leaves one free anion **A** (see Scheme 3.2).

$$2 * A \; + \; 2 * C \; \underset{}{\overset{K_{CAC}}{\rightleftharpoons}} \; A \; + \; CAC$$

Scheme 3.2: [Scheme S2]. General cationic sandwich association equilibrium for pyridinamide ion pairs.

The cationic sandwich association constant is defined as $k_1/k_2 = K_{CAC}$ with $k_2 = 1$ being a fixed value. The limited molar ionic conductivities for the anion and cation were calculated according to eq. 3.4. However, there was no established way to determine the limited molar ionic conductivity λ_{CAC} for the cation sandwich **CAC**. Therefore, instead of assigning all sandwich cations a fixed value, it was decided to treat λ_{CAC} as another variable. This required a slight modification of the optimization process since instead of one variable, the association constant K, there were two variables to be optimized, the sandwich association constant K_{CAC} (M^{-2}) and λ_{CAC} (S cm^2 mol^{-1}).

To simplify the process, the scaling factor δ_{CAC} was optimized rather than λ_{CAC} for the sandwich cation. Since the sandwich complex is formally positively charged, it is recommended to start the optimization process with $\delta_{CAC} = \delta_C = 0.63$ (exemplary for ion pair **3a**). The aim was to find a global minimum based on the sandwich association constant K_{CAC} with the RMSE being the quality control measure (see Table 3.5).

Table 3.5: [Table S5]. List of cationic sandwich association constants K_{CAC} (M^{-2}) and scaling factor δ_{CAC} of the optimization process to find the global minimum for both parameters for pyridinamide ion pair **3a** with its specific molar conductivity Λ_m (S cm^2 mol^1) and the limited ionic conductivities λ_i (S cm^2 mol^{-1}) for anion **3** and cation **a**.

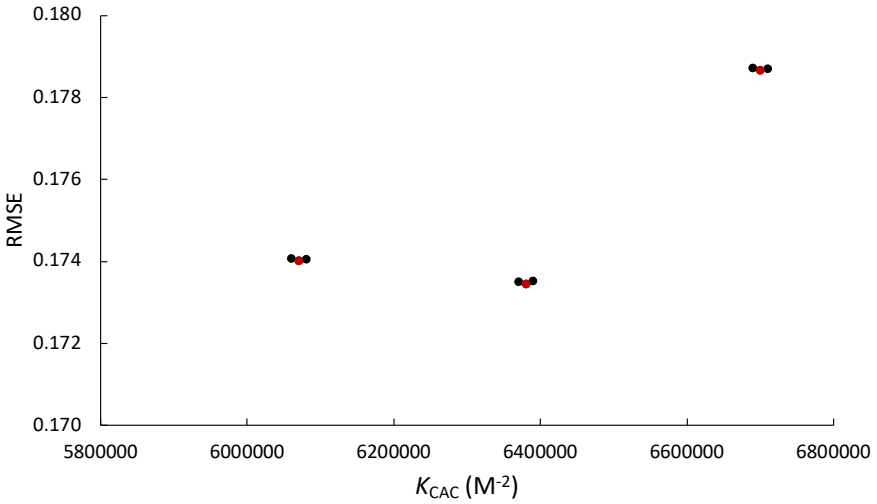

Ion Pair	Λ_m (S cm^2 mol^{-1})	δ_A/δ_C	δ_{CAC}	K_{CAC} (M^{-2})	RMSE
3a	79.2	37/63	0.66	6.06 x 10^6	0.1741
				6.07 x 10^6	0.1740
				6.08 x 10^6	0.1741
			0.67	6.37 x 10^6	0.1735
				6.38 x 10^6	**0.1734**
				6.39 x 10^6	0.1735
			0.68	6.69 x 10^6	0.1787
				6.70 x 10^6	0.1786
				6.71 x 10^6	0.1787

The obtained sandwich association constants for all ion pair systems are summarized in Table 3.6.

Table 3.6: [Table S6]. Cationic sandwich association constants K_{CAC} (M^{-2}) with the specific molar conductivities Λ_m (S cm^2 mol^{-1}) and the scaling factor δ_i of all charged species for pyridinamide ion pairs.

Ion Pair	Λ_m (S cm^2 mol^{-1})	$\delta_A/\delta_C/\delta_{CAC}$	K_{CAC} (M^{-2})	RMSE
3d	56.0	40/60/15	1.07 x 10^7	0.094
3c	57.9	41/59/22	1.01 x 10^7	0.100
3b	80.3	28/72/91	4.65 x 10^6	0.105
3a	79.2	37/63/67	6.38 x 10^6	0.173
5a	73.2	42/58/57	5.15 x 10^6	0.130
4a	73.6	44/56/54	6.50 x 10^6	0.122
6a	74.2	45/55/60	6.75 x 10^6	0.161

In comparing the RMSE value obtained for the 1:1 ion pair association and the cationic sandwich association, a better fit for the cationic sandwich association model was observed. As a secondary quality control measure, the ion volumes based on DOSY NMR were compared to ion volumes calculated based on the numerical simulation data. Therefore, the anion and cation volumes were calculated according to eq. 3.7.

$$\mathrm{vol}_{\mathrm{cat}} = \left(\frac{[\mathrm{C}]}{[\mathrm{IP}]_{\mathrm{tot}}}\right) \times 362 + \left(\frac{2 \times [\mathrm{CAC}]}{[\mathrm{IP}]_{\mathrm{tot}}}\right) \times 925 \qquad (3.7a)$$

$$\mathrm{vol}_{\mathrm{an}} = \left(\frac{[\mathrm{A}]}{[\mathrm{IP}]_{\mathrm{tot}}}\right) \times 215 + \left(\frac{[\mathrm{CAC}]}{[\mathrm{IP}]_{\mathrm{tot}}}\right) \times 925 \qquad (3.7b)$$

Figure 3.6 shows the data and model comparison for ion pair **3a** as an example.

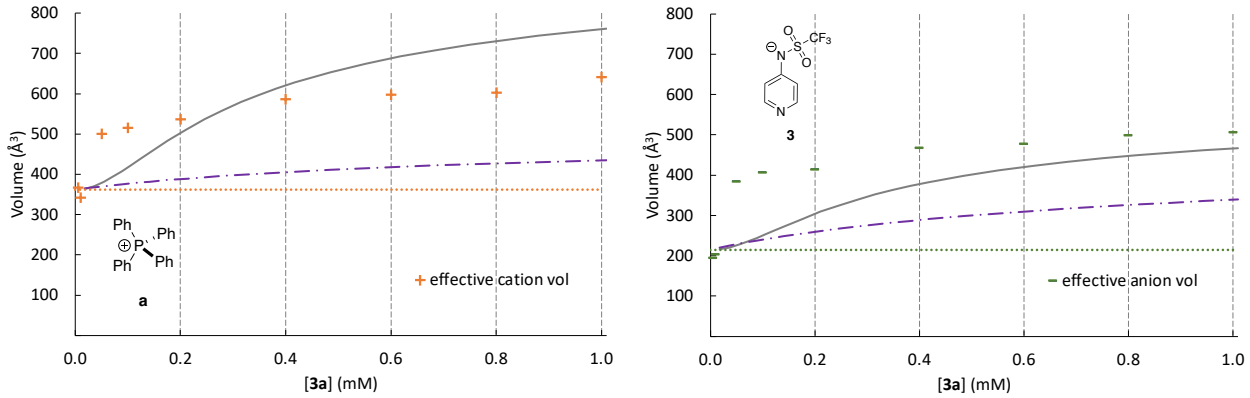

Figure 3.6: [Figure S6]. Concentration-dependent volumes of cations **a** (orange "+" symbols) and anions **3** (green "–" symbols) of salt **3a** in CD_2Cl_2 as calculated from DOSY experiments (with data from ref. [2]) with the respective free ion volumes (dotted line; cation in orange; anion in green), the calculated trend for 1:1 ion association for each ion volume (purple dotted line), and for the cationic sandwich model (grey line).

In this case the simulated volume curves for the cation and anion (orange and green lines, respectively) were closer to the experimental data than the 1:1 ion pair association model. First indications wer that cationic sandwich association provides indeed an excellent fit for both the conductivity as well as the DOSY NMR data.

3.1.4.5 Model IIb – Anionic Sandwich Association

Further comprehensive DOSY studies of all ion pair systems showed that the more nucleophilic ion pairs **4-6a** displayed results that indicated an anionic sandwich association rather than a cationic sandwich association (see SI of ref. [2]). Adjustment of the cationic sandwich association to incorporate an anion sandwich consisting of four ions, two anions **A** and two cations **C** which associate into a formally negative charged sandwich complex **ACA** with one free cation **C** left over(see Scheme 3.3).

$$2 * A + 2 * C \rightleftharpoons[K_{ACA}] C + ACA$$

Scheme 3.3: [Scheme S3]. General anionic sandwich association equilibrium for pyridinamide ion pairs.

The anion sandwich association constant was defined as $k_1/k_2 = K_{ACA}$ with $k_2 = 1$ being a fixed value. The limited molar ionic conductivities for the anion and cation were calculated according to eq. 3.4. The limited molar ionic conductivity λ_{ACA} of the anionic sandwich complex was treated as another variable. To find the global minimum for both the limited molar ionic conductivity λ_{ACA} and the anionic sandwich association constant K_{ACA} the same fitting process as described above for the cationic sandwich association model was followed. Since the sandwich complex is formally negatively charged, it is recommended to start the optimization process with $\delta_{ACA} = \delta_A$. The results are summarized in Table 3.7.

Table 3.7: [Table S7]. Anionic sandwich association constants K_{ACA} (M^{-2}) with the specific molar conductivities Λ_m (S cm^2 mol^{-1}) and the scaling factors δ_i of all charged species for pyridinamide ion pairs.

Ion Pair	Λ_m (S cm^2 mol^{-1})	δ_A /δ_C /δ_{ACA} (%)	K_{ACA} (M^{-2})	RMSE
3d	56.0	40/60/–	–	–
3c	57.9	41/59/4	1.01 x 10^7	0.100
3b	80.3	28/72/47	4.65 x 10^6	0.105
3a	79.2	37/63/41	6.38 x 10^6	0.173
5a	73.2	42/58/41	5.15 x 10^6	0.130
4a	73.6	44/56/42	6.50 x 10^6	0.122
6a	74.2	45/55/50	6.75 x 10^6	0.161

Numerical simulation of both sandwich association types gave identical association constants and RMSE values. Thus, based on conductivity data alone, those two association types cannot be distinguished. The sole exception is ion pair **3d**. Here the global minimum could not be found in the anionic sandwich association without allowing negative values for the limited molar ionic conductivity λ_{ACA}. This indicates either that for this ion pair, an anionic sandwich association is not feasible or that model II ran into a numerical boundary. In both cases, no optimized anionic sandwich association constant K_{ACA} could be found for ion pair **3d**.

For the comparison of the experimental and simulated ion volumes, the simulated volumes were calculated according to eq. 3.8 for the anionic sandwich association model.

$$\mathrm{vol_{cat}} = \left(\frac{[\mathrm{C}]}{[\mathrm{IP}]_{\mathrm{tot}}}\right) \times 362 + \left(\frac{[\mathrm{ACA}]}{[\mathrm{IP}]_{\mathrm{tot}}}\right) \times 782 \tag{3.8a}$$

$$\mathrm{vol_{an}} = \left(\frac{[\mathrm{A}]}{[\mathrm{IP}]_{\mathrm{tot}}}\right) \times 215 + \left(\frac{2 \times [\mathrm{ACA}]}{[\mathrm{IP}]_{\mathrm{tot}}}\right) \times 782 \tag{3.8b}$$

The comparison showed that the anionic sandwich association model does not offer a better overlap between the experimentally obtained and simulated ion volumes. Figure 3.7 shows the simulated ion volumes for both the cationic and the anionic sandwich association model exemplary for pyridinamide ion pair **3a**.

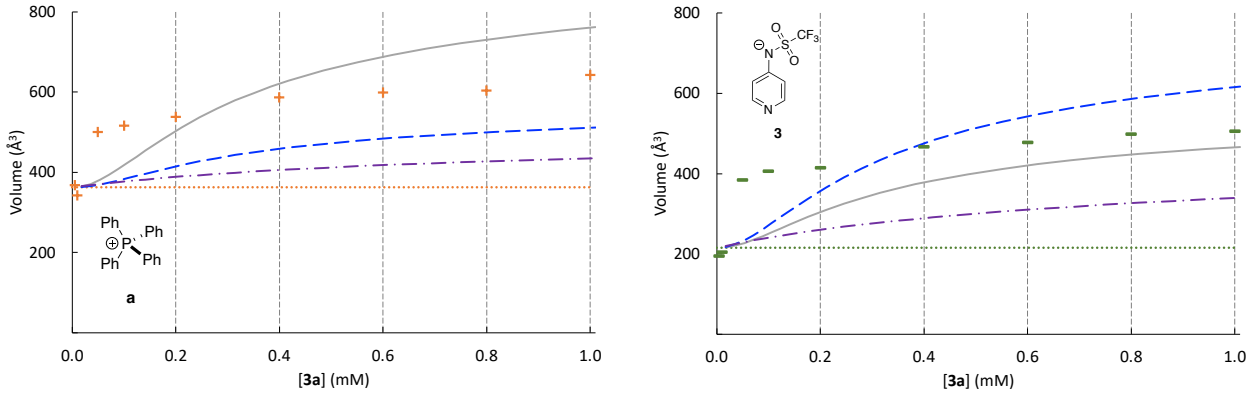

Figure 3.7: [Figure S7]. Concentration-dependent volumes of cations **a** (orange "+" symbols) and anions **3** (green "–" symbols) of salt **3a** in CD_2Cl_2 as calculated from DOSY experiments (with data from ref. [2]) with the respective free ion volumes (dotted line; cation in orange; anion in green), the calculated trend for 1:1 ion association for each ion volume (purple dotted line), and for the cationic (grey line) and anionic (blue dashed line) sandwich model.

While the simulated cation volumes based on the cationic sandwich association model are larger than the experimental values, the simulated cation volumes based on the anionic sandwich association are smaller than them. For the simulated anion volumes, the opposite holds true. For pyridinamide ion pair **3a** the cationic sandwich model is preferred since the increase in anion volumes should be obvious in the DOSY measurements, with the anion volumes surpassing the cation volumes as it can be seen for pyridinamide ion pair **4a** (for further details see Chapter 2)

3.1.4.6 Model III – Mixed Sandwich Association

Since the separate analysis of the conductivity data for both cationic and anionic sandwich association still revealed significant deviations in comparing the experimental and simulated ion volumes, the combination of both sandwich association types in the *mixed sandwich association model* was the next step. Therefore, both sandwich association constants, K_{CAC} and $K_{ACA,}$ were assigned a *scaling factor* α and β, respectively (see Scheme 3.4).

$$2 * A + 2 * C \xrightleftharpoons{\alpha \times K_{CAC}} A + CAC$$

$$2 * A + 2 * C \xrightleftharpoons{\beta \times K_{ACA}} C + ACA$$

Scheme 3.4: [Scheme S4]. Association equations for mixed sandwich association model.

To find the right ratio between cationic and anionic sandwich association one contribution factor would be set to a fixed value, while the other one would be treated as a variable and be optimized by using numerical simulation to find the minimum of the RMSE value. The optimization of the contribution factor was limited to two relevant decimals.

Cation and anion volumes obtained by DOSY NMR measurements at 1.0 mM salt concentration were used as reference to determine the optimal ratio for the factors, α and β. The simulated ion volumes were calculated according to eq. 3.9.

$$\mathrm{vol_{cat}} = \frac{[\mathrm{C}]}{[\mathrm{IP}]_{\mathrm{tot}}} \times 362 + \left(\frac{2 \times [\mathrm{CAC}]}{[\mathrm{IP}]_{\mathrm{tot}}}\right) \times 925 + \left(\frac{[\mathrm{ACA}]}{[\mathrm{IP}]_{\mathrm{tot}}}\right) \times 782 \qquad (3.9a)$$

$$\mathrm{vol_{an}} = \frac{[\mathrm{A}]}{[\mathrm{IP}]_{\mathrm{tot}}} \times 215 + \left(\frac{[\mathrm{CAC}]}{[\mathrm{IP}]_{\mathrm{tot}}}\right) \times 925 + \left(\frac{2 \times [\mathrm{ACA}]}{[\mathrm{IP}]_{\mathrm{tot}}}\right) \times 782 \qquad (3.9b)$$

The percentual residual between experimental and simulated ion volumes determined the optimal ratio for the factors, α and β in the mixed sandwich association. For more details see Chapter 2

Examining the simulated ion volumes based on Model II for the cationic and anionic sandwich association against the newly introduced mixed model showed a significantly improved overlap for the experimental data than any other association model (see Figure 3.8, exemplary for ion pair **3a**).

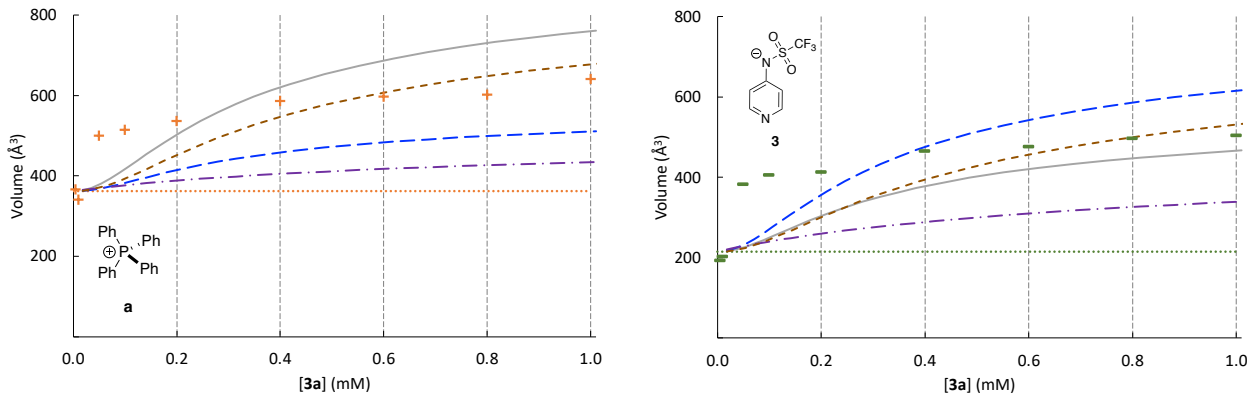

Figure 3.8: [Figure S8]. Concentration-dependent volumes of cations **a** (orange "+" symbols) and anions **3** (green "–" symbols) of salt **3a** in CD_2Cl_2 as calculated from DOSY experiments (with data from ref. [2]) with the respective free ion volumes (dotted line; cation in orange; anion in green), the calculated trend for 1:1 ion association for each ion volume (purple dotted line), for the cationic (grey line) and anionic (blue dashed line) sandwich model and the mixed sandwich association model (brown short-dash line).

The mixed model gave the best results when checking the experimental and simulated ion volumes against each other. The results of model 3 for all ion pairs are summarized in Table 3.8.

Table 3.8: [Table S8]. Final cationic and anionic sandwich association constants K_{CAC} (M^{-2}) and K_{ACA} (M^{-2}) with the specific molar conductivities Λ_m (S cm^2 mol^{-1}) and the scaling factors δ_i of all charged species with their respective scaling factors α and β for pyridinamide ion pairs.

Ion Pair	Λ_m (S cm^2 mol^{-1})	δ_A /δ_C /δ_{CAC}//δ_{ACA}	$\alpha \times K_{CAC}$ [M^{-2}]	$\beta \times K_{ACA}$ [M^{-2}]	α/β (%)	RMSE
3d	56.0	40/60/15/–	–	–	–	–
3c	57.9	41/59/22/4	3.33×10^6	2.32×10^6	33/23	0.61

3b	80.3	28/72/91/47	4.65×10^6	0.00	100/0	0.11
3a	79.2	37/63/67/41	2.81×10^6	1.34×10^6	44/21	0.43
5a	73.2	42/58/57/41	5.67×10^5	3.45×10^6	11/67	0.29
4a	73.6	44/56/54/42	7.80×10^5	3.97×10^6	12/61	0.35
6a	74.2	45/55/60/50	1.08×10^6	3.51×10^6	16/52	0.38

Notable is the result of the analysis of pyridinamide ion pair **3b** in the mixed model. For the **3b** the best result was achieved for the purely cationic sandwich association without any participation of the anionic sandwich association. However, the percentual residual for both cation and anion volume are rather large with +25% for the anion volume and +14% for the cation volume (see Figure 3.9A) compared to the results of the other ion pairs, e.g. ± 6.0% for ion volume in pyridinamide ion pair **3a** (see Figure 3.9B).

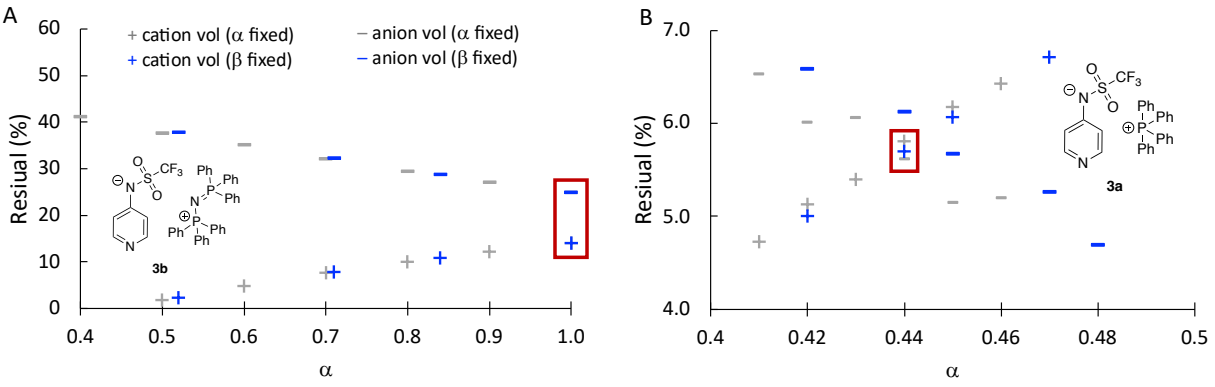

Figure 3.9: [Figure S9]. A) Percentual residue for calculated cation (blue (for β fixed) and grey (for α fixed) "+") and anion (blue (for β fixed) and grey (for α fixed) "–") volumes in mixed sandwich association model for pyridinamide ion pair **3b**. B) Percentual residue for calculated cation (blue (for β fixed) and grey (for α fixed) "+") and anion (blue (for β fixed) and grey (for α fixed) "–") volumes in mixed sandwich association model for pyridinamide ion pair **3a**.

This might be an indication for other ionic species or ionic effects taking place in solution for **3b** that are not yet accounted for in the current conductivity model. Moving forward, pyridinamide ion pairs **3b** as well as **3d** will be analyzed with the cationic sandwich association model.

3.1.4.7 Workflow summary

For the determination of ion pairing constant K_{IP} and sandwich association constant K_{CAC} for ionic compounds like **3a** based on conductivity measurements in DCM, the following steps were carried out:

<u>Determination of ion pairing constant K_{IP} (M^{-2}) for salt **3a**</u>

a) Measure conductivity for **3a**.
b) Determine the molar conductivity Λ_m by linear extrapolation of the first three data points.
c) Use eq. 3.3 or the respective biochemical model (for details see Scheme 3.1 or 3.2) concentrations for all compound involved in the model, copy the concentrations into excel to convert them into conductivity values by assigning both ion 50% contribution towards Λ_m.
d) Compare sum of theoretical conductivity with experimental values (without solvent background conductivity).
e) Use the RMSE value as a quality control measure.
f) Adjust k_1 in $K_{CAC} = k_1/k_2$ until the minimum RMSE is found, to obtain K_{IP}.

<u>Determination of sandwich association constant K_{CAC} (M^{-2}) for salt **3a**</u>

g) Measure conductivity for **3a**.
h) Determine the molar conductivity Λ_m by linear extrapolation of the first three data points.

i) Set the limited molar ionic conductivity for the anion λ_A and cation λ_C to the calculated values for the scaling factor δ_i based on eq. 3.8. The sum of $\delta_A+\delta_C$ cannot exceed 1.
j) Treat $\delta_{CAC} = \lambda_{CAC}/\Lambda_m$(**3a**) as a second variable. Select at starting value e.g. $\delta_{CAC} = 0.67$ and start the optimization process for K_{CAC}.
k) Use the respective sandwich association model (Model 3) to obtain concentrations for all species involved, copy them into Excel to convert them into conductivity values using eq. 3.5.
l) Compare sum of theoretical conductivity with experimental values (without solvent background conductivity).
m) Use the RMSE values as a quality control measure.
n) Adjust k_1 in $K_{CAC} = k_1/k_2$ until minimum RMSE is found, to obtain the final K_{CAC}.
o) Adjust the limited molar ionic conductivity for the sandwich ion λ_{CAC} to find the percentual distribution that fits the conductivity data the best. For each new percentual distribution, repeat step k) – n) until the global minimum RMSE is found.

For analysis of the additive **7a-d** the same steps are followed, only step q deviates since the determination of the specific molar conductivity Λ_m of BF_4^- is done slightly differently:

p) Measure conductivity for salt **7a-d**.
q) Determine the molar conductivity Λ_m by linear extrapolation of the first three data points.
r) Follow step i) – o) as described above to obtain K_{CAC} for additive **7a-d**.

<u>Determination of composition of cationic and anionic sandwich association for salt **3a** (Model 3)</u>

After determination of the cationic sandwich association constant K_{CAC} and the anionic sandwich association K_{ACA} the mix of both association types that fits the experimental data best is ascertained.

s) Assign each association constant a *scaling factor*: K_{CAC} x α and K_{ACA} x β.
t) Set α to a fixed value starting at 1.0 and going down in steps of 0.1. Optimize β to achieve the smallest RMSE value for the conductivity data using numerical simulations. Limit each factor to two relevant decimals.
u) Repeat step s) vice versa for factor β.
v) Determine the composition of cationic and anionic sandwich association in reference to the measured DOSY volume at 1.0 mM by calculating the percentual residual between experimental and simulated ion volumes.
w) Take further optimization steps until finding the α/β ratio with the smallest percentual residual for both cation and anion volume.

3.1.4.8 Data of Conductivity Measurements in MeCN

Concentration dependent conductivity data of **3b** in MeCN at 20 °C

[3b]/M	Conductivity κ (µS/cm)
0.00	0.80
1.68 x 10^{-5}	3.36
3.36 x 10^{-5}	5.28
5.04 x 10^{-5}	7.20
6.71 x 10^{-5}	9.76
8.38 x 10^{-5}	11.7
1.00 x 10^{-4}	13.6
1.17 x 10^{-4}	16.0
1.34 x 10^{-4}	17.9
1.50 x 10^{-4}	20.2
1.67 x 10^{-4}	22.1
1.83 x 10^{-4}	24.2
2.00 x 10^{-4}	26.4
2.33 x 10^{-4}	30.6
2.65 x 10^{-4}	34.7
2.98 x 10^{-4}	38.7
3.30 x 10^{-4}	42.9
3.63 x 10^{-4}	46.7
3.95 x 10^{-4}	50.7
4.59 x 10^{-4}	58.7
5.22 x 10^{-4}	66.4
5.85 x 10^{-4}	74.2
6.48 x 10^{-4}	81.9
7.10 x 10^{-4}	89.6
7.71 x 10^{-4}	96.8
8.32 x 10^{-4}	104
8.93 x 10^{-4}	111
9.53 x 10^{-4}	118
1.01 x 10^{-3}	125
1.07 x 10^{-3}	132
1.13 x 10^{-3}	139
1.25 x 10^{-3}	153
1.36 x 10^{-3}	166
1.48 x 10^{-3}	179
1.59 x 10^{-3}	192
1.70 x 10^{-3}	205
1.80 x 10^{-3}	217
1.91 x 10^{-3}	229
2.02 x 10^{-3}	240
2.12 x 10^{-3}	252

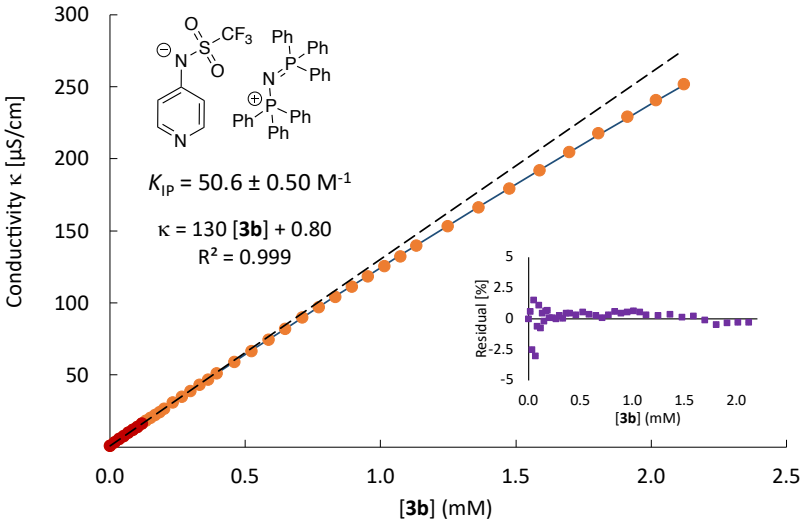

Concentration dependent conductivity data of **3c** in MeCN at 20 °C

[3c]/M	Conductivity κ (µS/cm)
0.00	0.80
1.99 x 10^{-5}	3.36
3.97 x 10^{-5}	6.24
5.94 x 10^{-5}	8.80
7.92 x 10^{-5}	11.4
9.89 x 10^{-5}	14.0
1.19 x 10^{-4}	16.4
1.38 x 10^{-4}	19.1
1.58 x 10^{-4}	21.8
1.77 x 10^{-4}	24.2
1.97 x 10^{-4}	26.9
2.36 x 10^{-4}	32.0
2.74 x 10^{-4}	37.0
3.13 x 10^{-4}	42.0
3.51 x 10^{-4}	47.0
3.90 x 10^{-4}	51.8
4.66 x 10^{-4}	61.4
5.41 x 10^{-4}	71.1
6.16 x 10^{-4}	80.6
6.90 x 10^{-4}	89.8
8.37 x 10^{-4}	108
9.82 x 10^{-4}	126
1.12 x 10^{-3}	143
1.27 x 10^{-3}	159
1.40 x 10^{-3}	177
1.54 x 10^{-3}	192
1.67 x 10^{-3}	208
1.81 x 10^{-3}	223
1.94 x 10^{-3}	238
2.07 x 10^{-3}	253
2.19 x 10^{-3}	268
2.32 x 10^{-3}	282
2.44 x 10^{-3}	296

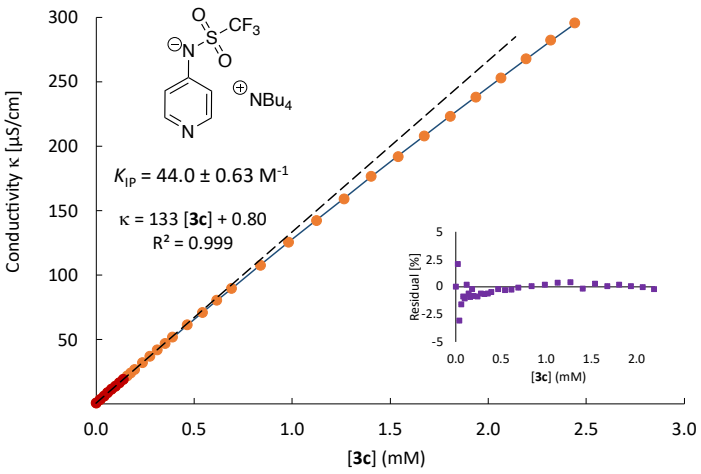

Concentration dependent conductivity data of **3d** in MeCN at 20 °C

[3d]/M	Conductivity κ (µS/cm)
0.00	0.80
2.01 x 10^{-5}	3.20
4.01 x 10^{-5}	5.92
6.01 x 10^{-5}	8.48
8.00 x 10^{-5}	11.0
9.99 x 10^{-5}	13.8
1.20 x 10^{-4}	16.3
1.40 x 10^{-4}	18.7
1.59 x 10^{-4}	21.3
1.79 x 10^{-4}	23.7
1.99 x 10^{-4}	26.2
2.18 x 10^{-4}	28.8
2.38 x 10^{-4}	31.2
2.58 x 10^{-4}	33.6
2.77 x 10^{-4}	36.2
2.97 x 10^{-4}	38.4
3.16 x 10^{-4}	41.1
3.56 x 10^{-4}	46.1
3.94 x 10^{-4}	50.6
4.32 x 10^{-4}	55.4
4.71 x 10^{-4}	60.3
5.09 x 10^{-4}	64.8
5.47 x 10^{-4}	69.6
6.23 x 10^{-4}	78.4
6.98 x 10^{-4}	87.2
7.72 x 10^{-4}	96.3
8.46 x 10^{-4}	105
9.20 x 10^{-4}	114
9.93 x 10^{-4}	123
1.06 x 10^{-3}	131
1.14 x 10^{-3}	140
1.21 x 10^{-3}	149
1.28 x 10^{-3}	157
1.42 x 10^{-3}	173
1.56 x 10^{-3}	189
1.69 x 10^{-3}	205
1.83 x 10^{-3}	220
1.96 x 10^{-3}	234
2.09 x 10^{-3}	249
2.22 x 10^{-3}	263
2.34 x 10^{-3}	277
2.47 x 10^{-3}	291

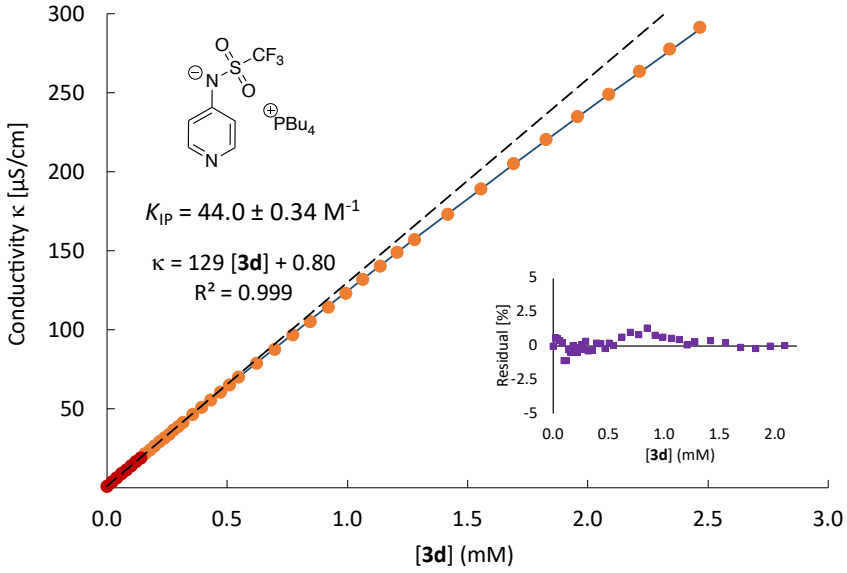

Concentration dependent conductivity data of **5a** in MeCN at 20 °C

[5a]/M	Conductivity κ (µS/cm)
0.00	0.80
1.98 x 10^{-5}	2.96
3.95 x 10^{-5}	5.36
5.92 x 10^{-5}	7.52
7.89 x 10^{-5}	9.68
9.85 x 10^{-5}	11.8
1.18 x 10^{-4}	14.2
1.38 x 10^{-4}	16.3
1.57 x 10^{-4}	18.4
1.77 x 10^{-4}	20.7
1.96 x 10^{-4}	22.9
2.35 x 10^{-4}	27.2
2.73 x 10^{-4}	31.4
3.12 x 10^{-4}	35.8
3.50 x 10^{-4}	40.0
3.88 x 10^{-4}	44.2
4.64 x 10^{-4}	53.1
5.39 x 10^{-4}	60.6
6.14 x 10^{-4}	68.8
6.88 x 10^{-4}	76.9
7.61 x 10^{-4}	84.7
8.34 x 10^{-4}	92.3
9.78 x 10^{-4}	107
1.12 x 10^{-3}	121
1.26 x 10^{-3}	136
1.40 x 10^{-3}	150
1.53 x 10^{-3}	164
1.67 x 10^{-3}	177
1.80 x 10^{-3}	189

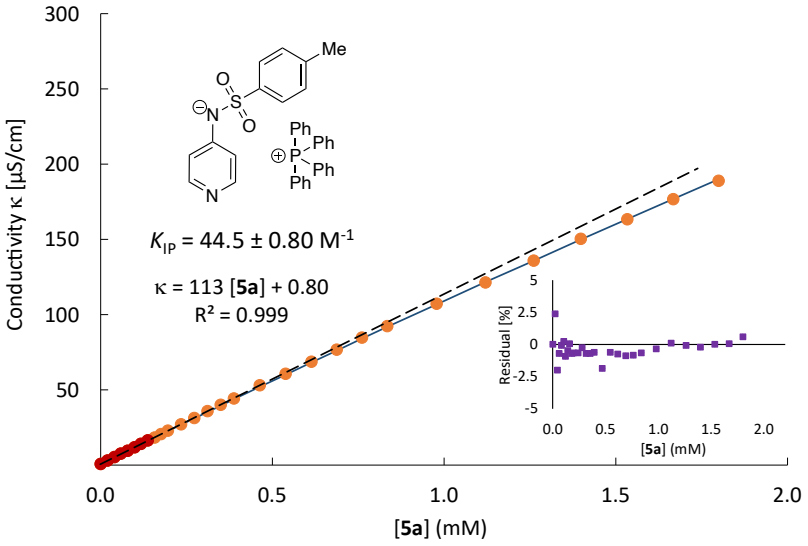

Concentration dependent conductivity data of **6a** in MeCN at 20 °C

[6a]/M	Conductivity κ (µS/cm)
0.00 x 10^{0}	8.00 x 10^{-1}
1.88 x 10^{-5}	2.72 x 10^{0}
3.75 x 10^{-5}	5.28 x 10^{0}
5.62 x 10^{-5}	7.20 x 10^{0}
7.48 x 10^{-5}	9.28 x 10^{0}
9.35 x 10^{-5}	1.17 x 10^{1}
1.12 x 10^{-4}	1.38 x 10^{1}
1.31 x 10^{-4}	1.58 x 10^{1}
1.49 x 10^{-4}	1.78 x 10^{1}
1.68 x 10^{-4}	1.97 x 10^{1}
1.86 x 10^{-4}	2.19 x 10^{1}
2.04 x 10^{-4}	2.38 x 10^{1}
2.23 x 10^{-4}	2.61 x 10^{1}
2.59 x 10^{-4}	3.02 x 10^{1}
2.96 x 10^{-4}	3.42 x 10^{1}
3.32 x 10^{-4}	3.82 x 10^{1}
3.68 x 10^{-4}	4.24 x 10^{1}
4.04 x 10^{-4}	4.62 x 10^{1}
4.40 x 10^{-4}	5.04 x 10^{1}
5.12 x 10^{-4}	5.80 x 10^{1}
5.82 x 10^{-4}	6.56 x 10^{1}
6.53 x 10^{-4}	7.33 x 10^{1}
7.22 x 10^{-4}	8.08 x 10^{1}
7.92 x 10^{-4}	8.86 x 10^{1}
8.60 x 10^{-4}	9.56 x 10^{1}
9.28 x 10^{-4}	1.03 x 10^{2}
9.96 x 10^{-4}	1.10 x 10^{2}
1.06 x 10^{-3}	1.17 x 10^{2}
1.13 x 10^{-3}	1.24 x 10^{2}
1.20 x 10^{-3}	1.30 x 10^{2}
1.26 x 10^{-3}	1.37 x 10^{2}
1.39 x 10^{-3}	1.51 x 10^{2}
1.52 x 10^{-3}	1.64 x 10^{2}
1.65 x 10^{-3}	1.77 x 10^{2}
1.77 x 10^{-3}	1.89 x 10^{2}
1.89 x 10^{-3}	2.02 x 10^{2}
2.01 x 10^{-3}	2.14 x 10^{2}
2.13 x 10^{-3}	2.26 x 10^{2}
2.25 x 10^{-3}	2.37 x 10^{2}
2.36 x 10^{-3}	2.48 x 10^{2}

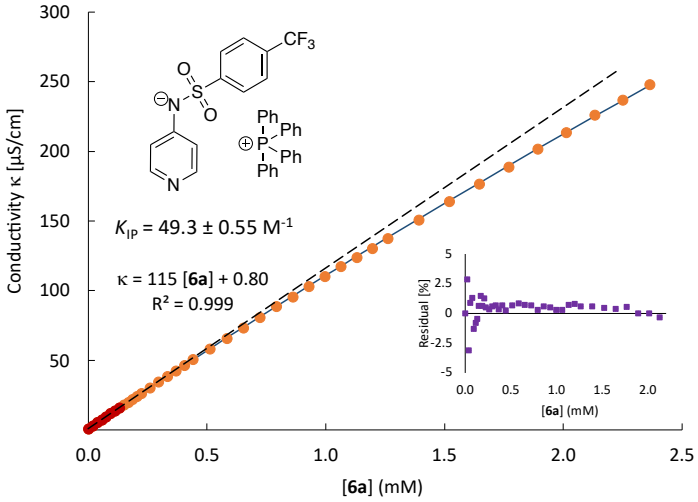

3.1.4.9 Pyridinamide Ion Pairs – Data of Conductivity Measurements in DCM

Concentration dependent conductivity data of **3a** in DCM at 20 °C

[3a]/M	Conductivity κ (µS/cm)
0.00 x 10^{0}	0.80
1.78 x 10^{-5}	2.24
3.55 x 10^{-5}	3.60
5.40 x 10^{-5}	5.12
7.09 x 10^{-5}	6.48
8.86 x 10^{-5}	7.44
1.06 x 10^{-4}	8.80
1.24 x 10^{-4}	9.92
1.41 x 10^{-4}	11.0
1.76 x 10^{-4}	13.2
2.11 x 10^{-4}	15.4
2.46 x 10^{-4}	17.0
2.80 x 10^{-4}	19.2
3.15 x 10^{-4}	21.1
3.49 x 10^{-4}	23.0
3.83 x 10^{-4}	24.8
4.17 x 10^{-4}	26.4
4.85 x 10^{-4}	29.6
5.52 x 10^{-4}	32.8
6.19 x 10^{-4}	36.0
6.85 x 10^{-4}	39.2
7.50 x 10^{-4}	42.4
8.15 x 10^{-4}	45.1
8.80 x 10^{-4}	48.0
9.44 x 10^{-4}	50.6
1.01 x 10^{-3}	53.1
1.07 x 10^{-3}	56.2
1.13 x 10^{-3}	58.4
1.20 x 10^{-3}	60.8
1.32 x 10^{-3}	66.4
1.44 x 10^{-3}	71.2
1.56 x 10^{-3}	76.0
1.68 x 10^{-3}	80.3
1.79 x 10^{-3}	84.0
2.02 x 10^{-3}	92.8
2.24 x 10^{-3}	101
2.51 x 10^{-3}	111
2.77 x 10^{-3}	120
3.26 x 10^{-3}	138
3.72 x 10^{-3}	153
4.15 x 10^{-3}	167
4.56 x 10^{-3}	181
4.94 x 10^{-3}	194

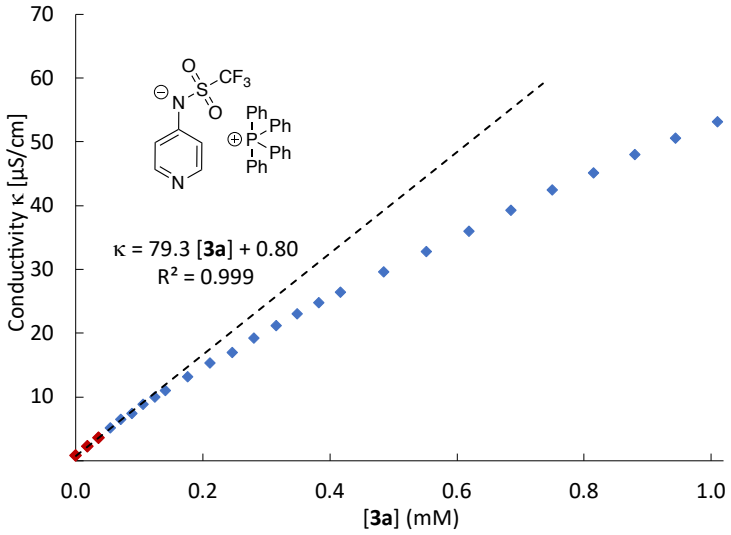

Concentration dependent conductivity data of **3b** in DCM at 20 °C

[3b]/M	Conductivity κ (µS/cm)
0.00	0.80
1.79×10^{-5}	2.24
3.58×10^{-5}	3.68
5.37×10^{-5}	5.12
7.16×10^{-5}	6.48
8.94×10^{-5}	7.84
1.08×10^{-4}	9.12
1.25×10^{-4}	10.4
1.43×10^{-4}	11.7
1.60×10^{-4}	12.8
1.78×10^{-4}	14.0
1.95×10^{-4}	15.1
2.13×10^{-4}	16.3
2.48×10^{-4}	18.6
2.83×10^{-4}	20.6
3.18×10^{-4}	22.7
3.52×10^{-4}	24.8
3.87×10^{-4}	26.9
4.21×10^{-4}	28.8
4.55×10^{-4}	30.7
4.89×10^{-4}	32.6
5.57×10^{-4}	36.5
6.24×10^{-4}	39.8
6.91×10^{-4}	43.2
7.57×10^{-4}	46.9
8.23×10^{-4}	50.1
8.88×10^{-4}	53.6
9.52×10^{-4}	57.1
1.02×10^{-3}	60.2
1.08×10^{-3}	63.4
1.14×10^{-3}	66.4
1.27×10^{-3}	72.8
1.39×10^{-3}	78.4
1.51×10^{-3}	84.5
1.63×10^{-3}	90.1
1.75×10^{-3}	95.4
1.87×10^{-3}	100
2.09×10^{-3}	111
2.32×10^{-3}	121
2.58×10^{-3}	132
2.84×10^{-3}	143
3.33×10^{-3}	162
3.80×10^{-3}	182
4.23×10^{-3}	201
4.64×10^{-3}	217

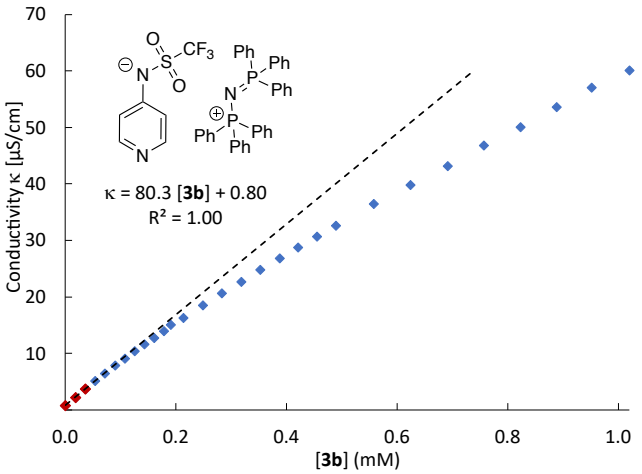

Concentration dependent conductivity data of **3c** in DCM at 20 °C

[3c]/M	Conductivity κ (µS/cm)
0.00 x 10^{0}	0.80
2.00 x 10^{-5}	2.00
3.99 x 10^{-5}	3.09
5.98 x 10^{-5}	4.24
7.97 x 10^{-5}	5.28
9.95 x 10^{-5}	6.24
1.19 x 10^{-4}	6.96
1.39 x 10^{-4}	7.68
1.59 x 10^{-4}	8.40
1.98 x 10^{-4}	9.76
2.37 x 10^{-4}	10.9
2.76 x 10^{-4}	12.1
3.15 x 10^{-4}	13.3
3.54 x 10^{-4}	14.3
3.92 x 10^{-4}	15.4
4.30 x 10^{-4}	16.3
4.69 x 10^{-4}	17.4
5.45 x 10^{-4}	19.1
6.20 x 10^{-4}	20.8
6.95 x 10^{-4}	22.6
7.69 x 10^{-4}	23.9
8.43 x 10^{-4}	25.5
9.16 x 10^{-4}	27.1
9.88 x 10^{-4}	28.5
1.06 x 10^{-3}	29.8
1.20 x 10^{-3}	32.3
1.34 x 10^{-3}	35.0
1.48 x 10^{-3}	37.4
1.62 x 10^{-3}	39.6
1.75 x 10^{-3}	41.9
1.88 x 10^{-3}	43.8
2.14 x 10^{-3}	48.2
2.39 x 10^{-3}	52.0
2.70 x 10^{-3}	56.3
2.99 x 10^{-3}	60.8
3.55 x 10^{-3}	68.1
4.08 x 10^{-3}	75.5
4.57 x 10^{-3}	82.7
5.03 x 10^{-3}	88.8

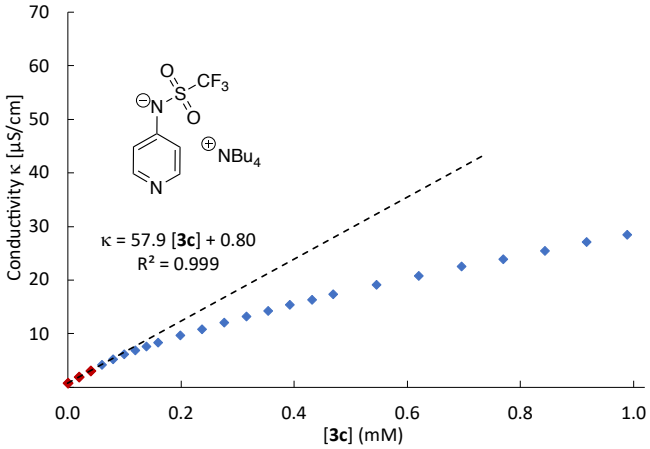

Concentration dependent conductivity data of **3d** in DCM at 20 °C

[3d]/M	Conductivity κ (µS/cm)
0.00	0.80
2.00×10^{-5}	1.92
4.00×10^{-5}	3.04
5.99×10^{-5}	4.16
7.98×10^{-5}	4.96
9.97×10^{-5}	5.92
1.20×10^{-4}	6.72
1.39×10^{-4}	7.36
1.59×10^{-4}	8.00
1.79×10^{-4}	8.80
1.98×10^{-4}	9.28
2.38×10^{-4}	10.4
2.77×10^{-4}	11.5
3.16×10^{-4}	12.3
3.54×10^{-4}	13.3
3.93×10^{-4}	14.4
4.70×10^{-4}	16.0
5.46×10^{-4}	17.6
6.21×10^{-4}	18.9
6.96×10^{-4}	20.5
7.71×10^{-4}	22.1
8.44×10^{-4}	23.2
9.18×10^{-4}	24.5
9.90×10^{-4}	25.8
1.06×10^{-3}	26.9
1.13×10^{-3}	28.0
1.28×10^{-3}	30.2
1.42×10^{-3}	32.3
1.55×10^{-3}	34.6
1.69×10^{-3}	35.7
1.82×10^{-3}	38.4
1.95×10^{-3}	40.5
2.08×10^{-3}	42.1
2.27×10^{-3}	44.5
2.46×10^{-3}	47.2
2.70×10^{-3}	50.1
2.94×10^{-3}	52.8
3.23×10^{-3}	56.5
3.50×10^{-3}	59.8
4.03×10^{-3}	65.6
4.53×10^{-3}	71.5
4.99×10^{-3}	77.3

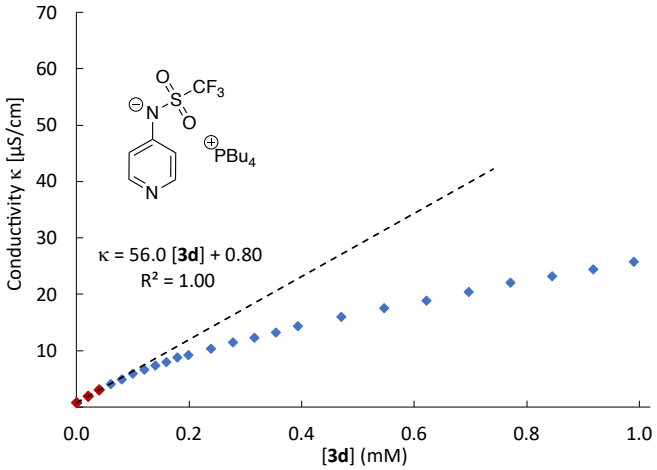

Concentration dependent conductivity data of **4a** in DCM at 20 °C

[4a]/M	Conductivity κ (µS/cm)
0.00	0.80
1.96 x 10^{-5}	2.24
3.91 x 10^{-5}	3.68
5.86 x 10^{-5}	5.04
7.81 x 10^{-5}	6.40
9.75 x 10^{-5}	7.52
1.17 x 10^{-4}	8.96
1.36 x 10^{-4}	9.92
1.56 x 10^{-4}	11.0
1.76 x 10^{-4}	12.2
1.94 x 10^{-4}	13.1
2.13 x 10^{-4}	14.2
2.32 x 10^{-4}	15.3
2.71 x 10^{-4}	17.0
3.09 x 10^{-4}	19.0
3.47 x 10^{-4}	20.8
3.84 x 10^{-4}	22.6
4.22 x 10^{-4}	24.2
4.59 x 10^{-4}	25.9
4.97 x 10^{-4}	27.5
5.34 x 10^{-4}	29.2
5.71 x 10^{-4}	30.7
6.08 x 10^{-4}	32.5
6.81 x 10^{-4}	35.4
7.54 x 10^{-4}	38.2
8.26 x 10^{-4}	41.1
8.98 x 10^{-4}	43.7
9.69 x 10^{-4}	46.6
1.04 x 10^{-3}	49.1
1.11 x 10^{-3}	51.5
1.18 x 10^{-3}	54.6
1.25 x 10^{-3}	57.0
1.32 x 10^{-3}	59.5
1.45 x 10^{-3}	64.3
1.59 x 10^{-3}	69.0
1.72 x 10^{-3}	73.3
1.85 x 10^{-3}	77.6
1.97 x 10^{-3}	82.1
2.10 x 10^{-3}	86.6
2.35 x 10^{-3}	94.2
2.59 x 10^{-3}	102
2.88 x 10^{-3}	111
3.16 x 10^{-3}	120
3.69 x 10^{-3}	136
4.19 x 10^{-3}	151
4.66 x 10^{-3}	165
5.10 x 10^{-3}	178

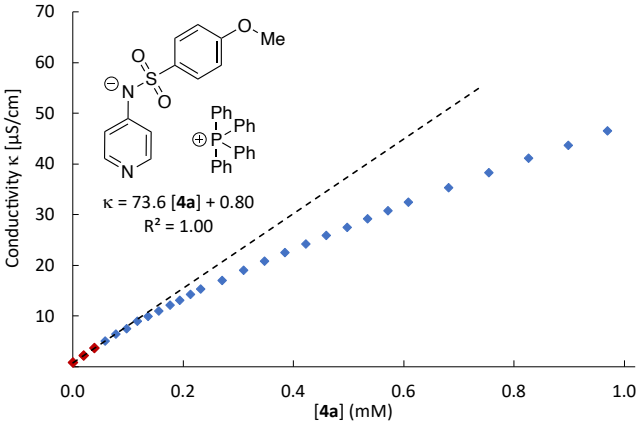

Concentration dependent conductivity data of **5a** in DCM at 20 °C

[5a]/M	Conductivity κ (µS/cm)
0.00	0.80
1.97×10^{-5}	2.24
3.94×10^{-5}	3.68
5.90×10^{-5}	5.12
7.85×10^{-5}	6.56
9.81×10^{-5}	7.92
1.18×10^{-4}	9.04
1.37×10^{-4}	10.1
1.56×10^{-4}	11.2
1.95×10^{-4}	13.4
2.34×10^{-4}	15.5
2.72×10^{-4}	17.4
3.10×10^{-4}	19.4
3.49×10^{-4}	21.3
3.87×10^{-4}	23.1
4.24×10^{-4}	24.8
4.62×10^{-4}	26.6
5.37×10^{-4}	29.9
6.11×10^{-4}	33.1
6.85×10^{-4}	36.3
7.58×10^{-4}	39.3
8.31×10^{-4}	42.1
9.03×10^{-4}	45.0
9.75×10^{-4}	47.8
1.05×10^{-3}	50.4
1.12×10^{-3}	53.0
1.19×10^{-3}	55.7
1.32×10^{-3}	60.6
1.46×10^{-3}	65.4
1.59×10^{-3}	70.3
1.73×10^{-3}	74.9
1.86×10^{-3}	79.2
1.99×10^{-3}	83.5
2.24×10^{-3}	91.8
2.48×10^{-3}	100
2.78×10^{-3}	109
3.06×10^{-3}	118
3.61×10^{-3}	135
4.12×10^{-3}	150
4.60×10^{-3}	164
5.05×10^{-3}	177

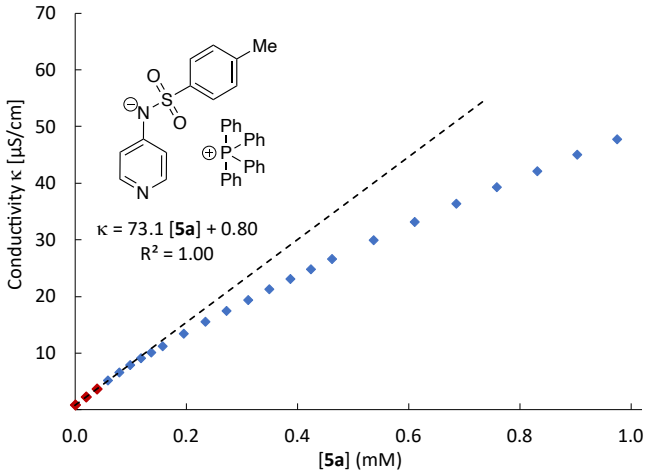

Concentration dependent conductivity data of **6a** in DCM at 20 °C

[6a]/M	Conductivity κ (µS/cm)
0.00	0.80
1.94 x 10^{-5}	2.24
3.88 x 10^{-5}	3.68
5.81 x 10^{-5}	5.12
7.74 x 10^{-5}	6.40
9.67 x 10^{-5}	7.60
1.16 x 10^{-4}	8.88
1.35 x 10^{-4}	10.0
1.54 x 10^{-4}	11.1
1.73 x 10^{-4}	12.2
1.92 x 10^{-4}	13.3
2.11 x 10^{-4}	14.2
2.30 x 10^{-4}	15.4
2.68 x 10^{-4}	17.3
3.06 x 10^{-4}	19.2
3.44 x 10^{-4}	21.2
3.81 x 10^{-4}	23.2
4.18 x 10^{-4}	24.6
4.56 x 10^{-4}	26.4
4.93 x 10^{-4}	28.3
5.29 x 10^{-4}	30.0
5.66 x 10^{-4}	31.5
6.03 x 10^{-4}	33.2
6.75 x 10^{-4}	36.3
7.69 x 10^{-4}	40.2
8.19 x 10^{-4}	42.4
8.90 x 10^{-4}	45.3
9.61 x 10^{-4}	48.2
1.03 x 10^{-3}	50.9
1.10 x 10^{-3}	53.6
1.17 x 10^{-3}	56.3
1.24 x 10^{-3}	58.7
1.31 x 10^{-3}	61.4
1.44 x 10^{-3}	66.4
1.57 x 10^{-3}	71.4
1.70 x 10^{-3}	76.0
1.83 x 10^{-3}	80.6
1.96 x 10^{-3}	85.0
2.14 x 10^{-3}	91.5
2.33 x 10^{-3}	97.6
2.56 x 10^{-3}	106
2.85 x 10^{-3}	115
3.13 x 10^{-3}	124
3.66 x 10^{-3}	141
4.16 x 10^{-3}	157

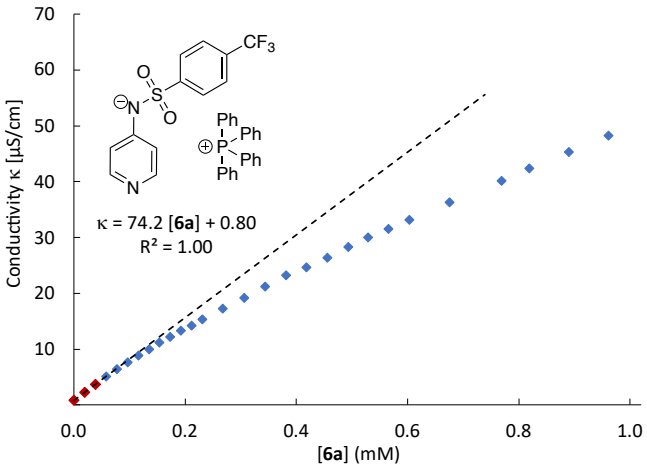

3.1.4.10 Additive Salts – Data of Conductivity Measurements in DCM

Concentration dependent conductivity data of **7a** in DCM at 20 °C

[7a]/M	Conductivity κ (µS/cm)
0.00	0.80
1.93×10^{-5}	2.64
3.86×10^{-5}	4.48
5.79×10^{-5}	6.24
7.71×10^{-5}	7.84
9.63×10^{-5}	9.36
1.15×10^{-4}	10.6
1.35×10^{-4}	12.3
1.54×10^{-4}	13.8
1.92×10^{-4}	16.4
2.30×10^{-4}	19.0
2.67×10^{-4}	21.4
3.05×10^{-4}	23.9
3.42×10^{-4}	26.1
3.80×10^{-4}	28.4
4.17×10^{-4}	30.5
4.54×10^{-4}	32.6
5.27×10^{-4}	36.6
6.00×10^{-4}	40.6
6.73×10^{-4}	44.1
7.45×10^{-4}	47.9
8.16×10^{-4}	51.4
8.87×10^{-4}	55.0
9.57×10^{-4}	58.2
1.03×10^{-3}	61.7
1.10×10^{-3}	64.6
1.16×10^{-3}	67.9
1.23×10^{-3}	71.1
1.30×10^{-3}	74.1
1.43×10^{-3}	79.9
1.57×10^{-3}	85.8
1.70×10^{-3}	91.3
1.82×10^{-3}	96.6
1.95×10^{-3}	102
2.20×10^{-3}	112
2.44×10^{-3}	122
2.73×10^{-3}	133
3.01×10^{-3}	145
3.54×10^{-3}	165
4.04×10^{-3}	184
4.51×10^{-3}	201

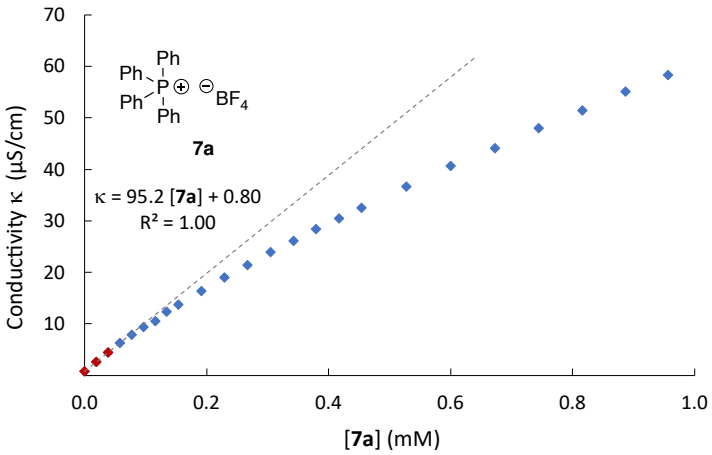

Concentration dependent conductivity data of **7b** in DCM at 20 °C

[7b]/M	Conductivity **κ** (µS/cm)
0.00	0.80
1.93×10^{-5}	2.56
3.85×10^{-5}	4.32
5.77×10^{-5}	6.08
7.69×10^{-5}	7.68
9.61×10^{-5}	9.36
1.15×10^{-4}	10.6
1.34×10^{-4}	12.2
1.53×10^{-4}	13.8
1.91×10^{-4}	16.4
2.29×10^{-4}	19.0
2.67×10^{-4}	21.8
3.04×10^{-4}	24.2
3.41×10^{-4}	26.6
3.79×10^{-4}	29.3
4.16×10^{-4}	31.4
4.52×10^{-4}	33.8
5.26×10^{-4}	38.1
5.99×10^{-4}	42.6
6.71×10^{-4}	46.7
7.43×10^{-4}	50.6
8.14×10^{-4}	54.9
8.84×10^{-4}	58.8
9.54×10^{-4}	62.6
1.02×10^{-3}	66.6
1.09×10^{-3}	70.2
1.16×10^{-3}	73.8
1.23×10^{-3}	77.2
1.30×10^{-3}	80.8
1.43×10^{-3}	87.7
1.56×10^{-3}	94.2
1.69×10^{-3}	101
1.82×10^{-3}	107
1.94×10^{-3}	113
2.19×10^{-3}	125
2.43×10^{-3}	136
2.72×10^{-3}	150
3.00×10^{-3}	163
3.53×10^{-3}	187
4.03×10^{-3}	210
4.50×10^{-3}	231
4.94×10^{-3}	250

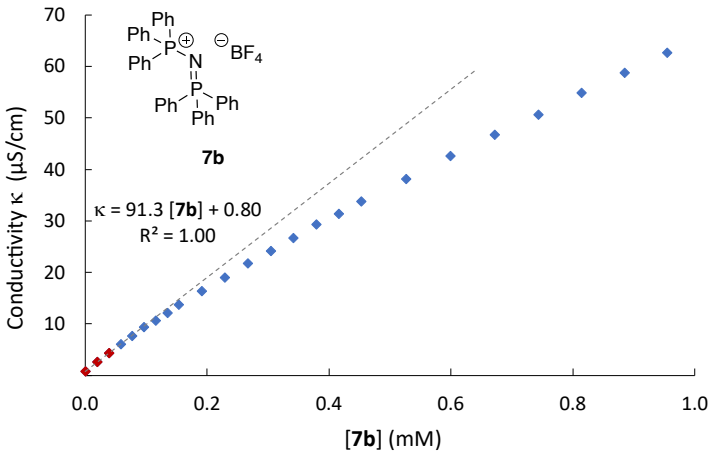

Concentration dependent conductivity data of **7c** in DCM at 20 °C

[7c]/M	Conductivity κ (µS/cm)
0.00	0.80
2.02×10^{-5}	2.24
4.03×10^{-5}	3.52
6.04×10^{-5}	4.32
8.05×10^{-5}	5.28
1.01×10^{-4}	6.24
1.21×10^{-4}	6.72
1.40×10^{-4}	7.36
1.60×10^{-4}	8.08
2.00×10^{-4}	9.20
2.40×10^{-4}	10.4
2.79×10^{-4}	11.2
3.18×10^{-4}	12.3
3.57×10^{-4}	13.1
3.96×10^{-4}	14.2
4.74×10^{-4}	16.0
5.50×10^{-4}	17.3
6.27×10^{-4}	18.9
7.02×10^{-4}	20.2
7.77×10^{-4}	21.8
8.52×10^{-4}	23.1
9.25×10^{-4}	24.3
9.99×10^{-4}	25.6
1.07×10^{-3}	26.9
1.14×10^{-3}	28.0
1.22×10^{-3}	29.2
1.29×10^{-3}	30.2
1.43×10^{-3}	32.3
1.57×10^{-3}	34.4
1.70×10^{-3}	36.5
1.84×10^{-3}	38.2
1.97×10^{-3}	40.2
2.23×10^{-3}	43.7
2.48×10^{-3}	46.9
2.79×10^{-3}	50.6
3.08×10^{-3}	54.4
3.64×10^{-3}	61.1
4.17×10^{-3}	67.1
4.66×10^{-3}	73.0
5.13×10^{-3}	78.2

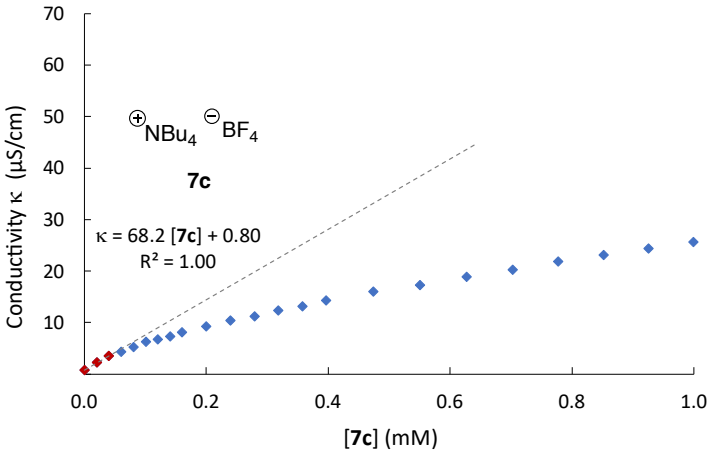

Concentration dependent conductivity data of **7d** in DCM at 20 °C

[7d]/M	Conductivity **κ** (µS/cm)
0.00	0.80
2.03×10^{-5}	2.08
4.06×10^{-5}	3.20
6.08×10^{-5}	4.08
8.10×10^{-5}	4.80
1.01×10^{-4}	5.44
1.21×10^{-4}	6.08
1.61×10^{-4}	7.12
2.01×10^{-4}	8.16
2.41×10^{-4}	9.04
2.81×10^{-4}	9.92
3.20×10^{-4}	10.6
3.60×10^{-4}	11.4
3.99×10^{-4}	12.2
4.77×10^{-4}	13.7
5.54×10^{-4}	15.0
6.31×10^{-4}	16.3
7.07×10^{-4}	17.4
7.82×10^{-4}	18.4
8.57×10^{-4}	19.7
9.32×10^{-4}	20.7
1.01×10^{-3}	21.8
1.08×10^{-3}	22.8
1.15×10^{-3}	23.7
1.29×10^{-3}	25.4
1.44×10^{-3}	27.4
1.58×10^{-3}	29.1
1.71×10^{-3}	30.6
1.85×10^{-3}	32.3
1.98×10^{-3}	33.8
2.24×10^{-3}	36.5
2.50×10^{-3}	39.2
2.81×10^{-3}	42.6
3.10×10^{-3}	45.4
3.67×10^{-3}	50.9
4.20×10^{-3}	56.0
4.69×10^{-3}	60.6
5.16×10^{-3}	65.0

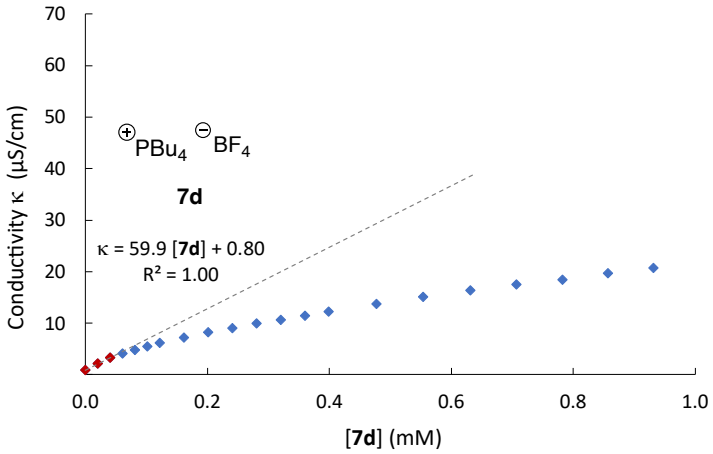

3.1.5 Nucleophilicity Data

The reaction rates of ion pair catalysts and TCAP (**2**) and the reference electrophiles were measured photometrically on a stop-flow spectrophotometer. The temperature was controlled with a circulating bath thermostat. The kinetic reactions were carried out under pseudo-first-order conditions (ion pair = nucleophile, excess compound) at the absorption maximum of benzhydrylium ion in the respective solvent as described previously by the H. Mayr group.[10] First-order rate constants k_{obs} (s^{-1}) were derived by fitting the absorbance according to the mono-exponential curve $A_t = A_0 \exp(-k_{obs}\, t) + C$ (see Figure 3.10).

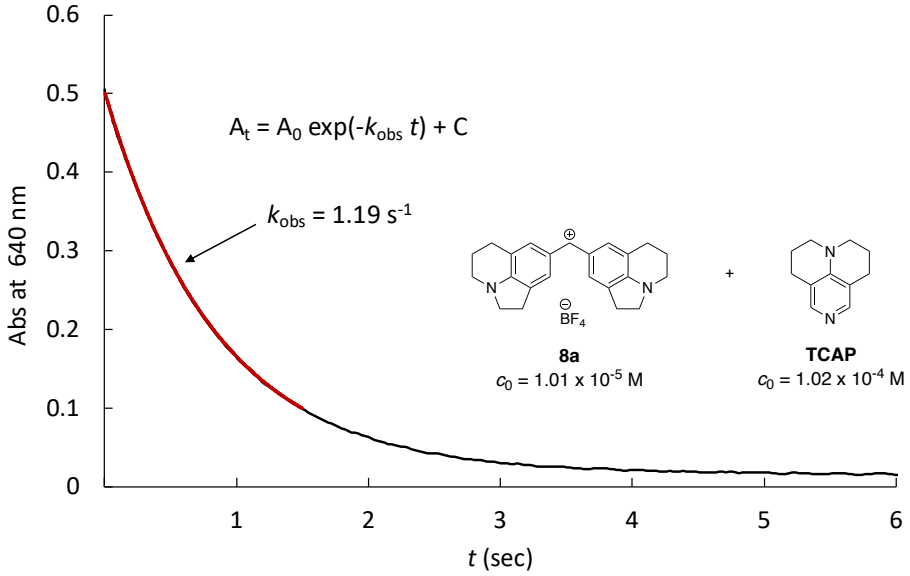

Figure 3.10: [Figure S11]. Absorbance decay of benzhydrylium salt **8a** reacting with nucleophile TCAP (**2**) in DCM at 20°C, fitted by mono-exponential decay function resulting in k_{obs} = 1.19 s^{-1}.

Then the second-order rate constant k_2 (L mol^{-1} s^{-1}) is obtained from the slope of the linear plots of k_{obs} (s^{-1}) vs [Nu] since $k_{obs} = k_2$[Nu]. The subsequent characterization is based on the Mayr-Patz eq. 3.10 where the reaction rates for the reaction of the nucleophile with the electrophile is expressed as a function of the nucleophilicity parameter *N*, the associated sensitivity parameter s_N, and the electrophilicity parameter *E*. Both, *N* parameter and nucleophile-specific s_N parameter are solvent dependent.[10–12]

$$\log k_2^{20\,^\circ C} = s_N(N + E) \qquad (3.10)$$

3.1.5.1 Kinetic Data Analysis

Measurements of ionic compounds performed in non-polar solvents require more consideration due to the influence of ion association on the first-order rate constant k_{obs}. To negate the effect of ion association in solution, the ionic strength controlled benzhydrylium method was developed where a non-nucleophilic, structurally related salt was added as additive to keep ionic strength *I* constant throughout the kinetic.

Kinetic data gathered under conditions of ionic strength control *I* = 1.0 mM, can be analyzed in multiple ways (for full discussion see Chapter 2). The most practical way would be to assume that the amount of weighted salt equals the amount of nucleophile in solution. Here, the standard Mayr method would be employed to obtain the second-order rate constant k_2 and subsequently gain the *N* parameter and s_N parameter.

The combination of conductivity and DOSY NMR, however, revealed a complex ion association taking place in solution, where the single ions associate into distinctive triple ion complexes of the type, **CAC,** and **ACA**. It is assumed that the remaining free anion **A** is the only reactive nucleophile in solution. To determine the concentration of free nucleophile **A** in solution, the conductivity model III was used as basis. Since the association of the pyridinamide ion pair is controlled *via* the addition of the additive salt, the association of the additive itself has to be considered. The existing model III was extended by adding the association equation for the additive to it (see Scheme 3.5).

$$2 * A + 2 * C \overset{\alpha \times K_{CAC}}{\rightleftharpoons} A + CAC$$

$$2 * A + 2 * C \overset{\beta \times K_{ACA}}{\rightleftharpoons} C + ACA$$

$$2 * C + 2 * B \overset{K_{CAC}(add)}{\rightleftharpoons} B + CBC$$

Scheme 3.5: [Scheme S5]. Numerical simulation equations of mixed sandwich association model extension for evaluation of ionic strength controlled kinetic data.

Since there are two pyridinamide ion pairs, **3b** and **3d**, whose association pattern could not be analyzed with the mixed sandwich association model, an alternative extension for the nucleophilicity data evaluation will be included here. DOSY NMR data revelated the cationic sandwich association as a suitable association model for pyridinamide ion pairs with the deprotonated 1,1,1-trifluoro-*N*-(pyridin-4(1*H*)-ylidene)methanesulfonamide as anion (see ref. [2]). As an alternative, model IIa was used as basis for another extension for the analysis of the ionic strength-controlled benzhydrylium method (see Scheme 3.6).

$$2 * A + 2 * C \overset{K_{CAC}}{\rightleftharpoons} A + CAC$$

$$2 * C + 2 * B \overset{K_{CAC}(add)}{\rightleftharpoons} B + CBC$$

Scheme 3.6: [Scheme S6]. Numerical simulation equations of cationic sandwich association model extension for evaluation of ionic strength controlled kinetic data.

Now, both models were used to evaluate the gathered kinetic data. For completeness, all kinetic data sets were analyzed utilizing both association extensions to obtain the respective nucleophilicity parameters *N* and s_N. Numerical simulation to obtain the relevant ion concentrations were performed using COPASI, whereas the individual starting concentrations are defined as:

– [**A**] = concentration of pyridinamide salt

– [**C**] = concentration of pyridinamide salt + concentration of additive

– [**B**] = concentration of additive + concentration of the respective benzhydrylium salt.

The resulting *N*- and s_N-parameter of the ionic-strength controlled benzhydrylium method for pyridinamide ion pairs in DCM are summarized in Table 3.9. The applied models are distinguished by superscripts: "HC" = $[\mathbf{A}]_{tot}$ with *I* = 1.0 mM, "HC,sw" = [**A**] obtained by model IIa extension with *I* = 1.0 mM, and "HC,mix" = [**A**] obtained by model III extension with *I* = 1.0 mM.

Table 3.9: [Table S14]. List of *N*- and s_N-parameter obtained with different evaluation models for pyridinamide ion pairs in DCM.

Ion Pair	*N*/s_N parameter		
	HC	HC,sw	HC,mix
3d	17.12/0.77	17.25/0.77	–
3c	17.20/0.76	17.33/0.76	17.32/0.76
3b	17.41/0.75	17.65/0.75	17.65/0.75
3a	17.40/0.75	17.61/0.75	17.88/0.73

5a	19.24/0.66	19.47/0.66	19.42/0.66
4a	19.35/0.65	19.65/0.65	19.63/0.65
6a	17.66/0.72	18.53/0.72	18.43/0.72

3.1.5.2 Nucleophilicity data in MeCN

Nucleophilicity of ion pair 3b in MeCN at 20 °C

Reaction of **3b** with $(lil)_2CH^+BF_4^-$ (stopped-flow, λ = 632 nm)

[8a] (mol L^{-1})	[3b] (mol L^{-1})	k_{obs} (s^{-1})
9.41 x 10^{-7}	9.81 x 10^{-6}	0.38
	1.47 x 10^{-5}	0.42
	1.96 x 10^{-5}	0.46
	2.45 x 10^{-5}	0.51
	2.94 x 10^{-5}	0.54

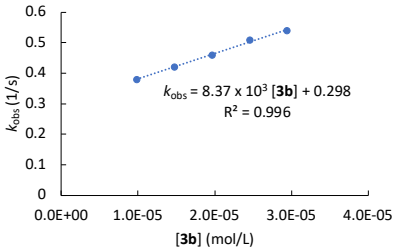

k_2 = 8.37 x 10^3 L mol^{-1} s^{-1}

Reaction of **3b** with $(jul)_2CH^+BF_4^-$ (stopped-flow, λ = 635 nm)

[8b] (mol L^{-1})	[3b] (mol L^{-1})	k_{obs} (s^{-1})
9.67 x 10^{-7}	9.81 x 10^{-6}	0.82
	1.47 x 10^{-5}	0.89
	1.96 x 10^{-5}	0.95
	2.45 x 10^{-5}	
	2.94 x 10^{-5}	1.09

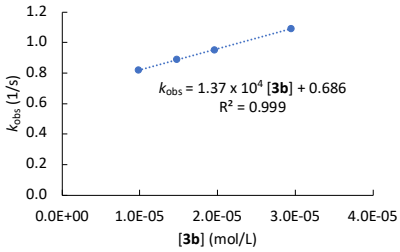

k_2 = 1.37 x 10^4 L mol^{-1} s^{-1}

Reaction of **3b** with $(ind)_2CH^+BF_4^-$ (stopped-flow, λ = 616 nm)

[8c] (mol L^{-1})	[3b] (mol L^{-1})	k_{obs} (s^{-1})
1.07 x 10^{-6}	9.81 x 10^{-6}	0.56
	1.47 x 10^{-5}	0.86
	1.96 x 10^{-5}	1.08
	2.45 x 10^{-5}	1.30
	2.94 x 10^{-5}	1.50

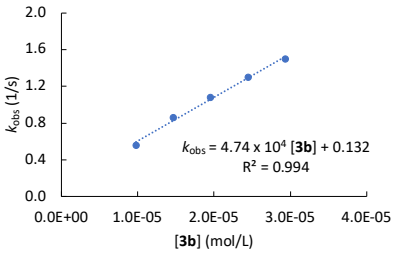

k_2 = 4.74 x 10^4 L mol^{-1} s^{-1}

Determination of *N* and s_N parameter for **3b** in MeCN

Electrophile	*E*	k_2 (M^{-1} s^{-1})
8a	-10.04	8.37 x 10^3
8b	-9.45	1.37 x 10^4
8c	-8.76	4.74 x 10^4

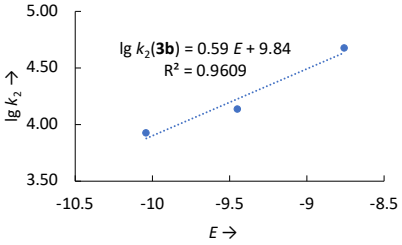

N = 16.68 **s_N = 0.59**

Nucleophilicity of ion pair 3c in MeCN at 20 °C

Reaction of **3c** with $(lil)_2CH^+BF_4^-$ (stopped-flow, λ = 632 nm)

[8a] (mol L^{-1})	[3c] (mol L^{-1})	k_{obs} (s^{-1})
1.09 x 10^{-6}	9.94 x 10^{-6}	0.33
	1.49 x 10^{-5}	0.38
	1.99 x 10^{-5}	0.41
	2.49 x 10^{-5}	0.46
	2.98 x 10^{-5}	0.50

k_2 = 8.45 x 10^3 L mol^{-1} s^{-1}

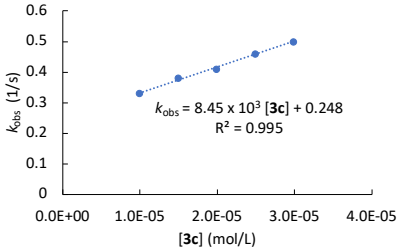

Reaction of **3c** with $(jul)_2CH^+BF_4^-$ (stopped-flow, λ = 635 nm)

[8b] (mol L^{-1})	[3c] (mol L^{-1})	k_{obs} (s^{-1})
1.04 x 10^{-6}	9.94 x 10^{-6}	0.82
	1.49 x 10^{-5}	0.89
	1.99 x 10^{-5}	0.92
	2.49 x 10^{-5}	1.01
	2.98 x 10^{-5}	1.10

k_2 = 1.37 x 10^4 L mol^{-1} s^{-1}

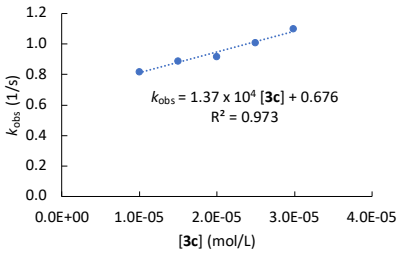

Reaction of **3c** with $(ind)_2CH^+BF_4^-$ (stopped-flow, λ = 616 nm)

[8c] (mol L^{-1})	[3c] (mol L^{-1})	k_{obs} (s^{-1})
9.27 x 10^{-7}	9.94 x 10^{-6}	0.54
	1.49 x 10^{-5}	0.86
	1.99 x 10^{-5}	1.06
	2.49 x 10^{-5}	1.34
	2.98 x 10^{-5}	1.49

k_2 = 4.97 x 10^4 L mol^{-1} s^{-1}

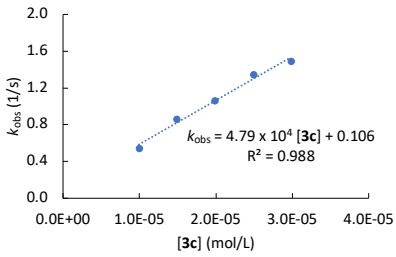

Determination of *N* and s_N parameter for **3c** in MeCN

Electrophile	*E*	k_2 (m^{-1} s^{-1})
8a	-10.04	8.45 x 10^3
8b	-9.45	1.37 x 10^4
8c	-8.76	4.79 x 10^4

N = 16.68 **s_N = 0.59**

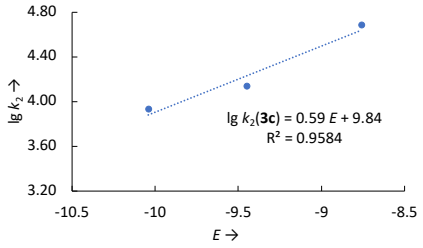

Nucleophilicity of ion pair 3d in MeCN at 20 °C

Reaction of **3d** with $(lil)_2CH^+BF_4^-$ (stopped-flow, λ = 632 nm)

[8a] (mol L^{-1})	[3d] (mol L^{-1})	k_{obs} (s^{-1})
9.69 x 10^{-7}	9.82 x 10^{-6}	0.33
	1.47 x 10^{-5}	0.38
	1.96 x 10^{-5}	0.42
	2.45 x 10^{-5}	0.46
	2.95 x 10^{-5}	

k_2 = 8.79 x 10^3 L mol^{-1} s^{-1}

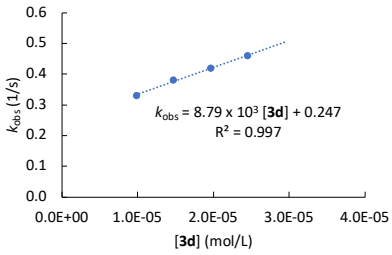

Reaction of **3d** with $(jul)_2CH^+BF_4^-$ (stopped-flow, λ = 635 nm)

[8b] (mol L^{-1})	[3d] (mol L^{-1})	k_{obs} (s^{-1})
	9.82 x 10^{-6}	0.81
	1.47 x 10^{-5}	0.88
9.56 x 10^{-7}	1.96 x 10^{-5}	0.96
	2.45 x 10^{-5}	1.05
	2.95 x 10^{-5}	

k_2 = 1.63 x 10^4 L mol^{-1} s^{-1}

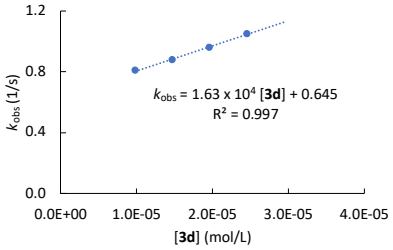

Reaction of **3d** with $(ind)_2CH^+BF_4^-$ (stopped-flow, λ = 616 nm)

[8c] (mol L^{-1})	[3d] (mol L^{-1})	k_{obs} (s^{-1})
	9.82 x 10^{-6}	0.56
	1.47 x 10^{-5}	0.86
8.98 x 10^{-7}	1.96 x 10^{-5}	1.10
	2.45 x 10^{-5}	1.30
	2.95 x 10^{-5}	

k_2 = 5.03 x 10^4 L mol^{-1} s^{-1}

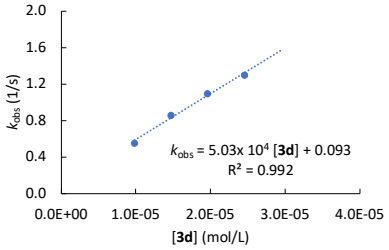

Determination of *N* and s_N parameter for **3d** in MeCN

Electrophile	*E*	k_2 (M^{-1} s^{-1})
8a	-10.04	8.79 x 10^3
8b	-9.45	1.63 x 10^4
8c	-8.76	5.03 x 10^4

N = 16.48 **s_N = 0.60**

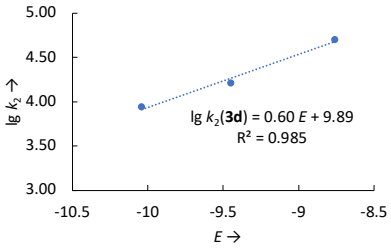

Nucleophilicity of ion pair 5a in MeCN at 20 °C

Reaction of **5a** with $(lil)_2CH^+BF_4^-$ (stopped-flow, λ = 632 nm)

[8a] (mol L^{-1})	[5a] (mol L^{-1})	k_{obs} (s^{-1})
	1.00 x 10^{-5}	
	2.01 x 10^{-5}	0.64
9.41 x 10^{-7}	3.01 x 10^{-5}	1.08
	4.02 x 10^{-5}	1.42
	5.02 x 10^{-5}	1.68

k_2 = 3.45 x 10^4 L mol^{-1} s^{-1}

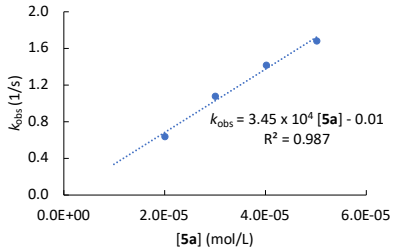

Reaction of **5a** with $(jul)_2CH^+BF_4^-$ (stopped-flow, λ = 635 nm)

[8b] (mol L^{-1})	[5a] (mol L^{-1})	k_{obs} (s^{-1})
	1.00 x 10^{-5}	0.38
	2.01 x 10^{-5}	1.54
1.17 x 10^{-6}	3.01 x 10^{-5}	2.51
	4.02 x 10^{-5}	3.31
	5.02 x 10^{-5}	4.20

k_2 = 9.36 x 10^4 L mol^{-1} s^{-1}

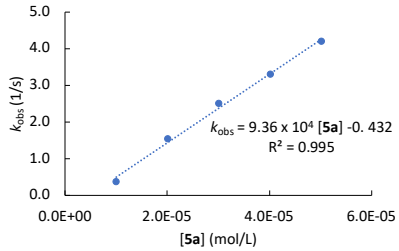

Reaction of **5a** with $(ind)_2CH^+BF_4^-$ (stopped-flow, λ = 616 nm)

[8c] (mol L^{-1})	[5a] (mol L^{-1})	k_{obs} (s^{-1})
1.14 x 10^{-6}	1.00 x 10^{-5}	1.46
	2.01 x 10^{-5}	3.6
	3.01 x 10^{-5}	5.91
	4.02 x 10^{-5}	8.42
	5.02 x 10^{-5}	10.6

k_2 = 2.30 x 10^5 L mol^{-1} s^{-1}

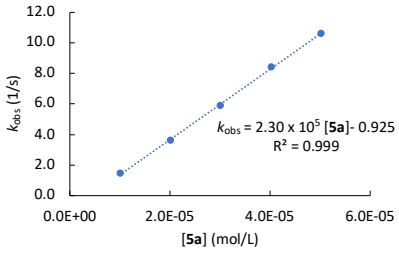

Determination of *N* and s_N parameter for **5a** in MeCN

Electrophile	*E*	k_2 (M^{-1} s^{-1})
8a	-10.04	3.45 x 10^4
8b	-9.45	9.36 x 10^4
8c	-8.76	2.30 x 10^5

***N* = 17.19** **s_N = 0.64**

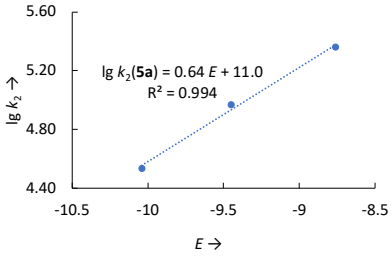

Nucleophilicity of ion pair 6a in MeCN at 20 °C

Reaction of **6a** with $(lil)_2CH^+BF_4^-$ (stopped-flow, λ = 632 nm)

[8a] (mol L^{-1})	[6a] (mol L^{-1})	k_{obs} (s^{-1})
9.96 x 10^{-7}	9.92 x 10^{-6}	0.16
	1.49 x 10^{-5}	0.32
	1.98 x 10^{-5}	0.48
	2.48 x 10^{-5}	0.64
	2.98 x 10^{-5}	0.75

k_2 = 3.02 x 10^4 L mol^{-1} s^{-1}

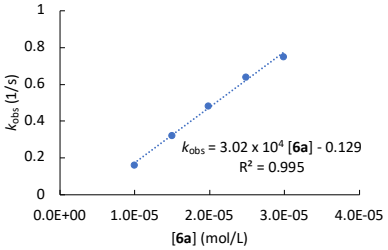

Reaction of **6a** with $(jul)_2CH^+BF_4^-$ (stopped-flow, λ = 635 nm)

[8b] (mol L^{-1})	[6a] (mol L^{-1})	k_{obs} (s^{-1})
1.02 x 10^{-6}	9.92 x 10^{-6}	0.58
	1.49 x 10^{-5}	0.85
	1.98 x 10^{-5}	1.18
	2.48 x 10^{-5}	1.50
	2.98 x 10^{-5}	1.73

k_2 = 5.94 x 10^4 L mol^{-1} s^{-1}

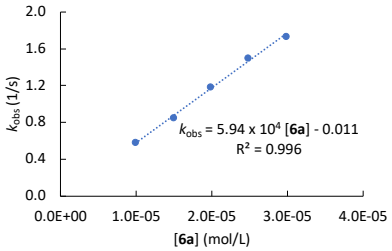

Reaction of **6a** with $(ind)_2CH^+BF_4^-$ (stopped-flow, λ = 616 nm)

[8c] (mol L^{-1})	[6a] (mol L^{-1})	k_{obs} (s^{-1})
9.13 x 10^{-7}	9.92 x 10^{-6}	1.22
	1.49 x 10^{-5}	1.97
	1.98 x 10^{-5}	2.50
	2.48 x 10^{-5}	3.12
	2.98 x 10^{-5}	3.61

k_2 = 1.19 x 10^5 L mol^{-1} s^{-1}

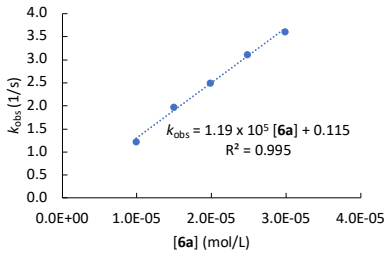

Determination of *N* and s_N parameter for **6a** in MeCN

Electrophile	*E*	k_2 (M^{-1} s^{-1})
8a	-10.04	3.02×10^4
8b	-9.45	6.26×10^4
8c	-8.76	1.19×10^5

***N* = 19.47** **s_N = 0.47**

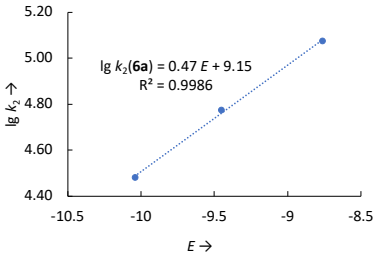

3.1.5.3 Nucleophilicity data in DCM at 0.01 – 0.03 mM

Nucleophilicity of ion pair 3b in DCM at 20 °C

Reaction of **3b** with $(lil)_2CH^+BF_4^-$ (stopped-flow, λ = 640 nm)

[8a] (mol L^{-1})	[3b] (mol L^{-1})	k_{obs} (s^{-1})
	9.88×10^{-6}	
	1.48×10^{-5}	21.0
1.05×10^{-6}	1.98×10^{-5}	27.6
	2.47×10^{-5}	35.8
	2.96×10^{-5}	41.9

k_2 = 1.44 x 10^6 L mol^{-1} s^{-1}

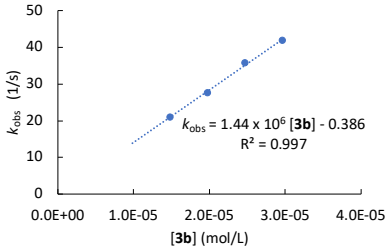

Reaction of **3b** with $(jul)_2CH^+BF_4^-$ (stopped-flow, λ = 643 nm)

[8b] (mol L^{-1})	[3b] (mol L^{-1})	k_{obs} (s^{-1})
	9.88×10^{-6}	29.7
	1.48×10^{-5}	
9.80×10^{-7}	1.98×10^{-5}	60.4
	2.47×10^{-5}	78.0
	2.96×10^{-5}	90.5

k_2 = 3.13 x 10^6 L mol^{-1} s^{-1}

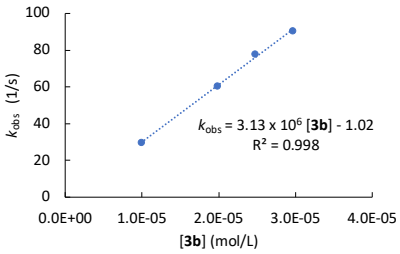

Reaction of **3b** with $(ind)_2CH^+BF_4^-$ (stopped-flow, λ = 626 nm)

[8c] (mol L^{-1})	[3b] (mol L^{-1})	k_{obs} (s^{-1})
	9.88×10^{-6}	119
	1.48×10^{-5}	202
1.01×10^{-6}	1.98×10^{-5}	266
	2.47×10^{-5}	342
	2.96×10^{-5}	

k_2 = 1.48 x 10^7 L mol^{-1} s^{-1}

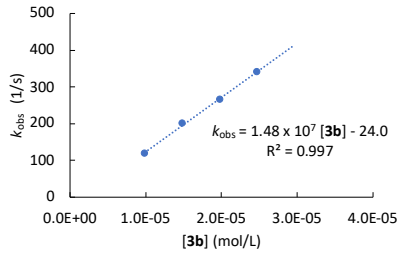

Determination of *N* and s_N parameter for **3b** in DCM

Electrophile	*E*	k_2 (M^{-1} s^{-1})
8a	-10.04	1.44×10^6
8b	-9.45	3.13×10^6
8c	-8.76	1.48×10^7

***N* = 17.63** **s_N = 0.80**

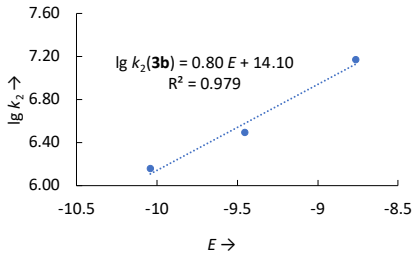

Nucleophilicity of ion pair 3c in DCM at 20 °C

Reaction of **3c** with $(lil)_2CH^+BF_4^-$ (stopped-flow, λ = 640 nm)

[8a] (mol L^{-1})	[3c] (mol L^{-1})	k_{obs} (s^{-1})
	9.49 x 10^{-6}	14.1
	1.42 x 10^{-5}	23.8
1.11 x 10^{-6}	1.90 x 10^{-5}	29.4
	2.37 x 10^{-5}	
	2.85 x 10^{-5}	

k_2 = 1.61 x 10^6 L mol^{-1} s^{-1}

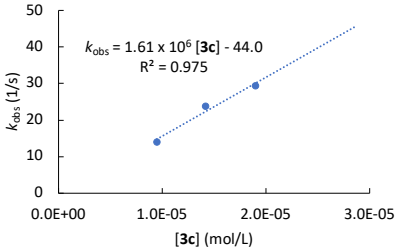

Reaction of **3c** with $(jul)_2CH^+BF_4^-$ (stopped-flow, λ = 643 nm)

[8b] (mol L^{-1})	[3c] (mol L^{-1})	k_{obs} (s^{-1})
	9.49 x 10^{-6}	
	1.42 x 10^{-5}	38.1
9.80 x 10^{-7}	1.90 x 10^{-5}	48.6
	2.37 x 10^{-5}	62.6
	2.85 x 10^{-5}	78.6

k_2 = 2.85 x 10^6 L mol^{-1} s^{-1}

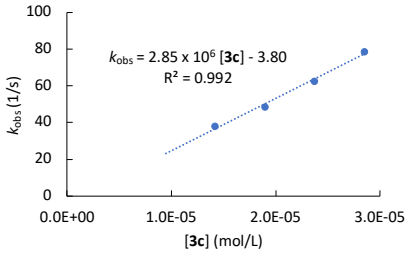

Reaction of **3c** with $(ind)_2CH^+BF_4^-$ (stopped-flow, λ = 626 nm)

[8c] (mol L^{-1})	[3c] (mol L^{-1})	k_{obs} (s^{-1})
	9.49 x 10^{-6}	
	1.42 x 10^{-5}	170
8.02 x 10^{-7}	1.90 x 10^{-5}	285
	2.37 x 10^{-5}	359
	2.85 x 10^{-5}	435

k_2 = 1.83 x 10^7 L mol^{-1} s^{-1}

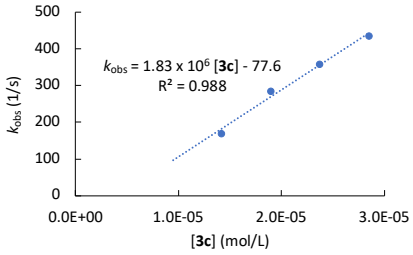

Determination of *N* and s_N parameter for **3c** in DCM

Electrophile	*E*	k_2 (M^{-1} s^{-1})
8a	-10.04	1.61 x 10^6
8b	-9.45	2.85 x 10^6
8c	-8.76	1.83 x 10^7

***N* = 17.47** **s_N = 0.83**

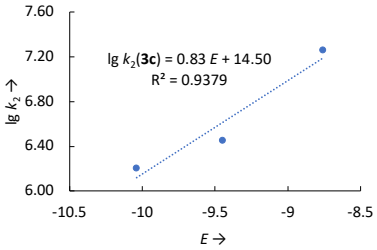

Nucleophilicity of ion pair 3d in DCM at 20 °C

Reaction of **3d** with $(lil)_2CH^+BF_4^-$ (stopped-flow, λ = 640 nm)

[8a] (mol L^{-1})	[3d] (mol L^{-1})	k_{obs} (s^{-1})
	9.98 x 10^{-6}	
	1.48 x 10^{-5}	24.6
9.50 x 10^{-7}	2.00 x 10^{-5}	32.6
	2.48 x 10^{-5}	37.4
	2.99 x 10^{-5}	45.3

k_2 = 1.33 x 10^6 L mol^{-1} s^{-1}

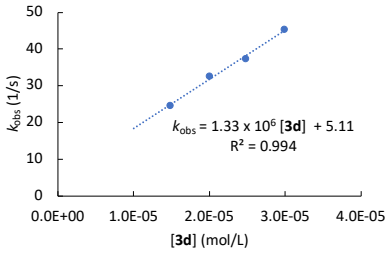

Reaction of **3d** with $(jul)_2CH^+BF_4^-$ (stopped-flow, λ = 643 nm)

[8b] (mol L^{-1})	[3d] (mol L^{-1})	k_{obs} (s^{-1})
	9.98 x 10^{-6}	28.8
	1.48 x 10^{-5}	47.7
1.03 x 10^{-6}	2.00 x 10^{-5}	
	2.48 x 10^{-5}	74.5
	2.99 x 10^{-5}	92.7

k_2 = 3.10 x 10^6 L mol^{-1} s^{-1}

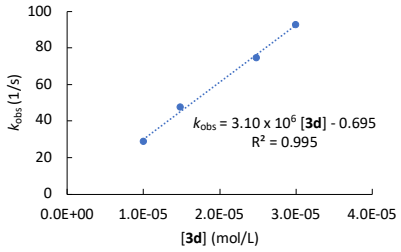

Reaction of **3d** with $(ind)_2CH^+BF_4^-$ (stopped-flow, λ = 626 nm)

[8c] (mol L^{-1})	[3d] (mol L^{-1})	k_{obs} (s^{-1})
	9.98 x 10^{-6}	111
	1.48 x 10^{-5}	188
9.56 x 10^{-7}	2.00 x 10^{-5}	265
	2.48 x 10^{-5}	
	2.99 x 10^{-5}	411

k_2 = 1.50 x 10^7 L mol^{-1} s^{-1}

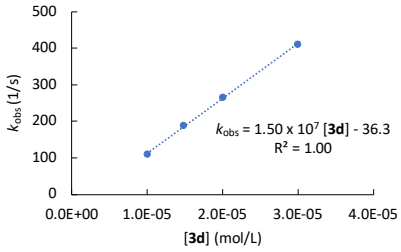

Determination of *N* and s_N parameter for **3d** in DCM

Electrophile	*E*	k_2 (M^{-1} s^{-1})
8a	-10.04	1.33 x 10^6
8b	-9.45	3.10 x 10^6
8c	-8.76	1.50 x 10^7

***N* = 17.33** **s_N = 0.83**

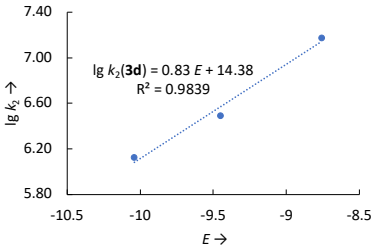

Nucleophilicity of ion pair 4a in DCM at 20 °C

Reaction of **4a** with $(lil)_2CH^+BF_4^-$ (stopped-flow, λ = 640 nm)

[8a] (mol L^{-1})	[4a] (mol L^{-1})	k_{obs} (s^{-1})
	1.01 x 10^{-5}	83.6
	1.49 x 10^{-5}	137
9.87 x 10^{-7}	2.01 x 10^{-5}	193
	2.49 x 10^{-5}	218
	3.02 x 10^{-5}	

k_2 = 9.24 x 10^7 L mol^{-1} s^{-1}

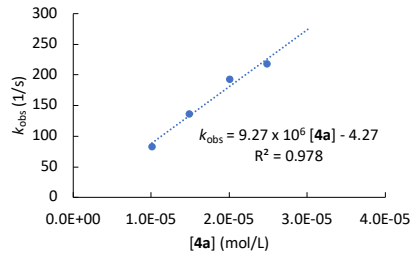

Reaction of **4a** with $(jul)_2CH^+BF_4^-$ (stopped-flow, λ = 643 nm)

[8b] (mol L^{-1})	[4a] (mol L^{-1})	k_{obs} (s^{-1})
	1.01 x 10^{-5}	
	1.49 x 10^{-5}	257
9.80 x 10^{-7}	2.01 x 10^{-5}	347
	2.49 x 10^{-5}	394
	3.02 x 10^{-5}	477

k_2 = 1.40 x 10^7 L mol^{-1} s^{-1}

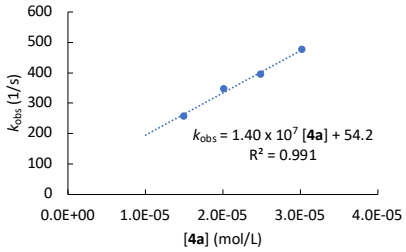

Determination of *N* and s_N parameter for **4a** in DCM

Electrophile	*E*	k_2 (M^{-1} s^{-1})
8a	-10.04	9.24×10^6
8b	-9.45	1.40×10^7
8c	-8.76	

***N* = 18.05** **s_N = 0.87[a]** (assumption based on **5a**)

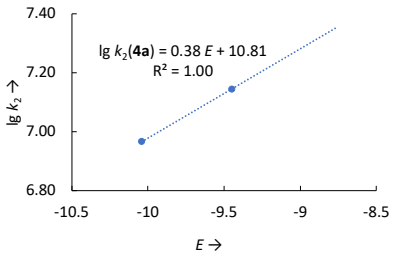

Nucleophilicity of ion pair 5a in DCM at 20 °C

Reaction of **5a** with $(lil)_2CH^+BF_4^-$ (stopped-flow, λ = 640 nm)

[8a] (mol L^{-1})	[5a] (mol L^{-1})	k_{obs} (s^{-1})
	9.96×10^{-6}	
	1.47×10^{-5}	111
9.87×10^{-7}	1.99×10^{-5}	
	2.47×10^{-5}	250
	2.99×10^{-5}	310

k_2 = 1.32 x 10^7 L mol^{-1} s^{-1}

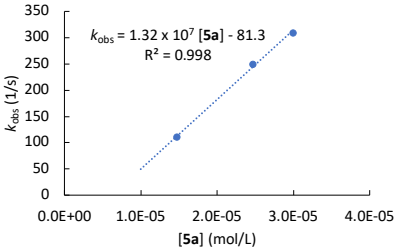

Reaction of **5a** with $(jul)_2CH^+BF_4^-$ (stopped-flow, λ = 643 nm)

[8b] (mol L^{-1})	[5a] (mol L^{-1})	k_{obs} (s^{-1})
	9.96×10^{-6}	
	1.47×10^{-5}	195
9.80×10^{-7}	1.99×10^{-5}	
	2.47×10^{-5}	432
	2.99×10^{-5}	564

k_2 = 2.42 x 10^7 L mol^{-1} s^{-1}

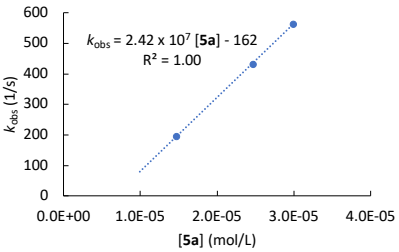

Reaction of **5a** with $(ind)_2CH^+BF_4^-$ (stopped-flow, λ = 626 nm)

[8c] (mol L^{-1})	[5a] (mol L^{-1})	k_{obs} (s^{-1})
	9.96×10^{-6}	186
	1.47×10^{-5}	969
1.01×10^{-6}	1.99×10^{-5}	
	2.47×10^{-5}	
	2.99×10^{-5}	

k_2 = 1.65 x 10^8 L mol^{-1} s^{-1}

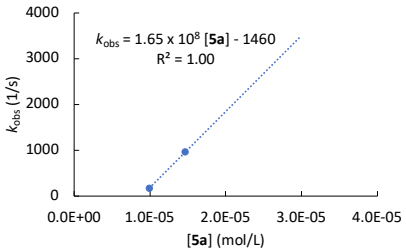

Determination of *N* and s_N parameter for **5a** in DCM

Electrophile	*E*	k_2 (M^{-1} s^{-1})
8a	-10.04	1.32×10^7
8b	-9.45	2.42×10^7
8c	-8.76	1.65×10^8

***N* = 18.05** **s_N = 0.84**

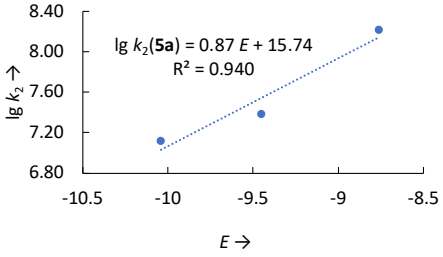

Nucleophilicity of ion pair 6a in DCM at 20 °C

Reaction of **6a** with $(lil)_2CH^+BF_4^-$ (stopped-flow, λ = 640 nm)

[8a] (mol L^{-1})	[6a] (mol L^{-1})	k_{obs} (s^{-1})
	9.93 x 10^{-6}	
	1.49 x 10^{-5}	54.2
9.00 x 10^{-7}	1.99 x 10^{-5}	82.7
	2.48 x 10^{-5}	99.1
	2.98 x 10^{-5}	126

k_2 = 4.68 x 10^6 L mol^{-1} s^{-1}

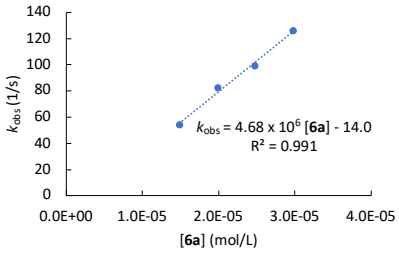

Reaction of **6a** with $(jul)_2CH^+BF_4^-$ (stopped-flow, λ = 643 nm)

[8b] (mol L^{-1})	[6a] (mol L^{-1})	k_{obs} (s^{-1})
	9.93 x 10^{-6}	
	1.49 x 10^{-5}	106
9.80 x 10^{-7}	1.99 x 10^{-5}	150
	2.48 x 10^{-5}	189
	2.98 x 10^{-5}	232

k_2 = 8.41 x 10^6 L mol^{-1} s^{-1}

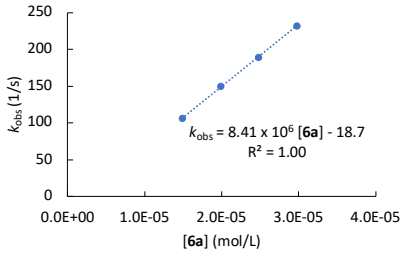

Reaction of **6a** with $(ind)_2CH^+BF_4^-$ (stopped-flow, λ = 626 nm)

[8c] (mol L^{-1})	[6a] (mol L^{-1})	k_{obs} (s^{-1})
	9.93 x 10^{-6}	133
	1.49 x 10^{-5}	346
9.00 x 10^{-7}	1.99 x 10^{-5}	486
	2.48 x 10^{-5}	629
	2.98 x 10^{-5}	

k_2 = 3.28 x 10^7 L mol^{-1} s^{-1}

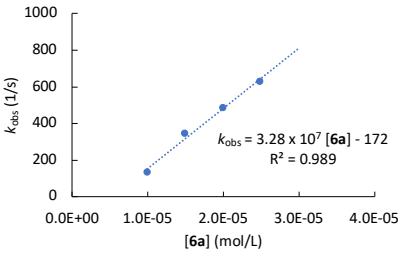

Determination of *N* and s_N parameter for **6a** in DCM

Electrophile	*E*	k_2 (M^{-1} s^{-1})
8a	-10.04	4.66 x 10^6
8b	-9.45	8.41 x 10^6
8c	-8.76	3.28 x 10^7

***N* = 19.87** **s_N = 0.67**

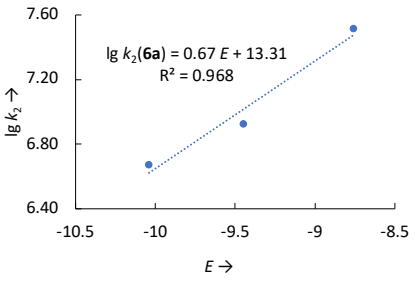

3.1.5.4 Nucleophilicity data in DCM at constant ionic strength *I* = 1.0 mM

Kinetic data of ion pair 3b in DCM at 20 °C

Association constants for numerical simulations: K_{CAC}(**3b**) = 4.65 x 10^6 M^{-2}, K_{CAC}(**7c**) = 4.61 x 10^6 M^{-2}.

Reaction of **3b + 7b** with $(lil)_2CH^+BF_4^-$ (stopped-flow, λ = 640 nm)

[8a] (mol L^{-1})	$[3b]_{tot}$ (mol L^{-1})	[C] (mol L^{-1})	$[3]^{HC,sw}$ (mol L^{-1})	$[3]^{HC,mix}$ (mol L^{-1})	k_{obs} (s^{-1})
	4.02 x 10^{-5}	9.57 x 10^{-4}	2.67 x 10^{-5}	–	15.0
	8.04 x 10^{-5}	9.18 x 10^{-4}	5.34 x 10^{-5}	–	28.8
4.04 x 10^{-6}	1.21 x 10^{-4}	8.79 x 10^{-4}	8.04 x 10^{-5}	–	43.2
	1.61 x 10^{-4}	8.41 x 10^{-4}	1.07 x 10^{-4}	–	55.1
	2.01 x 10^{-4}	8.02 x 10^{-4}	1.34 x 10^{-4}	–	67.8

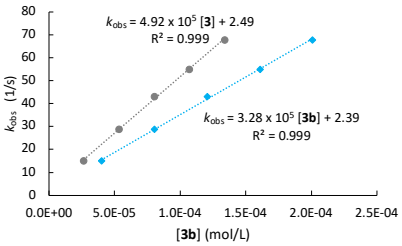

k_2^{HC} = 3.28 x 10^5 L mol^{-1} s^{-1} for $[3b]_{tot}$

$k_2^{HC,sw}$ = 4.92 x 10^5 L mol^{-1} s^{-1} for [**3**]

Reaction of **3b + 7b** with $(jul)_2CH^+BF_4^-$ (stopped-flow, λ = 643 nm)

[8b] (mol L^{-1})	$[3b]_{tot}$ (mol L^{-1})	[C] (mol L^{-1})	$[3]^{HC,sw}$ (mol L^{-1})	$[3]^{HC,mix}$ (mol L^{-1})	k_{obs} (s^{-1})
	4.02 x 10^{-5}	9.57 x 10^{-4}	2.67 x 10^{-5}	–	31.5
	8.04 x 10^{-5}	9.18 x 10^{-4}	5.34 x 10^{-5}	–	60.5
4.03 x 10^{-6}	1.21 x 10^{-4}	8.79 x 10^{-4}	8.04 x 10^{-5}	–	95.6
	1.61 x 10^{-4}	8.41 x 10^{-4}	1.07 x 10^{-4}	–	133
	2.01 x 10^{-4}	8.02 x 10^{-4}	1.34 x 10^{-4}	–	170

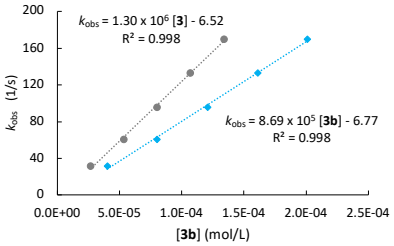

k_2^{HC} = 8.69 x 10^5 L mol^{-1} s^{-1} for $[3b]_{tot}$

$k_2^{HC,sw}$ = 1.30 x 10^6 L mol^{-1} s^{-1} for [**3**]

Reaction of **3b + 7b** with $(jul)_2CH^+BF_4^-$ (stopped-flow, λ = 643 nm)

[8c] (mol L^{-1})	$[3b]_{tot}$ (mol L^{-1})	[C] (mol L^{-1})	$[3]^{HC,sw}$ (mol L^{-1})	$[3]^{HC,mix}$ (mol L^{-1})	k_{obs} (s^{-1})
	4.02 x 10^{-5}	9.57 x 10^{-4}	2.67 x 10^{-5}	–	88.7
	8.04 x 10^{-5}	9.18 x 10^{-4}	5.34 x 10^{-5}	–	199
3.71 x 10^{-6}	1.21 x 10^{-4}	8.79 x 10^{-4}	8.04 x 10^{-5}	–	318
	1.61 x 10^{-4}	8.41 x 10^{-4}	1.07 x 10^{-4}	–	445
	2.01 x 10^{-4}	8.02 x 10^{-4}	1.34 x 10^{-4}	–	570

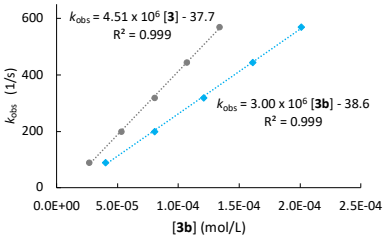

k_2^{HC} = 3.00 x 10^6 L mol^{-1} s^{-1} for $[3b]_{tot}$

$k_2^{HC,sw}$ = 4.51 x 10^6 L mol^{-1} s^{-1} for [**3**]

Determination of *N* and s_N parameter for **3b** in DCM

Electrophile	*E*	k_2^{HC} (M^{-1} s^{-1}) for $[3b]_{tot}$	$k_2^{HC,sw}$ (M^{-1} s^{-1}) for [**3**]	$k_2^{HC,mix}$ (M^{-1} s^{-1}) for [**3**]
8a	-10.04	3.28 x 10^5	4.92 x 10^5	–
8b	-9.45	8.69 x 10^5	1.30 x 10^6	–
8c	-8.76	3.00 x 10^6	4.51 x 10^6	–

N = 17.41 **s_N = 0.75** for $[3b]_{tot}$

N = 17.65 **s_N = 0.75** for $[3]^{HC,sw}$

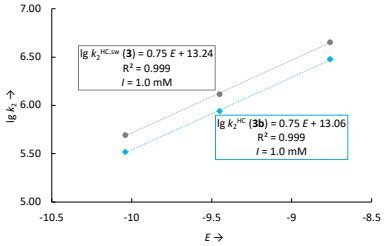

Data of ion pair 3c in DCM at 20 °C

Association constants for numerical simulations: K_{CAC}(**3c**) = 1.01 x 10^7 M^{-2}, K_{CAC}(**7c**) = 3.51 x 10^7 M^{-2},α x K_{CAC} = 3.33 x 10^6 M^{-2}, and β x K_{ACA} = 2.32 x 10^6 M^{-2}.

Reaction of **3c + 7c** with $(lil)_2CH^+BF_4^-$ (stopped-flow, λ = 640 nm)

[8a] (mol L^{-1})	$[3c]_{tot}$ (mol L^{-1})	[7c] (mol L^{-1})	$[3]^{HC,sw}$ (mol L^{-1})	$[3]^{HC,mix}$ (mol L^{-1})	k_{obs} (s^{-1})
	3.96 x 10^{-5}	9.550 x 10^{-}	1.80 x 10^{-5}	3.60 x 10^{-5}	10.9
	7.91 x 10^{-5}	9.160 x 10^{-}	3.70 x 10^{-5}	7.01 x 10^{-5}	23.4
3.90 x 10^{-6}	1.19 x 10^{-}	8.760 x 10^{-}	5.74 x 10^{-5}	1.03 x 10^{-}	34.2
	1.58 x 10^{-}	8.360 x 10^{-}	7.80 x 10^{-5}	1.33 x 10^{-}	45.1
	1.98 x 10^{-}	7.960 x 10^{-}	1.00 x 10^{-}	1.63 x 10^{-}	53.5

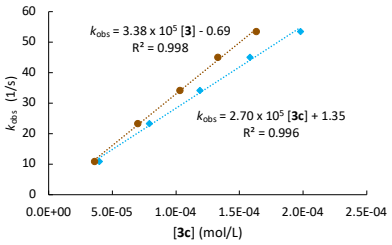

k_2^{HC} = 2.70 x 10^5 L mol^{-1} s^{-1} for $[3c]_{tot}$

$k_2^{HC,sw}$ = 3.41 x 10^5 L mol^{-1} s^{-1} for [3]

$k_2^{HC,mix}$ = 3.38 x 10^5 L mol^{-1} s^{-1} for [3]

Reaction of **3c + 7c** with $(jul)_2CH^+BF_4^-$ (stopped-flow, λ = 643 nm)

[8b] (mol L^{-1})	$[3c]_{tot}$ (mol L^{-1})	[7c] (mol L^{-1})	$[3]^{HC,sw}$ (mol L^{-1})	$[3]^{HC,mix}$ (mol L^{-1})	k_{obs} (s^{-1})
	3.96 x 10^{-5}	9.550 x 10^{-}	1.80 x 10^{-5}	3.60 x 10^{-5}	24.7
	7.91 x 10^{-5}	9.160 x 10^{-}	3.70 x 10^{-5}	7.01 x 10^{-5}	49.1
3.92 x 10^{-6}	1.19 x 10^{-}	8.760 x 10^{-}	5.74 x 10^{-5}	1.03 x 10^{-}	74.0
	1.58 x 10^{-}	8.360 x 10^{-}	7.80 x 10^{-5}	1.33 x 10^{-}	98.8
	1.98 x 10^{-}	7.960 x 10^{-}	1.00 x 10^{-}	1.63 x 10^{-}	132

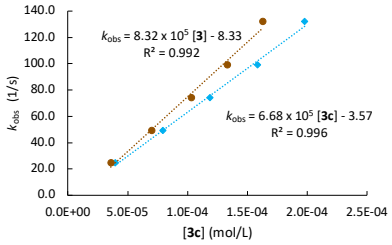

k_2^{HC} = 6.68 x 10^5 L mol^{-1} s^{-1} for $[3c]_{tot}$

$k_2^{HC,sw}$ = 8.42 x 10^5 L mol^{-1} s^{-1} for [3]

$k_2^{HC,mix}$ = 8.32 x 10^5 L mol^{-1} s^{-1} for [3]

Reaction of **3c + 7c** with $(jul)_2CH^+BF_4^-$ (stopped-flow, λ = 643 nm)

[8c] (mol L^{-1})	$[3c]_{tot}$ (mol L^{-1})	[7c] (mol L^{-1})	$[3]^{HC,sw}$ (mol L^{-1})	$[3]^{HC,mix}$ (mol L^{-1})	k_{obs} (s^{-1})
	3.96 x 10^{-5}	9.550 x 10^{-}	1.80 x 10^{-5}	3.60 x 10^{-5}	79.2
	7.91 x 10^{-5}	9.160 x 10^{-}	3.70 x 10^{-5}	7.01 x 10^{-5}	180
3.97 x 10^{-6}	1.19 x 10^{-}	8.760 x 10^{-}	5.74 x 10^{-5}	1.03 x 10^{-}	278
	1.58 x 10^{-}	8.360 x 10^{-}	7.80 x 10^{-5}	1.33 x 10^{-}	375
	1.98 x 10^{-}	7.960 x 10^{-}	1.00 x 10^{-}	1.63 x 10^{-}	485

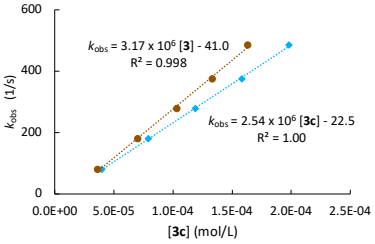

k_2^{HC} = 2.45 x 10^6 L mol^{-1} s^{-1} for $[3c]_{tot}$

$k_2^{HC,sw}$ = 3.21 x 10^6 L mol^{-1} s^{-1} for [3]

$k_2^{HC,mix}$ = 3.17 x 10^6 L mol^{-1} s^{-1} for [3]

Determination of N and s_N parameter for **3c** in DCM

Electrophile	E	k_2^{HC} (M^{-1} s^{-1}) for $[3c]_{tot}$	$k_2^{HC,sw}$ (M^{-1} s^{-1}) for [3]	$k_2^{HC,mix}$ (M^{-1} s^{-1}) for [3]
8a	-10.04	2.70 x 10^5	3.41 x 10^5	3.38 x 10^5
8b	-9.45	6.68 x 10^5	8.42 x 10^5	8.32 x 10^5

8c	-8.76	2.45 x 10^6	3.21 x 10^6	3.17 x 10^6

N = 17.20 **s_N = 0.76** for $[\mathbf{3c}]_{tot}$

N = 17.33 **s_N = 0.76** for $[\mathbf{3}]^{HC,sw}$

N = 17.32 **s_N = 0.76** for $[\mathbf{3}]^{HC,mix}$

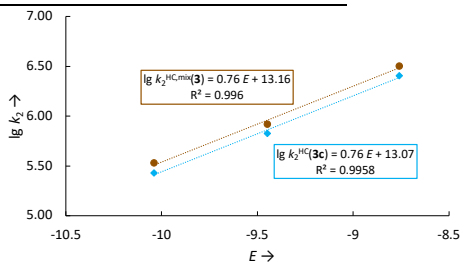

Kinetic data of ion pair 3d in DCM at 20 °C

Association constants for numerical simulations: K_{CAC}(**3d**) = 1.07 x 10^7 M^{-2}, K_{CAC}(**7d**) = 3.74 x 10^7 M^{-2}.

Reaction of **3d + 7d** with $(lil)_2CH^+BF_4^-$ (stopped-flow, λ = 640 nm)

[8a] (mol L^{-1})	$[3d]_{tot}$ (mol L^{-1})	[7d] (mol L^{-1})	$[3]^{HC,sw}$ (mol L^{-1})	$[3]^{HC,mix}$ (mol L^{-1})	k_{obs} (s^{-1})
	4.00 x 10^{-5}	9.51 x 10^{-4}	3.24 x 10^{-5}	–	12.0
	7.79 x 10^{-5}	9.21 x 10^{-4}	6.26 x 10^{-5}	–	25.0
4.03 x 10^{-6}	1.20 x 10^{-4}	8.77 x 10^{-4}	9.58 x 10^{-5}	–	36.6
	1.60 x 10^{-4}	8.32 x 10^{-4}	1.27 x 10^{-4}	–	45.8
	2.00 x 10^{-4}	8.02 x 10^{-4}	1.57 x 10^{-4}	–	57.6

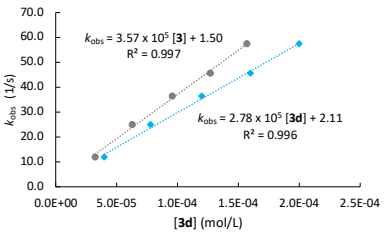

k_2^{HC} = 2.78 x 10^5 L mol^{-1} s^{-1} for $[\mathbf{3d}]_{tot}$

$k_2^{HC,sw}$ = 3.57 x 10^5 L mol^{-1} s^{-1} for $[\mathbf{3}]$

Reaction of **3d + 7d** with $(jul)_2CH^+BF_4^-$ (stopped-flow, λ = 643 nm)

[8b] (mol L^{-1})	$[3d]_{tot}$ (mol L^{-1})	[7d] (mol L^{-1})	$[3]^{HC,sw}$ (mol L^{-1})	$[3]^{HC,mix}$ (mol L^{-1})	k_{obs} (s^{-1})
	4.00 x 10^{-5}	9.51 x 10^{-4}	3.24 x 10^{-5}	–	24.8
	7.79 x 10^{-5}	9.21 x 10^{-4}	6.26 x 10^{-5}	–	50.0
4.02 x 10^{-6}	1.20 x 10^{-4}	8.77 x 10^{-4}	9.58 x 10^{-5}	–	76.7
	1.60 x 10^{-4}	8.32 x 10^{-4}	1.27 x 10^{-4}	–	108
	2.00 x 10^{-4}	8.02 x 10^{-4}	1.57 x 10^{-4}	–	138

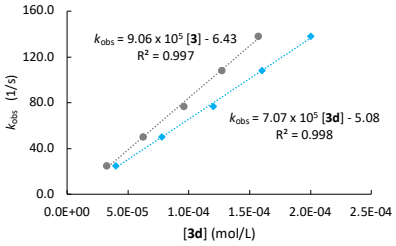

k_2^{HC} = 7.07 x 10^5 L mol^{-1} s^{-1} for $[\mathbf{3d}]_{tot}$

$k_2^{HC,sw}$ = 9.06 x 10^5 L mol^{-1} s^{-1} for $[\mathbf{3}]$

Reaction of **3d + 7d** with $(jul)_2CH^+BF_4^-$ (stopped-flow, λ = 643 nm)

[8c] (mol L^{-1})	$[3d]_{tot}$ (mol L^{-1})	[7d] (mol L^{-1})	$[3]^{HC,sw}$ (mol L^{-1})	$[3]^{HC,mix}$ (mol L^{-1})	k_{obs} (s^{-1})
	4.00 x 10^{-5}	9.51 x 10^{-4}	3.24 x 10^{-5}	–	80.2
	7.79 x 10^{-5}	9.21 x 10^{-4}	6.26 x 10^{-5}	–	191
4.14 x 10^{-6}	1.20 x 10^{-4}	8.77 x 10^{-4}	9.58 x 10^{-5}	–	282
	1.60 x 10^{-4}	8.32 x 10^{-4}	1.27 x 10^{-4}	–	400
	2.00 x 10^{-4}	8.02 x 10^{-4}	1.57 x 10^{-4}	–	517

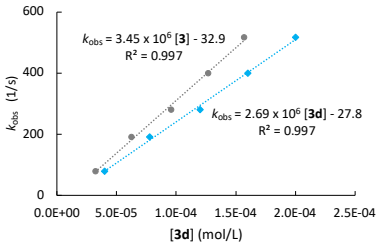

k_2^{HC} = 2.69 x 10^6 L mol^{-1} s^{-1} for $[\mathbf{3d}]_{tot}$

$k_2^{HC,sw}$ = 3.45 x 10^6 L mol^{-1} s^{-1} for $[\mathbf{3}]$

Determination of *N* and s_N parameter for **3d** in DCM

Electrophile	*E*	k_2^{HC} (M^{-1} s^{-1}) for [**3d**]$_{tot}$	$k_2^{HC,sw}$ (M^{-1} s^{-1}) for [**3**]	$k_2^{HC,mix}$ (M^{-1} s^{-1}) for [**3**]
8a	-10.04	2.78 x 10^5	3.57 x 10^5	–
8b	-9.45	7.07 x 10^5	9.06 x 10^5	–
8c	-8.76	2.69 x 10^6	3.45 x 10^6	–

***N* = 17.12** **s_N = 0.77** for [**3d**]$_{tot}$

***N* = 17.25** **s_N = 0.77** for [**3**]^{HC,sw}

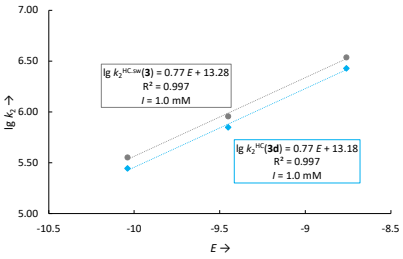

Kinetic data of ion pair 5a in DCM at 20 °C

Association constants for numerical simulations: K_{CAC}(**5a**) = 5.15 x 10^6 M^{-2}, K_{CAC}(**7a**) = 7.05 x 10^6 M^{-2},α x K_{CAC} = 5.67 x 10^5 M^{-2}, and β x K_{ACA} = 3.45 x 10^6 M^{-2}.

Reaction of **5a + 7a** with $(lil)_2CH^+BF_4^-$ (stopped-flow, λ = 640 nm)

[8a] (mol L^{-1})	[5a]$_{tot}$ (mol L^{-1})	[7a] (mol L^{-1})	[5]^{HC,sw} (mol L^{-1})	[5]^{HC,mix} (mol L^{-1})	k_{obs} (s^{-1})
	4.02 x 10^{-5}	9.59 x 10^{-4}	2.85 x 10^{-5}	3.60 x 10^{-5}	35.2
	6.02 x 10^{-5}	9.45 x 10^{-4}	4.25 x 10^{-5}	5.22 x 10^{-5}	55.3
4.00 x 10^{-6}	8.03 x 10^{-5}	9.18 x 10^{-4}	5.68 x 10^{-5}	6.77 x 10^{-5}	80.5
	1.00 x 10^{-4}	9.04 x 10^{-4}	7.07 x 10^{-5}	8.22 x 10^{-5}	113
	1.20 x 10^{-4}	8.76 x 10^{-4}	8.46 x 10^{-5}	9.61 x 10^{-5}	141

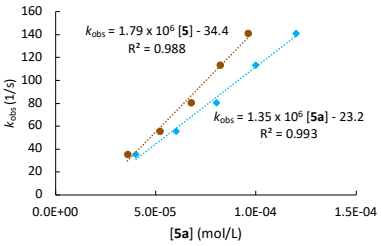

k_2^{HC} = 1.35 x 10^6 L mol^{-1} s^{-1} for [**5a**]$_{tot}$

$k_2^{HC,sw}$ = 1.92 x 10^6 L mol^{-1} s^{-1} for [**5**]

$k_2^{HC,mix}$ = 1.79 x 10^6 L mol^{-1} s^{-1} for [**5**]

Reaction of **5a + 7a** with $(jul)_2CH^+BF_4^-$ (stopped-flow, λ = 643 nm)

[8b] (mol L^{-1})	[5a]$_{tot}$ (mol L^{-1})	[7a] (mol L^{-1})	[5]^{HC,sw} (mol L^{-1})	[5]^{HC,mix} (mol L^{-1})	k_{obs} (s^{-1})
	4.02 x 10^{-5}	9.59 x 10^{-4}	2.85 x 10^{-5}	3.60 x 10^{-5}	74
	6.02 x 10^{-5}	9.45 x 10^{-4}	4.25 x 10^{-5}	5.22 x 10^{-5}	137
3.82 x 10^{-6}	8.03 x 10^{-5}	9.18 x 10^{-4}	5.68 x 10^{-5}	6.77 x 10^{-5}	196
	1.00 x 10^{-4}	9.04 x 10^{-4}	7.07 x 10^{-5}	8.22 x 10^{-5}	251
	1.20 x 10^{-4}	8.76 x 10^{-4}	8.46 x 10^{-5}	9.61 x 10^{-5}	317

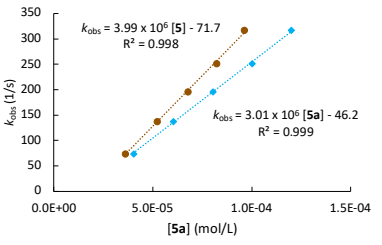

k_2^{HC} = 3.01 x 10^6 L mol^{-1} s^{-1} for [**5a**]$_{tot}$

$k_2^{HC,sw}$ = 4.27 x 10^6 L mol^{-1} s^{-1} for [**5**]

$k_2^{HC,mix}$ = 3.99 x 10^6 L mol^{-1} s^{-1} for [**5**]

Reaction of **5a + 7a** with $(jul)_2CH^+BF_4^-$ (stopped-flow, λ = 643 nm)

[8c] (mol L^{-1})	[5a]$_{tot}$ (mol L^{-1})	[7a] (mol L^{-1})	[5]^{HC,sw} (mol L^{-1})	[5]^{HC,mix} (mol L^{-1})	k_{obs} (s^{-1})
4.08 x 10^{-6}	4.02 x 10^{-5}	9.59 x 10^{-4}	2.85 x 10^{-5}	3.60 x 10^{-5}	270

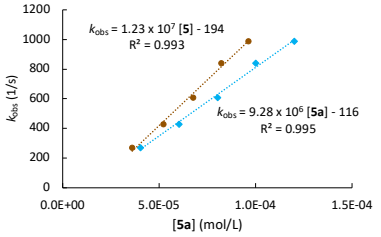

6.02 x 10^{-5}	9.45 x 10^{-4}	4.25 x 10^{-5}	5.22 x 10^{-5}	430
8.03 x 10^{-5}	9.18 x 10^{-4}	5.68 x 10^{-5}	6.77 x 10^{-5}	608
1.00 x 10^{-4}	9.04 x 10^{-4}	7.07 x 10^{-5}	8.22 x 10^{-5}	842
1.20 x 10^{-4}	8.76 x 10^{-4}	8.46 x 10^{-5}	9.61 x 10^{-5}	989

k_2^{HC} = 9.28 x 10^6 L mol^{-1} s^{-1} for **[5a]**$_{tot}$

$k_2^{HC,sw}$ = 1.32 x 10^7 L mol^{-1} s^{-1} for **[5]**

$k_2^{HC,mix}$ = 1.23 x 10^7 L mol^{-1} s^{-1} for **[5]**

Determination of *N* and s_N parameter for **5a** in DCM

Electrophile	*E*	k_2^{HC} (M^{-1} s^{-1}) for [5a]$_{tot}$	$k_2^{HC,sw}$ (M^{-1} s^{-1}) for [5]	$k_2^{HC,mix}$ (M^{-1} s^{-1}) for [5]
8a	-10.04	1.35 x 10^6	1.92 x 10^6	1.79 x 10^6
8b	-9.45	3.01 x 10^6	4.27 x 10^6	3.99 x 10^6
8c	-8.76	9.28 x 10^6	1.32 x 10^7	1.23 x 10^7

N = 19.24 **s_N = 0.66** for **[5a]**$_{tot}$

N = 19.47 **s_N = 0.66** for **[5]**^{HC,sw}

N = 19.42 **s_N = 0.66** for **[5]**^{HC,mix}

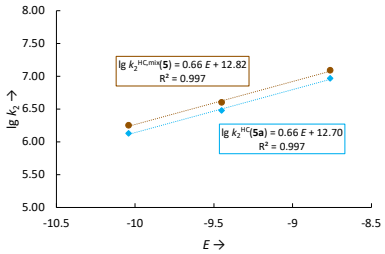

Kinetic data of ion pair 6a in DCM at 20 °C

Association constants for numerical simulations: K_{CAC}(**6a**) = 6.75 x 10^6 M^{-2}, K_{CAC}(**7a**) = 7.05 x 10^6 M^{-2},α x K_{CAC} = 1.08 x 10^6 M^{-2}, and β x K_{ACA} = 3.51 x 10^6 M^{-2}.

Reaction of **6a + 7a** with $(lil)_2CH^+BF_4^-$ (stopped-flow, λ = 640 nm)

[8a] (mol L^{-1})	[6a]$_{tot}$ (mol L^{-1})	[7a] (mol L^{-1})	[6]^{HC,sw} (mol L^{-1})	[6]^{HC,mix} (mol L^{-1})	k_{obs} (s^{-1})
	3.98 x 10^{-5}	9.59 x 10^{-4}	2.60 x 10^{-5}	3.44 x 10^{-5}	27.9
	5.97 x 10^{-5}	9.44 x 10^{-4}	3.90 x 10^{-5}	5.01 x 10^{-5}	44.4
3.82 x 10^{-6}	7.96 x 10^{-5}	9.16 x 10^{-4}	5.19 x 10^{-5}	6.50 x 10^{-5}	57.9
	9.95 x 10^{-5}	9.02 x 10^{-4}	6.48 x 10^{-5}	7.92 x 10^{-5}	75.5
	1.19 x 10^{-4}	8.74 x 10^{-4}	7.76 x 10^{-5}	9.25 x 10^{-5}	95.1

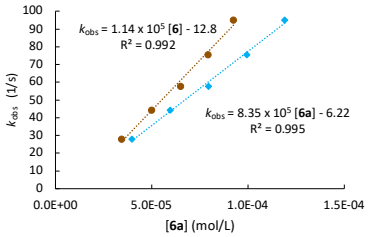

k_2^{HC} = 8.35 x 10^5 L mol^{-1} s^{-1} for **[6a]**$_{tot}$

$k_2^{HC,sw}$ = 1.28 x 10^6 L mol^{-1} s^{-1} for **[6]**

$k_2^{HC,mix}$ = 1.14 x 10^6 L mol^{-1} s^{-1} for **[6]**

Reaction of **6a + 7a** with $(jul)_2CH^+BF_4^-$ (stopped-flow, λ = 643 nm)

[8b] (mol L^{-1})	[6a]$_{tot}$ (mol L^{-1})	[7a] (mol L^{-1})	[6]^{HC,sw} (mol L^{-1})	[6]^{HC,mix} (mol L^{-1})	k_{obs} (s^{-1})
	3.98 x 10^{-5}	9.59 x 10^{-4}	2.60 x 10^{-5}	3.44 x 10^{-5}	58.3
	5.97 x 10^{-5}	9.44 x 10^{-4}	3.90 x 10^{-5}	5.01 x 10^{-5}	102
4.04 x 10^{-6}	7.96 x 10^{-5}	9.16 x 10^{-4}	5.19 x 10^{-5}	6.50 x 10^{-5}	153
	9.95 x 10^{-5}	9.02 x 10^{-4}	6.48 x 10^{-5}	7.92 x 10^{-5}	193
	1.19 x 10^{-4}	8.74 x 10^{-4}	7.76 x 10^{-5}	9.25 x 10^{-5}	237

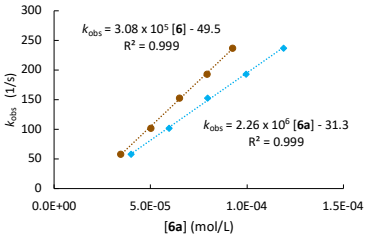

k_2^{HC} = 2.26 x 10^6 L mol^{-1} s^{-1} for **[6a]**$_{tot}$

$k_2^{HC,sw}$ = **3.48 x 10⁶ L mol⁻¹ s⁻¹** for [6]

$k_2^{HC,mix}$ = **3.08 x 10⁶ L mol⁻¹ s⁻¹** for [6

Reaction of **6a + 7a** with $(jul)_2CH^+BF_4^-$ (stopped-flow, λ = 643 nm)

[8c] (mol L⁻¹)	$[6a]_{tot}$ (mol L⁻¹)	[7a] (mol L⁻¹)	$[6]^{HC,sw}$ (mol L⁻¹)	$[6]^{HC,mix}$ (mol L⁻¹)	k_{obs} (s⁻¹)
	3.98 x 10⁻⁵	9.59 x 10⁻⁴	2.60 x 10⁻⁵	3.44 x 10⁻⁵	198
	5.97 x 10⁻⁵	9.44 x 10⁻⁴	3.90 x 10⁻⁵	5.01 x 10⁻⁵	350
4.02 x 10⁻⁶	7.96 x 10⁻⁵	9.16 x 10⁻⁴	5.19 x 10⁻⁵	6.50 x 10⁻⁵	514
	9.95 x 10⁻⁵	9.02 x 10⁻⁴	6.48 x 10⁻⁵	7.92 x 10⁻⁵	626
	1.19 x 10⁻⁴	8.74 x 10⁻⁴	7.76 x 10⁻⁵	9.25 x 10⁻⁵	748

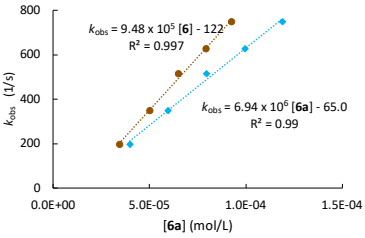

k_2^{HC} = **6.94 x 10⁶ L mol⁻¹ s⁻¹** for $[6a]_{tot}$

$k_2^{HC,sw}$ = **1.07 x 10⁷ L mol⁻¹ s⁻¹** for [6]

$k_2^{HC,mix}$ = **9.48 x 10⁶ L mol⁻¹ s⁻¹** for [6]

Determination of *N* and s_N parameter for **6a** in DCM

Electrophile	*E*	k_2^{HC} (M⁻¹ s⁻¹) for $[6a]_{tot}$	$k_2^{HC,sw}$ (M⁻¹ s⁻¹) for [6]	$k_2^{HC,mix}$ (M⁻¹ s⁻¹) for [6]
8a	-10.04	8.35 x 10⁵	1.28 x 10⁶	1.14 x 10⁶
8b	-9.45	2.26 x 10⁶	3.48 x 10⁶	3.08 x 10⁶
8c	-8.76	6.94 x 10⁶	1.07 x 10⁷	9.48 x 10⁶

***N* = 18.25** **s_N = 0.72** for $[6a]_{tot}$

***N* = 18.53** **s_N = 0.72** for $[6]^{HC,sw}$

***N* = 18.43** **s_N = 0.72** for $[6]^{HC,mix}$

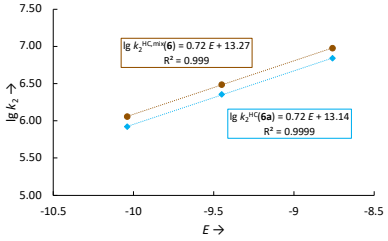

3.1.5.5 Effects of Ion Association on Nucleophilicity Measurements

The so-called wide range measurements employ the same principle as the benzhydrylium kinetics except for covering a much larger concentration range (1 x 10^{-5} to 4 x 10^{-3}). The aim of these measurement to illustrate the influence of ion pair formation with increasing concentration on the first-order reaction rate k_{obs} (s^{-1}) and obtained second order rate constants k_2 (M^{-1} s^{-1}) are generally not included in the N and s_N parameter determination. The benzhydrylium salt $(lil)_2CH^+BF_4^-$ (**8a**) was used as electrophile at λ = 640 nm.

Measurement of 3b at 20°C

Reaction of **3b** with $(lil)_2CH^+BF_4^-$ in DCM (stopped-flow, λ = 640 nm)

[8a] (mol L^{-1})	[3b] (mol L^{-1})	k_{obs} (s^{-1})
1.23 x 10^{-6}	1.00 x 10^{-5}	11.0
	2.00 x 10^{-5}	34.5
	4.01 x 10^{-5}	64.5
	6.21 x 10^{-5}	92.7
	8.01 x 10^{-5}	112
	1.00 x 10^{-4}	133
	2.00 x 10^{-4}	212
	4.01 x 10^{-4}	303
	6.01 x 10^{-4}	356
	8.01 x 10^{-4}	380
	1.00 x 10^{-3}	417
	2.00 x 10^{-3}	460
	4.01 x 10^{-3}	541

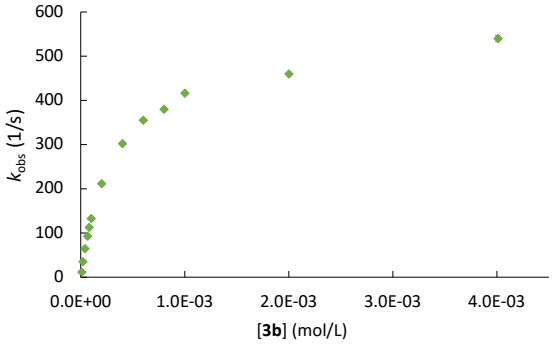

Measurement of 3c at 20°C

Reaction of **3c** with $(lil)_2CH^+BF_4^-$ in DCM (stopped-flow, λ = 640 nm)

[8a] (mol L^{-1})	[3c] (mol L^{-1})	k_{obs} (s^{-1})
1.06 x 10^{-6}	1.00 x 10^{-5}	15.0
	2.00 x 10^{-5}	28.9
	4.01 x 10^{-5}	52.1
	6.01 x 10^{-5}	71.9
	8.02 x 10^{-5}	88.1
	1.00 x 10^{-4}	100
	2.00 x 10^{-4}	142
	4.01 x 10^{-4}	196
	6.01 x 10^{-4}	238
	8.02 x 10^{-4}	266
	1.00 x 10^{-3}	294
	2.00 x 10^{-3}	367
	4.01 x 10^{-3}	469

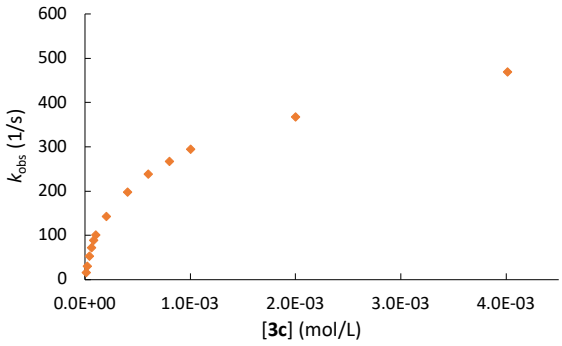

Measurement of 3d at 20°C

Reaction of **3d** with $(lil)_2CH^+BF_4^-$ in DCM (stopped-flow, λ = 640 nm)

[8a] (mol L^{-1})	[3d] (mol L^{-1})	k_{obs} (s^{-1})
1.03 x 10^{-6}	9.98 x 10^{-6}	14.0
	2.00 x 10^{-5}	31.1
	3.99 x 10^{-5}	50.3
	5.99 x 10^{-5}	72.6
	7.99 x 10^{-5}	86.1
	9.98 x 10^{-5}	98.2
	2.00 x 10^{-4}	149
	3.99 x 10^{-4}	188
	5.99 x 10^{-4}	242
	7.99 x 10^{-4}	269
	9.98 x 10^{-4}	294
	2.00 x 10^{-3}	379
	3.99 x 10^{-3}	475

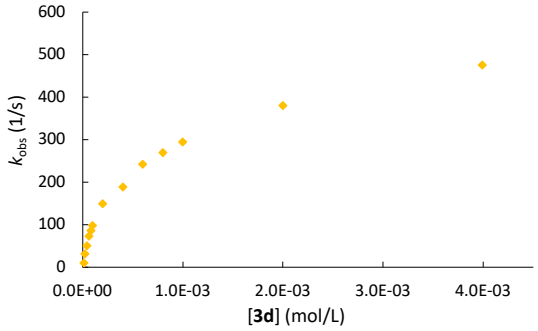

Reaction of **3d** with $(lil)_2CH^+BF_4^-$ in MeCN (stopped-flow, λ = 632 nm)

[8a] (mol L^{-1})	[3d] (mol L^{-1})	k_{obs} (s^{-1})
1.26 x 10^{-6}	9.91 x 10^{-6}	0.31
	1.98 x 10^{-5}	0.40
	3.96 x 10^{-5}	0.50
	5.94 x 10^{-5}	0.65
	7.92 x 10^{-5}	0.78
	9.91 x 10^{-5}	0.92
	1.98 x 10^{-4}	1.43
	3.96 x 10^{-4}	2.43
	5.94 x 10^{-4}	3.51
	7.92 x 10^{-4}	4.48
	9.91 x 10^{-4}	5.63
	1.98 x 10^{-3}	10.4
	3.96 x 10^{-3}	25.5

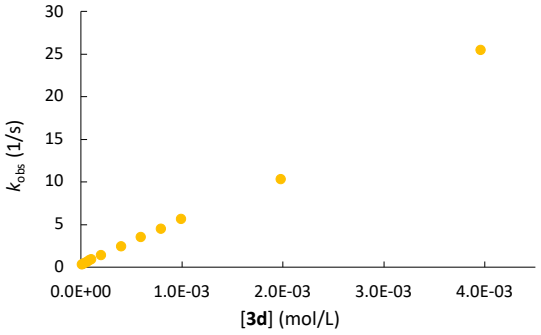

Measurement of 5a at 20°C

Reaction of **5a** with $(lil)_2CH^+BF_4^-$ in DCM (stopped-flow, λ = 640 nm)

[8a] (mol L^{-1})	[5a] (mol L^{-1})	k_{obs} (s^{-1})
9.74 x 10^{-7}	9.96 x 10^{-6}	49.5
	1.99 x 10^{-5}	205
	3.98 x 10^{-5}	354
	5.98 x 10^{-5}	502
	7.97 x 10^{-5}	672
	9.96 x 10^{-5}	828

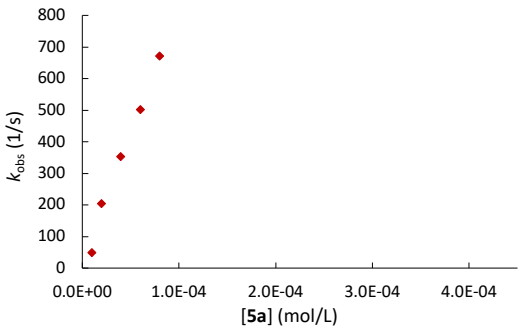

Measurement of 6a at 20°C

Reaction of **6a** with $(lil)_2CH^+BF_4^-$ in DCM (stopped-flow, λ = 640 nm)

[8a] (mol L^{-1})	[6a] (mol L^{-1})	k_{obs} (s^{-1})
1.04 x 10^{-6}	9.72 x 10^{-6}	20.7
	1.94 x 10^{-5}	71.6
	3.89 x 10^{-5}	173
	5.83 x 10^{-5}	228
	7.77 x 10^{-5}	291
	9.72 x 10^{-5}	358
	1.99 x 10^{-4}	535
	3.98 x 10^{-4}	680

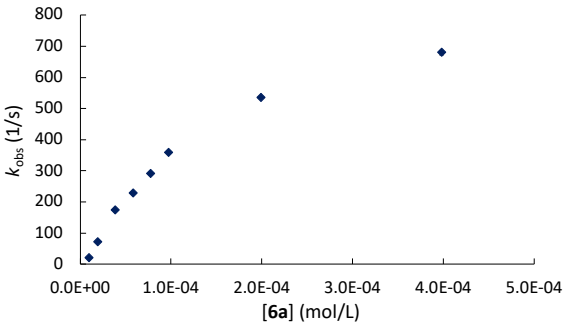

3.1.6 pK_a Measurements

3.1.6.1 General information – pK_a measurements in aqueous solutions

The neutral pyridinamides as well as the respective ion pairs were stored under nitrogen atmosphere. Hygroscopic salts were dried *in vacuo* for 12 h prior to being used in the buffer preparation. Pure water was used for the preparation of buffer solutions and stock solutions. For pipetting the buffer and stock solutions *Eppendorf* pipettes were used. All calibration solutions and the baseline solutions were tempered at 25 °C using a circulating water bath.

UV-Vis Spectra were recorded on a Varian Cary 100 Bio Spectrophotometer (version 9.00) maintained at 25 °C using the "scan software" (version 3.00(182)) and the "kinetics software" (version 3.00(182)). The scan software was used to record the full UV-Vis spectrum of the respective compound between 200 - 400 nm, while the kinetics software was used to validate the stability of the compound at a fixed wavelength, whereas the absorbance was measured every 0.1 min for 1.0 min. Before starting the measurement, the respective wavelength was selected, and the instrument was "zeroed" to air. The baseline function of the program was not used. Instead, a baseline spectrum would be measured for each data point where the solution had the same composition as the actual measurement but without the compound in it. The baseline spectrum was then subtracted from the measurement spectrum using Excel. The p*H* value of each baseline mixture was determined using a Radiometer Analytical RadioLab p*H* 210 standard p*H* meter connected to a radiometer electrode filled with saturated KCl solution. The electrode was stored in 3.0 M KCl solution in between measurements. Calibration of the setup was done at intervals of p*H* = 1.4 – 4.0, 4.0 – 7.0, and 7.0 – 10.0 shortly before measuring the respective baseline mixtures, which were tempered to 25 °C using a circulating water bath for at least 30 min prior to measuring.

For the aqueous pK_a measurements the neutral pyridinamides were dissolved in premixed MeCN/pure water mixtures (ratio = 50/50 of volume) and added to aqueous buffer solutions (c = 0.05 M or 0.1 M, I = 0.3 M) to give measurement solutions with a compound concentration of c = 0.05 mM. The absorbance of the neutral pyridinamide or respective anion was measured across the p*H* range and the resulting absorbance-p*H* plots were fitted using Origin. To obtain the necessary equation for the fitting, equations 3.11-3.15 are used, with eq. 3.12-3.14 being inserted into eq. 3.11 to give eq. 3.15 with K_a being the acid dissociation constant for the compound, p*H* is the one of the used buffers, A_{obs} being the observed absorbance, A_{max} the maximum absorbance (where the compound is either protonated or deprotonated) and A_{min} is the minimum absorbance (where the compound is either fully protonated or fully deprotonated).

When the chosen wavelength is following the neutral pyridinamide, e.g. 285 nm for pyridinamide **5**, the absorbance is increasing with the p*H* (p*H* < 6), thus A_{max} reflects the neutral pyridinamide (one proton at the pyridine nitrogen) and A_{min} the fully protonated pyridinamide form, which is depicted in eq. 3.13 and eq. 3.14.

$$K_a = \frac{[H^+][A^-]}{[HA]} \tag{3.11}$$

$$[H^+] = 10^{-pH} \tag{3.12}$$

$$[A^-] = A_{obs} - A_{min} \tag{3.13}$$

$$[HA] = A_{max} - A_{obs} \tag{3.14}$$

$$K_a = \frac{10^{-pH}(A_{obs} - A_{min})}{(A_{max} - A_{obs})} \quad (3.15)$$

Increase in absorbance: $$A_{obs} = \frac{10^{-pH} \times A_{min} + K_a \times A_{max}}{10^{-pH} \times K_a} \quad (3.16)$$

When further increasing p*H* (p*H* > 6) the absorbance of the neutral pyridinamide decreases due to deprotonation of the neutral pyridinamide towards the fully deprotonated anion. Here, A_{max} reflects the neutral pyridinamide and A_{min} the fully deprotonated anion. Therefore, eq. 3.13 and 3.14 are rewritten into eq. 3.17 and eq. 3.18. Inserting those equations into eq. 3.11 and solving it for A_{obs} results in eq. 3.19 with which the decrease in absorbance can be fitted in Origin to obtain K_a. In Origin A_{max} and A_{min} are treated as variables.

$$[A^-] = A_{max} - A_{obs} \quad (3.17)$$

$$[HA] = A_{obs} - A_{min} \quad (3.18)$$

Decrease in absorbance: $$A_{obs} = \frac{10^{-pH} \times A_{max} + K_a \times A_{min}}{K_a + 10^{-pH}} \quad (3.19)$$

Taking the logarithm of K_a (see eq. 3.20) gives the final value for pK_a.

$$pK_a = -\log_{10} K_a \quad (3.20)$$

Preparation of buffer solutions

The buffer solutions are prepared according to the Henderson-Hasselbalch equation (see eq. 3.21). Several acid-base pairs with variating amounts of free base were chosen to obtain the wanted p*H* value in the final buffer solution (see Table 3.10).

$$pH = pK_a + \log\frac{A^-}{HA} \quad (3.21)$$

The ionic strength *I* of the buffer solution is calculated according to eq. 3.22 with c_i being the concentration of ions in solution and z_i^2 the charge of ions squared.

$$I = \frac{1}{2}\sum c_i z_i^2 \quad (3.22)$$

For comparable results, all buffer solutions must have to the same ionic strength *I* independent of the concentration and composition regarding the acid and base of the final buffer solutions.

All prepared buffer solutions for the aqueous p*H*-titration with their acid-base pairs, amount of free base (fb) and measured p*H* value are listed below. All buffer solutions are prepared to have a concentration of 0.1 M and an ionic strength *I* of 0.3 M which is achieved by addition of potassium chloride (KCl).

Table 3.10: [Table S15]. List of prepared aqueous buffer solution with the involved acid and bases, the pK_a value of the respective acid, the amount of free base (fb) in percentage, the final buffer concentration, and the resulting p*H*

No.	Buffer System	Acid	Base	pK_a of acid	%fb	Concentration (M)	p*H*
1	HCl	HCl	–	–	–	0.1	1.08
2	HCl	HCl	–	–	–	0.03	1.60
3	HCl	HCl	–	–	–	0.01	2.10
4	Formate	HCl	$KCHCO_2$	3.75	10	0.1	2.51
5		HCl	$KCHCO_2$		50	0.1	3.55
6	Acetate	HCl	$KMeCO_2$	4.76	30	0.1	4.17
7		HCl	$KMeCO_2$		70	0.1	4.94
8	Phosphate	KH_2PO_4	K_2HPO_4	6.86	10	0.1	5.68

9		KH_2PO_4	K_2HPO_4		50	0.1	6.72
10	Triethanolamine-HCl	TEOA-HCl	KOH	7.76	10	0.1	6.94
11		TEOA-HCl	KOH		20	0.05	7.37
12		TEOA-HCl	KOH		30	0.1	7.55
13		TEOA-HCl	KOH		40	0.05	7.81
14		TEOA-HCl	KOH		50	0.1	7.95
15		TEOA-HCl	KOH		70	0.05/0.1	8.37
16		TEOA-HCl	KOH		80	0.05	8.62
17		TEOA-HCl	KOH		90	0.1	8.96
18	Carbonate	$KHCO_3$	K_2CO_3	10.30	10	0.1	9.04
19		$KHCO_3$	K_2CO_3		25	0.1	9.46
20		$KHCO_3$	K_2CO_3		50	0.1	9.97
21	Piperidine-HCl	PIP-HCl	KOH	11.20	20	0.1	10.71
22		PIP-HCl	KOH		60	0.1	11.47

DMAP – aqueous pK_a

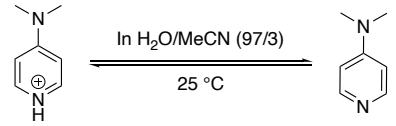

DMAP-H **DMAP**

VB24. Stock solution A with 3.04 mg DMAP (**1**) in 25 mL H_2O/MeCN mix (1:1), diluted to c = 0.05 mM, measured at λ_{max} = 280 nm.

Buffer	%fb	pH_{buffer}	p$H_{baseline}$	Abs (280nm)
Phosphate	50	6.72	6.75	0.87
TEOA	20	7.37	7.35	0.85
	40	7.81	7.79	0.89
	70	8.37	8.35	0.85
	80	8.62	8.59	0.87
Carbonate	10	9.04	9.09	0.79
	25	9.49	9.53	0.67
	50	9.97	10.03	0.51
PIP	20	10.71	10.71	0.34
	60	11.47	11.48	0.28

$K_a = 1.42 \times 10^{-10}$ → pK_a = 9.85, Lit: pK_a = 9.66[13]

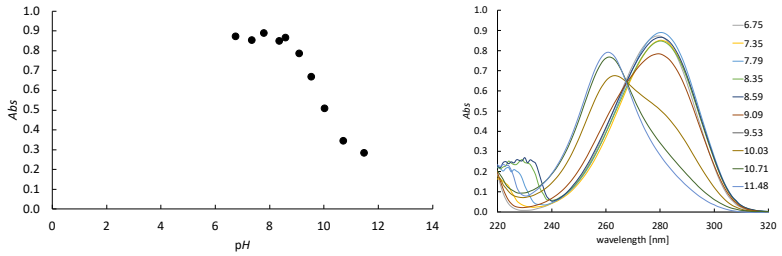

Pyridinamide 3 – aqueous pK_a

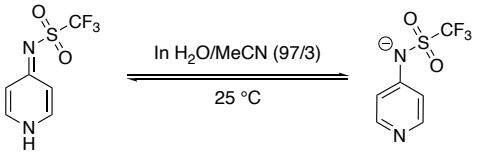

PA_3 **an3**

VB09. Stock solution A with 2.30 mg PA_**3** in 10 mL H_2O/MeCN mix (1:1), diluted to c = 0.05 mM, measured at λ_{max} = 272 nm. Not included in pK_a determination.

Buffer	%fb	pH_{buffer}	p$H_{baseline}$	Abs (272nm)
HCl	–	2.1	2.14	1.33

Formate	10	2.51	2.55	1.33
	50	3.55	3.59	1.30
Acetate	30	4.17	4.23	1.30
	70	4.94	5.00	1.24
Phosphate	10	5.68	5.74	1.31
TEOA-HCl	10	6.94	6.98	1.11
	30	7.55	7.58	0.70
	50	7.95	7.97	0.44
	70	8.36	8.36	0.25
	90	8.96	8.96	0.09
Carbonate	10	9.02	9.13	0.07
	25	9.45	9.54	0.04
	50	9.93	9.99	0.03
PIP-HCl	20	10.74	10.71	0.03
	60	11.50	11.47	0.04

$K_a = 2.24 \times 10^{-8}$ → $pK_a = 7.65$

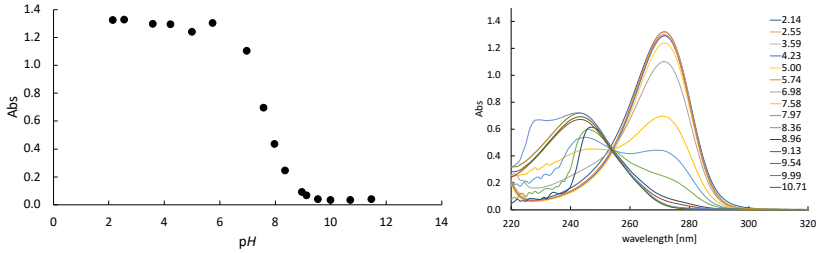

VB13. Stock solution A with 2.25 mg PA_**3** in 10 mL H_2O/MeCN mix (1:1), diluted to *c* = 0.05 mM, measured at λ_{max} = 272 nm.

Buffer	**%fb**	**p*H*$_{buffer}$**	**p*H*$_{baseline}$**	**Abs (272nm)**
Acetate	30	4.17	4.19	1.72
Phosphate	10	5.68	5.72	1.71
TEOA-HCl	10	6.94	6.96	1.42
	30	7.55	7.55	0.95
	50	7.95	7.93	0.61
	70	8.36	8.33	0.34
	90	8.96	8.91	0.13
Carbonate	10	9.02	9.1	0.11
	25	9.45	9.49	0.07
	50	9.93	9.95	0.05

$K_a = 2.38 \times 10^{-8}$ → $pK_a = 7.62$

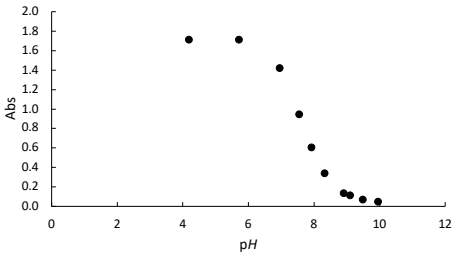

VB16. Stock solution A with 2.26 mg PA_**3** in 10 mL H_2O/MeCN mix (1:1), diluted to *c* = 0.05 mM, measured at λ_{max} = 272 nm.

Buffer	**%fb**	**p*H*$_{buffer}$**	**p*H*$_{baseline}$**	**Abs (272nm)**
HCl	–	1.09	1.12	1.09
HCl	–	1.6	1.64	1.10
HCl	–	2.1	2.12	1.09
Formate	10	2.51	2.52	1.13
	50	3.55	3.59	1.12
Acetat	30	4.17	4.24	1.11
	70	4.94	4.99	1.13
Phosphate	10	5.68	5.75	1.09

TEOA-HCl	10	6.94	6.95	0.98
	30	7.55	7.55	0.53
	50	7.95	7.93	0.38
	70	8.36	8.33	0.22
	90	8.96	8.89	0.13
Carbonate	10	9.02	9.12	0.06
	25	9.45	9.53	0.04
	50	9.93	9.98	0.02
PIP-HCl	20	10.74	10.72	0.03
	60	11.50	11.50	0.03

$K_a = 2.60 \times 10^{-8}$ → $pK_a = 7.59$

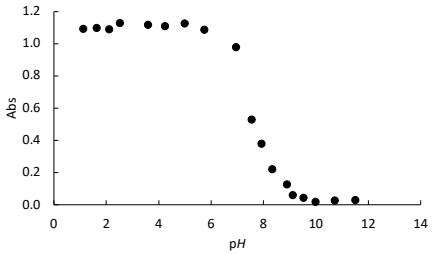

Pyridinamide 3 – aqueous pK_a with I = 0.15 M

Stock solutions were prepared according to procedure for pK_a measurements in 1:1 water/MeCN mixtures to verify that the change in overall ionic strength I by dilutions has no significant influence on the pK_a value.

VB35. Stock solution A with 2.31 mg PA_**3** in 10 mL H_2O/MeCN mix (1:1), diluted to c = 0.05 mM, measured at λ_{max} = 272 nm.

Buffer	**%fb**	**pH_{buffer}**	**p$H_{baseline}$**	**Abs (272nm)**
Acetat	30	4.17	4.23	1.23
	70	4.94	5.01	1.23
Phosphate	10	5.68	5.96	1.20
	50	6.72	6.87	1.07
TEOA	20	7.37	7.30	0.87
	40	7.81	7.75	0.60
	70	8.37	8.29	0.31
	80	8.62	8.53	0.24
Carbonate	10	9.04	9.25	0.13
	25	9.46	9.65	0.11
	50	9.97	10.12	0.11
PIP	20	10.71	10.59	0.11

$K_a = 2.29 \times 10^{-8}$ → $pK_a = 7.64$

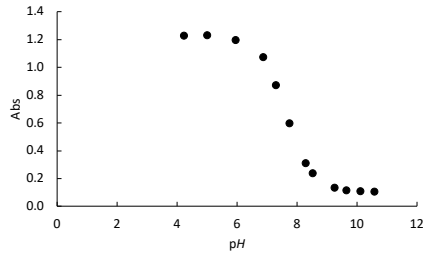

Pyridinamide 5 – aqueous pK_a

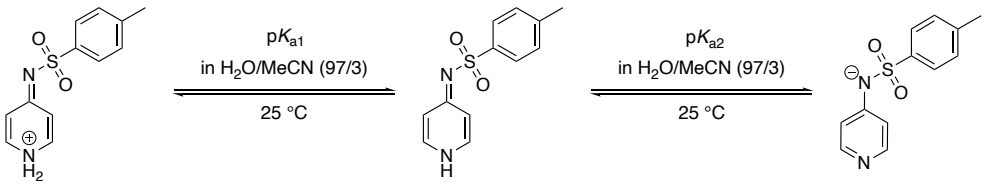

PAH_5 **PA_5** **an5**

VB12. Stock solution A with 2.48 mg PA_**5** in 10 mL H_2O/MeCN mix (1:1), diluted to *c* = 0.05 mM, measured at λ_{max} = 285 nm.

Buffer	%fb	pH_{buffer}	p$H_{baseline}$	Abs (285nm)	pKa_1	pKa_2
HCl	–	1.09	1.12	0.05	X	
HCl	–	1.6	1.64	0.07	X	
HCl	–	2.1	2.14	0.16	X	
Formate	10	2.51	2.55	0.21	X	
	50	3.55	3.59	0.79	X	
Acetat	30	4.17	4.24	1.20	X	
	70	4.94	5.00	1.33	X	
Phosphate	10	5.68	5.75	1.33	X	X
TEOA	10	6.94	6.96	1.35		X
	30	7.55	7.56	1.28		X
	50	7.95	7.93	1.22		X
	70	8.36	8.34	1.04		X
	90	8.96	8.91	0.68		X
Carbonate	10	9.02	9.2	0.52		X
	25	9.45	9.51	0.36		X
	50	9.93	9.98	0.23		X
PIP	20	10.74	10.71	0.16		X
	60	11.5	11.47	0.16		X

$K_{a1} = 3.72 \times 10^{-4}$ → pK_{a1} = 3.43

$K_{a2} = 1.51 \times 10^{-9}$ → pK_{a2} = 8.82

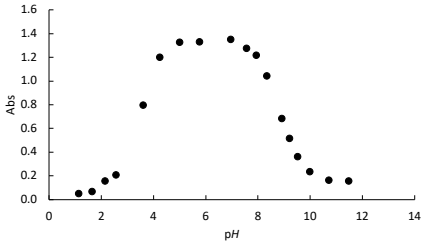

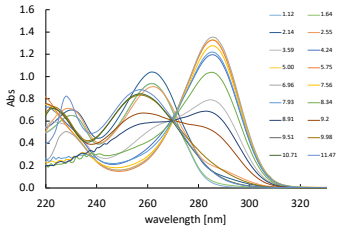

VB17. Stock solution A with 2.50 mg PA_**5** in 10 mL H_2O/MeCN mix (1:1), diluted to *c* = 0.05 mM, measured at λ_{max} = 285 nm.

Buffer	%fb	pH_{buffer}	p$H_{baseline}$	Abs (285nm)	pKa_1	pKa_2
HCl	–	1.09	1.12	0.05	X	
HCl	–	1.6	1.64	0.07	X	
HCl	–	2.1	2.12	0.13	X	
Formate	10	2.51	2.52	0.21	X	
	50	3.55	3.59	0.85	X	
Acetat	30	4.17	4.24	1.24	X	
	70	4.94	4.99	1.37	X	
Phosphate	10	5.68	5.75	1.43	X	X
TEOA	10	6.94	6.95	1.41		X
	30	7.55	7.55	1.30		X
	50	7.95	7.93	1.26		X
	70	8.36	8.33	1.11		X
	90	8.96	8.89	0.75		X

Carbonate	10	9.02	9.12	0.56	X
	25	9.45	9.53	0.36	X
	50	9.93	9.98	0.23	X
PIP	20	10.74	10.72	0.16	X
	60	11.50	11.50	0.15	X

K_{a1} = 3.63 x 10^{-4} → pK_{a1} = 3.44

K_{a2} = 1.48 x 10^{-9} → pK_{a2} = 8.83

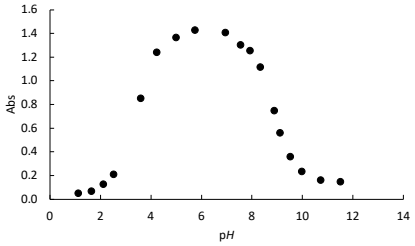

Pyridinamide ion pair 5a – aqueous pK_a

Stock solution prepared using pyridinamide ion pair **5a** rather than pyridinamide **5** to examine the potential influence of the counter-cation **a** on the measurement. The measurement was performed following two wavelengths: at 285 nm for the pyridinamide and at 258 nm for the pyridinamide anion **5**.

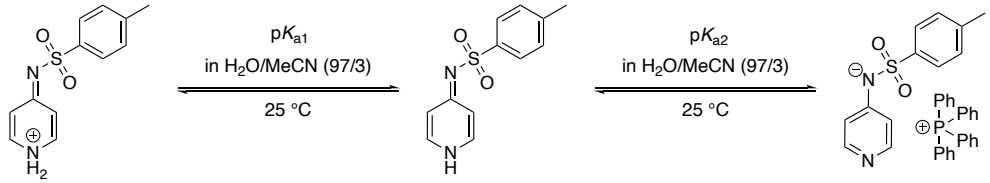

PAH_5 **PA_5** **5a**

VB25. Stock solution A with 5.89 mg **5a** in 10 mL H_2O/MeCN mix (1:1), diluted to *c* = 0.05 mM, measured at λ_{max}(PA_**5**) = 285 nm and λ_{max}(**5a**) = 258 nm.

Buffer	**%fb**	**pH_{buffer}**	**p$H_{baseline}$**	**Abs (258nm)**	**Abs (285nm)**	**pKa_1**	**pKa_2**
HCl	0.1	1.09	1.11	1.41	0.18	X	
HCl	0.03	1.60	1.62	1.42	0.19	X	
HCl	0.01	2.10	2.10	–	0.24	X	
Formate	10	2.51	2.51	1.31	0.34	X	
	50	3.55	3.59	0.83	1.15	X	
Acetat	30	4.17	4.21	0.58	1.57	X	
	70	4.94	5.00	0.51	1.78	X	
Phosphate	10	5.68	5.86	0.47	1.78	X	X
	50	6.72	6.75	0.48	1.78		X
TEOA	20	7.37	7.35	0.49	1.72		X
	40	7.81	7.81	0.54	1.64		X
	70	8.37	8.37	0.68	1.39		X
	80	8.62	8.62	0.77	1.20		X
Carbonate	10	9.04	9.13	1.00	0.78		X
	25	9.46	9.57	1.15	0.51		X
	50	9.97	10.05	1.26	0.37		X
PIP	20	10.71	10.72	1.28	0.29		X
	60	11.47	11.51	1.30	0.27		X

258 nm: K_{a1} = 4.36 x 10^{-4} → pK_{a1} = 3.36; K_{a2} = 1.35 x 10^{-9} → pK_{a2} = 8.87

285 nm: K_{a1} = 3.85 x 10^{-4} → pK_{a1} = 3.41; K_{a2} = 1.48 x 10^{-9} → pK_{a2} = 8.83

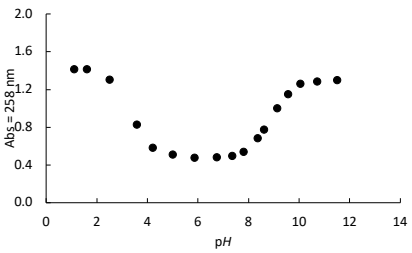

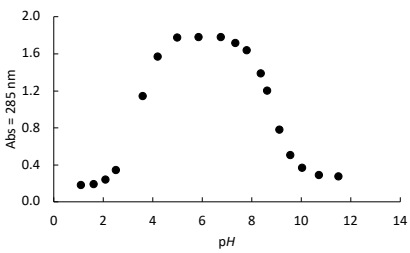

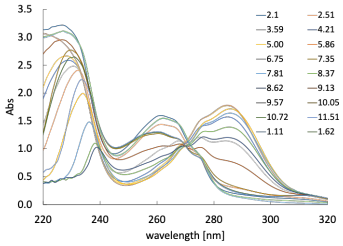

Pyridinamide 4 – aqueous pK_a

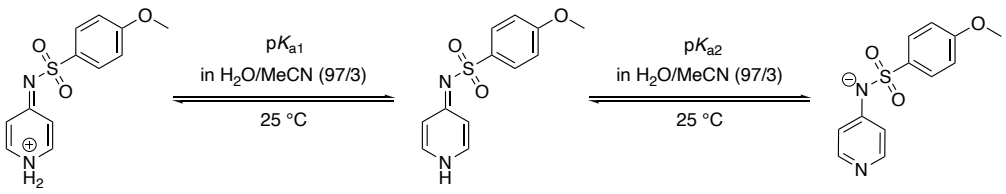

PAH_4 **PA_4** **an4**

VB10. Stock solution A with 2.65 mg PA_**4** in 10 mL H_2O/MeCN mix (1:1), diluted to *c* = 0.05 mM, measured at λ_{max} = 286 nm.

Buffer	%fb	pH_{buffer}	p$H_{baseline}$	Abs (286nm)	pKa_1	pKa_2
HCl	–	1.09	1.12	0.33	X	
HCl	–	1.6	1.64	0.34	X	
HCl	–	2.1	2.14	0.42	X	
Formate	10	2.51	2.55	0.47	X	
	50	3.55	3.59	1.10	X	
Acetat	30	4.17	4.23	1.46	X	
	70	4.94	5.00	1.72	X	
Phosphate	10	5.68	5.75	1.75	X	
TEOA	10	6.94	6.96	1.73		X
	30	7.55	7.57	1.67		X
	50	7.95	7.95	1.57		X
	70	8.36	8.35	1.46		X
	90	8.96	8.93	0.90		X
Carbonate	10	9.02	9.16	0.71		X
	25	9.45	9.51	0.48		X
	50	9.93	9.97	0.32		X
PIP	20	10.74	10.71	0.22		X
	60	11.5	11.47	0.21		X

K_{a1} = 2.84 x 10^{-4} → pK_{a1} = 3.55

K_{a2} = 1.35 x 10^{-9} → pK_{a2} = 8.87

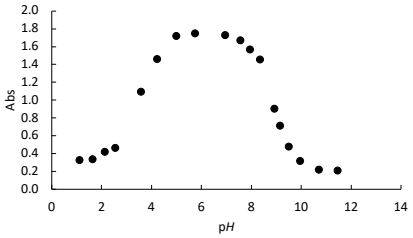

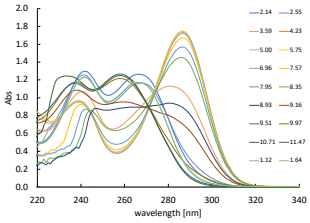

VB18. Stock solution A with 2.62 mg PA_**4** in 10 mL H_2O/MeCN mix (1:1), diluted to *c* = 0.05 mM, measured at λ_{max} = 285 nm.

Buffer	%fb	pH_{buffer}	p$H_{baseline}$	Abs (285nm)	pKa_1	pKa_2
HCl	–	1.09	1.12	0.26	X	
HCl	–	1.6	1.64	0.27	X	
HCl	–	2.1	2.12	0.31	X	
Formate	10	2.51	2.52	0.36	X	
	50	3.55	3.59	0.78	X	

Acetat	30	4.17	4.24	1.08	X	
	70	4.94	4.99	1.24	X	
Phosphate	10	5.68	5.75	1.28	X	X
TEOA	10	6.94	6.95	1.25		X
	30	7.55	7.55	1.15		X
	50	7.95	7.93	1.12		X
	70	8.36	8.33	0.95		X
	90	8.96	8.89	0.68		X
Carbonate	10	9.02	9.12	0.53		X
	25	9.45	9.53	0.35		X
	50	9.97	10.03	0.22		X
PIP	20	10.74	10.72	0.17		X
	60	11.50	11.50	0.17		X

K_{a1} = 2.60 x 10^{-4} → pK_{a1} = 3.59

K_{a2} = 1.48 x 10^{-9} → pK_{a2} = 8.83

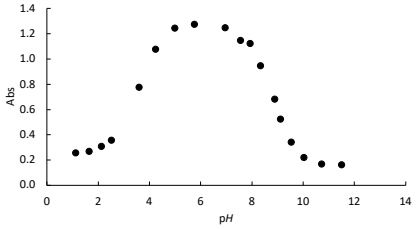

Pyridinamide 6 – aqueous pK_a

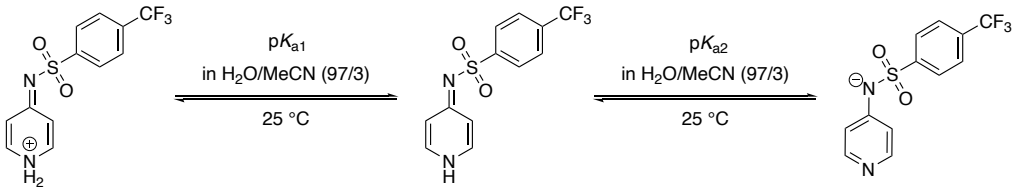

PAH_6 **PA_6** **an6**

VB11. Stock solution A with 3.03 mg PA_**6** in 10 mL H_2O/MeCN mix (1:1), diluted to *c* = 0.05 mM, measured at λ_{max} = 284 nm.

Buffer	%fb	pH_{buffer}	p$H_{baseline}$	Abs (284nm)	pKa_1	pKa_2
HCl	–	1.09	1.12	0.07	X	
HCl	–	1.6	1.64	0.15	X	
HCl	–	2.1	2.14	0.37	X	
Formate	10	2.51	2.55	0.62	X	
	50	3.55	3.59	1.34	X	
Acetat	30	4.17	4.17	1.44	X	
	70	4.94	5.00	1.49	X	
Phosphate	10	5.68	5.76	1.53	X	X
TEOA	10	6.94	6.95	1.46		X
	30	7.55	7.56	1.52		X
	50	7.95	7.94	1.30		X
	70	8.36	8.35	1.06		X
	90	8.96	8.96	0.66		X
Carbonate	10	9.02	9.19	0.52		X
	25	9.45	9.54	0.38		X
	50	9.93	9.98	0.29		X
PIP	20	10.74	10.71	0.23		X
	60	11.50	11.47	0.23		X

K_{a1} = 2.91 x 10^{-3} → pK_{a1} = 2.72

K_{a2} = 2.31 x 10^{-9} → pK_{a2} = 8.64

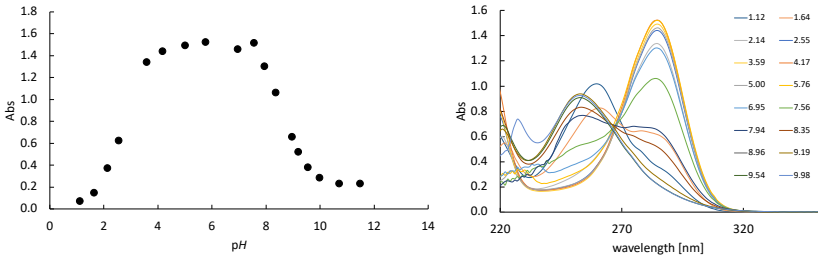

VB19. Stock solution A with 3.01 mg PA_**6** in 10 mL H_2O/MeCN mix (1:1), diluted to *c* = 0.05 mM, measured at λ_{max} = 285 nm.

Buffer	%fb	pH_{buffer}	p$H_{baseline}$	Abs (285nm)	pKa_1	pKa_2
HCl	–	1.09	1.12	0.04	X	
HCl	–	1.6	1.64	0.11	X	
HCl	–	2.1	2.12	0.27	X	
Formate	10	2.51	2.52	0.54	X	
	50	3.55	3.59	1.10	X	
Acetat	30	4.17	4.24	1.22	X	
	70	4.94	4.99	1.21	X	
Phosphate	10	5.68	5.75	1.26	X	X
TEOA	10	6.94	6.95	1.20		X
	30	7.55	7.55	1.10		X
	50	7.95	7.93	1.03		X
	70	8.36	8.33	0.84		X
	90	8.96	8.89	0.65		X
Carbonate	10	9.02	9.12	0.40		X
	25	9.45	9.53	0.28		X
	50	9.97	10.03	0.21		X
PIP	20	10.74	10.72	0.19		X
	60	11.50	11.50	0.18		X

$K_{a1} = 2.24 \times 10^{-3}$ → pK_{a1} = 2.65

$K_{a2} = 2.25 \times 10^{-9}$ → pK_{a2} = 8.65

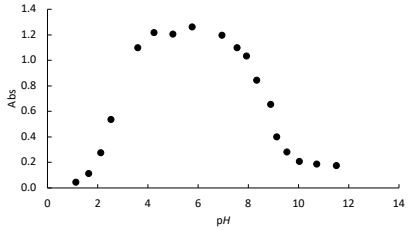

3.1.6.2 General information – pK_a measurements in MeCN mixtures

The respective ion pairs **3-6a** were used for stock solutions due to solubility issues of the pyridinamides for the pK_a determination in water/MeCN mixtures with a ratio of 50/50. Stock solution A with c = 1.0 mM of the respective neutral pyridinamides in MeCN was prepared and diluted with MeCN to give stock solution B with c = 0.1 mM. Subsequently, 0.5 mL of stock solution B was combined with 0.5 mL of buffer solution to give the final measurement mixture with a compound concentration of c = 0.05 mM.

However, due to dilution the final ionic strength of the measurement solution was reduced to *I* = 0.15 M. To verify that the reduced ionic strength would not influence the final pK_a value a test measurement with neutral pyridinamide PA_**3** was performed with the same conditions as for the aqueous pK_a measurement with the exception that the stock solution was diluted in a way that the ionic strength of the measurement mixture would be *I* = 0.15 M. The resulting pK_a value of this measurement did not deviate from the pK_a value obtained with *I* = 0.3 M. To the observed pH_{obs} of the water/MeCN mixtures a correction factor δ_{MeCN} must be applied since the pH_{obs} was determined with an electrode calibrated in

aqueous solutions. Therefore, a correction of -0.257 was added to the measured output of the p*H* probe.[14]

DMAP –pK_a in MeCN mixture

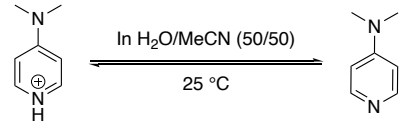

DMAP-H **DMAP**

VB30. Stock solution A with 12.2 mg DMAP (**1**) in 20 mL MeCN mix, diluted to *c* = 0.05 mM, measured at λ_{max} = 280 nm.

Buffer	%fb	pH_{buffer}	p$H_{baseline}$	pH(corr)	Abs (280nm)
Phosphate	50	6.72	7.52	7.263	0.94
TEOA	20	7.37	7.25	6.993	0.95
	40	7.81	7.68	7.423	0.94
	70	8.37	8.22	7.963	0.87
	80	8.62	8.49	8.233	0.81
Carbonate	10	9.04	10.12	9.863	0.31
	25	9.46	10.56	10.303	0.28
	50	9.97	11.03	10.773	0.27
PIP	20	10.71	10.19	9.933	0.31
	60	11.47	11	10.743	0.27

K_a = 1.65 x 10^{-9} → pK_a = 8.78

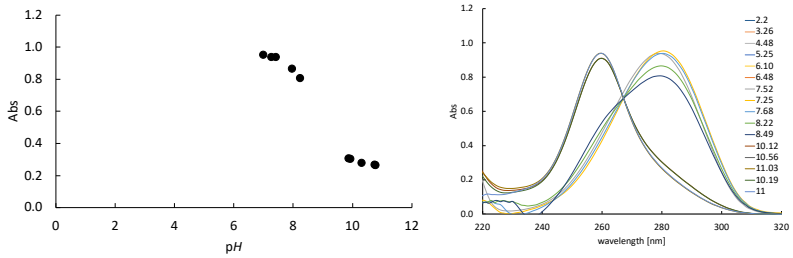

VB37. Stock solution A with 12.0 mg DMAP (**1**) in 20 mL MeCN mix, diluted to *c* = 0.05 mM, measured at λ_{max} = 280 nm.

Buffer	%fb	pH_{buffer}	p$H_{baseline}$	pH(corr)	Abs (280nm)
Acetat	30	4.17	5.29	5.033	1.06
	70	4.94	6.09	5.833	1.05
Phosphate	10	5.68	6.49	6.233	1.05
	50	6.72	7.52	7.263	1.02
TEOA	20	7.37	7.19	6.933	1.03
	40	7.81	7.64	7.383	1.01
	70	8.37	8.18	7.923	0.93
	80	8.62	8.42	8.163	0.87
Carbonate	10	9.04	10.16	9.903	0.33
	25	9.46	10.49	10.233	0.30
	50	9.97	11.04	10.783	0.29
PIP	20	10.71	10.11	9.853	0.34
	60	11.47	10.96	10.703	0.29

K_a = 2.16 x 10^{-9} → pK_a = 8.67

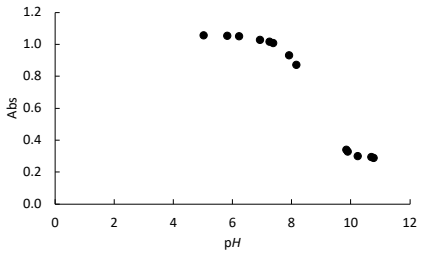

Ion Pair 3a –pK_a in MeCN mixture

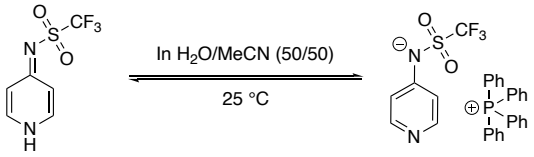

PA_3 **3a**

VB26. Stock solution A with 5.65 mg **3a** in 10 mL MeCN, diluted to *c* = 0.05 mM, measured at λ_{max} = 272 nm.

Buffer	%fb	pH_{buffer}	p$H_{baseline}$	pH(corr)	Abs (272nm)	pKa
HCl	0.1	1.08	1.17	0.913	1.65	
HCl	0.03	1.6	1.71	1.453	1.67	
HCl	0.01	2.1	2.2	1.943	1.66	
Formate	10	2.51	3.26	3.003	1.66	X
	50	3.55	4.48	4.223	1.66	X
Acetat	30	4.17	5.25	4.993	1.64	X
	70	4.94	6.10	5.84	1.62	X
Phosphate	10	5.68	6.48	6.223	1.56	X
	50	6.72	7.52	7.263	1.10	X
TEOA	20	7.37	7.18	6.923	1.30	X
	40	7.81	7.66	7.403	1.01	X
	70	8.37	8.2	7.943	0.69	X
	80	8.62	8.46	8.203	0.60	X
Carbonate	10	9.04	10.13	9.873	0.46	X
	25	9.46	10.56	10.303	0.44	X
	50	9.97	11.03	10.773	0.44	X
PIP	20	10.71	10.19	9.933	0.44	X
	60	11.47	11.00	10.743	0.44	X

$K_a = 4.60 \times 10^{-8}$ → pK_a = 7.34

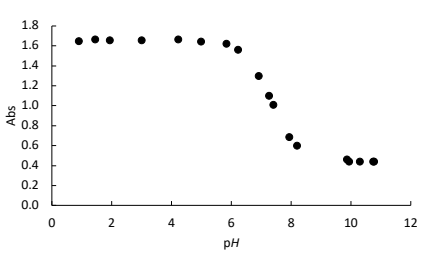

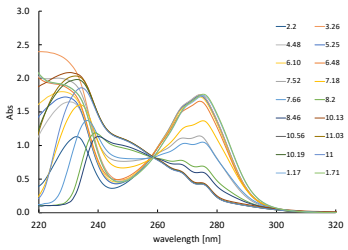

VB36. Stock solution A with 11.2 mg **3a** in 10 mL MeCN, diluted to *c* = 0.05 mM, measured at λ_{max} = 272 nm.

Buffer	%fb	pH_{buffer}	p$H_{baseline}$	pH(corr)	Abs (272nm)
Formate	10	2.51	3.24	2.983	1.33
	50	3.55	4.48	4.223	1.33
Acetat	30	4.17	5.29	5.033	1.33
	70	4.94	6.09	5.833	1.30
Phosphate	10	5.68	6.49	6.233	1.24
	50	6.72	7.52	7.263	0.80
TEOA	20	7.37	7.19	6.933	0.98
	40	7.81	7.64	7.383	0.70

	70	8.37	8.18	7.923	0.43
	80	8.62	8.42	8.163	0.38
Carbonate	10	9.04	10.16	9.903	0.22
	25	9.46	10.49	10.233	0.22
	50	9.97	11.04	10.783	0.22
PIP	20	10.71	10.11	9.853	0.22

K_a = 5.22 x 10^{-8} → pK_a = 7.28

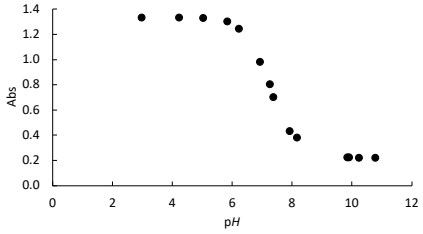

Ion Pair 5a –pK_a in MeCN mixture

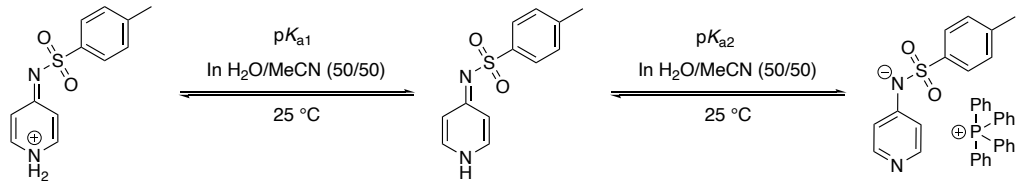

PAH_5 **PA_5** **5a**

VB27. Stock solution A with 5.85 mg **5a** in 10 mL MeCN, diluted to *c* = 0.05 mM, measured at λ_{max} = 290 nm.

Buffer	%fb	pH_{buffer}	p$H_{baseline}$	pH(corr)	Abs (290nm)	pKa1	pKa2
HCl	0.1	1.08	1.17	0.913	0.08	X	
HCl	0.03	1.6	1.71	1.453	0.08	X	
HCl	0.01	2.1	2.2	1.943	0.11	X	
Formate	10	2.51	3.26	3.003	0.45	X	
	50	3.55	4.48	4.223	1.17	X	
Acetat	30	4.17	5.25	4.993	1.26	X	
	70	4.94	6.10	5.843	1.29	X	X
Phosphate	10	5.68	6.48	6.223	1.28	X	X
	50	6.72	7.52	7.263	1.23		X
TEOA	20	7.37	7.18	6.923	1.27		X
	40	7.81	7.66	7.403	1.23		X
	70	8.37	8.2	7.943	1.10		X
	80	8.62	8.46	8.203	1.01		X
Carbonate	10	9.04	10.13	9.873	0.26		X
	25	9.46	10.56	10.303	0.21		X
	50	9.97	11.03	10.773	0.19		X
PIP	20	10.71	10.19	9.933	0.24		X
	60	11.47	11.00	10.743	0.19		X

K_{a1} = 4.65 x 10^{-4} → pK_{a1} = 3.33

K_{a2} = 2.14 x 10^{-9} → pK_{a2} = 8.67

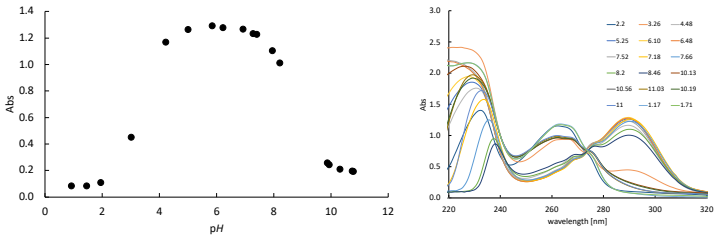

VB38. Stock solution A with 12.0 mg **5a** in 10 mL MeCN, diluted to *c* = 0.05 mM, measured at λ_{max} = 290 nm.

Buffer	%fb	pH_{buffer}	p$H_{baseline}$	pH(corr)	Abs (290nm)	pKa_1	pKa_2

HCl	0.1	1.08	1.2	0.943	0.07	X	
HCl	0.03	1.6	1.73	1.473	0.07	X	
HCl	0.01	2.1	2.21	1.953	0.10	X	
Formate	10	2.51	3.24	2.983	0.43	X	
	50	3.55	4.48	4.223	1.13	X	
Acetat	30	4.17	5.29	5.033	1.23	X	
	70	4.94	6.07	5.813	1.24	X	
Phosphate	10	5.68	6.5	6.243	1.23	X	X
	50	6.72	7.52	7.263	1.21		X
TEOA	20	7.37	7.21	6.953	1.21		X
	40	7.81	7.67	7.413	1.18		X
	70	8.37	8.21	7.953	1.07		X
	80	8.62	8.45	8.193	0.97		X
Carbonate	10	9.04	10.21	9.953	0.23		X
	25	9.46	10.48	10.223	0.20		X
	50	9.97	11.02	10.763	0.19		X
PIP	20	10.71	10.08	9.823	0.24		X
	60	11.47	10.95	10.693	0.19		X

K_{a1} = 4.88 x 10^{-4} → pK_{a1} = 3.31

K_{a2} = 2.14 x 10^{-9} → pK_{a2} = 8.67

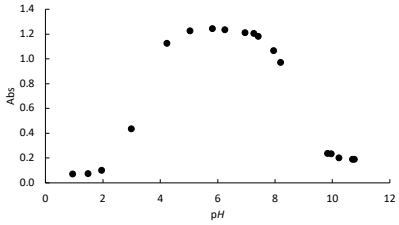

Ion Pair 4a –pK_a in MeCN mixture

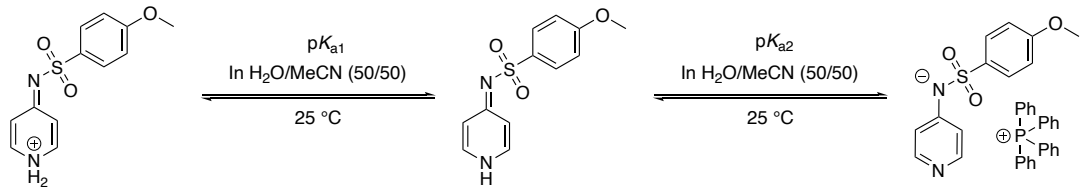

PAH_4 **PA_4** **4a**

VB28. Stock solution A with 6.02 mg **4a** in 10 mL MeCN, diluted to *c* = 0.05 mM, measured at λ_{max} = 290 nm.

Buffer	%fb	pH_{buffer}	p$H_{baseline}$	pH(corr)	Abs (290nm)	pKa_1	pKa_2
HCl	0.1	1.08	1.17	0.913	0.16	X	
HCl	0.03	1.6	1.71	1.453	0.17	X	
HCl	0.01	2.1	2.2	1.943	0.19	X	
Formate	10	2.51	3.26	3.003	0.41	X	
	50	3.55	4.48	4.223	1.03	X	
Acetat	30	4.17	5.25	4.993	1.15	X	
	70	4.94	6.10	5.843	1.17	X	X
Phosphate	10	5.68	6.48	6.223	1.17	X	X
	50	6.72	7.52	7.263	1.14		X
TEOA	20	7.37	7.18	6.923	1.15		X
	40	7.81	7.66	7.403	1.12		X
	70	8.37	8.2	7.943	1.01		X
	80	8.62	8.46	8.203	0.93		X
Carbonate	10	9.04	10.13	9.873	0.23		X
	25	9.46	10.56	10.303	0.19		X
	50	9.97	11.03	10.773	0.18		X
PIP	20	10.71	10.19	9.933	0.22		X
	60	11.47	11.00	10.743	0.17		X

K_{a1} = 3.36 x 10^{-4} → pK_{a1} = 3.47

K_{a2} = 2.04 x 10^{-9} → pK_{a2} = 8.69

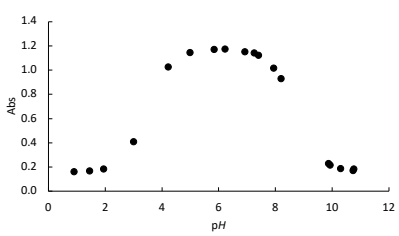

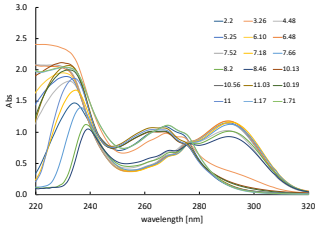

VB39. Stock solution A with 12.3 mg **4a** in 10 mL MeCN, diluted to *c* = 0.05 mM, measured at λ_{max} = 290 nm.

Buffer	%fb	pH_{buffer}	p$H_{baseline}$	pH(corr)	Abs (290nm)	pKa_1	pKa_2
HCl	0.1	1.08	1.2	0.943	0.18	X	
HCl	0.03	1.6	1.73	1.473	0.19	X	
HCl	0.01	2.1	2.21	1.953	0.21	X	
Formate	10	2.51	3.24	2.983	0.45	X	
	50	3.55	4.48	4.223	1.10	X	
Acetat	30	4.17	5.29	5.033	1.22	X	
	70	4.94	6.07	5.813	1.24	X	X
Phosphate	10	5.68	6.5	6.243	1.24	X	X
	50	6.72	7.52	7.263	1.20		X
TEOA	20	7.37	7.21	6.953	1.23		X
	40	7.81	7.67	7.413	1.19		X
	70	8.37	8.21	7.953	1.08		X
	80	8.62	8.45	8.193	0.99		X
Carbonate	10	9.04	10.21	9.953	0.24		X
	25	9.46	10.48	10.223	0.20		X
	50	9.97	11.02	10.763	0.19		X
PIP	20	10.71	10.08	9.823	0.29		X
	60	11.47	10.95	10.693	0.19		X

K_{a1} = 3.64 x 10^{-4} → pK_{a1} = 3.44

K_{a2} = 1.95 x 10^{-9} → pK_{a2} = 8.71

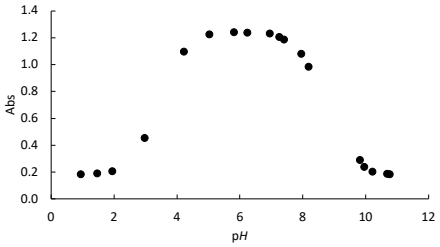

Ion Pair 6a –pK_a in MeCN mixture

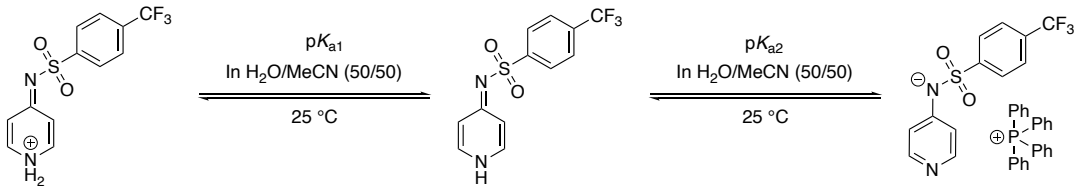

PAH_6 **PA_6** **6a**

VB29. Stock solution A with 6.41 mg **4a** in 10 mL MeCN, diluted to *c* = 0.05 mM, measured at λ_{max} = 290 nm.

Buffer	%fb	pH_{buffer}	p$H_{baseline}$	pH(corr)	Abs (290nm)	pKa_1	pKa_2
HCl	0.1	1.08	1.17	0.913	0.08	X	
HCl	0.03	1.6	1.71	1.453	0.16	X	
HCl	0.01	2.1	2.2	1.943	0.33	X	
Formate	10	2.51	3.26	3.003	0.98	X	

	50	3.55	4.48	4.223	1.22	X	
Acetat	30	4.17	5.25	4.993	1.24	X	X
	70	4.94	6.10	5.843	1.24	X	X
Phosphate	10	5.68	6.48	6.223	1.23		X
	50	6.72	7.52	7.263	1.16		X
TEOA	20	7.37	7.18	6.923	1.20		X
	40	7.81	7.66	7.403	1.14		X
	70	8.37	8.2	7.943	0.95		X
	80	8.62	8.46	8.203	0.83		X
Carbonate	10	9.04	10.13	9.873	0.27		X
	25	9.46	10.56	10.303	0.25		X
	50	9.97	11.03	10.773	0.24		X
PIP	20	10.71	10.19	9.933	0.27		X
	60	11.47	11.00	10.743	0.25		X

K_{a1} = 3.54 x 10^{-3} → pK_{a1} = 2.45

K_{a2} = 4.47 x 10^{-9} → pK_{a2} = 8.35

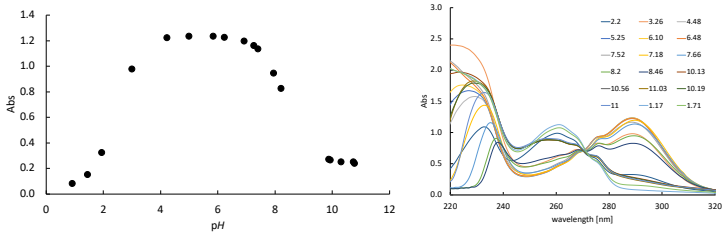

VB40. Stock solution A with 12.9 mg **4a** in 10 mL MeCN, diluted to *c* = 0.05 mM, measured at λ_{max} = 290 nm.

Buffer	**%fb**	**p*H*$_{buffer}$**	**p*H*$_{baseline}$**	**pH(corr)**	**Abs (290nm)**	**p*K*a$_1$**	**p*K*a$_2$**
HCl	0.1	1.09	1.2	0.943	0.07	X	
HCl	0.03	1.6	1.73	1.473	0.15	X	
HCl	0.01	2.1	2.21	1.953	0.32	X	
Formate	10	2.51	3.24	2.983	0.99	X	
	50	3.55	4.48	4.223	1.24	X	
Acetat	30	4.17	5.29	5.033	1.26	X	X
	70	4.94	6.07	5.813	1.26	X	X
Phosphate	10	5.68	6.5	6.243	1.23		X
	50	6.72	7.52	7.263	1.17		X
TEOA	20	7.37	7.21	6.953	1.20		X
	40	7.81	7.67	7.413	1.13		X
	70	8.37	8.21	7.953	0.95		X
	80	8.62	8.45	8.193	0.83		X
Carbonate	10	9.04	10.21	9.953	0.26		X
	25	9.46	10.48	10.223	0.24		X
	50	9.97	11.02	10.763	0.23		X
PIP	20	10.71	10.08	9.823	0.26		X
	60	11.47	10.95	10.693	0.23		X

K_{a1} = 3.54 x 10^{-3} → pK_{a1} = 2.45

K_{a2} = 4.58 x 10^{-9} → pK_{a2} = 8.34

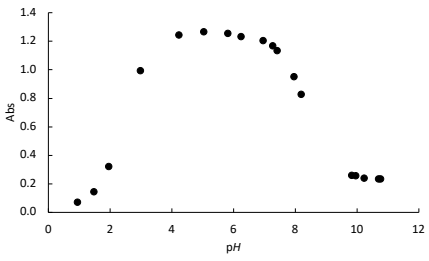

3.1.6.3 General information – pK_a measurements in DMSO mixtures

Stock solution A with c = 1.0 mM of the respective neutral pyridinamides in DMSO was prepared and diluted with DMSO to give stock solution B with c = 0.1 mM. 0.5 mL of stock solution B was combined with 0.5 mL of buffer solution to give the final measurement mixture with a compound concentration of c = 0.05 mM. In this chapter only observed p*H* values are reported for the deprotonation of the neutral pyridinamide to the fully deprotonated anion.

Pyridinamide 3 –pK_a in DMSO

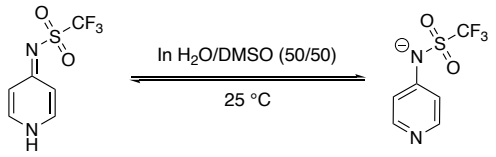

PA_3 **an3**

VB31. Stock solution A with 2.29 mg PA_**3** in 10 mL DMSO, diluted to *c* = 0.05 mM, measured at λ_{max} = 275 nm.

Buffer	%fb	pH_{buffer}	p$H_{baseline}$	Abs (275nm)
Acetat	30	4.17	5.9	1.39
	70	4.94	6.75	1.25
Phosphate	50	6.94	9	0.14
TEOA	20	7.55	7.54	0.71
	40	7.95	7.9	0.39
	70	8.36	8.51	0.18
	80	8.96	8.75	0.14
Carbonate	10	9.02	11.79	0.06
PIP	20	10.74	10.63	0.06
	60	11.50	11.46	0.06

$K_a = 3.47 \times 10^{-8}$ → pK_a = 7.46

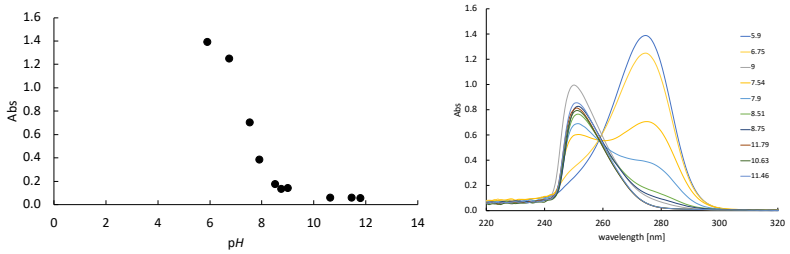

Pyridinamide 5 –pK_a in DMSO

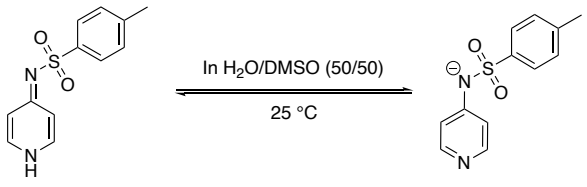

PA_5 **an5**

VB32. Stock solution A with 2.47 mg PA_**5** in 10 mL DMSO, diluted to *c* = 0.05 mM, measured at λ_{max} = 292 nm.

Buffer	%fb	pH_{buffer}	p$H_{baseline}$	Abs (292nm)
Acetat	30	4.17	5.9	1.53
	70	4.94	6.75	1.54
Phosphate	50	6.94	9	0.81
TEOA	20	7.55	7.54	1.50
	40	7.95	7.9	1.40
	70	8.36	8.51	1.17
	80	8.96	8.75	1.00

Carbonate	10	9.02	11.79	0.21
PIP	20	10.74	10.63	0.24
	60	11.50	11.46	0.20

K_a = 1.21 x 10^{-9} → pK_a = 8.92

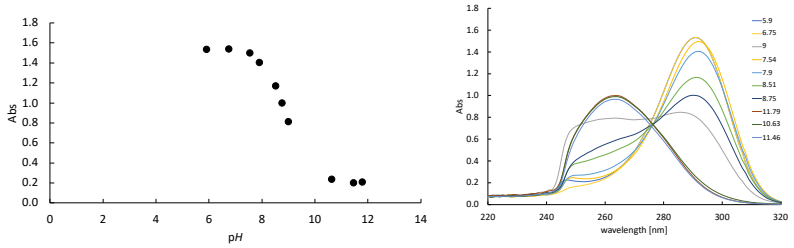

Pyridinamide 4 –pK_a in DMSO

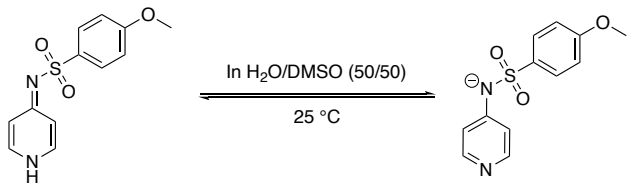

PA_4 **an4**

VB33. Stock solution A with 3.63 mg PA_**4** in 10 mL DMSO, diluted to *c* = 0.05 mM, measured at λ_{max} = 292 nm.

Buffer	**%fb**	**pH_{buffer}**	**p$H_{baseline}$**	**Abs (292nm)**
Acetat	30	4.17	5.9	1.57
	70	4.94	6.75	1.57
Phosphate	50	6.94	9	0.88
TEOA	20	7.55	7.54	1.54
	40	7.95	7.9	1.45
	70	8.36	8.51	1.23
	80	8.96	8.75	1.08
Carbonate	10	9.02	11.79	0.24
	25	9.45	12.25	0.25
PIP	20	10.74	10.63	0.28
	60	11.50	11.46	0.25

K_a = 1.08 x 10^{-9} → pK_a = 8.97

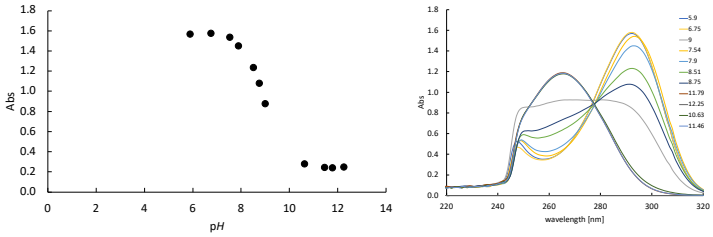

Pyridinamide 6 –pK_a in DMSO

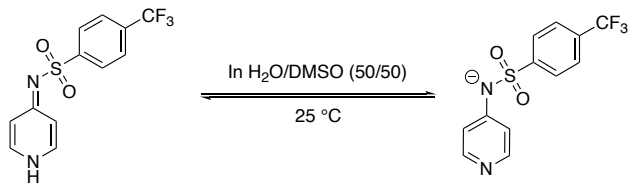

PA_6 **an6**

VB34. Stock solution A with 3.04 mg PA_**6** in 10 mL DMSO, diluted to *c* = 0.05 mM, measured at λ_{max} = 292 nm.

Buffer	**%fb**	**pH_{buffer}**	**p$H_{baseline}$**	**Abs (292nm)**
Acetat	30	4.17	5.90	1.26

	70	4.94	6.75	1.27
Phosphate	50	6.94	9.00	0.51
TEOA	20	7.55	7.54	1.20
	40	7.95	7.90	1.08
	70	8.36	8.51	0.80
	80	8.96	8.75	0.65
Carbonate	10	9.02	11.79	0.24
	25	9.45	12.25	0.23
PIP	20	10.74	10.63	0.25
	60	11.50	11.46	0.24

$K_a = 2.70 \times 10^{-9}$ $\rightarrow$ $pK_a = 8.57$

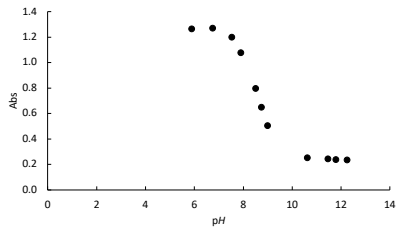

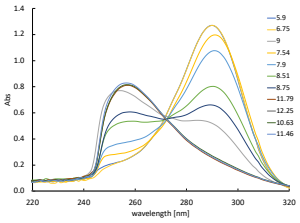

3.1.7 NMR Kinetics

The urethane synthesis was chosen as benchmark reaction to insert the newly designed ion pair catalyst into to existing reactivity library and compare their reactivity with already known ion pair catalysts. The benchmark reaction was performed with pyridinamide ion pair **3a**, **3b**, **5a,** and **6a**. The effective rate constants for **3c** and **4a** were taken from Helberg and Zipse.[3]

The reactant *p*-tosyl isocyanate (**9**, reagent grade) was distilled prior to use. The reactant 1-butanol (**10**, reagent grade) was distilled and stored over 4Å MS and under N_2 prior to use.

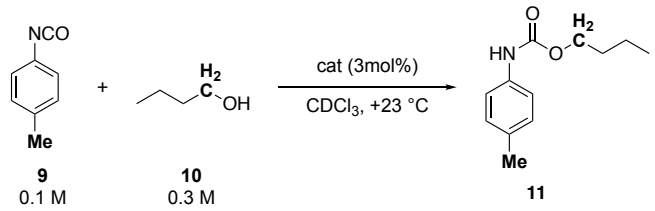

Scheme 3.7: [Scheme S7]. Urethane synthesis with *p*-tosyl isocyanate (**9**) and 1-butanol (**10**) giving urethane **11**.

The experimental procedure and evaluation of the urethane synthesis was done as described as in Helberg and Zipse.[3] There the conversion was calculated according to eq. 3.23.

$$\text{Conversion } [\%] = \frac{3 \times \text{product(CH2)}}{2 \times (\text{prod(me)} + \text{isocyanat(Me)})} \times 100 \tag{3.23}$$

The conversion is then used to calculate the concentration of urethane at the time *t* c_t[product] based on the initial concentration c_0 (eq. 3.24).

$$c_t = c(\mathbf{9})_0 - \left(\frac{c(\mathbf{9})_0 \times (100 - \text{conversion})}{100}\right) \tag{3.24}$$

Numerical simulation according to eq. 3.25 were performed using the program COPASI to obtain the respective effective rate constants k_{eff}.

$$[\mathbf{9}] + [\mathbf{10}] = [\text{urethane } \mathbf{11}] \tag{3.25}$$

The benchmark reaction was performed with three different catalyst loadings and in two independent runs each. The resulting averaged effective rate constants k_{eff} are summarized in Table 3.11.

Table 3.11: [Table S16]. List of averaged k_{eff} values obtained for the urethane synthesis with 1.0 mol%, 3.0 mol%, and 6.0 mol% catalyst loading.

IP	k_{eff}(1) / M^{-1} s^{-1}	k_{eff}(3) / M^{-1} s^{-1}	k_{eff}(6) / M^{-1} s^{-1}	k_{cat} / M^{-2} s^{-1}
1[a]	–	2.80 x 10^{-4}	–	0.086
2[a]	2.78 x 10^{-4}	7.50 x 10^{-4}	–	0.364
3a	2.26 x 10^{-4} ± 3.67 x 10^{-6}	6.01 x 10^{-4} ± 1.50 x 10^{-6}	1.20 x 10^{-3} ± 2.19 x 10^{-5}	0.196
3b	2.45 x 10^{-4} ± 1.86 x 10^{-6}	7.15 x 10^{-4} ± 1.56 x 10^{-5}	1.27 x 10^{-3} ± 1.61 x 10^{-5}	0.205
3c[a]	–	3.65 x 10^{-4}	–	0.115
4a[a]	8.04 x 10^{-4}[b]	1.99 x 10^{-3}	3.96 x 10^{-3}	0.661
5a	5.28 x 10^{-4} ± 1.95 x 10^{-6}	1.53 x 10^{-3} ± 8.03 x 10^{-6}	2.90 x 10^{-3} ± 1.20 x 10^{-4}	0.477
6a	4.30 x 10^{-4} ± 3.14 x 10^{-6}	1.25 x 10^{-3} ± 2.50 x 10^{-6}	2.58 x 10^{-3} ± 4.34 x 10^{-5}	0.433

[a] values taken from ref. [3]. [b] measured with 1.2 mol% catalyst load.

Subsequently the effective rate constants can be used to determine the concentration-independent rate constant of each catalyst according to eq. 3.26.

$$k_{eff} = k_{cat} \text{ x [catalyst]} \tag{3.26}$$

Plotting the effective rate constant k_{eff} against the respective catalyst load [catalyst] reveals a clear linear correlation for all investigated systems with a very small Y-intercept, thus, indicating that any potential uncatalyzed background reaction is negligible.

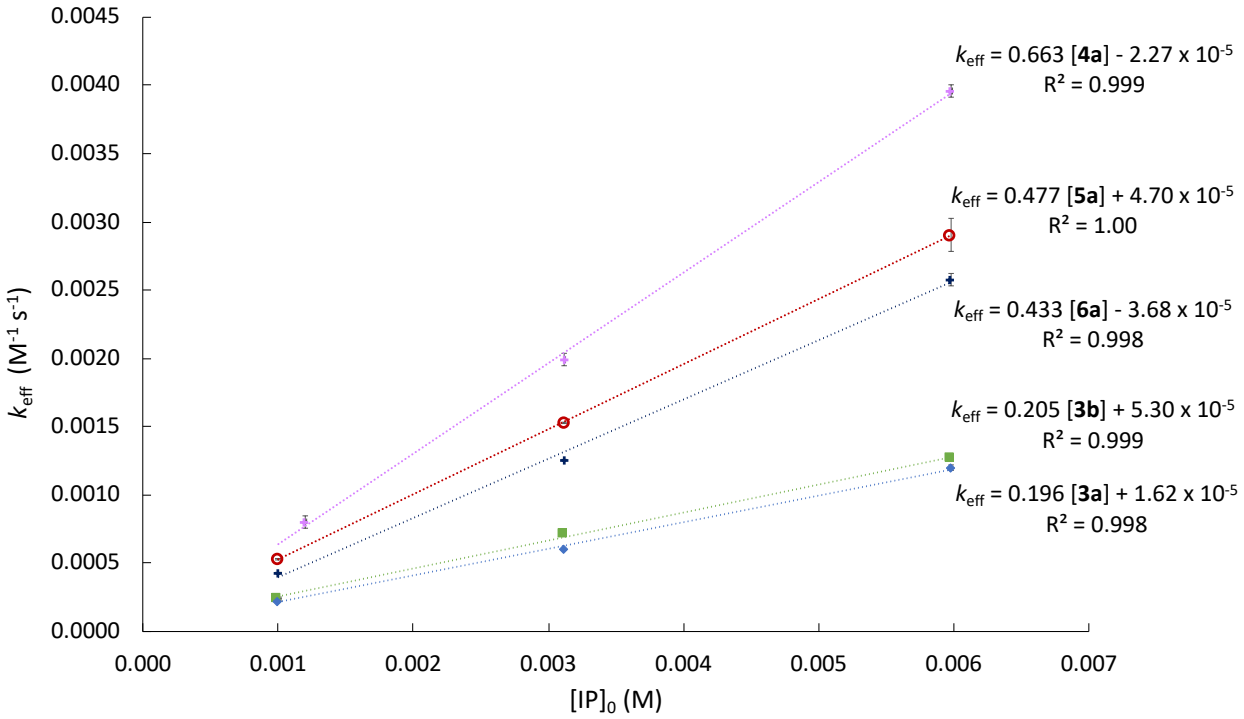

Figure 3.11: [Figure S12]. Correlation of catalytic activity at increasing catalyst loadings for the urethane synthesis with data from ref. [3] for **4a**.

The relative catalytic performance of the pyridinamide ion pair is reflected in the slope of the correlation as the concentration-independent rate constant k_{cat} (M^{-2} s^{-1}).

The fitted values of the effective rate constants k_{eff} by COPASI with a catalyst load of 3.0 mol% are summarized in Table 3.12.

Table 3.12: [Table S17]. List of k_{eff} values obtained for the urethane synthesis (3.0 mol%).

Catalyst	Run	Yield [%]	k_{eff}	Average k_{eff}
3a	1	99	6.00×10^{-4}	$6.01 \times 10^{-4} \pm 1.50 \times 10^{-6}$
	2	99	6.03×10^{-4}	
3b	1	99	7.30×10^{-4}	$7.15 \times 10^{-4} \pm 1.56 \times 10^{-5}$
	2	99	6.99×10^{-4}	
5a	1	98	1.54×10^{-3}	$1.53 \times 10^{-3} \pm 8.03 \times 10^{-6}$
	2	98	1.52×10^{-3}	
6a	1	99	1.26×10^{-3}	$1.25 \times 10^{-3} \pm 2.50 \times 10^{-6}$
	2	99	1.25×10^{-3}	

The raw data of the absolute kinetics with 3.0 mol% catalyst load are summarized in Table 3.13 to Table 3.16.

Table 3.13: [Table S18]. Raw data of absolute kinetic of urethane synthesis with **5a** (3.0 mol%) in $CDCl_3$.

Time (min)	Integ. Limits (ppm)		Integ	Absol.	Integ. Limits (ppm)		Integ	Absol.	Integ. Limits (ppm)		Integ	Absol.	$Conv_{exp}$ (%)
VB178a	**Product**				**Educt**				**Product+Educt**				**$Conv_{exp}$**
12	4.08	4.20	1.0	49294.1	3.56	3.71	9.7	476294.3	2.23	2.37	5.86	288770.5	25.6
15	4.09	4.20	1.0	55914.8	3.55	3.71	7.7	430175.9	2.22	2.39	4.88	273068.0	30.7
17	4.07	4.20	1.0	62846.1	3.55	3.70	6.7	423653.9	2.22	2.39	4.34	272685.0	34.6
34	4.07	4.20	1.0	98334.9	3.56	3.70	3.8	376780.0	2.25	2.37	2.68	263525.0	56.0
36	4.08	4.21	1.0	102344.9	3.56	3.69	3.6	372393.1	2.25	2.36	2.57	262921.2	58.4
50	4.07	4.20	1.0	122784.0	3.54	3.71	2.9	355569.3	2.21	2.38	2.18	267832.6	68.8
56	4.06	4.21	1.0	129615.9	3.54	3.70	2.7	350760.2	2.23	2.36	2.05	265973.5	73.1
69	4.07	4.21	1.0	138972.5	3.55	3.72	2.4	336015.9	2.24	2.37	1.89	262415.3	79.4
76	4.07	4.21	1.0	146500.3	3.53	3.71	2.3	337052.4	2.24	2.36	1.82	266753.2	82.4
94	4.00	4.16	1.0	156155.9	3.47	3.64	2.1	330238.6	2.19	2.30	1.71	267455.4	87.6
106	4.06	4.22	1.0	160783.5	3.57	3.70	2.0	325588.1	2.24	2.37	1.67	268897.9	89.7
136	4.07	4.23	1.0	168225.4	3.55	3.71	1.9	320733.0	2.24	2.37	1.60	269475.2	93.6
181	4.08	4.21	1.0	111998.1	3.57	3.71	1.8	205954.2	2.24	2.36	1.57	175523.0	95.7
204	4.07	4.21	1.0	171467.4	3.56	3.71	1.8	313087.9	2.25	2.36	1.55	266295.1	96.6
259	4.06	4.23	1.0	174991.4	3.54	3.71	1.8	315640.4	2.25	2.37	1.54	269731.8	97.3
319	4.06	4.23	1.0	175396.0	3.57	3.70	1.8	315181.3	2.25	2.37	1.54	270341.7	97.3
397	4.07	4.21	1.0	192169.9	3.56	3.71	1.8	347963.4	2.25	2.34	1.53	294564.8	97.9
454	4.06	4.22	1.0	172974.0	3.56	3.70	1.8	311679.1	2.25	2.34	1.54	265550.6	97.7
VB178b	**Product**				**Educt**				**Product+Educt**				**$Conv_{exp}$**

10	4.09	4.19	1.0	37893.4	3.56	3.70	11.41	432371.0	2.24	2.36	6.86	259805.7	21.9
13	4.08	4.19	1.0	47001.4	3.54	3.69	9.25	434932.5	2.25	2.35	5.64	265131.7	26.6
23	4.08	4.20	1.0	76538.2	3.56	3.70	5.33	407883.4	2.25	2.35	3.48	266070.6	43.1
42	4.07	4.21	1.0	112354.8	3.55	3.69	3.34	374759.4	2.24	2.36	2.38	267505.2	63.0
50	4.08	4.20	1.0	122211.4	3.56	3.69	3.00	366277.5	2.24	2.37	2.20	268516.7	68.3
72	4.07	4.20	1.0	93844.7	3.56	3.69	2.43	227976.5	2.24	2.35	1.88	176461.3	79.8
82	4.07	4.20	1.0	147132.3	3.55	3.70	2.28	335092.8	2.24	2.36	1.79	263607.9	83.7
118	4.07	4.20	1.0	161421.5	3.56	3.69	2.02	325616.8	2.25	2.36	1.65	265795.5	91.1
144	4.08	4.20	1.0	166541.9	3.54	3.69	1.94	322736.7	2.25	2.34	1.59	265081.5	94.2
173	4.07	4.20	1.0	170024.8	3.55	3.71	1.89	321623.8	2.24	2.34	1.57	267074.8	95.5
206	4.06	4.21	1.0	171642.3	3.56	3.69	1.86	318640.6	2.24	2.34	1.55	266157.9	96.7
244	4.07	4.20	1.0	171051.2	3.55	3.69	1.85	317160.7	2.25	2.34	1.55	264423.0	97.0
265	4.08	4.20	1.0	171900.8	3.56	3.69	1.85	317940.4	2.23	2.34	1.55	266886.2	96.6
323	4.06	4.21	1.0	172777.9	3.56	3.70	1.84	317965.8	2.24	2.35	1.54	266884.4	97.1
386	4.07	4.20	1.0	171132.6	3.56	3.70	1.85	315950.8	2.23	2.35	1.55	265461.2	96.7
448	4.06	4.21	1.0	196983.9	3.56	3.70	1.84	362400.7	2.25	2.34	1.54	302637.4	97.6
509	4.07	4.20	1.0	196566.2	3.55	3.70	1.85	363477.6	2.25	2.33	1.54	302865.7	97.4
570	4.08	4.19	1.0	198972.9	3.54	3.70	1.86	369253.6	2.25	2.35	1.54	307097.3	97.2
654	4.08	4.19	1.0	171821.6	3.55	3.70	1.85	318272.0	2.23	2.35	1.56	267421.0	96.4
728	4.06	4.23	1.0	172803.0	3.55	3.70	1.84	317268.7	2.23	2.35	1.54	266391.1	97.3

Table 3.14: [Table S19]. Raw data of absolute kinetic of urethane synthesis with 6a (3.0 mol%) in $CDCl_3$.

Time (min)	**Integ. Limits (ppm)**		**Integ**	**Absol.**	**Integ. Limits (ppm)**		**Integ**	**Absol.**	**Integ. Limits (ppm)**		**Integ**	**Absol.**	**$Conv_{exp}$ (%)**
VB179a	**Product**				**Educt**				**Product+Educt**				**$Conv_{exp}$**
7	4.10	4.19	1.0	21119.5	3.54	3.70	21.03	444081.1	2.24	2.37	12.10	255583.1	12.4
13	4.10	4.19	1.0	38513.7	3.55	3.70	11.13	428476.9	2.24	2.37	6.66	256415.1	22.5
23	4.07	4.20	1.0	64161.0	3.55	3.70	6.35	407122.9	2.25	2.36	4.01	257123.4	37.4
35	4.08	4.20	1.0	88042.4	3.55	3.70	4.39	386299.8	2.25	2.36	2.94	258846.2	51.0
53	4.08	4.20	1.0	112183.9	3.57	3.69	3.25	364042.0	2.26	2.35	2.31	258768.2	65.0
58	4.08	4.20	1.0	116953.6	3.56	3.69	3.07	358822.3	2.25	2.35	2.22	259096.4	67.7
93	4.07	4.20	1.0	146224.2	3.54	3.70	2.33	340964.5	2.25	2.35	1.80	263350.4	83.3
128	4.07	4.20	1.0	154824.2	3.54	3.70	2.05	317812.4	2.25	2.34	1.64	254342.1	91.3
151	4.07	4.20	1.0	160536.5	3.55	3.70	1.95	312903.5	2.25	2.35	1.59	256039.8	94.0
184	4.06	4.20	1.0	168818.8	3.55	3.70	1.86	314146.1	2.25	2.35	1.55	261326.1	96.9
210	4.07	4.22	1.0	171490.6	3.55	3.71	1.83	313455.0	2.26	2.34	1.52	260572.1	98.7
269	4.07	4.20	1.0	170644.1	3.57	3.69	1.79	304736.0	2.25	2.34	1.50	256627.1	99.7

330	4.08	4.20	1.0	170195.9	3.56	3.69	1.78	302412.0	2.25	2.34	1.50	254918.7	100.1
394	4.07	4.21	1.0	174777.5	3.55	3.70	1.77	308676.8	2.26	2.35	1.49	260655.1	100.6
455	4.08	4.21	1.0	169826.6	3.55	3.71	1.77	300827.9	2.25	2.35	1.49	253125.1	100.6
529	4.05	4.21	1.0	173616.0	3.54	3.71	1.76	306288.9	2.25	2.35	1.49	258404.8	100.8
601	4.08	4.20	1.0	173080.7	3.56	3.71	1.77	306534.7	2.24	2.34	1.50	259269.6	100.1
737	4.08	4.22	1.0	174241.5	3.55	3.70	1.77	308299.3	2.25	2.35	1.49	259882.2	100.6
VB179b	**Product**				**Educt**				**Product+Educt**				**$Conv_{exp}$**
8	4.08	4.20	1.0	24630.2	3.54	3.71	18.84	464151.3	2.24	2.36	10.57	260311.6	14.2
10	4.09	4.20	1.0	31628.5	3.54	3.71	14.48	457851.2	2.22	2.37	8.28	261910.8	18.1
25	4.07	4.21	1.0	69395.3	3.53	3.71	6.13	425178.0	2.22	2.39	3.81	264609.5	39.3
40	4.08	4.20	1.0	96043.3	3.56	3.71	4.16	399441.7	2.26	2.36	2.73	262339.7	54.9
58	4.08	4.21	1.0	118526.6	3.56	3.71	3.17	376155.2	2.24	2.37	2.21	262533.0	67.7
70	4.08	4.21	1.0	130089.9	3.54	3.71	2.83	367516.1	2.25	2.36	2.02	262345.0	74.4
87	4.08	4.20	1.0	143368.3	3.56	3.71	2.49	357482.1	2.24	2.37	1.85	265717.8	80.9
118	4.07	4.22	1.0	153762.7	3.56	3.71	2.19	335982.7	2.24	2.36	1.69	259428.1	88.9
145	4.08	4.20	1.0	160291.4	3.57	3.69	2.05	328527.5	2.24	2.35	1.62	259755.3	92.6
175	4.07	4.22	1.0	166496.1	3.56	3.71	1.95	325310.9	2.24	2.35	1.57	261136.9	95.6
207	4.07	4.22	1.0	169453.4	3.57	3.71	1.90	322588.5	2.25	2.35	1.53	260054.9	97.7
270	4.04	4.22	1.0	174752.1	3.55	3.72	1.86	324492.4	2.24	2.35	1.51	263627.8	99.4
333	4.05	4.22	1.0	173673.4	3.54	3.70	1.85	320440.0	2.24	2.36	1.51	262786.7	99.1
398	4.06	4.21	1.0	174802.4	3.55	3.70	1.84	322096.1	2.24	2.34	1.50	262549.3	99.9
459	4.07	4.21	1.0	172237.9	3.55	3.70	1.84	317275.6	2.24	2.35	1.50	258657.8	99.9
518	4.07	4.22	1.0	171481.0	3.55	3.71	1.84	315688.2	2.24	2.35	1.50	257702.8	99.8

Table 3.15: [Table S20]. Raw data of absolute kinetic of urethane synthesis with **3a** (3.0 mol%) in $CDCl_3$.

Time (min)	**Integ. Limits (ppm)**		**Integ**	**Absol.**	**Integ. Limits (ppm)**		**Integ**	**Absol.**	**Integ. Limits (ppm)**		**Integ**	**Absol.**	**$Conv_{exp}$ (%)**
VB180a	**Product**				**Educt**				**Product+Educt**				**$Conv_{exp}$**
8	4.09	4.19	1.0	12106.7	3.51	3.72	37.62	455470.7	2.24	2.37	21.05	254885.6	7.1
23	4.06	4.21	1.0	34660.7	3.53	3.72	12.42	430344.0	2.21	2.38	7.35	254677.0	20.4
44	4.06	4.20	1.0	61201.0	3.54	3.71	6.71	410922.0	2.23	2.37	4.23	258719.7	35.5
59	4.08	4.20	1.0	77216.4	3.53	3.72	5.23	403646.8	2.22	2.36	3.41	263495.9	44.0
70	4.08	4.20	1.0	86814.1	3.55	3.71	4.56	395843.8	2.22	2.38	3.06	265873.9	49.0
96	4.08	4.20	1.0	105104.0	3.54	3.71	3.57	374777.2	2.24	2.36	2.50	263257.0	59.9
127	4.06	4.21	1.0	121294.5	3.54	3.72	2.95	357899.8	2.24	2.36	2.16	261926.2	69.5
191	4.08	4.21	1.0	140897.3	3.54	3.72	2.37	333724.4	2.22	2.37	1.85	261289.1	80.9
246	4.06	4.20	1.0	155473.6	3.54	3.70	2.12	329236.5	2.22	2.36	1.72	267487.1	87.2

311	4.06	4.22	1.0	168453.1	3.54	3.71	1.96	330192.5	2.22	2.35	1.63	274495.2	92.1
375	4.07	4.21	1.0	174820.0	3.55	3.70	1.88	328765.2	2.24	2.35	1.58	276855.8	94.7
428	4.06	4.22	1.0	173903.6	3.54	3.72	1.84	320645.1	2.22	2.35	1.57	272185.2	95.8
490	4.06	4.23	1.0	175021.6	3.55	3.72	1.80	315648.3	2.22	2.35	1.54	269905.5	97.3
549	4.07	4.21	1.0	174387.5	3.54	3.73	1.80	313152.8	2.22	2.36	1.54	268564.2	97.4
610	4.08	4.21	1.0	173563.7	3.56	3.71	1.79	310251.8	2.22	2.35	1.54	266766.7	97.6
676	4.08	4.21	1.0	208267.6	3.56	3.71	1.78	371527.8	2.24	2.35	1.52	317593.6	98.4
737	4.07	4.22	1.0	198501.8	3.57	3.71	1.77	352000.2	2.23	2.36	1.53	303099.3	98.2
855	4.08	4.22	1.0	201673.4	3.55	3.71	1.77	357559.8	2.23	2.35	1.52	307452.2	98.4
VB180b	**Product**				**Educt**				**Product+Educt**				**$Conv_{exp}$**
8	4.10	4.19	1.0	10202.0	3.55	3.70	43.50	443824.4	2.24	2.37	23.32	237942.0	6.4
21	4.09	4.19	1.0	31387.3	3.56	3.69	14.21	445884.5	2.24	2.36	7.99	250754.4	18.8
31	4.07	4.21	1.0	45353.7	3.55	3.70	9.66	438069.9	2.23	2.36	5.60	254067.6	26.8
35	4.08	4.20	1.0	49194.4	3.55	3.71	8.85	435173.7	2.24	2.36	5.17	254116.6	29.0
56	4.08	4.20	1.0	46588.9	3.56	3.70	5.70	265557.5	2.22	2.37	3.53	164491.9	42.5
71	4.08	4.20	1.0	54869.3	3.57	3.70	4.71	258373.3	2.24	2.36	3.01	165081.9	49.9
97	4.08	4.21	1.0	67253.2	3.56	3.71	3.70	248698.5	2.24	2.36	2.47	166118.5	60.7
112	4.09	4.20	1.0	71585.6	3.55	3.71	3.37	241389.1	2.22	2.36	2.31	165109.7	65.0
148	4.07	4.21	1.0	127575.3	3.56	3.71	2.82	359489.7	2.23	2.36	2.01	256172.2	74.7
173	4.08	4.21	1.0	152312.3	3.54	3.72	2.60	396249.6	2.22	2.36	1.89	288615.0	79.2
211	4.08	4.21	1.0	144549.4	3.56	3.70	2.36	340705.2	2.22	2.36	1.78	256707.3	84.5
237	4.07	4.20	1.0	150186.8	3.54	3.71	2.25	337989.8	2.23	2.35	1.71	256934.8	87.7
270	4.09	4.20	1.0	152319.3	3.57	3.70	2.16	328817.8	2.22	2.36	1.67	254604.0	89.7
290	4.07	4.22	1.0	155610.2	3.55	3.71	2.10	327249.1	2.23	2.36	1.63	254297.4	91.8
320	4.07	4.21	1.0	157869.5	3.55	3.71	2.05	324154.9	2.22	2.37	1.61	254235.3	93.1
356	4.08	4.21	1.0	163634.7	3.55	3.71	2.00	328020.6	2.22	2.35	1.59	259391.6	94.6
415	4.08	4.21	1.0	179040.6	3.56	3.71	1.97	352363.3	2.22	2.36	1.56	278514.3	96.4
472	4.07	4.21	1.0	189082.0	3.55	3.71	1.93	364100.1	2.23	2.35	1.54	290916.0	97.5
533	4.07	4.22	1.0	163454.0	3.55	3.72	1.90	310119.0	2.23	2.35	1.52	248915.8	98.5
593	4.06	4.21	1.0	166964.1	3.58	3.71	1.87	312704.2	2.23	2.35	1.52	253385.2	98.8
655	4.07	4.21	1.0	165202.8	3.56	3.71	1.88	309988.3	2.23	2.35	1.51	250084.6	99.1
716	4.08	4.21	1.0	166852.0	3.55	3.71	1.88	312914.5	2.23	2.36	1.52	252851.0	99.0
777	4.09	4.21	1.0	165015.3	3.56	3.71	1.87	309295.2	2.22	2.36	1.52	250642.9	98.8
898	4.07	4.21	1.0	166530.3	3.55	3.70	1.87	310898.4	2.23	2.36	1.51	251766.7	99.2
1019	4.09	4.20	1.0	111250.7	3.56	3.70	1.87	207821.0	2.23	2.35	1.51	168346.4	99.1

Table 3.16: [Table S21]. Raw data of absolute kinetic of urethane synthesis with **3b** (3.0 mol%) in $CDCl_3$.

Time (min)	Integ. Limits (ppm)		Integ	Absol.	Integ. Limits (ppm)		Integ	Absol.	Integ. Limits (ppm)		Integ	Absol.	$Conv_{exp}$ (%)
VB181a	**Product**				**Educt**				**Product+Educt**				**$Conv_{exp}$**
10	4.09	4.19	1.0	22448.5	3.55	3.69	24.33	546069.3	2.23	2.35	13.25	297484.3	11.3
19	4.09	4.19	1.0	42333.5	3.55	3.70	12.49	528830.4	2.23	2.37	7.07	299283.2	21.2
31	4.08	4.20	1.0	62820.1	3.55	3.70	8.13	510560.6	2.22	2.37	4.79	300876.9	31.3
46	4.08	4.20	1.0	86236.3	3.55	3.71	5.68	490049.6	2.22	2.36	3.51	302259.1	42.8
61	4.06	4.20	1.0	104143.7	3.56	3.71	4.54	472966.0	2.22	2.37	2.91	303300.2	51.5
78	4.09	4.20	1.0	70978.8	3.55	3.71	3.80	269475.2	2.23	2.36	2.52	179064.3	59.5
99	4.08	4.21	1.0	80825.3	3.56	3.70	3.24	261786.2	2.22	2.36	2.23	180470.6	67.2
133	4.08	4.20	1.0	90538.9	3.55	3.70	2.71	245261.7	2.23	2.36	1.95	176774.5	76.8
161	4.07	4.21	1.0	98101.9	3.56	3.70	2.47	241854.5	2.23	2.36	1.83	179056.8	82.2
192	4.07	4.22	1.0	104311.6	3.55	3.70	2.29	238487.5	2.23	2.35	1.73	180480.5	86.7
225	4.08	4.21	1.0	108755.7	3.55	3.70	2.16	235182.8	2.21	2.36	1.67	181717.2	89.8
253	4.07	4.21	1.0	111600.7	3.56	3.71	2.09	233003.4	2.22	2.36	1.63	182073.9	91.9
281	4.07	4.21	1.0	113808.2	3.56	3.70	2.03	231558.6	2.23	2.35	1.60	182103.9	93.7
312	4.06	4.22	1.0	113997.5	3.55	3.71	1.99	226852.6	2.22	2.35	1.58	179580.2	95.2
377	4.07	4.23	1.0	116117.7	3.56	3.70	1.94	224689.5	2.23	2.36	1.55	179839.1	96.9
438	4.08	4.21	1.0	117570.3	3.55	3.70	1.92	225247.5	2.23	2.34	1.54	180721.1	97.6
498	4.07	4.20	1.0	114485.8	3.56	3.70	1.90	218083.3	2.23	2.35	1.53	175251.6	98.0
553	4.07	4.21	1.0	114461.0	3.56	3.70	1.89	216567.8	2.22	2.36	1.53	174887.5	98.2
615	4.07	4.21	1.0	115384.7	3.56	3.70	1.89	217794.2	2.22	2.35	1.52	175794.7	98.5
675	4.06	4.22	1.0	114030.0	3.56	3.71	1.88	214640.1	2.22	2.35	1.52	172944.6	98.9
VB181b	**Product**				**Educt**				**Product+Educt**				**$Conv_{exp}$**
7	4.09	4.19	1.0	13710.0	3.56	3.71	34.08	467245.9	2.24	2.37	19.65	269351.0	7.6
23	4.09	4.20	1.0	41798.3	3.55	3.71	10.55	440800.3	2.25	2.36	6.44	269355.0	23.3
43	4.09	4.20	1.0	46273.2	3.53	3.71	5.88	271873.6	2.23	2.36	3.85	177993.9	39.0
58	4.09	4.19	1.0	87975.9	3.56	3.69	4.59	403953.5	2.22	2.37	3.14	276296.3	47.8
79	4.08	4.20	1.0	106883.8	3.55	3.71	3.60	384683.5	2.23	2.36	2.57	275093.8	58.3
108	4.08	4.20	1.0	123349.0	3.57	3.71	2.88	355121.5	2.23	2.36	2.17	268172.1	69.0
139	4.07	4.22	1.0	138162.9	3.55	3.71	2.47	341350.7	2.23	2.36	1.94	268601.5	77.2
167	4.08	4.20	1.0	146150.0	3.56	3.70	2.25	328996.5	2.22	2.36	1.83	266786.6	82.2
195	4.07	4.21	1.0	155650.7	3.57	3.71	2.09	324777.0	2.23	2.36	1.73	269502.7	86.6
215	4.07	4.21	1.0	160956.8	3.56	3.71	2.02	324641.0	2.22	2.37	1.70	272898.2	88.5
257	4.08	4.21	1.0	164760.7	3.56	3.71	1.91	314618.1	2.22	2.36	1.63	269276.9	91.8
275	4.07	4.21	1.0	165753.8	3.56	3.71	1.88	311138.6	2.22	2.36	1.62	267854.9	92.8
318	4.08	4.22	1.0	199454.8	3.55	3.70	1.82	362315.5	2.23	2.35	1.58	315214.5	94.9

379	4.07	4.21	1.0	171945.1	3.56	3.71	1.76	303430.8	2.22	2.36	1.55	267060.1	96.6
441	4.08	4.20	1.0	202047.0	3.54	3.70	1.74	352121.4	2.22	2.37	1.54	311594.4	97.3
502	4.07	4.20	1.0	202205.8	3.55	3.71	1.73	349564.1	2.20	2.35	1.53	310244.9	97.8
579	4.07	4.21	1.0	204730.1	3.55	3.71	1.71	350597.1	2.22	2.35	1.52	311548.7	98.6
624	4.06	4.21	1.0	203172.8	3.56	3.71	1.71	347389.4	2.21	2.36	1.52	309359.7	98.5
684	4.06	4.22	1.0	202490.7	3.56	3.71	1.71	345301.6	2.22	2.36	1.52	307293.7	98.8
746	4.07	4.21	1.0	203387.3	3.56	3.71	1.71	346977.5	2.22	2.35	1.52	308443.1	98.9

The absolute kinetics of the urethane reaction were done with 6.0 mol% catalyst. The results are summarized in Table 3.17.

Table 3.17: [Table S22]. List of k_{eff} values obtained for the urethane synthesis (6.0 mol%).

Catalyst	Run	Yield [%]	k_{eff}	Average k_{eff}
3a	1	99	1.17×10^{-3}	$1.20 \times 10^{-3} \pm 2.19 \times 10^{-5}$
	2	99	1.22×10^{-3}	
3b	1	99	1.25×10^{-3}	$1.27 \times 10^{-3} \pm 1.61 \times 10^{-5}$
	2	99	1.29×10^{-3}	
5a	1	94	2.78×10^{-3}	$2.90 \times 10^{-3} \pm 1.20 \times 10^{-4}$
	2	94	3.02×10^{-3}	
6a	1	99	2.62×10^{-3}	$2.58 \times 10^{-3} \pm 4.34 \times 10^{-5}$
	2	99	2.53×10^{-3}	

The raw data of absolute kinetics with 6.0 mol% catalyst are summarized in Table 3.18 to Table 3.21.

Table 3.18: [Table S23]. Raw data of absolute kinetic of urethane synthesis with **5a** (6.0 mol%) in $CDCl_3$.

Time (min)	Integ. Limits (ppm)		Integ	Absol.	Integ. Limits (ppm)		Integ	Absol.	Integ. Limits (ppm)		Integ	Absol.	$Conv_{exp}$ (%)
VB148a	**Product**				**Educt**				**Product+Educt**				$Conv_{exp}$
8	4.09	4.18	1.0	29185.0	3.56	3.69	9.30	271306.7	2.24	2.35	5.69	166208.1	26.3
10	4.09	4.18	1.0	59227.1	3.56	3.71	6.98	413205.8	2.24	2.36	4.40	260880.1	34.1
12	4.08	4.19	1.0	71187.4	3.54	3.70	5.66	402809.9	2.23	2.37	3.68	262096.6	40.7
17	4.09	4.19	1.0	58203.6	3.55	3.69	4.25	247297.0	2.23	2.35	2.89	168302.2	51.9
22	4.08	4.19	1.0	69779.6	3.56	3.68	3.41	238296.2	2.23	2.35	2.43	169707.5	61.7
27	4.08	4.20	1.0	78221.0	3.55	3.70	2.96	231383.6	2.23	2.35	2.17	169958.2	69.0
45	4.07	4.20	1.0	148303.5	3.56	3.70	2.23	330735.0	2.24	2.35	1.76	261273.4	85.1
49	4.07	4.20	1.0	150486.5	3.55	3.70	2.18	328273.0	2.23	2.34	1.73	261053.3	86.5
57	4.07	4.21	1.0	155900.6	3.56	3.69	2.08	324180.4	2.24	2.35	1.68	261781.6	89.3
67	4.06	4.20	1.0	160640.7	3.56	3.69	2.01	322507.9	2.24	2.34	1.64	263201.6	91.6

87	4.07	4.21	1.0	163389.5	3.55	3.69	1.95	317842.8	2.24	2.35	1.60	261982.7	93.5
97	4.07	4.21	1.0	164771.4	3.56	3.69	1.93	317761.2	2.24	2.35	1.60	263296.9	93.9
114	4.07	4.20	1.0	164387.3	3.56	3.70	1.93	316867.2	2.23	2.35	1.60	263070.8	93.7
137	4.06	4.22	1.0	166393.9	3.55	3.70	1.91	318151.6	2.23	2.35	1.59	264277.0	94.4
205	4.07	4.20	1.0	166060.0	3.54	3.69	1.92	318604.0	2.23	2.35	1.60	264971.5	94.0
232	4.07	4.20	1.0	165119.6	3.57	3.69	1.92	316459.3	2.24	2.34	1.59	261878.0	94.6
259	4.08	4.20	1.0	165620.4	3.55	3.70	1.92	317924.4	2.24	2.34	1.59	263065.6	94.4
292	4.08	4.20	1.0	165821.4	3.56	3.70	1.92	318132.1	2.24	2.34	1.59	263490.2	94.4
VB148b	**Product**				**Educt**				**Product+Educt**				**$Conv_{exp}$**
8	4.08	4.19	1.0	47747.8	3.56	3.70	8.68	414514.0	2.25	2.37	5.43	259419.5	27.6
19	4.07	4.20	1.0	103050.3	3.56	3.69	3.59	369901.9	2.25	2.35	2.56	263556.5	58.6
22	4.07	4.20	1.0	110270.1	3.56	3.69	3.30	363801.4	2.25	2.35	2.39	264007.5	62.7
24	4.09	4.19	1.0	115854.2	3.57	3.70	3.09	358255.6	2.24	2.35	2.28	264336.0	65.7
26	4.07	4.20	1.0	121937.8	3.57	3.69	2.90	353083.0	2.23	2.35	2.17	264921.5	69.0
36	4.08	4.20	1.0	139135.3	3.56	3.70	2.42	336126.5	2.23	2.35	1.90	263977.5	79.1
38	4.07	4.20	1.0	142251.9	3.58	3.69	2.34	332825.0	2.24	2.35	1.85	263857.6	80.9
48	4.08	4.20	1.0	152991.0	3.56	3.70	2.15	328785.7	2.23	2.35	1.75	267110.8	85.9
63	4.07	4.20	1.0	159359.0	3.56	3.69	1.99	317805.2	2.24	2.34	1.65	263423.6	90.7
73	4.07	4.20	1.0	162087.7	3.57	3.69	1.94	315235.1	2.24	2.34	1.62	263239.7	92.4
88	4.08	4.20	1.0	164490.2	3.57	3.69	1.91	314633.4	2.25	2.35	1.61	264561.5	93.3
98	4.08	4.20	1.0	165074.1	3.57	3.69	1.90	313714.9	2.23	2.33	1.60	264202.9	93.7
131	4.08	4.20	1.0	166136.5	3.57	3.69	1.88	313109.0	2.24	2.33	1.59	264379.8	94.3
161	4.09	4.20	1.0	167512.0	3.57	3.69	1.89	316039.8	2.25	2.33	1.59	266051.2	94.4
190	4.09	4.19	1.0	167308.2	3.55	3.68	1.89	315590.2	2.24	2.33	1.59	266756.4	94.1
221	4.06	4.20	1.0	168539.3	3.56	3.69	1.87	315961.5	2.25	2.33	1.58	266660.7	94.8
277	4.08	4.19	1.0	166523.6	3.56	3.69	1.89	313924.4	2.24	2.33	1.59	264813.4	94.3
339	4.06	4.20	1.0	166788.4	3.56	3.70	1.88	313455.6	2.23	2.35	1.59	265520.8	94.2
404	4.07	4.20	1.0	165905.3	3.57	3.70	1.88	311843.9	2.23	2.34	1.59	263533.8	94.4
464	4.08	4.20	1.0	167065.1	3.56	3.70	1.88	314615.3	2.23	2.35	1.60	266675.3	94.0
582	4.08	4.20	1.0	166197.5	3.55	3.69	1.88	313076.0	2.22	2.33	1.59	265011.1	94.1
703	4.08	4.20	1.0	166849.9	3.57	3.69	1.88	313756.0	2.24	2.34	1.59	265064.7	94.4

Table 3.19: [Table S24]. Raw data of absolute kinetic of urethane synthesis with **6a** (6.0 mol%) in $CDCl_3$.

Time (min)	**Integ. Limits (ppm)**		**Integ**	**Absol.**	**Integ. Limits (ppm)**		**Integ**	**Absol.**	**Integ. Limits (ppm)**		**Integ**	**Absol.**	**$Conv_{exp}$ (%)**
VB149b	**Product**				**Educt**				**Product+Educt**				**$Conv_{exp}$**
8	4.10	4.18	1.0	42807.5	3.53	3.70	9.45	404583.4	2.24	2.35	5.56	238155.5	27.0

11	4.08	4.19	1.0	54341.0	3.56	3.69	7.25	394059.7	2.24	2.36	4.40	238883.1	34.1
20	4.08	4.19	1.0	90368.1	3.55	3.70	4.00	361602.8	2.23	2.37	2.66	240357.1	56.4
23	4.07	4.20	1.0	96708.7	3.55	3.71	3.69	356485.2	2.24	2.37	2.49	240666.5	60.3
25	4.08	4.21	1.0	102716.9	3.56	3.70	3.42	351085.0	2.21	2.36	2.36	242262.4	63.6
36	4.08	4.20	1.0	123801.3	3.55	3.70	2.69	332410.3	2.24	2.36	1.95	241698.4	76.8
38	4.07	4.20	1.0	149671.3	3.55	3.70	2.59	387700.9	2.24	2.36	1.90	284964.1	78.8
49	4.07	4.20	1.0	139718.0	3.56	3.70	2.30	320853.3	2.24	2.36	1.75	244059.1	85.9
51	4.08	4.20	1.0	141802.0	3.56	3.70	2.25	319471.4	2.23	2.36	1.73	244888.7	86.9
54	4.07	4.21	1.0	144471.4	3.56	3.70	2.20	317838.5	2.23	2.35	1.70	244889.4	88.5
68	4.07	4.20	1.0	152312.1	3.56	3.71	2.04	309962.6	2.24	2.35	1.60	244227.6	93.5
78	4.07	4.20	1.0	155162.5	3.57	3.70	1.97	305499.3	2.25	2.34	1.56	242781.7	95.9
93	4.08	4.20	1.0	157954.3	3.56	3.70	1.91	302330.6	2.24	2.34	1.54	243087.0	97.5
95	4.07	4.21	1.0	186571.0	3.57	3.69	1.90	354687.5	2.24	2.34	1.53	285760.7	97.9
111	4.07	4.20	1.0	161009.5	3.57	3.69	1.87	300984.5	2.24	2.34	1.52	243932.6	99.0
132	4.07	4.20	1.0	161771.6	3.56	3.69	1.85	299937.3	2.25	2.34	1.50	243285.0	99.7
160	4.07	4.20	1.0	164362.5	3.56	3.69	1.84	302820.0	2.24	2.33	1.50	246339.4	100.1
187	4.07	4.20	1.0	164685.3	3.56	3.70	1.84	302388.8	2.25	2.34	1.49	245888.3	100.5
245	4.08	4.20	1.0	163030.5	3.56	3.70	1.84	299643.5	2.24	2.34	1.50	244430.7	100.0
VB149c	**Product**				**Educt**				**Product+Educt**				**$Conv_{exp}$**
10	4.08	4.19	1.0	46050.9	3.55	3.70	8.88	408956.5	2.25	2.36	5.25	241937.7	28.6
21	4.09	4.19	1.0	91277.2	3.57	3.69	4.09	373301.4	2.23	2.35	2.70	246878.5	55.5
23	4.09	4.19	1.0	97854.8	3.57	3.69	3.76	367793.0	2.25	2.35	2.52	246782.4	59.5
25	4.08	4.19	1.0	103814.3	3.56	3.69	3.49	362742.3	2.23	2.35	2.39	247833.5	62.8
27	4.09	4.19	1.0	108987.2	3.56	3.70	3.29	358586.2	2.24	2.35	2.27	247795.3	66.0
38	4.08	4.19	1.0	129136.3	3.57	3.69	2.64	341432.5	2.25	2.35	1.93	249602.9	77.6
48	4.02	4.13	1.0	143426.4	3.51	3.63	2.35	336603.8	2.18	2.29	1.77	254406.5	84.6
50	4.08	4.19	1.0	145282.3	3.58	3.69	2.30	334284.8	2.24	2.34	1.75	253867.0	85.8
57	4.09	4.20	1.0	151155.3	3.58	3.69	2.18	329770.6	2.24	2.34	1.68	254399.9	89.1
74	4.07	4.20	1.0	160457.2	3.57	3.69	2.00	320635.5	2.26	2.33	1.57	252526.9	95.3
90	4.06	4.20	1.0	164379.9	3.57	3.69	1.92	316103.9	2.24	2.33	1.54	252808.0	97.5
108	4.07	4.20	1.0	160969.2	3.57	3.69	1.88	303151.4	2.26	2.33	1.51	242862.9	99.4
117	4.07	4.20	1.0	161798.8	3.57	3.69	1.87	302581.1	2.25	2.33	1.51	243921.6	99.5
158	4.08	4.20	1.0	163303.9	3.58	3.69	1.85	301648.9	2.25	2.33	1.50	244479.4	100.2
177	4.08	4.20	1.0	163460.0	3.57	3.70	1.85	301688.8	2.24	2.33	1.50	245247.6	100.0
210	4.08	4.20	1.0	163795.1	3.56	3.69	1.84	301684.9	2.25	2.33	1.49	244616.0	100.4
240	4.09	4.19	1.0	163494.8	3.58	3.69	1.84	301356.7	2.25	2.33	1.50	244846.4	100.2
299	4.06	4.20	1.0	163912.3	3.56	3.69	1.84	301021.6	2.25	2.33	1.49	244513.7	100.6
363	4.08	4.20	1.0	163587.4	3.58	3.70	1.84	301007.6	2.24	2.33	1.50	244717.4	100.3

425	4.07	4.20	1.0	163892.2	3.58	3.69	1.84	301066.0	2.24	2.33	1.49	244930.8	100.4

Table 3.20: [Table S25]. Raw data of absolute kinetic of urethane synthesis with **3a** (6.0 mol%) in $CDCl_3$.

Time (min)	Integ. Limits (ppm)		Integ	Absol.	Integ. Limits (ppm)		Integ	Absol.	Integ. Limits (ppm)		Integ	Absol.	$Conv_{exp}$ (%)
VB150b	**Product**				**Educt**				**Product+Educt**				**$Conv_{exp}$**
7	4.10	4.18	1.0	16975.7	3.57	3.69	23.60	400550.1	2.26	2.35	12.88	218569.1	11.7
9	4.10	4.18	1.0	22743.8	3.56	3.70	17.41	395871.3	2.25	2.36	9.65	219396.1	15.5
14	4.10	4.18	1.0	33728.6	3.57	3.69	11.42	385024.3	2.25	2.36	6.52	219916.2	23.0
19	4.09	4.19	1.0	44866.6	3.56	3.70	8.41	377201.5	2.25	2.36	4.93	221260.3	30.4
24	4.09	4.19	1.0	55034.5	3.57	3.69	6.72	369620.8	2.24	2.36	4.06	223499.5	36.9
29	4.10	4.19	1.0	63898.5	3.56	3.70	5.69	363632.9	2.25	2.35	3.51	224263.4	42.7
34	4.09	4.19	1.0	72009.0	3.56	3.70	4.97	357675.4	2.24	2.36	3.14	226364.2	47.7
51	4.10	4.19	1.0	90964.2	3.56	3.70	3.64	331436.5	2.23	2.35	2.45	222920.0	61.2
60	4.07	4.20	1.0	100193.8	3.56	3.69	3.21	321730.0	2.23	2.35	2.22	222283.8	67.6
64	4.10	4.20	1.0	102327.1	3.56	3.70	3.12	318812.4	2.23	2.37	2.17	222471.7	69.0
84	4.07	4.20	1.0	120684.9	3.55	3.71	2.63	317398.6	2.23	2.35	1.91	230951.6	78.4
112	4.09	4.20	1.0	124247.3	3.57	3.70	2.31	286982.0	2.25	2.35	1.73	215539.6	86.5
141	4.08	4.20	1.0	143192.5	3.57	3.69	2.11	302664.9	2.25	2.35	1.63	233950.3	91.8
172	4.08	4.20	1.0	144498.7	3.56	3.70	2.01	290303.5	2.24	2.35	1.58	228917.6	94.7
205	4.09	4.20	1.0	147750.5	3.57	3.71	1.95	288467.7	2.24	2.35	1.56	230195.8	96.3
235	4.08	4.20	1.0	154688.5	3.57	3.70	1.91	295719.1	2.23	2.35	1.54	238367.9	97.3
359	4.09	4.20	1.0	167525.7	3.56	3.70	1.87	313036.4	2.24	2.34	1.51	253762.2	99.0
420	4.08	4.20	1.0	167099.2	3.56	3.70	1.86	310884.2	2.24	2.33	1.51	251979.5	99.5
482	4.08	4.20	1.0	166607.4	3.56	3.70	1.86	309469.7	2.23	2.33	1.51	251046.4	99.5
533	4.08	4.20	1.0	164303.9	3.57	3.70	1.86	305123.5	2.23	2.33	1.51	247375.5	99.6
599	4.07	4.20	1.0	170235.8	3.57	3.69	1.85	315358.7	2.23	2.34	1.51	256223.6	99.7
659	4.08	4.20	1.0	165639.7	3.57	3.69	1.86	307591.4	2.22	2.34	1.51	250266.8	99.3
VB150c	**Product**				**Educt**				**Product+Educt**				**$Conv_{exp}$**
6	4.09	4.18	1.0	20151.8	3.53	3.73	24.3	490320.0	2.24	2.37	13.56	273187.3	11.1
16	4.08	4.19	1.0	49860.8	3.55	3.72	9.31	464309.3	2.24	2.37	5.55	276667.0	27.0
18	4.09	4.19	1.0	55754.9	3.54	3.72	8.24	459227.5	2.23	2.38	4.97	277283.7	30.2
20	4.08	4.20	1.0	61729.0	3.56	3.72	7.35	453735.4	2.22	2.39	4.51	278519.4	33.2
30	4.09	4.20	1.0	84272.2	3.55	3.71	5.14	433369.2	2.24	2.36	3.30	278341.5	45.4
33	4.08	4.19	1.0	88920.2	3.54	3.69	4.82	428764.2	2.22	2.35	3.14	279331.4	47.7
35	4.09	4.20	1.0	92922.6	3.55	3.71	4.57	424963.8	2.23	2.38	3.01	280085.7	49.8
41	4.08	4.20	1.0	102791.3	3.56	3.70	4.04	415188.2	2.22	2.37	2.73	280363.1	55.0

53	4.08	4.20	1.0	120675.6	3.57	3.70	3.33	401345.5	2.24	2.36	2.34	281894.8	64.2
64	4.08	4.20	1.0	115425.7	3.56	3.70	2.94	339027.1	2.23	2.36	2.13	245928.0	70.4
84	4.09	4.20	1.0	151515.1	3.57	3.70	2.50	379055.4	2.21	2.36	1.90	287791.9	79.0
94	4.08	4.21	1.0	157817.5	3.56	3.70	2.37	373773.0	2.23	2.36	1.83	288156.3	82.2
126	4.08	4.21	1.0	167218.9	3.55	3.70	2.11	352184.0	2.24	2.35	1.67	280062.2	89.6
157	4.09	4.20	1.0	176820.4	3.57	3.70	1.97	348924.7	2.23	2.35	1.61	284733.3	93.2
188	4.09	4.20	1.0	181696.9	3.57	3.70	1.90	344527.2	2.24	2.36	1.57	284948.4	95.6
220	4.09	4.20	1.0	160988.9	3.57	3.69	1.85	297860.2	2.23	2.35	1.55	248820.9	97.1
289	4.08	4.20	1.0	185655.0	3.57	3.71	1.81	336780.2	2.22	2.35	1.53	283602.1	98.2
334	4.08	4.20	1.0	175196.0	3.56	3.70	1.81	317013.2	2.24	2.34	1.51	264951.1	99.2
394	4.08	4.20	1.0	161682.9	3.57	3.70	1.80	290507.4	2.22	2.35	1.52	245212.9	98.9
454	4.07	4.21	1.0	190082.3	3.54	3.71	1.79	340744.2	2.20	2.34	1.51	287011.4	99.3
514	4.07	4.21	1.0	190528.2	3.57	3.70	1.79	340183.4	2.23	2.36	1.51	287437.7	99.4
576	4.08	4.20	1.0	188852.2	3.57	3.70	1.79	338501.1	2.25	2.34	1.50	283272.4	100.0
644	4.06	4.21	1.0	187939.8	3.57	3.70	1.79	336237.9	2.21	2.35	1.51	283847.0	99.3
705	4.07	4.20	1.0	187200.9	3.56	3.70	1.79	335462.7	2.23	2.35	1.51	282801.5	99.3

Table 3.21: [Table S26]. Raw data of absolute kinetic of urethane synthesis with **3b** (6.0 mol%) in $CDCl_3$.

Time (min)	**Integ. Limits (ppm)**		**Integ**	**Absol.**	**Integ. Limits (ppm)**		**Integ**	**Absol.**	**Integ. Limits (ppm)**		**Integ**	**Absol.**	**$Conv_{exp}$ (%)**
VB151a	**Product**				**Educt**				**Product+Educt**				**$Conv_{exp}$**
7	4.09	4.19	1.0	19017.1	3.55	3.71	23.2	440423.3	2.24	2.36	12.78	243094.3	11.7
9	4.10	4.19	1.0	24022.1	3.55	3.69	18.0	431570.6	2.25	2.36	10.04	241240.6	14.9
12	4.09	4.20	1.0	33803.6	3.54	3.70	12.7	429442.2	2.25	2.36	7.25	245108.3	20.7
17	4.10	4.19	1.0	47243.6	3.56	3.70	8.87	418899.0	2.24	2.37	5.23	247242.9	28.7
27	4.09	4.20	1.0	69016.2	3.56	3.69	5.63	388310.4	2.23	2.36	3.52	243095.8	42.6
29	4.09	4.20	1.0	73232.3	3.56	3.69	5.25	384158.3	2.22	2.37	3.32	243435.6	45.1
32	4.09	4.20	1.0	77101.1	3.57	3.70	4.93	380001.7	2.23	2.36	3.15	242873.2	47.6
42	4.08	4.20	1.0	93920.6	3.55	3.71	3.94	369804.8	2.23	2.37	2.62	246325.2	57.2
52	4.07	4.21	1.0	107040.0	3.56	3.70	3.35	358868.4	2.24	2.37	2.31	247545.6	64.9
54	4.06	4.20	1.0	109431.2	3.55	3.70	3.26	356332.1	2.23	2.35	2.26	247487.5	66.3
62	4.08	4.20	1.0	116738.5	3.56	3.70	2.99	348945.6	2.23	2.35	2.12	247488.2	70.8
72	4.09	4.19	1.0	124082.7	3.54	3.70	2.75	341564.1	2.24	2.36	2.00	247661.1	75.2
87	4.08	4.20	1.0	133953.4	3.56	3.69	2.47	331507.8	2.23	2.35	1.85	247975.8	81.0
102	4.08	4.21	1.0	142432.0	3.56	3.71	2.30	326884.5	2.23	2.36	1.75	249895.3	85.5
134	4.08	4.20	1.0	151650.9	3.55	3.70	2.08	315627.5	2.24	2.35	1.64	248030.3	91.7
195	4.09	4.20	1.0	158526.6	3.57	3.70	1.93	305635.0	2.24	2.34	1.55	246447.5	96.5
222	4.09	4.20	1.0	160994.2	3.55	3.70	1.90	305233.5	2.23	2.35	1.54	248598.5	97.1

257	4.08	4.19	1.0	161266.4	3.57	3.70	1.87	301507.2	2.22	2.35	1.53	246917.1	98.0
282	4.08	4.20	1.0	160862.1	3.57	3.70	1.86	298989.3	2.23	2.35	1.52	244876.0	98.5
346	4.08	4.21	1.0	166365.8	3.55	3.70	1.84	306246.5	2.22	2.34	1.51	251547.2	99.2
407	4.07	4.20	1.0	165204.2	3.57	3.70	1.84	303574.8	2.21	2.35	1.51	250220.0	99.0
467	4.08	4.20	1.0	160596.4	3.56	3.70	1.85	296374.0	2.22	2.35	1.52	243735.0	98.8
528	4.07	4.21	1.0	160677.1	3.56	3.70	1.84	295400.3	2.22	2.34	1.51	242429.7	99.4
590	4.09	4.20	1.0	160363.1	3.57	3.70	1.84	295591.3	2.22	2.35	1.52	243093.3	99.0
651	4.07	4.20	1.0	160307.5	3.56	3.70	1.84	294893.4	2.22	2.34	1.51	241933.9	99.4
711	4.09	4.20	1.0	158890.1	3.56	3.70	1.84	293066.7	2.22	2.34	1.51	240611.7	99.1
VB151b	**Product**				**Educt**				**Product+Educt**				**$Conv_{exp}$**
11	4.10	4.18	1.0	31178.5	3.55	3.70	13.1	408195.5	2.24	2.36	7.61	237358.2	19.7
13	4.09	4.19	1.0	44174.4	3.56	3.70	10.7	474147.3	2.24	2.36	6.34	279939.4	23.7
21	4.08	4.20	1.0	55885.2	3.54	3.72	6.91	386346.9	2.25	2.37	4.25	237719.6	35.3
31	4.09	4.19	1.0	75614.9	3.57	3.69	4.87	368239.3	2.25	2.35	3.17	239833.4	47.3
40	4.10	4.19	1.0	90430.9	3.56	3.70	3.94	356417.2	2.24	2.35	2.68	242127.6	56.0
43	4.08	4.19	1.0	110242.7	3.57	3.70	3.77	416012.7	2.24	2.35	2.58	284826.3	58.1
45	4.10	4.19	1.0	113582.7	3.58	3.70	3.63	412456.2	2.25	2.35	2.50	283932.8	60.0
47	4.09	4.19	1.0	116688.9	3.57	3.70	3.51	409807.6	2.25	2.35	2.43	283756.2	61.7
63	4.09	4.19	1.0	118778.9	3.58	3.69	2.87	341373.1	2.25	2.35	2.09	248578.6	71.7
65	4.08	4.20	1.0	121231.5	3.57	3.70	2.81	340961.2	2.25	2.35	2.06	249661.6	72.8
80	4.09	4.19	1.0	132074.7	3.57	3.69	2.50	330434.3	2.24	2.34	1.90	250501.5	79.1
112	4.08	4.20	1.0	141949.4	3.57	3.70	2.15	304524.6	2.24	2.35	1.71	242487.1	87.8
122	4.09	4.20	1.0	145845.5	3.58	3.70	2.08	303274.5	2.24	2.35	1.67	243647.6	89.8
132	4.09	4.20	1.0	148250.9	3.57	3.70	2.03	300307.1	2.24	2.35	1.64	243691.2	91.3
147	4.03	4.14	1.0	152969.4	3.51	3.63	1.97	301299.2	2.16	2.28	1.62	247463.7	92.7
177	4.09	4.21	1.0	162094.9	3.57	3.70	1.89	305911.0	2.22	2.35	1.57	255100.8	95.3
201	4.09	4.20	1.0	164280.0	3.57	3.70	1.85	304229.9	2.24	2.34	1.55	254778.2	96.7
237	4.08	4.21	1.0	163332.8	3.57	3.70	1.81	296299.2	2.23	2.34	1.53	249844.7	98.1
263	4.08	4.20	1.0	163736.6	3.57	3.69	1.80	294760.7	2.23	2.34	1.52	249435.8	98.5
296	4.08	4.19	1.0	163723.4	3.57	3.69	1.79	293616.9	2.23	2.33	1.52	248622.2	98.8
357	4.08	4.19	1.0	164008.4	3.57	3.69	1.79	292938.3	2.23	2.34	1.52	248779.3	98.9
419	4.08	4.20	1.0	163654.8	3.58	3.69	1.78	291186.5	2.24	2.33	1.51	246346.5	99.6
487	4.09	4.19	1.0	190682.2	3.57	3.69	1.79	340553.9	2.22	2.34	1.52	289407.1	98.8
548	4.10	4.20	1.0	190691.0	3.58	3.70	1.78	340099.0	2.24	2.33	1.51	287927.7	99.3
599	4.09	4.20	1.0	189898.1	3.58	3.69	1.78	338163.2	2.24	2.33	1.51	286409.2	99.5
665	4.08	4.20	1.0	180069.0	3.58	3.69	1.79	321510.8	2.24	2.33	1.51	271479.6	99.5

The absolute kinetics of the urethane reaction were done with 1.0 mol% catalyst. The results are summarized in Table 3.22.

Table 3.22: [Table S27]. List of k_{eff} values obtained for the urethane synthesis (1.0 mol%).

Catalyst	Run	Yield [%]	k_{eff}	Average k_{eff}
3a	1	99	2.23×10^{-4}	$2.26 \times 10^{-4} \pm 3.67 \times 10^{-6}$
	2	99	2.30×10^{-4}	
3b	1	99	2.43×10^{-4}	$2.45 \times 10^{-4} \pm 1.86 \times 10^{-6}$
	2	99	2.47×10^{-4}	
5a	1	97	5.26×10^{-4}	$5.28 \times 10^{-4} \pm 1.95 \times 10^{-6}$
	2	98	5.30×10^{-4}	
6a	1	98	4.33×10^{-4}	$4.30 \times 10^{-4} \pm 3.14 \times 10^{-6}$
	2	98	4.27×10^{-4}	

The raw data of absolute kinetics with 1.0 mol% catalyst is summarized in Table 3.23 to Table 3.26.

Table 3.23: [Table S28]. Raw data of absolute kinetic of urethane synthesis with **5a** (1.0 mol%) in $CDCl_3$.

Time (min)	Integ. Limits (ppm)		Integ	Absol.	Integ. Limits (ppm)		Integ	Absol.	Integ. Limits (ppm)		Integ	Absol.	$Conv_{exp}$ (%)
VB229a	**Product**				**Educt**				**Product+Educt**				**$Conv_{exp}$**
6	4.11	4.19	1.0	9517.4	3.53	3.70	40.8	388705.2	2.22	2.38	23.1	220155.6	6.5
8	4.09	4.20	1.0	12138.0	3.53	3.71	31.9	386786.2	2.23	2.38	18.1	220157.0	8.3
15	4.08	4.19	1.0	19520.3	3.52	3.71	19.5	381095.0	2.22	2.38	11.3	221394.3	13.2
25	4.09	4.19	1.0	29774.7	3.54	3.71	12.5	372002.5	2.24	2.37	7.45	221700.4	20.1
35	4.09	4.20	1.0	39190.5	3.54	3.71	9.28	363859.8	2.24	2.36	5.67	222336.4	26.4
55	4.08	4.20	1.0	57560.0	3.56	3.71	6.18	355654.7	2.22	2.37	3.98	228934.0	37.7
68	4.08	4.20	1.0	67136.0	3.54	3.71	5.20	348930.4	2.20	2.38	3.44	230729.4	43.6
99	4.08	4.20	1.0	84246.7	3.57	3.70	3.83	322627.6	2.24	2.37	2.67	225086.0	56.1
127	4.09	4.20	1.0	96337.5	3.54	3.70	3.26	313659.6	2.22	2.35	2.35	226711.4	63.7
191	4.06	4.20	1.0	117625.6	3.56	3.70	2.51	295219.5	2.23	2.36	1.94	228307.4	77.3
259	4.08	4.22	1.0	130258.4	3.56	3.69	2.18	283687.6	2.21	2.35	1.76	229818.7	85.0
319	4.08	4.21	1.0	135787.0	3.57	3.71	2.03	275873.0	2.22	2.37	1.68	228165.2	89.3
373	4.07	4.22	1.0	143944.6	3.53	3.70	1.95	280740.1	2.21	2.35	1.63	235150.3	91.8
434	4.05	4.23	1.0	147826.5	3.55	3.71	1.89	279116.4	2.22	2.35	1.60	236226.5	93.9
495	4.01	4.16	1.0	192545.2	3.49	3.64	1.85	356939.0	2.16	2.29	1.58	304056.9	95.0
557	4.06	4.21	1.0	191386.1	3.55	3.71	1.83	350576.0	2.22	2.35	1.57	300045.9	95.7
617	4.06	4.22	1.0	192679.0	3.55	3.71	1.82	350758.9	2.21	2.35	1.56	301332.9	95.9
679	4.07	4.22	1.0	187290.9	3.56	3.70	1.82	340269.2	2.21	2.37	1.56	292418.5	96.1
729	4.06	4.22	1.0	194953.1	3.54	3.70	1.81	352439.1	2.21	2.35	1.55	303145.9	96.5
848	4.07	4.22	1.0	168555.7	3.54	3.72	1.80	303378.6	2.20	2.36	1.55	261692.3	96.6

970	4.08	4.22	1.0	193918.4	3.52	3.71	1.81	350314.5	2.21	2.35	1.55	301052.1	96.6
1090	4.06	4.22	1.0	169184.6	3.56	3.72	1.79	303395.9	2.23	2.37	1.54	261305.8	97.1
1216	4.08	4.21	1.0	194798.6	3.56	3.70	1.80	350549.1	2.21	2.35	1.55	302558.9	96.6
1333	4.05	4.23	1.0	194271.0	3.55	3.70	1.79	348164.4	2.18	2.35	1.55	300832.1	96.9
1453	4.02	4.14	1.0	165813.2	3.50	3.64	1.80	298902.8	2.15	2.28	1.55	257828.9	96.5
1574	4.05	4.23	1.0	167347.2	3.53	3.70	1.79	300342.3	2.20	2.35	1.55	259004.0	96.9
VB229b	**Product**				**Educt**				**Product+Educt**				**$Conv_{exp}$**
6	4.10	4.18	1.0	11351.0	3.55	3.70	44.6	506743.2	2.26	2.37	24.6	278814.4	6.1
22	4.09	4.18	1.0	33760.8	3.56	3.71	14.3	484114.4	2.24	2.37	8.29	279928.3	18.1
24	4.03	4.14	1.0	36790.5	3.49	3.64	13.1	481479.0	2.16	2.30	7.63	280714.8	19.7
44	4.09	4.20	1.0	60773.0	3.54	3.71	7.63	463442.3	2.23	2.37	4.66	283386.5	32.2
57	4.08	4.20	1.0	73048.7	3.55	3.70	6.19	451881.5	2.25	2.36	3.88	283077.4	38.7
68	4.08	4.20	1.0	83214.3	3.56	3.70	5.30	441260.0	2.24	2.36	3.40	283230.3	44.1
96	4.08	4.20	1.0	102807.1	3.56	3.70	4.00	410721.3	2.23	2.36	2.70	277781.6	55.5
124	4.08	4.20	1.0	119550.8	3.55	3.70	3.37	402306.3	2.23	2.37	2.37	282841.0	63.4
188	4.07	4.20	1.0	142930.0	3.57	3.70	2.60	371297.1	2.24	2.36	1.94	277542.2	77.2
247	4.09	4.20	1.0	159996.6	3.56	3.70	2.29	365874.2	2.23	2.35	1.78	284811.7	84.3
313	4.09	4.20	1.0	173349.3	3.56	3.70	2.10	364448.5	2.24	2.35	1.68	290823.4	89.4
367	4.07	4.23	1.0	182233.1	3.58	3.70	2.00	365132.5	2.22	2.36	1.63	296433.5	92.2
428	4.08	4.21	1.0	177320.9	3.57	3.70	1.94	344816.1	2.22	2.35	1.59	282518.9	94.1
488	4.08	4.21	1.0	193534.6	3.57	3.71	1.91	370372.9	2.23	2.35	1.57	304662.8	95.3
549	4.08	4.21	1.0	179373.8	3.56	3.71	1.89	339445.0	2.22	2.34	1.56	280462.2	95.9
609	4.08	4.23	1.0	180607.5	3.56	3.70	1.87	338196.1	2.24	2.34	1.54	278902.5	97.1
671	4.07	4.21	1.0	200253.2	3.56	3.70	1.87	373900.1	2.23	2.35	1.55	310178.3	96.8
733	4.09	4.20	1.0	166837.8	3.57	3.70	1.88	313056.4	2.23	2.36	1.56	259626.1	96.4
854	4.08	4.22	1.0	191221.4	3.56	3.71	1.85	353471.6	2.23	2.35	1.54	295258.7	97.1
968	4.07	4.20	1.0	185569.1	3.56	3.70	1.85	343373.2	2.24	2.35	1.54	285920.4	97.4
1088	4.07	4.21	1.0	186093.2	3.55	3.70	1.85	343617.1	2.22	2.36	1.55	287697.3	97.0
1210	4.08	4.21	1.0	184869.5	3.57	3.70	1.85	341673.6	2.23	2.35	1.54	285308.2	97.2
1330	4.08	4.21	1.0	187723.9	3.55	3.70	1.85	347441.6	2.23	2.35	1.54	289291.1	97.3
1453	4.07	4.20	1.0	189093.3	3.56	3.70	1.85	348977.3	2.22	2.36	1.55	292393.6	97.0

Table 3.24: [Table S29]. Raw data of absolute kinetic of urethane synthesis with **6a** (1.0 mol%) in $CDCl_3$.

Time (min)	**Integ. Limits (ppm)**		**Integ**	**Absol.**	**Integ. Limits (ppm)**		**Integ**	**Absol.**	**Integ. Limits (ppm)**		**Integ**	**Absol.**	**$Conv_{exp}$ (%)**
VB230a	**Product**				**Educt**				**Product+Educt**				**$Conv_{exp}$**
10	4.10	4.19	1.0	12717.5	3.56	3.71	30.7	389892.1	2.24	2.37	17.2	219324.1	8.7

12	4.10	4.19	1.0	14623.3	3.57	3.71	26.4	386709.0	2.24	2.37	15.0	219305.5	10.0
27	4.09	4.19	1.0	28146.7	3.53	3.71	13.4	376967.3	2.23	2.36	7.84	220606.9	19.1
37	4.09	4.19	1.0	36486.6	3.56	3.70	10.1	368385.6	2.23	2.36	6.05	220837.5	24.8
47	4.09	4.20	1.0	43743.4	3.56	3.70	8.28	362292.1	2.23	2.36	5.07	221712.9	29.6
68	4.09	4.20	1.0	57734.8	3.55	3.71	6.09	351826.3	2.22	2.37	3.87	223614.1	38.7
91	4.09	4.20	1.0	73080.3	3.55	3.71	4.80	351038.3	2.23	2.36	3.17	231384.8	47.4
139	4.09	4.20	1.0	89800.4	3.54	3.71	3.54	317837.6	2.23	2.36	2.47	221885.1	60.7
192	4.09	4.20	1.0	108911.6	3.56	3.70	2.87	312683.2	2.23	2.35	2.12	230485.5	70.9
253	4.09	4.20	1.0	122596.8	3.56	3.70	2.47	303139.9	2.23	2.36	1.90	232604.6	79.1
314	4.08	4.21	1.0	144488.3	3.55	3.71	2.24	323453.0	2.24	2.36	1.77	255242.3	84.9
375	4.07	4.21	1.0	175320.6	3.53	3.70	2.10	367959.8	2.21	2.36	1.69	296739.9	88.6
437	4.07	4.21	1.0	181169.9	3.56	3.71	2.00	363190.6	2.24	2.34	1.64	296264.7	91.7
498	4.09	4.20	1.0	178316.0	3.57	3.69	1.95	348539.3	2.22	2.35	1.62	288511.7	92.7
558	4.08	4.21	1.0	162220.6	3.56	3.71	1.90	308028.1	2.23	2.35	1.58	256630.2	94.8
619	4.06	4.21	1.0	165173.9	3.56	3.71	1.87	308235.3	2.22	2.36	1.57	258926.8	95.7
679	4.07	4.21	1.0	167093.2	3.55	3.70	1.85	308296.3	2.22	2.35	1.56	259886.2	96.4
741	4.08	4.21	1.0	192719.8	3.57	3.71	1.84	353746.0	2.23	2.34	1.55	298310.2	96.9
862	4.07	4.21	1.0	168563.7	3.56	3.71	1.81	305401.2	2.20	2.36	1.54	260055.1	97.2
971	4.09	4.20	1.0	168732.3	3.56	3.70	1.81	305452.1	2.23	2.34	1.54	259170.5	97.7
1098	4.08	4.21	1.0	187166.4	3.56	3.70	1.81	338226.9	2.21	2.36	1.53	287162.9	97.8
1215	4.07	4.20	1.0	191171.5	3.55	3.71	1.80	344999.3	2.21	2.36	1.53	292980.4	97.9
1337	4.09	4.21	1.0	167458.7	3.56	3.70	1.80	301536.6	2.24	2.35	1.53	255733.8	98.2
1457	4.08	4.21	1.0	167998.9	3.57	3.70	1.80	301697.7	2.23	2.36	1.53	256338.7	98.3
1572	4.08	4.23	1.0	168468.5	3.55	3.71	1.80	302612.6	2.23	2.36	1.52	256859.3	98.4
VB230b	**Product**				**Educt**				**Product+Educt**				**$Conv_{exp}$**
10	4.09	4.19	1.0	15012.1	3.54	3.70	34.6	519985.9	2.24	2.36	18.7	279992.1	8.0
20	4.09	4.19	1.0	26562.7	3.54	3.71	19.2	510582.9	2.23	2.36	10.6	281736.1	14.1
22	4.09	4.20	1.0	29260.3	3.55	3.71	17.4	508036.7	2.24	2.37	9.63	281826.7	15.6
46	4.09	4.20	1.0	54493.7	3.55	3.71	9.06	493571.4	2.23	2.37	5.28	287875.5	28.4
61	4.08	4.20	1.0	68017.5	3.56	3.71	7.06	480252.4	2.23	2.38	4.24	288588.2	35.4
81	4.09	4.20	1.0	84020.7	3.55	3.71	5.55	466669.3	2.23	2.37	3.45	289635.1	43.5
101	4.09	4.20	1.0	92579.8	3.55	3.71	4.66	431723.3	2.22	2.38	2.98	276115.5	50.3
130	4.08	4.21	1.0	114044.3	3.55	3.71	3.91	445437.8	2.23	2.37	2.58	293915.1	58.2
207	4.08	4.21	1.0	148451.7	3.55	3.71	2.90	430075.1	2.22	2.36	2.05	304527.3	73.1
262	4.08	4.21	1.0	163190.0	3.56	3.72	2.56	417610.8	2.23	2.35	1.87	305370.2	80.2
317	4.07	4.21	1.0	160034.3	3.55	3.71	2.35	375380.8	2.21	2.37	1.76	282243.6	85.1
379	4.08	4.21	1.0	184516.8	3.55	3.71	2.20	406695.6	2.22	2.37	1.69	311842.8	88.8
434	4.05	4.22	1.0	172706.8	3.56	3.72	2.11	364603.0	2.21	2.36	1.64	283014.8	91.5

496	4.06	4.22	1.0	162313.5	3.55	3.71	2.05	332890.6	2.22	2.36	1.61	260917.2	93.3
557	4.06	4.22	1.0	187089.8	3.55	3.71	2.00	373341.2	2.22	2.37	1.58	296022.0	94.8
617	4.08	4.23	1.0	189967.1	3.55	3.71	1.97	374178.8	2.23	2.35	1.57	297376.7	95.8
676	4.06	4.22	1.0	163587.9	3.55	3.72	1.94	317985.1	2.23	2.36	1.55	253500.9	96.8
738	4.07	4.22	1.0	185517.8	3.55	3.71	1.93	358265.9	2.23	2.36	1.54	286435.7	97.2
858	4.08	4.20	1.0	188398.7	3.56	3.70	1.92	361114.7	2.21	2.35	1.54	290540.9	97.3
980	4.08	4.21	1.0	186455.2	3.56	3.71	1.91	355971.1	2.22	2.35	1.53	285859.8	97.8
1094	4.07	4.21	1.0	191379.1	3.55	3.71	1.90	363698.2	2.23	2.35	1.53	292415.8	98.2
1216	4.06	4.23	1.0	192969.6	3.55	3.70	1.89	364546.1	2.22	2.34	1.52	294266.7	98.4
1335	4.07	4.21	1.0	191797.7	3.56	3.70	1.90	363491.4	2.22	2.34	1.53	292731.9	98.3
1457	4.08	4.21	1.0	191807.1	3.56	3.71	1.90	363624.4	2.23	2.34	1.53	292889.3	98.2
1575	4.08	4.21	1.0	191224.3	3.56	3.70	1.90	362792.7	2.22	2.35	1.53	292704.3	98.0

Table 3.25: [Table S30]. Raw data of absolute kinetic of urethane synthesis with **3a** (1.0 mol%) in $CDCl_3$.

Time (min)	**Integ. Limits (ppm)**		**Integ**	**Absol.**	**Integ. Limits (ppm)**		**Integ**	**Absol.**	**Integ. Limits (ppm)**		**Integ**	**Absol.**	**$Conv_{exp}$ (%)**
VB227a	**Product**				**Educt**				**Product+Educt**				**$Conv_{exp}$**
5	4.10	4.19	1.0	3929.2	3.53	3.73	113.8	447214.5	2.23	2.38	62.7	246385.3	2.4
28	4.09	4.19	1.0	17551.3	3.53	3.73	24.9	436583.1	2.22	2.37	14.1	248195.5	10.6
33	4.07	4.20	1.0	20512.5	3.54	3.72	21.1	433740.4	2.22	2.38	12.1	248444.0	12.4
48	4.08	4.21	1.0	28371.3	3.54	3.73	15.1	427186.6	2.20	2.38	8.80	249601.0	17.0
63	4.02	4.15	1.0	35704.2	3.48	3.66	11.8	421135.0	2.16	2.32	7.00	249906.2	21.4
95	4.08	4.20	1.0	50425.1	3.53	3.72	8.09	407904.0	2.22	2.37	4.97	250533.3	30.2
128	4.06	4.21	1.0	63311.3	3.53	3.73	6.27	396912.4	2.21	2.38	3.98	251973.5	37.7
186	4.01	4.14	1.0	82268.5	3.47	3.66	4.62	380085.0	2.15	2.30	3.08	253299.2	48.7
246	4.08	4.22	1.0	98353.5	3.56	3.71	3.71	365160.4	2.22	2.38	2.59	254414.6	58.0
307	4.04	4.22	1.0	111236.5	3.54	3.71	3.18	353187.1	2.21	2.37	2.29	254279.2	65.6
369	4.06	4.21	1.0	121736.3	3.53	3.72	2.84	345633.5	2.21	2.36	2.10	256129.5	71.3
429	4.05	4.23	1.0	130674.2	3.52	3.72	2.60	339408.5	2.22	2.36	1.97	257350.0	76.2
491	4.07	4.22	1.0	135646.4	3.55	3.72	2.43	329417.2	2.22	2.37	1.88	254920.5	79.8
546	4.06	4.22	1.0	163320.2	3.54	3.71	2.31	377062.0	2.20	2.35	1.81	295890.3	82.8
606	4.06	4.22	1.0	167817.5	3.53	3.72	2.21	370359.6	2.21	2.36	1.75	294281.8	85.5
665	4.05	4.22	1.0	171460.3	3.56	3.74	2.12	363662.2	2.20	2.36	1.71	292881.4	87.8
727	4.05	4.22	1.0	174760.6	3.54	3.73	2.06	359152.0	2.20	2.37	1.67	292142.7	89.7
846	4.07	4.22	1.0	184868.8	3.53	3.72	1.96	361589.8	2.22	2.36	1.62	299052.1	92.7
966	4.04	4.22	1.0	163046.6	3.53	3.72	1.89	307481.4	2.22	2.36	1.58	257519.2	95.0
1087	4.05	4.23	1.0	163628.3	3.54	3.71	1.85	303077.8	2.21	2.36	1.56	255560.1	96.0

1225	4.06	4.23	1.0	144252.4	3.55	3.71	1.82	263091.8	2.21	2.37	1.55	222920.9	97.1
1330	4.06	4.22	1.0	130121.2	3.56	3.72	1.81	235849.2	2.20	2.37	1.54	200232.6	97.5
1445	4.05	4.22	1.0	143255.7	3.53	3.71	1.79	256651.8	2.21	2.35	1.53	218498.2	98.3
1581	4.06	4.21	1.0	147706.8	3.56	3.72	1.78	263113.4	2.20	2.36	1.53	225327.4	98.3
1812	4.05	4.23	1.0	152622.9	3.55	3.73	1.76	268937.8	2.21	2.36	1.51	230812.0	99.2
1994	4.05	4.24	1.0	193812.7	3.52	3.74	1.76	340360.2	2.20	2.36	1.51	292462.1	99.4
VB227b	**Product**				**Educt**				**Product+Educt**				**$Conv_{exp}$**
5	4.09	4.19	1.0	4626.8	3.54	3.72	110.0	508927.5	2.23	2.37	60.3	278789.9	2.5
15	4.10	4.19	1.0	11772.9	3.54	3.71	42.7	503045.3	2.24	2.37	23.7	279468.7	6.3
31	4.10	4.19	1.0	22232.8	3.55	3.72	22.3	494983.7	2.22	2.37	12.7	281709.0	11.8
38	4.09	4.19	1.0	26592.0	3.55	3.72	18.5	491850.0	2.23	2.37	10.6	281921.7	14.1
62	4.08	4.21	1.0	40520.3	3.55	3.71	11.7	474354.7	2.23	2.37	6.91	279981.1	21.7
75	4.08	4.20	1.0	46775.2	3.53	3.72	9.90	462999.8	2.23	2.38	5.93	277256.5	25.3
101	4.09	4.20	1.0	59597.0	3.55	3.72	7.61	453244.9	2.21	2.38	4.69	279380.7	32.0
132	4.08	4.21	1.0	73681.5	3.55	3.71	5.98	440740.6	2.22	2.38	3.80	280151.5	39.5
192	4.08	4.21	1.0	96907.8	3.55	3.70	4.41	427440.1	2.22	2.37	2.95	285618.8	50.9
254	4.08	4.20	1.0	115324.7	3.55	3.72	3.57	412071.3	2.22	2.37	2.49	287263.1	60.2
315	4.07	4.21	1.0	129653.1	3.54	3.73	3.08	399768.3	2.21	2.38	2.22	288414.2	67.4
380	4.06	4.22	1.0	141767.5	3.55	3.72	2.74	388063.4	2.20	2.37	2.04	288697.6	73.7
436	4.08	4.22	1.0	150827.9	3.55	3.72	2.53	381706.2	2.21	2.37	1.92	290172.4	78.0
497	4.06	4.21	1.0	158641.1	3.55	3.72	2.37	375263.0	2.22	2.36	1.83	290672.3	81.9
564	4.05	4.21	1.0	164750.8	3.54	3.72	2.24	368817.1	2.22	2.37	1.76	290283.2	85.1
610	4.06	4.23	1.0	169501.8	3.53	3.72	2.16	366547.8	2.19	2.37	1.73	292417.6	86.9
670	4.06	4.22	1.0	172321.8	3.55	3.72	2.09	360065.6	2.22	2.36	1.68	290019.2	89.1
741	4.06	4.23	1.0	176677.8	3.55	3.72	2.02	357076.6	2.22	2.36	1.64	290111.8	91.3
852	4.08	4.21	1.0	180632.5	3.54	3.72	1.95	353021.1	2.22	2.36	1.61	290736.6	93.2
973	4.06	4.22	1.0	187691.5	3.54	3.72	1.89	354577.1	2.19	2.36	1.58	296268.0	95.0
1093	3.98	4.16	1.0	188788.3	3.49	3.65	1.85	349175.9	2.15	2.31	1.55	292736.2	96.7
1216	4.07	4.21	1.0	191280.7	3.54	3.71	1.83	349770.9	2.22	2.35	1.54	294854.0	97.3
1331	4.06	4.23	1.0	164903.5	3.55	3.71	1.81	297956.7	2.21	2.35	1.53	252277.1	98.0
1457	4.00	4.16	1.0	189227.8	3.48	3.65	1.80	340425.1	2.14	2.30	1.52	287959.3	98.6
1702	4.05	4.23	1.0	191959.9	3.54	3.73	1.78	342190.7	2.22	2.35	1.51	289726.2	99.4
1938	4.05	4.23	1.0	204185.3	3.56	3.73	1.78	362741.5	2.21	2.35	1.51	307796.4	99.5
2178	4.07	4.22	1.0	193553.9	3.55	3.72	1.77	342398.5	2.20	2.37	1.51	292336.0	99.3
2415	4.08	4.23	1.0	183498.1	3.54	3.72	1.78	326171.6	2.21	2.35	1.51	276624.9	99.5

Table 3.26: [Table S31]. Raw data of absolute kinetic of urethane synthesis with **3b** (1.0 mol%) in $CDCl_3$.

Time (min)	Integ. Limits (ppm)		Integ	Absol.	Integ. Limits (ppm)		Integ	Absol.	Integ. Limits (ppm)		Integ	Absol.	$Conv_{exp}$ (%)
VB228a	**Product**				**Educt**				**Product+Educt**				**$Conv_{exp}$**
5	4.09	4.20	1.0	4643.0	3.56	3.72	97.3	451622.2	2.23	2.38	54.3	251915.5	2.8
16	4.10	4.19	1.0	11511.3	3.54	3.72	38.8	446083.7	2.23	2.38	21.9	252138.6	6.8
36	4.07	4.20	1.0	24810.5	3.54	3.72	17.5	434843.9	2.23	2.37	10.2	252917.8	14.7
46	4.09	4.19	1.0	29983.2	3.54	3.71	14.3	430233.6	2.22	2.37	8.46	253682.0	17.7
64	4.08	4.20	1.0	39729.8	3.53	3.72	10.6	420722.1	2.23	2.38	6.38	253358.5	23.5
93	4.09	4.19	1.0	53929.7	3.55	3.71	7.59	409242.8	2.23	2.36	4.74	255464.9	31.7
124	4.07	4.21	1.0	67115.5	3.55	3.71	5.92	397304.0	2.22	2.37	3.82	256409.4	39.3
183	4.09	4.21	1.0	87481.8	3.54	3.72	4.33	378391.5	2.21	2.37	2.94	257143.5	51.0
245	4.08	4.21	1.0	105211.2	3.53	3.72	3.47	364603.8	2.22	2.36	2.46	259093.7	60.9
310	4.07	4.21	1.0	118694.6	3.54	3.71	2.96	351170.6	2.23	2.36	2.18	259095.3	68.7
370	4.06	4.21	1.0	129238.8	3.54	3.71	2.65	342491.2	2.22	2.36	2.01	260053.2	74.5
424	4.08	4.21	1.0	134017.1	3.52	3.72	2.47	331499.3	2.21	2.36	1.92	256657.1	78.3
491	4.07	4.22	1.0	165012.6	3.54	3.72	2.29	378695.6	2.23	2.36	1.81	299074.4	82.8
547	4.08	4.22	1.0	168610.0	3.56	3.72	2.19	369352.2	2.21	2.36	1.76	296524.5	85.3
605	4.05	4.23	1.0	173236.0	3.53	3.72	2.10	363621.2	2.21	2.38	1.71	295431.2	88.0
668	4.08	4.21	1.0	176028.0	3.53	3.71	2.04	358521.2	2.22	2.36	1.67	294207.5	89.7
722	4.07	4.22	1.0	182772.0	3.54	3.71	1.98	361608.9	2.21	2.36	1.64	300516.9	91.2
846	4.07	4.22	1.0	164235.8	3.55	3.71	1.89	309895.0	2.23	2.35	1.59	261674.5	94.1
967	4.07	4.21	1.0	167706.1	3.55	3.73	1.84	308744.6	2.21	2.36	1.57	263560.1	95.4
1123	4.08	4.20	1.0	171157.4	3.54	3.71	1.84	314528.2	2.22	2.35	1.55	265132.5	96.8
1204	4.07	4.21	1.0	149226.9	3.53	3.72	1.79	267395.7	2.21	2.36	1.54	229942.0	97.3
1326	4.07	4.21	1.0	152878.8	3.54	3.72	1.77	271070.3	2.21	2.35	1.53	233694.8	98.1
1443	4.07	4.23	1.0	151022.3	3.55	3.73	1.76	265414.1	2.22	2.35	1.52	229133.7	98.9
1564	4.08	4.21	1.0	156143.0	3.56	3.73	1.75	273851.8	2.23	2.36	1.52	237137.1	98.8
1805	4.08	4.22	1.0	195715.1	3.55	3.71	1.75	341838.3	2.21	2.36	1.52	297217.1	98.8
2049	4.07	4.22	1.0	200730.4	3.54	3.71	1.74	348682.8	2.21	2.36	1.51	303278.6	99.3
VB228b	**Product**				**Educt**				**Product+Educt**				**$Conv_{exp}$**
5	4.09	4.19	1.0	5184.1	3.52	3.73	102.3	530218.9	2.21	2.39	54.9	284855.9	2.7
9	4.10	4.20	1.0	7770.8	3.54	3.71	67.8	526864.0	2.22	2.37	36.6	284421.7	4.1
19	4.08	4.20	1.0	15263.9	3.54	3.72	34.1	521142.1	2.22	2.38	18.7	285514.3	8.0
36	4.09	4.20	1.0	27814.9	3.55	3.71	18.3	509968.1	2.22	2.36	10.3	286217.6	14.6
49	4.08	4.20	1.0	35653.6	3.53	3.71	14.1	503038.7	2.21	2.38	8.05	286967.7	18.6
72	4.08	4.20	1.0	49189.4	3.55	3.71	10.0	489760.3	2.23	2.36	5.83	287009.3	25.7
96	4.08	4.21	1.0	62427.5	3.55	3.72	7.66	478184.5	2.21	2.37	4.62	288497.5	32.5

126	4.08	4.21	1.0	76661.8	3.51	3.72	6.09	467038.2	2.21	2.37	3.78	289765.2	39.7
191	4.08	4.22	1.0	102749.0	3.55	3.71	4.29	441135.8	2.23	2.38	2.83	290405.4	53.1
246	4.08	4.21	1.0	119491.3	3.55	3.71	3.57	426131.9	2.23	2.37	2.44	291362.9	61.5
307	4.05	4.21	1.0	134573.2	3.54	3.71	3.07	413342.0	2.22	2.36	2.17	292601.7	69.0
366	4.06	4.22	1.0	145942.8	3.54	3.72	2.77	403560.7	2.22	2.36	2.01	293251.2	74.7
427	4.06	4.21	1.0	154296.5	3.55	3.72	2.54	391905.3	2.23	2.36	1.89	291294.1	79.5
488	4.07	4.22	1.0	161117.3	3.55	3.73	2.38	383970.8	2.23	2.37	1.80	290800.9	83.1
549	4.06	4.21	1.0	167574.2	3.55	3.72	2.27	379939.7	2.23	2.36	1.75	292683.2	85.9
607	4.07	4.22	1.0	172069.5	3.57	3.71	2.18	375104.7	2.24	2.36	1.70	292485.1	88.2
667	4.07	4.22	1.0	175248.6	3.54	3.71	2.12	371388.9	2.22	2.36	1.67	292019.7	90.0
727	4.08	4.22	1.0	181721.1	3.55	3.71	2.06	375236.5	2.21	2.36	1.64	298727.3	91.2
846	4.07	4.22	1.0	158597.6	3.56	3.71	1.98	314655.2	2.21	2.37	1.60	253786.1	93.7
968	4.07	4.22	1.0	160980.6	3.55	3.71	1.93	311273.7	2.22	2.36	1.57	252734.1	95.5
1086	4.07	4.21	1.0	163661.5	3.56	3.71	1.90	311255.4	2.23	2.35	1.55	254220.6	96.6
1207	4.06	4.21	1.0	189361.5	3.55	3.71	1.88	356773.6	2.21	2.36	1.54	292054.1	97.3
1328	4.07	4.21	1.0	190116.1	3.56	3.71	1.87	355558.4	2.22	2.36	1.54	291836.0	97.7
1453	4.07	4.22	1.0	191263.9	3.55	3.70	1.86	355621.3	2.23	2.34	1.52	291648.6	98.4
1567	4.07	4.22	1.0	205200.0	3.56	3.71	1.85	380436.2	2.23	2.36	1.52	312490.2	98.5
1807	4.07	4.21	1.0	203826.6	3.54	3.71	1.85	376804.8	2.22	2.34	1.52	309123.3	98.9
2052	4.08	4.21	1.0	194504.9	3.56	3.70	1.84	357286.8	2.23	2.36	1.52	294868.6	98.9
2290	4.07	4.20	1.0	192043.4	3.55	3.71	1.84	352656.8	2.22	2.35	1.52	291384.5	98.9

3.1.8 Crystallographic Data

Triphenyl ((triphenyl-λ5-phosphaneylidene)amino) phosphonium pyridin-4-yl (trifluoromethyl) sulfonyl) amide (**3b**)

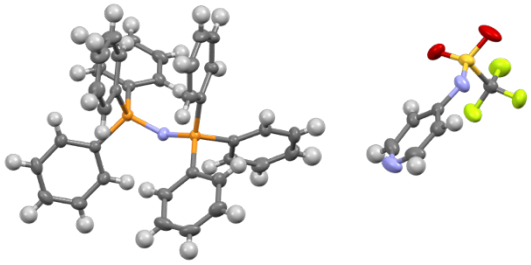

Table 3.27: [Table S32]. Crystallographic details for **3b**.

net formula	$C_{42}H_{34}F_3N_3O_2P_2S$
M_r/g mol^{-1}	763.72
crystal size/mm	0.170 × 0.140 × 0.120
T/K	173.(2)
radiation	MoKα
diffractometer	'Bruker D8 Venture TXS'
crystal system	triclinic
space group	'P -1'
a/Å	10.3726(12)
b/Å	11.4051(12)
c/Å	16.5612(19)
α/°	97.926(4)
β/°	106.882(4)
γ/°	90.907(4)
V/Å^3	1853.6(4)
Z	2
calc. density/g cm^{-3}	1.368
μ/mm^{-1}	0.230
absorption correction	Multi-Scan
transmission factor range	0.93–0.97
refls. measured	32931
R_{int}	0.0504
mean σ(I)/I	0.0487
θ range	2.377–27.485
observed refls.	7124
x, y (weighting scheme)	0.0419, 0.9450
hydrogen refinement	constr
Flack parameter	?
refls in refinement	8480
parameters	478
restraints	0
$R(F_{obs})$	0.0412
$R_w(F^2)$	0.1105
S	1.027
shift/error$_{max}$	0.001
max electron density/e Å^{-3}	0.405
min electron density/e Å^{-3}	−0.367

Tetraphenylphosphonium pyridin-4-yl(tosyl)amide (**5a**)

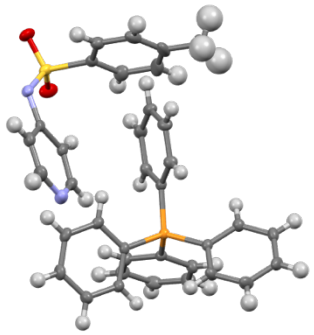

Table 3.28: [Table S33]. Crystallographic details for **5a**

net formula	$C_{36}H_{31}N_2O_2PS$
M_r/g mol^{-1}	586.66
crystal size/mm	0.120 × 0.100 × 0.090
T/K	103.(2)
radiation	MoKα
diffractometer	'Bruker D8 Venture TXS'
crystal system	triclinic
space group	'P -1'
a/Å	10.7903(5)
b/Å	12.0043(5)
c/Å	13.0598(5)
α/°	98.1020(10)
β/°	105.4840(10)
γ/°	107.2340(10)
V/Å^3	1511.90(11)
Z	2
calc. density/g cm^{-3}	1.289
μ/mm^{-1}	0.196
absorption correction	Multi-Scan
transmission factor range	0.96–0.98
refls. measured	37059
R_{int}	0.0493
mean σ(*I*)/*I*	0.0411
θ range	2.754–28.278
observed refls.	5838
x, y (weighting scheme)	0.0284, 1.1454
hydrogen refinement	constr
Flack parameter	?
refls in refinement	7485
parameters	380
restraints	0
$R(F_{obs})$	0.0429
$R_w(F^2)$	0.1037
S	1.054
shift/error$_{max}$	0.001
max electron density/e Å^{-3}	0.375
min electron density/e Å^{-3}	−0.412

Tetraphenylphosphonium pyridin-4-yl((4-(trifluoromethyl)phenyl)sulfonyl)amide (**6a**)

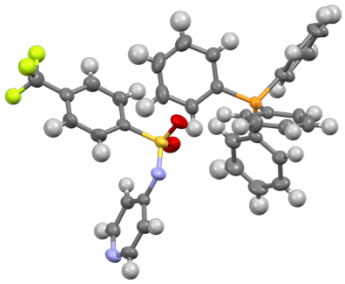

Table 3.29: [Table S34]. Crystallographic details for **6a**.

net formula	$C_{36}H_{28}F_3N_2O_2PS$
M_r/g mol^{-1}	640.63
crystal size/mm	0.110 × 0.050 × 0.040
T/K	173.(2)
radiation	MoKα
diffractometer	'Bruker D8 Venture TXS'
crystal system	triclinic
space group	'P -1'
a/Å	10.5191(6)
b/Å	12.8560(7)
c/Å	14.7858(7)
α/°	66.648(2)
β/°	81.861(2)
γ/°	73.088(2)
V/Å^3	1755.57(16)
Z	2
calc. density/g cm^{-3}	1.212
μ/mm^{-1}	0.186
absorption correction	Multi-Scan
transmission factor range	0.96–0.99
refls. measured	31372
R_{int}	0.0509
mean σ(I)/I	0.0464
θ range	2.861–27.102
observed refls.	5983
x, y (weighting scheme)	0.0792, 1.0326
hydrogen refinement	constr
Flack parameter	?
refls in refinement	7726
parameters	431
restraints	133
$R(F_{obs})$	0.0572
$R_w(F^2)$	0.1681
S	1.044
shift/error$_{max}$	0.001
max electron density/e Å^{-3}	0.393
min electron density/e Å^{-3}	−0.545

Triphenyl((triphenyl-λ5-phosphaneylidene)amino)phosphonium tetrafluoroborate (**7b**)

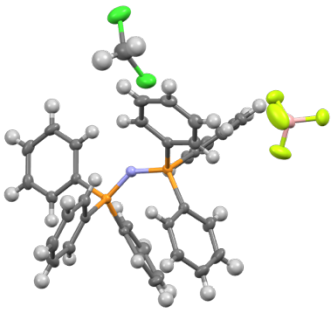

Table 3.30: [Table S35]. Crystallographic details for additive **7b** ($PNPBF_4 \times CH_2Cl_2$).

net formula	$C_{37}H_{32}BCl_2F_4NP_2$
M_r/g mol^{-1}	710.28
crystal size/mm	0.100 × 0.060 × 0.050
T/K	173.(2)
radiation	MoKα
diffractometer	'Bruker D8 Venture TXS'
crystal system	triclinic
space group	'P -1'
a/Å	9.5185(5)
b/Å	10.6730(6)
c/Å	17.0550(9)
α/°	90.353(2)
β/°	94.638(2)
γ/°	93.483(2)
V/Å^3	1723.66(16)
Z	2
calc. density/g cm^{-3}	1.369
μ/mm^{-1}	0.331
absorption correction	Multi-Scan
transmission factor range	0.95–0.98
refls. measured	29933
R_{int}	0.0464
mean σ(I)/I	0.0408
θ range	2.965–26.372
observed refls.	6153
x, y (weighting scheme)	0.0362, 1.2966
hydrogen refinement	constr
Flack parameter	?
refls in refinement	7035
parameters	424
restraints	0
$R(F_{obs})$	0.0398
$R_w(F^2)$	0.1016
S	1.011
shift/error$_{max}$	0.001
max electron density/e Å^{-3}	0.399
min electron density/e Å^{-3}	−0.638

The X-ray crystal structure of compound **7a** has previously been reported (without the DCM solvate).[15–17]

3.1.9 NMR Spectra

The recorded NMR spectra of compounds PA_**3**, PA_**4**, PA_**5**, **3c**, **3d**, and **4a** were identical to the ones published in ref. [3].

N-(pyridin-4(1*H*)-ylidene)-4-(trifluoromethyl)benzenesulfonamide (**6**)

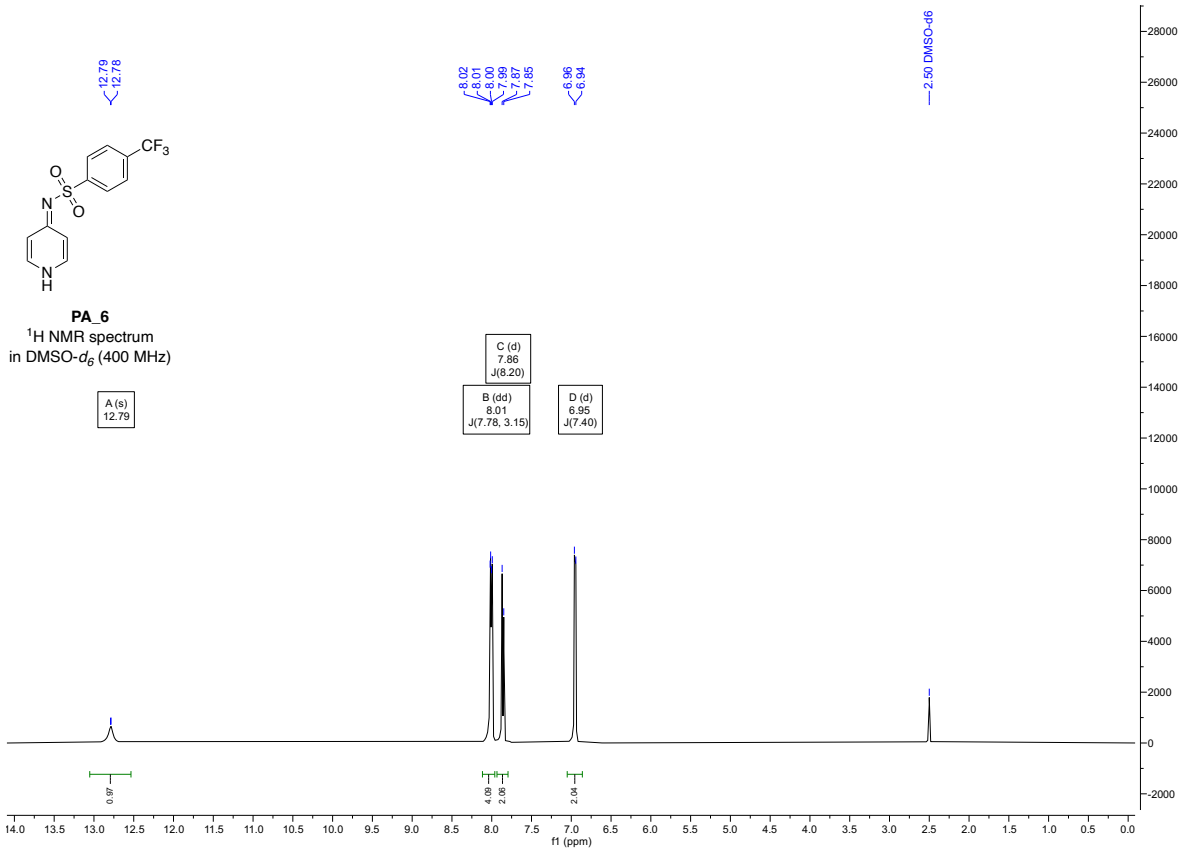

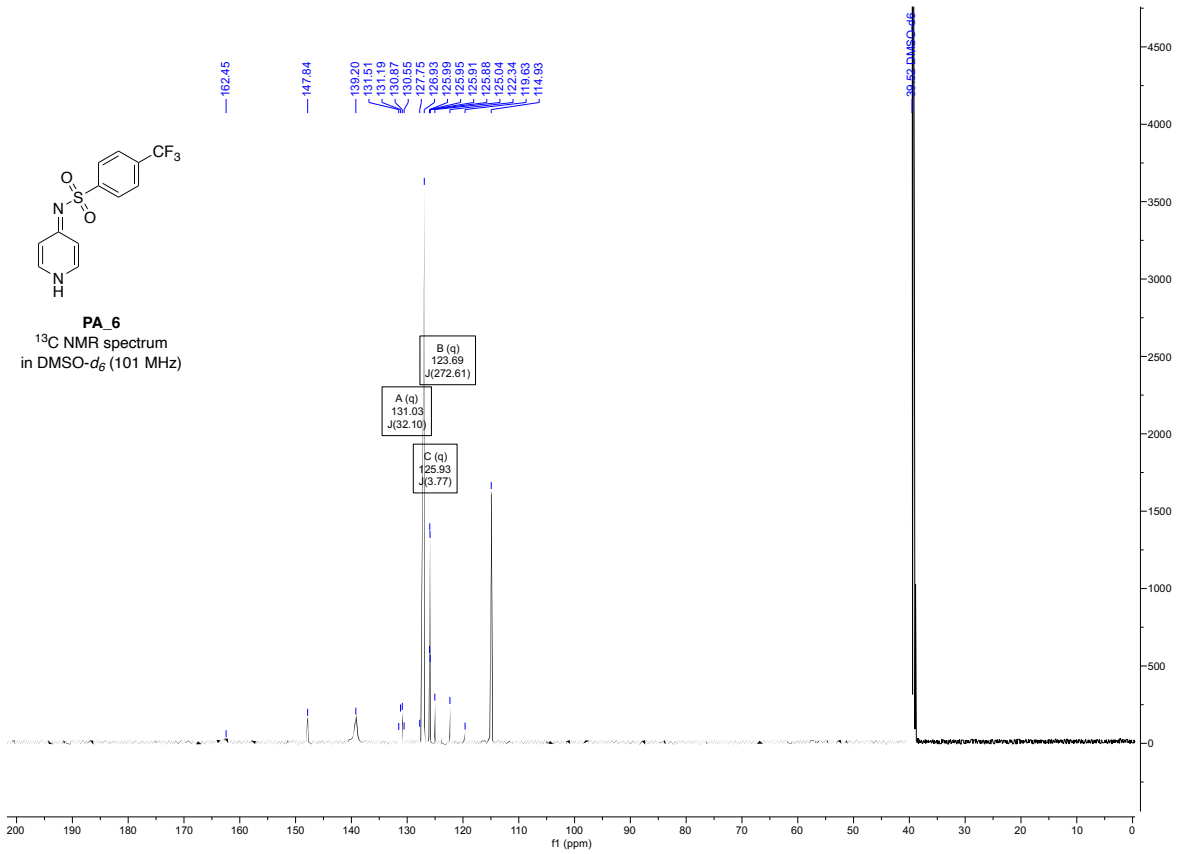

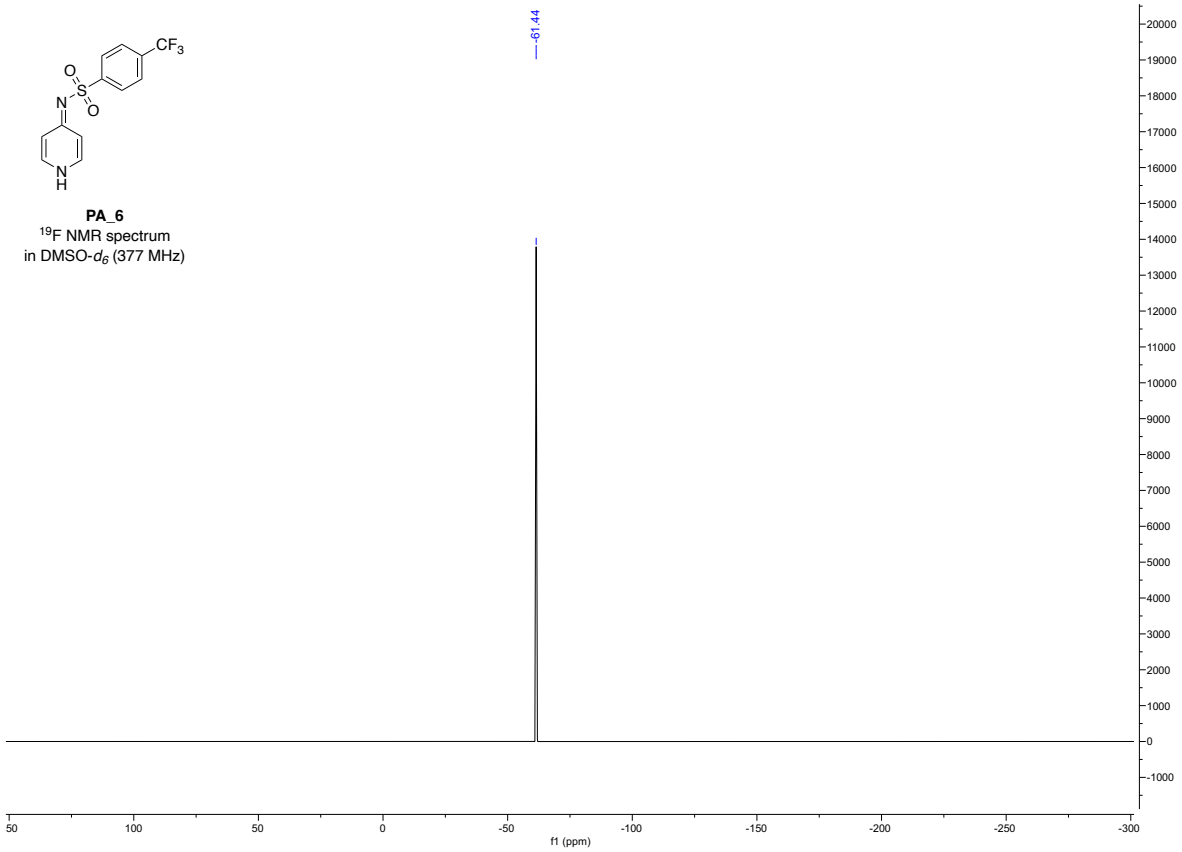

PA_6
^{19}F NMR spectrum
in DMSO-d_6 (377 MHz)

Triphenyl ((triphenyl-λ5-phosphaneylidene)amino) phosphonium pyridin-4-yl (trifluoromethyl) sulfonyl) amide (**3b**)

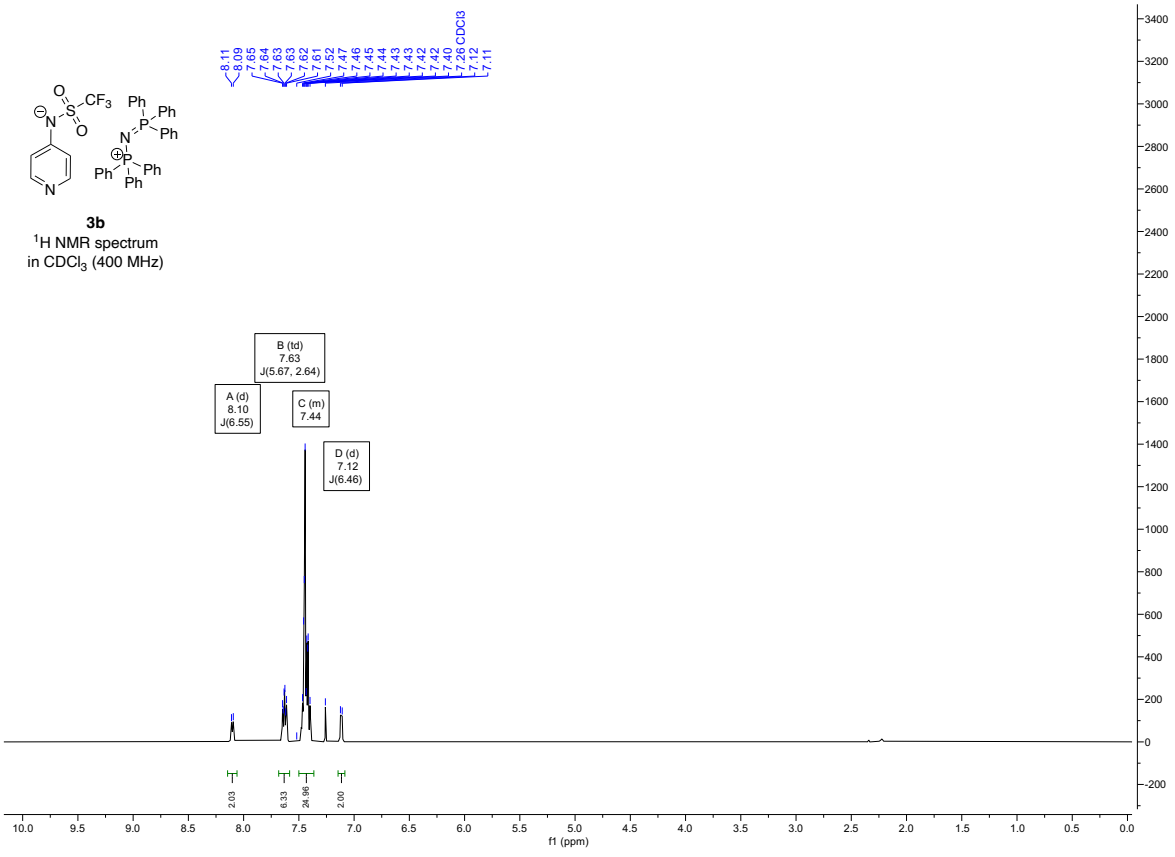

3b
^{1}H NMR spectrum
in $CDCl_3$ (400 MHz)

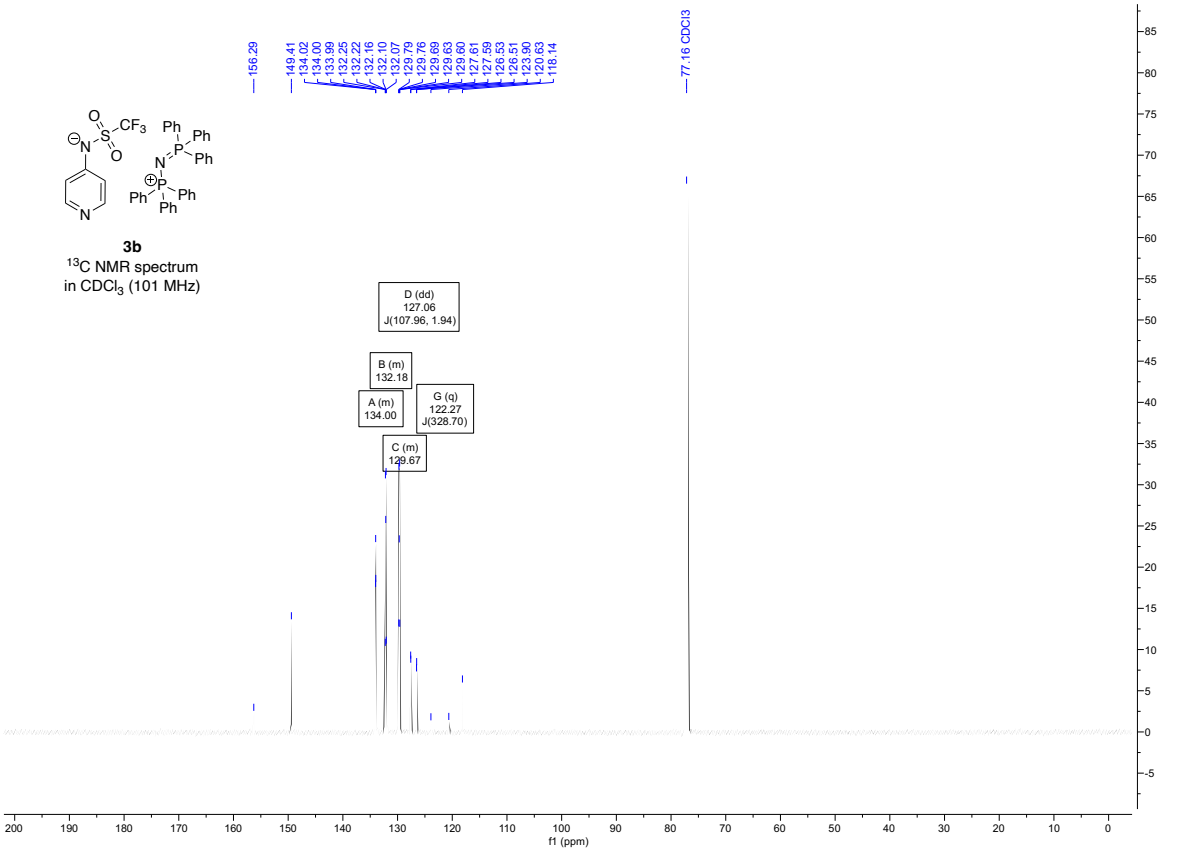

3b
^{13}C NMR spectrum
in $CDCl_3$ (101 MHz)

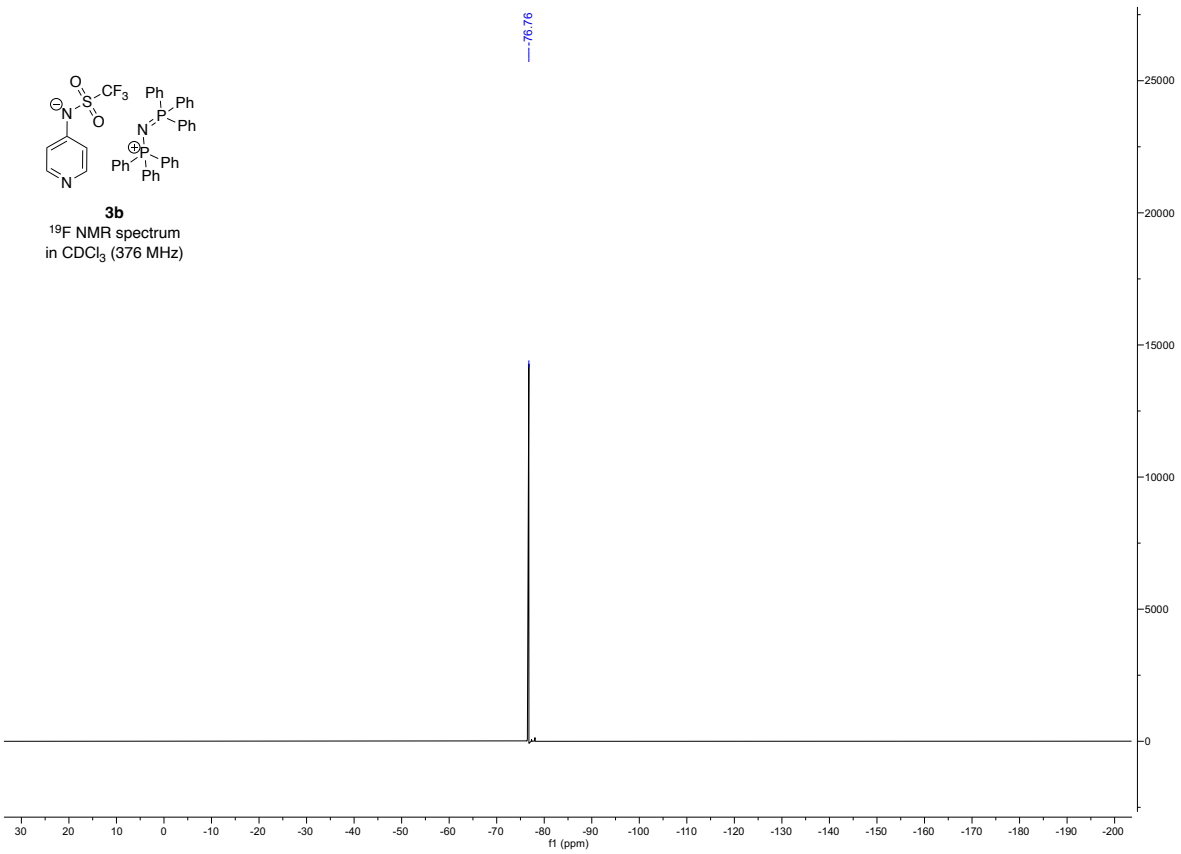

3b
^{19}F NMR spectrum
in $CDCl_3$ (376 MHz)

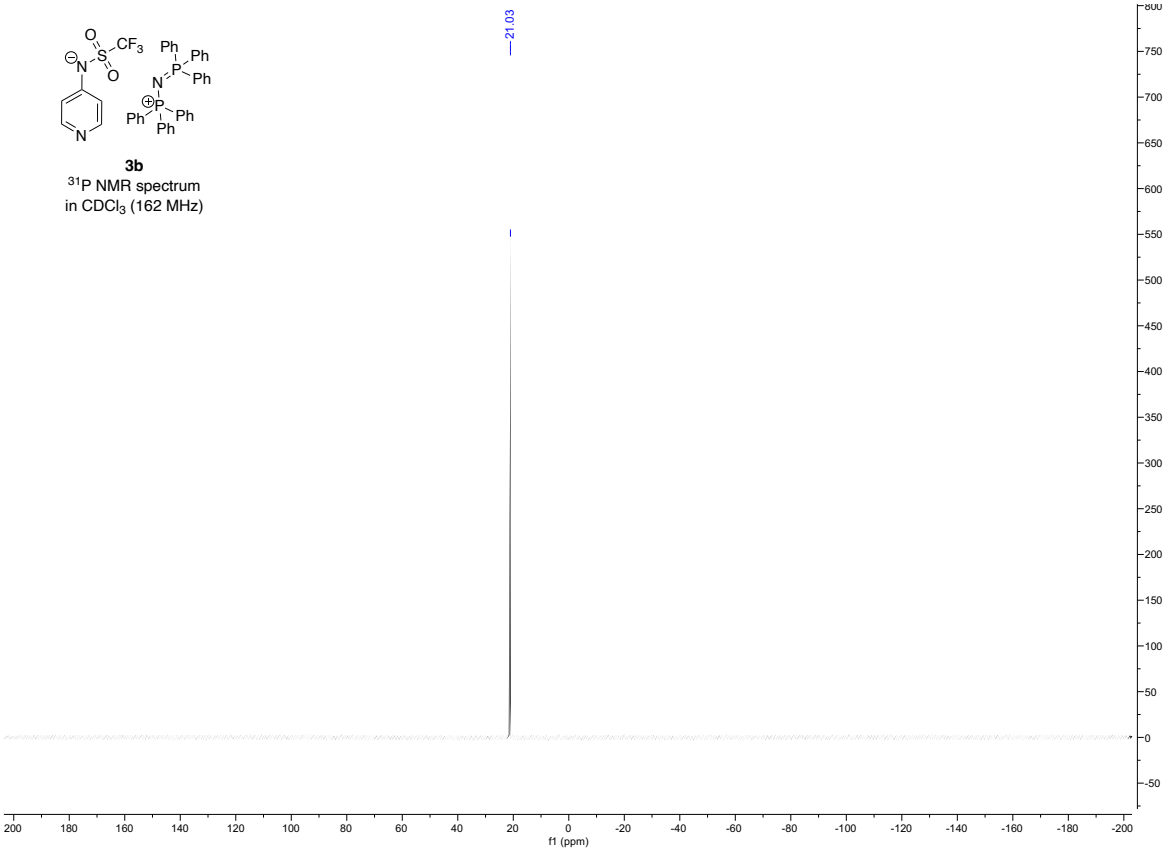

3b
^{31}P NMR spectrum
in $CDCl_3$ (162 MHz)

Tetraphenylphosphonium pyridin-4-yl(tosyl)amide (**5a**)

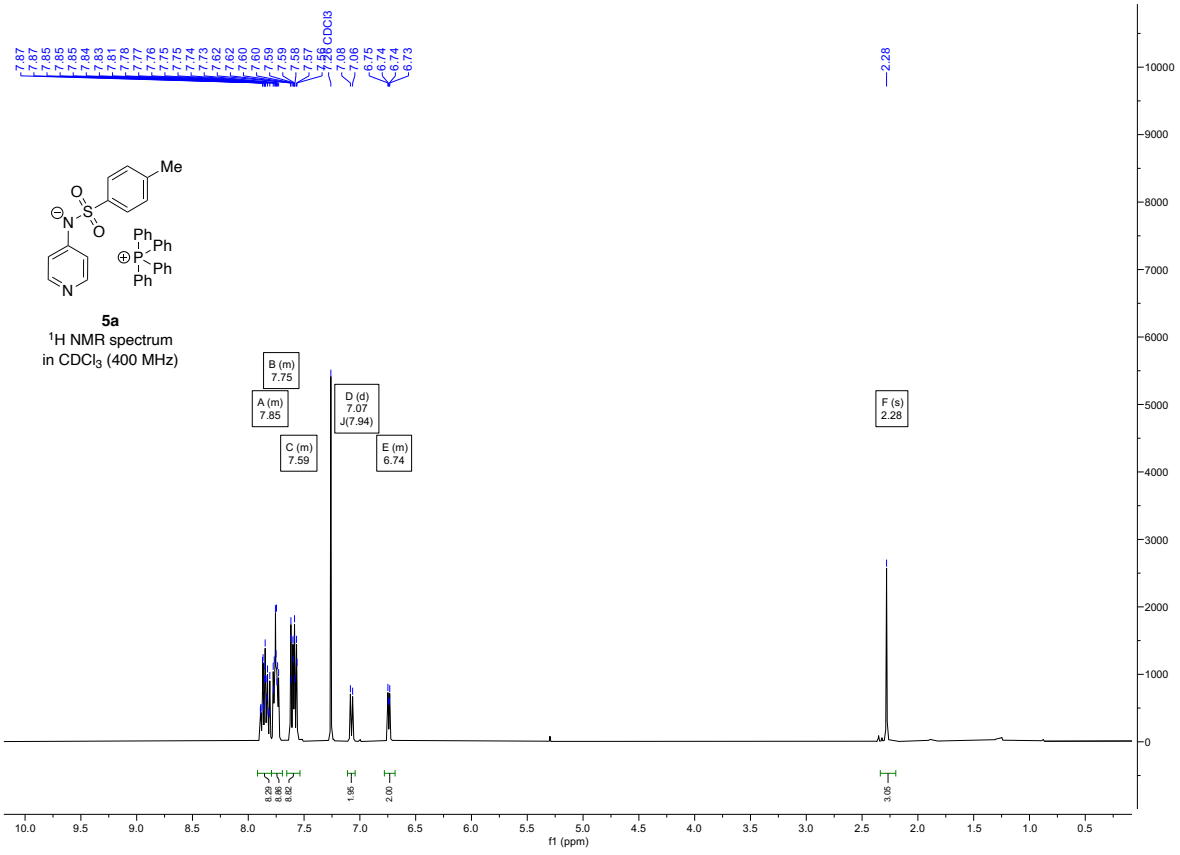

5a
^{1}H NMR spectrum
in $CDCl_3$ (400 MHz)

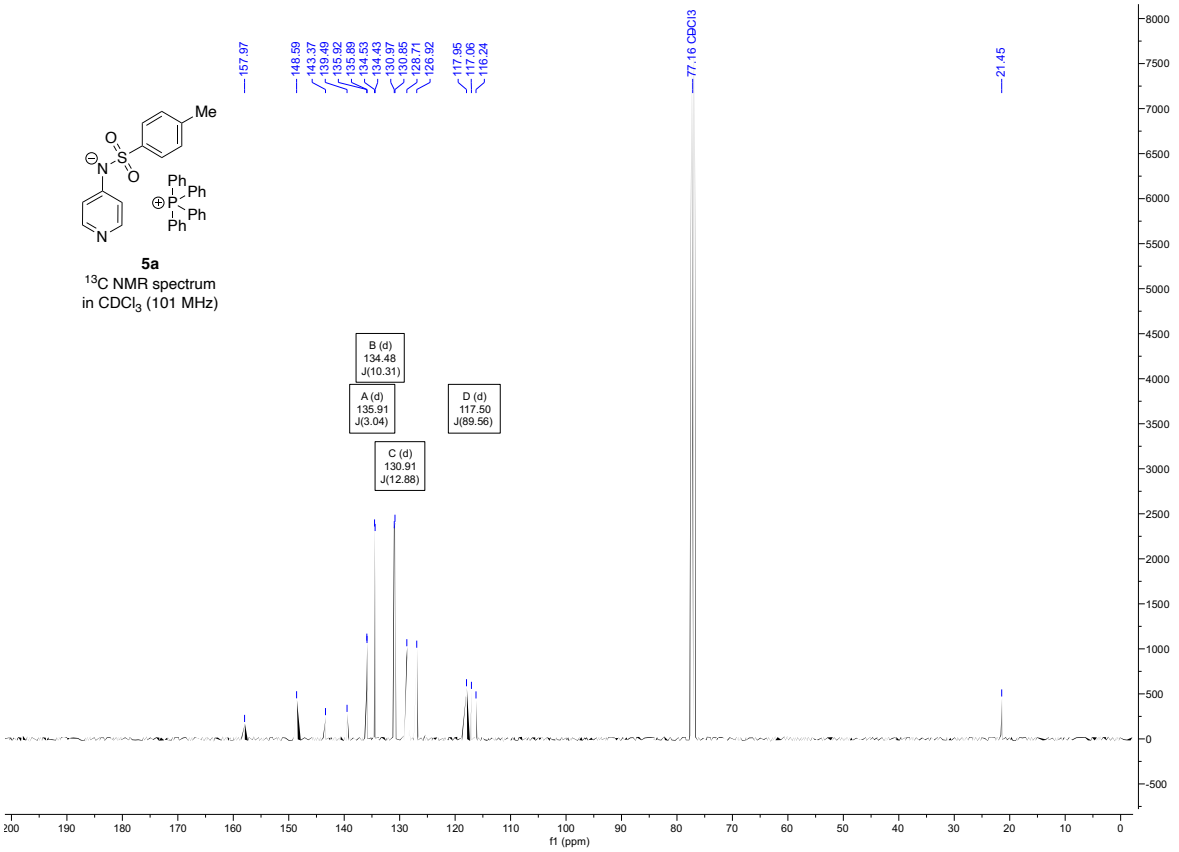

5a
^{13}C NMR spectrum
in $CDCl_3$ (101 MHz)

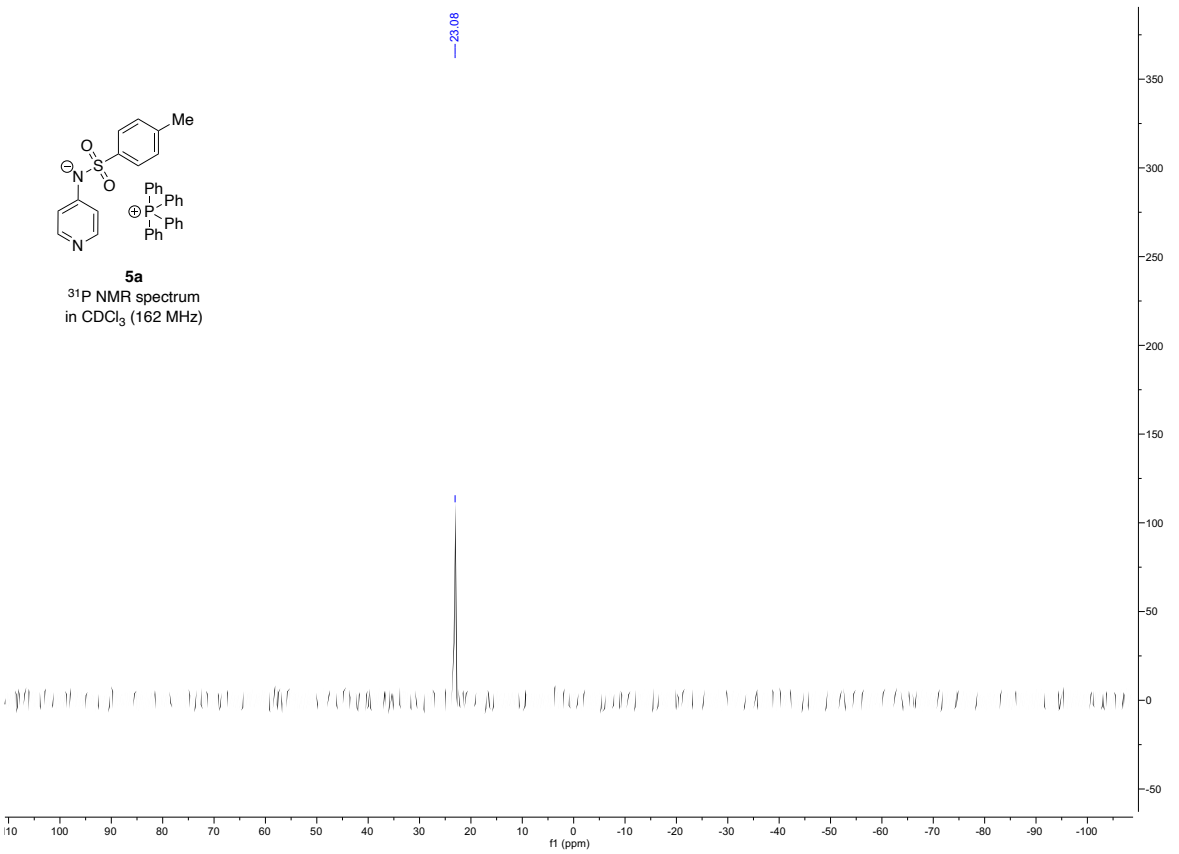

5a
^{31}P NMR spectrum
in $CDCl_3$ (162 MHz)

Tetraphenylphosphonium pyridin-4-yl((4-(trifluoromethyl)phenyl)sulfonyl)amide (**6a**)

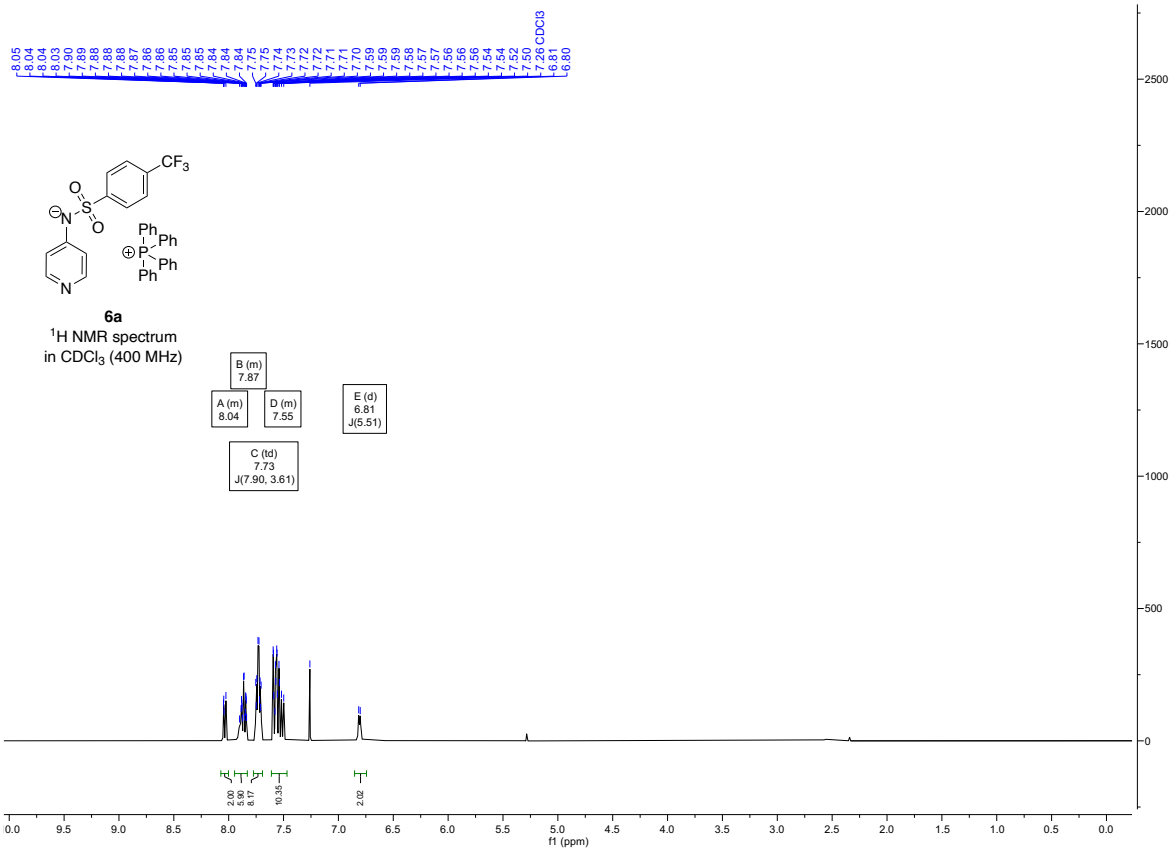

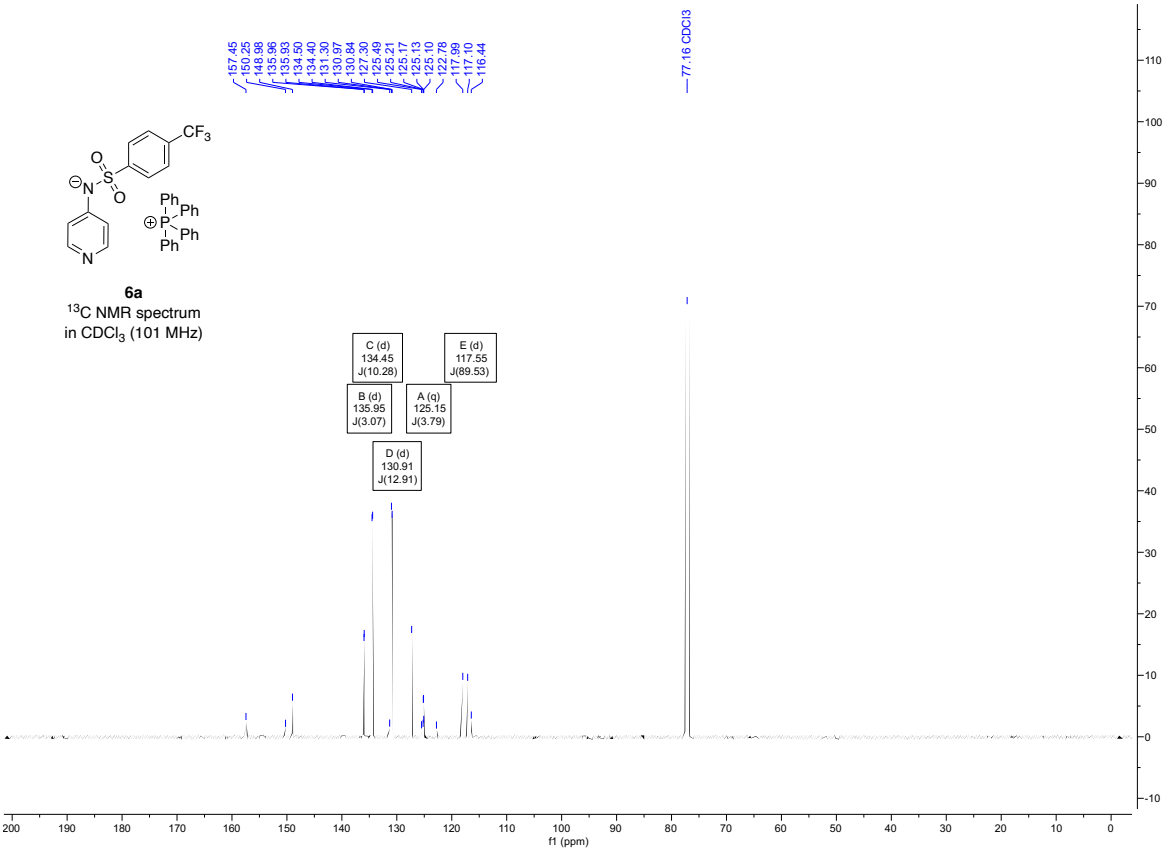

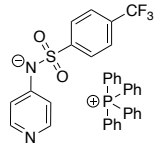

6a
^{19}F NMR spectrum
in $CDCl_3$ (376 MHz)

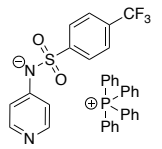

6a
^{31}P NMR spectrum
in $CDCl_3$ (162 MHz)

Triphenyl((triphenyl-λ5-phosphaneylidene)amino)phosphonium tetrafluoroborate (**7b**)

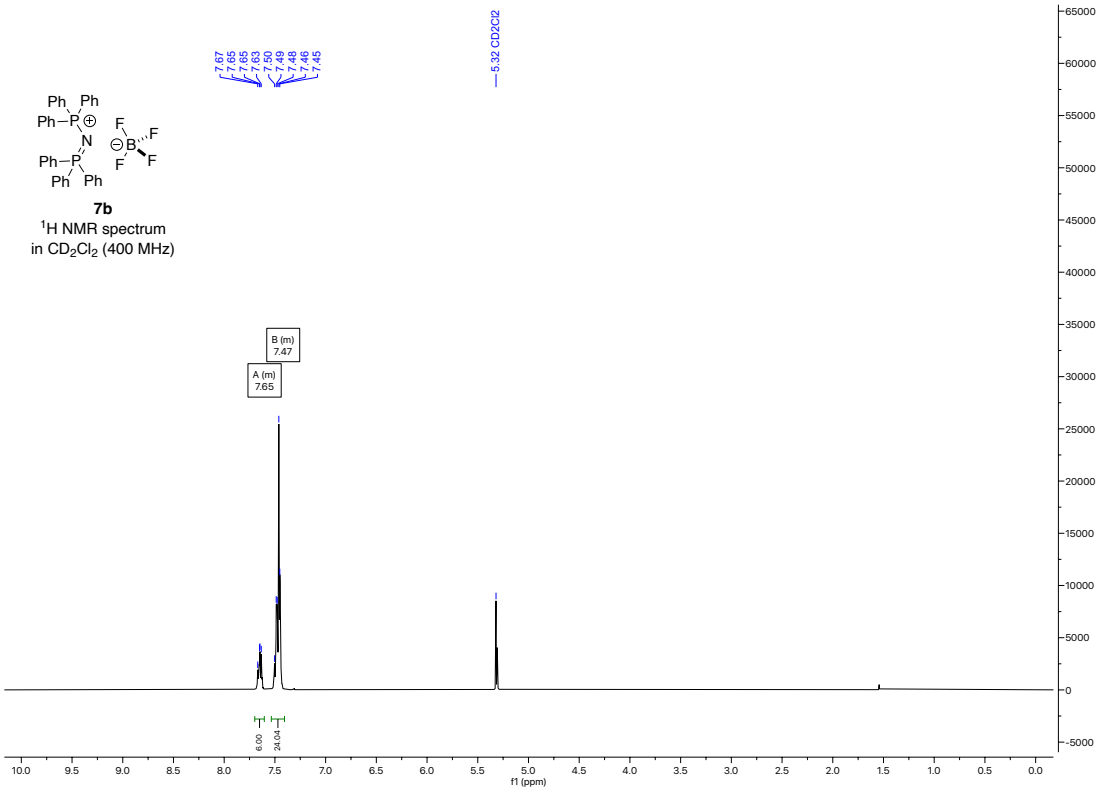

7b
^{1}H NMR spectrum
in CD_2Cl_2 (400 MHz)

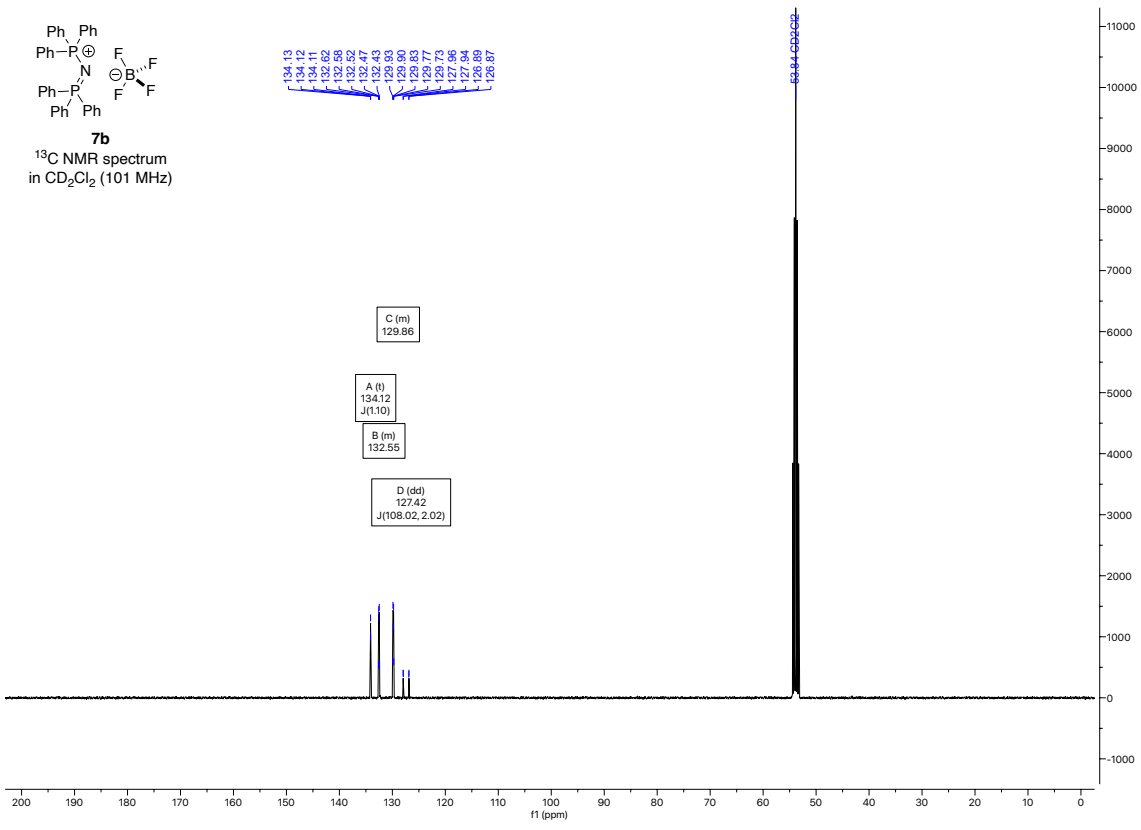

7b
^{13}C NMR spectrum
in CD_2Cl_2 (101 MHz)

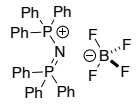

7b
^{19}F NMR spectrum
in CD_2Cl_2 (377 MHz)

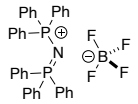

7b
^{31}P NMR spectrum
in CD_2Cl_2 (162 MHz)

Tetrabutylammonium tetrafluoroborate (**7c**)

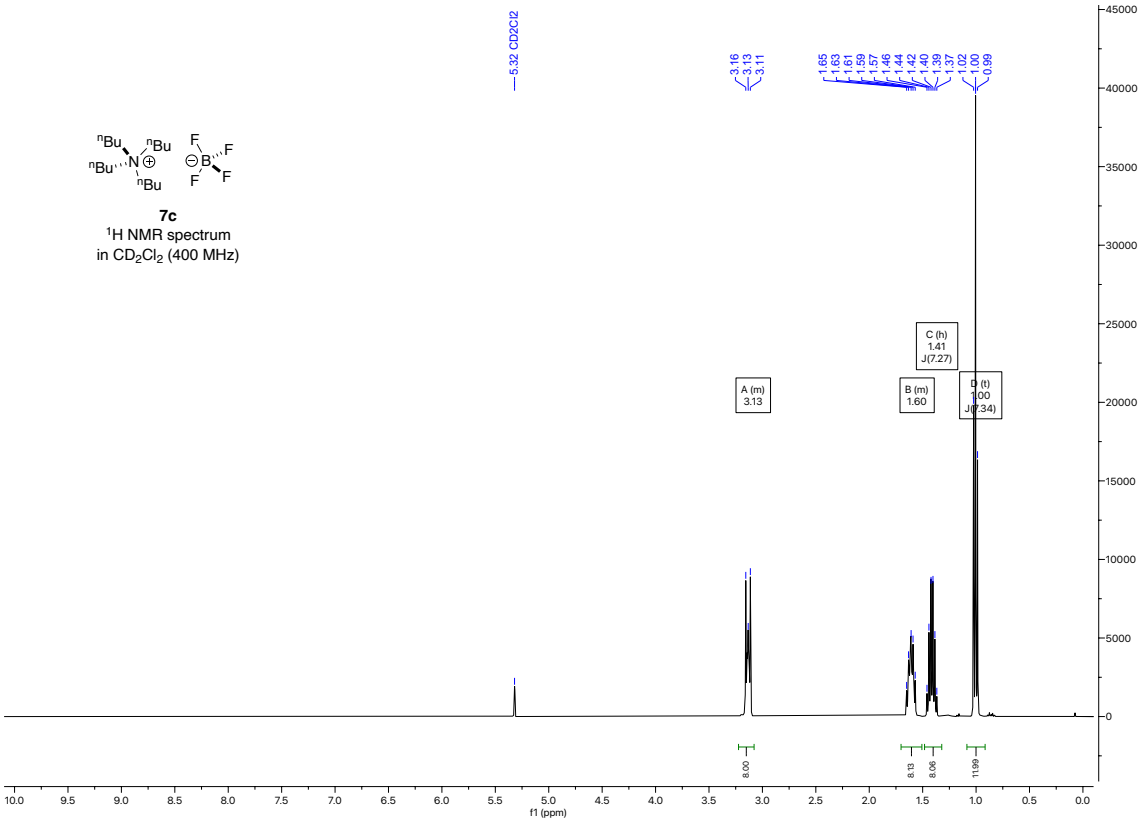

7c
^{1}H NMR spectrum
in CD_2Cl_2 (400 MHz)

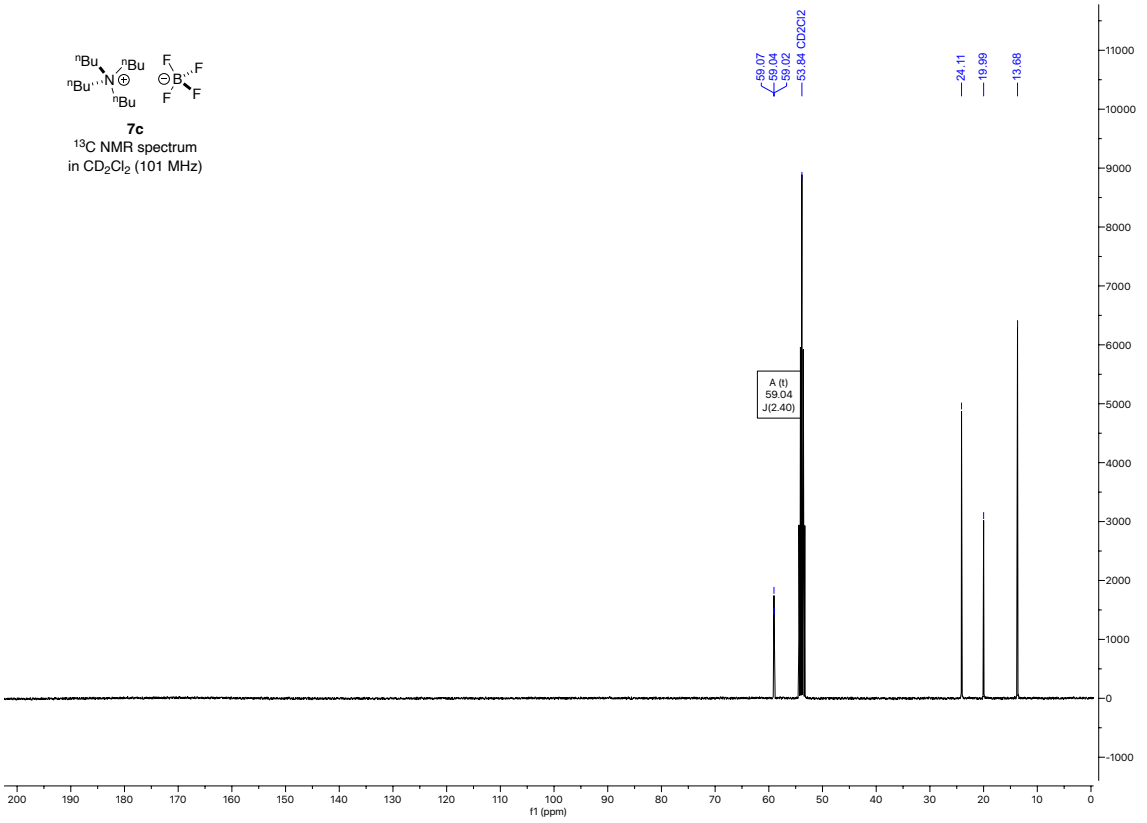

7c
^{13}C NMR spectrum
in CD_2Cl_2 (101 MHz)

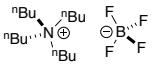

7c
^{19}F NMR spectrum
in CD_2Cl_2 (376 MHz)

Tetrabutylphosphonium tetrafluoroborate (**7d**)

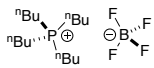

7d
^{1}H NMR spectrum
in CD_2Cl_2 (400 MHz)

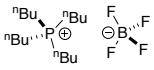

7d
^{13}C NMR spectrum
in CD_2Cl_2 (101 MHz)

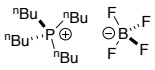

7d
^{19}F NMR spectrum
in CD_2Cl_2 (376 MHz)

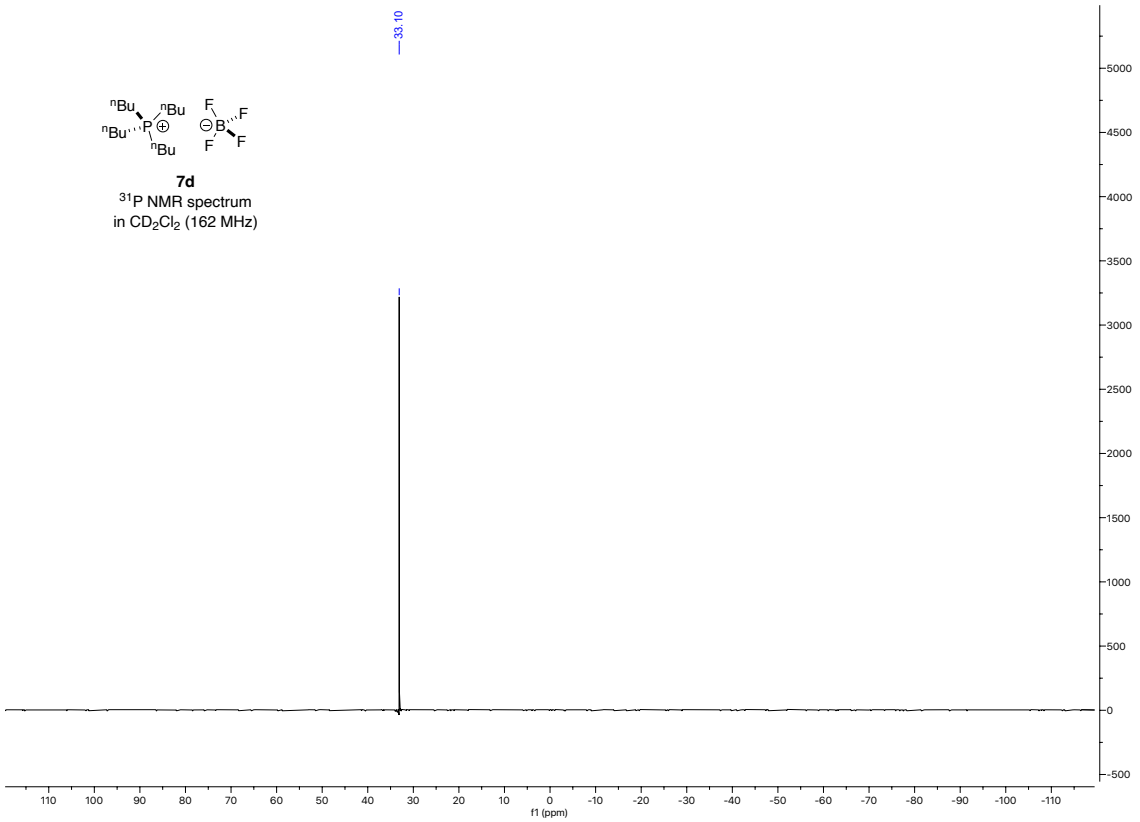

7d
^{31}P NMR spectrum
in CD_2Cl_2 (162 MHz)

3.1.10 Computational Studies

All substrate structures were optimized with the B3LYP-D3 hybrid functional[18–20] with the 6-31+G(d) basis set.[21] Solvent effects for dichloromethane have been calculated with the SMD continuum solvation model.[22] This combination has worked well in previous studies of charge-separated intermediates.[23–26] Frequency and single point calculations were performed at the same level of theory. Thermochemical correction to 198.15 K has been applied to all found minima from unscaled vibrational frequencies obtained at the same level of theory. To lessen the impact of low-lying frequencies of large systems on entropy and enthalpy in an unpredictable manner, a free-rotor approximation for entropy as proposed by Grimme[27] and a quasi-harmonic treatment with a cutoff value of 100 cm^{-1} using Goodvibes[28] was applied. Free energies in solution have been corrected to the reference state of 1.0 mol L^{-1} at 298.15 K by adding 7.925 kJ mol^{-1} to the free energies ($G_{298,qh,corr}$). All reported calculations were done with Gaussian 16, Revision A.03[29] and B.01[30].

The conformational search was performed with Maestro-. For ion pair and additive salt systems, a set of 150 starting points was obtained by using the stochastic kick procedure invented by Saunders[32] and further developed by Sakic.[33] At a time, a set of 50 starting points was generated by a combination of the best, the second-best conformer, and the third-best conformer of the prior separately optimized anion and cation. In case on ion does not have more than two anion conformers, the last 50 starting points were obtained from the combination of the best anion conformer with the third best cation conformer. The following kick settings were used: Distance parameter: 3 Å, Minimal Distance 1.5 Å, Number of Fragments: 1, Number of Files: 50.

Starting points for the conformers of the ion pair systems were obtained from Julian Helberg. Conformers for the new systems with tetraphenyl phosphonium as cation (**3-6a**) were obtained by manual modification of the corresponding triphenyl methyl phosphonium containing systems, initially calculated by Helberg[3], whereby the methyl group was replaced by a phenyl group. The starting point of ion pair **6a** were obtained by manual modification of the starting points of ion pair **5a** whereas the methyl group was manually fluorinated. Starting points for the *n*-butyl chained cations were generated by manually extending the methylated ion conformers of Julian Helberg. To represent tetraalkyl ammonium and tetraalkyl phosphonium cations (present in substrates **3c** and **3d**) without having to cover the entire conformational spaces of these largely flexible systems, the alkyl chains were restricted to their fully elongated, trans oriented state.

Starting points for the conformers of the sandwich cation and sandwich anion were obtained by sorting the optimized structures of the respective ion pair according to the total energy. The best six conformers were chosen and in combination with the best cation conformer the stochastic kick procedure invented by Saunders[32] and further developed by Sakic[33] was applied to generate 60 new substrate structures in total. The following kick settings were used: Distance parameter: 3 Å, Minimal Distance 1.5 Å, Number of Fragments: 1, Number of Files: 10.

The goal in calculating the respective triple ion conformers was to obtain the volumes based on the van der Waals cavities employed in the SMD continuum solvation model at the SMD(DCM)/B3LYP-D3/6-31+G(d) level of theory for the calculation of the volumes of ions based on the simulated concentrations in each respective conductivity model to compare the DOSY results with the results of the numerical simulations. Due to the heavy nature of the calculated systems (between 81 – 119 atoms) the less costly r^2SCAN-3c developed by Grimme[34] with Orca 5.0.3[35] was used for pre-optimizations, followed by single point calculations at the SMD(DCM)/B3LYP-D3/6-31+G(d) level of theory with Gaussian 16, Revision C.01[36].

The calculated ion volumes based on the van der Waals cavities employed in the SMD continuum solvation model at the SMD(DCM)/B3LYP-D3/6-31+G(d) level of theory with Gaussian 16 were used in the conductivity analysis (see Chapter 2.1.4 and Chapter 3.1.4). The calculated ion volumes of all computed species are summarized in Table 3.31.

Table 3.31: [Table S36]. Calculated isotropic polarizabilities and ion volumes for cations, anions, and ion aggregates based on the van der Waals cavity used in the SMD solvation model at the SMD(DCM)/B3LYP-D3/6-31+G(d) level of theory.

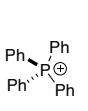

a_PPh$_4$

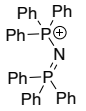

b_PNP

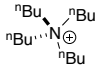

c_NBu$_4$

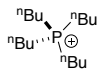

d_PBu$_4$

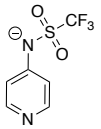

3

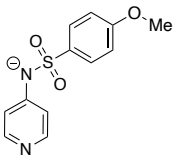

4

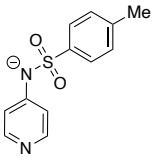

5

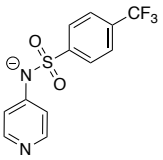

6

7

Ion Volume Values

Single Ions				1:1 Ion Pair		Triple Ion Complexes			
Anion	**Vol (Å³)**	**Cation**	**Vol (Å³)**	**Ion Pair**	**Vol (Å³)**	**CAC**	**Vol (Å³)**	**ACA**	**Vol (Å³)**
3	215	**a_PPh4**	362	**3a**	570	**a3a**	925	**3a3**	782
5	266	**b_PNP**	559	**3b**	769	**b3b**	1321	**3b3**	981
4	285	**c_NBu4**	313	**3c**	522	**c3c**	830	**3c3**	733
6	295	**d_PBu4**	326	**3d**	536	**d3d**	859	**3d3**	748
7	69.7			**4a**	641	**a4a**	995	**4a4**	920
				5a	624	**a5a**	980	**5a5**	887
				6a	651	**a6a**	1007	**6a6**	941
				7a	430				
				7b	629				
				7c	382				
				7d	396				

Polarizability Values

Single Ions				1:1 Ion Pair		Triple Ion Complexes			
Anion	**Iso Pol (Å³)**	**Cation**	**Iso Pol (Å³)**	**Ion Pair**	**Iso Pol (Å³)**	**CAC**	**Iso Pol (Å³)**	**ACA**	**Iso Pol (Å³)**
3	82.8	**a_PPh4**	214	**3a**	300	**a3a**	509	**3a3**	383
5	137	**b_PNP**	335	**3b**	421	**b3b**	748	**3b3**	504
4	140	**c_NBu4**	132	**3c**	219	**c3c**	351	**3c3**	305
6	137	**d_PBu4**	144	**3d**	230	**d3d**	373	**3d3**	316
7	12.5			**4a**	354	**a4a**	563	**4a4**	490
				5a	351	**a5a**	559	**5a5**	484
				6a	350	**a6a**	557	**6a6**	481
				7a	227				
				7b	348				
				7c	145				
				7d	157				

Calculating the volume of the ion pair by summing up the respective single cation and anion volumes and comparing it to the computed ion pair volume, we check if there is a problem regarding the additivity of these ions. The results are listed in Table 3.32.

Table 3.32: [Table S37]. Additivity analysis of ion aggregate volumes relative to the constituent ions based on SMD cavities calculated at the SMD(DCM)/B3LYP-D3/6-31+G(d) level of theory.

Ion aggregate	Constituent cation(s)	Constituent anion(s)	Sum of constituent volumes	Calculate volume	Volume difference[a]

3a	**a_PPh4**	**3**	577	570	-7.00
3b	**b_PNP**	**3**	774	769	-5.00
3c	**c_NBu4**	**3**	528	522	-6.00
3d	**d_PBu4**	**3**	541	536	-5.00
4a	**a_PPh4**	**4**	647	641	-6.00
5a	**a_PPh4**	**5**	628	624	-4.00
6a	**a_PPh4**	**6**	657	651	-6.00
7a	**a_PPh4**	**7**	432	430	-1.70
7b	**b_PNP**	**7**	629	629	0.30
7c	**c_NBu4**	**7**	383	382	-0.70
7d	**d_PBu4**	**7**	396	396	0.30
a3a	**a_PPh4**	**3**	939	925	-14.0
a4a	**b_PNP**	**3**	1333	1321	-12.0
c3c	**c_NBu4**	**3**	841	830	-11.0
d3d	**d_PBu4**	**3**	867	859	-8.00
a4a	**a_PPh4**	**4**	1009	995	-14.0
a5a	**a_PPh4**	**5**	990	980	-10.0
a6a	**a_PPh4**	**6**	1019	1007	-12.0
3a3	**a_PPh4**	**3**	792	782	-10.0
4a4	**b_PNP**	**3**	989	981	-8.00
3c3	**c_NBu4**	**3**	743	733	-10.0
3d3	**d_PBu4**	**3**	756	748	-8.00
4a4	**a_PPh4**	**4**	932	920	-12.0
5a5	**a_PPh4**	**5**	894	887	-7.00
6a6	**a_PPh4**	**6**	952	941	-11.0

[a] Volume difference = Calculated volume - Sum of constituent volumes.

Comparing calculated volumes with the sum of constituent ion volumes of a charged species show comparably low deviations. Therefore, the additivity for the ion volumes is given.

Another property we looked at is the isotropic polarizability ions at the SMD(DCM)/B3LYP-D3/6-31+G(d) level of theory which is given in Bohr^3 in the output file using Gaussian 16. With 1 Bohr = 0.529177 Å, we can convert these values to Å^3 by multiplying with $(0.529177)^3$ = 0.14818. The obtained isotropic polarizability values are summarized in Table 3.31 and correlated with the respective ion volumes in Figure 3.12.

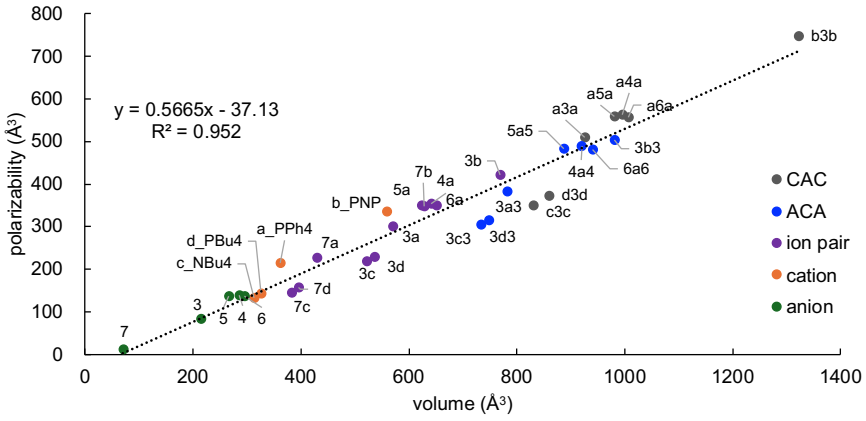

Figure 3.12: [Figure S13]. Correlation of calculated ion volumes (Å^3) vs. isotropic polarizability (Å^3) for all calculated single anions (green dots) and cations (orange dots), ion pairs (purple dots), cationic and anionic sandwich complexes (grey and blue dots).

Plotting the ion volumes vs. the isotropic polarizability gives a strong correlation which is remarkable considering the various type of species involved in this data set.

So far, the cation size seems to be a key factor regarding the final association pattern of the ion pair. To check whether the ion size is correlating with another association parameter, we calculated the mol fraction $\alpha/(\alpha+\beta)$ for the scaling factor α of the cationic sandwich association in the mixed model. The results are listed in Table 3.33. Additionally, we calculated the volume difference Δvolume (Å^3) between the cation and anion volumes.

Table 3.33: [Table S38]. List of cation volumes (Å^3).

Ion aggregate	Constituent cation(s)	Volume cation (Å^3)	Constituent anion(s)	α/β	$\alpha/(\alpha+\beta)$	Volume anion (Å^3)	Volume difference[a]
3a	**a_PPh4**	362	**3**	44/21	0.68	215	147
3b	**b_PNP**	559	**3**	100/0	1.00	215	344
3c	**c_NBu4**	313	**3**	33/23	0.59	215	98.0
4a	**a_PPh4**	362	**4**	12/61	0.16	285	77.0
5a	**a_PPh4**	362	**5**	11/67	0.14	266	96.0
6a	**a_PPh4**	362	**6**	16/52	0.24	295	67.0

[a] Volume difference = cation volume - anion volume.

The mol fraction as well as the scaling factor α was plotted against the calculated volume difference Δvolume (Å^3). Both graphs in Figure 3.13 show a strong correlation for ion pairs **3a**, **3b**, and **3c** where cation changes while the anion remains the same. The is no correlation when comparing ion pairs with changing anions and constant cation.

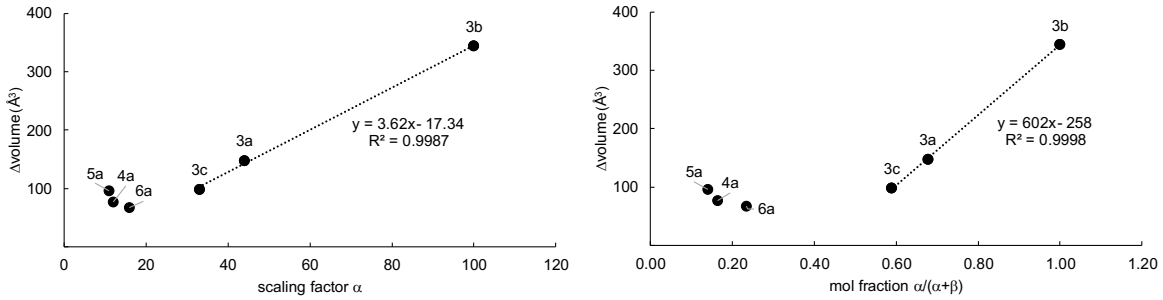

Figure 3.13: [Figure S14]. Left: correlation of scaling factor α with ion volume difference Δvolume (Å^3). Right: correlation of mol fraction $\alpha/(\alpha+\beta)$ with ion volume difference Δvolume (Å^3).

Assuming that other ion pairs such as **4a** would display a correlation with a similar slope when exchanging cation **a** (PPh_4^+) for cation **b** (PNP^+) we could predict the mol fraction for theoretical ion pair **4b** (see Figure 3.14).

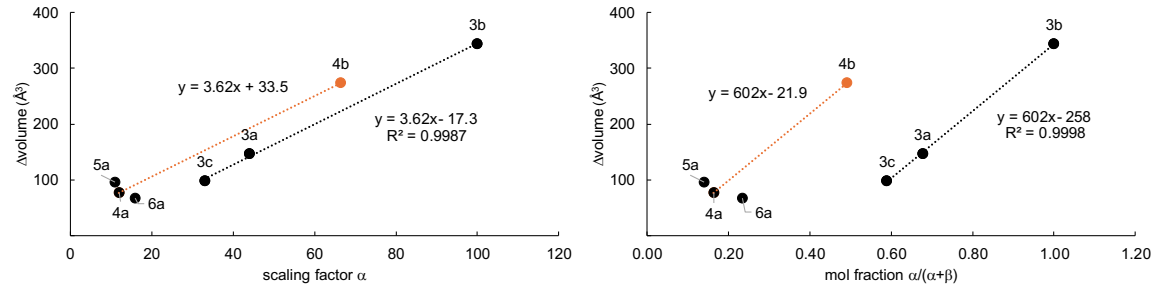

Figure 3.14: [Figure S15]. Left: correlation of scaling factor α with ion volume difference Δvolume (Å^3). Right: correlation of mol fraction $\alpha/(\alpha+\beta)$ with ion volume difference Δvolume (Å^3).

Thus, ion pair **4b** would have a scaling factor α of 66 and a mol fraction of 0.49 if this assumption is correct, which would indicate a predominated cationic sandwich association.

3.1.10.1 Optimized Conformers of Pyridinamide Ion Pairs in DCM

System 3b – computational data

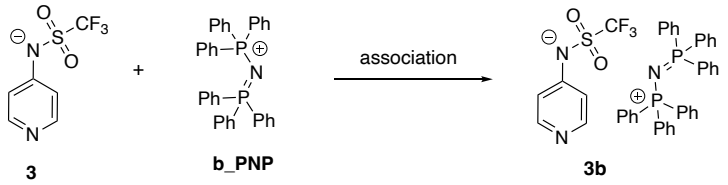

Figure 3.15: [Figure S16]. Ion association of pyridinamide ion pair **3b** and the single ions

The Boltzmann-averaged free reaction energy of the ion pairing of **3b** amounts to $\Delta G_{qh,298,corr}$ = 1.3 kJ mol^{-1} in DCM solution. Focusing only on the best conformers of the reactants and product the free reaction energy of the ion pairing of **3b** changes to $\Delta G_{qh,298,corr}$ = -1.8 kJ mol^{-1} in DCM solution. This result is mainly due to solvation effects since the gas phase free energy of the ion pairing amounts to $\Delta G_{qh,298}$ = -213.4 kJ mol^{-1}. In addition, we note that the contribution of the D3-dispersion correction amounts to ΔE_{disp} = -67.0 kJ mol^{-1} for the free energy in the DCM solution and in the gas phase. The blue marked cells show the Boltzmann-averaged values.

According to $\Delta G_{qh,298,corr}$ = -RT ln*K* and assuming R = 8.314 J K^{-1} mol^{-1} and T = 298.15 K, the respective equilibrium constant amounts to *K*(**3b**, DCM) = +2.06 for the best conformer of **3b** and to *K*(**3b**, DCM) = +0.60 for the Boltzmann-averaged free reaction energy. In this case the equilibrium constant *K* corresponds to the concentration of the reactants and products in the following way: *K* = [**3b**]/[**3**] [**b_PNP**] = [**3b**]/[**3**]^2.

Table 3.34: [Table S39]. Energies for all systems shown in Figure 3.15.

System	E_{tot} SMD(DCM)/ B3LYP-D3/ 6-31+G(d)	H_{298} SMD(DCM)/ B3LYP-D3/ 6-31+G(d)	$G_{qh,298}$ SMD(DCM)/ B3LYP-D3/ 6-31+G(d)	$G_{qh,298,corr}$ SMD(DCM)/ B3LYP-D3/ 6-31+G(d)	Cavity Volume (Å^3)	Relative Population Parameter based on $G_{qh,298}$
3						
an3_001	**-1188.8384606**	**-1188.7186926**	**-1188.769809**	**-1188.766790**	**215**	0.91
an3_002	-1188.8357192	-1188.7160622	-1188.7673382	-1188.7643197	214	0.09
			-1188.7693051	**-1188.7662866**	**215**	
b_PNP						
cation_c_002	**-2127.413003**	**-2126.821082**	**-2126.913057**	**-2126.910039**	**560**	0.51
cation_c_003	-2127.412921	-2126.820643	-2126.912356	-2126.909338	559	0.24
cation_c_001	-2127.412908	-2126.820541	-2126.912386	-2126.909367	559	0.25

			-2126.912720	**-2126.909702**	**559**	
3b[a]						
cat3b_124_dcm_fr	**-3316.275809**	**-3315.561663**	**-3315.680224**	**-3315.677206**	**768**	0.29
cat3b_020_dcm_fr	-3316.275058	-3315.560851	-3315.679373	-3315.676355	770	0.12
cat3b_147_dcm_fr	-3316.274602	-3315.560287	-3315.678876	-3315.675857	768	0.07
cat3b_136m_dcm	-3316.274338	-3315.560086	-3315.678610	-3315.675591	770	0.05
cat3b_140_dcm_fr	-3316.274329	-3315.560084	-3315.678552	-3315.675533	771	0.05
cat3b_053_dcm_fr	-3316.273923	-3315.559646	-3315.677960	-3315.674942	763	0.03
cat3b_104_dcm_fr	-3316.274181	-3315.559715	-3315.677871	-3315.674853	770	0.02
cat3b_145_dcm_fr	-3316.273835	-3315.559443	-3315.677862	-3315.674844	771	0.02
cat3b_059_dcm_fr	-3316.272931	-3315.559001	-3315.677746	-3315.674727	766	0.02
cat3b_043_dcm_fr	-3316.273208	-3315.559194	-3315.677712	-3315.674693	769	0.02
cat3b_073_dcm_fr	-3316.272688	-3315.558601	-3315.677594	-3315.674576	771	0.02
cat3b_096_dcm_fr	-3316.273468	-3315.559242	-3315.677589	-3315.674570	772	0.02
cat3b_015_dcm_fr	-3316.272868	-3315.558895	-3315.677588	-3315.674570	769	0.02
cat3b_108_dcm_fr	-3316.273117	-3315.559030	-3315.677570	-3315.674552	770	0.02
cat3b_022_dcm_fr	-3316.272537	-3315.558623	-3315.677469	-3315.674450	770	0.02
cat3b_042_dcm_fr	-3316.272400	-3315.558590	-3315.677322	-3315.674304	772	0.01
cat3b_030_dcm_fr	-3316.272439	-3315.558496	-3315.677313	-3315.674295	770	0.01
cat3b_032_dcm_fr	-3316.273425	-3315.558924	-3315.677248	-3315.674230	772	0.01
cat3b_048_dcm_fr	-3316.272623	-3315.558500	-3315.677195	-3315.674177	769	0.01
cat3b_021_dcm_fr	-3316.272520	-3315.558424	-3315.677002	-3315.673984	770	0.01
all			**-3315.678519**	**-3315.675501**	**769**	
ΔE	-63.92	-57.47	+6.14	-1.79		
all			**+9.21**	**+1.28**		

[a] best 20 conformers according to $G_{qh,298}$ at SMD(DCM)/B3LYP-D3/6-31+G(d) level of theory.

Table 3.35:[Table S40]. Energies of the best conformer for all systems shown in Figure 3.15 at different level of theory.

System	E_{tot}[a] B3LYP-D3/ 6-31+G(d)	$G_{qh,298}$[a] B3LYP-D3/ 6-31+G(d)	E_{tot}[a] B3LYP/ 6-31+G(d)	$G_{qh,298}$[a] B3LYP/ 6-31+G(d)	E_{tot}[a] SMD(DCM)/ B3LYP/ 6-31+G(d)	$G_{qh,298,corr}$[a] SMD(DCM)/ B3LYP/ 6-31+G(d)
3						
an3_001	-1188.770301	-1188.701344	-1188.753230	-1188.684273	-1188.821390	-1188.7494140

b_PNP						
cation_c_002	-2127.324579	-2126.824633	-2127.229977	-2126.730031	-2127.318402	-2126.815438
3b[a]						
cat3b_124	-3316.202835	-3315.607250	-3316.06563	-3315.470045	-3316.138605	-3315.540001
ΔE(3b, 3, b)	**-283.44**	**-213.38**	**-216.40**	**-146.35**	**+3.12**	**+65.25**

[a] using geometries optimized at SMD(DCM)/B3LYP-D3/6-31+G(d) level.

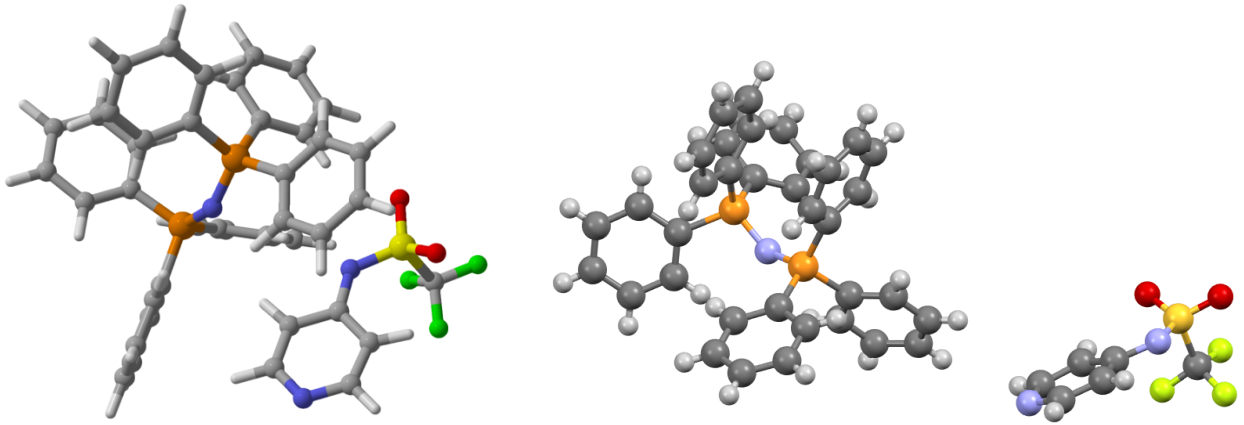

Figure 3.16: [Figure S17]. left: structure of conformer cat3b_124 calculated at SMD(DCM)/ B3LYP-D3/6-31+G(d) level of theory; right: crystal structure of one ion pair in catalyst **3b**.

System 3c – computational data

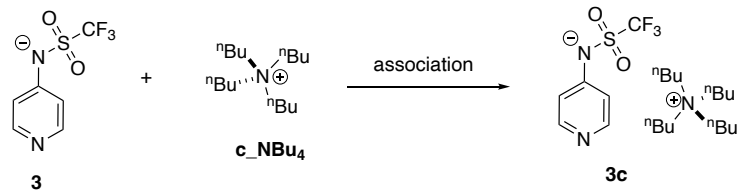

Figure 3.17: [Figure S18]. Ion association of pyridinamide ion pair **3c** and the single ions.

The Boltzmann-averaged free reaction energy of the ion pairing of **3c** amounts to $\Delta G_{qh,298,corr}$ = 7.3 kJ mol^{-1} in DCM solution. Focusing only on the best conformers of the reactants and product the free reaction energy of the ion pairing of **3c** changes to $\Delta G_{qh,298,corr}$ = +5.2 kJ mol^{-1} in DCM solution. This result is mainly due to solvation effects since the gas phase free energy of the ion pairing amounts to $\Delta G_{qh,298}$ = -243.8 kJ mol^{-1}. In addition, we note that the contribution of the D3-dispersion correction amounts to ΔE_{disp} = -50.0 kJ mol^{-1} for the free energy in the DCM solution and in the gas phase. The blue marked cells show the Boltzmann-averaged values.

According to $\Delta G_{qh,298,corr}$ = -RT ln*K* and assuming R = 8.314 J K^{-1} mol^{-1} and T = 298.15 K, the respective equilibrium constant amounts to *K*(**3c**, DCM) = +0.12 for the best conformer of **3c** and to *K*(**3c**, DCM) = +0.05 for the Boltzmann-averaged free reaction energy. In this case the equilibrium constant *K* corresponds to the concentration of the reactants and products in the following way: *K* = [**3c**]/[**3**] [**c_NBu4**] = [**3c**]/[**3**]^2.

Table 3.36: [Table S41]. Energies for all systems shown in Figure 3.17.

System	E_{tot} SMD(DCM)/ B3LYP-D3/ 6-31+G(d)	H_{298} SMD(DCM)/ B3LYP-D3/ 6-31+G(d)	$G_{qh,298}$ SMD(DCM)/ B3LYP-D3/ 6-31+G(d)	$G_{qh,298,corr}$ SMD(DCM)/ B3LYP-D3/ 6-31+G(d)	Cavity Volume (Å^3)	Relative Population Parameter based on $G_{qh,298}$
3						
an3_001	**-1188.8384606**	**-1188.7186926**	**-1188.769809**	**-1188.766790**	215	0.91
an3_002	-1188.8357192	-1188.7160622	-1188.7673382	-1188.7643197	214	0.09
			-1188.7693051	**-1188.7662866**	**215**	
c_NBu4						
NBu4_002	**-686.095346**	**-685.564482**	**-685.637042**	**-685.634023**	313	0.99
NBu4_001c	-686.094074	-685.564092	-685.632815	-685.629797	313	0.01
NBu4_006	-686.090709	-685.558999	-685.630636	-685.627618	312	0.00
NBu4_005	-686.089721	-685.557688	-685.629512	-685.626493	312	0.00
NBu4_003	-686.089384	-685.557149	-685.628989	-685.625971	312	0.00
NBu4_004	-686.086662	-685.553694	-685.624302	-685.621283	312	0.00

			-685.6369831	**-685.6339647**	**313**	
3c[a]						
cat3c_001_dcm	-1874.956418	**-1874.302434**	**-1874.401539**	**-1874.398520**	522	0.10
cat3c_034_dcm	-1874.956217	-1874.302034	-1874.401302	-1874.398284	523	0.08
cat3c_028_dcm	-1874.956268	-1874.302058	-1874.401246	-1874.398228	522	0.07
cat3c_003m_dcm_fr	-1874.956347	-1874.302312	-1874.401237	-1874.398219	522	0.07
cat3c_027_dcm	**-1874.957013**	-1874.302207	-1874.401158	-1874.398140	521	0.07
cat3c_036mm_dcm_fr	-1874.956034	-1874.301936	-1874.401090	-1874.398072	523	0.06
cat3c_009_dcm	-1874.956094	-1874.301719	-1874.400973	-1874.397954	521	0.05
cat3c_031_dcm	-1874.956330	-1874.301906	-1874.400938	-1874.397920	520	0.05
cat3c_026_dcm	-1874.956044	-1874.301623	-1874.400868	-1874.397849	524	0.05
cat3c_029_dcm	-1874.955676	-1874.301445	-1874.400546	-1874.397528	523	0.03
cat3c_035bp_dcm_fr	-1874.956082	-1874.301776	-1874.400515	-1874.397497	523	0.03
cat3c_021_dcm	-1874.955681	-1874.301376	-1874.400392	-1874.397374	522	0.03
cat3c_057_dcm	-1874.955604	-1874.301212	-1874.400303	-1874.397284	522	0.03
cat3c_023_dcm	-1874.954437	-1874.300508	-1874.400231	-1874.397212	522	0.02
cat3c_033aa_dcm	-1874.955485	-1874.301102	-1874.400056	-1874.397038	522	0.02
cat3c_054_dcm	-1874.955693	-1874.301116	-1874.399912	-1874.396893	522	0.02
cat3c_072_dcm	-1874.955489	-1874.300937	-1874.399899	-1874.396880	521	0.02
cat3c_041a_dcm	-1874.955713	-1874.301023	-1874.399884	-1874.396866	521	0.02
cat3c_042_dcm	-1874.954777	-1874.300537	-1874.399813	-1874.396794	523	0.02
cat3c_002_dcm	-1874.955041	-1874.300786	-1874.399681	-1874.396663	523	0.01
all			**-1874.400652**	**-1874.397634**	**522**	
ΔE	-60.93	-52.57	+13.14	+5.22		
all			**+15.21**	**+7.28**		

[a] best 20 conformers according to $G_{qh,298}$ at SMD(DCM)/B3LYP-D3/6-31+G(d) level of theory.

Table 3.37: [Table S42]. Energies of the best conformer for all systems shown in Figure 3.17 at different level of theory.

System	E_{tot}[a] B3LYP-D3/ 6-31+G(d)	$G_{qh,298}$[a] B3LYP-D3/ 6-31+G(d)	E_{tot}[a] B3LYP/ 6-31+G(d)	$G_{qh,298}$[a] B3LYP/ 6-31+G(d)	E_{tot}[a] SMD(DCM)/ B3LYP/ 6-31+G(d)	$G_{qh,298,corr}$[a] SMD(DCM)/ B3LYP/ 6-31+G(d)
3						
an3_001	-1188.770301	-1188.701344	-1188.753230	-1188.684273	-1188.821390	-1188.7494140
c_NBu4						
NBu4_002	-686.009748	-685.551444	-685.954640	-685.496336	-686.040238	-685.578915
3c[a]						
cat3c_001_dcm	-1874.900521	-1874.345642	-1874.809296	-1874.254417	-1874.865193	-1874.307295
ΔE(3c, 3, c)	-316.30	-243.79	-266.29	-193.78	-9.36	+55.23

[a] using geometries optimized at SMD(DCM)/B3LYP-D3/6-31+G(d) level.

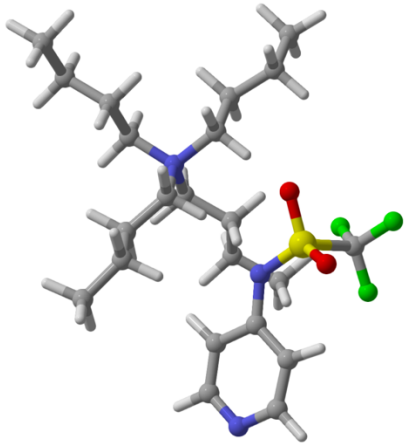

Figure 3.18: [Figure S19]. Structure of conformer cat3c_001 calculated at SMD(DCM)/ B3LYP-D3/6-31+G(d) level of theory

System 3d – computational data

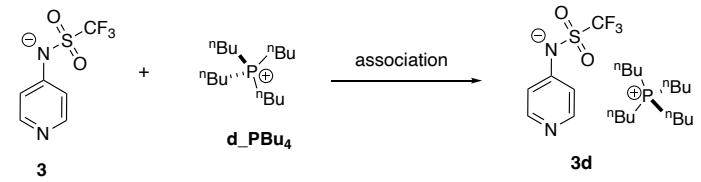

Figure 3.19: [Figure S20]. Ion association of pyridinamide ion pair **3d** and the single ions.

The Boltzmann-averaged free reaction energy of the ion pairing of **3d** amounts to $\Delta G_{qh,298,corr}$ = +1.1 kJ mol^{-1} in DCM solution. Focusing only on the best conformers of the reactants and product the free reaction energy of the ion pairing of **3d** changes to $\Delta G_{qh,298,corr}$ = +1.3 kJ mol^{-1} in DCM solution. This result is mainly due to solvation effects since the gas phase free energy of the ion pairing amounts to $\Delta G_{qh,298}$ = -250.4 kJ mol^{-1}. In addition, we note that the contribution of the D3-dispersion correction amounts to ΔE_{disp} = +176.3 kJ mol^{-1} for the free energy in the DCM solution and in the gas phase. The blue marked cells show the Boltzmann-averaged values.

According to $\Delta G_{qh,298,corr}$ = -RT ln*K* and assuming R = 8.314 J K^{-1} mol^{-1} and T = 298.15 K, the respective equilibrium constant amounts to *K*(**3d**, DCM) = +0.59 for the best conformer of **3d** and to *K* (**3d**, DCM) = +0.65 for the Boltzmann-averaged free reaction energy. In this case the equilibrium constant K corresponds to the concentration of the reactants and products in the following way: *K* = [**3d**]/[**3**] [**d_PBu4**] = [**3d**]/[**3**]^2.

Table 3.38: [Table S43]. Energies for all systems shown in Figure 3.19.

System	E_{tot} SMD(DCM)/ B3LYP-D3/ 6-31+G(d)	H_{298} SMD(DCM)/ B3LYP-D3/ 6-31+G(d)	$G_{qh,298}$ SMD(DCM)/ B3LYP-D3/ 6-31+G(d)	$G_{qh,298,corr}$ SMD(DCM)/ B3LYP-D3/ 6-31+G(d)	Cavity Volume (Å^3)	Relative Population Parameter based on $G_{qh,298}$
3						
an3_001	**-1188.8384606**	**-1188.7186926**	**-1188.769809**	**-1188.766790**	**215**	0.91
an3_002	-1188.8357192	-1188.7160622	-1188.7673382	-1188.7643197	214	0.09
			-1188.7693051	**-1188.7662866**	**215**	
d_PBu4						
PBu4_001_dcm_fr	**-972.730410**	**-972.207922**	**-972.283263**	**-972.280245**	**326**	0.71
PBu4_002b_pos	-972.729488	-972.206599	-972.282049	-972.279030	327	0.20
PBu4_003_dcm_fr	-972.727645	-972.204727	-972.280491	-972.277472	326	0.04
PBu4_005_dcm_fr	-972.728208	-972.205291	-972.280338	-972.277319	326	0.03
PBu4_004_dcm_fr	-972.727749	-972.204384	-972.279426	-972.276408	326	0.01
PBu4_006_dcm_fr	-972.726367	-972.203286	-972.278751	-972.275732	326	0.01

PBu4_007_dcm_fr	-972.725758	-972.202871	-972.278552	-972.275534	327	0.00
			-972.282730	**-972.279711**	**326**	
cat3d[a]						
cat3d_031_dcm_fr	-2161.591204	-2160.946455	**-2161.049248**	**-2161.046230**	536	0.05
cat3d_041a_dcm_fr	-2161.590889	-2160.946323	-2161.049170	-2161.046152	535	0.04
cat3d_027_dcm_fr	**-2161.591598**	**-2160.946633**	-2161.049140	-2161.046122	536	0.04
cat3d_029_dcm_fr	-2161.590751	-2160.946099	-2161.049124	-2161.046106	537	0.04
cat3d_001_dcm_fr	-2161.591275	-2160.946562	-2161.049074	-2161.046055	536	0.04
cat3d_013_dcm_fr	-2161.591276	-2160.946557	-2161.049068	-2161.046049	536	0.04
cat3d_034_dcm_fr	-2161.590791	-2160.946235	-2161.049054	-2161.046035	537	0.04
cat3d_057_dcm_fr	-2161.591600	-2160.946514	-2161.049037	-2161.046019	536	0.04
cat3d_004_dcm_fr	-2161.590797	-2160.946216	-2161.049006	-2161.045988	537	0.04
cat3d_020p_dcm_fr	-2161.590748	-2160.945995	-2161.048963	-2161.045945	536	0.04
cat3d_011_dcm_fr	-2161.590818	-2160.946070	-2161.048929	-2161.045911	537	0.03
cat3d_033a_dcm_fr	-2161.590646	-2160.945991	-2161.048913	-2161.045895	538	0.03
cat3d_025p_dcm_fr	-2161.591113	-2160.946250	-2161.048881	-2161.045862	537	0.03
cat3d_052_dcm_fr	-2161.590437	-2160.945840	-2161.048854	-2161.045835	535	0.03
cat3d_028_dcm_fr	-2161.590914	-2160.946146	-2161.048824	-2161.045805	536	0.03
cat3d_008_dcm_fr	-2161.590811	-2160.946001	-2161.048782	-2161.045764	537	0.03
cat3d_018_dcm_fr	-2161.591009	-2160.946197	-2161.048743	-2161.045724	537	0.03
cat3d_003_dcm_fr	-2161.591285	-2160.946372	-2161.048742	-2161.045723	536	0.03
cat3d_054_dcm_fr	-2161.591052	-2160.946085	-2161.048724	-2161.045706	535	0.03
cat3d_007p_dcm_fr	-2161.591297	-2160.946399	-2161.048721	-2161.045702	536	0.03
all			**-2161.048612**	**-2161.045594**	**536**	
ΔE	-59.68	-52.56	+9.24	+1.31		
all			**+8.99**	**+1.06**		

[a] best 20 conformers according to $G_{qh,298}$ at SMD(DCM)/B3LYP-D3/6-31+G(d) level of theory.

Table 3.39: [Table S44]. Energies of the best conformer for all systems shown in Figure 3.19 at different level of theory.

System	E_{tot}[a] B3LYP-D3/ 6-31+G(d)	$G_{qh,298}$[a] B3LYP-D3/ 6-31+G(d)	E_{tot}[a] B3LYP/ 6-31+G(d)	$G_{qh,298}$[a] B3LYP/ 6-31+G(d)	E_{tot}[a] SMD(DCM)/ B3LYP/ 6-31+G(d)	$G_{qh,298,corr}$[a] SMD(DCM)/ B3LYP/ 6-31+G(d)
3						
an3_001	-1188.770301	-1188.701344	-1188.753230	-1188.684273	-1188.821390	-1188.7494140
d_PBu4						
PBu4_001	-972.643814	-972.196667	-972.679808	-972.232661	-972.593212	-972.143046
cat3d[a]						
cat3d_031	-2161.535344	-2160.993388	-2161.448224	-2160.906268	-2161.504084	-2160.959110
ΔE(3d, 3, d)	**-318.29**	**-250.41**	**-39.87**	**+28.00**	**-234.94**	**-174.99**

[a] using geometries optimized at SMD(DCM)/B3LYP-D3/6-31+G(d) level.

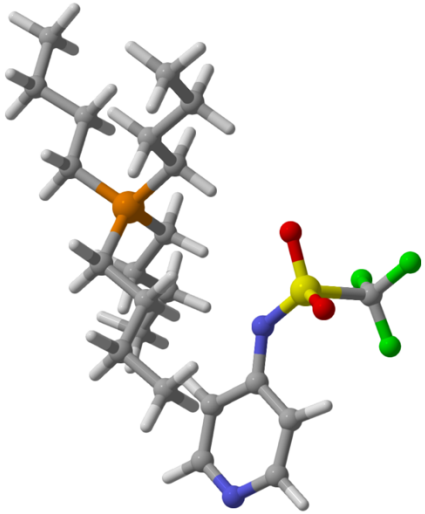

Figure 3.20: [Figure S21]. structure of conformer cat**3d**_008 calculated at SMD(DCM)/ B3LYP-D3/6-31+G(d) level of theory.

System 5a – computational data

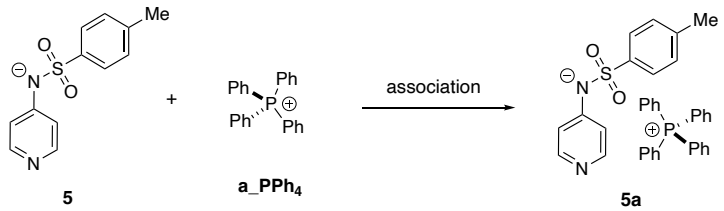

Figure 3.21: [Figure S22]. Ion association of pyridinamide ion pair **5a** and the single ions.

The Boltzmann-averaged free reaction energy of the ion pairing of **5a** amounts to $\Delta G_{qh,298,corr}$ = -3.8 kJ mol^{-1} in DCM solution. Focusing only on the best conformers of the reactants and product the free reaction energy of the ion pairing of **5a** changes to $\Delta G_{qh,298,corr}$ = -4.8 kJ mol^{-1} in DCM solution. This result is mainly due to solvation effects since the gas phase free energy of the ion pairing amounts to $\Delta G_{qh,298}$ = -224.4 kJ mol^{-1}. In addition, we note that the contribution of the D3-dispersion correction amounts to ΔE_{disp} = +136.5 kJ mol^{-1} for the free energy in the DCM solution and in the gas phase. The blue marked cells show the Boltzmann-averaged values.

According to $\Delta G_{qh,298,corr}$ = -RT ln*K* and assuming R = 8.314 J K^{-1} mol^{-1} and T = 298.15 K, the respective equilibrium constant amounts to *K*(**5a**, DCM) = +7.0 for the best conformer of **5a** and to *K*(**5a**, DCM) = +4.5 for the Boltzmann-averaged free reaction energy. In this case the equilibrium constant *K* corresponds to the concentration of the reactants and products in the following way: *K* = [**5a**]/[**5**] [**a_PPh4**] = [**5a**]/[**5**]^2.

Table 3.40: [Table S45]. Energies for all systems shown in Figure 3.21.

System	E_{tot} SMD(DCM)/ B3LYP-D3/ 6-31+G(d)	H_{298} SMD(DCM)/ B3LYP-D3/ 6-31+G(d)	$G_{qh,298}$ SMD(DCM)/ B3LYP-D3/ 6-31+G(d)	$G_{qh,298,corr}$ SMD(DCM)/ B3LYP-D3/ 6-31+G(d)	Cavity Volume (Å^3)	Relative Population Parameter based on $G_{qh,298}$
5						
an5_001_dcm	**-1122.186986**	**-1121.960277**	**-1122.016776**	**-1122.013757**	**266**	0.82
an5_002a_dcm	-1122.184655	-1121.958007	-1122.014729	-1122.011711	267	0.09
an5_003_dcm	-1122.184683	-1121.957984	-1122.014655	-1122.011636	267	0.09
			-1122.016400	**-1122.013381**	**266**	
a_PPh4						
PPh4_003a	-1267.9099858	**-1267.5207058**	**-1267.5885298**	**-1267.5855113**	**360**	0.46
PPh4_001	-1267.9100736	-1267.5203936	-1267.5881566	-1267.5851381	364	0.31
PPh4_002f	**-1267.9100864**	-1267.5202704	-1267.5878314	-1267.5848129	362	0.22
			-1267.5882580	**-1267.5852395**	**362**	

5a[a]						
cat5a_012_dcm_fr	**-2390.123118**	**-2389.504272**	**-2389.604120**	**-2389.601102**	**625**	0.13
cat5a_078m_dcm_fr	-2390.122167	-2389.503803	-2389.603890	-2389.600871	621	0.10
cat5a_041_dcm_fr	-2390.121537	-2389.503322	-2389.603789	-2389.600771	624	0.09
cat5a_032_dcm_fr	-2390.121516	-2389.503282	-2389.603532	-2389.600514	623	0.07
cat5a_028_dcm_fr	-2390.121504	-2389.503143	-2389.603493	-2389.600474	625	0.07
cat5a_013_dcm_fr	-2390.121659	-2389.503236	-2389.603382	-2389.600363	624	0.06
cat5a_063_dcm_fr	-2390.122080	-2389.503363	-2389.603183	-2389.600164	625	0.05
cat5a_069_dcm_fr	-2390.121584	-2389.503089	-2389.603162	-2389.600143	626	0.05
cat5a_026_dcm_fr	-2390.121046	-2389.502972	-2389.603153	-2389.600135	623	0.05
cat5a_037_dcm_fr	-2390.120816	-2389.502607	-2389.602888	-2389.599869	624	0.04
cat5a_065am_dcm_fr	-2390.121449	-2389.502741	-2389.602660	-2389.599641	625	0.03
cat5a_057_dcm_fr	-2390.121561	-2389.502919	-2389.602533	-2389.599515	623	0.02
cat5a_046_dcm_fr	-2390.119762	-2389.501712	-2389.602329	-2389.599311	620	0.02
cat5a_018_dcm_fr	-2390.120212	-2389.502005	-2389.602274	-2389.599256	622	0.02
cat5a_048a_dcm_fr	-2390.120156	-2389.501910	-2389.602252	-2389.599233	625	0.02
cat5a_070a_dcm_fr	-2390.120100	-2389.501971	-2389.602233	-2389.599215	621	0.02
cat5a_061_dcm_fr	-2390.120222	-2389.501959	-2389.602151	-2389.599133	625	0.02
cat5a_083_dcm_fr	-2390.121484	-2389.502563	-2389.602024	-2389.599005	624	0.01
cat5a_003_dcm_fr	-2390.121455	-2389.502636	-2389.602022	-2389.599004	621	0.01
cat5a_020_dcm_fr	-2390.120352	-2389.501930	-2389.602002	-2389.598984	624	0.01
all			**-2389.603068**	**-2389.600049**	**624**	
ΔE	-68.38	-61.15	+3.11	-4.81		
all			**+4.18**	**-3.75**		

[a] best 20 conformers according to $G_{qh,298}$ at SMD(DCM)/B3LYP-D3/6-31+G(d) level of theory.

Table 3.41: [Table S46]. Energies of the best conformer for all systems shown in Figure 3.21 at different level of theory.

System	E_{tot}[a] B3LYP-D3/ 6-31+G(d)	$G_{qh,298}$[a] B3LYP-D3/ 6-31+G(d)	E_{tot}[a] B3LYP/ 6-31+G(d)	$G_{qh,298}$[a] B3LYP/ 6-31+G(d)	E_{tot}[a] SMD(DCM)/ B3LYP/ 6-31+G(d)	$G_{qh,298,corr}$[a] SMD(DCM)/ B3LYP/ 6-31+G(d)
5						
an5_001	-1122.102832	-1121.932622	-1122.158865	-1121.988655	-1122.074711	-1121.901483
a_PPh4						

PPh4_003a	-1267.828115	-1267.506659	-1267.778739	-1267.457283	-1267.860609	-1267.5361348
5a[a]						
cat5a_012	-2390.043728	-2389.524730	-2389.934069	-2389.415071	-2390.013459	-2389.491443
ΔE(5a, 5, a)	**-285.83**	**-218.53**	**-228.13**	**-160.83**	**-0.54**	**+58.83**

[a] using geometries optimized at SMD(DCM)/B3LYP-D3/6-31+G(d) level.

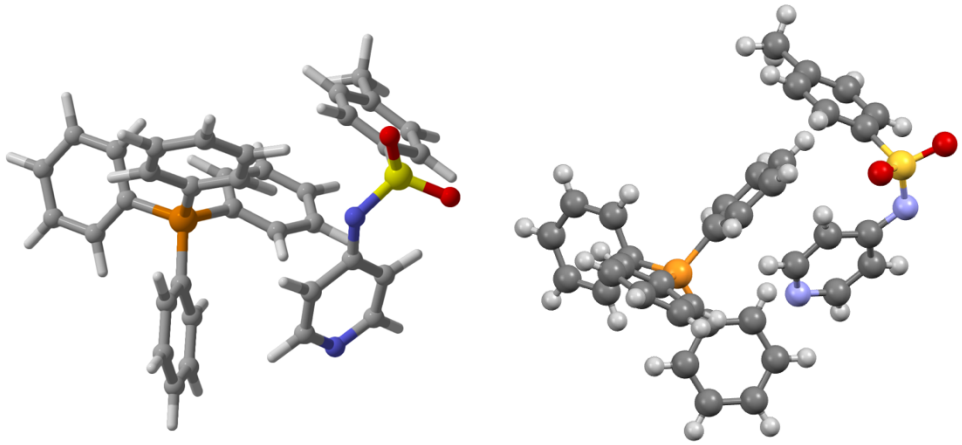

Figure 3.22: [Figure S23]. left: structure of conformer cat**5a**_012 calculated at SMD(DCM)/ B3LYP-D3/6-31+G(d) level of theory; right: crystal structure of one ion pair in catalyst **5a**.

System 6a – computational data

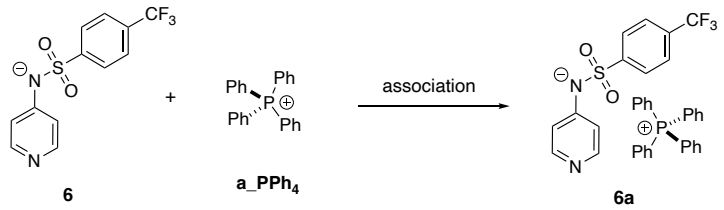

Figure 3.23: [Figure S24]. Ion association of pyridinamide ion pair **6a** and the single ions.

The Boltzmann-averaged free reaction energy of the ion pairing of **6a** amounts to $\Delta G_{qh,298,corr}$ = -3.8 kJ mol^{-1} in DCM solution. Focusing only on the best conformers of the reactants and product the free reaction energy of the ion pairing of **6a** changes to $\Delta G_{qh,298,corr}$ = -5.3 kJ mol^{-1} in DCM solution. This result is mainly due to solvation effects since the gas phase free energy of the ion pairing amounts to $\Delta G_{qh,298}$ = -216.2 kJ mol^{-1}. In addition, we note that the contribution of the D3-dispersion correction amounts to ΔE_{disp} = +115.8 kJ mol^{-1} for the free energy in the DCM solution and in the gas phase. The blue marked cells show the Boltzmann-averaged values.

According to $\Delta G_{qh,298,corr}$ = -RT ln*K* and assuming R = 8.314 J K^{-1} mol^{-1} and T = 298.15 K, the respective equilibrium constant amounts to *K*(**6a**, DCM) = 8.5 for the best conformer of **6a** and to *K*(**6a**, DCM) = 4.6 for the Boltzmann-averaged free reaction energy. In this case the equilibrium constant *K* corresponds to the concentration of the reactants and products in the following way: *K* = [**6a**]/[**6**] [**a_PPh4**] = [**6a**]/[**6**]^2.

Table 3.42: [Table S47]. Energies for all systems shown in Figure 3.23.

System	E_{tot} SMD(DCM)/ B3LYP-D3/ 6-31+G(d)	H_{298} SMD(DCM)/ B3LYP-D3/ 6-31+G(d)	$G_{qh,298}$ SMD(DCM)/ B3LYP-D3/ 6-31+G(d)	$G_{qh,298,corr}$ SMD(DCM)/ B3LYP-D3/ 6-31+G(d)	Cavity Volume (Å^3)	Relative Population Parameter based on $G_{qh,298}$
6						
an6_001	**-1419.929810**	**-1419.724473**	**-1419.784896**	**-1419.781877**	**295**	0.89
an6_002	-1419.927369	-1419.722133	-1419.782897	-1419.779879	294	0.11
			-1419.784681	**-1419.781662**	**295**	
a_PPh4						
PPh4_003a	-1267.9099858	**-1267.5207058**	**-1267.5885298**	**-1267.5855113**	**360**	0.46
PPh4_001	-1267.9100736	-1267.5203936	-1267.5881566	-1267.5851381	364	0.31
PPh4_002f	**-1267.9100864**	-1267.5202704	-1267.5878314	-1267.5848129	362	0.22
			-1267.5882580	**-1267.5852395**	**362**	

6a[a]						
cat6a_012_dcm	-2687.866218	**-2687.269030**	**-2687.372424**	**-2687.369405**	**651**	0.16
cat6a_062_dcm	-2687.865545	-2687.268462	-2687.371852	-2687.368833	652	0.09
cat6a_077_dcm	-2687.865538	-2687.268342	-2687.371699	-2687.368681	649	0.07
cat6a_049_dcm	-2687.864657	-2687.267827	-2687.371664	-2687.368645	650	0.07
cat6a_003_dcm	**-2687.866341**	-2687.268788	-2687.371615	-2687.368597	651	0.07
cat6a_075p_dcm	-2687.865276	-2687.268285	-2687.371478	-2687.368459	651	0.06
cat6a_040_dcm	-2687.864450	-2687.267618	-2687.371469	-2687.368450	648	0.06
cat6a_056_dcm	-2687.865655	-2687.268398	-2687.371412	-2687.368394	653	0.05
cat6a_032_dcm	-2687.864713	-2687.267699	-2687.371402	-2687.368384	651	0.05
cat6a_028m_dcm	-2687.864474	-2687.267546	-2687.371337	-2687.368319	649	0.05
cat6a_002_dcm	-2687.865084	-2687.268002	-2687.371209	-2687.368190	653	0.04
cat6a_021_dcm	-2687.864480	-2687.267547	-2687.371013	-2687.367994	653	0.04
cat6a_026p_dcm	-2687.864470	-2687.267495	-2687.370956	-2687.367937	652	0.03
cat6a_068_dcm	-2687.864753	-2687.267464	-2687.370856	-2687.367837	653	0.03
cat6a_064m_dcm	-2687.864473	-2687.267166	-2687.370527	-2687.367509	652	0.02
cat6a_041_dcm	-2687.863090	-2687.266142	-2687.370069	-2687.367051	649	0.01
cat6a_047_dcm	-2687.863096	-2687.266094	-2687.369983	-2687.366965	649	0.01
cat6a_016_dcm	-2687.863649	-2687.266488	-2687.369931	-2687.366912	652	0.01
cat6a_048_dcm	-2687.862693	-2687.265908	-2687.369813	-2687.366795	651	0.01
cat6a_018_dcm	-2687.862898	-2687.266030	-2687.369766	-2687.366748	649	0.01
all			**-2687.371356**	**-2687.368337**	**641**	
ΔE	-69.43	-62.62	+2.63	-5.30		
all			**+4.16**	**-3.77**		

[a] best 20 conformers according to $G_{qh,298}$ at SMD(DCM)/B3LYP-D3/6-31+G(d) level of theory.

Table 3.43: [Table S48]. Energies of the best conformer for all systems shown in Figure 3.23 at different level of theory.

System	**E_{tot}[a] B3LYP-D3/ 6-31+G(d)**	**$G_{qh,298}$[a] B3LYP-D3/ 6-31+G(d)**	**E_{tot}[a] B3LYP/ 6-31+G(d)**	**$G_{qh,298}$[a] B3LYP/ 6-31+G(d)**	**E_{tot}[a] SMD(DCM)/ B3LYP/ 6-31+G(d)**	**$G_{qh,298,corr}$[a] SMD(DCM)/ B3LYP/ 6-31+G(d)**
6						
an6_001	-1419.853500	-1419.708586	-1419.823428	-1419.678514	-1419.823428	-1419.675496
a_PPh4						
PPh4_003a	-1267.828115	-1267.506659	-1267.778739	-1267.457283	-1267.860609	-1267.5361348

6a[a]						
cat6a_012	-2687.791372	-2687.297578	-2687.679722	-2687.185928	-2687.754568	-2687.257755
ΔE(6a, 6, a)	**-288.17**	**-216.17**	**-203.62**	**-131.62**	**-185.18**	**-121.10**

[a] using geometries optimized at SMD(DCM)/B3LYP-D3/6-31+G(d) level.

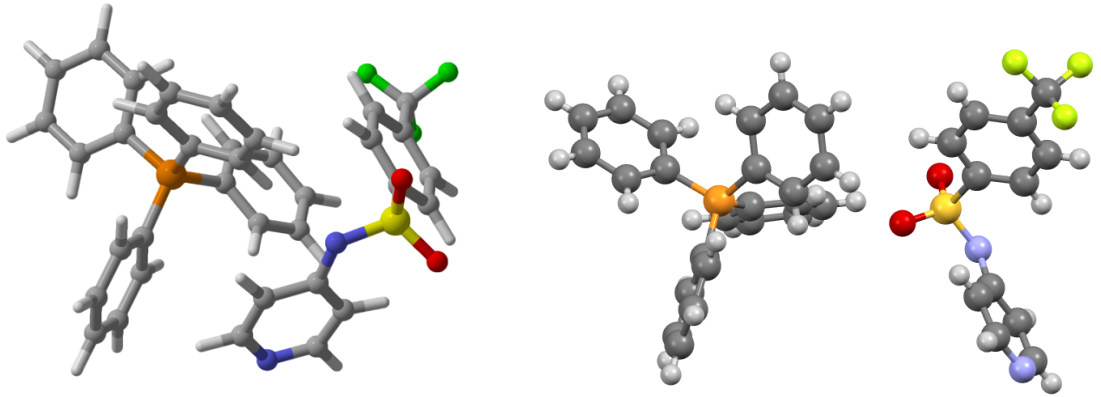

Figure 3.24: [Figure S25]. left: structure of conformer cat**6a**_012 calculated at SMD(DCM)/ B3LYP-D3/6-31+G(d) level of theory; right: crystal structure of one ion pair in catalyst **6a**.

3.1.10.2 Calculations of Methyl Cation Affinity (MCA) values

A way to describe the Lewis basicity of organocatalysts is the calculation of methyl cation affinity value (ΔMCA). Therefore, the difference in free reaction energy is determined of the methyl transfer from pyridine ma_py to the more Lewis basic ion pair **3a-d,4-6a** forming the methylated pyridinamide Me_**3a-d,4-6a** according to the equations shown in Figure 3.25 to Figure 3.31.

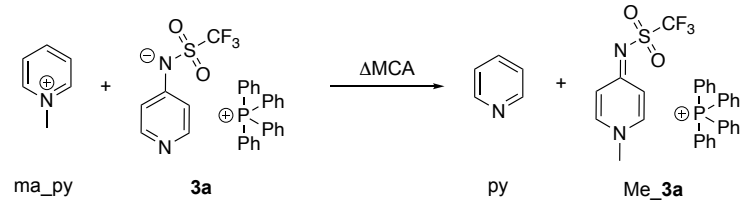

Figure 3.25: [Figure S26]. Equation used for calculation of relative Lewis basicity of ion pair **3a** with pyridine as reference.

Table 3.44: [Table S49]. Energy for all systems shown in Figure 3.25.

System	E_{tot} SMD(DCM)/ B3LYP-D3/ 6-31+G(d)	H_{298} SMD(DCM)/ B3LYP-D3/ 6-31+G(d)	$G_{qh,298}$ SMD(DCM)/ B3LYP-D3/ 6-31+G(d)	$G_{qh,298,corr}$ SMD(DCM)/ B3LYP-D3/ 6-31+G(d)
Pyridine				
py_001_dcm_fr	-248.3117009	-248.2175679	-248.2502039	-248.2471854
ma_py_001_dcm_fr	-288.0755143	-287.9375633	-287.9743763	-287.9713578
3a				
cat3a_008	-2456.770628	**-2456.259420**	**-2456.354582**	**-2456.351563**
cat3a_002	-2456.770669	-2456.259399	-2456.354514	-2456.351496
cat3a_018	**-2456.770818**	-2456.259384	-2456.354496	-2456.351478
cat3a_029	-2456.770644	-2456.259350	-2456.354385	-2456.351367
cat3a_033m	-2456.770628	-2456.259315	-2456.354345	-2456.351327
		-2456.2588145	**-2456.353922**	**-2456.350904**
Me_3a				
ma_cat3a_003pp_dcm_ofr	-2496.547562	**-2495.992855**	**-2496.091673**	**-2496.088654**
ma_cat3a_033m_dcm	-2496.547742	-2495.992686	-2496.091213	-2496.088194
ma_cat3a_036ma_dcm_ofr	-2496.547841	-2495.992493	-2496.090755	-2496.087736
ma_cat3a_018_dcm	-2496.547747	-2495.992344	-2496.090674	-2496.087656
ma_cat3a_008_dcm	**-2496.548009**	-2495.992669	-2496.090602	-2496.087583

ma_cat3a_035m_dcm_ofr	-2496.547339	-2495.991834	-2496.090023	-2496.087005
		-2495.9925766	**-2496.0911053**	**-2496.0880868**
ΔMCA		-35.28		-33.92
all		**-36.14**		**-34.16**

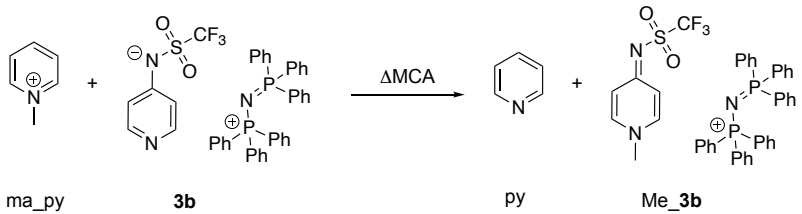

Figure 3.26: [Figure S27]. Equation used for calculation of relative Lewis basicity of ion pair **3b** with pyridine as reference.

Table 3.45: [Table S50]. Energy for all systems shown in Figure 3.26.

System	**E_{tot} SMD(DCM)/ B3LYP-D3/ 6-31+G(d)**	**H_{298} SMD(DCM)/ B3LYP-D3/ 6-31+G(d)**	**$G_{qh,298}$ SMD(DCM)/ B3LYP-D3/ 6-31+G(d)**	**$G_{qh,298,corr}$ SMD(DCM)/ B3LYP-D3/ 6-31+G(d)**
Pyridine				
py_001_dcm_fr	-248.3117009	-248.2175679	-248.2502039	-248.2471854
ma_py_001_dcm_fr	-288.0755143	-287.9375633	-287.9743763	-287.9713578
3b				
cat3b_124_dcm_fr	**-3316.275809**	**-3315.561663**	**-3315.680224**	**-3315.677206**
cat3b_020_dcm_fr	-3316.275058	-3315.560851	-3315.679373	-3315.676355
cat3b_147_dcm_fr	-3316.274602	-3315.560287	-3315.678876	-3315.675857
cat3b_136m_dcm	-3316.274338	-3315.560086	-3315.678610	-3315.675591
cat3b_140_dcm_fr	-3316.274329	-3315.560084	-3315.678552	-3315.675533
		-3315.559900	**-3315.678519**	**-3315.675501**
Me_3b				
ma_cat3b_124_dcm	**-3356.0547111**	**-3355.2966571**	**-3355.4184931**	**-3355.4154746**
ma_cat3b_136mb_gas_dcm_ofr	-3356.0544600	-3355.2961920	-3355.4177030	-3355.4146845
ma_cat3b_027m_dcm_ofr	-3356.0531658	-3355.2950028	-3355.4165188	-3355.4135003

ma_cat3b_053_dcm_ofr	-3356.0541933	-3355.2956923	-3355.4164783	-3355.4134598
ma_cat3b_147m_dcm_ofr	-3356.0522264	-3355.2944324	-3355.4164324	-3355.4134139
ma_cat3b_147p_dcm_ofr	-3356.0522644	-3355.2940784	-3355.4160154	-3355.4129969
ma_cat3b_104b_gas_dcm_ofr	-3356.0523916	-3355.2937736	-3355.4150656	-3355.4120471
ma_cat3b_020_dcm_fr	-3356.0533789	-3355.2939939	-3355.4137099	-3355.4106914
		-3355.2959969	**-3355.4177759**	**-3355.4147575**
ΔMCA		-39.38		-37.01
all		**-42.27**		**-39.60**

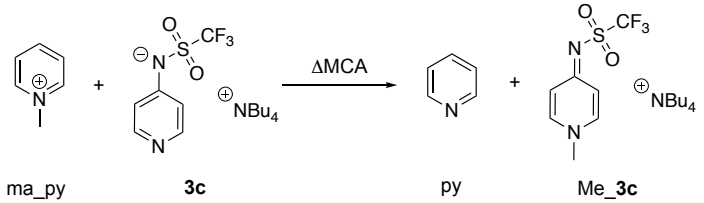

Figure 3.27: [Figure S28]. Equation used for calculation of relative Lewis basicity of ion pair **3c** with pyridine as reference.

Table 3.46: [Table S51]. Energy for all systems shown in Figure 3.27.

System	**E_{tot} SMD(DCM)/ B3LYP-D3/ 6-31+G(d)**	**H_{298} SMD(DCM)/ B3LYP-D3/ 6-31+G(d)**	**$G_{qh,298}$ SMD(DCM)/ B3LYP-D3/ 6-31+G(d)**	**$G_{qh,298,corr}$ SMD(DCM)/ B3LYP-D3/ 6-31+G(d)**
Pyridine				
py_001_dcm_fr	-248.3117009	-248.2175679	-248.2502039	-248.2471854
ma_py_001_dcm_fr	-288.0755143	-287.9375633	-287.9743763	-287.9713578
3c				
cat3c_001_dcm	-1874.956418	**-1874.302434**	**-1874.401539**	**-1874.398520**
cat3c_034_dcm	-1874.956217	-1874.302034	-1874.401302	-1874.398284
cat3c_028_dcm	-1874.956268	-1874.302058	-1874.401246	-1874.398228
cat3c_003m_dcm_fr	-1874.956347	-1874.302312	-1874.401237	-1874.398219
cat3c_027_dcm	**-1874.957013**	-1874.302207	-1874.401158	-1874.398140
		-1874.301555	**-1874.400652**	**-1874.397634**

Me_3c				
ma_cat3c_007Ab_dcm_ofr	-1914.7331121	-1914.0350321	**-1914.1374141**	**-1914.1343956**
ma_cat3c_001m_dcm_ofr	-1914.7330948	**-1914.0350398**	-1914.1373738	-1914.1343553
ma_cat3c_003ma_gas_dcm_ofr	-1914.7332517	-1914.0347557	-1914.1367767	-1914.1337582
ma_cat3c_028f_gas_dcm_ofr	-1914.7330784	-1914.0347214	-1914.1365864	-1914.1335679
ma_cat3c_006p_dcm_ofr	**-1914.7333896**	-1914.0346546	-1914.1362436	-1914.1332251
ma_cat3c_027_dcm_fr	-1914.7317967	-1914.0332237	-1914.1350997	-1914.1320812
		-1914.0348127	**-1914.1370318**	**-1914.1340133**
ΔMCA		-33.11		-30.73
all		**-34.82**		**-32.05**

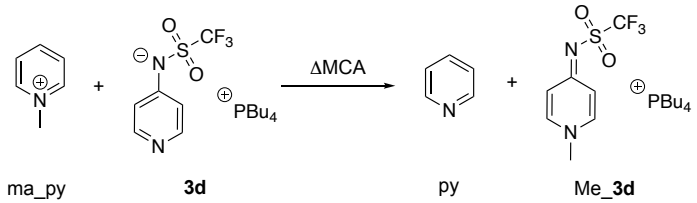

Figure 3.28: [Figure S29]. Equation used for calculation of relative Lewis basicity of ion pair **3d** with pyridine as reference.

Table 3.47: [Table S52]. Energy for all systems shown in Figure 3.28.

System	**E_{tot} SMD(DCM)/ B3LYP-D3/ 6-31+G(d)**	**H_{298} SMD(DCM)/ B3LYP-D3/ 6-31+G(d)**	**$G_{qh,298}$ SMD(DCM)/ B3LYP-D3/ 6-31+G(d)**	**$G_{qh,298,corr}$ SMD(DCM)/ B3LYP-D3/ 6-31+G(d)**
Pyridine				
py_001_dcm_fr	-248.3117009	-248.2175679	-248.2502039	-248.2471854
ma_py_001_dcm_fr	-288.0755143	-287.9375633	-287.9743763	-287.9713578
3d				
cat3d_031_dcm_fr	-2161.591204	-2160.946455	**-2161.049248**	**-2161.046230**
cat3d_041a_dcm_fr	-2161.590889	-2160.946323	-2161.049170	-2161.046152
cat3d_027_dcm_fr	**-2161.591598**	**-2160.946633**	-2161.049140	-2161.046122
cat3d_029_dcm_fr	-2161.590751	-2160.946099	-2161.049124	-2161.046106
cat3d_001_dcm_fr	-2161.591275	-2160.946562	-2161.049074	-2161.046055

		-2160.942902	**-2161.048612**	**-2161.045594**
Me_3d				
ma_cat3d_034a_gas_dcm_ofr	-2201.3680129	**-2200.6794399**	**-2200.7851839**	**-2200.7821654**
ma_cat3d_013_dcm_fr	-2201.3679147	-2200.6790277	-2200.7848337	-2200.7818152
ma_cat3d_031_dcm	**-2201.3682858**	-2200.6791278	-2200.7843968	-2200.7813783
ma_cat3d_004p_dcm_ofr	-2201.3671572	-2200.6784452	-2200.7839092	-2200.7808907
ma_cat3d_057_dcm_fr	-2201.3676727	-2200.6783757	-2200.7838607	-2200.7808422
		-2200.6790507	**-2200.7847125**	**-2200.7816940**
ΔMCA		-33.64		-30.88
all		**-34.49**		**-31.32**

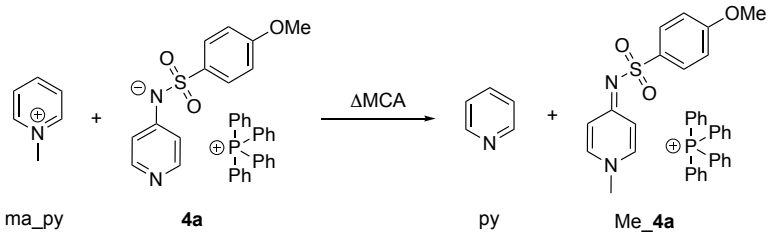

Figure 3.29: [Figure S30]. Equation used for calculation of relative Lewis basicity of ion pair **4a** with pyridine as reference.

Table 3.48: [Table S53]. Energy for all systems shown in Figure 3.29.

System	**E_{tot} SMD(DCM)/ B3LYP-D3/ 6-31+G(d)**	**H_{298} SMD(DCM)/ B3LYP-D3/ 6-31+G(d)**	**$G_{qh,298}$ SMD(DCM)/ B3LYP-D3/ 6-31+G(d)**	**$G_{qh,298,corr}$ SMD(DCM)/ B3LYP-D3/ 6-31+G(d)**
Pyridine				
py_001_dcm_fr	-248.3117009	-248.2175679	-248.2502039	-248.2471854
ma_py_001_dcm_fr	-288.0755143	-287.9375633	-287.9743763	-287.9713578
4a				
cat4a_050_dcm	**-2465.334938**	**-2464.710187**	**-2464.811281**	**-2464.808262**
cat4a_030_dcm	-2465.334896	-2464.710055	-2464.811095	-2464.808077
cat4a_026_dcm	-2465.333194	-2464.708774	-2464.810286	-2464.807268

cat4a_108_dcm	-2465.333336	-2464.708800	-2464.810174	-2464.807155
cat4a_105_dcm	-2465.332334	-2464.708102	-2464.809786	-2464.806767
		-2464.708811	**-2464.809896**	**-2464.806877**
Me_4a				
ma_cat4a_025b_gas_dcm_ofr	-2505.1179139	**-2504.4496129**	**-2504.5548899**	**-2504.5518714**
ma_cat4a_108p_dcm_ofr	-2505.1176995	-2504.4495725	-2504.5548515	-2504.5518330
ma_cat4a_030_dcm_fr	-2505.1183124	-2504.4491904	-2504.5529494	-2504.5499309
ma_cat4a_026a_gas_dcm_ofr	-2505.1168195	-2504.4477005	-2504.5521365	-2504.5491180
ma_cat4a_037_dcm_ofr	-2505.1177474	-2504.4484204	-2504.5519874	-2504.5489689
ma_cat4a_050_dcm	**-2505.1188272**	-2504.4484902	-2504.5501182	-2504.5470997
		-2504.4492390	**-2504.5546169**	**-2504.5515985**
ΔMCA		-51.02		-51.03
all		**-53.64**		**-53.95**

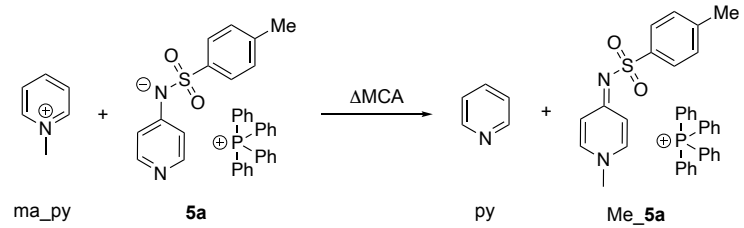

Figure 3.30: [Figure S31]. Equation used for calculation of relative Lewis basicity of ion pair **5a** with pyridine as reference.

Table 3.49: [Table S54]. Energy for all systems shown in Figure 3.30.

System	**E_{tot} SMD(DCM)/ B3LYP-D3/ 6-31+G(d)**	**H_{298} SMD(DCM)/ B3LYP-D3/ 6-31+G(d)**	**$G_{qh,298}$ SMD(DCM)/ B3LYP-D3/ 6-31+G(d)**	**$G_{qh,298,corr}$ SMD(DCM)/ B3LYP-D3/ 6-31+G(d)**
Pyridine				
py_001_dcm_fr	-248.3117009	-248.2175679	-248.2502039	-248.2471854
ma_py_001_dcm_fr	-288.0755143	-287.9375633	-287.9743763	-287.9713578
5a				
cat5a_012_dcm_fr	**-2390.123118**	**-2389.504272**	**-2389.604120**	**-2389.601102**

cat5a_078m_dcm_fr	-2390.122167	-2389.503803	-2389.603890	-2389.600871
cat5a_041_dcm_fr	-2390.121537	-2389.503322	-2389.603789	-2389.600771
cat5a_032_dcm_fr	-2390.121516	-2389.503282	-2389.603532	-2389.600514
cat5a_028_dcm_fr	-2390.121504	-2389.503143	-2389.603493	-2389.600474
		-2389.503006	**-2389.603068**	**-2389.600049**
Me_5a				
ma_cat5a_032_dcm_ofr	-2429.9057838	-2429.2438118	**-2429.3477648**	**-2429.3447463**
ma_cat5a_012_dcm	**-2429.9064585**	**-2429.2438815**	-2429.3471655	-2429.3441470
ma_cat5a_041p_dcm_ofr	-2429.9060414	-2429.2438664	-2429.3471074	-2429.3440889
ma_cat5a_078m_dcm_fr	-2429.9047560	-2429.2425950	-2429.3461140	-2429.3430955
ma_cat5a_063b_gas_dcm_ofr	-2429.9040312	-2429.2417902	-2429.3456412	-2429.3426227
ma_cat5a_013_dcm_ofr	-2429.9052240	-2429.2425910	-2429.3455130	-2429.3424945
		-2429.2436080	**-2429.3471965**	**-2429.3441780**
ΔMCA		-51.50		-51.12
all		**-54.10**		**-52.40**

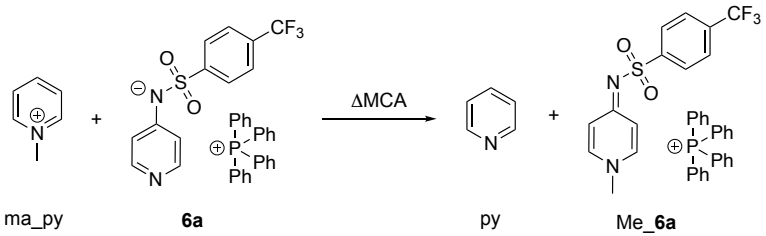

Figure 3.31: [Figure S34]. Equation used for calculation of relative Lewis basicity of ion pair **6a** with pyridine as reference.

Table 3.50: [Table S55]. Energy for all systems shown in Figure 3.31.

System	**E_{tot} SMD(DCM)/ B3LYP-D3/ 6-31+G(d)**	**H_{298} SMD(DCM)/ B3LYP-D3/ 6-31+G(d)**	**$G_{qh,298}$ SMD(DCM)/ B3LYP-D3/ 6-31+G(d)**	**$G_{qh,298,corr}$ SMD(DCM)/ B3LYP-D3/ 6-31+G(d)**
Pyridine				
py_001_dcm_fr	-248.3117009	-248.2175679	-248.2502039	-248.2471854
ma_py_001_dcm_fr	-288.0755143	-287.9375633	-287.9743763	-287.9713578

6a				
cat6a_012_dcm	-2687.866218	**-2687.269030**	**-2687.372424**	**-2687.369405**
cat6a_062_dcm	-2687.865545	-2687.268462	-2687.371852	-2687.368833
cat6a_077_dcm	-2687.865538	-2687.268342	-2687.371699	-2687.368681
cat6a_049_dcm	-2687.864657	-2687.267827	-2687.371664	-2687.368645
cat6a_003_dcm	**-2687.866341**	-2687.268788	-2687.371615	-2687.368597
		-2687.268042	**-2687.371356**	**-2687.368337**
Me_6a				
ma_cat6a_032_dcm_ofr	-2727.6473085	**-2727.0070385**	**-2727.1146215**	**-2727.1116030**
ma_cat6a_040_dcm_ofr	-2727.6472324	-2727.0066464	-2727.1141994	-2727.1111809
ma_cat6a_049_dcm_ofr	-2727.6473434	-2727.0066284	-2727.1139164	-2727.1108979
ma_cat6a_003m_dcm_ofr	**-2727.6479245**	-2727.0060155	-2727.1109755	-2727.1079570
		-2727.0067095	**-2727.1143026**	**-2727.1112841**
ΔMCA		-47.29		-47.33
all		**-49.02**		**-49.29**

Previous studies of ΔMCA indicate that the catalytic active center is situated on the pyridine N rather than the amide N. Since anion **6** is a newly designed compound ΔMCA were calculated for the pyridine N methylated and the amide N methylated conformer according to the equation shown in Figure 3.32. The energy values are listed in Table 3.51.

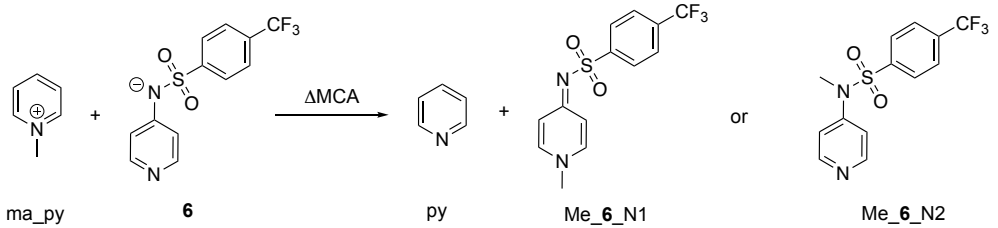

Figure 3.32: [Figure S33]. Comparison of MCA at pyridine-N position (N1) and amide-N position (N2) for anion **6** with pyridine as reference system.

The resulting ΔMCA show that the methylation on the pyridine N leads to the thermodynamic more stable product by 13.7 kJ mol^{-1} in reaction enthalpy and by 16.6 kJ mol^{-1} in the free reaction energy.

Table 3.51: [Table S56]. Energy for all systems shown in Figure 3.32.

System	E_{tot} SMD(DCM)/ B3LYP-D3/	H_{298} SMD(DCM)/ B3LYP-D3/	$G_{qh,298}$ SMD(DCM)/ B3LYP-D3/	$G_{qh,298,corr}$ SMD(DCM)/ B3LYP-D3/

	6-31+G(d)	6-31+G(d)	6-31+G(d)	6-31+G(d)
Pyridine				
py_001_dcm_fr	-248.3117009	-248.2175679	-248.2502039	-248.2471854
ma_py_001_dcm_fr	-288.0755143	-287.9375633	-287.9743763	-287.9713578
6				
an6_001	**-1419.929810**	**-1419.724473**	**-1419.784896**	**-1419.781877**
Me_6				
ma_an6_001_n1_dcm_fr	-1459.7173223	-1459.4683223	-1459.5325203	-1459.5295018
ma_an6_001_n2_dcm_fr	-1459.7118231	-1459.4630761	-1459.5262031	-1459.5231846
ΔMCA				
ma_an6_n1[a]		-62.6		-61.6
ma_an6_n2[b]		-48.9		-45.0

[a] N1 = methylation on pyridine N, [b] N2 = methylation on amide N.

3.1.10.3 Conformers of Pyridinamide Triple Ion Complexes in DCM

Starting points of pyridinamide ion triple complexes were pre-optimized using SMD(DCM)/r^{2}SCAN-3c level of theory with Orca 5.0.3[35], followed by single point calculations at SMD(DCM)/B3LYP-D3/6-31+G(d) with Gaussian 16, Revision C.01[36] to obtain calculated triple ion volumes based on the van der Waals cavities employed in the SMD continuum solvation model employed in Gaussian 16 so they are comparable to the calculated ion volumes of ion pair systems and the respective single cation and anions optimized at the SMD(DCM)/B3LYP-D3/6-31+G(d) with Gaussian 16.

Table 3.52: [Table S57]. Single point energies for all triple ion systems of ion pair **3a** calculated at the SMD(DCM)/B3LYP-D3/6-31+G(d) level of theory with Gaussian 16

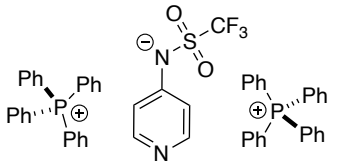 **a3a**				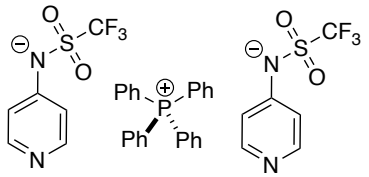 **3a3**			
System[a]	**E_{tot} SMD(DCM)/ B3LYP-D3/6-31+G(d)**	**Cavity Volume (Å^3)**	**Relative Population Parameter based on E_{298}**	**System[a]**	**E_{tot} SMD(DCM)/ B3LYP-D3/6-31+G(d)**	**Cavity Volume (Å^3)**	**Relative Population Parameter based on E_{298}**
sw_a3a_new_033b_dcm_sp	**-3724.7011753**	**925**	**0.39**	asw_3a3_058b_dcm_sp	**-3645.6244701**	**781**	**0.23**
sw_a3a_new_030a_dcm_sp	-3724.7008822	923	0.28	asw_3a3_011a_dcm_sp	-3645.6233739	780	0.07
sw_a3a_new_005na_dcm_sp	-3724.6995552	925	0.07	asw_3a3_044a_dcm_sp	-3645.6233403	781	0.07
sw_a3a_new_039a_dcm_sp	-3724.6993743	926	0.06	asw_3a3_032a_dcm_sp	-3645.6231043	783	0.05
sw_a3a_new_015b_dcm_sp	-3724.6989764	926	0.04	asw_3a3_053a_dcm_sp	-3645.6231020	783	0.05
sw_a3a_new_042a_dcm_sp	-3724.6989336	927	0.04	asw_3a3_006_dcm_sp	-3645.6230698	781	0.05
sw_a3a_new_010b_dcm_sp	-3724.6985369	927	0.02	asw_3a3_047a_dcm_sp	-3645.6230374	782	0.05
sw_a3a_new_045c_dcm_sp	-3724.6984005	926	0.02	asw_3a3_039b_dcm_sp	-3645.6229589	782	0.05
sw_a3a_new_014_dcm_sp	-3724.6980441	926	0.01	asw_3a3_045b_dcm_sp	-3645.6228896	780	0.04
sw_a3a_new_047a_dcm_sp	-3724.6976338	926	0.01	asw_3a3_049a_dcm_sp	-3645.6228146	783	0.04
sw_a3a_new_018a_dcm_sp	-3724.6975821	926	0.01	asw_3a3_048b_dcm_sp	-3645.6227627	784	0.04
sw_a3a_new_038a_dcm_sp	-3724.6975740	927	0.01	asw_3a3_057b_dcm_sp	-3645.6226849	781	0.03
sw_a3a_new_020a_dcm_sp	-3724.6971852	926	0.01	asw_3a3_050_dcm_sp	-3645.6223597	781	0.02
sw_a3a_new_004a_dcm_sp	-3724.6970783	926	0.01	asw_3a3_059b_dcm_sp	-3645.6223396	782	0.02
sw_a3a_new_003_dcm_sp	-3724.6968941	928	0.00	asw_3a3_022a_dcm_sp	-3645.6220941	781	0.02
sw_a3a_new_052b_dcm_sp	-3724.6967130	925	0.00	asw_3a3_037_dcm_sp	-3645.6219701	785	0.02
sw_a3a_new_013b_dcm_sp	-3724.6964818	925	0.00	asw_3a3_008a_dcm_sp	-3645.6217232	783	0.01

sw_a3a_new_029a_dcm_sp	-3724.6964377	925	0.00	asw_3a3_051b_dcm_sp	-3645.6217229	785	0.01
sw_a3a_new_040a_dcm_sp	-3724.6963431	924	0.00	asw_3a3_033_dcm_sp	-3645.6216873	780	0.01
sw_a3a_new_055b_dcm_sp	-3724.6963343	928	0.00	asw_3a3_004a_dcm_sp	-3645.6216535	780	0.01
	-3724.7002363	**925**			**-3645.6230836**	**782**	

[a] best 20 conformers according to E_{tot} at SMD(DCM)/B3LYP-D3/6-31+G(d) level of theory.

Table 3.53: [Table S58]. Single point energies for all triple ion systems of ion pair **3b** calculated at the SMD(DCM)/B3LYP-D3/6-31+G(d) level of theory with Gaussian 16.

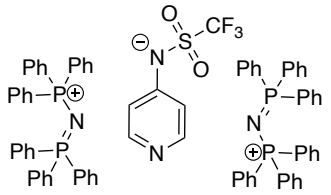

b3b

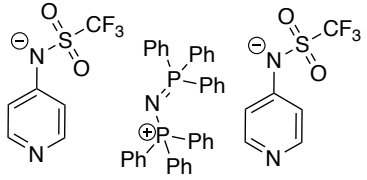

3b3

System[a]	E_{tot} SMD(DCM)/ B3LYP-D3/6-31+G(d)	Cavity Volume (Å³)	Relative Population Parameter based on E_{298}	System[a]	E_{tot} SMD(DCM)/ B3LYP-D3/6-31+G(d)	Cavity Volume (Å³)	Relative Population Parameter based on E_{298}
sw_b3b_013a_dcm_sp	**-5443.7140126**	**1320**	**0.61**	asw_3b3_005_dcm_sp	**-4505.1275635**	**981**	**0.24**
sw_b3b_017a_dcm_sp	-5443.7127269	1321	0.16	asw_3b3_011_dcm_sp	-4505.1272391	982	0.17
sw_b3b_006a_dcm_sp	-5443.7119224	1323	0.07	asw_3b3_052_dcm_sp	-4505.1266092	978	0.09
sw_b3b_020_dcm_sp	-5443.7114798	1320	0.04	asw_3b3_059_dcm_sp	-4505.1263098	983	0.06
sw_b3b_009a_dcm_sp	-5443.7112347	1323	0.03	asw_3b3_015_dcm_sp	-4505.1262657	980	0.06
sw_b3b_032a_dcm_sp	-5443.7109708	1326	0.02	asw_3b3_021_dcm_sp	-4505.1262106	979	0.06
sw_b3b_035_dcm_sp	-5443.7109331	1320	0.02	asw_3b3_040_dcm_sp	-4505.1259597	978	0.04
sw_b3b_018_dcm_sp	-5443.7108530	1325	0.02	asw_3b3_006_dcm_sp	-4505.1258741	979	0.04
sw_b3b_007a_dcm_sp	-5443.7099513	1322	0.01	asw_3b3_017_dcm_sp	-4505.1257747	982	0.04
sw_b3b_034_dcm_sp	-5443.7099490	1322	0.01	asw_3b3_060_dcm_sp	-4505.1257439	977	0.04
sw_b3b_044_dcm_sp	-5443.7095511	1324	0.01	asw_3b3_019n_dcm_sp	-4505.1257036	977	0.03
sw_b3b_054a_dcm_sp	-5443.7085566	1325	0.00	asw_3b3_012_dcm_sp	-4505.1252592	985	0.02
sw_b3b_058a_dcm_sp	-5443.7077099	1323	0.00	asw_3b3_035_dcm_sp	-4505.1249856	980	0.02
sw_b3b_015a_dcm_sp	-5443.7077063	1322	0.00	asw_3b3_049_dcm_sp	-4505.1244954	983	0.01
sw_b3b_012a_dcm_sp	-5443.7076373	1324	0.00	asw_3b3_018_dcm_sp	-4505.1244067	980	0.01
sw_b3b_055a_dcm_sp	-5443.7070373	1322	0.00	asw_3b3_008_dcm_sp	-4505.1241883	980	0.01

sw_b3b_025_dcm_sp	-5443.7067425	1322	0.00	asw_3b3_043_dcm_sp	-4505.1241157	984	0.01
sw_b3b_008a_dcm_sp	-5443.7061014	1320	0.00	asw_3b3_038_dcm_sp	-4505.1240810	981	0.01
sw_b3b_004n_dcm_sp	-5443.7060467	1325	0.00	asw_3b3_036_dcm_sp	-4505.1240283	980	0.01
sw_b3b_014a_dcm_sp	-5443.7059537	1325	0.00	asw_3b3_025_dcm_sp	-4505.1240232	980	0.01
	-5443.7131383	**1321**			**-4505.1264153**	**981**	

[a] best 20 conformers according to E_{tot} at SMD(DCM)/B3LYP-D3/6-31+G(d) level of theory.

Table 3.54: [Table S59]. Single point energies for all triple ion systems of ion pair **3c** calculated at the SMD(DCM)/B3LYP-D3/6-31+G(d) level of theory with Gaussian 16.

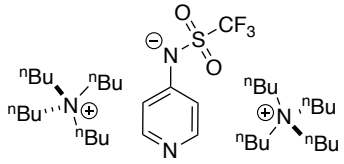

c3c

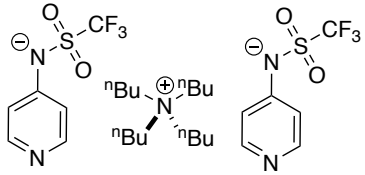

3c3

System[a]	E_{tot} SMD(DCM)/ B3LYP-D3/6-31+G(d)	Cavity Volume (Å³)	Relative Population Parameter based on E_{298}	System[a]	E_{tot} SMD(DCM)/ B3LYP-D3/6-31+G(d)	Cavity Volume (Å³)	Relative Population Parameter based on E_{298}
sw_c3c_052_dcm_sp	**-2561.0719269**	**830**	**0.38**	asw_3c3_007_dcm_sp	**-3063.8103134**	**733**	**0.12**
sw_c3c_028_dcm_sp	-2561.0717762	830	0.33	asw_3c3_060a_dcm_sp	-3063.8102955	733	0.12
sw_c3c_038_dcm_sp	-2561.0705711	830	0.09	asw_3c3_057_dcm_sp	-3063.8102873	733	0.12
sw_c3c_018_dcm_sp	-2561.0705085	830	0.09	asw_3c3_046_dcm_sp	-3063.8101185	735	0.10
sw_c3c_034_dcm_sp	-2561.0692660	830	0.02	asw_3c3_059_dcm_sp	-3063.8101059	732	0.10
sw_c3c_048_dcm_sp	-2561.0692481	827	0.02	asw_3c3_030_dcm_sp	-3063.8099630	733	0.09
sw_c3c_001_dcm_sp	-2561.0692174	832	0.02	asw_3c3_005_dcm_sp	-3063.8094223	734	0.05
sw_c3c_050_dcm_sp	-2561.0682378	829	0.01	asw_3c3_047_dcm_sp	-3063.8092563	734	0.04
sw_c3c_017_dcm_sp	-2561.0680673	828	0.01	asw_3c3_027_dcm_sp	-3063.8090680	733	0.03
sw_c3c_051_dcm_sp	-2561.0680099	829	0.01	asw_3c3_006_dcm_sp	-3063.8089166	732	0.03
sw_c3c_057_dcm_sp	-2561.0678695	831	0.01	asw_3c3_043a_dcm_sp	-3063.8086977	733	0.02
sw_c3c_022_dcm_sp	-2561.0676726	832	0.00	asw_3c3_045a_dcm_sp	-3063.8086730	736	0.02
sw_c3c_011_dcm_sp	-2561.0676605	830	0.00	asw_3c3_058_dcm_sp	-3063.8086506	735	0.02
sw_c3c_012_dcm_sp	-2561.0676197	829	0.00	asw_3c3_051a_dcm_sp	-3063.8086414	734	0.02
sw_c3c_037_dcm_sp	-2561.0671134	830	0.00	asw_3c3_038a_dcm_sp	-3063.8083860	732	0.02

sw_c3c_005n_dcm_sp	-2561.0661687	833	0.00	asw_3c3_012_dcm_sp	-3063.8083259	734	0.02
sw_c3c_039_dcm_sp	-2561.0659415	830	0.00	asw_3c3_018_dcm_sp	-3063.8082924	734	0.01
sw_c3c_004_dcm_sp	-2561.0657957	833	0.00	asw_3c3_010b_dcm_sp	-3063.8081661	732	0.01
sw_c3c_054_dcm_sp	-2561.0655312	831	0.00	asw_3c3_024_dcm_sp	-3063.8078301	737	0.01
sw_c3c_059_dcm_sp	-2561.0639387	828	0.00	asw_3c3_053_dcm_sp	-3063.8077583	733	0.01
	-2561.0712698	**830**			**-3063.8096410**	**733**	

[a] best 20 conformers according to E_{tot} at SMD(DCM)/B3LYP-D3/6-31+G(d) level of theory.

Table 3.55: [Table S60]. Single point energies for all triple ion systems of ion pair **3d** calculated at the SMD(DCM)/B3LYP-D3/6-31+G(d) level of theory with Gaussian 16.

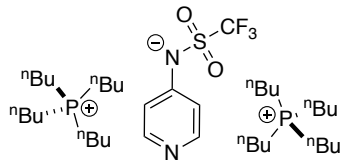

d3d

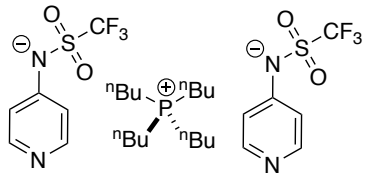

3d3

System[a]	E_{tot} SMD(DCM)/ B3LYP-D3/6-31+G(d)	Cavity Volume (Å³)	Relative Population Parameter based on E_{298}	System[a]	E_{tot} SMD(DCM)/ B3LYP-D3/6-31+G(d)	Cavity Volume (Å³)	Relative Population Parameter based on E_{298}
sw_d3d_025a_dcm_sp	**-3134.3408192**	**860**	**0.18**	asw_3d3_012_dcm_sp	**-3350.4463795**	**749**	**0.24**
sw_d3d_006_dcm_sp	-3134.3407523	859	0.17	asw_3d3_026na_dcm_sp	-3350.4457333	748	0.12
sw_d3d_029_dcm_sp	-3134.3406891	860	0.16	asw_3d3_039a_dcm_sp	-3350.4455166	748	0.09
sw_d3d_005_dcm_sp	-3134.3405380	857	0.13	asw_3d3_057_dcm_sp	-3350.4454886	748	0.09
sw_d3d_028a_dcm_sp	-3134.3402854	861	0.10	asw_3d3_050_dcm_sp	-3350.4450766	747	0.06
sw_d3d_001_dcm_sp	-3134.3398077	861	0.06	asw_3d3_021_dcm_sp	-3350.4447109	750	0.04
sw_d3d_047a_dcm_sp	-3134.3396429	857	0.05	asw_3d3_022_dcm_sp	-3350.4446535	747	0.04
sw_d3d_011_dcm_sp	-3134.3392396	857	0.03	asw_3d3_020a_dcm_sp	-3350.4445641	748	0.03
sw_d3d_048b_dcm_sp	-3134.3389328	857	0.02	asw_3d3_052_dcm_sp	-3350.4445564	747	0.03
sw_d3d_018_dcm_sp	-3134.3382911	859	0.01	asw_3d3_030a_dcm_sp	-3350.4445371	749	0.03
sw_d3d_019_dcm_sp	-3134.3382483	859	0.01	asw_3d3_036_dcm_sp	-3350.4444546	750	0.03
sw_d3d_054b_dcm_sp	-3134.3381786	861	0.01	asw_3d3_004_dcm_sp	-3350.4441409	747	0.02
sw_d3d_060_dcm_sp	-3134.3379861	860	0.01	asw_3d3_031_dcm_sp	-3350.4438600	750	0.02
sw_d3d_041a_dcm_sp	-3134.3379353	860	0.01	asw_3d3_006_dcm_sp	-3350.4437393	746	0.01
sw_d3d_003a_dcm_sp	-3134.3378059	860	0.01	asw_3d3_003_dcm_sp	-3350.4437379	750	0.01
sw_d3d_044n_dcm_sp	-3134.3371015	858	0.00	asw_3d3_015_dcm_sp	-3350.4436902	749	0.01

sw_d3d_039a_dcm_sp	-3134.3370776	859	0.00	asw_3d3_002a_dcm_sp	-3350.4436816	747	0.01
sw_d3d_017a_dcm_sp	-3134.3369477	858	0.00	asw_3d3_011_dcm_sp	-3350.4436606	750	0.01
sw_d3d_056_dcm_sp	-3134.3369464	859	0.00	asw_3d3_017_dcm_sp	-3350.4435234	745	0.01
sw_d3d_004_dcm_sp	-3134.3367814	857	0.00	asw_3d3_019a_dcm_sp	-3350.4431721	748	0.01
	-3134.3402174	**859**			**-3350.4451207**	**748**	

[a] best 20 conformers according to E_{tot} at SMD(DCM)/B3LYP-D3/6-31+G(d) level of theory.

Table 3.56: [Table S61]. Single point energies for all triple ion systems of ion pair **4a** calculated at the SMD(DCM)/B3LYP-D3/6-31+G(d) level of theory with Gaussian 16.

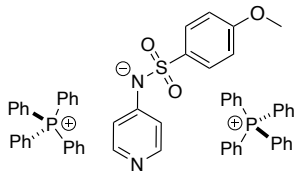

a4a

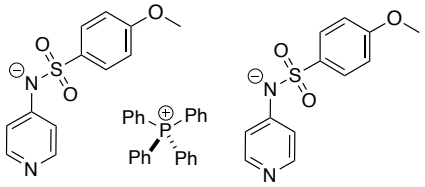

4a4

System[a]	E_{tot} SMD(DCM)/ B3LYP-D3/6-31+G(d)	Cavity Volume (Å³)	Relative Population Parameter based on E_{298}	System[a]	E_{tot} SMD(DCM)/ B3LYP-D3/6-31+G(d)	Cavity Volume (Å³)	Relative Population Parameter based on E_{298}
sw_a4a_018_dcm_sp	**-3733.2653541**	**993**	**0.39**	asw_4a4_005a_dcm_sp	**-3662.7548378**	**921**	**0.53**
sw_a4a_049a_dcm_sp	-3733.2653444	995	0.39	asw_4a4_016_dcm_sp	-3662.7535339	921	0.13
sw_a4a_004b_dcm_sp	-3733.2635672	998	0.06	asw_4a4_011a_dcm_sp	-3662.7534663	920	0.12
sw_a4a_040b_dcm_sp	-3733.2629560	999	0.03	asw_4a4_015a_dcm_sp	-3662.7532492	920	0.10
sw_a4a_022_dcm_sp	-3733.2629292	997	0.03	asw_4a4_006_dcm_sp	-3662.7526111	915	0.05
sw_a4a_017a_dcm_sp	-3733.2628530	997	0.03	asw_4a4_031a_dcm_sp	-3662.7516599	923	0.02
sw_a4a_005a_dcm_sp	-3733.2626049	998	0.02	asw_4a4_024a_dcm_sp	-3662.7515888	923	0.02
sw_a4a_011a_dcm_sp	-3733.2619594	998	0.01	asw_4a4_059n_dcm_sp	-3662.7514401	922	0.01
sw_a4a_008a_dcm_sp	-3733.2613398	998	0.01	asw_4a4_001_dcm_sp	-3662.7495052	924	0.00
sw_a4a_028a_dcm_sp	-3733.2612325	995	0.01	asw_4a4_034_dcm_sp	-3662.7493973	923	0.00
sw_a4a_007_dcm_sp	-3733.2611335	999	0.00	asw_4a4_021a_dcm_sp	-3662.7488765	923	0.00
sw_a4a_039a_dcm_sp	-3733.2608890	999	0.00	asw_4a4_002_dcm_sp	-3662.7486765	922	0.00
sw_a4a_016_dcm_sp	-3733.2606781	998	0.00	asw_4a4_014_dcm_sp	-3662.7485596	922	0.00
sw_a4a_047a_dcm_sp	-3733.2603097	994	0.00	asw_4a4_023a_dcm_sp	-3662.7485027	920	0.00
sw_a4a_038b_dcm_sp	-3733.2602851	997	0.00	asw_4a4_042b_dcm_sp	-3662.7484625	918	0.00
sw_a4a_044_dcm_sp	-3733.2601809	994	0.00	asw_4a4_035a_dcm_sp	-3662.7480696	923	0.00

sw_a4a_037a_dcm_sp	-3733.2601341	995	0.00	asw_4a4_050a_dcm_sp	-3662.7480102	915	0.00
sw_a4a_013a_dcm_sp	-3733.2597333	998	0.00	asw_4a4_057n_dcm_sp	-3662.7479483	923	0.00
sw_a4a_023b_dcm_sp	-3733.2595989	996	0.00	asw_4a4_019b_dcm_sp	-3662.7477695	921	0.00
sw_a4a_015a_dcm_sp	-3733.2593335	998	0.00	asw_4a4_028b_dcm_sp	-3662.7477203	922	0.00
	-3733.2647588	**995**			**-3662.7539922**	**920**	

[a] best 20 conformers according to E_{tot} at SMD(DCM)/B3LYP-D3/6-31+G(d) level of theory.

Table 3.57: [Table S62]. Single point energies for all triple ion systems of ion pair **5a** calculated at the SMD(DCM)/B3LYP-D3/6-31+G(d) level of theory with Gaussian 16.

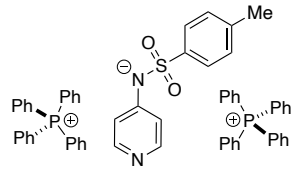

a5a

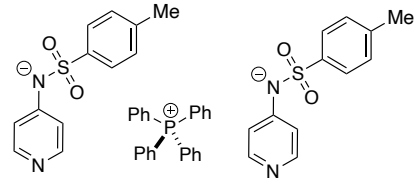

5a5

System[a]	E_{tot} SMD(DCM)/ B3LYP-D3/6-31+G(d)	Cavity Volume (Å³)	Relative Population Parameter based on E_{298}	System[a]	E_{tot} SMD(DCM)/ B3LYP-D3/6-31+G(d)	Cavity Volume (Å³)	Relative Population Parameter based on E_{298}
sw_a5a_002_dcm_sp	**-3658.0547888**	**979**	**0.79**	asw_5a5_002_dcm_sp	**-3512.3318260**	**886**	**0.64**
sw_a5a_042_dcm_sp	-3658.0527891	981	0.10	asw_5a5_047_dcm_sp	-3512.3306211	889	0.18
sw_a5a_039_dcm_sp	-3658.0515452	981	0.03	asw_5a5_040_dcm_sp	-3512.3299469	885	0.09
sw_a5a_057_dcm_sp	-3658.0509115	979	0.01	asw_5a5_003_dcm_sp	-3512.3289716	887	0.03
sw_a5a_007a_dcm_sp	-3658.0508619	983	0.01	asw_5a5_043_dcm_sp	-3512.3282751	889	0.01
sw_a5a_014_dcm_sp	-3658.0507259	976	0.01	asw_5a5_049_dcm_sp	-3512.3280050	884	0.01
sw_a5a_016_dcm_sp	-3658.0506566	975	0.01	asw_5a5_017_dcm_sp	-3512.3276961	885	0.01
sw_a5a_055_dcm_sp	-3658.0504648	978	0.01	asw_5a5_028_dcm_sp	-3512.3275307	890	0.01
sw_a5a_026_dcm_sp	-3658.0501218	979	0.01	asw_5a5_045_dcm_sp	-3512.3274238	888	0.01
sw_a5a_037_dcm_sp	-3658.0498951	978	0.00	asw_5a5_039_dcm_sp	-3512.3273996	880	0.01
sw_a5a_019a_dcm_sp	-3658.0497402	976	0.00	asw_5a5_038_dcm_sp	-3512.3268988	884	0.00
sw_a5a_033_dcm_sp	-3658.0497270	981	0.00	asw_5a5_011_dcm_sp	-3512.3265133	888	0.00
sw_a5a_041_dcm_sp	-3658.0490194	984	0.00	asw_5a5_033_dcm_sp	-3512.3264806	883	0.00
sw_a5a_005_dcm_sp	-3658.0489046	982	0.00	asw_5a5_058_dcm_sp	-3512.3262658	890	0.00
sw_a5a_038_dcm_sp	-3658.0488603	979	0.00	asw_5a5_013_dcm_sp	-3512.3262106	882	0.00
sw_a5a_045n_dcm_sp	-3658.0484830	982	0.00	asw_5a5_027_dcm_sp	-3512.3261552	889	0.00

sw_a5a_011_dcm_sp	-3658.0484258	980	0.00	asw_5a5_018_dcm_sp	-3512.3258251	886	0.00
sw_a5a_036a_dcm_sp	-3658.0483335	979	0.00	asw_5a5_053_dcm_sp	-3512.3255224	889	0.00
sw_a5a_010_dcm_sp	-3658.0481000	982	0.00	asw_5a5_051_dcm_sp	-3512.3250416	886	0.00
sw_a5a_006_dcm_sp	-3658.0479113	977	0.00	asw_5a5_015_dcm_sp	-3512.3246455	884	0.00
	-3658.0541301	**980**			**-3512.3310521**	**887**	

[a] best 20 conformers according to E_{tot} at SMD(DCM)/B3LYP-D3/6-31+G(d) level of theory.

Table 3.58: [Table S63]. Single point energies for all triple ion systems of ion pair **6a** calculated at the SMD(DCM)/B3LYP-D3/6-31+G(d) level of theory with Gaussian 16.

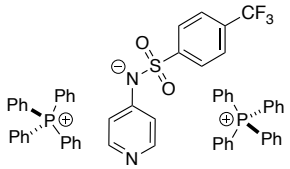

a6a

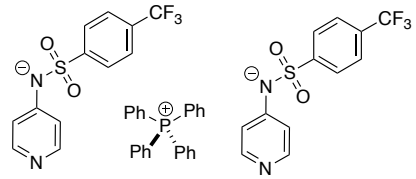

6a6

System[a]	E_{tot} SMD(DCM)/ B3LYP-D3/6-31+G(d)	Cavity Volume (Å³)	Relative Population Parameter based on E_{298}	System[a]	E_{tot} SMD(DCM)/ B3LYP-D3/6-31+G(d)	Cavity Volume (Å³)	Relative Population Parameter based on E_{298}
sw_a6a_016a_dcm_sp	**-3955.7953706**	**1008**	**0.36**	asw_6a6_040a_dcm_sp	**-4107.8137166**	**942**	**0.39**
sw_a6a_032n_dcm_sp	-3955.7945098	1006	0.15	asw_6a6_022_dcm_sp	-4107.8123392	943	0.09
sw_a6a_057a_dcm_sp	-3955.7944884	1007	0.14	asw_6a6_050a_dcm_sp	-4107.8123121	939	0.09
sw_a6a_019a_dcm_sp	-3955.7941140	1008	0.10	asw_6a6_021b_dcm_sp	-4107.8120945	942	0.07
sw_a6a_028a_dcm_sp	-3955.7932440	1004	0.04	asw_6a6_012_dcm_sp	-4107.8120813	941	0.07
sw_a6a_007b_dcm_sp	-3955.7932155	1008	0.04	asw_6a6_017a_dcm_sp	-4107.8118183	942	0.05
sw_a6a_043a_dcm_sp	-3955.7931982	1006	0.04	asw_6a6_052_dcm_sp	-4107.8113834	942	0.03
sw_a6a_044b_dcm_sp	-3955.7928419	1002	0.02	asw_6a6_035_dcm_sp	-4107.8112172	942	0.03
sw_a6a_033b_dcm_sp	-3955.7925148	1006	0.02	asw_6a6_031a_dcm_sp	-4107.8112095	940	0.03
sw_a6a_046a_dcm_sp	-3955.7921923	1003	0.01	asw_6a6_018_dcm_sp	-4107.8109963	940	0.02
sw_a6a_009a_dcm_sp	-3955.7921595	1005	0.01	asw_6a6_027b_dcm_sp	-4107.8109782	941	0.02
sw_a6a_018a_dcm_sp	-3955.7920784	1006	0.01	asw_6a6_026b_dcm_sp	-4107.8107390	941	0.02
sw_a6a_054a_dcm_sp	-3955.7918627	1008	0.01	asw_6a6_038_dcm_sp	-4107.8106768	943	0.02
sw_a6a_050a_dcm_sp	-3955.7918518	1006	0.01	asw_6a6_043a_dcm_sp	-4107.8106361	940	0.01
sw_a6a_042a_dcm_sp	-3955.7917440	1005	0.01	asw_6a6_058_dcm_sp	-4107.8102195	936	0.01
sw_a6a_025a_dcm_sp	-3955.7914750	1006	0.01	asw_6a6_004a_dcm_sp	-4107.8101148	943	0.01

sw_a6a_027a_dcm_sp	-3955.7913930	1006	0.01	asw_6a6_036n_dcm_sp	-4107.8098943	941	0.01
sw_a6a_053a_dcm_sp	-3955.7912338	1004	0.00	asw_6a6_028_dcm_sp	-4107.8097038	939	0.01
sw_a6a_041b_dcm_sp	-3955.7911459	1002	0.00	asw_6a6_011a_dcm_sp	-4107.8096103	938	0.01
sw_a6a_049b_dcm_sp	-3955.7910002	1007	0.00	asw_6a6_054_dcm_sp	-4107.8094442	941	0.00
	-3955.7942465	**1007**			**-4107.8123916**	**941**	

[a] best 20 conformers according to E_{tot} at SMD(DCM)/B3LYP-D3/6-31+G(d) level of theory.

3.1.10.4 Optimized Conformers of Additive Salts in DCM

System $PNPBF_4$ – computational data

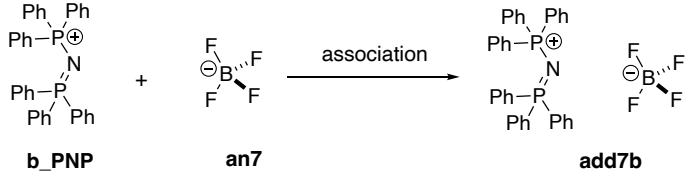

Figure 3.33: [Figure S34]. Ion association of additive **7b** and the single ions.

The Boltzmann-averaged free reaction energy of the ion pairing of **7b** amounts to $\Delta G_{qh,298,corr}$ = +13.9 kJ mol^{-1} in DCM solution. Focusing only on the best conformers of the reactants and product the free reaction energy of the ion pairing of **7b** changes to $\Delta G_{qh,298,corr}$ = +12.5 kJ mol^{-1} in DCM solution. The blue marked cells show the Boltzmann-averaged values.

According to $\Delta G_{qh,298,corr}$ = -RT ln*K* and assuming R = 8.314 J K^{-1} mol^{-1} and T = 298.15 K, the respective equilibrium constant amounts to *K*(**7b**, DCM) = 0.007 for the best conformer of **7b** and to *K*(**7b**, DCM) = 0.004 for the Boltzmann-averaged free reaction energy. In this case the equilibrium constant *K* corresponds to the concentration of the reactants and products in the following way: *K* = [**7b**]/[$\mathbf{BF_4}$] [**b_PNP**] = [**7b**]/[$\mathbf{BF_4}$]^2.

Table 3.59: [Table S64]. Energies for all systems shown in Figure 3.33.

System	E_{tot} SMD(DCM)/ B3LYP-D3/ 6-31+G(d)	H_{298} SMD(DCM)/ B3LYP-D3/ 6-31+G(d)	$G_{qh,298}$ SMD(DCM)/ B3LYP-D3/ 6-31+G(d)	$G_{qh,298,corr}$ SMD(DCM)/ B3LYP-D3/ 6-31+G(d)	Cavity Volume (Å^3)	Relative Population Parameter based on $G_{qh,298}$
BF_4						
borate_001_dcm	**-424.6525330**	**-424.6336440**	**-424.6644660**	**-424.6614475**	**69.7**	1.00
			-424.6644660	**-424.6614475**	**69.7**	

b_PNP						
cation_c_002	**-2127.413003**	**-2126.821082**	**-2126.913057**	**-2126.910039**	**560**	0.51
cation_c_003	-2127.412921	-2126.820643	-2126.912356	-2126.909338	559	0.24
cation_c_001	-2127.412908	-2126.820541	-2126.912386	-2126.909367	559	0.25
			-2126.912720	**-2126.909702**	**559**	
7b[a]						
add7b_012_dcm	**-2552.0780873**	**-2551.4650303**	**-2551.5697613**	**-2551.5667428**	**628**	0.08
add7b_112_dcm	-2552.0779330	-2551.4648320	-2551.5696060	-2551.5665875	629	0.07
add7b_145_dcm	-2552.0780671	-2551.4649881	-2551.5695071	-2551.5664886	628	0.06
add7b_080_dcm	-2552.0775340	-2551.4646350	-2551.5693790	-2551.5663605	629	0.05
add7b_040_dcm	-2552.0777464	-2551.4645434	-2551.5691644	-2551.5661459	629	0.04
add7b_025_dcm	-2552.0775889	-2551.4644939	-2551.5690929	-2551.5660744	629	0.04
add7b_008_dcm	-2552.0777622	-2551.4645002	-2551.5690812	-2551.5660627	629	0.04
add7b_031_dcm	-2552.0775467	-2551.4644087	-2551.5690747	-2551.5660562	629	0.04
add7b_142_dcm	-2552.0774378	-2551.4643418	-2551.5690398	-2551.5660213	629	0.04
add7b_044_dcm	-2552.0774876	-2551.4643126	-2551.5689506	-2551.5659321	629	0.03
add7b_075_dcm	-2552.0772426	-2551.4641026	-2551.5689176	-2551.5658991	629	0.03
add7b_124_dcm	-2552.0772946	-2551.4640796	-2551.5688946	-2551.5658761	629	0.03
add7b_004_dcm	-2552.0771107	-2551.4640887	-2551.5688207	-2551.5658022	628	0.03
add7b_056_dcm	-2552.0770696	-2551.4640306	-2551.5686996	-2551.5656811	628	0.03
add7b_024_dcm	-2552.0772159	-2551.4639719	-2551.5686949	-2551.5656764	630	0.03
add7b_107_dcm	-2552.0771499	-2551.4639409	-2551.5686399	-2551.5656214	629	0.02
add7b_058_dcm	-2552.0768889	-2551.4638929	-2551.5686269	-2551.5656084	629	0.02
add7b_027_dcm	-2552.0771886	-2551.4639656	-2551.5686256	-2551.5656071	630	0.02
add7b_010_dcm	-2552.0769587	-2551.4638597	-2551.5686037	-2551.5655852	629	0.02
add7b_147_dcm	-2552.0767477	-2551.4637577	-2551.5685927	-2551.5655742	628	0.02
all			**-2551.5688566**	**-2551.5658381**	**629**	
ΔE	-33.0	-27.1	+20.4	+12.5		
all			**+21.9**	**+13.9**		

[a] best 20 conformers according to $G_{qh,298}$ at SMD(DCM)/B3LYP-D3/6-31+G(d) level of theory.

System NBu_4BF_4 – computational data

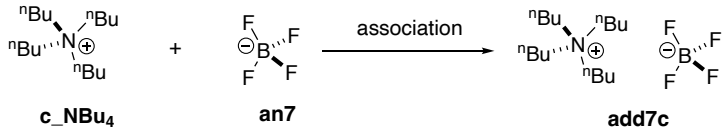

Figure 3.34: [Figure S35]. Ion association of additive **7c** and the single ions.

The Boltzmann-averaged free reaction energy of the ion pairing of **7c** amounts to $\Delta G_{qh,298,corr}$ = +11.2 kJ mol^{-1} in DCM solution. Focusing only on the best conformers of the reactants and product the free reaction energy of the ion pairing of **7c** changes to $\Delta G_{qh,298,corr}$ = +9.58 kJ mol^{-1} in DCM solution. The blue marked cells show the Boltzmann-averaged values.

According to $\Delta G_{qh,298,corr}$ = -RT ln*K* and assuming R = 8.314 J K^{-1} mol^{-1} and T = 298.15 K, the respective equilibrium constant amounts to *K*(**7c**, DCM) = 0.021 for the best conformer of **7c** and to *K*(**7c**, DCM) = 0.011 for the Boltzmann-averaged free reaction energy. In this case the equilibrium constant *K* corresponds to the concentration of the reactants and products in the following way: *K* = [**7c**]/[$\mathbf{BF_4}$] [**c_NBu4**] = [**7c**]/[$\mathbf{BF_4}$]^2.

Table 3.60: [Table S65]. Energies for all systems shown in Figure 3.34.

System	E_{tot} SMD(DCM)/ B3LYP-D3/ 6-31+G(d)	H_{298} SMD(DCM)/ B3LYP-D3/ 6-31+G(d)	$G_{qh,298}$ SMD(DCM)/ B3LYP-D3/ 6-31+G(d)	$G_{qh,298,corr}$ SMD(DCM)/ B3LYP-D3/ 6-31+G(d)	Cavity Volume (Å^3)	Relative Population Parameter based on $G_{qh,298}$
BF_4						
borate_001_dcm	**-424.6525330**	**-424.6336440**	**-424.6644660**	**-424.6614475**	**69.7**	1.00
			-424.6644660	**-424.6614475**	**69.7**	
c_NBu4						
NBu4_002	**-686.095346**	**-685.564482**	**-685.637042**	**-685.634023**	**313**	0.99
NBu4_001c	-686.094074	-685.564092	-685.632815	-685.629797	313	0.01
NBu4_006	-686.090709	-685.558999	-685.630636	-685.627618	312	0.00
NBu4_005	-686.089721	-685.557688	-685.629512	-685.626493	312	0.00
NBu4_003	-686.089384	-685.557149	-685.628989	-685.625971	312	0.00
NBu4_004	-686.086662	-685.553694	-685.624302	-685.621283	312	0.00
			-685.6369831	**-685.6339647**	**313**	
7c[a]						
add7c_054_dcm	-1110.7624593	-1110.2095593	**-1110.2948393**	**-1110.2918208**	**382**	0.08
add7c_055_dcm	**-1110.7628299**	**-1110.2095709**	-1110.2948259	-1110.2918074	381	0.08

add7c_071_dcm	-1110.7628267	-1110.2095787	-1110.2948067	-1110.2917882	381	0.08
add7c_069_dcm	-1110.7628682	-1110.2095592	-1110.2947382	-1110.2917197	381	0.07
add7c_044_dcm	-1110.7628513	-1110.2095313	-1110.2947053	-1110.2916868	381	0.07
add7c_025_dcm	-1110.7624997	-1110.2093367	-1110.2945137	-1110.2914952	383	0.06
add7c_046_dcm	-1110.7624132	-1110.2091262	-1110.2943952	-1110.2913767	381	0.05
add7c_031_dcm	-1110.7623732	-1110.2093152	-1110.2942822	-1110.2912637	380	0.05
add7c_039_dcm	-1110.7628326	-1110.2093826	-1110.2942296	-1110.2912111	382	0.04
add7c_019_dcm	-1110.7625147	-1110.2091387	-1110.2941467	-1110.2911282	381	0.04
add7c_074_dcm	-1110.7625037	-1110.2091167	-1110.2938947	-1110.2908762	381	0.03
add7c_067_dcm	-1110.7625069	-1110.2090839	-1110.2938629	-1110.2908444	382	0.03
add7c_103_dcm	-1110.7616967	-1110.2088647	-1110.2938257	-1110.2908072	382	0.03
add7c_096_dcm	-1110.7617889	-1110.2087909	-1110.2937699	-1110.2907514	381	0.03
add7c_007_dcm	-1110.7620485	-1110.2087845	-1110.2937495	-1110.2907310	383	0.03
add7c_123_dcm	-1110.7617894	-1110.2087484	-1110.2937474	-1110.2907289	382	0.03
add7c_105_dcm	-1110.7617380	-1110.2088000	-1110.2937460	-1110.2907275	382	0.03
add7c_075_dcm	-1110.7620559	-1110.2087609	-1110.2936939	-1110.2906754	383	0.02
add7c_094_dcm	-1110.7617982	-1110.2087672	-1110.2936892	-1110.2906707	381	0.02
add7c_104_dcm	-1110.7617631	-1110.2086991	-1110.2936601	-1110.2906416	382	0.02
all			**-1110.2941800**	**-1110.2911615**	**382**	
ΔE	-39.4	-30.1	+17.5	+9.58		
all			**+19.1**	**+11.2**		

[a] best 20 conformers according to $G_{qh,298}$ at SMD(DCM)/B3LYP-D3/6-31+G(d) level of theory.

System PBu_4BF_4 – computational data

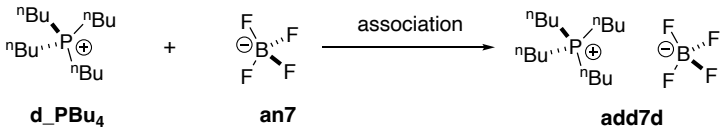

Figure 3.35: [Figure S36]. Ion association of additive **7d** and the single ions.

The Boltzmann-averaged free reaction energy of the ion pairing of **7d** amounts to $\Delta G_{qh,298,corr}$ = +5.97 kJ mol^{-1} in DCM solution. Focusing only on the best conformers of the reactants and product the free reaction energy of the ion pairing of **7d** changes to $\Delta G_{qh,298,corr}$ = +5.82 kJ mol^{-1} in DCM solution. The blue marked cells show the Boltzmann-averaged values.

According to $\Delta G_{qh,298,corr}$ = -RT ln*K* and assuming R = 8.314 J K^{-1} mol^{-1} and T = 298.15 K, the respective equilibrium constant amounts to *K*(**7d**, DCM) = 0.096 for the best conformer of **7d** and to *K*(**7d**, DCM) = 0.090 for the Boltzmann-averaged free reaction energy. In this case the equilibrium constant *K* corresponds to the concentration of the reactants and products in the following way: *K* = [**7d**]/[$\mathbf{BF_4}$] [**d_PBu4**] = [**7d**]/[$\mathbf{BF_4}$]^2.

Table 3.61: [Table S66]. Energies for all systems shown in Figure 3.35.

System	E_{tot} SMD(DCM)/ B3LYP-D3/ 6-31+G(d)	H_{298} SMD(DCM)/ B3LYP-D3/ 6-31+G(d)	$G_{qh,298}$ SMD(DCM)/ B3LYP-D3/ 6-31+G(d)	$G_{qh,298,corr}$ SMD(DCM)/ B3LYP-D3/ 6-31+G(d)	Cavity Volume (Å^3)	Relative Population Parameter based on $G_{qh,298}$
BF_4						
borate_001_dcm	**-424.6525330**	**-424.6336440**	**-424.6644660**	**-424.6614475**	**69.7**	1.00
			-424.6644660	**-424.6614475**	**69.7**	
d_PBu4						
PBu4_001_dcm_fr	**-972.730410**	**-972.207922**	**-972.283263**	**-972.280245**	**326**	0.71
PBu4_002b_pos	-972.729488	-972.206599	-972.282049	-972.279030	327	0.20
PBu4_003_dcm_fr	-972.727645	-972.204727	-972.280491	-972.277472	326	0.04
PBu4_005_dcm_fr	-972.728208	-972.205291	-972.280338	-972.277319	326	0.03
PBu4_004_dcm_fr	-972.727749	-972.204384	-972.279426	-972.276408	326	0.01
PBu4_006_dcm_fr	-972.726367	-972.203286	-972.278751	-972.275732	326	0.01
PBu4_007_dcm_fr	-972.725758	-972.202871	-972.278552	-972.275534	327	0.00
			-972.282730	**-972.279711**	**326**	
7d[a]						
add7d_062_dcm	-1397.3971810	-1396.8536460	**-1396.9424950**	**-1396.9394765**	**396**	0.06
add7d_015_dcm	**-1397.3975433**	**-1396.8537783**	-1396.9423173	-1396.9392988	396	0.05
add7d_097_dcm	-1397.3965382	-1396.8531322	-1396.9421622	-1396.9391437	396	0.04
add7d_082_dcm	-1397.3970628	-1396.8535218	-1396.9421588	-1396.9391403	395	0.04
add7d_134_dcm	-1397.3970898	-1396.8534568	-1396.9421548	-1396.9391363	396	0.04
add7d_031_dcm	-1397.3971864	-1396.8534744	-1396.9421394	-1396.9391209	396	0.04
add7d_081_dcm	-1397.3970494	-1396.8534964	-1396.9421364	-1396.9391179	395	0.04
add7d_091_dcm	-1397.3965428	-1396.8530588	-1396.9421358	-1396.9391173	396	0.04
add7d_089_dcm	-1397.3970672	-1396.8534242	-1396.9421092	-1396.9390907	396	0.04
add7d_138_dcm	-1397.3970898	-1396.8534328	-1396.9420748	-1396.9390563	396	0.04
add7d_135_dcm	-1397.3965485	-1396.8530665	-1396.9420705	-1396.9390520	396	0.04
add7d_085_dcm	-1397.3970885	-1396.8534225	-1396.9420565	-1396.9390380	396	0.04
add7d_046_dcm	-1397.3970089	-1396.8532869	-1396.9420429	-1396.9390244	396	0.04
add7d_117_dcm	-1397.3970913	-1396.8534273	-1396.9420413	-1396.9390228	396	0.04

add7d_032_dcm	-1397.3967888	-1396.8533268	-1396.9419428	-1396.9389243	396	0.03
add7d_131_dcm	-1397.3970733	-1396.8533643	-1396.9419293	-1396.9389108	396	0.03
add7d_056_dcm	-1397.3967936	-1396.8533546	-1396.9419266	-1396.9389081	396	0.03
add7d_084_dcm	-1397.3969363	-1396.8531233	-1396.9418323	-1396.9388138	397	0.03
add7d_001_dcm	-1397.3970497	-1396.8532797	-1396.9418177	-1396.9387992	396	0.03
add7d_139_dcm	-1397.3964290	-1396.8527250	-1396.9415420	-1396.9385235	395	0.02
all			**-1396.9419027**	**-1396.9388842**	**396**	
ΔE	-38.3	-32.1	+13.7	+5.82		
all			**+13.9**	**+5.97**		

[a] best 20 conformers according to $G_{qh,298}$ at SMD(DCM)/B3LYP-D3/6-31+G(d) level of theory.

3.1.10.5 Optimized Conformers and Methyl Cation Affinities of Neutral Lewis Base Catalysts in DCM

Neutral organocatalysts DMAP (**1**) and TCAP (**2**) were used as reference compounds. Their energies and methyl cation affinities were calculated at at SMD(DCM)/B3LYP-D3/6-31+G(d) level of theory. The blue marked cells show the Boltzmann-averaged values.

System DMAP – computational data

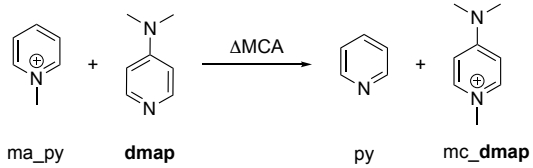

Figure 3.36: Figure S37. Equation used for calculation of relative Lewis basicity of DMAP (**1**) with pyridine as reference.

Table 3.62: Table S67. Energy for all systems shown in Figure 3.36.

System	E_{tot} SMD(DCM)/ B3LYP-D3/ 6-31+G(d)	H_{298} SMD(DCM)/ B3LYP-D3/ 6-31+G(d)	$G_{qh,298}$ SMD(DCM)/ B3LYP-D3/ 6-31+G(d)	$G_{qh,298,corr}$ SMD(DCM)/ B3LYP-D3/ 6-31+G(d)
Pyridine				
py_001_dcm_fr	-248.3117009	-248.2175679	-248.2502039	-248.2471854
ma_py_001_dcm_fr	-288.0755143	-287.9375633	-287.9743763	-287.9713578

DMAP (1)				
dmap_001_dcm	-382.301346	-382.129303	-382.171771	-382.168753
mc_dmap_001_dcm_ofr	-422.0778555	-421.8616535	-421.9077655	-421.9047470
ΔMCA		**-32.44**		**-31.04**

System TCAP – computational data

Figure 3.37: Figure S38. Equation used for calculation of relative Lewis basicity of TCAP (**2**) with pyridine as reference.

Table 3.63: Table S68. Energy for all systems shown in Figure 3.37.

System	E_{tot} SMD(DCM)/ B3LYP-D3/ 6-31+G(d)	H_{298} SMD(DCM)/ B3LYP-D3/ 6-31+G(d)	$G_{qh,298}$ SMD(DCM)/ B3LYP-D3/ 6-31+G(d)	$G_{qh,298,corr}$ SMD(DCM)/ B3LYP-D3/ 6-31+G(d)
Pyridine				
py_001_dcm_fr	-248.3117009	-248.2175679	-248.2502039	-248.2471854
ma_py_001_dcm_fr	-288.0755143	-287.9375633	-287.9743763	-287.9713578
TCAP (2)				
tcap_001_dcm	**-537.180523**	**-536.933789**	**-536.980044**	**-536.977026**
tcap_002_dcm	-537.180206	-536.933432	-536.979826	-536.976808
		-536.9336439	**-536.9799476**	**-536.9769292**
Me_TCAP				
mc_tcap_002_dcm_ofr	**-576.9609333**	**-576.6701483**	**-576.7200573**	**-576.7170388**
mc_tcap_001_dcm_ofr	-576.9603169	-576.6692849	-576.7192719	-576.7162534
		-576.6699013	**-576.7198191**	**-576.7168006**
ΔMCA		-42.70		-41.59
all		**-42.96**		**-41.22**

3.2 Additional Results

3.2.1 Solvent Effects on Pyridinamide Ion Pairs

Conductivity measurements of pyridinamide ion pairs were carried out in tetrahydrofuran (THF) and chloroform ($CHCl_3$). The conductivity profiles were analyzed with the simple 1:1 association model (see Chapter 2.1.4) and the resulting association constants K_{IP} (M^{-1}) together with the association constant obtained from conductivity measurements performed in MeCN and DCM are listed in Table 3.64. Further evaluation using other association models were not performed.

Table 3.64. Association constant K_{IP} (M^{-1}) obtained by employing eq. 3.6 of pyridinamide ion pairs in various solvents.

	MeCN		DCM		THF		$CHCl_3$	
IP	**Λ_m (S cm² mol⁻¹)**	**K_{IP} (M^{-1})**	**Λ_m (S cm² mol⁻¹)**	**K_{IP} (M^{-1})**	**Λ_m (S cm² mol⁻¹)**	**K_{IP} (M^{-1})**	**Λ_m (S cm² mol⁻¹)**	**K_{IP} (M^{-1})**
3a	126	34.6 ± 0.29	79.2	828 ± 8.27	44.8	2453 ± 33.1	6.97	3012 ± 146
3b	130	50.6 ± 0.50	80.3	544 ± 6.03	60.8	2760 ± 33.9	16.3	5587 ± 200
3c	133	44.0 ± 0.63	57.9	2237 ± 24.9	18.2	5698 ± 134	n.d.[b]	n.d.[b]
3d	129	44.0 ± 0.34	56.0	2707 ± 39.1	19.1	8129 ± 167	n.d.[b]	n.d.[b]
4a	110	42.9 ± 0.33	73.6	938 ± 8.53	n.d.[a]	n.d.[a]	7.97	9422 ± 210
5a	113	44.5 ± 0.80	73.2	832 ± 6.82	n.d.[a]	n.d.[a]	7.89	8795 ± 248
6a	115	49.3 ± 0.55	74.2	830 ± 8.92	39.1	4993 ± 44.3	9.74	6518 ± 155

[a] not determined due to solubility problem. [b] reliable conductivity measurement not possible due to pronounced ion association at low concentration.

The association constants of all pyridinamide ion pair increased significantly with decreasing solvent polarity when transitioning from MeCN to DCM to THF to $CHCl_3$, indicating the weakest association in the polar protic solvent MeCN and the strongest in the apolar solvent $CHCl_3$. Simultaneously, the specific molar conductivities Λ_m decreased with decreasing solvent polarity, reflecting the same trend in ion association. The association constants K_{IP} (M^{-1}) were analyzed in relation to several solvent descriptors (see Table 3.65). These included the relative permittivity ε_r, which measures the solvent's ability to reduce electrostatic interactions between charges species[37], and the $E_T(30)$ values, which reflect the solvent polarity based on the solvatochromic shift of the Reichardt's dye[38–41]. Additionally, the Gutmann acceptor number (AN), representing the solvent's Lewis acidity, and the Gutmann donor number (DN), reflecting the solvent's Lewis basicity, were considered.[42,43]

Table 3.65. List of solvent descriptors: relative permittivity ε_r values[37], $E_T(30)$[38–41], and Gutmann acceptor (AN) and Gutmann donor (DN) numbers[42,43] for selected solvents.

	ε_r	**$E_T(30)$ (kcal mol⁻¹)**	**AN**	**DN**
MeCN	36.6	45.6	18.9	14.1
DCM	9.08	40.7	20.4	1.0
THF	7.52	37.4	8.0	20.0
$CHCl_3$	4.81	39.1	23.1	4.0

Correlating the association constant of each ion pair with the relative permittivity ε_r or the Gutmann's AN and DN across all four solvents gave only weak correlations (R^2 = 0.7 – 0.5) at best. Stronger correlation (R^2 > 0.7) were observed between the association constant and the $E_T(30)$ values, as exemplified for salt **3a** in Figure 3.38A. Due to overly strong associations in $CHCl_3$ at low concentrations (c < 0.03 mM), the earlier made assumption of fully dissociated ions may not hold. Therefore, the association constant obtained in $CHCl_3$ was excluded from the final analysis, which resulted in a stronger correlation between K_{IP} and the $E_T(30)$ values as exemplary shown for salt **3a** in Figure 3.38B).

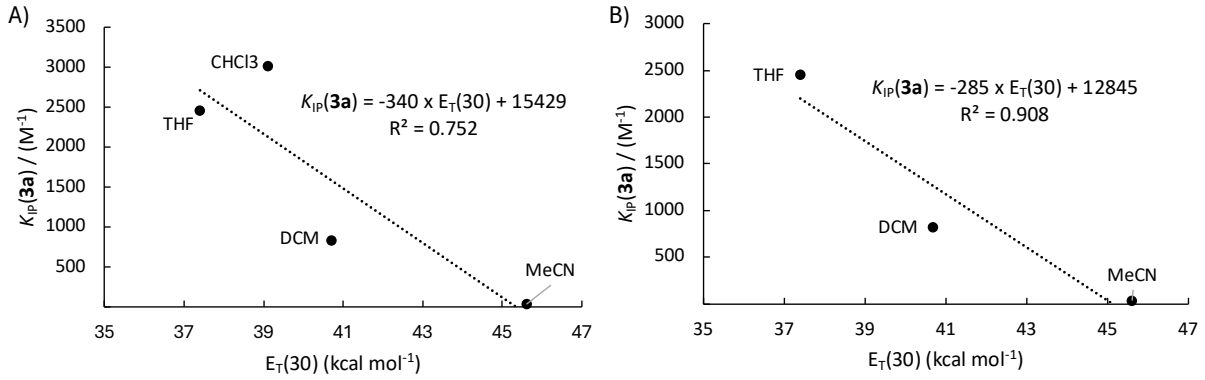

Figure 3.38. A) The correlation between the $E_T(30)$ values and K_{IP} for salt **3a** in MeCN, DCM, THF, and $CHCl_3$, and B) the correlation between the $E_T(30)$ and K_{IP} for salt **3a** in MeCN, DCM, and THF.

Plotting the logarithmic association constants against the solvent descriptors according to the Eyring equation significantly improved the respective correlations. While the correlation of the logarithmic association constants with the Gutmann's AN and DN across all four solvents remained weak ($R^2 < 0.3$), the correlation of the logarithmic association constants with the relative permittivity ε_r and the $E_T(30)$ values was strong ($R^2 > 0.9$), as shown exemplary for salt **3a** in Figure 3.39A for the $E_T(30)$ values. Here, excluding the association constant determined in $CHCl_3$ for salt **3a**, due to potentially overly strong ion association at low concentration, had only a minor effect on the correlation between log K_{IP} and the $E_T(30)$ values (see Figure 3.39B).

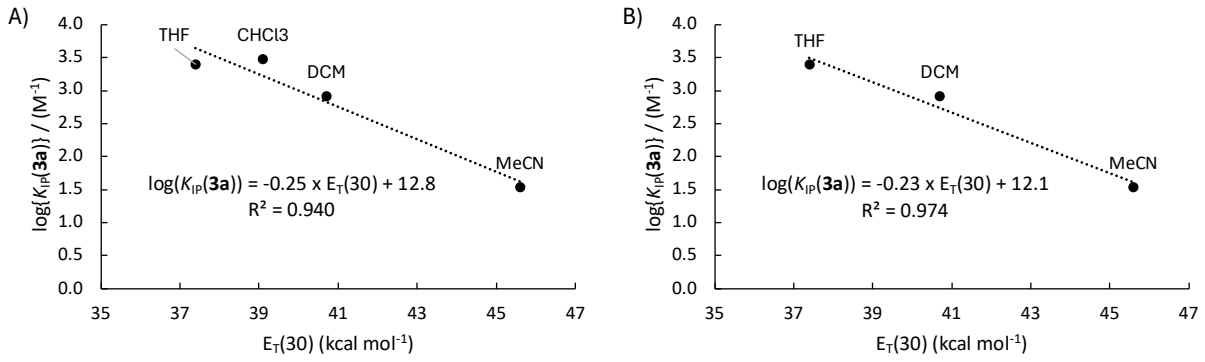

Figure 3.39. A) The correlation between the $E_T(30)$ values and log(K_{IP}) for salt **3a** in MeCN, DCM, THF, and $CHCl_3$, and B) the correlation between the $E_T(30)$ and log(K_{IP}) for salt **3a** in MeCN, DCM, and THF.

To access the effect of solvent polarity on the reactivity of pyridinamide ion pairs, the reaction rates of electrophile **8a** reacting with salt **3a** were measured across a salt concentration of [**3a**] = 0.01 – 4.0 mM in MeCN, DCM, THF, and $CHCl_3$ (see Figure 3.40).

In MeCN, a linear correlation is observed between the pseudo-first order rate constant k_{obs} and the salt concentration [**3a**]. In DCM, the initial correlation is linear ([**3a**] < 0.04 mM) until the association equilibrium shifted towards a higher fraction of ion aggregates as the concentration increased. A similar observation is made in THF and $CHCl_3$, though, the pseudo-first order rate constants k_{obs} are significantly higher than in MeCN and DCM. Furthermore, k_{obs} values measured in THF are higher than in $CHCl_3$. This is likely caused by a reduced reactivity of the salt due to a stronger association in $CHCl_3$ than in THF, as already indicated by the association constants K_{IP} (M^{-1}) in Table 3.64. In $CHCl_3$ the association equilibrium shifts towards higher aggregates at lower concentrations than in THF, thus impacting the reaction rates at lower concentrations. It should be noted that the visible plateaus in THF and $CHCl_3$ cannot be conclusively ascribed to the diminished reactivity caused by a shift in the association equilibrium since

k_{obs} values higher than 500 s^{-1} are no longer reliable since the boundaries of the stopped-flow machine are reached according to the manufacturer.

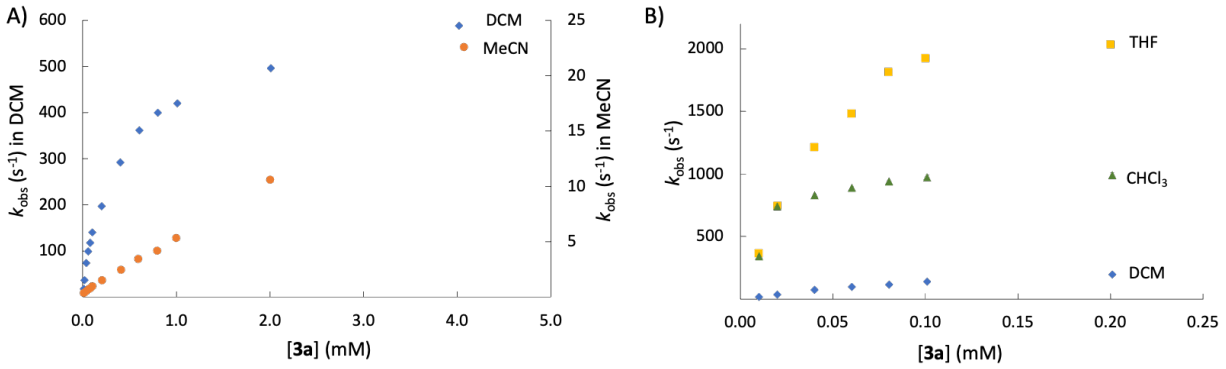

Figure 3.40. A) Correlation of k_{obs} for the reaction of **8a** with **3a** for salt concentrations [**3a**] = 0.01 – 4.0 mM in MeCN and DCM at 20 °C. B) Correlation of k_{obs} for the reaction of **8a** with **3a** for salt concentrations [**3a**] = 0.01 – 0.2 mM in DCM, THF, and $CHCl_3$ at 20 °C.

To check for correlation with solvent descriptor, the second-order rate constant k_2 of salt **3a** were used. The rate constants $k_{2,MeCN}$(**3a**) = 7.16 x 10^3 M^{-1} s^{-1} and $k_{2,DCM}$(**3a**) = 1.82 x 10^6 M^{-1} s^{-1} were obtained using five data points for a concentration window of [**3a**] = 0.01 – 0.03 mM (see Chapter 2.1.7). Rate constants in THF and $CHCl_3$ were extrapolated using the first two data points of the wide range measurement, which gave $k_{2,THF}$(**3a**) = 3.78 x 10^7 M^{-1} s^{-1} and $k_{2,CHCl3}$(**3a**) = 3.98 x 10^7 M^{-1} s^{-1}. Correlating the logarithmic values of these second-order rate constants with the solvent descriptors listed in Table 3.65 revealed no correlation with the Gutmann's AN and DN (R^2 < 0.1), but a strong correlation (R^2 > 0.9) between log k_2(**3a**) with the relative permittivity ε_r and with the $E_T(30)$ values (see Figure 3.38). This trends, which were also observed for the logarithmic association constants log K_{IP}, suggests that the solvent polarity plays a significant role in the association behavior and reactivity of pyridinamide ion pairs.

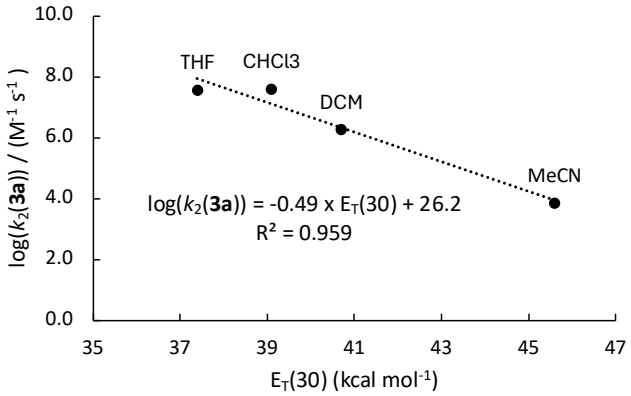

Figure 3.41. Correlation between the $E_T(30)$ values and logarithmic second-order rate constants log k_2 (M^{-1} s^{-1}) for salt **3a** in MeCN, DCM, THF, and $CHCl_3$.

Finally, it should be noted that no further kinetic measurements in THF and MeCN have been performed due to the high reaction speed of **8a** reacting with **3a**. The benzhydrylium salt **8a**, with an electrophilicity parameter E = -10.04 is the least reactive benzhydrylium salt. Therefore, any other benzhydrylium salt would react even faster when used as electrophile in this measurement.

3.2.2 Association Model Validity at Higher Concentrations.

The conductivity profiles of pyridinamide ion pairs in dichloromethane (DCM) have been studied at salt concentrations up to 1.0 mM, with a thorough analysis of three possible ion association models (see

Chapter 2.1.4 and 3.1.4). Although this concentration range has been extensively studied and optimized, typical synthetic applications often involve catalyst concentrations of 1.0 mM or higher. To assess the robustness of the established association models beyond 1.0 mM, conductivity measurements were extended to 5.0 mM, and the root mean square error (RMSE) between experimental data and simulations using previously optimized association constants was calculated. The RMSE values, summarized in Table 3.2 and Table 3.3, show that at 1.0 mM, the RMSE is below 1.0 mM across all models, indicating a good fit between experimental and simulated data. However, when extending the concentration to 5.0 mM, the RMSE increases (see Table 3.66).

Table 3.66. List of specific molar conductivities Λ_m (S cm² mol^{-1}) and the resulting ion association constant K_{IP} (M^{-2}, Model 1), the cationic and anionic sandwich association constants K_{CAC} and K_{ACA} (M^{-2}, Model 2), and the scaling factors α and β to obtain the association constants of the mixed association (model 3) with the respective RMSE values for salt concentration up to 5.0 mM for all pyridinamide ion pairs in DCM.

Ion Pair	Λ_m (S cm² mol^{-1})	Model 1 K_{IP} (M^{-2}) (RMSE)	Model 2a K_{CAC} (M^{-2}) (RMSE)	Model 2b K_{ACA} (M^{-2}) (RMSE)	Model 3 [α|β] x K_{CAC} (M^{-2}) (RMSE)
3d	56.0	7.35 x 10^6 (2.55)	1.07 x 10^7 (3.32)	–	–
3c	57.9	5.00 x 10^6 (3.44)	1.01 x 10^7 (4.25)	1.01 x 10^7 (4.25)	[33|23] x 1.01 x 10^7 (6.17)
3b	80.3	2.96 x 10^5 (11.4)	4.65 x 10^6 (4.85)	4.65 x 10^6 (4.85)	[100|0] x 4.65 x 10^6 (4.85)
3a	79.2	6.86 x 10^5 (11.4)	6.38 x 10^6 (6.71)	6.38 x 10^6 (6.71)	[44|21] x 6.38 x 10^6 (2.29)
4a	73.6	8.79 x 10^5 (10.5)	6.50 x 10^6 (5.16)	6.50 x 10^6 (5.16)	[12|61] x 6.50 x 10^6 (2.23)
5a	73.2	6.92 x 10^5 (9.31)	5.15 x 10^6 (5.71)	5.15 x 10^6 (5.71)	[11|67] x 5.15 x 10^6 (1.12)
6a	74.2	6.89 x 10^5 (7.16)	6.75 x 10^6 (4.41)	6.75 x 10^6 (4.41)	[16|52] x 6.75 x 10^6 (1.12)

A progressive decrease in RMSE is observed as the model evolves from the 1:1 ion association to the sandwich association and finally to the mixed sandwich association model. This is graphically depicted in Figure 3.42 for salt **3a** as example. In the 1:1 association model beyond 1.0 mM the simulated conductivity profile is clearly below the experimental data point, yielding a RMSE of 11.4. Opposed to this, in the sandwich association model (Model 2) the simulated curve runs above the experimental data, however, the deviation is smaller, yielding an RMSE of 6.71. In the final association model, the mixed sandwich association model, the experimental data points, and the simulated curve are almost overlapping as indicated by the significantly reduced RMSE of 2.29.

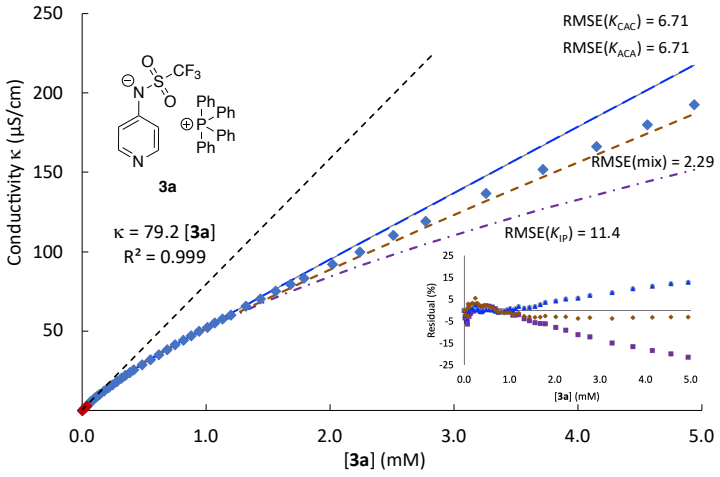

Figure 3.42. Conductivity profile for salt **3a** in DCM with fits to the calculated conductivity data for the 1:1 association model (purple dotted-dashed line), the cationic and anionic sandwich association models (grey line and blue long dashed line), and mixed sandwich association model (brown short-dashed line) with their respective percentual residue.

The RMSE for the final mixed sandwich model at 5.0 mM is notably lower compared to the initial 1:1 ion association model, indicating substantial improvements in the accuracy of the association model with increasing complexity. This demonstrates that the mixed sandwich association model is more accurate

for predicting the behavior of pyridinamide ion pairs at higher concentrations, relevant to practical synthetic conditions. This trend is observed for all pyridinamide ion pairs, except salt **3c** and **3d**.

While the RMSE at 1.0 mM decreases during the model refinement (see Table 3.2 and Table 3.3), a different trend is observed when extending to 5.0 mM. Here, the RMSE progressively increases as the model transitions from the 1:1 ion association to the sandwich association and finally to the mixed sandwich association model. As salt **3c** and **3d** contain *n*-butyl chained cations, their association behavior at higher concentration might differ from other ion pairs carrying cations with aromatic substituents (cation **a** and **b**). The association constants of salt **3c** and **3d** suggest a stronger ion association, which could potentially lead to 1:1 ion pairs or other symmetric higher-order aggregates rather than following an asymmetric sandwich association at higher concentrations as observed with other pyridinamide salts.

Looking forward, future synthesis efforts for pyridinamide ion pair will focus on selecting ion combination that preferentially favor the cationic sandwich association, thereby ensuring a high concentration of free anions, which are responsible for the enhanced reactivity observed for these systems in apolar solvents.

3.2.3 Additional Experimental Data

3.2.3.1 Pyridinamide Ion Pairs – Data of Conductivity Measurements in THF

Concentration dependent conductivity data of **3a** in THF at 20 °C

[3a]/M	Conductivity κ (µS/cm)
0.00	0.80
1.79×10^{-5}	1.60
3.57×10^{-5}	2.40
5.35×10^{-5}	3.20
7.13×10^{-5}	3.92
8.90×10^{-5}	4.48
1.07×10^{-4}	5.20
1.24×10^{-4}	5.76
1.42×10^{-4}	6.24
1.77×10^{-4}	7.12
2.12×10^{-4}	7.92
2.47×10^{-4}	8.72
2.82×10^{-4}	9.52
3.16×10^{-4}	10.2
3.51×10^{-4}	10.9
3.85×10^{-4}	11.6
4.19×10^{-4}	12.2
4.87×10^{-4}	13.5
5.55×10^{-4}	14.7
6.21×10^{-4}	15.9
6.88×10^{-4}	17.0
7.54×10^{-4}	18.0
8.19×10^{-4}	19.1
8.84×10^{-4}	20.0
9.48×10^{-4}	21.0
1.01×10^{-3}	22.0
1.08×10^{-3}	22.9
1.20×10^{-3}	24.6
1.32×10^{-3}	26.3
1.45×10^{-3}	28.0
1.57×10^{-3}	29.7
1.68×10^{-3}	31.1
1.80×10^{-3}	32.8
1.92×10^{-3}	34.2
2.03×10^{-3}	35.7
2.14×10^{-3}	37.0
2.25×10^{-3}	38.5
2.41×10^{-3}	40.6
2.57×10^{-3}	42.5
2.78×10^{-3}	44.9
3.03×10^{-3}	47.9
3.27×10^{-3}	50.6
3.51×10^{-3}	53.6
3.74×10^{-3}	56.2
3.96×10^{-3}	58.7
4.17×10^{-3}	61.2
4.38×10^{-3}	63.5
4.58×10^{-3}	65.8

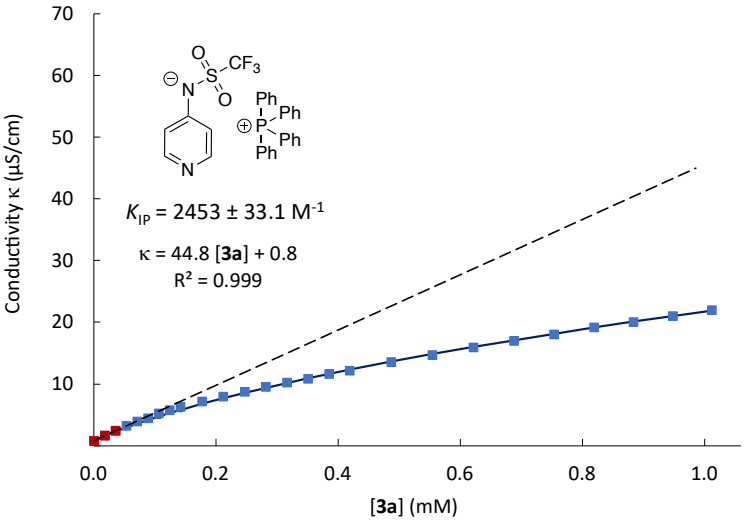

Concentration dependent conductivity data of **3b** in THF at 20 °C

[3b]/M	Conductivity κ (µS/cm)
0.00	0.80
1.90×10^{-5}	2.00
3.80×10^{-5}	3.09
5.70×10^{-5}	3.92
7.59×10^{-5}	4.88
9.48×10^{-5}	5.60
1.14×10^{-4}	6.32
1.32×10^{-4}	7.09
1.51×10^{-4}	7.84
1.70×10^{-4}	8.48
1.89×10^{-4}	9.04
2.26×10^{-4}	10.2
2.63×10^{-4}	11.1
3.00×10^{-4}	12.2
3.37×10^{-4}	13.2
3.73×10^{-4}	14.3
4.46×10^{-4}	16.3
5.19×10^{-4}	18.4
5.91×10^{-4}	19.7
6.62×10^{-4}	21.4
7.33×10^{-4}	22.9
8.03×10^{-4}	24.3
9.41×10^{-4}	27.4
1.08×10^{-3}	30.0
1.21×10^{-3}	32.5
1.35×10^{-3}	35.2
1.54×10^{-3}	38.8
1.73×10^{-3}	42.3
1.92×10^{-3}	45.7
2.10×10^{-3}	49.0
2.34×10^{-3}	53.0
2.63×10^{-3}	57.9
2.91×10^{-3}	62.6
3.17×10^{-3}	67.1
3.43×10^{-3}	71.4
3.69×10^{-3}	75.7
3.93×10^{-3}	79.6
4.17×10^{-3}	83.4
4.40×10^{-3}	87.0
4.62×10^{-3}	90.6
4.83×10^{-3}	94.2

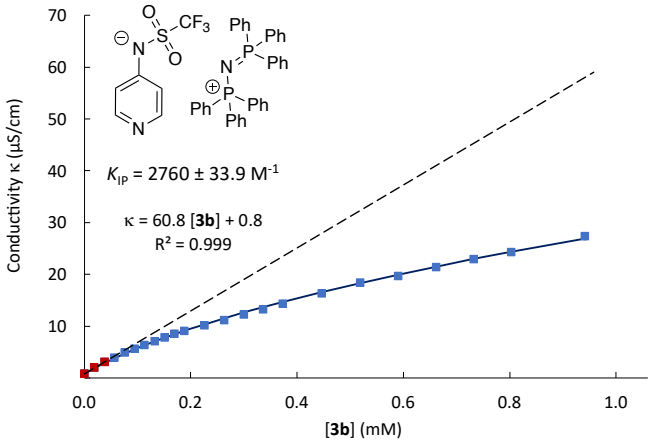

Concentration dependent conductivity data of **3c** in THF at 20 °C

[3c]/M	Conductivity κ (µS/cm)
0.00	0.80
1.97×10^{-5}	1.15
3.93×10^{-5}	1.52
5.90×10^{-5}	1.79
7.85×10^{-5}	2.00
9.81×10^{-5}	2.24
1.18×10^{-4}	2.40
1.56×10^{-4}	2.75
1.95×10^{-4}	2.99
2.34×10^{-4}	3.20
2.72×10^{-4}	3.41
3.10×10^{-4}	3.65
3.87×10^{-4}	4.13
4.62×10^{-4}	4.43
5.37×10^{-4}	4.88
6.11×10^{-4}	5.33
7.58×10^{-4}	5.92
9.03×10^{-4}	6.72
1.05×10^{-3}	7.41
1.19×10^{-3}	8.00
1.32×10^{-3}	8.56
1.46×10^{-3}	8.96
1.66×10^{-3}	9.71
1.86×10^{-3}	10.5
2.05×10^{-3}	11.0
2.30×10^{-3}	11.8
2.60×10^{-3}	12.9
2.89×10^{-3}	13.8
3.18×10^{-3}	14.7
3.45×10^{-3}	15.7
3.71×10^{-3}	16.4
3.97×10^{-3}	17.2
4.22×10^{-3}	18.1
4.46×10^{-3}	18.7

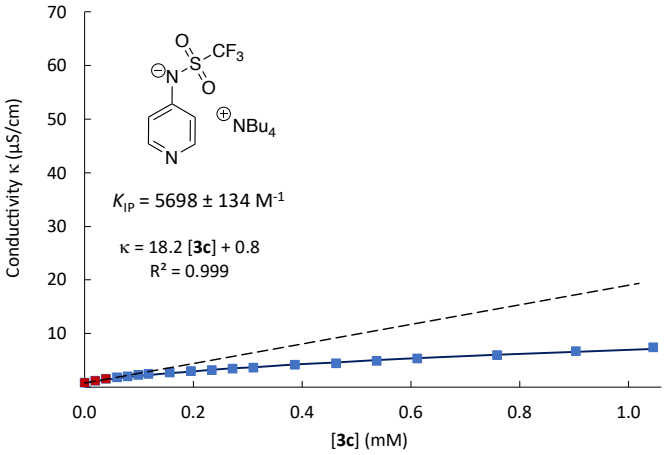

Concentration dependent conductivity data of **3d** in THF at 20 °C

[3d]/M	Conductivity κ (µS/cm)
0.00	0.72
2.04×10^{-5}	1.11
4.15×10^{-5}	1.51
6.10×10^{-5}	1.76
8.13×10^{-5}	1.93
1.01×10^{-4}	2.18
1.22×10^{-4}	2.35
1.62×10^{-4}	2.60
2.02×10^{-4}	2.86
2.42×10^{-4}	3.11
2.82×10^{-4}	3.28
3.21×10^{-4}	3.53
4.00×10^{-4}	3.91
4.78×10^{-4}	4.25
5.56×10^{-4}	4.62
6.32×10^{-4}	4.96
7.84×10^{-4}	5.59
9.34×10^{-4}	6.10
1.08×10^{-3}	6.55
1.23×10^{-3}	7.06
1.37×10^{-3}	7.56
1.58×10^{-3}	8.18
1.79×10^{-3}	8.74
1.99×10^{-3}	9.29
2.19×10^{-3}	9.91
2.44×10^{-3}	10.6
2.75×10^{-3}	11.3
3.05×10^{-3}	12.1
3.34×10^{-3}	12.9
3.62×10^{-3}	13.7
3.89×10^{-3}	14.4
4.16×10^{-3}	15.1
4.41×10^{-3}	15.8
4.66×10^{-3}	16.5
4.90×10^{-3}	17.1
5.13×10^{-3}	17.6
5.35×10^{-3}	18.2
2.04×10^{-5}	0.72
4.15×10^{-5}	1.11
6.10×10^{-5}	1.51
8.13×10^{-5}	1.76
1.01×10^{-4}	1.93

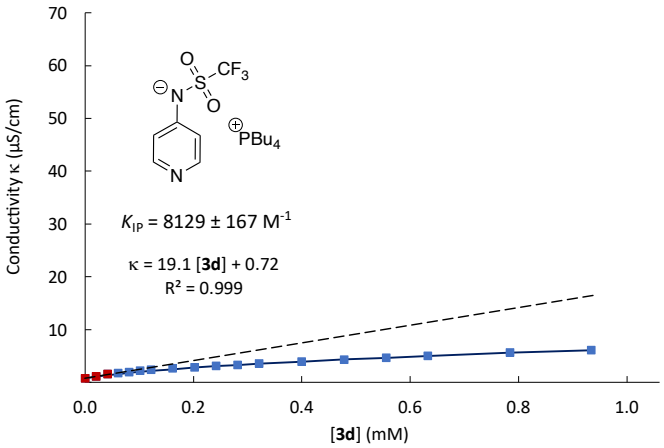

Concentration dependent conductivity data of **6a** in THF at 20 °C

[6a]/M	Conductivity κ (µS/cm)
0.00	0.72
1.87×10^{-5}	1.49
3.74×10^{-5}	2.16
5.60×10^{-5}	2.72
7.46×10^{-5}	3.12
9.31×10^{-5}	3.52
1.12×10^{-4}	4.00
1.30×10^{-4}	4.24
1.49×10^{-4}	4.72
1.85×10^{-4}	5.44
2.22×10^{-4}	6.00
2.58×10^{-4}	6.56
2.95×10^{-4}	7.12
3.31×10^{-4}	7.60
3.67×10^{-4}	8.08
4.39×10^{-4}	8.96
5.10×10^{-4}	9.76
5.80×10^{-4}	10.6
6.50×10^{-4}	11.3
7.20×10^{-4}	12.0
7.89×10^{-4}	12.8
9.25×10^{-4}	14.1
1.06×10^{-3}	15.4
1.19×10^{-3}	16.6
1.32×10^{-3}	17.8
1.45×10^{-3}	18.7
1.64×10^{-3}	20.6
1.82×10^{-3}	22.0
2.01×10^{-3}	23.4
2.24×10^{-3}	25.2
2.53×10^{-3}	27.3
2.80×10^{-3}	29.5
3.07×10^{-3}	31.4
3.33×10^{-3}	33.3
3.57×10^{-3}	35.3
3.82×10^{-3}	37.0

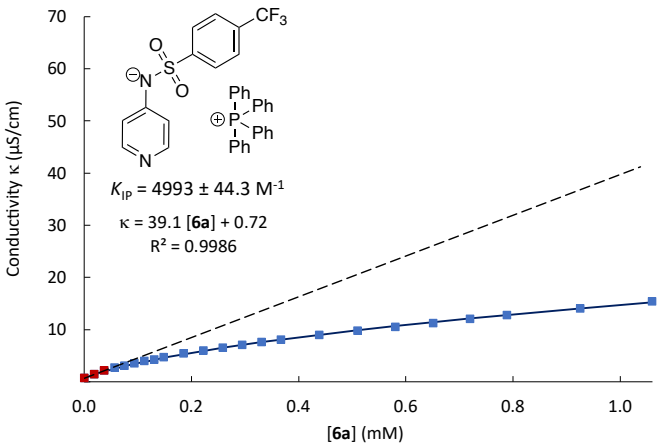

3.2.3.2 Pyridinamide Ion Pairs – Data of Conductivity Measurements in $CHCl_3$

Concentration dependent conductivity data of **3a** in $CHCl_3$ at 20 °C

[3a]/M	Conductivity κ (µS/cm)
0.00	0.80
1.76×10^{-5}	0.93
3.51×10^{-5}	1.04
7.00×10^{-5}	1.25
1.05×10^{-4}	1.44
1.39×10^{-4}	1.60
2.08×10^{-4}	1.76
2.77×10^{-4}	1.92
3.45×10^{-4}	2.24
4.79×10^{-4}	2.48
6.11×10^{-4}	2.88
7.41×10^{-4}	3.36
9.95×10^{-4}	3.92
1.24×10^{-3}	4.48
1.54×10^{-3}	5.20
1.83×10^{-3}	5.76
2.10×10^{-3}	6.48
2.37×10^{-3}	7.04
2.63×10^{-3}	7.60
2.88×10^{-3}	8.16
3.12×10^{-3}	8.80
3.36×10^{-3}	9.44
3.58×10^{-3}	10.0
3.80×10^{-3}	10.4
4.01×10^{-3}	11.0
4.22×10^{-3}	11.5
4.42×10^{-3}	12.1
4.61×10^{-3}	12.6

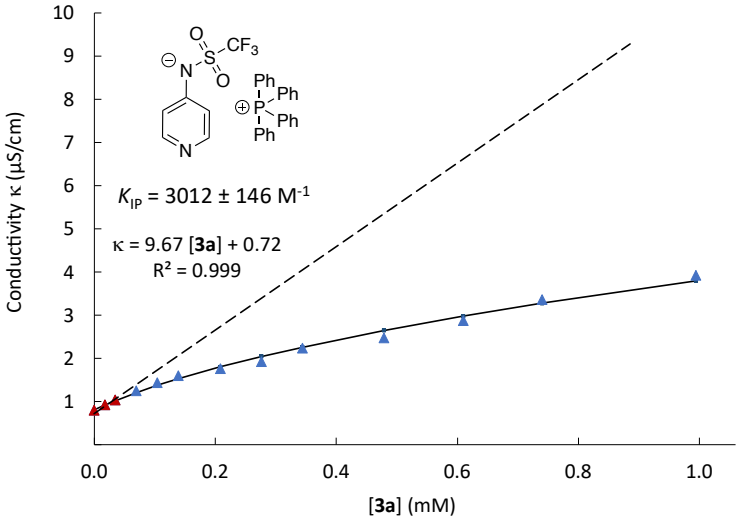

Concentration dependent conductivity data of **3b** in $CHCl_3$ at 20 °C

[3b]/M	Conductivity κ (µS/cm)
0.00	0.80
1.90×10^{-5}	1.14
3.80×10^{-5}	1.41
5.70×10^{-5}	1.63
7.59×10^{-5}	1.76
9.48×10^{-5}	1.89
1.14×10^{-4}	2.08
1.51×10^{-4}	2.29
1.89×10^{-4}	2.56
2.26×10^{-4}	2.80
3.00×10^{-4}	3.12
3.73×10^{-4}	3.60
4.46×10^{-4}	3.95
5.19×10^{-4}	4.29
5.91×10^{-4}	4.80
6.62×10^{-4}	5.04
8.03×10^{-4}	5.76

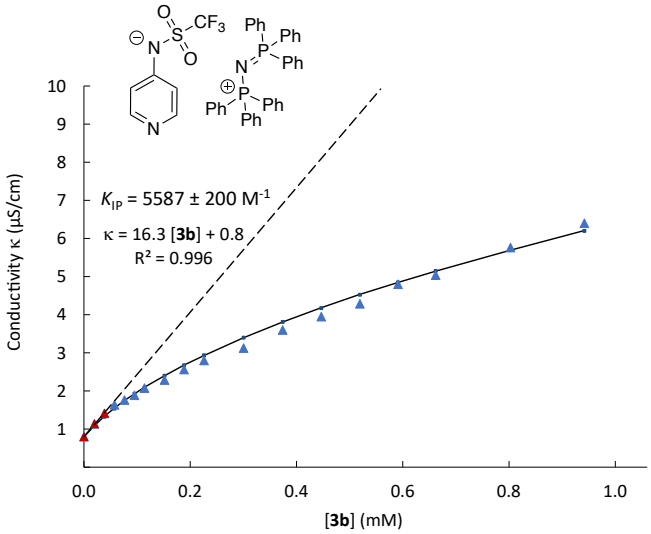

9.41 x 10^{-4}	6.40
1.08 x 10^{-3}	7.07
1.21 x 10^{-3}	7.63
1.41 x 10^{-3}	8.51
1.60 x 10^{-3}	9.44
1.79 x 10^{-3}	10.2
2.04 x 10^{-3}	11.3
2.34 x 10^{-3}	12.7
2.63 x 10^{-3}	14.1
2.91 x 10^{-3}	15.6
3.17 x 10^{-3}	16.8
3.43 x 10^{-3}	18.1
3.69 x 10^{-3}	19.4
3.93 x 10^{-3}	20.8
4.17 x 10^{-3}	22.2
4.40 x 10^{-3}	23.2
4.62 x 10^{-3}	24.5

Concentration dependent conductivity data of **4a** in $CHCl_3$ at 20 °C

[4a]/M	Conductivity κ (µS/cm)
0.00	0.72
1.86 x 10^{-5}	0.88
3.71 x 10^{-5}	1.01
7.41 x 10^{-5}	1.17
1.48 x 10^{-4}	1.39
2.21 x 10^{-4}	1.60
3.65 x 10^{-4}	1.86
5.07 x 10^{-4}	2.16
6.46 x 10^{-4}	2.45
7.84 x 10^{-4}	2.64
9.87 x 10^{-4}	2.93
1.20 x 10^{-3}	3.26
1.44 x 10^{-3}	3.68
1.75 x 10^{-3}	4.11
2.05 x 10^{-3}	4.64
2.34 x 10^{-3}	5.12
2.62 x 10^{-3}	5.52
2.89 x 10^{-3}	5.98
3.15 x 10^{-3}	6.40
3.40 x 10^{-3}	6.80
3.65 x 10^{-3}	7.25
3.89 x 10^{-3}	7.60
4.11 x 10^{-3}	8.08
4.34 x 10^{-3}	8.53
4.55 x 10^{-3}	8.88
4.76 x 10^{-3}	9.31
4.96 x 10^{-3}	9.68

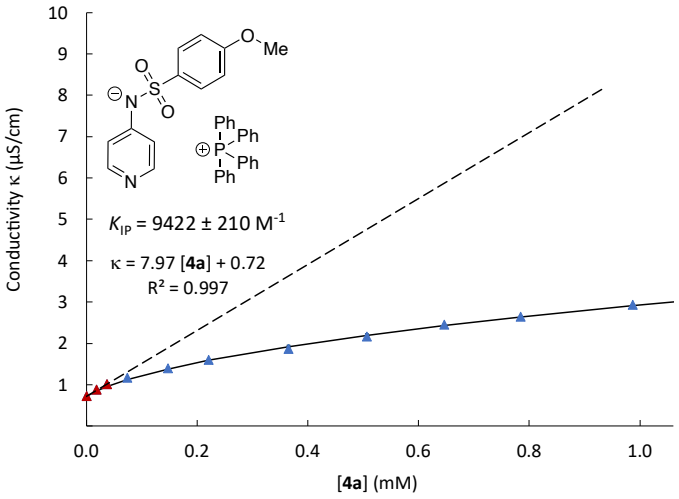

Concentration dependent conductivity data of **5a** in $CHCl_3$ at 20 °C

[5a]/M	Conductivity κ (µS/cm)
0.00	0.72
2.03 x 10^{-5}	0.88
4.05 x 10^{-5}	1.04
6.08 x 10^{-5}	1.12
8.09 x 10^{-5}	1.20
1.01 x 10^{-4}	1.28
1.21 x 10^{-4}	1.36
1.61 x 10^{-4}	1.52
2.01 x 10^{-4}	1.60
2.41 x 10^{-4}	1.68
3.20 x 10^{-4}	1.84
3.98 x 10^{-4}	2.00
5.53 x 10^{-4}	2.32
7.06 x 10^{-4}	2.48
8.56 x 10^{-4}	2.72
1.00 x 10^{-3}	2.99
1.15 x 10^{-3}	3.25
1.29 x 10^{-3}	3.52
1.50 x 10^{-3}	3.73
1.71 x 10^{-3}	4.08
1.91 x 10^{-3}	4.40
2.18 x 10^{-3}	4.91
2.49 x 10^{-3}	5.47
2.80 x 10^{-3}	5.89
3.10 x 10^{-3}	6.35
3.39 x 10^{-3}	6.88
3.66 x 10^{-3}	7.36
3.93 x 10^{-3}	7.84
4.19 x 10^{-3}	8.24
4.44 x 10^{-3}	8.75
4.69 x 10^{-3}	9.28
4.92 x 10^{-3}	9.68
5.15 x 10^{-3}	10.1
5.38 x 10^{-3}	10.5

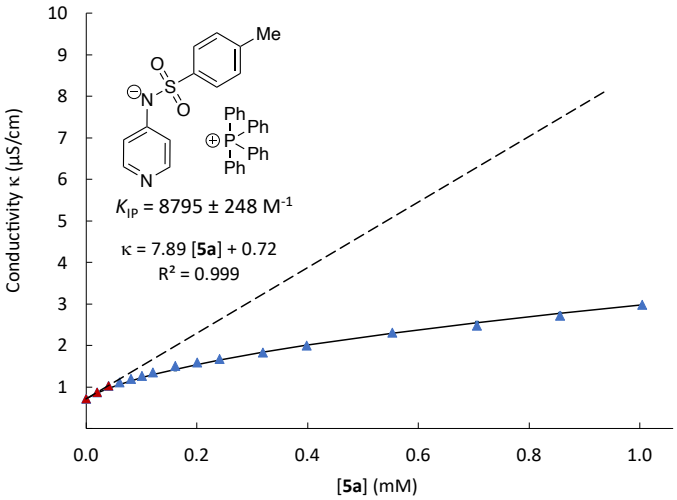

Concentration dependent conductivity data of **6a** in $CHCl_3$ at 20 °C

[6a]/M	Conductivity κ (µS/cm)
0.00	0.72
1.93 x 10^{-5}	0.93
3.72 x 10^{-5}	1.07
5.57 x 10^{-5}	1.20
7.42 x 10^{-5}	1.36
9.26 x 10^{-5}	1.49
1.11 x 10^{-4}	1.57
1.48 x 10^{-4}	1.65
1.84 x 10^{-4}	1.76
2.21 x 10^{-4}	1.97
2.93 x 10^{-4}	2.21
3.65 x 10^{-4}	2.40
4.36 x 10^{-4}	2.53
5.07 x 10^{-4}	2.77
6.47 x 10^{-4}	3.09
7.85 x 10^{-4}	3.41
9.20 x 10^{-4}	3.68
1.05 x 10^{-3}	4.00
1.19 x 10^{-3}	4.24
1.38 x 10^{-3}	4.88
1.57 x 10^{-3}	5.28
1.75 x 10^{-3}	5.60
1.94 x 10^{-3}	6.08
2.17 x 10^{-3}	6.56
2.46 x 10^{-3}	7.15
2.73 x 10^{-3}	7.76
3.00 x 10^{-3}	8.40
3.26 x 10^{-3}	8.96
3.51 x 10^{-3}	9.60
3.75 x 10^{-3}	10.1
3.98 x 10^{-3}	10.6
4.21 x 10^{-3}	11.2
4.43 x 10^{-3}	11.8
4.64 x 10^{-3}	12.4

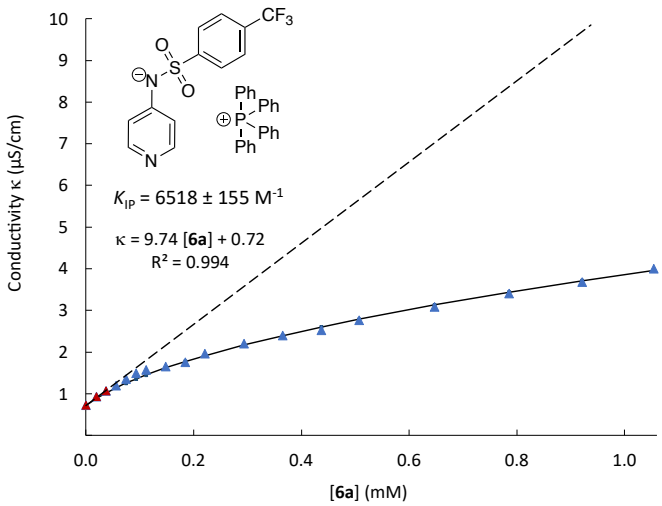

3.2.3.3 Data of kinetic Measurements

Measurement of 3a at 20°C

Reaction of **3a** with $(lil)_2CH^+BF_4^-$ in THF (stopped-flow, λ = 635 nm)

[8a] (mol L^{-1})	[3a] (mol L^{-1})	k_{obs} (s^{-1})
9.25 x 10^{-7}	1.00 x 10^{-5}	368
	2.00 x 10^{-5}	746
	4.00 x 10^{-5}	1214
	6.01 x 10^{-5}	1484
	8.01 x 10^{-5}	1814
	1.00 x 10^{-4}	1923
	2.00 x 10^{-4}	2035

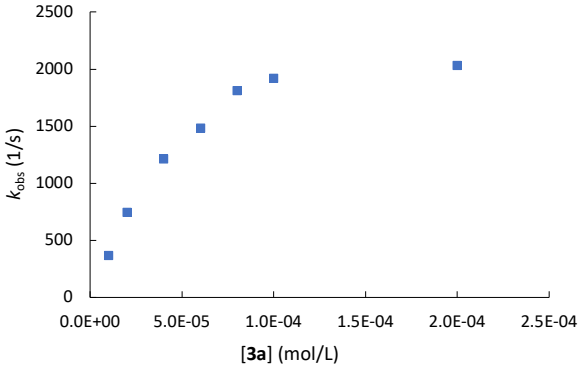

Reaction of **3a** with $(lil)_2CH^+BF_4^-$ in $CHCl_3$ (stopped-flow, λ = 636 nm)

[8a] (mol L^{-1})	[3a] (mol L^{-1})	k_{obs} (s^{-1})
1.11 x 10^{-6}	1.01 x 10^{-5}	342
	2.01 x 10^{-5}	740
	4.02 x 10^{-5}	828
	6.03 x 10^{-5}	890
	8.04 x 10^{-5}	940
	1.01 x 10^{-4}	972
	2.01 x 10^{-4}	990
	4.02 x 10^{-4}	1009
	6.03 x 10^{-4}	1020

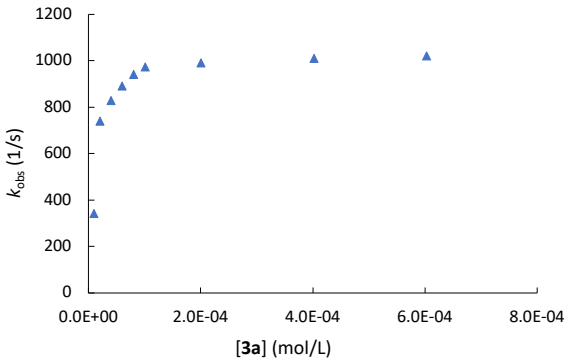

3.3 References

[1] R. K. Harris, E. D. Becker, S. M. C. de Menezes, R. Goodfellow, P. Granger, *Pure Appl. Chem.* **2001**, *73*, 1795–1818.

[2] V. Burger, M. Franta, A. R. Ofial, R. M. Gschwind, H. Zipse, *J. Am. Chem. Soc.* **2024**, accepted.

[3] J. Helberg, T. Ampßler, H. Zipse, *J. Org. Chem.* **2020**, *85*, 5390–5402.

[4] R. J. Mayer, A. R. Ofial, H. Mayr, C. Y. Legault, *J. Am. Chem. Soc.* **2020**, *142*, 5221–5233.

[5] Y. C. Wu, W. F. Koch, K. W. Pratt, *J. Res. Natl. Inst. Stand. Technol.* **1991**, *96*, 191–201.

[6] A. M. Brown, R. M. Fuoss, *J. Am. Chem. Soc.* **1960**, *64*, 1341–1342.

[7] R. M. Fuoss, E. Hirsch, *J. Am. Chem. Soc.* **1960**, *82*, 1013–1017.

[8] S. Hoops, S. Sahle, R. Gauges, C. Lee, J. Pahle, N. Simus, M. Singhal, L. Xu, P. Mendes, U. Kummer, *Bioinformatics* **2006**, *22*, 3067–3074.

[9] F. Zott, *GitHub repository*, "fabianzott/steadystate_analysis", **2023**, available at https://github.com/fabianzott/steadystate_analysis.

[10] H. Mayr, T. Bug, M. F. Gotta, N. Hering, B. Irrgang, B. Janker, B. Kempf, R. Loos, A. R. Ofial, G. Remennikov, H. Schimmel, *J. Am. Chem. Soc.* **2001**, *123*, 9500–9512.

[11] F. Brotzel, B. Kempf, T. Singer, H. Zipse, H. Mayr, *Chem. Eur. J.* **2007**, *13*, 336–345.

[12] N. De Rycke, G. Berionni, F. Couty, H. Mayr, R. Goumont, O. R. P. David, *Org. Lett.* **2011**, *13*, 530–533.

[13] L. Sooväli, T. Rodima, I. Kaljurand, A. Kütt, I. A. Koppel, I. Leito, *Org. Biomol. Chem.* **2006**, *4*, 2100–2105.

[14] L. G. Gagliardi, C. B. Castells, C. Ràfols, M. Rosés, E. Bosch, *Anal. Chem.* **2007**, *79*, 3180–3187.

[15] A. Folda, V. Scalcon, M. Ghazzali, M. H. Jaafar, R. A. Khan, A. Casini, A. Citta, A. Bindoli, M. P. Rigobello, K. Al-Farhan, A. Alsalme, J. Reedijk, *J. Inorg. Biochem.* **2015**, *153*, 346–354.

[16] P. Bertocco, C. Bolli, B. A. Correia Bicho, C. Jenne, B. Erken, R. S. Laitinen, H. A. Seeger, T. T. Takaluoma, *Inorg. Chem.* **2016**, *55*, 3599–3604.

[17] J. A. Denny, M. Y. Darensbourg, *CSD Commun.* **2016**.

[18] A. D. Becke, *J. Chem. Phys.* **1993**, *98*, 1372–1377.

[19] S. Grimme, *J. Chem. Phys.* **2006**, *124*, 034108.

[20] C. Lee, W. Yang, R. G. Parr, *Phys. Rev.* **1988**, *37*, 785–789.

[21] G. W. Spitznagel, T. Clark, J. Chandrasekhar, P. V. R. Schleyer, *J. Comput. Chem.* **1982**, *3*, 363–371.

[22] A. V. Marenich, C. J. Cramer, D. G. Truhlar, *J. Phys. Chem. B* **2009**, *113*, 6378–6396.

[23] M. Marin-Luna, P. Patschinski, H. Zipse, *Chem. Eur. J.* **2018**, *24*, 15052–15058.

[24] M. Marin-Luna, B. Pölloth, F. Zott, H. Zipse, *Chem. Sci.* **2018**, *9*, 6509–6515.

[25] B. Pölloth, M. P. Sibi, H. Zipse, *Angew. Chem. Int. Ed.* **2021**, *60*, 774–778.

[26] S. Mayr, M. Marin-Luna, H. Zipse, *J. Org. Chem.* **2021**, *86*, 3456–3489.

[27] S. Grimme, *Chem. - Eur. J.* **2012**, *18*, 9955–9964.

[28] G. Luchini, J. V. Alegre-Requena, I. Funes-Ardoiz, R. S. Paton, *F1000Research* **2020**, *9*, 1–14.

[29] Gaussian 16, Revision A.03, M. J. Frisch, G. W. Trucks, H. B. Schlegel, G. E. Scuseria, M. A. Robb, J. R. Cheeseman, G. Scalmani, V. Barone, G. A. Petersson, H. Nakatsuji, X. Li, M. Caricato, A. V. Marenich, J. Bloino, B. G. Janesko, R. Gomperts, B. Mennucci, H. P. Hratchian, J. V. Ortiz, A. F. Izmaylov, J. L. Sonnenberg, D. Williams-Young, F. Ding, F. Lipparini, F. Egidi, J. Goings, B. Peng, A. Petrone, T. Henderson, D. Ranasinghe, V. G. Zakrzewski, J. Gao, N. Rega, G. Zheng, W. Liang, M. Hada, M. Ehara, K. Toyota, R. Fukuda, J. Hasegawa, M. Ishida, T. Nakajima, Y. Honda, O. Kitao, H. Nakai, T. Vreven, K. Throssell, J. A. Jr. Montgomery, J. E. Peralta, F. Ogliaro, M. J. Bearpark, J. J. Heyd, E. N. Brothers, K. N. Kudin, V. N. Staroverov, T. A. Keith, R. Kobayashi, J. Normand, K. Raghavachari, A. P. Rendell, J. C. Burant, S. S. Iyengar, J. Tomasi, M. Cossi, J. M. Millam, M. Klene, C. Adamo, R. Cammi, J. W. Ochterski, R. L. Martin, K. Morokuma, O. Farkas, J. B. Foresman, D. J. Fox, **2016**, p Gaussian, Inc, Wallingford CT.

[30] Gaussian 16, Revision B.01, M. J. Frisch, G. W. Trucks, H. B. Schlegel, G. E. Scuseria, M. A. Robb, J. R. Cheeseman, G. Scalmani, V. Barone, G. A. Petersson, H. Nakatsuji, X. Li, M. Caricato, A. V. Marenich, J. Bloino, B. G. Janesko, R. Gomperts, B. Mennucci, H. P. Hratchian, J. V. Ortiz, A. F. Izmaylov, J. L. Sonnenberg, D. Williams-Young, F. Ding, F. Lipparini, F. Egidi, J. Goings, B. Peng, A. Petrone, T. Henderson, D. Ranasinghe, V. G. Zakrzewski, J. Gao, N. Rega, G. Zheng, W. Liang, M. Hada, M. Ehara, K. Toyota, R. Fukuda, J. Hasegawa, M. Ishida, T. Nakajima, Y. Honda, O. Kitao, H. Nakai, T. Vreven, K. Throssell, J. A. Jr. Montgomery, J. E. Peralta, F.

Ogliaro, M. J. Bearpark, J. J. Heyd, E. N. Brothers, K. N. Kudin, V. N. Staroverov, T. A. Keith, R. Kobayashi, J. Normand, K. Raghavachari, A. P. Rendell, J. C. Burant, S. S. Iyengar, J. Tomasi, M. Cossi, J. M. Millam, M. Klene, C. Adamo, R. Cammi, J. W. Ochterski, R. L. Martin, K. Morokuma, O. Farkas, J. B. Foresman, D. J. Fox, **2016**, p Gaussian, Inc, Wallingford CT.

[31] Maestro, rev 12.2.012. Schrödinger, New York, **2019**.

[32] M. Saunders, *J. Comput. Chem.* **2004**, *25*, 621–626.

[33] D. Šakić, M. Hanževački, D. M. Smith, V. Vrček, *Org. Biomol. Chem.* **2015**, *13*, 11740–11752.

[34] S. Grimme, A. Hansen, S. Ehlert, J. M. Mewes, *J. Chem. Phys.* **2021**, *154*, DOI 10.1063/5.0040021.

[35] F. Neese, *WIREs Comput. Mol. Sci.* **2022**, *12*, e1606.

[36] Gaussian 16, Revision C.01, M. J. Frisch, G. W. Trucks, H. B. Schlegel, G. E. Scuseria, M. A. Robb, J. R. Cheeseman, G. Scalmani, V. Barone, G. A. Petersson, H. Nakatsuji, X. Li, M. Caricato, A. V. Marenich, J. Bloino, B. G. Janesko, R. Gomperts, B. Mennucci, H. P. Hratchian, J. V. Ortiz, A. F. Izmaylov, J. L. Sonnenberg, D. Williams-Young, F. Ding, F. Lipparini, F. Egidi, J. Goings, B. Peng, A. Petrone, T. Henderson, D. Ranasinghe, V. G. Zakrzewski, J. Gao, N. Rega, G. Zheng, W. Liang, M. Hada, M. Ehara, K. Toyota, R. Fukuda, J. Hasegawa, M. Ishida, T. Nakajima, Y. Honda, O. Kitao, H. Nakai, T. Vreven, K. Throssell, J. A. Jr. Montgomery, J. E. Peralta, F. Ogliaro, M. J. Bearpark, J. J. Heyd, E. N. Brothers, K. N. Kudin, V. N. Staroverov, T. A. Keith, R. Kobayashi, J. Normand, K. Raghavachari, A. P. Rendell, J. C. Burant, S. S. Iyengar, J. Tomasi, M. Cossi, J. M. Millam, M. Klene, C. Adamo, R. Cammi, J. W. Ochterski, R. L. Martin, K. Morokuma, O. Farkas, J. B. Foresman, D. J. Fox, **2016**, p Gaussian, Inc, Wallingford CT.

[37] D. R. Lide, *CRC Handbook of Chemistry and Physics, 85th Edition*, CRC Press, Washington DC, **2004**.

[38] C. Reichardt, *Chem. Rev.* **1994**, *94*, 2319–2358.

[39] C. Reichardt, G. Schäfer, *Liebigs Ann.* **1995**, *1995*, 1579–1582.

[40] C. Reichardt, *Green Chem.* **2005**, *7*, 339–351.

[41] V. G. Machado, R. I. Stock, C. Reichardt, *Chem. Rev.* **2014**, *114*, 10429–10475.

[42] V. Gutmann, *Electrochimica Acta* **1976**, *21*, 661–670.

[43] C. Reichardt, T. Welton, *Solvents and Solvent Effects in Organic Chemistry: Fourth Edition*, Wiley-VCH, Weinheim, **2011**.

Chapter 4. Application of Ion Pair Catalysts in Acylation Reactions

4.1 Introduction

Lewis base catalyzed acylation reaction are among the most relevant organocatalytic transformations due to their extensive use in protection chemistry and in enantioselective applications[1] and they have been widely studied utilizing Lewis base catalysts such as DMAP (**1**) and its analogs.[2–5] The currently accepted mechanism of acylation of alcohols catalyzed by DMAP-based Lewis bases is shown in Scheme 4.1 and starts with the preequilibrium between DMAP and the acyl donor forming an acyl pyridinium cation **12**. This intermediate subsequently reacts with the alcohol in the rate-determining step via transition state **13** to form the ester product **14** and the deactivated (protonated) catalyst. The regeneration of the active catalyst usually requires an auxiliary base such as triethylamine (NEt_3).[2,6]

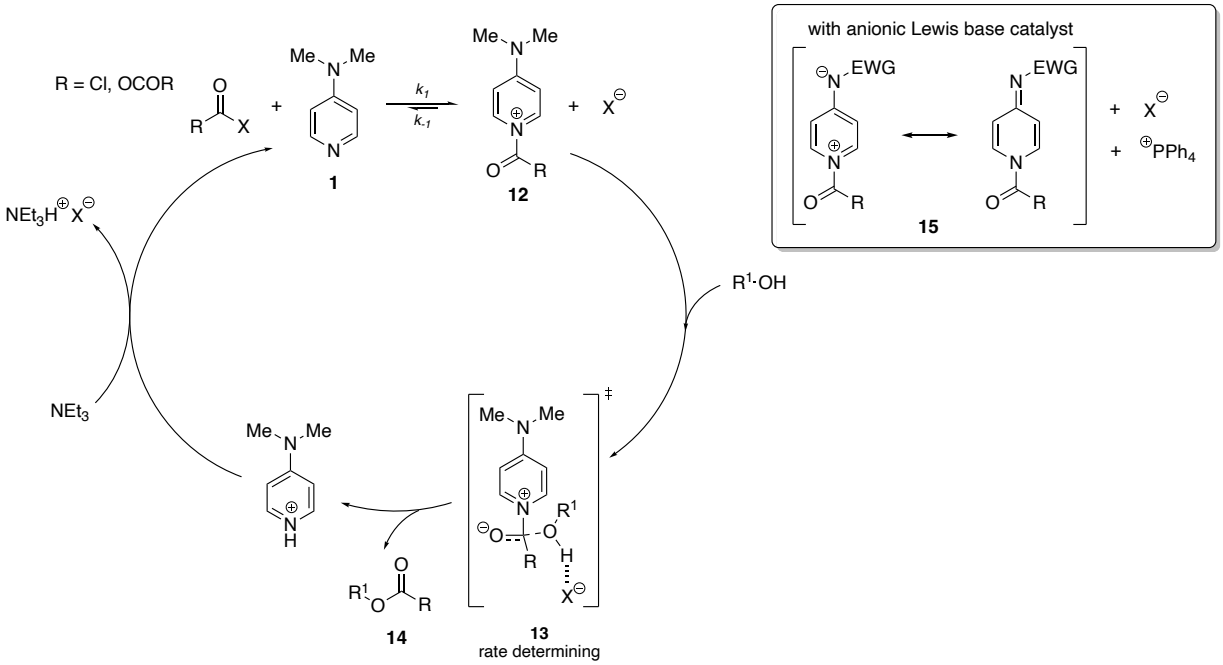

Scheme 4.1. Reaction mechanism of acylation reaction with DMAP (**1**).

When using an anionic catalyst, the catalytic pathway is expected to be almost identical with the main difference being the charge distribution of the substrate-catalyst adduct **15** as shown in Scheme 4.1. The catalytic efficiency of DMAP-type catalysts in acyl-transfer reactions is influence by two main factors. The first one being the formation and stabilization of the acylpyridinium **12**. The second is the type of acyl donor, since the counterion X^- of the acylpyridinium cation **12** formed in the preequilibrium critically affects the transition state **13**. It was found, that acylation reactions of tertiary alcohols employing anhydrides proceed faster than with acetyl chloride.[7] The importance of the counterion X^- on the reaction rate was noted by several researchers.[8–10] It was suggested that the acetyl anion promotes the deprotonation of the hydroxyl group in transition state **13** best in comparison to otherwise generated acids using other acyl donors. Therefore, anhydrides are most often used for acylation reactions.[6,11]

In the past, the acylation reaction of 1-ethinylcyclohexanol (**16**) with acetic anhydride (**17**) yielding ester **18**, as it is shown in Scheme 4.2, has been used as a benchmark reaction for newly developed Lewis base catalyst.[3,4] Therefore, it was also used to test the catalytic potential of pyridinamide salts and to investigate their behavior in reactions that produce an acidic byproduct in the catalytic cycle.

4.2 Results and Discussion

4.2.1 Steglich Acylation

The catalytic efficiency of pyridinamide ion pairs was investigated using the in Scheme 4.2 depicted *Steglich*[12] acylation reaction as a secondary benchmark reaction following the synthesis of urethane **11** as the primary benchmark reaction (see Chapter 3). In this reaction, 1-ethinylcyclohexanol (**16**, 0.2 M) was reacted with acetic anhydride (**17**, 0.4 M) and NEt_3 (0.6 M) as an auxiliary base in deuterated Chloroform ($CDCl_3$). The progress was monitored by ^{1}H-NMR using the protons marked in bold in Scheme 4.2. The objective was to assess the performance of pyridinamide ion pairs in reactions that generate an acid as a side product, as it commonly observed in acylation reactions involving anhydrides.

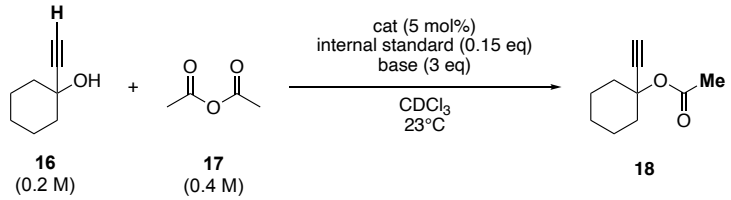

Scheme 4.2. Acylation reaction of 1-ethinylcyclohexanol (**16**) with acetic anhydride (**17**) in $CDCl_3$.

The catalytic performance of organocatalysts **1** and **2** was compared with that of pyridinamide ion pair catalysts **3a-d** and **4-6a**. The corresponding effective reaction rates k_{eff} (M^{-1} s^{-1}) are listed in Table 4.1, showing the reaction rates for each catalyst alongside their respective half-life times $t_{1/2}$ (sec). The results demonstrate a range of catalytic activity across different classes of catalysts.

Table 4.1. Effective reaction rates k_{eff} (M^{-1} s^{-1}) and half-life times $t_{1/2}$ (sec) for the acylation benchmark reaction using DMAP (**1**), TCAP (**2**) and pyridinamide salts **3a-d** and **4**-**6a** in $CDCl_3$.

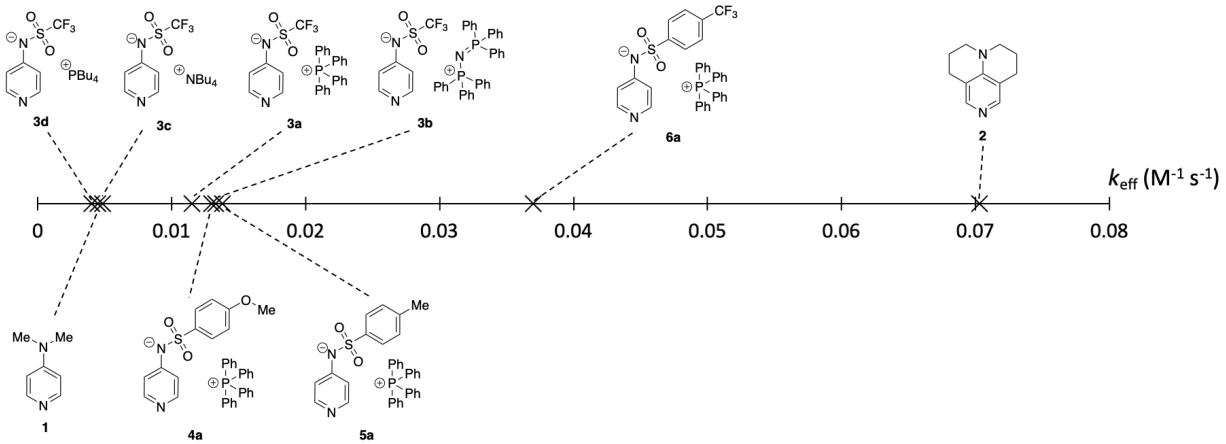

catalyst	k_{eff} (M^{-1} s^{-1})[a]	$t_{1/2}$ (s)[a,b]	$t_{1/2}$ (min)[a,b]
2	7.03 x 10^{-2}	1792	29.9
6a	3.70 x 10^{-2}	3011	50.2
5a	1.38 x 10^{-2}	6968	116
3b	1.33 x 10^{-2}	6698	112
4a	1.30 x 10^{-2}	7416	124
3a	1.15 x 10^{-2}	7494	125
3c	4.85 x 10^{-3}	17200	287
1	4.50 x 10^{-3}	17750	296
3d	4.05 x 10^{-3}	20750	346

[a] average values of two measurement. [b] extracted from simulation data generated with COPASI.

Based on the turnover curves of the Steglich acylation reaction, the ion pair catalysts were classified into three distinct groups. Group A consisted of ion pairs **3c** and **3d**, which contain unbranched alkyl cations. Their catalytic activity was comparable to DMAP (**1**) in this acylation. Group B included ion pairs **3a**, **3b**,

4a, and **5a**, all of which contain aromatic cations. The ion pairs in Group B demonstrated approximately three times higher catalytic activity than those in Group A. Interestingly, despite the higher Lewis and Brønsted basicity and nucleophilicity of ion pairs **4a** and **5a**, their effective reaction rates were comparable to those of ion pair **3a** and **3b**. Group C, represented solely by ion pair **6a**, displayed the highest catalytic efficiency among the ion pair catalysts, although the neutral organocatalyst TCAP (**2**) remained the most efficient catalyst in this series, outperforming ion pair **6a** by a factor of two.

To further explore the relationship between catalytic efficiency and molecular properties, the logarithmic effective reaction rates log(k_{eff}) of the pyridinamide salts were correlated in Figure 4.1 with the logarithmic bimolecular rate constant log($k_{2,8a}$), methyl cation affinities (ΔMCA), and pK_{a2} values, all introduced in Chapter 3. This correlation analysis provided insights into how nucleophilicity and basicity contribute to the overall catalytic performance of pyridinamide ion pairs.

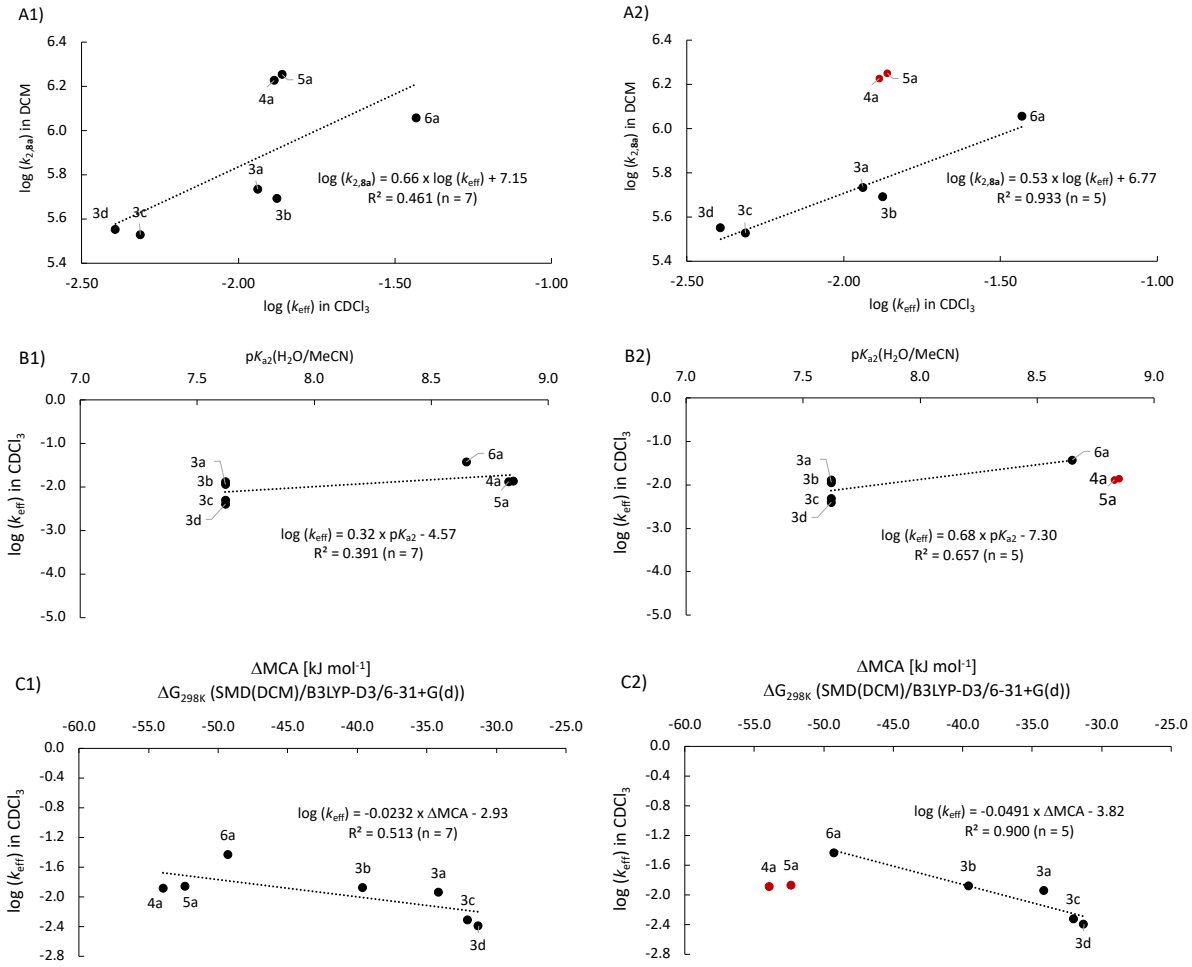

Figure 4.1. Correlation of A) log (k_{eff}) vs. bimolecular rate constant log $k_{2,8a}$ for pyridinamide ion pair catalysts. B) log (k_{eff}) vs. pK_{a2} values in H_2O/MeCN = 1:1. C) log (k_{eff}) vs. Lewis basicity parameter ΔMCA (calculation are listed in Chapter 3.1.10.2).

The effective reaction rates k_{eff} of pyridinamide salts in the urethane benchmark reaction showed a strong linear correlation with each reactivity parameter (R^2 > 0.9, see Chapter 3), indicating a clear relationship between nucleophilicity, Brønsted basicity, Lewis basicity, and catalytic efficiency. However, in the Steglich acylation reaction, no such correlation was observed when all seven pyridinamide ion pairs were analyzed (see Figure 4.1_A1/B1/C1). When salts **4a** and **5a** were excluded from the analysis, the effective reaction rates k_{eff} of the remaining five pyridinamide catalysts correlated linearly with the logarithmic bimolecular rate constants k_2 for their reaction with benzhydryl cation **8a** (see Figure 4.1_A2).

Similarly, a linear correlation was observed with their relative Lewis basicity parameter ∆MCA (see Figure 4.1_C2).

Thus, the high nucleophilicity and basicity of salts **4a** and **5a** do not translate into the expected high catalytic reactivity. Comparable observations have been made for 3,4,5-triaminopyridines of type **D** (see Chapter 1, Chart 1.1) which also displayed a lower catalytic activity than their high Lewis basicity and high nucleophilicity values would have suggested.[4] One possible explanation for the comparably low catalytic activity of salts **4a** and **5a** could be an increased stabilization of the acylpyridinium **12** formed in the first reaction step. This might raise the energy barrier of the subsequent alcohol acylation *via* intermediate **13** (see Scheme 4.1).[13,14] To test this hypothesis, quantum chemical calculations comparing the Gibbs free reaction energies of anhydride **17** reacting with catalyst **1**, **3a**, and **5a** are recommended. Additionally, spectroscopic analysis of the mixtures of anhydride **17** with these catalysts could be conducted to detect the acylated intermediate **12**. This approach has been proven effective in previous studies.[14]

4.2.2 Influence of the Auxiliary Base

The reduced catalytic efficiency of salts **4a** and **5a** could also be attributed to partial deactivation of the catalyst via protonation. This deactivation might occur at the end of the catalytic cycle, where NEt_3 might be unable to fully regenerate the pyridinamide anion, thus leaving the catalyst inactive. Another possible source of protonation could be the acetic acid formed as a byproduct during the consumption of acetic anhydride, which would further neutralize the basic catalyst. To investigate this hypothesis, the benchmark reaction was repeated using ion pair catalyst **5a** in combination with various bases. Ion pair **6a**, which demonstrated the highest catalytic activity in this benchmark reaction, was used as the reference salt. The corresponding effective reaction rates k_{eff} (M^{-1} s^{-1}) are presented in Table 4.2.

Table 4.2. Effective reaction rate k_{eff} (M^{-1} s^{-1}) for salt **5a** and **6a** with various auxiliary bases in $CDCl_3$.

	k_{eff} (M^{-1} s^{-1})			
cat	**NEt_3**	**NPr_3**	**DIPEA**	**HMPN**
5a	1.38×10^{-2}	1.30×10^{-2}	1.32×10^{-2}[a]	1.27×10^{-3}[a]
6a	3.70×10^{-2}	3.37×10^{-2}	–	–

[a] k_{eff} obtained in a single measurement.

Replacing NEt_3 with tri-propylamine (NPr_3) did not result in an increase in catalytic activity either for salt **5a** or **6a**. Instead, a slight decrease in reaction rate for salt **6a** was noted. Similarly, the use of the stronger, sterically hindered base diisopropylethylamine (DIPEA, Hünig base) or 1,8-bis(hexamethyltriaminophosphazenyl)naphthalene (HMPN) failed to enhance the benchmark reaction catalyzed by salt **5a**. It is notable that the significant steric hindrance presented by the proton sponge resulted in a 10-fold reduction in the effective reaction rate k_{eff}(**5a**) (see Table 4.2). These findings are in agreement with previous studies where more sterically hindered auxiliary bases would slow down the reaction.[15] Based on these results, it can be concluded that the reduced catalytic activity of salt **4a** and **5a** was unlikely caused by deactivation through protonation.

4.2.3 Solvent Effects

Before starting the investigation of the Steglich acylation with various catalysts, the benchmark reaction was performed in three selected organic solvents. Previous research has shown that Lewis-base catalyzed acylation reactions perform optimally in apolar organic solvents, while reaction rates tend to decrease in polar solvents.[4,16,17] In both conductometric measurements and nucleophilicity measurements, the choice of solvent was found to significantly affect the behavior of the ion pairs (see Chapter 2 and 3). Thus, catalyst **5a**, one of the most active pyridinamide catalysts in previous benchmark reactions, was

selected to further evaluate solvent effects on ion pair catalysts in this benchmark reaction. For comparison, these kinetic studies were conducted using DMAP (**1**) as a neutral organocatalyst.

The influence of solvents on the benchmark reaction was evident for both investigated catalysts. For DMAP, a stepwise increase in the reaction rates was noted with increasing solvent polarity (MeCN-d_3 < DCM-d_2 < $CDCl_3$). Simultaneously, the effect was more pronounced for **5a**. Upon replacing MeCN-d_3 with DCM-d_2, the rate constant increased by a factor of 1.7, whereas the difference between the rate constants in $CDCl_3$ and DCM-d_2 was approximately half of this value.

Table 4.3. List of effective reaction rate k_{eff} (M^{-1} s^{-1}) and half-life times (min) for DMAP (**1**) and salt **5a** in the Steglich benchmark acylation in $CDCl_3$, DCM-d_2, and MeCN-d_3.

Catalyst	Solvent	k_{eff} (M^{-1} s^{-1})	$t_{1/2}$ (sec)	$t_{1/2}$ (min)
1	$CDCl_3$	4.50×10^{-3}	17750	296
	DCM-d_2	2.58×10^{-3}[a]	31800[a]	530[a]
	MeCN-d_3	1.53×10^{-3}[a]	54400[a]	907[a]
5a	$CDCl_3$	1.38×10^{-2}	6968	116
	DCM-d_2	7.81×10^{-3}[a]	12000[a]	200[a]
	MeCN-d_3	7.39×10^{-4}	11550	1925

[a] k_{eff} obtained in a single measurement.

The effective reaction rates k_{eff} were analyzed in relation to several solvent descriptors listed in Table 4.4. These included the relative permittivity ε_r, which measures the solvent's ability to reduce electrostatic interactions between charged species, and the $E_T(30)$ values, which reflect the solvent polarity based on the solvatochromic shift of the Reichardt's dye. Additionally, the Gutmann acceptor number (AN), representing the solvent's Lewis acidity, and the Gutmann donor number (DN), reflecting the solvent's Lewis basicity, were considered.

Table 4.4. List of solvent descriptors: relative permittivity ε_r values[18], $E_T(30)$[19–22], and Gutmann acceptor (AN) and Gutmann donor (DN) numbers[23,24] for selected solvents $CDCl_3$, DCM-d_2 and MeCN-d_2.

	ε_r	$E_T(30)$ (kcal mol^{-1})	AN	DN
$CDCl_3$	4.81	39.1	23.1	4.0
DCM-d_2	9.08	40.7	20.4	1.0
MeCN-d_3	36.6	45.6	18.9	14.1

Correlating the logarithmic effective reaction rate log k_{eff} with the respective solvent descriptors using the Eyring equation gave the following results: all correlation were solid to strong, with the exception of the weak correlation of log k_{eff}(**1**) with the Gutmann donor numbers (DN) which had an R^2 of 0.5 (see Table 4.5). For pyridinamide ion pair **5a**, the strongest correlation were observed between log k_{eff} with the relative permittivity ε_r as well as the $E_T(30)$ values (R^2 < 0.9).

These findings suggested that the most decisive solvent properties are its ability to permit electrostatic interactions between charged species, and its polarity. Subsequent kinetic measurements of the remaining ion pair catalysts were carried out in $CDCl_3$, where the highest catalytic activity for both catalysts was observed.

Table 4.5. Correlations between the logarithmic effective reaction rate log(k_{eff}) (M^{-1} s^{-1}) with the respective solvent descriptors relative permittivity ε_r[18], E_T(30) (kcal mol^{-1})[19–22], and Gutmann acceptor (AN) and Gutmann donor (DN) numbers[23,24] for catalysts **1** and **5a**.

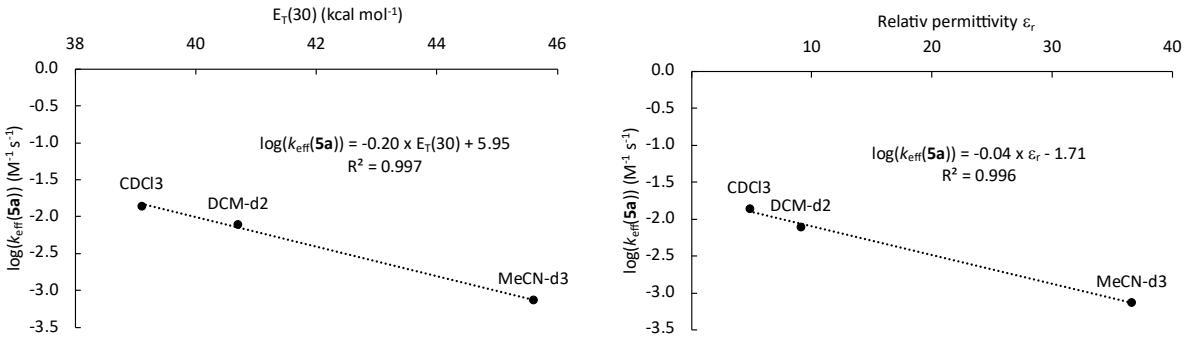

	5a		1	
	Equation	**R^2**	**Equation**	**R^2**
E_T(30) (kcal mol^{-1})	log k_{eff}(**5a**) = -0.20 x E_T(30) + 5.95	0.997	log k_{eff}(**1**) = -0.07 x E_T(30) + 0.18	0.911
ε_r	log k_{eff}(**5a**) = -0.04 x ε_r - 1.71	0.996	log k_{eff}(**1**) = -0.01 x ε_r – 2.38	0.846
AN	log k_{eff}(**5a**) = 0.28 x AN - 8.14	0.769	log k_{eff}(**1**) = 0.11 x AN – 4.85	0.979
DN	log k_{eff}(**5a**) = -0.09 x DN -1.79	0.844	log k_{eff}(**1**) = -0.03 x DN -2.43	0.523

4.2.4 Acylation with Benzoic Anhydride

The response of pyridinamide ion pair catalysts to changes in the steric demand of the acylation reagent was tested by reacting tertiary alcohol **16** with benzoic anhydride **19** to obtain ester **20**, as shown in Scheme 4.3. These studies were performed under the same reaction conditions as the Steglich acylation benchmark reaction, utilizing the four selected ion pair catalysts **3a**, **3d**, **4a**, and **6a**, along with TCAP (**2**) as neutral reference organocatalyst. Due to the prolonged reaction time (approx. 4 weeks) required for ion pair catalyst **3a** and **3d**, kinetic measurements were only conducted once. The reaction was monitored over a 30-day period without achieving full conversion for **3a** and **3d**. In contrast, the reaction times of the other selected catalysts, **2**, **4a**, and **6a**, were significantly shorter, taking approx. 14 days or less.

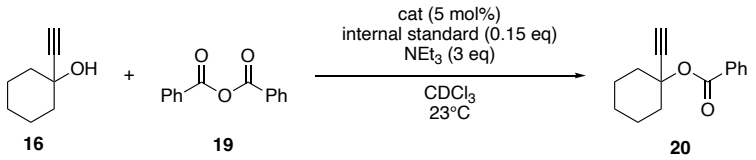

Scheme 4.3. Acylation reaction of 1-ethinylcyclohexanol (**16**) with benzoic anhydride (**19**).

The observed effective reaction rates k_{eff} for acylation using benzoic anhydride **19** were generally slower compared to acylation using acetic anhydride **17** across the examined catalysts (see Table 4.6). The ratio of the k_{eff} values for both benchmark reactions indicated how sensitive each catalyst responded to the increase in steric demand. The ratio showed a similar trend in the lower catalytic activity for catalysts **2**, **3a**, **3d**, and **6a**. In contrast, catalyst **4a** exhibited the least sensitivity to the increased steric demand of the acylating agent, resulting in a smaller disparity in catalytic performance between catalysts **6a** and **4a**. Specifically, the difference in activity decreased from an approx. threefold difference in the acylation with acetic anhydride **17** to a factor of 1.3 in the acylation with benzoic anhydride **19**.

Table 4.6. Comparison of effective reaction rates k_{eff} (M^{-1} s^{-1}) for acylation with acetic anhydride **17** ($k_{eff,AA}$) and benzoic anhydride **19** ($k_{eff,BA}$) and the ratio of those two parameters.

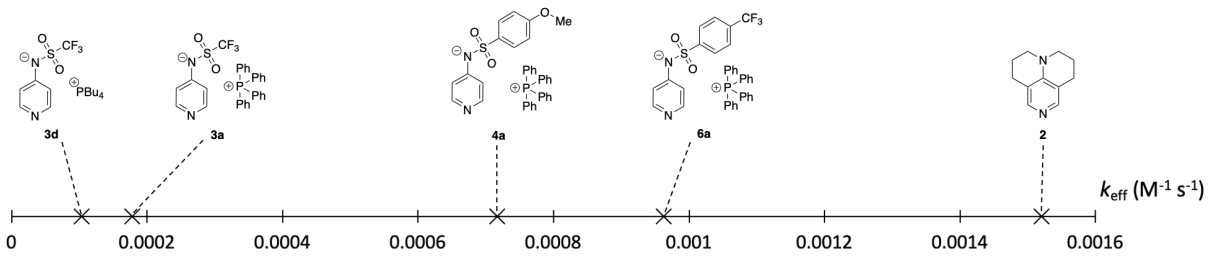

cat	$k_{eff,AA}$ (M^{-1} s^{-1})	$k_{eff,BA}$ (M^{-1} s^{-1})	Ratio of k_{eff} values
2	7.03 x 10^{-2}	1.52 x 10^{-3}	46
3a	1.15 x 10^{-2}	1.78 x 10^{-4}[a]	65
3d	4.05 x 10^{-3}	1.03 x 10^{-4}[a]	39
4a	1.30 x 10^{-2}	7.17 x 10^{-4}	18
6a	3.70 x 10^{-2}	9.63 x 10^{-4}	38

[a] $k_{eff,BA}$ obtained in a single measurement.

A comparable effect was noted between catalysts **6a** and **2**, though the magnitude of change was significantly smaller and catalyst **2** remained the most active in this series. Quantum chemical calculations are recommended to assess the stability of the respective acylpyridinium intermediate **12** generated in the acylation reaction with benzoic anhydride. Future studies in this direction might reveal the reason for the lower sensitivity of catalyst **4a** towards the increased steric demand of the acylating reagent. Meanwhile, these observations suggest that, with careful selection of reagents and optimization of reaction conditions, ion pair catalysts might have the potential to match the catalytic efficiency of **2** in acylation reactions.

4.2.5 Comparison with Neutral Lewis Base Catalysts

The Steglich acylation reaction (see Scheme 4.2) has been extensively studied by the Zipse group, which has investigated a library of pyridine-based Lewis base catalysts. Over the years, different concepts were explored to enhance the catalytic activity. The most promising Lewis base catalysts, with a catalytic activity comparable to or better than TCAP (**2**), are listed in Table 4.7.

Table 4.7. Half-life time $t_{1/2}$ (min) of Lewis base catalysts measured for acylation reaction of alcohol **16** with anhydride **17**.

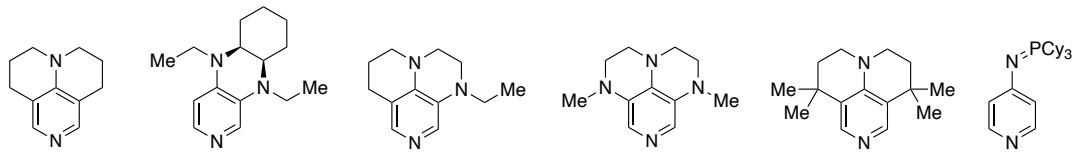

Catalyst	$t_{1/2}$ (min) for 10 mol% of cat.	$t_{1/2}$ (min) for 5.0 mol% of cat.
2	14.7 ± 0.1[3]	29.9[a]
6a	–	50.2[a]
21	18.0 ± 0.1[3]	36.0[b]
22	13.8 ± 0.4[4]	27.6[b]
23	38.0 ± 1.5[4]	76.0[b]
24	12.0[25]	24.0[b]
25	5.7 ± 0.1[5]	11.4[b]

[a] this work. [b] estimated assuming a linear correlation between $t_{1/2}$ and catalyst load.

In previous studies, the benchmark reaction of alcohol **16** with anhydride **17** was conducted using 10 mol% of catalyst. To compare the half-life times $t_{1/2}$ (min) of the neutral Lewis base catalysts with the most catalytically active pyridinamide salt **6a**, the half-life time $t_{1/2}$ of the benchmark acylation with 5.0

The evaluation of the catalytic activity of pyridinamide ion pairs using the Steglich acylation reaction revealed three distinguishable groups, based on their catalytic performance. Pyridinamide salts **3c** and **3d** displayed a catalytic efficiency comparable to DMAP (**1**), whereas salts **3a**, **3b**, **4a**, and **5a** showed a threefold increase in activity. The most efficient pyridinamide ion pair catalyst was found to be **6a**, although TCAP (**2**) remained the best performing organocatalyst in this study, with a reaction rate twice as fast as that of salt **6a**.

Despite their high nucleophilicity and basicity, pyridinamide salts **4a** and **5a** displayed only moderate catalytic activity. This lack in catalytic activity led to investigations of potential deactivation *via* protonation, which was ruled out by testing various auxiliary bases in the benchmark reaction. However, quantum chemical calculations comparing the Gibbs free reaction energies of anhydride **17** reacting with catalyst **1**, **3a**, and **5a** are recommended as an increased stabilization of the acylated pyridinium intermediate **12** might negatively affect the energy barrier of the following reaction steps. The choice of solvent as well as the steric demand of the anhydride had a considerable impact on the reaction rates, emphasizing the importance of these variables in acylation reactions.

While pyridinamide salts were effective in acylation reaction, several other Lewis base catalysts proved to be more efficient. Nevertheless, the majority of these organocatalysts are either expensive or require a complex synthetic procedure. Pyridinamide ion pairs, which can be synthesized in a straightforward, rapid, and cost-effective manner, offer a viable alternative. To fully exploit their catalytic potential, it is recommended to employ pyridinamide salts primarily in addition reactions or rearrangement reactions, where acidic byproducts would not interfere with their catalytic effectiveness.

In summary, this study provided valuable insights into the performance of pyridinamide ion pairs in acylation reactions. The possibility to synthesize these catalysts easily and at low cost, combined with their moderate efficiency, presents a promising avenue for further exploration, particularly in reactions where acidic byproducts are not an issue.

mol% catalyst was estimated for catalysts **21**, **22**, **23**, **24**, and **25**, assuming a linear correlation between $t_{1/2}$ and the catalyst load. This linear correlation has been previously established for several catalysts in different benchmark reaction, including pyridinamide ion pair catalysts[4,26]. Comparing the measured and estimated half-life times $t_{1/2}$ of the Lewis bases catalysts listed in Table 4.7 showed that catalyst **25** is the most catalytically active catalyst, followed by TMAJ (**24**). 3,4-Diaminopyridine derivatives **21** and **22** exhibit catalytic activities directly comparable to TCAP (**2**), with **22** reacting slightly faster. As already mentioned, pyridinamide salt **6a** reacted slower than TCAP by a factor of two. However, the lowest catalytic activity was exhibited by 3,4,5-triaminopyridine derivative **24**.

4.3 Conclusion

The evaluation of the catalytic activity of pyridinamide ion pairs using the Steglich acylation reaction revealed three distinguishable groups, based on their catalytic performance. Pyridinamide salts **3c** and **3d** displayed a catalytic efficiency comparable to DMAP (**1**), whereas salts **3a**, **3b**, **4a**, and **5a** showed a threefold increase in activity. The most efficient pyridinamide ion pair catalyst was found to be **6a**, although TCAP (**2**) remained the best performing organocatalyst in this study, with a reaction rate twice as fast as that of salt **6a**.

Despite their high nucleophilicity and basicity, pyridinamide salts **4a** and **5a** displayed only moderate catalytic activity. This lack of catalytic activity led to investigations of potential deactivation *via* protonation, which was ruled out by testing various auxiliary bases in the benchmark reaction. However, quantum chemical calculations comparing the Gibbs free reaction energies of anhydride **17** reacting with

catalysts **1**, **3a**, and **5a** are recommended, as an increased stabilization of the acylated pyridinium intermediate **12** might raise the energy barrier of the following reaction steps. The choice of solvent, as well as the steric demand of the anhydride, had a considerable impact on the reaction rates, emphasizing the importance of these variables in acylation reactions.

While pyridinamide salts are effective in acylation reactions, several other Lewis base catalysts proved to be more efficient. Nevertheless, most of these organocatalysts are either expensive or require a complex synthetic procedure. Pyridinamide ion pairs, which can be synthesized in a straightforward, rapid, and cost-effective manner, offer a viable alternative. To fully exploit their catalytic potential, it is recommended to employ pyridinamide salts primarily in addition reactions or rearrangement reactions, where acidic byproducts would not interfere with their catalytic effectiveness.

In summary, this study provides valuable insights into the performance of pyridinamide ion pairs in acylation reactions. The possibility to synthesize these catalysts easily and at low cost, combined with their moderate efficiency, offers promising opportunities for further applications, particularly in reactions where acidic byproducts are not an issue.

4.4 Experimental Part

4.4.1 General Information

All reagents were purchased from Sigma Aldrich, TCI, or Acros and used without further purification unless otherwise noted. Solvents were obtained from Acros Organics, Sigma Aldrich, or Merck and purified by simple distillation in a rotary evaporator, unless otherwise specified.

All air- and moisture-sensitive reactions were performed under a nitrogen atmosphere and the glassware and magnetic stirrers were dried in a dry oven at 110 °C overnight. $CDCl_3$ and NEt_3 were dried over CaH_2 and distilled prior to use. MeCN-d_3, CD_2Cl_2 and $CDCl_3$ were dried over 4 Å molecular sieves.

Nuclear magnetic resonance (NMR) spectra were recorded on Bruker 400 MHz or INOVA 400 and 600 MHz machines. The following abbreviations were used in the analysis of NMR spectra: s = singlet, d = doublet, t = triplet, q = quartet, m = multiplet, br s = broad singlet. NMR signals were assigned based on 2D spectra (COSY, HSQC, HMBC) analysis. Chemical shifts were given in ppm. The internal reference was set to the residual solvent signals (CD_2Cl_2, $CDCl_3$, DMSO-d_6, MeCN-d_3). ^{19}F NMR spectra were referenced using the solvent signal.[27] The spectra were processed using MestreNova (version 14.1.1).

4.4.2 Experimental Design

As a benchmark reaction the acylation of 1-ethynylcyclohexanol (**16**, 1.0 eq) with acetic anhydride (**17**, 2.0 eq) was chosen. 1,3,5-Trimethoxybenzene was used as internal standard and NEt_3 as the auxiliary base. The reaction progress was traced via ^1H NMR.

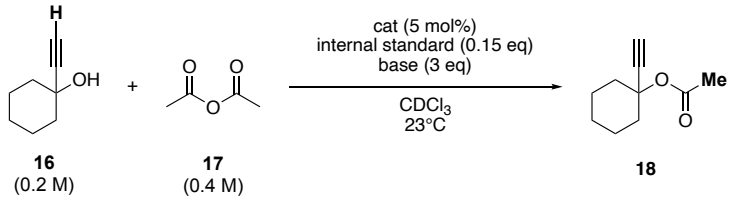

Scheme 4.4. Acylation of 1-ethynylcyclohexanol (**16**) with acetic anhydride **(17**) and NEt_3 in deuterated chloroform.

Three stock solutions were prepared in oven-dried 1.0 mL volumetric flasks under N_2 atmosphere. Stock solution A contained 0.6 M 1-ethynylcyclohexanol **16** with 1.8 M NEt_3. Stock solution B contained 1.2 M acetic anhydride **17** with 0.09 M standard, and stock solution C contained 0.03 M catalyst. Hamilton syringes were used to transfer 0.2 mL of each stock solution in a N_2 flushed NMR tube. ^1H NMR measurements were then taken of the sample in defined time intervals and the bold-marked protons were traced (see Scheme 4.4 and Figure 4.2).

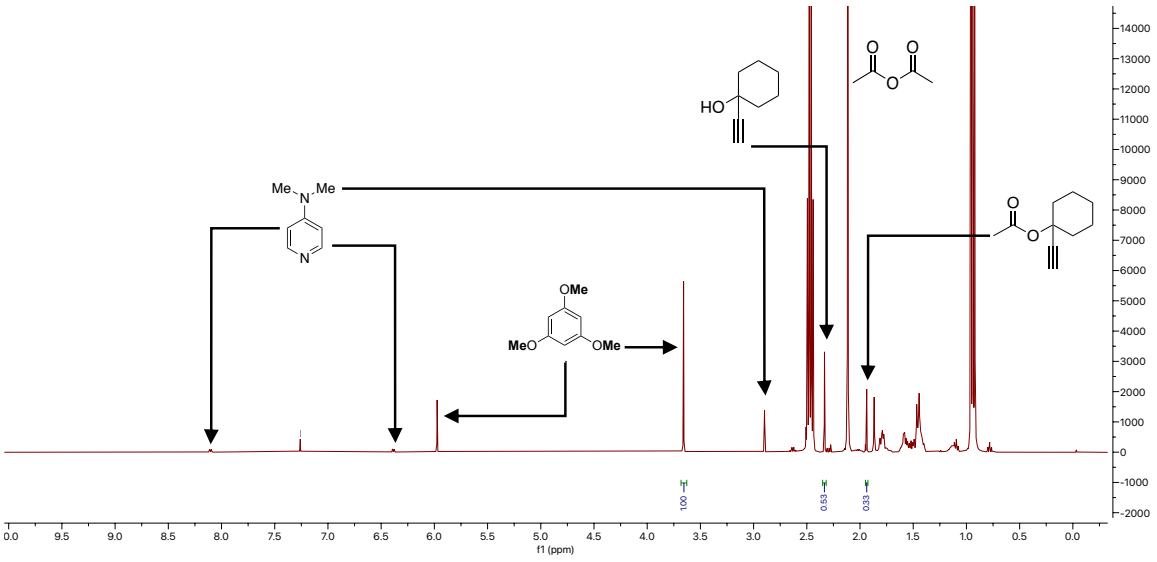

Figure 4.2. NMR spectra of Steglich benchmark reaction with assigned ^1H shift of all compounds.

Eq. 4.1 was used to calculate the conversion of the acylation product at time *t,* with *I* being the absolute NMR integral of the ester or the internal standard (Std), *N* being number of protons of the selected integral, *M* being the molar mass of the respective compound, *m* being the weighted mass of the internal standard and the ester at 100 % conversion, and c_0 representing the starting concentration of the alcohol.

$$c_t[\text{ester}] = \frac{I_{\text{ester}}}{I_{\text{Std}}} \times \frac{N_{\text{Std}}}{N_{\text{ester}}} \times \frac{M_{\text{ester}}}{M_{\text{Std}}} \times \frac{m_{\text{Std}}}{m_{\text{ester,100\%}}} \times c_0[\text{alcohol}] \quad (4.1)$$

In previous studies, the kinetic half-life time $t_{1/2}$ of the reaction was calculated with eq. 4.2.[3,4]

$$t_{1/2} = \frac{\ln 1.5}{k_{\text{eff}}[\text{alcohol}]_0} \quad (4.2)$$

In this work the half-life times are extracted in seconds (s) from the kinetic simulations performed in COPASI and converted into minutes (min) for better comparability.

4.4.3 Simulation of Kinetic Experiments – Steglich Acylation with Acetic Anhydride

The secondary rate constants k_{eff} of the acylation reaction were simulated using the program COPASi[28]. Figure 4.3 shows the simplified mechanism used for the simulation and the equations used for numerical simulation with COPASI.

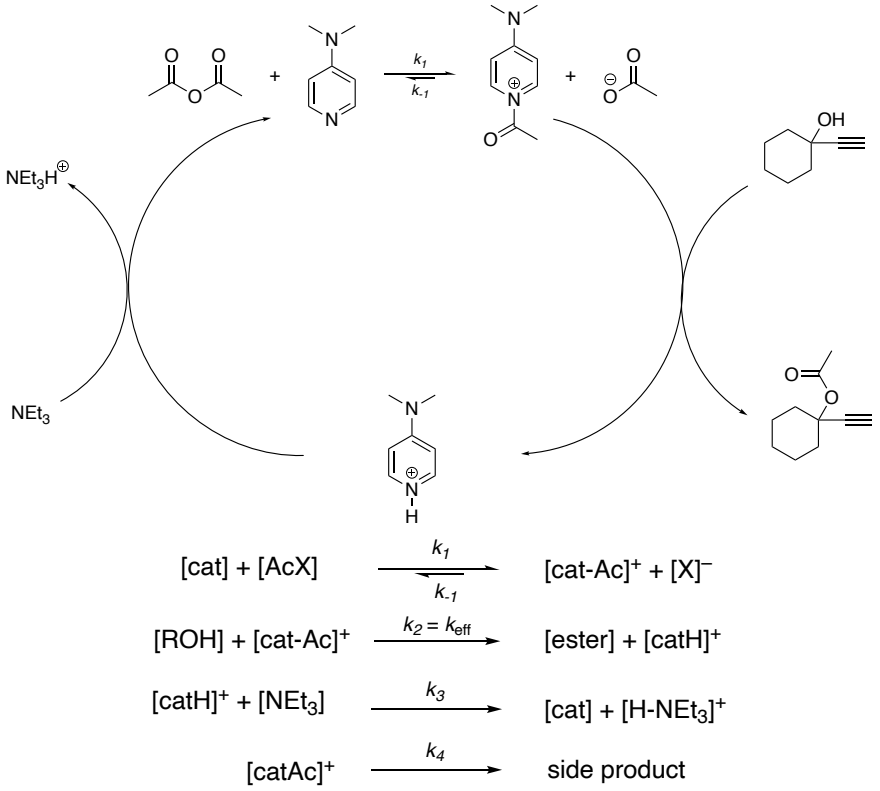

Figure 4.3. Proposed mechanism of acylation reaction and the employed numerical simulation equation in COPASI to obtain effective rate constant k_{eff}.

Therefore, the time *t* (sec) and c_t[ester] were imported into COPASi as a .txt file. With the function "Parameter Estimation" (default settings) the rate constant k_{eff} (= k_2) were simulated. The catalyst loading was set to be on the product side with k_1 = 0.1 M^{-1} s^{-1} and k_{-1} = 0.001 M^{-1} s^{-1}. The catalyst restoration was set to be k_3 = 0.1 M^{-1} s^{-1}. For reaction that did not run to completion the fourth equation "side" reaction" was added and the rate constant k_4 was simultaneously simulated with k_{eff}. The results of the simulations are summarized in Table 4.8.

Table 4.8. Effective reaction rates k_{eff} (M^{-1} s^{-1}) and half-life times $t_{1/2}$ (min)for the acylation of 1-ethynylcyclohexanol **16** with acetic anhydride **17** in $CDCl_3$.

Catalyst	k_{eff} (M^{-1} s^{-1})	Average k_{eff} (M^{-1} s^{-1})	$t_{1/2}$ (s)	$t_{1/2}$ (min)	Average $t_{1/2}$ (min)
DMAP	4.30 x 10^{-3}	4.50 x 10^{-3} ± 2.00 x 10^{-4}	18300	305	296 ± 9.17

	4.70×10^{-3}		17200	287	
TCAP	7.80×10^{-2}	$7.03 \times 10^{-2} \pm 7.70 \times 10^{-3}$	1813	30.2	29.9 ± 0.35
	6.26×10^{-2}		1771	29.5	
3a	1.20×10^{-2}	$1.15 \times 10^{-2} \pm 5.00 \times 10^{-4}$	7176	120	125 ± 5.29
	1.10×10^{-2}		7811	130	
3b	1.30×10^{-2}	$1.33 \times 10^{-2} \pm 3.00 \times 10^{-4}$	6712	112	112 ± 0.23
	1.36×10^{-2}		6684	111	
3c	5.00×10^{-3}	$4.85 \times 10^{-3} \pm 1.50 \times 10^{-4}$	16900	282	287 ± 5.00
	4.70×10^{-3}		17500	292	
3d	3.90×10^{-3}	$4.05 \times 10^{-3} \pm 1.50 \times 10^{-4}$	21200	353	346 ± 7.50
	4.20×10^{-3}		20300	338	
4a	1.10×10^{-2}	$1.30 \times 10^{-2} \pm 2.00 \times 10^{-3}$	8402	140	124 ± 16.4
	1.50×10^{-2}		6429	107	
5a	1.62×10^{-2}	$1.38 \times 10^{-2} \pm 2.37 \times 10^{-3}$	5975	100	116 ± 16.6
	1.15×10^{-2}		7961	133	
6a	3.10×10^{-2}	$3.70 \times 10^{-2} \pm 6.00 \times 10^{-3}$	3384	56.4	50.2 ± 6.22
	4.30×10^{-2}		2638	44.0	

The raw data sets of the kinetic measurements are summarized in Table 4.9 – Table 4.17.

Table 4.9. Raw data of absolute kinetic of acylation reaction with DMAP (**1**) in $CDCl_3$.

Time (min)	Integ. limits (ppm)		Integ.	Absol.	Integ. limits (ppm)		Integ.	Absol.	Integ. limits (ppm)		Integ.	Absol.	$Yield_{ester}$ (%)
VB116a	**Standard**				**Educt**				**Product**				
7	3.61	3.70	1.0	64899.9	2.32	2.37	0.63	40875.2	1.93	1.95	0.05	3448.6	2.15
23	3.63	3.68	1.0	60150.9	2.32	2.35	0.60	35975.9	1.93	1.94	0.15	8949.3	6.03
41	3.62	3.69	1.0	64325.3	2.32	2.35	0.56	36063.9	1.93	1.95	0.26	16579.9	10.4
53	3.63	3.68	1.0	64441.3	2.32	2.35	0.53	34220.2	1.93	1.95	0.33	21280.5	13.4
72	3.64	3.67	1.0	62407.3	2.31	2.34	0.53	33075.3	1.93	1.94	0.43	26754.1	17.4
90	3.64	3.67	1.0	63105.2	2.31	2.34	0.51	32169.1	1.92	1.94	0.50	31729.2	20.4
95	3.63	3.67	1.0	63335.6	2.32	2.34	0.49	30954.2	1.91	1.94	0.56	35323.8	22.6
118	3.67	3.71	1.0	63309.9	2.35	2.38	0.48	30238.3	1.96	1.98	0.63	39795.7	25.5
133	3.64	3.67	1.0	63399.5	2.31	2.33	0.45	28531	1.92	1.94	0.69	44034.6	28.1
150	3.63	3.67	1.0	63471.0	2.31	2.33	0.45	28405.7	1.92	1.94	0.75	47380.5	30.3
184	3.63	3.67	1.0	60823.5	2.31	2.33	0.36	22062.7	1.92	1.94	0.85	51591.9	34.4
215	3.63	3.67	1.0	63115.2	2.30	2.33	0.37	23237.6	1.92	1.93	0.95	60013.3	38.5
271	3.63	3.66	1.0	62395.0	2.31	2.32	0.30	19004.8	1.91	1.93	1.16	72174.0	46.9
328	3.62	3.66	1.0	56750.6	2.30	2.32	0.27	15528.4	1.91	1.93	1.28	72627.2	51.9
382	3.62	3.66	1.0	59379.9	2.30	2.32	0.26	15192.3	1.90	1.93	1.44	85587.6	58.4
502	3.62	3.65	1.0	59216.4	2.30	2.31	0.19	11024.8	1.91	1.92	1.53	90322.0	61.8
623	3.61	3.65	1.0	65153.7	2.29	2.31	0.16	10365.4	1.89	1.93	1.76	114774.3	71.4
862	3.67	3.71	1.0	64048.7	2.35	2.37	0.10	6198.0	1.95	1.98	1.97	126175.3	79.8
1102	3.61	3.64	1.0	64118.2	2.29	2.30	0.07	4243.7	1.89	1.92	2.09	134156.2	84.8
1342	3.61	3.65	1.0	59498.5	2.29	2.31	0.05	3206.6	1.88	1.93	2.24	132983.8	90.6
1709	3.59	3.66	1.0	64908.9	2.28	2.30	0.03	2036.6	1.88	1.93	2.28	148223.2	92.5
2062	3.59	3.65	1.0	65069.4	2.28	2.30	0.02	1006.4	1.88	1.93	2.36	153622.4	95.7
2782	3.60	3.64	1.0	66000.5	2.29	2.30	0.01	482.9	1.88	1.93	2.39	157759.7	96.9
4222	3.60	3.65	1.0	65572.2	–		–	–	1.87	1.93	2.42	158537.8	98.0
VB116b	**Standard**				**Educt**				**Product**				**Yield (%)**
4	3.58	3.74	1.0	71391.1	2.32	2.37	0.5	35695	1.93	1.95	0.05	3755.0	2.43
44	3.6	3.7	1.0	70256.6	2.31	2.36	0.47	33092.1	1.92	1.95	0.29	20259.7	13.3
73	3.6	3.7	1.0	71169.6	2.31	2.36	0.45	31772.2	1.92	1.95	0.44	31051.3	20.2
127	3.59	3.69	1.0	71832.4	2.3	2.35	0.41	29344.1	1.91	1.95	0.65	46385.3	29.9
190	3.59	3.7	1.0	73017.5	2.30	2.35	0.36	26216.8	1.9	1.95	0.87	63169.3	40.0
251	3.59	3.69	1.0	71926.1	2.29	2.33	0.28	20355.9	1.9	1.94	1.01	72402.2	46.6
309	3.60	3.68	1.0	66455.1	2.3	2.33	0.24	15985.8	1.9	1.95	1.14	75607.1	52.6
364	3.60	3.68	1.0	73268.2	2.29	2.33	0.22	15866.3	1.89	1.95	1.25	91637.5	57.9
424	3.60	3.67	1.0	73188.7	2.29	2.32	0.19	13791.5	1.89	1.94	1.35	99170.6	62.7

487	3.59	3.67	1.0	71346.9	2.29	2.33	0.17	12143.1	1.89	1.94	1.42	101596.0	65.9
548	3.60	3.67	1.0	72459.9	2.28	2.32	0.15	11017.4	1.89	1.94	1.49	107945.0	68.9
607	3.59	3.67	1.0	71410.4	2.28	2.32	0.13	9569.5	1.89	1.94	1.55	110970.4	71.9
667	3.60	3.67	1.0	71212.4	2.28	2.32	0.12	8838.3	1.88	1.94	1.63	116245.4	75.5
727	3.60	3.67	1.0	72452.0	2.28	2.32	0.12	8346.2	1.89	1.94	1.66	120609.3	77.0
852	3.59	3.66	1.0	72454.4	2.28	2.32	0.1	6915.6	1.89	1.93	1.74	126132.9	80.5
966	3.60	3.66	1.0	72774.8	2.28	2.31	0.08	5780.6	1.88	1.93	1.82	132218.3	84.1
1092	3.59	3.66	1.0	72079.0	2.29	2.31	0.06	4473.8	1.88	1.94	1.88	135432.4	86.9
1207	3.60	3.66	1.0	73414.2	2.28	2.31	0.05	3944.7	1.88	1.93	1.91	139889.1	88.2
1328	3.58	3.66	1.0	70507.1	2.28	2.31	0.05	3381.1	1.88	1.93	1.94	136509.9	89.6
1447	3.59	3.67	1.0	70256.2	2.28	2.31	0.04	2773.6	1.88	1.93	1.97	138197.4	91.0
1567	3.58	3.67	1.0	71675.7	2.28	2.31	0.03	2490.1	1.88	1.93	1.98	142179.2	91.8
1806	3.59	3.66	1.0	71738.1	2.28	2.30	0.02	1746.9	1.88	1.93	2.03	145732.4	94.0
2047	3.59	3.66	1.0	71449.8	2.28	2.30	0.02	1229.7	1.88	1.93	2.04	145418.8	94.2
2286	3.58	3.66	1.0	71792.8	2.28	2.31	0.02	1078.1	1.88	1.93	2.07	148423.8	95.6
2527	3.59	3.65	1.0	71373.8	2.26	2.30	0.01	799.3	1.87	1.93	2.11	150355.0	97.5

Table 4.10. Raw data of absolute kinetic of acylation reaction with TCAP (**2**) in $CDCl_3$.

Time (min)	**Integ. limits (ppm)**		**Integ.**	**Absol.**	**Integ. Limits (ppm)**		**Integ.**	**Absol.**	**Integ. Limits (ppm)**		**Integ.**	**Absol.**	**$Yield_{ester}$ (%)**
VB129a	**Standard**				**Educt**				**Product**				
7	3.62	3.69	1.0	72660.5	2.32	2.35	0.41	29549.1	1.92	1.95	0.40	29166.9	15.8
19	3.62	3.67	1.0	71908.3	2.31	2.33	0.34	24147.4	1.91	1.94	0.85	61233.1	36.0
25	3.62	3.67	1.0	72303.6	2.30	2.33	0.29	20736.6	1.91	1.94	1.02	73436.4	48.2
40	3.62	3.66	1.0	71550.7	2.30	2.32	0.20	14333.8	1.90	1.94	1.34	95729.8	65.3
55	3.61	3.66	1.0	71765.8	2.29	2.31	0.15	10784.1	1.90	1.93	1.51	108482.1	69.7
70	3.61	3.65	1.0	72012.4	2.29	2.31	0.11	8123.1	1.89	1.93	1.65	118591.7	76.7
85	3.61	3.65	1.0	71181.4	2.29	2.31	0.09	6441.5	1.89	1.93	1.75	124442.4	88.4
127	3.61	3.65	1.0	71411.6	2.29	2.30	0.05	3680.3	1.89	1.93	1.91	136472.9	90.4
193	3.60	3.64	1.0	69816.5	2.28	2.30	0.02	1670.4	1.88	1.92	2.02	141000.2	96.4
253	3.60	3.65	1.0	73173.3	2.28	2.30	0.01	837.6	1.88	1.92	2.08	152297.6	97.1
308	3.60	3.65	1.0	71124.2	2.28	2.30	0.01	485.5	1.88	1.93	2.11	150284.4	98.6
367	3.60	3.65	1.0	72521.0	–	–	–	–	1.88	1.93	2.13	154109.4	98.6
427	3.60	3.65	1.0	72756.8	–	–	–	–	1.88	1.92	2.12	154187.3	99.2
487	3.60	3.64	1.0	71551.0	–	–	–	–	1.88	1.92	2.14	152800.8	98.7
547	3.61	3.65	1.0	72433.8	–	–	–	–	1.88	1.92	2.12	153906.2	99.9
VB129b	**Standard**				**Educt**				**Product**				**Yield (%)**

6	3.63	3.69	1.0	68547.6	2.31	2.35	0.48	33128.8	1.92	1.95	0.35	23986.7	15.8
16	3.62	3.68	1.0	69271.7	2.31	2.34	0.38	26334.3	1.91	1.94	0.80	55313.3	36.0
25	3.62	3.67	1.0	68581.8	2.31	2.33	0.31	21369.6	1.91	1.94	1.07	73401.1	48.2
43	3.62	3.66	1.0	69049.8	2.30	2.32	0.19	13196.4	1.90	1.94	1.45	100030.2	65.3
53	3.61	3.66	1.0	70581.0	2.29	2.31	0.17	11724.3	1.89	1.93	1.55	109169.7	69.7
68	3.62	3.66	1.0	69975.1	2.29	2.31	0.13	9303.9	1.89	1.93	1.70	119084.2	76.7
110	3.61	3.65	1.0	69952.0	2.29	2.30	0.07	4924.8	1.89	1.93	1.96	137286.7	88.4
131	3.61	3.65	1.0	70733.6	2.29	2.30	0.05	3639.0	1.89	1.93	2.01	141913.2	90.4
190	3.61	3.65	1.0	68159.6	2.29	2.30	0.02	1628.0	1.88	1.92	2.14	145905.9	96.4
250	3.60	3.65	1.0	68808.2	2.29	2.30	0.01	858.8	1.89	1.92	2.16	148361.9	97.1
310	3.60	3.65	1.0	68108.7	2.28	2.30	0.01	640.8	1.89	1.93	2.19	149003.1	98.6
373	3.60	3.65	1.0	67907.3	2.28	2.30	0.00	327.4	1.88	1.92	2.19	148581.7	98.6
430	3.60	3.65	1.0	68606.9	–	–	–	–	1.89	1.92	2.20	151030.1	99.2
494	3.61	3.65	1.0	69414.4	–	–	–	–	1.89	1.92	2.19	152117.1	98.7
550	3.60	3.65	1.0	69950.3	–	–	–	–	1.88	1.92	2.22	155095.2	99.9

Table 4.11. Raw data of absolute kinetic of acylation reaction with **3c** in $CDCl_3$.

Time (min)	**Integ. limits (ppm)**		**Integ.**	**Absol.**	**Integ. Limits (ppm)**		**Integ.**	**Absol.**	**Integ. Limits (ppm)**		**Integ.**	**Absol.**	**$Yield_{ester}$ (%)**
VB124a	**Standard**				**Educt**				**Product**				
7	3.62	3.70	1.0	63057.8	2.32	2.36	0.52	32785.9	1.93	1.94	0.06	3790.6	2.75
32	3.62	3.69	1.0	63045.6	2.32	2.35	0.46	29165.1	1.92	1.96	0.25	15656.8	11.4
51	3.63	3.68	1.0	63683.4	2.32	2.34	0.43	27468.8	1.92	1.94	0.31	19423.9	14.0
79	3.67	3.71	1.0	65236.3	2.35	2.38	0.42	27717.0	1.95	1.98	0.47	30803.1	21.6
96	3.62	3.67	1.0	67039.0	2.31	2.33	0.39	26178.3	1.91	1.94	0.52	35018.1	23.9
118	3.63	3.67	1.0	65808.9	2.31	2.33	0.38	24887.8	1.91	1.94	0.62	40864.6	28.4
134	3.62	3.67	1.0	66895.2	2.31	2.33	0.35	23463.9	1.91	1.93	0.66	43913.1	30.0
164	3.61	3.68	1.0	70256.6	2.30	2.33	0.33	23452.8	1.91	1.94	0.77	54128.4	35.2
196	3.66	3.72	1.0	68802.5	2.35	2.37	0.31	21379.0	1.96	1.99	0.87	60079.1	39.9
224	3.62	3.66	1.0	66716.6	2.30	2.32	0.29	19044.4	1.90	1.94	0.97	64932.1	44.5
252	3.61	3.67	1.0	67582.4	2.29	2.32	0.26	17546.1	1.90	1.93	1.02	68731.4	46.5
313	3.62	3.66	1.0	64681.6	2.29	2.32	0.23	14664.9	1.89	1.93	1.18	76016.9	53.8
372	3.61	3.66	1.0	68513.8	2.29	2.32	0.19	13259.9	1.89	1.93	1.25	85637.0	57.2
439	3.62	3.65	1.0	67773.6	2.29	2.31	0.17	11736.2	1.89	1.93	1.36	92208.9	62.2
488	3.61	3.65	1.0	69772.3	2.29	2.31	0.15	10663.1	1.89	1.93	1.42	99369.7	65.1
548	3.61	3.65	1.0	68259.8	2.29	2.31	0.14	9534.6	1.89	1.92	1.48	101025.8	67.7
608	3.61	3.65	1.0	66956.3	2.29	2.31	0.13	8678.9	1.89	1.92	1.55	103515.2	70.7
668	3.61	3.65	1.0	65919.4	2.29	2.30	0.11	7096.0	1.88	1.92	1.61	105833.1	73.4

728	3.61	3.65	1.0	68560.0	2.29	2.31	0.10	6664.5	1.89	1.92	1.64	112315.6	74.9
848	3.61	3.65	1.0	68491.5	2.28	2.30	0.09	6102.2	1.89	1.92	1.72	117924.2	78.8
967	3.60	3.65	1.0	69606.8	2.28	2.30	0.07	4866.0	1.88	1.92	1.77	123516.3	81.2
1093	3.60	3.65	1.0	65398.0	2.28	2.30	0.06	3771.2	1.88	1.92	1.83	119398.9	83.5
1222	3.60	3.65	1.0	70562.1	2.28	2.30	0.05	3340.4	1.88	1.92	1.84	129986.1	84.3
1329	3.60	3.65	1.0	65412.2	2.28	2.29	0.04	2432.2	1.88	1.92	1.86	121820.4	85.2
1454	3.60	3.64	1.0	65229.8	2.27	2.30	0.03	1653.0	1.88	1.92	1.96	127646.5	89.5
1687	3.59	3.65	1.0	68639.2	2.28	2.30	0.03	2256.2	1.88	1.92	1.91	130903.6	87.2
1939	3.61	3.64	1.0	64634.8	2.28	2.29	0.02	1015.6	1.88	1.92	2.00	129155.7	91.4
2304	3.60	3.64	1.0	73421.6	2.28	2.29	0.01	906.1	1.88	1.92	2.02	148561.5	92.6
VB124b	**Standard**				**Educt**				**Product**				**Yield (%)**
14	3.62	3.69	1.0	70836.5	2.31	2.35	0.58	41025.4	1.93	1.94	0.08	6016.5	4.00
34	3.62	3.68	1.0	72034.6	2.31	2.35	0.54	38834.7	1.92	1.94	0.21	15254.0	10.0
51	3.62	3.68	1.0	72510.1	2.31	2.34	0.51	37060.4	1.92	1.94	0.29	21220.2	13.8
75	3.62	3.67	1.0	73462.9	2.31	2.34	0.53	39129.6	1.92	1.94	0.41	30255.3	19.4
97	3.63	3.67	1.0	72626.3	2.31	2.33	0.45	32682.9	1.91	1.94	0.52	37993.8	24.7
111	3.62	3.68	1.0	73706.5	2.30	2.34	0.46	34189.2	1.91	1.94	0.58	42508.2	27.2
142	3.62	3.67	1.0	75213.1	2.30	2.33	0.43	32621.5	1.90	1.93	0.69	51802.8	32.5
197	3.62	3.66	1.0	70214.9	2.30	2.32	0.35	24735.8	1.90	1.94	0.87	61354.7	41.2
254	3.61	3.66	1.0	67885.4	2.29	2.32	0.29	20008.1	1.90	1.94	1.01	68577.5	47.6
310	3.62	3.66	1.0	70008.4	2.29	2.32	0.26	18386.5	1.90	1.93	1.12	78132.8	52.6
369	3.62	3.65	1.0	69498.4	2.29	2.31	0.22	15614.3	1.89	1.93	1.22	84695.7	57.4
430	3.61	3.66	1.0	69434.4	2.29	2.31	0.19	13177.1	1.89	1.93	1.30	90201.0	61.2
494	3.60	3.66	1.0	69560.0	2.29	2.31	0.17	11929.4	1.89	1.93	1.38	95761.1	64.9
554	3.61	3.66	1.0	71398.4	2.29	2.31	0.15	10565.3	1.89	1.92	1.42	101518.4	67.0
611	3.61	3.65	1.0	70953.9	2.28	2.31	0.14	10239.6	1.89	1.92	1.50	106300.6	70.6
670	3.61	3.65	1.0	69709.4	2.29	2.31	0.13	8825.0	1.89	1.92	1.55	108253.9	73.2
731	3.60	3.65	1.0	70275.9	2.28	2.30	0.12	8303.7	1.89	1.93	1.59	111641.0	74.9
851	3.60	3.65	1.0	73453.9	2.29	2.30	0.10	7027.7	1.89	1.93	1.66	121870.7	78.2
970	3.60	3.64	1.0	70493.7	2.28	2.30	0.08	5771.4	1.88	1.92	1.72	121408.7	81.2
1096	3.60	3.65	1.0	73879.4	2.28	2.30	0.07	5159.5	1.88	1.92	1.77	131126.2	83.6
1216	3.60	3.64	1.0	67566.0	2.28	2.30	0.06	3756.6	1.88	1.92	1.83	123407.8	86.1
1336	3.61	3.64	1.0	70324.0	2.28	2.30	0.05	3476.2	1.88	1.92	1.86	130601.7	87.5
1452	3.60	3.64	1.0	75946.1	2.28	2.29	0.04	3015.3	1.88	1.92	1.87	141737.2	87.9
1931	3.60	3.64	1.0	70733.9	2.27	2.29	0.02	1440.0	1.87	1.92	1.93	136857.0	91.2
2293	3.59	3.64	1.0	67887.8	2.28	2.29	0.01	964.6	1.87	1.92	1.97	133717.2	92.8
2653	3.59	3.63	1.0	75084.9	2.28	2.29	0.01	680.6	1.87	1.92	2.00	150354.9	94.4
3373	3.60	3.64	1.0	68557.8	2.28	2.29	0.00	238.3	1.88	1.92	1.99	136500.9	93.8
6110	3.59	3.64	1.0	69276.8	–	–	–	–	1.87	1.91	1.98	137212.8	93.3

Table 4.12. Raw data of absolute kinetic of acylation reaction with **3d** in $CDCl_3$.

Time (min)	Integ. limits (ppm)		Integ.	Absol.	Integ. Limits (ppm)		Integ.	Absol.	Integ. Limits (ppm)		Integ.	Absol.	$Yield_{ester}$ (%)
VB125a	**Standard**				**Educt**				**Product**				
16	3.64	3.68	1.00	60974.99	2.32	2.34	0.53	32348.04	1.93	1.94	0.10	6072.39	4.33
34	3.63	3.68	1.00	66234.84	2.32	2.34	0.48	31722.32	1.92	1.94	0.18	12212.99	8.01
51	3.63	3.67	1.00	59615.72	2.32	2.34	0.47	28166.13	1.92	1.94	0.27	16312.03	11.9
68	3.63	3.68	1.00	65300.96	2.32	2.34	0.46	29825.74	1.92	1.94	0.34	22065.52	14.7
86	3.62	3.68	1.00	66475.04	2.31	2.34	0.45	29670.15	1.91	1.94	0.45	29651.03	19.4
108	3.63	3.67	1.00	61698.50	2.31	2.33	0.43	26324.40	1.92	1.93	0.50	30728.97	21.6
127	3.63	3.67	1.00	67702.18	2.31	2.33	0.44	30006.19	1.91	1.93	0.58	38984.02	25.0
189	3.62	3.67	1.00	62215.46	2.31	2.32	0.35	21964.65	1.90	1.93	0.79	49040.92	34.2
255	3.62	3.66	1.00	64692.63	2.30	2.32	0.31	20346.31	1.90	1.93	0.95	61245.94	41.1
307	3.62	3.66	1.00	60966.63	2.30	2.32	0.28	17305.60	1.90	1.93	1.05	64248.30	45.8
367	3.61	3.66	1.00	61668.18	2.29	2.32	0.25	15194.26	1.90	1.93	1.17	72007.64	50.7
432	3.61	3.65	1.00	59565.18	2.29	2.31	0.22	13382.47	1.89	1.93	1.30	77568.08	56.6
489	3.61	3.65	1.00	62727.45	2.29	2.31	0.20	12796.09	1.90	1.92	1.36	85276.09	59.1
547	3.61	3.65	1.00	64607.33	2.29	2.31	0.19	12005.39	1.90	1.93	1.44	93267.54	62.7
617	3.60	3.66	1.00	63794.70	2.29	2.30	0.16	9954.39	1.89	1.92	1.50	95590.82	65.1
667	3.61	3.65	1.00	62936.70	2.29	2.31	0.15	9681.84	1.89	1.92	1.57	98730.33	68.2
729	3.61	3.65	1.00	64867.70	2.29	2.30	0.14	8904.89	1.88	1.92	1.61	104323.83	69.9
847	3.60	3.65	1.00	65682.54	2.29	2.30	0.12	7702.99	1.89	1.92	1.71	112166.63	74.2
971	3.61	3.65	1.00	63786.57	2.28	2.30	0.10	6405.40	1.88	1.92	1.80	114534.21	78.0
1088	3.60	3.64	1.00	64202.60	2.28	2.30	0.08	5221.84	1.88	1.92	1.85	118666.46	80.3
1209	3.60	3.64	1.00	65465.01	2.28	2.30	0.07	4720.11	1.89	1.92	1.87	122540.27	81.3
1328	3.67	3.71	1.00	63889.90	2.35	2.37	0.06	4118.42	1.95	1.99	1.92	122793.56	83.5
1450	3.61	3.64	1.00	64852.66	2.28	2.30	0.05	3417.47	1.88	1.92	1.97	127880.01	85.7
1696	3.60	3.64	1.00	67040.96	2.28	2.30	0.04	2849.89	1.88	1.92	2.03	136322.10	88.4
1934	3.60	3.64	1.00	62041.29	2.28	2.29	0.03	1972.14	1.88	1.92	2.06	127591.33	89.4
2170	3.60	3.64	1.00	63629.04	2.28	2.29	0.02	1395.82	1.88	1.92	2.10	133344.82	91.1
2410	3.60	3.65	1.00	65288.30	2.28	2.29	0.02	1219.97	1.88	1.92	2.09	136198.71	90.6
2773	3.59	3.64	1.00	62417.16	2.28	2.29	0.01	807.63	1.88	1.92	2.11	131815.81	91.8
3132	3.60	3.64	1.00	64190.36	2.28	2.29	0.01	601.54	1.88	1.92	2.14	137524.34	93.1
3497	3.59	3.64	1.00	64551.01	2.28	2.29	0.01	364.49	1.88	1.92	2.13	137754.68	92.7
3856	3.59	3.64	1.00	64289.22	2.27	2.29	0.01	420.10	1.88	1.92	2.16	138593.75	93.7
VB125b	**Standard**				**Educt**				**Product**				**Yield (%)**
8	3.62	3.69	1.0	73934.8	2.32	2.35	0.56	41113.4	1.93	1.95	0.05	3726.8	2.38

25	3.63	3.68	1.0	74228.2	2.32	2.35	0.51	38054.1	1.93	1.95	0.13	9844.2	6.27
47	3.63	3.68	1.0	74741.4	2.32	2.34	0.50	37325.4	1.92	1.95	0.26	19114.9	12.1
75	3.63	3.68	1.0	66977.5	2.32	2.34	0.45	30345.4	1.92	1.94	0.36	23999.0	16.9
88	3.62	3.68	1.0	72683.9	2.31	2.34	0.47	34521.1	1.91	1.94	0.41	29939.2	19.5
113	3.63	3.67	1.0	69239.1	2.31	2.34	0.45	30947.3	1.91	1.94	0.50	34325.2	23.4
139	3.62	3.67	1.0	67752.7	2.31	2.33	0.42	28621.3	1.91	1.94	0.59	39836.9	27.8
195	3.62	3.67	1.0	67398.5	2.30	2.33	0.38	25376.2	1.91	1.94	0.75	50848.4	35.7
248	3.62	3.66	1.0	68334.8	2.30	2.32	0.33	22641.7	1.90	1.93	0.88	60107.6	41.6
308	3.61	3.67	1.0	67467.1	2.29	2.32	0.28	19044.3	1.90	1.93	1.00	67691.1	47.5
372	3.61	3.66	1.0	70678.0	2.29	2.32	0.24	17126.2	1.90	1.93	1.11	78780.4	52.7
428	3.61	3.65	1.0	71747.6	2.29	2.32	0.22	15461.2	1.90	1.93	1.21	86548.3	57.0
489	3.61	3.66	1.0	73222.6	2.29	2.31	0.19	13930.9	1.89	1.93	1.27	93140.9	60.2
548	3.60	3.65	1.0	72416.6	2.28	2.31	0.17	12520.2	1.89	1.93	1.33	96644.2	63.1
608	3.61	3.66	1.0	71717.8	2.29	2.31	0.15	10912.7	1.89	1.93	1.39	99989.8	65.9
669	3.61	3.66	1.0	71451.5	2.28	2.31	0.14	10059.2	1.88	1.93	1.46	104395.9	69.1
738	3.60	3.65	1.0	72882.7	2.28	2.31	0.13	9115.9	1.89	1.92	1.47	107252.6	69.6
849	3.60	3.65	1.0	73305.0	2.28	2.30	0.11	7865.1	1.88	1.92	1.56	114427.8	73.8
976	3.60	3.65	1.0	73477.1	2.28	2.30	0.09	6570.2	1.88	1.92	1.62	119007.9	76.6
1095	3.59	3.65	1.0	71847.5	2.28	2.30	0.08	5538.5	1.88	1.92	1.66	119204.9	78.5
1217	3.60	3.65	1.0	67742.5	2.28	2.30	0.06	4093.3	1.88	1.93	1.72	116653.1	81.4
1338	3.60	3.64	1.0	72504.7	2.28	2.30	0.05	3797.0	1.88	1.92	1.74	126153.5	82.3
1454	3.60	3.64	1.0	71759.5	2.28	2.30	0.05	3331.3	1.88	1.93	1.77	127110.9	83.8
1698	3.60	3.65	1.0	71453.3	2.28	2.29	0.03	2434.0	1.88	1.92	1.79	127986.3	84.7
1943	3.59	3.65	1.0	72165.0	2.28	2.29	0.03	1831.1	1.88	1.92	1.82	131548.3	86.2
2183	3.60	3.64	1.0	75264.8	2.28	2.29	0.02	1424.8	1.88	1.92	1.86	140194.1	88.1
2419	3.59	3.64	1.0	72355.3	2.28	2.29	0.01	1043.5	1.88	1.92	1.86	134720.1	88.1
2781	3.59	3.65	1.0	69465.9	2.28	2.29	0.01	717.1	1.88	1.92	1.86	129451.0	88.1
3138	3.59	3.64	1.0	72642.9	2.28	2.29	0.01	547.9	1.88	1.92	1.87	135682.8	88.3
3496	3.59	3.65	1.0	73944.7	2.28	2.29	0.01	386.0	1.87	1.92	1.87	138245.6	88.4
3859	3.58	3.64	1.0	72545.9	2.28	2.29	0.00	239.2	1.87	1.91	1.88	136445.4	88.9
4220	3.59	3.65	1.0	68920.7	2.27	2.29	0.01	378.4	1.88	1.91	1.87	128960.1	88.5
4579	3.59	3.63	1.0	75244.8	–	–	–	–	1.87	1.91	1.90	142629.5	89.6
4940	3.59	3.64	1.0	68414.1	–	–	–	–	1.87	1.91	1.88	128935.6	89.1
5298	3.60	3.63	1.0	75147.2	–	–	–	–	1.88	1.91	1.89	141742.5	89.2
5659	3.59	3.64	1.0	76842.5	–	–	–	–	1.87	1.91	1.90	145712.2	89.7

Table 4.13. Raw data of absolute kinetic of acylation reaction with **3a** in $CDCl_3$

Time (min)	Integ. limits (ppm)		Integ.	Absol.	Integ. Limits (ppm)		Integ.	Absol.	Integ. Limits (ppm)		Integ.	Absol.	$Yield_{ester}$ (%)
VB123a	**Standard**				**Educt**				**Product**				
11	3.62	3.69	1.0	67216.4	2.32	2.35	0.56	37876.3	1.92	1.94	0.19	12565.7	8.55
28	3.60	3.69	1.0	68820.0	2.31	2.35	0.52	35930.3	1.91	1.95	0.42	28784.6	19.1
48	3.63	3.68	1.0	63641.5	2.31	2.34	0.47	29938.4	1.91	1.94	0.62	39343.7	28.3
68	3.62	3.67	1.0	61848.5	2.30	2.33	0.43	26468.9	1.91	1.94	0.77	47352.5	35.0
90	3.61	3.67	1.0	62729.3	2.30	2.33	0.37	23196.5	1.91	1.94	0.93	58039.9	42.3
108	3.62	3.67	1.0	63813.8	2.30	2.32	0.32	20485.5	1.90	1.94	1.06	67375.4	48.3
143	3.61	3.67	1.0	64424.8	2.29	2.32	0.28	17811.9	1.90	1.93	1.21	78078.4	55.4
177	3.61	3.66	1.0	60624.8	2.29	2.32	0.23	13874.0	1.89	1.93	1.34	81021.3	61.1
202	3.61	3.66	1.0	66821.9	2.29	2.31	0.20	13473.4	1.89	1.93	1.43	95230.6	65.2
236	3.61	3.66	1.0	69086.0	2.29	2.31	0.17	11961.1	1.89	1.93	1.50	103656.2	68.6
290	3.60	3.65	1.0	68090.6	2.29	2.31	0.15	9950.9	1.89	1.93	1.64	111346.6	74.8
352	3.60	3.65	1.0	72755.1	2.28	2.31	0.12	8719.6	1.88	1.93	1.74	126294.8	79.4
423	3.61	3.64	1.0	65431.2	2.28	2.30	0.10	6235.0	1.88	1.93	1.85	120817.9	84.5
478	3.60	3.65	1.0	66559.5	2.28	2.30	0.08	5239.0	1.89	1.93	1.87	124723.0	85.7
541	3.60	3.65	1.0	68566.2	2.28	2.30	0.06	4140.3	1.88	1.92	1.91	130931.8	87.3
597	3.60	3.65	1.0	67594.5	2.28	2.30	0.06	3771.4	1.88	1.92	1.95	131881.9	89.2
652	3.60	3.64	1.0	62327.0	2.27	2.30	0.05	3185.7	1.88	1.92	1.98	123408.1	90.6
707	3.60	3.64	1.0	67984.0	2.28	2.30	0.04	2704.0	1.88	1.92	2.01	136823.4	92.0
833	3.60	3.64	1.0	70426.5	2.28	2.29	0.03	2056.9	1.88	1.92	2.03	143063.7	92.9
953	3.60	3.65	1.0	66783.3	2.28	2.30	0.02	1563.3	1.88	1.92	2.09	139318.7	95.4
1068	3.59	3.65	1.0	69474.5	2.28	2.29	0.02	1134.3	1.87	1.92	2.09	145169.8	95.6
1192	3.60	3.64	1.0	68880.9	2.28	2.29	0.01	819.2	1.88	1.92	2.11	145413.7	96.6
1308	3.60	3.64	1.0	70295.1	2.28	2.29	0.01	624.0	1.88	1.92	2.10	147782.7	96.2
1432	3.59	3.65	1.0	63471.0	2.28	2.29	0.01	462.4	1.87	1.92	2.10	133368.8	96.1
1561	3.60	3.64	1.0	68873.3	2.28	2.29	0.00	342.5	1.87	1.92	2.13	146699.8	97.4
VB123b	**Standard**				**Educt**				**Product**				**Yield (%)**
8	3.63	3.68	1.0	71967.0	2.32	2.35	0.48	34819.6	1.93	1.94	0.12	8622.6	5.65
31	3.63	3.68	1.0	66561.1	2.31	2.34	0.44	29575.7	1.92	1.94	0.37	24882.2	17.6
51	3.62	3.67	1.0	66116.5	2.31	2.34	0.37	24492.8	1.91	1.94	0.60	39493.1	28.1
76	3.62	3.67	1.0	68945.4	2.31	2.32	0.32	22291.5	1.91	1.94	0.76	52542.6	35.9
88	3.62	3.67	1.0	65672.1	2.30	2.33	0.32	21309.8	1.90	1.93	0.82	53774.5	38.6
122	3.61	3.66	1.0	72190.8	2.30	2.32	0.26	18446.0	1.89	1.94	1.03	74708.4	48.8
133	3.62	3.66	1.0	71403.4	2.30	2.32	0.24	17263.4	1.90	1.94	1.08	76955.3	50.8
170	3.61	3.66	1.0	72949.1	2.29	2.31	0.20	14512.4	1.89	1.93	1.20	87549.6	56.6

196	3.61	3.66	1.0	73806.6	2.29	2.31	0.18	13432.6	1.89	1.93	1.29	94930.2	60.6
248	3.61	3.65	1.0	74754.6	2.29	2.31	0.14	10696.1	1.89	1.93	1.43	107209.4	67.6
310	3.60	3.65	1.0	70263.7	2.28	2.31	0.12	8084.6	1.89	1.92	1.55	109172.1	73.2
381	3.61	3.65	1.0	69655.5	2.28	2.30	0.09	6275.8	1.88	1.92	1.66	115830.9	78.4
437	3.60	3.64	1.0	69048.0	2.28	2.30	0.07	5169.5	1.88	1.92	1.71	117824.2	80.4
505	3.60	3.64	1.0	71437.0	2.28	2.30	0.06	4377.6	1.89	1.92	1.76	125781.1	83.0
560	3.60	3.64	1.0	74404.8	2.28	2.30	0.05	3928.9	1.87	1.92	1.83	136078.7	86.2
674	3.60	3.64	1.0	75302.1	2.28	2.29	0.03	2505.3	1.89	1.92	1.83	137590.5	86.1
799	3.59	3.64	1.0	69114.9	2.28	2.29	0.03	1845.4	1.88	1.91	1.88	130220.0	88.8
917	3.60	3.64	1.0	75483.5	2.28	2.29	0.02	1410.3	1.88	1.92	1.96	147740.1	92.2
1036	3.60	3.63	1.0	75380.7	2.28	2.29	0.01	1036.5	1.88	1.92	1.96	147719.1	92.3
1156	3.59	3.65	1.0	72757.1	2.28	2.29	0.01	751.5	1.87	1.92	1.95	142009.6	92.0
1276	3.59	3.64	1.0	68755.5	2.28	2.29	0.01	623.9	1.88	1.91	1.95	134354.9	92.1
1392	3.60	3.64	1.0	71968.4	2.27	2.30	0.01	470.3	1.88	1.92	1.98	142218.0	93.1
1402	3.60	3.64	1.0	72888.4	2.28	2.29	0.01	372.7	1.88	1.92	2.01	146558.9	93.2
1512	3.59	3.64	1.0	73075.0	2.28	2.29	0.00	241.4	1.88	1.92	1.97	143987.6	94.7
1632	3.60	3.64	1.0	74420.6	2.28	2.29	0.00	189.2	1.88	1.91	1.96	145759.1	92.8
1871	3.60	3.64	1.0	76185.4	–	–	–	–	1.87	1.92	2.00	152150.4	92.3
2112	3.60	3.64	1.0	71770.0	–	–	–	–	1.88	1.92	1.98	141905.7	94.1
2114	3.60	3.64	1.0	76270.1	–	–	–	–	1.88	1.92	1.98	150851.8	93.2

Table 4.14. Raw data of absolute kinetic of acylation reaction with **3b** in $CDCl_3$.

Time (min)	**Integ. limits (ppm)**		**Integ.**	**Absol.**	**Integ. Limits (ppm)**		**Integ.**	**Absol.**	**Integ. Limits (ppm)**		**Integ.**	**Absol.**	**$Yield_{ester}$ (%)**
VB126a	**Standard**				**Educt**				**Product**				
15	3.63	3.68	1.0	66608.8	2.32	2.34	0.48	31886.6	1.92	1.94	0.27	18282.0	11.9
32	3.63	3.67	1.0	65307.5	2.31	2.34	0.44	28436.3	1.92	1.94	0.49	32045.9	21.3
44	3.62	3.66	1.0	64731.6	2.31	2.33	0.41	26572.7	1.91	1.94	0.65	42109.4	28.3
70	3.62	3.66	1.0	64599.3	2.30	2.32	0.33	21387.4	1.91	1.93	0.89	57399.3	38.6
88	3.62	3.66	1.0	64037.9	2.30	2.32	0.29	18619.0	1.90	1.93	1.01	64453.5	43.7
108	3.62	3.66	1.0	65310.9	2.29	2.32	0.27	17532.3	1.90	1.93	1.14	74347.7	49.5
131	3.61	3.65	1.0	60768.9	2.30	2.31	0.23	13922.3	1.89	1.93	1.28	77853.7	55.7
158	3.61	3.65	1.0	61212.9	2.29	2.31	0.20	12390.9	1.89	1.92	1.38	84527.3	60.0
182	3.61	3.65	1.0	61159.4	2.29	2.31	0.18	10973.7	1.89	1.92	1.47	89617.8	63.7
247	3.61	3.65	1.0	68295.0	2.29	2.30	0.14	9313.4	1.89	1.92	1.62	110335.1	70.2
314	3.60	3.65	1.0	62163.5	2.28	2.30	0.10	5920.2	1.89	1.92	1.73	107431.3	75.1
372	3.60	3.64	1.0	64237.4	2.28	2.30	0.08	5369.5	1.89	1.92	1.83	117389.6	79.4

429	3.60	3.64	1.0	63949.8	2.28	2.30	0.07	4213.2	1.89	1.91	1.87	119326.7	81.1
492	3.60	3.64	1.0	62494.3	2.28	2.30	0.05	3392.8	1.89	1.92	1.95	122113.4	84.9
553	3.60	3.64	1.0	64511.4	2.28	2.29	0.04	2858.5	1.89	1.91	1.99	128443.6	86.5
608	3.60	3.64	1.0	64113.9	2.28	2.30	0.04	2303.9	1.88	1.92	2.04	130721.5	88.6
672	3.60	3.64	1.0	65143.3	2.28	2.30	0.03	2017.0	1.88	1.92	2.08	135536.5	90.4
728	3.60	3.64	1.0	63878.2	2.28	2.29	0.02	1572.5	1.88	1.91	2.06	131667.3	89.6
849	3.60	3.64	1.0	63514.1	2.28	2.29	0.02	1102.7	1.88	1.91	2.10	133288.0	91.2
968	3.60	3.64	1.0	65031.3	2.28	2.29	0.01	809.0	1.88	1.92	2.14	139426.2	93.2
1090	3.60	3.64	1.0	65534.2	2.28	2.29	0.01	514.1	1.88	1.92	2.14	140563.2	93.2
1212	3.60	3.64	1.0	65431.1	2.28	2.29	0.01	392.8	1.88	1.91	2.18	142381.6	94.6
1330	3.60	3.64	1.0	63550.4	2.28	2.29	0.00	250.1	1.88	1.92	2.18	138601.6	94.8
1451	3.60	3.64	1.0	66127.6	–	–	–	–	1.87	1.91	2.18	144138.9	94.7
1819	3.60	3.64	1.0	64034.6	–	–	–	–	1.87	1.92	2.20	140676.0	95.5
VB126b	**Standard**				**Educt**				**Product**				**Yield (%)**
8	3.63	3.68	1.0	72671.0	2.32	2.35	0.48	34759.3	1.93	1.94	0.14	10424.4	6.78
21	3.63	3.68	1.0	73226.2	2.32	2.34	0.43	31462.3	1.92	1.94	0.35	25325.3	16.4
35	3.62	3.67	1.0	73505.3	2.31	2.33	0.41	30036.0	1.91	1.94	0.52	37861.0	24.4
49	3.62	3.67	1.0	73319.5	2.31	2.33	0.38	27530.1	1.91	1.94	0.64	46767.6	30.2
65	3.62	3.67	1.0	72332.2	2.30	2.33	0.34	24350.0	1.91	1.94	0.79	57047.5	37.3
97	3.62	3.67	1.0	71498.1	2.30	2.32	0.25	17897.9	1.90	1.93	0.99	70781.2	46.8
129	3.61	3.66	1.0	74075.1	2.29	2.31	0.21	15912.5	1.89	1.93	1.17	86924.2	55.5
187	3.61	3.66	1.0	72985.1	2.29	2.31	0.16	11440.2	1.89	1.93	1.37	100324.8	65.0
247	3.60	3.65	1.0	71783.9	2.28	2.31	0.12	8414.3	1.89	1.93	1.52	109292.6	72.0
307	3.60	3.65	1.0	72350.6	2.29	2.30	0.09	6209.7	1.89	1.93	1.61	116778.7	76.3
367	3.61	3.65	1.0	74110.4	2.28	2.30	0.07	5251.1	1.88	1.92	1.69	125494.3	80.1
432	3.60	3.65	1.0	65538.8	2.28	2.30	0.05	3420.0	1.89	1.93	1.74	114350.1	82.5
493	3.60	3.65	1.0	76439.7	2.28	2.30	0.04	3360.9	1.87	1.92	1.82	139093.6	86.0
548	3.61	3.64	1.0	66788.1	2.28	2.29	0.03	2247.8	1.88	1.92	1.83	121950.9	86.3
607	3.60	3.65	1.0	76301.1	2.28	2.30	0.03	2226.6	1.88	1.92	1.85	141405.9	87.6
671	3.60	3.65	1.0	69017.7	2.28	2.29	0.02	1527.4	1.87	1.92	1.88	129634.3	88.8
729	3.60	3.65	1.0	70750.2	2.28	2.29	0.02	1360.6	1.88	1.92	1.89	133761.7	89.4
848	3.59	3.65	1.0	71246.2	2.28	2.29	0.01	863.3	1.88	1.92	1.90	135510.3	89.9
968	3.60	3.64	1.0	71255.8	2.28	2.29	0.01	635.7	1.88	1.92	1.92	136705.0	90.7
1088	3.60	3.64	1.0	71359.6	2.27	2.30	0.01	533.4	1.88	1.92	1.94	138301.0	91.6
1208	3.59	3.65	1.0	71854.6	2.28	2.29	0.00	301.6	1.87	1.92	1.94	139226.4	91.6
1330	3.60	3.65	1.0	69857.2	2.29	2.31	0.00	201.2	1.88	1.92	1.94	135320.8	91.6
1453	3.59	3.65	1.0	69515.7	2.29	2.30	0.00	208.4	1.87	1.92	1.95	135275.3	92.0

Table 4.15. Raw data of absolute kinetic of acylation reaction with **5a** in $CDCl_3$.

Time (min)	Integ. limits (ppm)		Integ.	Absol.	Integ. Limits (ppm)		Integ.	Absol.	Integ. Limits (ppm)		Integ.	Absol.	$Yield_{ester}$ (%)
VB118a	**Standard**				**Educt**				**Product**				
7	3.61	3.69	1.0	64104.0	2.30	2.34	0.55	35232.5	1.92	1.94	0.18	11711.9	7.40
10	3.62	3.67	1.0	62583.2	2.31	2.34	0.55	34285.8	1.91	1.94	0.28	17620.9	11.4
20	3.62	3.67	1.0	62629.9	2.31	2.33	0.50	31008.4	1.91	1.94	0.44	27632.4	17.9
22	3.62	3.67	1.0	61599.7	2.31	2.33	0.48	29319.1	1.91	1.93	0.48	29358.6	19.3
24	3.60	3.67	1.0	63557.2	2.30	2.33	0.49	31381.1	1.91	1.94	0.53	33491.5	21.4
27	3.62	3.66	1.0	62338.8	2.31	2.33	0.47	29014.2	1.91	1.94	0.56	35167.7	22.9
31	3.62	3.66	1.0	62371.7	2.30	2.32	0.47	29192.0	1.90	1.93	0.63	39255.4	25.5
41	3.61	3.67	1.0	65795.1	2.30	2.32	0.42	27493.8	1.90	1.93	0.73	48145.1	29.7
50	3.60	3.67	1.0	64331.9	2.29	2.32	0.41	26086.1	1.90	1.94	0.86	55424.1	34.9
56	3.61	3.66	1.0	63672.9	2.29	2.32	0.39	25105.5	1.90	1.93	0.89	56691.5	36.1
71	3.61	3.66	1.0	62147.4	2.30	2.31	0.31	19072.6	1.89	1.93	1.01	62815.6	41.0
103	3.60	3.67	1.0	62428.4	2.29	2.31	0.26	16024.4	1.89	1.93	1.21	75623.8	49.1
133	3.61	3.65	1.0	62062.7	2.29	2.31	0.23	14478.1	1.89	1.92	1.38	85867.7	56.1
168	3.61	3.65	1.0	64250.3	2.29	2.30	0.19	12007.0	1.89	1.92	1.47	94249.1	59.4
223	3.60	3.65	1.0	62271.7	2.28	2.30	0.14	8968.0	1.88	1.92	1.64	101874.9	66.3
288	3.60	3.64	1.0	65042.4	2.28	2.30	0.12	8091.8	1.88	1.92	1.74	112925.1	70.4
404	3.60	3.64	1.0	62305.6	2.28	2.29	0.08	5063.3	1.88	1.92	1.90	118140.5	76.8
534	3.59	3.64	1.0	64460.4	2.28	2.29	0.05	3387.2	1.87	1.91	1.98	127697.0	80.3
764	3.59	3.64	1.0	64258.1	2.27	2.29	0.02	1292.9	1.87	1.92	2.11	135420.1	85.4
1003	3.59	3.63	1.0	65622.3	2.27	2.29	0.02	1025.6	1.87	1.91	2.12	139181.5	86.0
1260	3.59	3.63	1.0	66637.2	2.27	2.29	0.01	684.3	1.87	1.91	2.15	143362.9	87.2
1483	3.58	3.64	1.0	66529.9	2.26	2.29	0.01	691.5	1.87	1.92	2.16	143613.5	87.5
2203	3.59	3.63	1.0	65170.4	–	–	–	–	1.87	1.91	2.17	141287.7	87.9
2923	3.59	3.63	1.0	66667.3	–	–	–	–	1.87	1.91	2.17	144726.4	88.0
VB118b	**Standard**				**Educt**				**Product**				**Yield (%)**
10	3.57	3.71	1.0	72457.1	2.29	2.35	0.58	42344.5	1.91	1.94	0.20	14211.6	9.10
27	3.58	3.69	1.0	72627.3	2.29	2.33	0.46	33283.7	1.90	1.94	0.42	30432.3	19.5
45	3.57	3.69	1.0	72565.3	2.29	2.32	0.39	28122.3	1.90	1.94	0.59	42456.5	27.2
76	3.59	3.68	1.0	72234.1	2.28	2.32	0.33	24044.1	1.89	1.93	0.82	58991.8	37.9
100	3.58	3.67	1.0	72154.9	2.28	2.32	0.29	21180.3	1.89	1.93	0.95	68574.0	44.1
131	3.58	3.68	1.0	70272.8	2.28	2.31	0.26	18530.9	1.88	1.94	1.11	77898.9	51.5
187	3.57	3.67	1.0	70871.8	2.28	2.31	0.21	14947.6	1.88	1.93	1.27	89794.5	58.8
248	3.58	3.66	1.0	70335.4	2.27	2.31	0.18	12444.3	1.87	1.93	1.43	100231.6	66.2
250	3.57	3.66	1.0	70688.2	2.27	2.31	0.18	12487.2	1.87	1.94	1.43	101404.5	66.6
307	3.57	3.66	1.0	70670.9	2.27	2.31	0.15	10933.5	1.87	1.93	1.51	106831.2	70.2

365	3.57	3.67	1.0	70848.9	2.27	2.30	0.13	8985.1	1.87	1.92	1.58	111987.3	73.4
432	3.56	3.67	1.0	66955.6	2.27	2.30	0.11	7239.1	1.87	1.92	1.63	109128.1	75.7
499	3.57	3.67	1.0	76038.0	2.26	2.30	0.09	7106.5	1.87	1.92	1.68	127973.0	78.1
502	3.58	3.66	1.0	68780.9	2.27	2.30	0.09	6438.2	1.87	1.92	1.69	116505.0	78.6
548	3.58	3.65	1.0	76108.2	2.27	2.30	0.08	6441.1	1.86	1.92	1.76	134005.1	81.7
608	3.58	3.65	1.0	76263.4	2.27	2.30	0.07	5066.8	1.87	1.92	1.76	134536.1	81.9
668	3.56	3.66	1.0	76775.3	2.26	2.30	0.06	4844.1	1.87	1.92	1.79	137044.4	82.9
728	3.56	3.67	1.0	70753.0	2.26	2.30	0.06	4250.3	1.87	1.92	1.81	127967.1	84.0
852	3.57	3.66	1.0	77679.9	2.26	2.30	0.05	3705.5	1.87	1.92	1.85	143820.1	85.9
977	3.57	3.66	1.0	75054.1	2.26	2.30	0.03	2418.3	1.87	1.91	1.87	140703.7	87.0
1088	3.57	3.66	1.0	75384.2	2.27	2.29	0.02	1844.4	1.87	1.91	1.89	142267.8	87.6
1234	3.57	3.66	1.0	77033.5	2.27	2.29	0.02	1237.1	1.87	1.92	1.90	146746.3	88.4
1334	3.57	3.65	1.0	73027.4	2.26	2.29	0.02	1275.6	1.87	1.91	1.91	139399.2	88.6
1452	3.55	3.66	1.0	71794.1	2.25	2.29	0.02	1523.4	1.86	1.92	1.94	139074.0	89.9
1685	3.55	3.66	1.0	72632.8	2.26	2.29	0.01	952.9	1.86	1.91	1.92	139659.0	89.3
1935	3.55	3.66	1.0	72677.1	2.26	2.29	0.01	762.6	1.87	1.92	1.93	140110.2	89.5

Table 4.16. Raw data of absolute kinetic of acylation reaction with **4a** in $CDCl_3$.

Time (min)	**Integ. limits (ppm)**		**Integ.**	**Absol.**	**Integ. Limits (ppm)**		**Integ.**	**Absol.**	**Integ. Limits (ppm)**		**Integ.**	**Absol.**	**$Yield_{ester}$ (%)**
VB127a	**Standard**				**Educt**				**Product**				
10	3.64	3.72	1.0	93061.1	2.35	2.39	0.45	41911.1	1.95	1.97	0.22	20747.4	10.3
25	3.64	3.71	1.0	81723.6	2.34	2.38	0.40	32893.9	1.94	1.97	0.46	37640.3	21.2
41	3.62	3.72	1.0	89029.3	2.34	2.38	0.33	29186.9	1.94	1.97	0.58	52001.2	26.9
59	3.63	3.70	1.0	81891.1	2.34	2.37	0.30	24617.8	1.94	1.97	0.73	59826.3	33.6
74	3.66	3.72	1.0	91729.9	2.36	2.39	0.28	25864.3	1.95	1.99	0.83	75708.3	38.0
83	3.65	3.69	1.0	91595.7	2.33	2.36	0.28	25367.4	1.93	1.97	0.88	80568.7	40.5
101	3.64	3.69	1.0	81473.6	2.33	2.36	0.25	20506.6	1.93	1.97	0.95	77692.9	43.9
116	3.64	3.70	1.0	83572.4	2.33	2.36	0.23	19364.7	1.93	1.97	1.00	83904.6	46.2
128	3.64	3.69	1.0	82637.9	2.33	2.36	0.23	18789.9	1.93	1.97	1.04	86306.5	48.1
190	3.64	3.69	1.0	82525.4	2.33	2.36	0.19	15332.0	1.93	1.96	1.21	99942.7	55.7
250	3.64	3.69	1.0	82294.7	2.33	2.35	0.15	12536.8	1.92	1.96	1.33	109532.8	61.3
307	3.63	3.69	1.0	87061.2	2.33	2.35	0.13	11396.7	1.92	1.96	1.40	122112.0	64.6
368	3.63	3.69	1.0	85993.4	2.32	2.35	0.12	10220.7	1.92	1.96	1.48	127133.2	68.0
428	3.63	3.69	1.0	85559.8	2.32	2.35	0.10	8762.1	1.92	1.96	1.52	130254.7	70.1
490	3.64	3.68	1.0	84580.7	2.32	2.35	0.10	8165.9	1.92	1.96	1.61	135835.4	73.9

552	3.63	3.68	1.0	82847.6	2.32	2.34	0.08	6970.3	1.91	1.96	1.64	136208.9	75.7
608	3.64	3.68	1.0	82793.6	2.32	2.34	0.08	6306.6	1.92	1.96	1.66	137842.4	76.6
669	3.62	3.69	1.0	79636.6	2.32	2.34	0.06	5131.5	1.91	1.96	1.72	136941.6	79.1
728	3.63	3.68	1.0	82989.7	2.32	2.34	0.07	5420.9	1.92	1.96	1.73	143599.9	79.6
848	3.63	3.68	1.0	82164.7	2.32	2.34	0.05	4281.8	1.92	1.96	1.77	145806.3	81.7
968	3.63	3.68	1.0	85962.4	2.32	2.34	0.04	3736.2	1.91	1.96	1.82	156084.7	83.6
1096	3.63	3.68	1.0	86882.0	2.32	2.34	0.03	3026.1	1.91	1.96	1.84	159779.2	84.6
1209	3.64	3.68	1.0	86719.8	2.32	2.33	0.03	2521.6	1.91	1.96	1.87	162374.5	86.2
1332	3.63	3.68	1.0	88722.0	2.32	2.33	0.02	2188.8	1.92	1.96	1.88	166223.1	86.2
1450	3.63	3.68	1.0	89093.3	2.32	2.33	0.02	1895.7	1.91	1.96	1.90	169696.8	87.7
1690	3.63	3.67	1.0	86540.7	2.32	2.34	0.02	1427.1	1.92	1.95	1.91	165385.2	88.0
1933	3.63	3.68	1.0	86673.3	2.32	2.34	0.01	1070.4	1.91	1.95	1.94	167728.6	89.1
2177	3.63	3.68	1.0	86275.2	2.32	2.33	0.01	726.5	1.91	1.96	1.95	168552.0	89.9
2420	3.63	3.68	1.0	83900.4	2.32	2.33	0.01	486.3	1.92	1.96	1.95	163256.5	89.6
2654	3.63	3.67	1.0	82438.7	2.32	2.33	0.00	380.7	1.91	1.95	1.96	161933.5	90.4
VB127b	**Standard**				**Educt**				**Product**				**Yield (%)**
7	3.61	3.68	1.0	68573.1	2.31	2.35	0.49	33583.9	1.92	1.94	0.19	12824.8	8.49
14	3.62	3.68	1.0	68215.2	2.31	2.34	0.47	31873.9	1.91	1.94	0.34	22876.2	15.2
51	3.62	3.66	1.0	68136.5	2.30	2.32	0.35	23829.1	1.90	1.93	0.77	52258.9	34.8
60	3.61	3.66	1.0	65697.9	2.29	2.32	0.33	21538.7	1.90	1.93	0.83	54604.1	37.7
81	3.61	3.66	1.0	67984.6	2.29	2.32	0.27	18266.4	1.89	1.93	0.99	67455.1	45.1
92	3.60	3.66	1.0	69799.7	2.29	2.31	0.25	17588.5	1.89	1.93	1.04	72696.4	47.3
106	3.61	3.66	1.0	68368.1	2.28	2.31	0.24	16210.0	1.89	1.93	1.11	76189.8	50.6
122	3.61	3.65	1.0	68253.1	2.28	2.31	0.22	15194.4	1.89	1.93	1.19	81020.3	53.9
137	3.60	3.65	1.0	68750.7	2.29	2.31	0.20	14010.5	1.89	1.93	1.24	85022.7	56.2
172	3.61	3.65	1.0	68739.0	2.28	2.31	0.17	11952.3	1.89	1.93	1.35	92883.3	61.4
199	3.61	3.65	1.0	68575.9	2.28	2.31	0.16	10869.3	1.89	1.93	1.41	96569.1	63.9
250	3.60	3.65	1.0	67708.5	2.28	2.30	0.12	8383.9	1.88	1.92	1.50	101719.3	68.2
309	3.60	3.65	1.0	70522.8	2.28	2.30	0.11	7544.0	1.88	1.92	1.61	113618.1	73.2
374	3.60	3.65	1.0	68451.4	2.27	2.30	0.09	5930.7	1.88	1.92	1.68	115076.6	76.3
433	3.60	3.64	1.0	67390.2	2.27	2.29	0.07	4999.4	1.88	1.92	1.73	116514.0	78.5
489	3.60	3.64	1.0	66644.0	2.27	2.29	0.05	3541.3	1.88	1.92	1.79	119512.7	81.4
549	3.59	3.64	1.0	68087.2	2.28	2.29	0.05	3504.2	1.88	1.92	1.80	122616.7	81.8
608	3.59	3.64	1.0	68243.4	2.27	2.29	0.05	3171.4	1.87	1.92	1.85	126089.9	83.9
669	3.59	3.64	1.0	69763.6	2.27	2.29	0.04	2893.9	1.88	1.92	1.86	129766.7	84.5
728	3.59	3.64	1.0	69767.6	2.27	2.29	0.03	2363.4	1.88	1.92	1.87	130279.6	84.8
850	3.59	3.64	1.0	66769.6	2.27	2.29	0.03	1922.4	1.87	1.92	1.91	127414.2	86.7
976	3.59	3.64	1.0	68716.9	2.27	2.29	0.02	1313.3	1.88	1.92	1.93	132922.3	87.8
1093	3.59	3.64	1.0	65325.1	2.27	2.29	0.02	1217.2	1.87	1.91	1.92	125723.7	87.4
1210	3.59	3.63	1.0	66873.9	2.27	2.29	0.01	760.2	1.88	1.91	1.93	129308.1	87.8

1332	3.59	3.63	1.0	67961.9	2.27	2.29	0.01	665.5	1.87	1.91	1.94	131745.0	88.0
1456	3.59	3.63	1.0	68274.2	2.27	2.28	0.01	496.1	1.87	1.92	1.98	134925.9	89.7
1691	3.59	3.63	1.0	68305.9	2.27	2.29	0.01	423.3	1.87	1.91	1.97	134418.6	89.4
1934	3.59	3.63	1.0	68672.8	2.27	2.28	0.00	190.9	1.87	1.91	1.97	135292.6	89.5
2175	3.59	3.63	1.0	69977.1	2.27	2.28	0.00	133.8	1.87	1.91	1.97	137886.4	89.5

Table 4.17. Raw data of absolute kinetic of acylation reaction with **6a** in $CDCl_3$.

Time (min)	**Integ. limits (ppm)**		**Integ.**	**Absol.**	**Integ. Limits (ppm)**		**Integ.**	**Absol.**	**Integ. Limits (ppm)**		**Integ.**	**Absol.**	**$Yield_{ester}$ (%)**
VB128a	**Standard**				**Educt**				**Product**				
6	3.64	3.72	1.0	83831.0	2.34	2.38	0.44	37040.9	1.95	1.98	0.32	26598.5	14.6
24	3.64	3.70	1.0	83042.0	2.34	2.37	0.31	26116.2	1.93	1.97	0.73	61004.2	33.8
32	3.64	3.70	1.0	82836.5	2.33	2.36	0.28	23414.9	1.93	1.97	0.86	71414.4	39.7
52	3.64	3.69	1.0	82862.6	2.33	2.36	0.23	19106.1	1.93	1.97	1.08	89721.5	49.8
66	3.64	3.69	1.0	83743.4	2.32	2.36	0.20	16909.2	1.93	1.97	1.17	98279.1	54.0
84	3.63	3.70	1.0	84311.3	2.32	2.35	0.17	14637.9	1.92	1.96	1.28	107561.4	58.7
100	3.63	3.69	1.0	83147.9	2.32	2.35	0.15	12871.1	1.92	1.96	1.37	113513.5	62.8
107	3.64	3.69	1.0	83884.1	2.32	2.35	0.15	12698.9	1.92	1.96	1.39	117018.3	64.2
131	3.63	3.68	1.0	85361.7	2.31	2.35	0.13	11265.2	1.92	1.96	1.47	125815.5	67.8
187	3.63	3.69	1.0	87845.4	2.32	2.35	0.09	8114.6	1.92	1.96	1.61	141282.7	74.0
250	3.63	3.69	1.0	86876.2	2.32	2.34	0.07	5912.3	1.91	1.96	1.72	149576.8	79.2
307	3.63	3.68	1.0	85750.7	2.32	2.34	0.05	4477.7	1.92	1.96	1.77	151499.0	81.3
376	3.63	3.68	1.0	84063.3	2.31	2.34	0.04	3348.6	1.91	1.96	1.84	154869.9	84.8
428	3.62	3.69	1.0	84648.0	2.31	2.34	0.03	2719.7	1.92	1.96	1.84	155772.9	84.7
491	3.63	3.68	1.0	94863.3	2.32	2.34	0.03	2375.1	1.91	1.96	1.88	178034.9	86.4
552	3.63	3.68	1.0	84243.7	2.31	2.34	0.02	1757.6	1.91	1.96	1.90	160335.9	87.6
607	3.63	3.68	1.0	83273.3	2.32	2.34	0.02	1317.3	1.92	1.95	1.90	158046.2	87.4
668	3.63	3.69	1.0	83589.2	2.32	2.33	0.01	1012.1	1.91	1.95	1.90	158881.2	87.5
727	3.62	3.68	1.0	87362.1	2.32	2.33	0.01	820.8	1.91	1.95	1.92	167406.1	88.2
848	3.62	3.68	1.0	88650.1	2.32	2.33	0.01	679.3	1.91	1.95	1.93	171450.6	89.0
968	3.66	3.72	1.0	89296.9	2.36	2.37	0.00	392.7	1.95	1.99	1.93	172059.5	88.7
1089	3.63	3.68	1.0	88021.2	2.32	2.33	0.00	208.1	1.91	1.96	1.96	172103.9	90.0
1211	3.63	3.68	1.0	90797.4	2.32	2.33	0.00	152.8	1.91	1.95	1.95	176616.3	89.5
1330	3.61	3.69	1.0	92344.7	–	–	–	–	1.91	1.96	1.93	177922.3	88.7
1458	3.63	3.68	1.0	87653.7	–	–	–	–	1.91	1.96	1.96	171716.4	90.2
VB128b	**Standard**				**Educt**				**Product**				**Yield (%)**
6	3.62	3.68	1.0	66526.9	2.31	2.34	0.46	30544.6	1.92	1.94	0.33	22162.9	15.1
17	3.61	3.67	1.0	67937.8	2.30	2.33	0.39	26529.1	1.91	1.94	0.67	45812.7	30.6

27	3.61	3.67	1.0	68484.5	2.29	2.32	0.30	20854.8	1.90	1.93	0.88	60448.8	40.1
46	3.61	3.66	1.0	69802.8	2.29	2.31	0.23	15710.6	1.89	1.93	1.16	80849.2	52.6
57	3.60	3.65	1.0	70390.2	2.29	2.31	0.19	13675.2	1.89	1.93	1.27	89661.7	57.8
73	3.61	3.65	1.0	69967.8	2.28	2.31	0.17	11567.9	1.89	1.93	1.40	97626.7	63.4
87	3.60	3.65	1.0	70154.3	2.28	2.30	0.14	10094.2	1.89	1.92	1.47	102991.2	66.7
105	3.60	3.65	1.0	70329.6	2.28	2.30	0.12	8638.2	1.88	1.92	1.56	109519.6	70.7
114	3.60	3.65	1.0	69388.0	2.27	2.30	0.11	7880.1	1.89	1.92	1.58	109807.3	71.9
127	3.60	3.65	1.0	70460.6	2.28	2.30	0.10	7120.0	1.88	1.92	1.62	113840.0	73.4
189	3.60	3.64	1.0	70719.2	2.28	2.29	0.06	4156.5	1.88	1.92	1.74	123266.4	79.2
249	3.59	3.64	1.0	69265.1	2.27	2.29	0.04	2931.0	1.88	1.92	1.82	126343.8	82.8
309	3.59	3.64	1.0	68434.8	2.27	2.29	0.03	1906.4	1.88	1.92	1.86	127389.6	84.5
370	3.59	3.64	1.0	69397.7	2.27	2.29	0.02	1322.6	1.88	1.91	1.88	130425.9	85.3
434	3.58	3.64	1.0	69489.2	2.27	2.29	0.01	771.8	1.88	1.91	1.89	130997.6	85.6
492	3.59	3.64	1.0	68909.4	2.27	2.29	0.01	592.3	1.88	1.91	1.89	130421.8	85.9
555	3.58	3.64	1.0	68828.0	2.27	2.29	0.01	644.5	1.88	1.92	1.91	131359.4	86.7
609	3.58	3.64	1.0	71277.1	2.27	2.29	0.01	480.8	1.87	1.92	1.94	138232.3	88.1
679	3.59	3.63	1.0	68826.5	2.26	2.29	0.01	760.4	1.88	1.91	1.92	132465.9	87.4
739	3.58	3.64	1.0	69025.9	2.27	2.30	0.01	469.2	1.88	1.91	1.90	130968.0	86.2
849	3.59	3.64	1.0	68926.4	2.25	2.29	0.01	563.8	1.87	1.91	1.92	132276.3	87.1
975	3.59	3.63	1.0	68782.8	2.26	2.30	0.01	494.9	1.87	1.91	1.93	132875.6	87.7
1089	3.58	3.64	1.0	71561.3	2.27	2.30	0.00	314.1	1.87	1.91	1.93	137930.2	87.5
1216	3.59	3.64	1.0	67140.1	2.26	2.29	0.01	673.0	1.87	1.91	1.94	130222.7	88.1
1331	3.58	3.64	1.0	64869.5	2.26	2.30	0.01	652.5	1.87	1.92	1.96	127049.4	88.9
1448	3.58	3.64	1.0	67547.6	2.27	2.29	0.00	243.8	1.87	1.91	1.92	129888.4	87.3

4.4.4 Simulation of Kinetic Experiments – Acylation with Different Auxiliary Bases

Kinetic measurements performed with different auxiliary bases were prepared and analyzed according to the procedure described in Chapter 4.3.2 and Chapter 4.3.3. The resulting effective reaction rates k_{eff} and half-life times $t_{1/2}$ (min) are summarized in Table 4.18.

Table 4.18. Effective reaction rates k_{eff} (M^{-1} s^{-1}) and half-life times $t_{1/2}$ (min)for the acylation of 1-ethynylcyclohexanol **16** with acetic anhydride **17** and various auxiliary bases in $CDCl_3$.

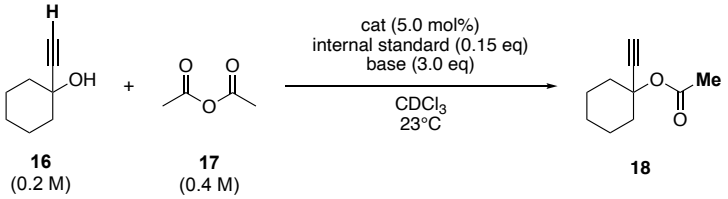

Catalyst	Base	k_{eff} (M^{-1} s^{-1})	Average k_{eff} (M^{-1} s^{-1})	$t_{1/2}$ (s)	$t_{1/2}$ (min)	Average $t_{1/2}$ (min)
5a	NEt_3	1.62×10^{-2}	$1.38 \times 10^{-2} \pm 2.37 \times 10^{-3}$	5975	100	116 ± 16.6
		1.15×10^{-2}		7961	133	
	NPr_3	1.21×10^{-2}	$1.30 \times 10^{-2} \pm 9.22 \times 10^{-4}$	7632	127	119 ± 8.12
		1.39×10^{-2}		6658	111	
	DIPEA	1.32×10^{-2}	–	6993	117	–
	Proton Sponge	1.27×10^{-3}	–	77800	1297	–
6a	NEt_3	3.09×10^{-2}	$3.70 \times 10^{-2} \pm 6.00 \times 10^{-3}$	3384	56	50.2 ± 6.22
		4.29×10^{-2}		2638	44	
	NPr_3	3.24×10^{-2}	$3.37 \times 10^{-2} \pm 1.25 \times 10^{-3}$	3128	52.1	51.9 ± 0.27
		3.49×10^{-2}		3096	51.6	

The raw data sets of the kinetic measurements are summarized in Table 4.19 – Table 4.22.

Table 4.19. Raw data of absolute kinetic of acylation reaction with **5a** with *tri*-propylamine (NPr_3) in $CDCl_3$.

Time (min)	Integ. limits (ppm)		Integ.	Absol.	Integ. limits (ppm)		Integ.	Absol.	Integ. limits (ppm)		Integ.	Absol.	$Yield_{ester}$ (%)
VB210a	**Standard**				**Educt (overlap with base)**				**Product**				
5	3.62	3.72	1.0	57016	–	–	–	–	1.94	1.97	0.20	11161	9.09
26	3.61	3.70	1.0	57130	–	–	–	–	1.93	1.97	0.52	29684	24.1
42	3.61	3.71	1.0	56274	–	–	–	–	1.92	1.97	0.67	37695	31.1
72	3.61	3.71	1.0	56915	–	–	–	–	1.91	1.96	0.87	49513	40.4
102	3.60	3.71	1.0	56475	–	–	–	–	1.90	1.96	1.02	57726	47.5
136	3.60	3.70	1.0	55474	–	–	–	–	1.90	1.96	1.15	63552	53.2
196	3.61	3.68	1.0	54741	–	–	–	–	1.90	1.96	1.30	71162	60.4
251	3.60	3.69	1.0	54721	–	–	–	–	1.90	1.96	1.40	76742	65.1
314	3.61	3.68	1.0	52881	–	–	–	–	1.90	1.95	1.51	79819	70.1
374	3.60	3.68	1.0	52332	–	–	–	–	1.90	1.95	1.57	82394	73.1
434	3.60	3.69	1.0	54294	–	–	–	–	1.90	1.95	1.64	88825	76.0
506	3.60	3.68	1.0	56076	–	–	–	–	1.89	1.95	1.71	96046	79.6
558	3.60	3.68	1.0	55506	–	–	–	–	1.88	1.95	1.75	96867	81.1
620	3.59	3.69	1.0	55468	–	–	–	–	1.89	1.94	1.75	97184	81.4
680	3.60	3.68	1.0	55106	–	–	–	–	1.90	1.95	1.79	98757	83.3
741	3.59	3.69	1.0	55422	–	–	–	–	1.89	1.95	1.81	100367	84.1
852	3.60	3.68	1.0	55608	–	–	–	–	1.88	1.95	1.89	105094	87.8
972	3.60	3.68	1.0	56522	–	–	–	–	1.89	1.95	1.89	106984	87.9
1093	3.60	3.68	1.0	56464	–	–	–	–	1.88	1.94	1.91	107756	88.7
1214	3.59	3.68	1.0	57182	–	–	–	–	1.88	1.94	1.91	108996	88.5

1337	3.60	3.68	1.0	55644	–	–	–	–	1.89	1.94	1.92	106883	89.2
1455	3.61	3.68	1.0	57463	–	–	–	–	1.88	1.94	1.95	111974	90.5
1575	3.60	3.67	1.0	59499	–	–	–	–	1.89	1.94	1.94	115231	90.0
1706	3.60	3.67	1.0	54582	–	–	–	–	1.88	1.94	1.97	107426	91.4
3136	3.60	3.68	1.0	56412	–	–	–	–	1.89	1.94	1.97	111338	91.7
4578	3.59	3.68	1.0	58659	–	–	–	–	1.88	1.93	1.96	114946	91.0
6026	3.59	3.66	1.0	54723	–	–	–	–	1.88	1.93	1.97	107912	91.6
7464	3.59	3.67	1.0	58188	–	–	–	–	1.87	1.94	2.01	116733	93.2
VB210b	**Standard**				**Educt (overlap with base)**				**Product**				**Yield (%)**
5	3.61	3.72	1.0	55347	–	–	–	–	1.94	1.97	0.23	12610	10.6
27	3.61	3.72	1.0	54704	–	–	–	–	1.92	1.98	0.55	30322	25.7
47	3.60	3.70	1.0	54158	–	–	–	–	1.91	1.97	0.75	40364	34.6
68	3.60	3.70	1.0	53650	–	–	–	–	1.91	1.97	0.88	47113	40.8
80	3.60	3.70	1.0	53529	–	–	–	–	1.91	1.96	0.94	50397	43.7
112	3.59	3.72	1.0	60674	–	–	–	–	1.90	1.97	1.10	66490	50.9
172	3.57	3.70	1.0	53877	–	–	–	–	1.90	1.96	1.28	68866	59.4
233	3.60	3.70	1.0	55056	–	–	–	–	1.90	1.96	1.41	77623	65.5
292	3.58	3.70	1.0	56450	–	–	–	–	1.90	1.95	1.50	84508	69.5
353	3.59	3.69	1.0	55932	–	–	–	–	1.90	1.95	1.58	88301	73.3
414	3.59	3.69	1.0	55873	–	–	–	–	1.90	1.95	1.64	91462	76.0
474	3.60	3.69	1.0	55444	–	–	–	–	1.89	1.95	1.72	95268	79.8
536	3.59	3.69	1.0	55834	–	–	–	–	1.88	1.95	1.76	98440	81.9
597	3.59	3.69	1.0	55887	–	–	–	–	1.88	1.95	1.81	101135	84.1
657	3.59	3.69	1.0	55900	–	–	–	–	1.88	1.95	1.85	103269	85.8
725	3.60	3.68	1.0	56524	–	–	–	–	1.89	1.94	1.83	103575	85.1
840	3.60	3.68	1.0	56658	–	–	–	–	1.88	1.94	1.88	106293	87.1
952	3.60	3.67	1.0	51637	–	–	–	–	1.88	1.95	1.93	99782	89.8
1088	3.60	3.68	1.0	55610	–	–	–	–	1.88	1.94	1.92	106869	89.3
1203	3.59	3.68	1.0	57453	–	–	–	–	1.89	1.94	1.92	110117	89.0
1325	3.59	3.68	1.0	59501	–	–	–	–	1.89	1.94	1.92	114526	89.4
1457	3.60	3.67	1.0	55354	–	–	–	–	1.88	1.94	1.97	108874	91.4
1570	3.59	3.68	1.0	55343	–	–	–	–	1.89	1.94	1.95	107743	90.4
1687	3.59	3.68	1.0	55874	–	–	–	–	1.88	1.94	1.96	109786	91.3
3127	3.58	3.68	1.0	59633	–	–	–	–	1.89	1.94	1.95	116390	90.7
4570	3.59	3.68	1.0	58562	–	–	–	–	1.88	1.94	1.98	116095	92.1
6010	3.59	3.67	1.0	59229	–	–	–	–	1.88	1.93	1.97	116543	91.4
7451	3.58	3.67	1.0	60124	–	–	–	–	1.88	1.93	1.99	119887	92.6

Table 4.20. Raw data of absolute kinetic of acylation reaction with **5a** with DIEPA in $CDCl_3$.

Time (min)	Integ. limits (ppm)		Integ.	Absol.	Integ. limits (ppm)		Integ.	Absol.	Integ. limits (ppm)		Integ.	Absol.	$Yield_{ester}$ (%)
VB219	**Standard**				**Educt**				**Product**				
14	3.63	3.72	1.0	52419	2.35	2.39	0.44	22979	1.93	1.98	0.45	23396	18.9
23	3.61	3.71	1.0	52982	2.34	2.38	0.39	20630	1.93	1.98	0.56	29643	23.7
47	3.60	3.71	1.0	51123	2.33	2.38	0.33	17105	1.92	1.97	0.85	43554	36.1
68	3.60	3.72	1.0	53488	2.32	2.38	0.30	15906	1.92	1.97	0.96	51288	40.6
103	3.60	3.71	1.0	53303	2.31	2.37	0.28	14829	1.91	1.97	1.14	60783	48.3
129	3.61	3.70	1.0	54728	2.31	2.37	0.25	13902	1.91	1.96	1.27	69267	53.6
191	3.60	3.70	1.0	55664	2.32	2.35	0.19	10352	1.90	1.96	1.45	80758	61.5
251	3.61	3.69	1.0	54220	2.31	2.35	0.16	8934	1.90	1.96	1.60	86572	67.6
313	3.60	3.69	1.0	52951	2.31	2.35	0.15	7730	1.90	1.95	1.66	87822	70.3
374	3.60	3.69	1.0	54919	2.30	2.34	0.12	6617	1.90	1.96	1.74	95413	73.6
426	3.58	3.70	1.0	55174	2.31	2.34	0.11	6023	1.90	1.95	1.81	99750	76.6
485	3.61	3.68	1.0	54701	2.31	2.34	0.09	4802	1.90	1.95	1.87	102062	79.1
546	3.60	3.69	1.0	55246	2.30	2.33	0.08	4363	1.89	1.95	1.90	104841	80.4
609	3.59	3.69	1.0	55120	2.30	2.33	0.06	3531	1.89	1.95	1.94	107197	82.4
669	3.59	3.68	1.0	53853	2.31	2.33	0.05	2915	1.89	1.95	1.97	106088	83.5
733	3.60	3.69	1.0	56583	2.30	2.33	0.06	3258	1.88	1.94	2.01	113577	85.0
851	3.59	3.68	1.0	57311	2.30	2.32	0.04	2155	1.88	1.95	2.07	118608	87.7
969	3.58	3.68	1.0	54914	2.29	2.33	0.04	1956	1.89	1.95	2.06	112935	87.1
1086	3.57	3.68	1.0	54985	2.30	2.33	0.03	1470	1.89	1.95	2.08	114425	88.2
1204	3.60	3.68	1.0	53518	2.34	2.37	0.04	1955	1.89	1.95	2.13	114214	90.4
1329	3.58	3.70	1.0	55286	2.30	2.33	0.02	1078	1.90	1.95	2.09	115779	88.7
1445	3.58	3.71	1.0	54533	2.30	2.33	0.02	984	1.88	1.95	2.16	117545	91.3
1567	3.56	3.70	1.0	56262	2.30	2.33	0.02	858	1.89	1.95	2.15	120983	91.1
1808	3.58	3.68	1.0	54484	2.30	2.33	0.01	643	1.88	1.95	2.18	118552	92.2
2163	3.58	3.70	1.0	55157	2.29	2.32	0.01	409	1.88	1.94	2.17	119667	91.9
3249	3.57	3.69	1.0	54571	2.30	2.33	0.00	269	1.89	1.94	2.16	117605	91.3
3604	3.57	3.69	1.0	54987	2.29	2.33	0.01	407	1.89	1.95	2.18	119781	92.3
5044	3.58	3.68	1.0	55929	2.28	2.32	0.01	619	1.88	1.94	2.20	122968	93.2

Table 4.21. Raw data of absolute kinetic of acylation reaction with **5a** with 1,8-bis(hexa-methyltriaminophosphazenyl)naphthalene (proton sponge) in $CDCl_3$.

Time (min)	Integ. limits (ppm)		Integ.	Absol.	Integ. limits (ppm)		Integ.	Absol.	Integ. limits (ppm)		Integ.	Absol.	$Yield_{ester}$ (%)
VB237	**Standard**				**Educt**				**Product**				

6	3.49	3.71	1.0	86953	2.27	2.35	0.32	27939	1.90	1.95	0.27	23112	11.4
13	3.54	3.65	1.0	63413	2.29	2.34	0.40	25148	1.90	1.95	0.41	25921	17.6
28	3.54	3.66	1.0	63368	2.29	2.34	0.38	24010	1.90	1.95	0.40	25059	17.0
43	3.56	3.65	1.0	61473	2.29	2.33	0.38	23509	1.90	1.94	0.42	25862	18.1
58	3.56	3.66	1.0	61297	2.28	2.34	0.40	24361	1.91	1.95	0.44	27191	19.1
88	3.55	3.66	1.0	61913	2.29	2.34	0.38	23610	1.91	1.95	0.46	28676	19.9
118	3.56	3.65	1.0	61755	2.29	2.34	0.39	24223	1.91	1.95	0.51	31644	22.0
181	3.54	3.65	1.0	61558	2.29	2.33	0.38	23121	1.91	1.95	0.58	35866	25.0
241	3.54	3.65	1.0	60151	2.30	2.33	0.37	22326	1.91	1.95	0.61	36675	26.2
301	3.55	3.65	1.0	59265	2.29	2.33	0.38	22418	1.91	1.96	0.66	38881	28.2
364	3.56	3.64	1.0	56333	2.29	2.32	0.37	20824	1.92	1.96	0.71	39745	30.3
422	3.52	3.68	1.0	55565	2.29	2.33	0.34	18779	1.91	1.95	0.76	42152	32.6
488	3.53	3.67	1.0	63042	2.29	2.33	0.38	23704	1.91	1.96	0.76	47945	32.7
544	3.55	3.65	1.0	61818	2.29	2.33	0.39	24264	1.91	1.96	0.79	48971	34.1
605	3.55	3.65	1.0	61050	2.29	2.33	0.39	24081	1.91	1.96	0.86	52532	37.0
670	3.55	3.65	1.0	55587	2.29	2.32	0.36	20229	1.91	1.96	0.87	48309	37.4
724	3.56	3.65	1.0	63102	2.30	2.33	0.33	20732	1.92	1.96	0.87	54979	37.5
845	3.52	3.67	1.0	63320	2.29	2.33	0.38	23895	1.91	1.96	0.93	59129	40.1
966	3.53	3.66	1.0	55842	2.29	2.33	0.37	20842	1.92	1.96	0.96	53709	41.3
1090	3.56	3.64	1.0	60227	2.28	2.33	0.40	23798	1.92	1.96	1.03	61837	44.1
1198	3.55	3.65	1.0	59828	2.28	2.33	0.39	23322	1.92	1.96	1.05	62973	45.2
1353	3.79	3.85	1.0	61610	2.50	2.55	0.39	23725	2.14	2.18	1.13	69682	48.6
1443	3.79	3.85	1.0	60410	2.50	2.55	0.37	22557	2.14	2.18	1.16	70008	49.8
1567	3.58	3.67	1.0	61325	2.30	2.36	0.36	22109	1.94	1.98	1.18	72306	50.7
1805	3.58	3.67	1.0	60015	2.30	2.36	0.35	20716	1.94	1.98	1.26	75844	54.3
2046	3.58	3.67	1.0	59430	2.30	2.36	0.33	19755	1.94	1.98	1.36	80742	58.4
2286	3.58	3.67	1.0	62178	2.30	2.36	0.32	19642	1.94	1.98	1.37	85180	58.9
2530	3.58	3.67	1.0	62356	2.30	2.36	0.30	18928	1.94	1.98	1.43	89092	61.4
2769	3.78	3.86	1.0	57442	2.50	2.53	0.24	13708	2.13	2.17	1.47	84492	63.2
3010	3.78	3.86	1.0	55261	2.50	2.54	0.24	13321	2.14	2.18	1.49	82458	64.1
3252	3.58	3.67	1.0	62041	2.30	2.36	0.28	17153	1.94	1.98	1.57	97518	67.6
3493	3.58	3.67	1.0	61685	2.30	2.36	0.27	16550	1.94	1.98	1.61	99115	69.1
3732	3.58	3.67	1.0	62160	2.30	2.36	0.25	15820	1.94	1.98	1.65	102448	70.8
4081	3.58	3.67	1.0	61840	2.30	2.36	0.24	15142	1.94	1.98	1.71	105623	73.4
4441	3.58	3.67	1.0	62136	2.30	2.36	0.23	14088	1.94	1.98	1.76	109149	75.5
4801	3.58	3.67	1.0	56163	2.30	2.36	0.20	11506	1.94	1.98	1.80	101331	77.6
5167	3.58	3.67	1.0	61405	2.30	2.36	0.19	11412	1.94	1.98	1.85	113490	79.4
5528	3.58	3.67	1.0	62739	2.30	2.36	0.17	10488	1.94	1.98	1.89	118520	81.2
5889	3.58	3.67	1.0	55044	2.30	2.36	0.16	8571	1.94	1.98	1.92	105602	82.5
6609	3.58	3.67	1.0	61647	2.30	2.36	0.14	8757	1.94	1.98	2.00	123571	86.2

7331	3.58	3.67	1.0	63978	2.30	2.36	0.13	8032	1.94	1.98	2.06	131693	88.5
8038	3.58	3.66	1.0	62134	2.30	2.34	0.12	7324	1.94	1.98	2.09	129561	89.6

Table 4.22. Raw data of absolute kinetic of acylation reaction with **6a** with *tri*-propylamine (NPr_3) in $CDCl_3$.

Time (min)	**Integ. limits (ppm)**		**Integ.**	**Absol.**	**Integ. limits (ppm)**		**Integ.**	**Absol.**	**Integ. limits (ppm)**		**Integ.**	**Absol.**	**$Yield_{ester}$ (%)**
VB211a	**Standard**				**Educt (overlap with base)**				**Product**				
7	3.59	3.73	1.0	56461	–	–	–	–	1.92	1.97	0.41	23168	19.1
30	3.60	3.70	1.0	56817	–	–	–	–	1.91	1.96	0.87	49613	40.6
50	3.60	3.70	1.0	54408	–	–	–	–	1.90	1.96	1.11	60252	51.4
68	3.60	3.70	1.0	51740	–	–	–	–	1.91	1.95	1.24	64072	57.5
100	3.61	3.69	1.0	54723	–	–	–	–	1.90	1.95	1.43	78130	66.3
130	3.60	3.68	1.0	54726	–	–	–	–	1.89	1.95	1.55	84893	72.1
201	3.61	3.68	1.0	56547	–	–	–	–	1.89	1.95	1.72	97243	79.9
258	3.60	3.68	1.0	57452	–	–	–	–	1.89	1.95	1.80	103472	83.7
315	3.60	3.68	1.0	58951	–	–	–	–	1.88	1.94	1.85	108791	85.7
378	3.59	3.69	1.0	59182	–	–	–	–	1.89	1.94	1.88	111088	87.2
449	3.59	3.67	1.0	54830	–	–	–	–	1.89	1.94	1.91	104801	88.8
509	3.58	3.67	1.0	54795	–	–	–	–	1.88	1.94	1.95	106913	90.6
559	3.60	3.67	1.0	54521	–	–	–	–	1.88	1.94	1.96	106834	91.0
618	3.59	3.67	1.0	54870	–	–	–	–	1.89	1.94	1.95	107263	90.8
729	3.64	3.74	1.0	55447	–	–	–	–	1.94	2.00	1.98	109851	92.0
851	3.58	3.68	1.0	59221	–	–	–	–	1.88	1.94	1.98	117150	91.9
971	3.60	3.68	1.0	58016	–	–	–	–	1.87	1.93	2.02	116958	93.6
1094	3.59	3.68	1.0	54221	–	–	–	–	1.89	1.93	1.97	106796	91.5
1213	3.59	3.67	1.0	60327	–	–	–	–	1.88	1.94	2.00	120723	93.0
1336	3.58	3.67	1.0	54530	–	–	–	–	1.88	1.93	1.99	108273	92.2
1450	3.59	3.67	1.0	55746	–	–	–	–	1.89	1.94	1.97	109994	91.7
1571	3.60	3.67	1.0	53973	–	–	–	–	1.88	1.94	2.00	108057	93.0
VB211b	**Standard**				**Educt (overlap with base)**				**Product**				**Yield (%)**
9	3.60	3.72	1.0	56599	–	–	–	–	1.93	1.97	0.48	27217	22.7
28	3.62	3.69	1.0	56143	–	–	–	–	1.92	1.96	0.83	46863	39.4
54	3.60	3.70	1.0	56326	–	–	–	–	1.91	1.96	1.12	62888	52.8
73	3.60	3.69	1.0	56303	–	–	–	–	1.90	1.96	1.27	71500	60.0
109	3.60	3.69	1.0	56593	–	–	–	–	1.90	1.96	1.42	80347	67.1
136	3.61	3.68	1.0	56110	–	–	–	–	1.90	1.96	1.52	85048	71.6
192	3.60	3.69	1.0	56539	–	–	–	–	1.88	1.95	1.67	94193	78.7
250	3.58	3.69	1.0	57185	–	–	–	–	1.89	1.95	1.71	97540	80.6

314	3.59	3.68	1.0	57599	–	–	–	–	1.89	1.95	1.77	101885	83.6
375	3.64	3.72	1.0	60602	–	–	–	–	1.93	2.00	1.82	110278	86.0
435	3.58	3.69	1.0	60476	–	–	–	–	1.88	1.94	1.84	111304	87.0
438	3.60	3.68	1.0	60207	–	–	–	–	1.88	1.94	1.83	110095	86.4
498	3.60	3.68	1.0	60475	–	–	–	–	1.88	1.95	1.87	112948	88.3
559	3.58	3.68	1.0	59845	–	–	–	–	1.88	1.94	1.86	111538	88.1
621	3.60	3.67	1.0	57702	–	–	–	–	1.87	1.94	1.94	112037	91.8
687	3.59	3.68	1.0	56194	–	–	–	–	1.89	1.94	1.87	105079	88.4
739	3.57	3.69	1.0	61911	–	–	–	–	1.88	1.95	1.91	118471	90.4
862	3.58	3.68	1.0	63059	–	–	–	–	1.88	1.94	1.89	118887	89.1
984	3.58	3.68	1.0	57815	–	–	–	–	1.89	1.94	1.86	107752	88.1
1106	3.58	3.68	1.0	62077	–	–	–	–	1.88	1.94	1.89	117024	89.1
1226	3.58	3.68	1.0	56051	–	–	–	–	1.88	1.94	1.89	106052	89.4
1347	3.58	3.68	1.0	62654	–	–	–	–	1.88	1.94	1.89	118161	89.1

4.4.5 Simulation of Kinetic Experiments – Acylation in Different Solvents

Kinetic measurements performed in different deuterated solvents were prepared and analyzed according to the procedure described in Chapter 4.3.2 and Chapter 4.3.3. The resulting effective reaction rates k_{eff} and half-life times $t_{1/2}$ (min) are summarized in Table 4.23.

Table 4.23. Effective reaction rates k_{eff} (M^{-1} s^{-1}) and half-life times $t_{1/2}$ (min) for the acylation of 1-ethynylcyclohexanol **16** with acetic anhydride **17** in $CDCl_3$, DCM-d_2 or MeCN-d_3.

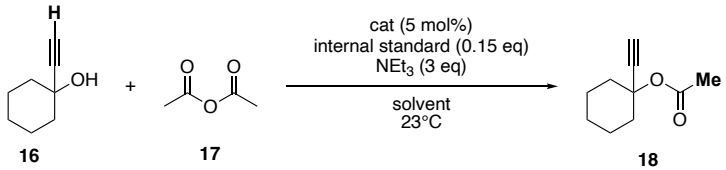

16 17 18

Catalyst	Base	k_{eff} (M^{-1} s^{-1})	Average k_{eff} (M^{-1} s^{-1})	$t_{1/2}$ (s)	$t_{1/2}$ (min)	Average $t_{1/2}$ (min)
1	$CDCl_3$	4.30×10^{-3}	$4.50 \times 10^{-3} \pm 2.00 \times 10^{-4}$	18300	305	296 ± 9.17
		4.70×10^{-3}		17200	287	
	DCM-d_2	2.58×10^{-3}	–	31800	530	–
	MeCN-d_3	1.53×10^{-3}	–	54400	907	–
5a	NEt_3	1.62×10^{-2}	$1.38 \times 10^{-2} \pm 2.37 \times 10^{-3}$	5975	100	116 ± 16.6
		1.15×10^{-2}		7961	133	
	DCM-d_2	7.81×10^{-3}	–	12000	200	–
	MeCN-d_3	7.61×10^{-4}	$7.39 \times 10^{-4} \pm 2.18 \times 10^{-5}$	112000	1867	1925 ± 58.3
		7.17×10^{-4}		119000	1983	

The raw data sets of the kinetic measurements are summarized in Table 4.24 – Table 4.27.

Table 4.24. Raw data of absolute kinetic of acylation reaction with DMAP (**1**) in DCM-d_2.

Time (min)	Integ. limits (ppm)		Integ.	Absol.	Integ. limits (ppm)		Integ.	Absol.	Integ. limits (ppm)		Integ.	Absol.	$Yield_{ester}$ (%)
VB117a	**Standard**				**Educt**				**Product**				
6	3.71	3.75	1.0	65625	–	–	–	–	1.98	2.00	0.03	1834	1.20
21	3.70	3.75	1.0	67683	–	–	–	–	1.98	2.00	0.08	5572	3.52
39	3.70	3.75	1.0	66781	–	–	–	–	1.97	2.00	0.15	10259	6.57
56	3.69	3.77	1.0	67610	–	–	–	–	1.97	2.00	0.21	14142	8.95
73	3.69	3.77	1.0	68258	–	–	–	–	1.96	2.00	0.27	18194	11.4
88	3.69	3.77	1.0	67841	–	–	–	–	1.95	2.00	0.32	21620	13.6
104	3.69	3.76	1.0	67921	–	–	–	–	1.96	2.00	0.37	24966	15.7
119	3.69	3.77	1.0	67876	–	–	–	–	1.96	2.00	0.40	27356	17.2
129	3.69	3.76	1.0	67510	–	–	–	–	1.96	2.00	0.43	28904	18.3
160	3.69	3.77	1.0	67507	2.45	2.47	0.38	25709	1.98	2.00	0.49	32745	20.8
186	3.68	3.77	1.0	68865	2.44	2.46	0.38	26257	1.96	2.00	0.58	39701	24.7
217	3.69	3.77	1.0	67139	2.44	2.47	0.37	24681	1.95	2.00	0.66	44143	28.1
246	3.70	3.77	1.0	65644	2.44	2.47	0.36	23406	1.96	2.00	0.72	47056	30.7
308	3.70	3.76	1.0	66505	2.44	2.47	0.32	21007	1.96	2.00	0.83	55191	35.5
373	3.68	3.76	1.0	70313	2.44	2.46	0.28	19425	1.97	2.00	0.93	65156	39.7
493	3.69	3.76	1.0	69033	2.44	2.46	0.24	16295	1.97	2.00	1.11	76590	47.5
613	3.70	3.75	1.0	68245	2.44	2.46	0.21	14494	1.96	2.00	1.25	85435	53.6
729	3.71	3.74	1.0	67777	2.44	2.46	0.19	12554	1.97	2.00	1.37	92733	58.5
853	3.68	3.76	1.0	69590	2.43	2.46	0.16	11416	1.96	2.00	1.45	100810	62.0
1088	3.71	3.74	1.0	68524	2.43	2.46	0.14	9416	1.96	2.00	1.62	110976	69.3
1331	3.70	3.75	1.0	66458	2.44	2.45	0.09	6267	1.96	2.00	1.76	116920	75.3
1686	3.70	3.74	1.0	67282	2.44	2.45	0.07	4712	1.95	2.00	1.89	126884	80.7
2046	3.70	3.74	1.0	68739	2.44	2.45	0.05	3357	1.96	2.00	1.95	133815	83.3
3487	3.71	3.73	1.0	67523	2.44	2.45	0.02	1410	1.96	1.99	2.12	143361	90.8
5646	3.70	3.74	1.0	65481	2.44	2.45	0.01	365	1.95	2.00	2.19	143434	93.7

Table 4.25. Raw data of absolute kinetic of acylation reaction with **5a** in DCM-d_2.

Time (min)	Integ. limits (ppm)		Integ.	Absol.	Integ. limits (ppm)		Integ.	Absol.	Integ. limits (ppm)		Integ.	Absol.	$Yield_{ester}$ (%)
VB119a	**Standard**				**Educt**				**Product**				
7	3.69	3.77	1.0	69903	–	–	–	–	1.97	2.00	0.13	9165	5.61
9	3.69	3.78	1.0	70368	–	–	–	–	1.97	2.00	0.15	10715	6.52

24	3.68	3.77	1.0	69814	–	–	–	–	1.97	2.00	0.36	24852	15.2
40	3.69	3.77	1.0	68373	–	–	–	–	1.96	2.00	0.49	33201	20.8
43	3.69	3.76	1.0	68069	–	–	–	–	1.97	2.00	0.50	34317	21.6
60	3.68	3.76	1.0	68069	–	–	–	–	1.96	2.00	0.62	41968	26.4
80	3.68	3.76	1.0	69726	–	–	–	–	1.96	2.00	0.74	51555	31.6
92	3.70	3.76	1.0	68725	–	–	–	–	1.96	2.00	0.79	54579	34.0
108	3.69	3.75	1.0	67787	2.43	2.46	0.32	21410	1.96	2.00	0.86	58039	36.6
125	3.70	3.75	1.0	68002	2.43	2.47	0.32	21410	1.96	2.00	0.93	63239	39.8
158	3.69	3.75	1.0	68649	2.43	2.46	0.27	21410	1.96	2.00	1.05	72319	45.1
191	3.69	3.75	1.0	67734	2.44	2.46	0.25	21410	1.96	1.99	1.10	74490	47.1
255	3.70	3.75	1.0	67350	2.42	2.46	0.22	21410	1.95	2.00	1.28	86251	54.8
316	3.69	3.75	1.0	67516	2.43	2.46	0.18	21410	1.96	2.00	1.38	92927	58.9
368	3.67	3.76	1.0	68395	2.44	2.46	0.16	21410	1.95	2.00	1.43	97887	61.2
428	3.69	3.75	1.0	67548	2.43	2.45	0.16	21410	1.95	2.00	1.53	103202	65.4
548	3.70	3.74	1.0	68054	2.43	2.45	0.13	21410	1.95	2.00	1.62	110533	69.5
668	3.69	3.75	1.0	68882	2.43	2.46	0.11	21410	1.96	2.00	1.69	116165	72.2
788	3.70	3.74	1.0	68616	2.44	2.45	0.09	21410	1.96	2.00	1.74	119100	74.3
1148	3.68	3.74	1.0	68888	2.44	2.45	0.06	21410	1.96	2.00	1.86	128229	79.6
1269	3.70	3.74	1.0	68159	2.43	2.45	0.07	21410	1.95	2.00	1.92	130848	82.1
1509	3.68	3.75	1.0	68390	2.43	2.45	0.05	21410	1.94	2.00	1.95	133512	83.5
2235	3.67	3.75	1.0	69193	2.43	2.45	0.04	21410	1.95	2.00	2.02	139468	86.2
4081	3.69	3.74	1.0	68877	2.47	2.48	0.01	21410	1.94	2.00	2.10	144572	89.8

Table 4.26. Raw data of absolute kinetic of acylation reaction with DMAP (**1**) in MeCN-d_3.

Time (min)	**Integ. limits (ppm)**		**Integ.**	**Absol.**	**Integ. limits (ppm)**		**Integ.**	**Absol.**	**Integ. limits (ppm)**		**Integ.**	**Absol.**	**$Yield_{ester}$ (%)**
VB121a	**Standard**				**Educt**				**Product**				
15	3.70	3.76	1.0	67227	2.63	2.68	0.55	36941	1.97	1.99	0.05	3043	2.04
17	3.70	3.76	1.0	67217	2.64	2.68	0.52	35037	1.97	1.99	0.05	3299	2.21
23	3.70	3.77	1.0	67519	2.64	2.68	0.55	37080	1.97	1.98	0.05	3712	2.48
45	3.71	3.76	1.0	67253	2.63	2.68	0.53	35337	1.97	1.99	0.11	7646	5.13
53	3.71	3.76	1.0	67354	2.63	2.67	0.50	33542	1.96	1.99	0.13	8958	6.00
68	3.69	3.76	1.0	67940	2.64	2.67	0.45	30471	1.96	1.99	0.17	11324	7.52
98	3.71	3.76	1.0	67305	2.65	2.66	0.37	24710	1.97	1.98	0.20	13419	8.99
131	3.71	3.75	1.0	66630	2.65	2.66	0.33	22046	1.97	1.99	0.27	17944	12.1
158	3.71	3.76	1.0	67063	2.65	2.66	0.32	21631	1.96	1.99	0.31	20796	14.0
227	3.71	3.75	1.0	66416	2.64	2.66	0.29	19568	1.97	1.99	0.42	27868	18.9
281	3.71	3.76	1.0	66677	2.64	2.66	0.27	18233	1.96	1.99	0.50	33133	22.4

345	3.72	3.75	1.0	67607	2.64	2.66	0.27	18389	1.96	1.99	0.60	40249	26.8
404	3.72	3.75	1.0	67025	2.64	2.67	0.26	17125	1.96	1.99	0.67	44673	30.1
461	3.72	3.75	1.0	65074	2.64	2.67	0.25	16052	1.96	1.99	0.74	48203	33.4
580	3.71	3.76	1.0	67138	2.64	2.66	0.22	14817	1.96	1.99	0.85	57281	38.5
701	3.71	3.75	1.0	67399	2.65	2.66	0.20	13369	1.96	1.99	0.95	64022	42.8
821	3.71	3.75	1.0	68919	2.64	2.66	0.17	11815	1.96	1.99	1.04	71836	47.0
941	3.71	3.76	1.0	68881	2.64	2.66	0.17	11432	1.96	1.99	1.09	74927	49.1
1061	3.71	3.75	1.0	67644	2.64	2.67	0.17	11407	1.96	1.99	1.18	80044	53.4
1304	3.70	3.76	1.0	68015	2.65	2.66	0.13	8686	1.95	1.99	1.33	90346	59.9
1549	3.71	3.75	1.0	65217	2.65	2.66	0.13	8284	1.96	1.99	1.40	91196	63.1
1914	3.70	3.75	1.0	65714	2.65	2.66	0.11	7383	1.96	1.99	1.52	99680	68.4
2273	3.71	3.75	1.0	63518	2.65	2.66	0.10	6404	1.96	1.99	1.64	104030	73.9
2630	3.71	3.75	1.0	64916	2.65	2.66	0.09	5690	1.96	1.99	1.72	111529	77.5
2975	3.71	3.75	1.0	63965	2.65	2.66	0.07	4752	1.96	1.99	1.75	111828	78.8
3334	3.72	3.75	1.0	63791	2.65	2.66	0.06	3567	1.96	1.99	1.82	116323	82.2
3715	3.71	3.75	1.0	66753	2.65	2.66	0.05	3452	1.96	1.99	1.83	122089	82.5
4076	3.71	3.75	1.0	65199	2.65	2.66	0.05	3524	1.96	1.99	1.86	121032	83.7
4450	3.70	3.76	1.0	67446	2.65	2.66	0.05	3112	1.96	1.99	1.88	126870	84.8
4803	3.71	3.75	1.0	65856	2.65	2.66	0.06	3633	1.96	1.99	1.94	127522	87.3
5516	3.71	3.75	1.0	68279	2.65	2.66	0.04	3037	1.96	1.99	1.94	132388	87.4
6958	3.71	3.75	1.0	68997	2.65	2.66	0.03	1772	1.96	1.99	1.99	137435	89.8
8397	3.71	3.76	1.0	66322	–	–	–	–	1.96	1.99	2.07	137540	93.5
9101	3.71	3.76	1.0	68018	–	–	–	–	1.96	1.99	2.04	139068	92.2
9821	3.72	3.75	1.0	71752	–	–	–	–	1.96	1.99	2.06	147829	92.9
10454	3.71	3.75	1.0	66760	–	–	–	–	1.96	1.99	2.05	136912	92.5

Table 4.27. Raw data of absolute kinetic of acylation reaction with **5a** in MeCN-d_3.

Time (min)	**Integ. limits (ppm)**		**Integ.**	**Absol.**	**Integ. limits (ppm)**		**Integ.**	**Absol.**	**Integ. limits (ppm)**		**Integ.**	**Absol.**	**$Yield_{ester}$ (%)**
VB122a	**Standard**				**Educt**				**Product**				
8	3.71	3.76	1.0	66931	2.64	2.68	0.57	37967	1.97	1.98	0.02	1610	1.09
18	3.70	3.76	1.0	67704	2.64	2.67	0.55	37155	1.97	1.99	0.05	3659	2.44
38	3.70	3.75	1.0	67312	2.64	2.67	0.51	34411	1.97	1.98	0.08	5437	3.64
51	3.72	3.75	1.0	66903	2.64	2.67	0.54	35854	1.97	1.98	0.10	6420	4.33
78	3.71	3.76	1.0	70671	2.64	2.66	0.45	31596	1.97	1.98	0.14	9608	6.13
80	3.71	3.76	1.0	70318	2.64	2.66	0.44	31011	1.97	1.98	0.14	9637	6.18
106	3.71	3.75	1.0	72560	2.64	2.67	0.43	30911	1.97	1.99	0.17	12564	7.81
108	3.71	3.75	1.0	63032	2.64	2.66	0.40	25174	1.96	1.99	0.18	11655	8.34

131	3.71	3.75	1.0	67279	2.65	2.67	0.38	25251	1.97	1.98	0.20	13289	8.91
164	3.71	3.75	1.0	67242	2.64	2.66	0.36	24125	1.97	1.98	0.23	15468	10.4
218	3.71	3.75	1.0	67221	2.65	2.67	0.33	21884	1.96	1.99	0.32	21536	14.4
254	3.71	3.76	1.0	68507	2.64	2.67	0.37	25251	1.96	1.99	0.33	22479	14.8
311	3.71	3.75	1.0	66959	2.64	2.66	0.32	21531	1.96	1.99	0.38	25349	17.1
369	3.70	3.76	1.0	67704	2.65	2.67	0.30	20632	1.96	1.99	0.41	28093	18.7
420	3.71	3.75	1.0	66961	2.64	2.66	0.31	20673	1.96	1.99	0.48	31891	21.5
486	3.71	3.75	1.0	66884	2.64	2.67	0.31	20701	1.96	1.98	0.49	33076	22.3
551	3.71	3.75	1.0	67400	2.64	2.67	0.28	18880	1.96	1.99	0.55	36747	24.6
609	3.71	3.75	1.0	67791	2.64	2.67	0.29	19333	1.96	1.99	0.58	39493	26.3
671	3.71	3.75	1.0	69720	2.64	2.66	0.26	17932	1.96	1.99	0.63	43759	28.3
729	3.71	3.75	1.0	69053	2.64	2.67	0.26	18155	1.96	1.99	0.65	44844	29.3
850	3.71	3.75	1.0	69917	2.65	2.67	0.24	17095	1.96	1.99	0.71	49543	32.0
966	3.72	3.75	1.0	69418	2.64	2.66	0.24	16972	1.96	1.99	0.77	53224	34.6
1090	3.70	3.75	1.0	70890	2.64	2.67	0.24	16960	1.96	1.99	0.81	57246	36.4
1211	3.71	3.75	1.0	69424	2.64	2.67	0.23	16030	1.96	1.99	0.86	59723	38.8
1337	3.70	3.75	1.0	69228	2.64	2.67	0.21	14858	1.96	1.99	0.90	62482	40.7
1754	3.71	3.75	1.0	65714	2.64	2.67	0.21	13534	1.96	1.99	1.07	70056	48.1
2113	3.70	3.75	1.0	64783	2.64	2.67	0.19	12464	1.96	1.99	1.16	74959	52.2
2471	3.71	3.75	1.0	65238	2.65	2.66	0.17	11098	1.96	1.99	1.25	81450	56.3
2847	3.70	3.76	1.0	66045	2.65	2.67	0.15	9798	1.96	1.99	1.30	86027	58.7
3207	3.71	3.75	1.0	64954	2.64	2.67	0.14	9213	1.96	1.99	1.37	89228	62.0
3565	3.71	3.75	1.0	67269	2.65	2.66	0.13	9016	1.96	1.99	1.44	96641	64.8
3926	3.71	3.75	1.0	65570	2.64	2.67	0.14	8886	1.96	1.99	1.49	97911	67.3
4299	3.71	3.75	1.0	67639	2.65	2.66	0.12	8094	1.96	1.99	1.57	106069	70.7
4653	3.71	3.76	1.0	67205	2.65	2.67	0.12	7979	1.96	1.99	1.58	106066	71.2
5012	3.71	3.75	1.0	70034	2.65	2.66	0.10	6977	1.96	1.99	1.61	112562	72.5
5356	3.71	3.75	1.0	68560	2.65	2.66	0.09	6278	1.96	1.99	1.66	113626	74.7
6077	3.71	3.75	1.0	68624	2.65	2.66	0.08	5653	1.96	1.99	1.67	114526	75.3
6798	3.71	3.75	1.0	68890	2.65	2.66	0.09	6150	1.96	1.99	1.72	118351	77.5
7517	3.71	3.75	1.0	67769	2.65	2.66	0.09	5841	1.96	1.99	1.76	119325	79.4
8237	3.71	3.75	1.0	67895	2.65	2.66	0.08	5190	1.96	1.99	1.84	124811	82.9
8962	3.71	3.75	1.0	66007	2.65	2.66	0.08	5239	1.96	1.99	1.85	122091	83.4
9681	3.71	3.75	1.0	73059	2.65	2.66	0.08	5640	1.96	1.99	1.84	134747	83.2
10362	3.70	3.75	1.0	64226	2.65	2.66	0.06	3860	1.96	1.99	1.89	121693	85.5
11801	3.71	3.75	1.0	71921	2.65	2.66	0.09	6351	1.96	1.99	1.95	140215	87.9
13238	3.71	3.75	1.0	64847	2.65	2.66	0.08	5404	1.96	1.99	1.95	126550	88.0
14672	3.71	3.75	1.0	66322	–	–	–	–	1.96	1.99	1.97	130550	88.8
16112	3.71	3.76	1.0	68691	–	–	–	–	1.96	1.99	1.98	135682	89.1
17551	3.70	3.75	1.0	66740	–	–	–	–	1.96	1.99	1.97	131807	89.1

VB122b	Standard				Educt				Product				Yield (%)
8	3.71	3.76	1.0	65399	2.64	2.67	0.51	33058	1.97	1.98	0.02	1503	1.0
50	3.70	3.76	1.0	65912	2.65	2.67	0.46	30045	1.97	1.98	0.08	5101	3.5
81	3.72	3.75	1.0	65954	2.65	2.66	0.41	26861	1.97	1.98	0.12	7597	5.2
107	3.71	3.75	1.0	63673	2.64	2.66	0.39	24592	1.97	1.98	0.15	9242	6.5
140	3.71	3.76	1.0	71987	2.64	2.66	0.36	25917	1.97	1.98	0.17	12509	7.8
173	3.71	3.75	1.0	70519	2.64	2.66	0.37	25761	1.96	1.99	0.22	15255	9.8
193	3.71	3.76	1.0	72607	2.64	2.67	0.37	26527	1.96	1.99	0.24	17248	10.7
258	3.72	3.75	1.0	64158	2.64	2.66	0.36	22883	1.97	1.99	0.28	18146	12.8
320	3.71	3.75	1.0	65433	2.64	2.67	0.34	22572	1.96	1.99	0.34	22059	15.2
376	3.71	3.76	1.0	65723	2.64	2.67	0.33	21648	1.96	1.99	0.38	25216	17.3
433	3.72	3.75	1.0	63868	2.64	2.66	0.32	20404	1.96	1.99	0.43	27273	19.3
556	3.71	3.75	1.0	64227	2.63	2.66	0.32	20735	1.96	1.99	0.51	32571	22.9
679	3.71	3.75	1.0	64281	2.64	2.67	0.30	19312	1.96	1.99	0.58	37369	26.2
798	3.71	3.75	1.0	64036	2.64	2.67	0.29	18706	1.96	1.99	0.65	41836	29.5
916	3.71	3.75	1.0	73764	2.64	2.66	0.28	20519	1.96	1.99	0.71	52481	32.1
1036	3.71	3.75	1.0	65151	2.64	2.67	0.26	17108	1.96	1.99	0.76	49676	34.4
1281	3.71	3.75	1.0	63004	2.64	2.67	0.25	15585	1.96	1.99	0.89	56082	40.1
1518	3.71	3.75	1.0	65044	2.64	2.66	0.22	14455	1.96	1.99	0.96	62271	43.2
1761	3.71	3.75	1.0	64690	2.65	2.66	0.20	12844	1.96	1.98	1.02	66227	46.2
2116	3.72	3.75	1.0	66582	2.65	2.66	0.18	12158	1.96	1.99	1.13	75048	50.8
2476	3.71	3.75	1.0	66093	2.65	2.67	0.17	11480	1.96	1.99	1.18	77867	53.1
2843	3.71	3.75	1.0	67262	2.65	2.66	0.16	10912	1.96	1.99	1.27	85745	57.5
3200	3.72	3.75	1.0	67442	2.65	2.66	0.16	11033	1.96	1.99	1.32	89305	59.7
3570	3.72	3.75	1.0	70135	2.65	2.66	0.14	9694	1.96	1.99	1.40	98017	63.0
3936	3.71	3.75	1.0	69232	2.65	2.66	0.15	10234	1.96	1.99	1.44	99499	64.8
4290	3.71	3.75	1.0	67630	2.65	2.66	0.13	8503	1.96	1.99	1.49	100694	67.1
5011	3.72	3.75	1.0	68818	2.65	2.66	0.12	8481	1.96	1.99	1.57	108058	70.8
5731	3.71	3.75	1.0	68676	2.65	2.66	0.10	6592	1.96	1.99	1.63	111778	73.4
6451	3.71	3.75	1.0	68674	2.65	2.66	0.12	7933	1.96	1.99	1.66	113705	74.7
7546	3.67	3.77	1.0	66779	2.65	2.66	0.09	6276	1.96	1.99	1.73	115258	77.8
8275	3.69	3.78	1.0	66351	2.65	2.66	0.10	6363	1.96	1.99	1.73	114529	77.8
8972	3.69	3.77	1.0	71449	2.65	2.66	0.09	6111	1.96	1.99	1.83	130419	82.3
10413	3.69	3.76	1.0	74942	–	–	–	–	1.96	1.99	1.87	139946	84.2
11852	3.68	3.77	1.0	67675	–	–	–	–	1.96	1.99	1.88	127500	85.0
13189	3.69	3.77	1.0	74160	–	–	–	–	1.96	1.99	1.90	141228	85.9
14623	3.69	3.77	1.0	68787	–	–	–	–	1.96	1.99	1.93	133098	87.3
16063	3.68	3.77	1.0	68671	–	–	–	–	1.96	1.99	1.94	133486	87.7
17606	3.67	3.78	1.0	65788	–	–	–	–	1.96	1.99	1.99	130672	89.6
19051	3.69	3.77	1.0	69179	–	–	–	–	1.96	1.99	1.99	137865	89.9

4.4.6 Simulation of Kinetic Experiments – Acylation with Benzoic Anhydride

Kinetic measurements performed with benzoic anhydride were prepared and analyzed according to the procedure described in Chapter 4.3.2 and Chapter 4.3.3. In this benchmark reaction other proton signals were used for the analysis. Figure 4.4 exemplary shows an ^{1}H-NMR spectrum of the acylation reaction catalyzed by salt **6a**. Proton shift used in the evaluation are marked.

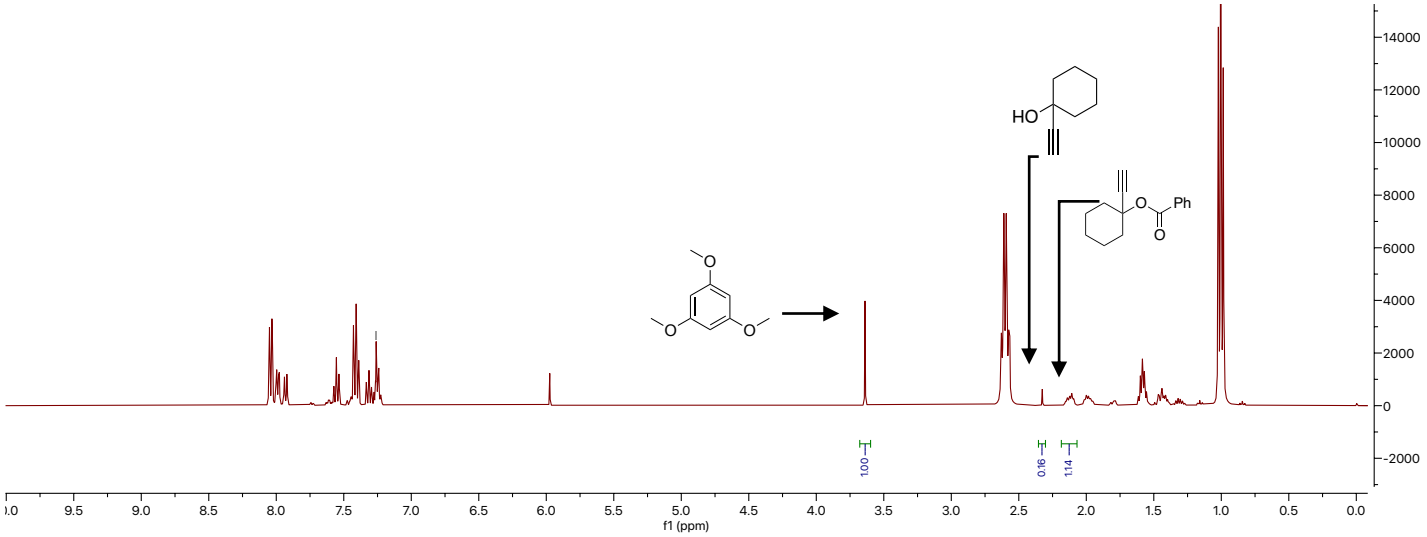

Figure 4.4. NMR spectra of acylation benchmark reaction with benzoic anhydride **19** catalyzed by salt **6a** with assigned ^{1}H shift necessary of analysis.

The resulting effective reaction rates k_{eff} and half-life times $t_{1/2}$ (min) are summarized in Table 4.28.

Table 4.28. Effective reaction rates k_{eff} (M^{-1} s^{-1}) and half-life times $t_{1/2}$ (min) for the acylation of 1-ethynylcyclohexanol **16** with benzoic anhydride **19** in $CDCl_3$.

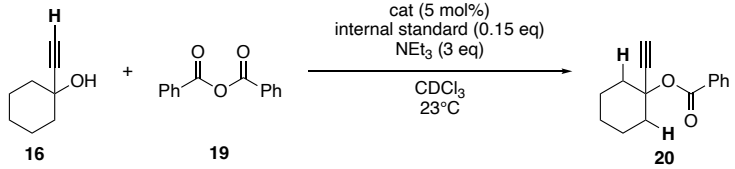

Catalyst	k_{eff} (M^{-1} s^{-1})	Average k_{eff} (M^{-1} s^{-1})	$t_{1/2}$ (s)	$t_{1/2}$ (min)	Average $t_{1/2}$ (min)
2	1.48×10^{-3}	$1.52 \times 10^{-3} \pm 4.39 \times 10^{-5}$	51000	850	814 ± 35.8
	1.57×10^{-3}		46700	778	

3a	1.78×10^{-4}	–	553000	9217	–
3d	1.03×10^{-4}	–	1190000	19833	–
4a	7.21×10^{-4}	$7.17 \times 10^{-4} \pm 4.14 \times 10^{-6}$	113000	1883	1892 ± 8.33
	7.13×10^{-4}		114000	1900	
6a	9.23×10^{-4}	$9.63 \times 10^{-4} \pm 4.01 \times 10^{-5}$	84500	1408	1347 ± 61.7
	1.00×10^{-3}		77100	1285	

The raw data sets of the kinetic measurements are summarized in Table 4.29 – Table 4.33.

Table 4.29. Raw data of absolute kinetic of acylation reaction with **2** with benzoic anhydride in $CDCl_3$.

Time (min)	**Integ. limits (ppm)**		**Integ.**	**Absol.**	**Integ. limits (ppm)**		**Integ.**	**Absol.**	**Integ. limits (ppm)**		**Integ.**	**Absol.**	**$Yield_{ester}$ (%)**
VB312a	**Standard**				**Educt**				**Product**				
11	3.59	3.69	1.0	61042	2.32	2.37	0.56	34266					0.0
129	3.62	3.68	1.0	62695	2.33	2.37	0.49	30530	2.09	2.19	0.18	11367	11.9
492	3.61	3.69	1.0	56055	2.32	2.37	0.44	24422	2.09	2.19	0.55	30766	36.0
613	3.59	3.70	1.0	63983	2.32	2.37	0.40	25362	2.09	2.20	0.64	41039	42.1
735	3.60	3.70	1.0	64140	2.31	2.38	0.38	24183	2.08	2.20	0.73	46679	47.7
855	3.61	3.69	1.0	56170	2.31	2.36	0.31	17162	2.09	2.19	0.79	44188	51.6
980	3.61	3.69	1.0	64081	2.31	2.37	0.29	18378	2.08	2.21	0.86	54950	56.2
1102	3.61	3.69	1.0	56181	2.31	2.37	0.25	14231	2.09	2.20	0.90	50538	59.0
1219	3.60	3.70	1.0	62466	2.31	2.37	0.24	15266	2.08	2.20	0.96	59902	62.9
1339	3.62	3.69	1.0	57253	2.32	2.35	0.20	11514	2.09	2.19	0.99	56758	65.0
1462	3.61	3.68	1.0	62665	2.32	2.36	0.19	11753	2.09	2.19	1.03	64369	67.4
1703	3.62	3.71	1.0	63271	2.32	2.36	0.17	10467	2.08	2.20	1.11	69921	72.5
1942	3.62	3.69	1.0	55582	2.32	2.36	0.14	7947	2.08	2.19	1.16	64708	76.4
2183	3.63	3.68	1.0	57117	2.33	2.35	0.12	6909	2.08	2.19	1.21	69317	79.6
2424	3.62	3.68	1.0	57780	2.32	2.36	0.11	6603	2.08	2.19	1.25	72308	82.1
2666	3.62	3.68	1.0	58214	2.32	2.36	0.10	5825	2.09	2.19	1.28	74471	83.9
2909	3.61	3.68	1.0	57633	2.32	2.36	0.09	5032	2.08	2.19	1.31	75585	86.0
3317	3.63	3.68	1.0	55304	2.32	2.36	0.08	4631	2.09	2.19	1.34	74081	87.9
3618	3.60	3.69	1.0	57013	2.31	2.37	0.08	4616	2.09	2.20	1.35	77027	88.6
3618	3.63	3.68	1.0	56933	2.32	2.36	0.07	3814	2.08	2.20	1.40	79865	92.0
3981	3.61	3.69	1.0	56934	2.32	2.35	0.06	3232	2.08	2.19	1.40	79572	91.7
4340	3.61	3.69	1.0	57632	2.32	2.36	0.05	2973	2.09	2.20	1.42	81964	93.3
4701	3.63	3.68	1.0	55879	2.32	2.35	0.04	2442	2.08	2.20	1.46	81723	95.9
5062	3.62	3.69	1.0	58397	2.32	2.35	0.04	2290	2.08	2.20	1.47	85623	96.2
5424	3.61	3.69	1.0	59117	2.31	2.36	0.04	2432	2.08	2.19	1.47	87019	96.5
5784	3.62	3.68	1.0	58294	2.31	2.36	0.04	2337	2.08	2.19	1.48	86238	97.0

7222	3.61	3.69	1.0	58350	2.32	2.36	0.03	1468	2.08	2.20	1.51	88357	99.3
8662	3.61	3.70	1.0	64799	2.32	2.35	0.02	1043	2.08	2.20	1.53	99324	100
10115	3.61	3.69	1.0	61685	2.32	2.35	0.01	720	2.08	2.20	1.54	95076	100
11545	3.62	3.69	1.0	59847	2.32	2.36	0.01	810	2.08	2.20	1.56	93176	100
12992	3.62	3.68	1.0	55902	2.31	2.37	0.02	1306	2.08	2.19	1.53	85785	100
14431	3.61	3.69	1.0	62275	2.31	2.37	0.02	1299	2.08	2.20	1.54	95739	100
15867	3.61	3.69	1.0	61373	2.31	2.37	0.02	1301	2.09	2.19	1.53	94029	100
17308	3.61	3.69	1.0	60550	2.31	2.37	0.02	1217	2.08	2.20	1.54	93257	100
18755	3.61	3.68	1.0	60272	2.31	2.37	0.02	1279	2.08	2.19	1.54	92926	100
20194	3.61	3.68	1.0	62380	2.31	2.37	0.02	1281	2.08	2.20	1.55	96610	100
VB312b	**Standard**				**Educt**				**Product**				**Yield (%)**
13	3.62	3.71	1.0	52076	2.34	2.38	0.67	34893					0.0
139	3.63	3.71	1.0	52779	2.35	2.38	0.61	32069	2.10	2.21	0.20	10814	13.3
255	3.63	3.70	1.0	52868	2.34	2.38	0.58	30709	2.10	2.20	0.34	18152	22.3
380	3.61	3.71	1.0	53053	2.32	2.38	0.58	30987	2.10	2.21	0.48	25302	31.0
497	3.62	3.70	1.0	53090	2.32	2.38	0.54	28745	2.09	2.21	0.59	31176	38.2
615	3.59	3.71	1.0	53321	2.32	2.38	0.49	26103	2.09	2.21	0.68	36045	43.9
735	3.61	3.71	1.0	53384	2.32	2.37	0.42	22661	2.09	2.20	0.76	40360	49.1
873	3.61	3.71	1.0	55450	2.32	2.38	0.39	21405	2.09	2.20	0.83	46233	54.2
981	3.61	3.70	1.0	53589	2.33	2.37	0.34	18083	2.09	2.20	0.90	48026	58.3
1106	3.62	3.69	1.0	59273	2.33	2.37	0.31	18103	2.09	2.20	0.95	56485	61.9
1219	3.62	3.69	1.0	59119	2.32	2.37	0.29	17201	2.09	2.19	1.01	59432	65.4
1345	3.62	3.68	1.0	59217	2.32	2.36	0.26	15473	2.08	2.19	1.05	62406	68.5
1462	3.61	3.69	1.0	59279	2.31	2.36	0.24	14505	2.09	2.19	1.08	64073	70.3
1705	3.61	3.69	1.0	54032	2.32	2.36	0.21	11579	2.09	2.19	1.16	62414	75.1
1944	3.62	3.68	1.0	54934	2.32	2.37	0.19	10271	2.09	2.19	1.22	66919	79.2
2184	3.62	3.69	1.0	54913	2.32	2.36	0.16	8792	2.09	2.19	1.27	69736	82.6
2425	3.62	3.69	1.0	58088	2.32	2.36	0.15	8461	2.09	2.19	1.31	75921	85.0
2671	3.62	3.69	1.0	52398	2.32	2.36	0.13	6712	2.08	2.19	1.36	71364	88.5
2908	3.61	3.69	1.0	53542	2.32	2.36	0.12	6311	2.08	2.20	1.39	74660	90.6
3148	3.61	3.69	1.0	59863	2.31	2.37	0.11	6707	2.08	2.19	1.42	84921	92.2
3372	3.61	3.69	1.0	53878	2.31	2.36	0.10	5286	2.07	2.19	1.46	78587	94.8
3621	3.62	3.69	1.0	54257	2.33	2.36	0.08	4611	2.08	2.19	1.46	79423	95.2
3862	3.61	3.68	1.0	54228	2.32	2.35	0.08	4215	2.08	2.19	1.48	80260	96.2
4105	3.61	3.69	1.0	59115	2.32	2.35	0.07	4098	2.08	2.19	1.50	88699	97.5
4344	3.62	3.68	1.0	58248	2.32	2.36	0.07	4137	2.08	2.20	1.53	89111	99.5
4711	3.60	3.70	1.0	54707	2.32	2.36	0.06	3374	2.09	2.18	1.52	82741	98.3
5071	3.61	3.69	1.0	55412	2.31	2.37	0.06	3369	2.09	2.19	1.54	85079	99.8
5426	3.60	3.70	1.0	55029	2.33	2.35	0.04	2252	2.08	2.18	1.56	85335	100
5788	3.60	3.70	1.0	55263	2.32	2.35	0.04	2148	2.09	2.19	1.56	85736	101

7231	3.60	3.70	1.0	55199	2.33	2.35	0.02	1256	2.09	2.18	1.59	87123	101
8672	3.60	3.70	1.0	53911	2.33	2.35	0.02	867	2.09	2.18	1.60	86068	101
10111	3.59	3.69	1.0	54648	2.33	2.35	0.01	717	2.09	2.18	1.62	88438	101
11553	3.60	3.69	1.0	58194	2.33	2.35	0.01	587	2.09	2.18	1.64	94189	101
12983	3.59	3.70	1.0	57369	2.33	2.35	0.01	519	2.08	2.18	1.64	93580	101
14415	3.59	3.69	1.0	57273	2.33	2.35	0.01	457	2.08	2.19	1.66	94088	101
15860	3.60	3.69	1.0	58148	2.33	2.35	0.01	456	2.08	2.19	1.65	95302	101
17301	3.60	3.69	1.0	57515	2.33	2.35	0.01	426	2.09	2.19	1.64	94056	101
18743	3.60	3.69	1.0	55792	2.33	2.35	0.01	412	2.08	2.19	1.66	91815	101
20189	3.60	3.70	1.0	58957	2.33	2.35	0.01	430	2.09	2.19	1.65	96512	101
21626	3.60	3.69	1.0	58150	2.33	2.35	0.01	446	2.09	2.19	1.65	95351	101

Table 4.30. Raw data of absolute kinetic of acylation reaction with **3a** with benzoic anhydride in $CDCl_3$.

Time (min)	**Integ. limits (ppm)**		**Integ.**	**Absol.**	**Integ. limits (ppm)**		**Integ.**	**Absol.**	**Integ. limits (ppm)**		**Integ.**	**Absol.**	**$Yield_{ester}$ (%)**
VB136	**Standard**				**Educt**				**Product**				
7	3.59	3.68	1.0	71589	2.32	2.36	0.53	38261	–	–	–	–	0.00
19	3.61	3.68	1.0	71952	2.32	2.36	0.51	36473	–	–	–	–	0.00
34	3.58	3.70	1.0	72718	2.32	2.35	0.51	36634	2.09	2.16	0.01	411	0.40
50	3.58	3.69	1.0	71860	2.32	2.35	0.51	35864	2.08	2.17	0.01	667	0.65
71	3.58	3.69	1.0	72477	2.32	2.35	0.50	35687	2.08	2.17	0.01	919	0.89
103	3.60	3.70	1.0	70701	2.31	2.36	0.50	35432	2.08	2.17	0.02	1169	1.16
137	3.59	3.69	1.0	72052	2.32	2.35	0.48	33449	2.08	2.17	0.02	1674	1.64
159	3.58	3.68	1.0	72485	2.32	2.35	0.48	33635	2.08	2.18	0.03	1894	1.84
190	3.57	3.70	1.0	73348	2.32	2.35	0.49	35116	2.09	2.17	0.03	2082	2.00
250	3.58	3.70	1.0	72931	2.32	2.35	0.49	34711	2.08	2.17	0.04	2665	2.57
310	3.58	3.70	1.0	72324	2.32	2.35	0.50	35717	2.08	2.18	0.05	3224	3.14
375	3.58	3.70	1.0	69670	2.32	2.35	0.49	33594	2.08	2.18	0.05	3631	3.67
435	3.59	3.69	1.0	70031	2.32	2.35	0.49	33705	2.08	2.17	0.06	4113	4.14
494	3.58	3.69	1.0	69282	2.32	2.35	0.49	33098	2.08	2.18	0.07	4515	4.59
551	3.59	3.69	1.0	69176	2.32	2.35	0.49	33242	2.08	2.17	0.08	5179	5.27
611	3.58	3.71	1.0	69362	2.32	2.35	0.47	31847	2.07	2.18	0.08	5688	5.78
671	3.57	3.71	1.0	69092	2.32	2.35	0.48	31804	2.08	2.18	0.09	6167	6.29
731	3.59	3.70	1.0	75836	2.32	2.35	0.50	37369	2.07	2.18	0.10	7673	7.13
850	3.59	3.69	1.0	75567	2.32	2.35	0.49	36606	2.07	2.18	0.12	8687	8.10
975	3.59	3.68	1.0	72499	2.32	2.35	0.50	35457	2.07	2.18	0.13	9488	9.22
1091	3.59	3.69	1.0	74213	2.32	2.35	0.50	36338	2.07	2.18	0.15	10776	10.2
1341	3.57	3.71	1.0	70847	2.32	2.34	0.47	32384	2.06	2.18	0.18	12489	12.4

1570	3.57	3.69	1.0	71690	2.31	2.35	0.51	36021	2.07	2.18	0.20	14155	13.9
1930	3.58	3.69	1.0	68389	2.31	2.35	0.47	31622	2.07	2.17	0.23	15439	15.9
2294	3.57	3.70	1.0	71884	2.31	2.34	0.46	32084	2.07	2.17	0.27	18720	18.3
2655	3.60	3.69	1.0	71710	2.31	2.35	0.43	31088	2.07	2.17	0.31	22412	22.0
3010	3.60	3.68	1.0	73882	2.31	2.34	0.42	31092	2.07	2.17	0.35	25522	24.3
3370	3.60	3.68	1.0	72578	2.31	2.34	0.42	30271	2.07	2.17	0.37	27118	26.3
3727	3.60	3.68	1.0	73268	2.31	2.34	0.41	29896	2.06	2.17	0.41	29788	28.6
4088	3.59	3.69	1.0	74092	2.31	2.34	0.39	28799	1.93	2.04	0.43	32008	30.4
4450	3.60	3.68	1.0	74965	2.31	2.34	0.38	28455	1.93	2.04	0.44	32740	30.8
5167	3.59	3.68	1.0	69003	2.31	2.35	0.35	24092	1.92	2.04	0.49	33718	34.4
5897	3.58	3.68	1.0	68615	2.31	2.34	0.34	23667	1.92	2.04	0.55	37634	38.6
6612	3.59	3.67	1.0	74539	2.31	2.34	0.31	22844	1.92	2.04	0.60	44499	42.1
7332	3.58	3.69	1.0	67608	2.31	2.34	0.29	19758	1.92	2.04	0.61	41461	43.2
8053	3.56	3.70	1.0	69129	2.30	2.35	0.30	20459	1.92	2.04	0.67	46303	47.2
8776	3.61	3.67	1.0	67844	2.30	2.35	0.27	18631	1.92	2.04	0.69	46749	48.5
9493	3.60	3.68	1.0	68229	2.31	2.35	0.27	18255	1.92	2.04	0.73	49844	51.5
10212	3.60	3.67	1.0	67593	2.30	2.35	0.27	17945	1.92	2.04	0.75	50490	52.6
10933	3.60	3.67	1.0	67436	2.31	2.35	0.25	17174	1.92	2.04	0.79	53193	55.6
11654	3.60	3.67	1.0	72521	2.31	2.35	0.24	17156	1.93	2.04	0.81	58516	56.8
12371	3.60	3.67	1.0	69584	2.31	2.35	0.23	15787	1.93	2.03	0.81	56086	56.8
13088	3.62	3.66	1.0	75263	2.31	2.34	0.22	16350	1.92	2.03	0.83	62759	58.7
13808	3.61	3.67	1.0	73363	2.32	2.34	0.21	15110	1.92	2.03	0.87	63736	61.2
14532	3.60	3.68	1.0	73868	2.31	2.35	0.21	15508	1.92	2.03	0.88	65082	62.1
15245	3.60	3.68	1.0	74270	2.30	2.34	0.20	14758	1.91	2.04	0.90	66605	63.2
15967	3.59	3.68	1.0	69341	2.30	2.35	0.18	12727	1.92	2.05	0.94	64859	65.9
16690	3.59	3.67	1.0	71924	2.30	2.35	0.18	13117	1.91	2.05	0.94	67322	65.9
17406	3.59	3.67	1.0	75264	2.31	2.35	0.18	13439	1.92	2.04	0.94	71112	66.6
18136	3.59	3.68	1.0	75101	2.29	2.35	0.18	13331	1.92	2.04	0.96	71963	67.5
18857	3.60	3.68	1.0	73794	2.30	2.35	0.18	13455	1.91	2.04	0.99	72974	69.7
19576	3.60	3.67	1.0	73630	2.30	2.35	0.17	12667	1.91	2.04	0.98	72058	68.9
21017	3.60	3.68	1.0	73124	2.29	2.36	0.17	12401	1.91	2.05	1.03	75309	72.6
22445	3.59	3.68	1.0	74721	2.30	2.34	0.15	11389	1.91	2.04	1.04	77467	73.0
23889	3.59	3.69	1.0	70151	2.30	2.35	0.14	9913	1.90	2.04	1.04	73134	73.4
25324	3.60	3.68	1.0	69749	2.30	2.35	0.14	9513	1.91	2.04	1.06	74053	74.8
26765	3.60	3.68	1.0	75600	2.30	2.35	0.13	10073	1.92	2.04	1.08	81630	76.1
28205	3.60	3.68	1.0	68900	2.30	2.35	0.13	8831	1.91	2.04	1.11	76426	78.1
29645	3.58	3.69	1.0	69138	2.30	2.35	0.12	8097	1.92	2.03	1.09	75392	76.8
31085	3.60	3.67	1.0	74994	2.31	2.34	0.11	8607	1.92	2.04	1.13	85028	79.9
32525	3.61	3.67	1.0	71016	2.30	2.35	0.12	8192	1.91	2.04	1.15	81675	81.0
33967	3.61	3.67	1.0	69349	2.30	2.34	0.11	7544	1.92	2.04	1.16	80241	81.5

35407	3.60	3.67	1.0	68899	2.29	2.35	0.11	7566	1.92	2.05	1.17	80949	82.8
36844	3.61	3.68	1.0	69113	2.30	2.35	0.10	7150	1.93	2.04	1.16	80410	82.0
38285	3.61	3.67	1.0	68699	2.31	2.34	0.10	6608	1.91	2.04	1.19	81627	83.7
39724	3.60	3.67	1.0	69161	2.31	2.34	0.09	6287	1.92	2.04	1.19	82291	83.8
41167	3.59	3.68	1.0	68802	2.31	2.34	0.09	6053	1.92	2.04	1.19	82095	84.1
42609	3.61	3.67	1.0	69242	2.31	2.34	0.09	6090	1.92	2.04	1.22	84322	85.8
44056	3.61	3.67	1.0	71091	2.31	2.35	0.09	6089	1.91	2.04	1.23	87267	86.5
45480	3.61	3.67	1.0	68835	2.30	2.34	0.08	5825	1.92	2.04	1.23	84339	86.3
46917	3.61	3.67	1.0	76937	2.30	2.35	0.08	6406	1.92	2.04	1.23	94613	86.6
48356	3.61	3.67	1.0	68430	2.30	2.35	0.08	5352	1.91	2.04	1.25	85612	88.1
49797	3.60	3.66	1.0	68975	2.30	2.35	0.08	5415	1.91	2.04	1.25	85938	87.8

Table 4.31. Raw data of absolute kinetic of acylation reaction with **3d** with benzoic anhydride in $CDCl_3$.

Time (min)	**Integ. limits (ppm)**		**Integ.**	**Absol.**	**Integ. limits (ppm)**		**Integ.**	**Absol.**	**Integ. limits (ppm)**		**Integ.**	**Absol.**	**$Yield_{ester}$ (%)**
VB137	**Standard**				**Educt**				**Product**				
8	3.56	3.70	1.0	66043	2.31	2.35	0.58	37986	1.91	1.99	0.02	1252	1.34
23	3.60	3.68	1.0	67139	2.31	2.35	0.58	38680	1.91	1.99	0.02	1188	1.25
40	3.58	3.68	1.0	71558	2.31	2.34	0.59	41252	1.91	1.99	0.02	1233	1.21
60	3.57	3.70	1.0	72030	2.32	2.34	0.58	40491	1.91	1.99	0.02	1244	1.22
74	3.55	3.72	1.0	72095	2.31	2.35	0.58	41293	1.91	1.99	0.01	922	0.90
97	3.61	3.66	1.0	65557	2.31	2.35	0.58	37721	1.90	1.99	0.02	1292	1.39
127	3.57	3.71	1.0	67626	2.32	2.34	0.56	37151	1.91	2.00	0.02	1345	1.40
187	3.59	3.69	1.0	65998	2.31	2.34	0.58	37318	1.90	2.00	0.02	1384	1.48
247	3.58	3.68	1.0	72984	2.31	2.34	0.58	41359	1.92	2.01	0.03	2109	2.04
312	3.58	3.68	1.0	68849	2.32	2.34	0.58	38938	1.92	2.02	0.03	2159	2.21
372	3.62	3.66	1.0	68691	2.32	2.34	0.56	38694	1.91	2.02	0.04	2666	2.73
431	3.58	3.69	1.0	69503	2.31	2.35	0.58	39569	1.91	2.01	0.04	2698	2.73
488	3.60	3.68	1.0	69407	2.31	2.35	0.58	39779	1.93	2.02	0.04	2926	2.97
548	3.59	3.68	1.0	69120	2.31	2.34	0.59	39815	1.93	2.02	0.04	3045	3.10
608	3.60	3.68	1.0	68887	2.32	2.35	0.57	38220	1.91	2.01	0.05	3454	3.53
669	3.62	3.66	1.0	67892	2.31	2.34	0.57	38641	1.92	2.02	0.06	3788	3.93
728	3.59	3.69	1.0	69299	2.32	2.34	0.57	38288	1.92	2.02	0.06	3997	4.06
848	3.59	3.68	1.0	67251	2.32	2.34	0.56	37296	1.91	2.02	0.07	4643	4.86
968	3.60	3.68	1.0	72992	2.32	2.35	0.56	40427	1.92	2.02	0.07	5024	4.85
1089	3.57	3.69	1.0	74673	2.32	2.35	0.56	41465	1.92	2.01	0.07	5028	4.74
1328	3.57	3.70	1.0	71981	2.31	2.34	0.56	40621	1.92	2.02	0.08	6028	5.90
1568	3.57	3.70	1.0	72192	2.31	2.35	0.56	40604	1.92	2.02	0.10	7199	7.03

1927	3.58	3.69	1.0	67005	2.31	2.35	0.55	36856	1.93	2.02	0.12	7838	8.24
2290	3.57	3.70	1.0	72264	2.31	2.35	0.55	39742	1.91	2.02	0.15	10545	10.3
2650	3.57	3.70	1.0	70992	2.31	2.35	0.54	38068	1.92	2.03	0.16	11359	11.3
3009	3.59	3.69	1.0	73539	2.31	2.34	0.54	39634	1.92	2.02	0.18	13516	12.9
3367	3.57	3.70	1.0	70053	2.31	2.35	0.53	37457	1.92	2.03	0.20	13889	14.0
3727	3.57	3.69	1.0	67731	2.30	2.34	0.53	35840	1.92	2.04	0.22	15181	15.8
4452	3.58	3.70	1.0	68351	2.31	2.35	0.51	35193	1.91	2.03	0.28	18834	19.4
5166	3.59	3.68	1.0	69466	2.32	2.34	0.48	33009	1.92	2.03	0.29	20257	20.5
5887	3.59	3.68	1.0	68225	2.31	2.34	0.48	32827	1.92	2.04	0.34	23206	24.0
6609	3.59	3.69	1.0	68869	2.31	2.35	0.46	31822	1.92	2.03	0.35	24265	24.8
7334	3.59	3.68	1.0	68673	2.31	2.35	0.45	30783	1.93	2.03	0.37	25670	26.3
8046	3.59	3.68	1.0	68668	2.31	2.34	0.43	29868	1.92	2.03	0.41	27811	28.5
8781	3.59	3.68	1.0	68254	2.31	2.34	0.40	27497	1.92	2.04	0.43	29354	30.3
9488	3.59	3.68	1.0	67460	2.31	2.34	0.39	26524	1.92	2.04	0.45	30680	32.0
10214	3.57	3.69	1.0	68066	2.30	2.35	0.39	26782	1.92	2.03	0.47	32186	33.3
10926	3.58	3.68	1.0	68274	2.31	2.34	0.38	25879	1.91	2.04	0.50	34287	35.4
11656	3.57	3.71	1.0	73712	2.31	2.34	0.35	25647	1.92	2.04	0.53	39219	37.5
12378	3.57	3.69	1.0	74493	2.30	2.34	0.36	26602	1.91	2.04	0.54	40312	38.1
13823	3.59	3.68	1.0	68302	2.30	2.34	0.34	23047	1.91	2.03	0.59	40514	41.8
15266	3.58	3.68	1.0	69603	2.30	2.34	0.32	22481	1.91	2.03	0.61	42527	43.0
16687	3.60	3.68	1.0	73727	2.30	2.34	0.30	21957	1.91	2.04	0.64	47416	45.3
18126	3.59	3.68	1.0	75723	2.30	2.35	0.30	22887	1.91	2.04	0.68	51690	48.1
19570	3.59	3.68	1.0	67443	2.30	2.34	0.29	19841	1.91	2.04	0.69	46633	48.7
21010	3.57	3.68	1.0	67461	2.30	2.35	0.29	19254	1.92	2.03	0.72	48668	50.8
22447	3.58	3.68	1.0	69007	2.30	2.35	0.27	18416	1.91	2.04	0.73	50563	51.6
23890	3.59	3.67	1.0	69765	2.31	2.35	0.26	18139	1.91	2.04	0.75	52434	53.0
25326	3.57	3.68	1.0	69742	2.31	2.35	0.25	17668	1.91	2.04	0.76	52996	53.5
26778	3.58	3.69	1.0	74084	2.30	2.35	0.25	18429	1.92	2.04	0.80	59502	56.6
28208	3.58	3.68	1.0	68689	2.30	2.35	0.25	17264	1.91	2.04	0.80	55146	56.6
29648	3.59	3.68	1.0	68780	2.31	2.34	0.23	16129	1.91	2.04	0.82	56196	57.6
31088	3.60	3.66	1.0	71294	2.30	2.35	0.24	16757	1.92	2.03	0.83	59496	58.8
32526	3.60	3.67	1.0	71178	2.31	2.34	0.22	15868	1.92	2.04	0.86	61285	60.7
33971	3.60	3.67	1.0	70182	2.29	2.35	0.23	16210	1.92	2.03	0.87	60906	61.1
35407	3.60	3.68	1.0	69385	2.30	2.35	0.22	15512	1.92	2.04	0.88	61253	62.2
36853	3.61	3.67	1.0	70890	2.30	2.35	0.22	15680	1.92	2.04	0.90	63755	63.4
38286	3.60	3.67	1.0	69109	2.30	2.35	0.22	14977	1.92	2.04	0.90	62325	63.5
39726	3.60	3.67	1.0	69272	2.31	2.34	0.21	14326	1.91	2.04	0.92	63733	64.8
41167	3.60	3.67	1.0	68139	2.30	2.35	0.21	14027	1.93	2.04	0.92	62407	64.5
42613	3.60	3.67	1.0	70619	2.30	2.35	0.21	14486	1.91	2.03	0.93	65909	65.8
44054	3.60	3.68	1.0	70472	2.30	2.35	0.20	13969	1.92	2.03	0.93	65560	65.5

45487	3.61	3.67	1.0	68675	2.30	2.34	0.19	13130	1.91	2.04	0.96	65975	67.7
46917	3.59	3.67	1.0	70967	2.30	2.35	0.19	13562	1.91	2.03	0.95	67541	67.1
48357	3.61	3.67	1.0	68775	2.30	2.35	0.19	12985	1.92	2.03	0.97	66656	68.3
49798	3.60	3.67	1.0	69169	2.30	2.35	0.18	12756	1.91	2.04	0.98	67968	69.2

Table 4.32. Raw data of absolute kinetic of acylation reaction with **4a** with benzoic anhydride in $CDCl_3$.

Time (min)	**Integ. limits (ppm)**		**Integ.**	**Absol.**	**Integ. limits (ppm)**		**Integ.**	**Absol.**	**Integ. limits (ppm)**		**Integ.**	**Absol.**	**$Yield_{ester}$ (%)**
VB313a	**Standard**				**Educt**				**Product**				
13	3.63	3.70	1.0	58038	2.33	2.37	0.64	37069					0.00
117	3.63	3.69	1.0	60697	2.33	2.37	0.59	35930	2.10	2.20	0.10	5935	6.36
236	3.62	3.70	1.0	62594	2.32	2.38	0.60	37700	2.09	2.20	0.18	11445	11.9
367	3.62	3.69	1.0	62928	2.33	2.37	0.55	34618	2.09	2.20	0.26	16621	17.2
476	3.61	3.69	1.0	63564	2.32	2.38	0.55	35159	2.09	2.19	0.32	20363	20.8
597	3.62	3.69	1.0	55910	2.33	2.37	0.52	28997	2.09	2.20	0.38	21491	25.0
716	3.62	3.69	1.0	58347	2.31	2.38	0.53	30682	2.09	2.20	0.43	25211	28.1
844	3.62	3.69	1.0	59048	2.32	2.38	0.51	30010	2.09	2.20	0.48	28426	31.3
956	3.62	3.69	1.0	59466	2.32	2.37	0.48	28688	2.09	2.20	0.52	31101	34.0
1076	3.61	3.69	1.0	59243	2.32	2.36	0.43	25664	2.09	2.20	0.56	33302	36.5
1206	3.61	3.69	1.0	59225	2.32	2.37	0.45	26433	2.09	2.19	0.60	35808	39.3
1327	3.61	3.68	1.0	58947	2.31	2.37	0.41	24258	2.09	2.20	0.64	37887	41.8
1449	3.61	3.68	1.0	62463	2.31	2.37	0.41	25417	2.08	2.19	0.68	42378	44.1
1676	3.61	3.68	1.0	64235	2.31	2.37	0.37	23665	2.09	2.20	0.74	47229	47.8
1916	3.62	3.69	1.0	58382	2.31	2.36	0.32	18966	2.08	2.20	0.78	45812	51.0
2157	3.61	3.68	1.0	65119	2.31	2.36	0.30	19705	2.09	2.20	0.83	53894	53.8
2518	3.61	3.68	1.0	58528	2.31	2.36	0.27	15677	2.08	2.19	0.89	52027	57.8
2882	3.62	3.68	1.0	58310	2.31	2.36	0.25	14555	2.08	2.19	0.96	55791	62.2
3240	3.61	3.68	1.0	58049	2.31	2.36	0.23	13064	2.08	2.20	0.98	56990	63.8
3601	3.61	3.68	1.0	58832	2.31	2.36	0.21	12266	2.08	2.19	1.04	61022	67.4
3962	3.61	3.68	1.0	59481	2.31	2.36	0.19	11480	2.07	2.19	1.07	63889	69.8
4323	3.61	3.68	1.0	59418	2.31	2.36	0.18	10744	2.08	2.19	1.10	65102	71.2
4684	3.61	3.68	1.0	59349	2.31	2.35	0.16	9542	2.07	2.18	1.13	67171	73.6
5037	3.61	3.68	1.0	59447	2.30	2.37	0.16	9554	2.08	2.19	1.15	68552	75.0
5396	3.61	3.68	1.0	59852	2.31	2.36	0.14	8627	2.07	2.19	1.18	70430	76.5
5757	3.61	3.67	1.0	59033	2.31	2.35	0.13	7932	2.08	2.18	1.20	70618	77.8
7206	3.61	3.67	1.0	58240	2.30	2.36	0.11	6388	2.07	2.19	1.29	74987	83.7
8641	3.61	3.68	1.0	63599	2.30	2.36	0.09	5706	2.08	2.18	1.31	83453	85.3
10080	3.61	3.68	1.0	61951	2.31	2.35	0.07	4230	2.08	2.19	1.35	83414	87.5

11522	3.61	3.67	1.0	62287	2.32	2.35	0.05	3371	2.08	2.19	1.42	88398	92.3
12964	3.62	3.67	1.0	63816	2.31	2.35	0.05	2930	2.07	2.18	1.41	89783	91.5
14404	3.62	3.66	1.0	61198	2.32	2.34	0.04	2182	2.08	2.18	1.47	90018	95.6
15836	3.62	3.66	1.0	60402	2.31	2.34	0.03	1915	2.08	2.18	1.46	88340	95.1
17285	3.61	3.66	1.0	56080	2.31	2.35	0.03	1725	2.08	2.18	1.46	81937	95.0
18725	3.62	3.67	1.0	56152	2.32	2.34	0.02	1220	2.07	2.18	1.49	83712	96.9
20158	3.61	3.67	1.0	63841	2.31	2.34	0.02	1307	2.08	2.18	1.48	94172	95.9
VB313b	**Standard**				**Educt**				**Product**				**Yield (%)**
10	3.62	3.70	1.0	59610	2.34	2.38	0.56	33670					0.00
250	3.63	3.69	1.0	58405	2.34	2.37	0.50	29032	2.10	2.21	0.19	11329	12.6
489	3.63	3.68	1.0	59968	2.34	2.37	0.45	27210	2.09	2.19	0.33	19806	21.5
730	3.62	3.69	1.0	60599	2.32	2.38	0.48	28872	2.09	2.21	0.44	26788	28.8
970	3.62	3.69	1.0	61320	2.31	2.37	0.43	26214	2.09	2.20	0.53	32333	34.3
1216	3.63	3.69	1.0	60425	2.32	2.36	0.36	21838	2.08	2.20	0.61	37083	39.9
1454	3.62	3.69	1.0	55897	2.31	2.37	0.35	19566	2.08	2.19	0.68	37822	44.0
1694	3.62	3.68	1.0	60686	2.32	2.36	0.30	18037	2.09	2.19	0.73	44526	47.7
1935	3.62	3.68	1.0	61610	2.32	2.36	0.28	16990	2.08	2.19	0.79	48705	51.4
2175	3.61	3.68	1.0	62744	2.32	2.36	0.25	15549	2.08	2.20	0.84	52757	54.7
2417	3.61	3.68	1.0	62558	2.31	2.36	0.23	14380	2.08	2.20	0.88	54998	57.2
2657	3.62	3.69	1.0	63076	2.30	2.36	0.22	13568	2.08	2.19	0.90	56891	58.7
2898	3.62	3.68	1.0	62755	2.32	2.36	0.20	12241	2.08	2.19	0.94	59111	61.3
3260	3.61	3.68	1.0	62733	2.31	2.37	0.19	11919	2.08	2.20	1.00	62699	65.0
3620	3.61	3.68	1.0	62567	2.32	2.36	0.17	10465	2.08	2.19	1.05	65404	68.0
3981	3.60	3.68	1.0	62896	2.31	2.36	0.15	9681	2.08	2.20	1.07	67564	69.9
4342	3.61	3.69	1.0	63215	2.31	2.36	0.14	9138	2.08	2.20	1.10	69649	71.7
4704	3.62	3.68	1.0	63120	2.31	2.36	0.13	8413	2.08	2.20	1.13	71530	73.7
5062	3.60	3.69	1.0	64265	2.31	2.36	0.12	7730	2.07	2.20	1.15	73832	74.7
5426	3.61	3.68	1.0	61892	2.31	2.36	0.11	6868	2.07	2.20	1.18	73051	76.8
5793	3.62	3.68	1.0	62287	2.31	2.36	0.11	6590	2.07	2.19	1.19	74344	77.6
7232	3.61	3.68	1.0	63115	2.31	2.36	0.08	5133	2.07	2.20	1.26	79479	81.9
8673	3.62	3.68	1.0	58546	2.32	2.35	0.06	3464	2.07	2.18	1.30	76214	84.7
10109	3.61	3.67	1.0	57254	2.31	2.35	0.05	2754	2.08	2.19	1.35	77136	87.6
11551	3.62	3.67	1.0	57673	2.31	2.35	0.04	2257	2.08	2.18	1.36	78452	88.5
12971	3.61	3.67	1.0	58602	2.31	2.35	0.03	1942	2.07	2.18	1.40	81988	91.0
14412	3.62	3.67	1.0	56750	2.32	2.34	0.02	1351	2.08	2.19	1.43	80960	92.8
15854	3.61	3.67	1.0	60462	2.31	2.34	0.02	1282	2.08	2.18	1.43	86485	93.0
17300	3.61	3.67	1.0	58609	2.32	2.34	0.02	966	2.08	2.18	1.43	83752	92.9
18736	3.61	3.67	1.0	63974	2.32	2.34	0.01	953	2.08	2.18	1.43	91659	93.2

Table 4.33. Raw data of absolute kinetic of acylation reaction with **4a** with benzoic anhydride in $CDCl_3$.

Time (min)	Integ. limits (ppm)		Integ.	Absol.	Integ. limits (ppm)		Integ.	Absol.	Integ. limits (ppm)		Integ.	Absol.	$Yield_{ester}$ (%)
VB194a	**Standard**				**Educt**				**Product**				
5	3.56	3.74	1.0	58625	2.32	2.37	0.63	37172	2.10	2.19	0.01	611	0.67
37	3.61	3.69	1.0	58722	2.31	2.37	0.62	36637	2.09	2.19	0.05	2737	3.02
67	3.61	3.69	1.0	58538	2.31	2.37	0.61	35958	2.08	2.20	0.08	4512	4.99
97	3.61	3.69	1.0	59071	2.31	2.37	0.61	36062	2.08	2.20	0.11	6213	6.82
156	3.61	3.69	1.0	59201	2.31	2.37	0.58	34571	2.07	2.19	0.16	9377	10.3
213	3.62	3.68	1.0	59053	2.31	2.36	0.58	34030	2.07	2.20	0.21	12364	13.6
281	3.61	3.68	1.0	58777	2.31	2.36	0.56	33076	2.08	2.18	0.25	14905	16.4
333	3.61	3.68	1.0	59215	2.30	2.36	0.55	32587	2.07	2.19	0.30	17706	19.4
392	3.61	3.68	1.0	59642	2.31	2.36	0.52	31081	2.08	2.19	0.34	20097	21.8
450	3.61	3.68	1.0	59715	2.31	2.36	0.49	29359	2.08	2.19	0.37	22229	24.1
514	3.61	3.68	1.0	63053	2.30	2.36	0.48	29990	2.07	2.19	0.42	26222	26.9
575	3.60	3.69	1.0	63339	2.30	2.36	0.47	29730	2.07	2.19	0.45	28267	28.9
635	3.61	3.68	1.0	63361	2.29	2.36	0.45	28690	2.08	2.19	0.48	30324	31.0
694	3.60	3.68	1.0	63732	2.30	2.37	0.46	29172	2.08	2.19	0.50	32156	32.7
755	3.60	3.68	1.0	63802	2.30	2.36	0.41	26468	2.07	2.19	0.54	34396	34.9
876	3.60	3.68	1.0	63986	2.30	2.36	0.38	24505	2.07	2.19	0.60	38225	38.7
997	3.60	3.68	1.0	64034	2.29	2.36	0.37	23784	2.07	2.19	0.64	41231	41.7
1118	3.59	3.69	1.0	64182	2.30	2.36	0.34	21902	2.07	2.19	0.69	44111	44.5
1251	3.60	3.68	1.0	63750	2.30	2.36	0.32	20676	2.07	2.19	0.74	46869	47.6
1364	3.60	3.69	1.0	52932	2.29	2.36	0.32	17007	2.07	2.19	0.77	40516	49.6
1484	3.61	3.67	1.0	61087	2.30	2.36	0.29	17638	2.07	2.19	0.81	49396	52.4
1725	3.60	3.68	1.0	58809	2.29	2.36	0.27	15996	2.07	2.19	0.86	50830	56.0
1965	3.60	3.69	1.0	58933	2.30	2.36	0.26	15161	2.07	2.18	0.91	53687	59.0
2207	3.60	3.68	1.0	55340	2.29	2.37	0.25	13650	2.08	2.19	0.95	52505	61.5
2210	3.60	3.68	1.0	58009	2.29	2.36	0.24	13738	2.07	2.19	0.97	56000	62.6
2448	3.61	3.68	1.0	56370	2.30	2.35	0.22	12261	2.07	2.19	1.00	56561	65.0
2692	3.61	3.67	1.0	61225	2.31	2.35	0.20	11946	2.07	2.18	1.04	63499	67.2
2930	3.61	3.67	1.0	60434	2.30	2.35	0.18	10888	2.07	2.19	1.08	65068	69.8
3178	3.60	3.67	1.0	60350	2.30	2.35	0.17	10319	2.07	2.18	1.11	66703	71.6
3418	3.60	3.68	1.0	60926	2.30	2.35	0.16	9798	2.07	2.18	1.14	69206	73.6
3773	3.61	3.67	1.0	60384	2.30	2.35	0.14	8755	2.07	2.18	1.18	71140	76.3
4136	3.60	3.68	1.0	61349	2.30	2.35	0.13	7947	2.06	2.18	1.22	74786	79.0
4495	3.60	3.67	1.0	61796	2.31	2.34	0.12	7196	2.07	2.18	1.24	76698	80.4
4857	3.60	3.68	1.0	60808	2.30	2.35	0.11	6693	2.06	2.19	1.28	77835	82.9
5218	3.60	3.68	1.0	61304	2.30	2.35	0.10	6304	2.07	2.19	1.30	79723	84.3

5579	3.59	3.68	1.0	60920	2.30	2.35	0.10	5811	2.07	2.19	1.31	80076	85.2
5940	3.60	3.68	1.0	60573	2.30	2.36	0.09	5501	2.06	2.19	1.35	81493	87.2
6301	3.60	3.68	1.0	60464	2.30	2.35	0.08	4790	2.06	2.19	1.36	82343	88.2
6661	3.60	3.67	1.0	60161	2.30	2.35	0.08	4653	2.06	2.18	1.37	82697	89.1
7386	3.60	3.67	1.0	61445	2.30	2.35	0.07	4054	2.07	2.19	1.39	85633	90.3
8104	3.60	3.68	1.0	61020	2.30	2.34	0.06	3498	2.07	2.18	1.41	86018	91.3
8829	3.60	3.68	1.0	62440	2.31	2.35	0.05	3100	2.06	2.19	1.43	89575	93.0
9545	3.60	3.67	1.0	61945	2.31	2.34	0.04	2730	2.06	2.19	1.45	90070	94.2
10277	3.60	3.67	1.0	60214	2.31	2.34	0.04	2187	2.07	2.18	1.45	87460	94.1
10987	3.60	3.68	1.0	60122	2.32	2.34	0.03	1934	2.07	2.19	1.47	88159	95.0
11710	3.60	3.67	1.0	60477	2.31	2.34	0.03	1867	2.07	2.18	1.47	89079	95.4
12431	3.61	3.68	1.0	58107	2.31	2.34	0.03	1608	2.06	2.18	1.49	86625	96.6
13151	3.60	3.68	1.0	60990	2.30	2.34	0.03	1687	2.07	2.18	1.48	90226	95.9
13872	3.59	3.68	1.0	59134	2.30	2.35	0.03	1643	2.07	2.18	1.49	87926	96.4
14594	3.60	3.68	1.0	62330	2.30	2.35	0.03	1618	2.06	2.18	1.52	94822	98.6
15314	3.59	3.68	1.0	60375	2.31	2.34	0.02	1125	2.06	2.18	1.52	91825	98.6
16034	3.59	3.68	1.0	59947	2.31	2.34	0.02	1039	2.06	2.18	1.52	91080	98.5
16756	3.60	3.68	1.0	60974	2.31	2.34	0.02	1076	2.06	2.18	1.52	92801	98.6
17476	3.60	3.67	1.0	61509	2.31	2.34	0.01	915	2.06	2.18	1.53	94379	99.4
VB194b	**Standard**				**Educt**				**Product**				**Yield (%)**
8	3.60	3.71	1.0	61736	2.33	2.37	0.58	35569	2.10	2.19	0.01	849	0.89
125	3.61	3.69	1.0	54543	2.32	2.36	0.56	30319	2.09	2.19	0.15	8125	9.65
255	3.62	3.68	1.0	61450	2.31	2.37	0.56	34562	2.08	2.19	0.26	16169	17.0
380	3.61	3.69	1.0	61470	2.30	2.36	0.52	31674	2.08	2.18	0.36	22276	23.5
498	3.60	3.68	1.0	61825	2.31	2.36	0.46	28732	2.08	2.19	0.45	27570	28.9
617	3.61	3.68	1.0	61757	2.31	2.36	0.42	26202	2.08	2.19	0.52	32052	33.6
738	3.61	3.68	1.0	61746	2.30	2.35	0.39	23845	2.08	2.18	0.57	35330	37.1
855	3.61	3.68	1.0	61431	2.31	2.35	0.37	22739	2.08	2.19	0.63	38888	41.0
975	3.61	3.68	1.0	61161	2.31	2.36	0.35	21466	2.08	2.19	0.68	41513	44.0
1098	3.61	3.68	1.0	60826	2.31	2.35	0.33	19817	2.07	2.19	0.73	44334	47.2
1216	3.60	3.68	1.0	61236	2.31	2.35	0.30	18650	2.08	2.19	0.76	46801	49.5
1340	3.60	3.68	1.0	61016	2.30	2.35	0.29	17993	2.07	2.19	0.81	49446	52.5
1461	3.61	3.68	1.0	61127	2.31	2.36	0.28	17200	2.07	2.19	0.85	51713	54.8
1701	3.60	3.68	1.0	60905	2.30	2.35	0.25	15438	2.07	2.18	0.90	55114	58.6
1943	3.61	3.68	1.0	60698	2.30	2.36	0.24	14455	2.07	2.19	0.97	58784	62.7
2185	3.61	3.68	1.0	60823	2.30	2.35	0.22	13169	2.07	2.19	1.02	61931	66.0
2422	3.61	3.68	1.0	60597	2.31	2.35	0.20	11948	2.06	2.19	1.06	64301	68.8
2663	3.60	3.68	1.0	60792	2.30	2.35	0.19	11378	2.07	2.18	1.08	65598	69.9
2909	3.59	3.68	1.0	60893	2.30	2.35	0.18	10819	2.07	2.18	1.12	68299	72.7
3268	3.60	3.68	1.0	61164	2.29	2.35	0.16	9647	2.07	2.18	1.17	71284	75.5

3628	3.60	3.68	1.0	61041	2.30	2.35	0.14	8731	2.06	2.19	1.22	74452	79.0
3995	3.60	3.68	1.0	61489	2.31	2.35	0.13	7733	2.07	2.18	1.23	75720	79.8
4351	3.60	3.68	1.0	62376	2.31	2.35	0.11	7115	2.07	2.18	1.26	78869	81.9
4711	3.60	3.67	1.0	61067	2.30	2.35	0.11	6473	2.07	2.18	1.30	79256	84.1
5058	3.61	3.67	1.0	61858	2.30	2.35	0.10	6286	2.07	2.18	1.31	81343	85.2
5418	3.61	3.68	1.0	55484	2.30	2.35	0.10	5281	2.07	2.18	1.34	74420	86.9
5779	3.60	3.67	1.0	61116	2.31	2.34	0.08	4965	2.07	2.18	1.35	82230	87.2
6140	3.61	3.67	1.0	55493	2.30	2.35	0.08	4350	2.07	2.18	1.38	76328	89.1
6501	3.61	3.67	1.0	60950	2.31	2.34	0.07	4323	2.07	2.18	1.39	84726	90.1
6870	3.61	3.67	1.0	59374	2.31	2.34	0.07	4063	2.07	2.18	1.40	83218	90.8
7233	3.60	3.67	1.0	60821	2.30	2.34	0.06	3722	2.07	2.18	1.42	86219	91.8
7584	3.60	3.67	1.0	60023	2.30	2.34	0.06	3565	2.07	2.18	1.42	85153	91.9
7946	3.60	3.67	1.0	59609	2.30	2.35	0.06	3407	2.07	2.18	1.43	85149	92.5
8672	3.60	3.67	1.0	57517	2.31	2.34	0.05	2902	2.07	2.19	1.46	84118	94.8
9388	3.60	3.68	1.0	56767	2.31	2.35	0.02	1331	2.07	2.18	1.47	83336	95.1
10110	3.61	3.67	1.0	60453	2.31	2.34	0.04	2281	2.06	2.18	1.49	90206	96.7
10830	3.60	3.67	1.0	61460	2.31	2.34	0.03	2080	2.07	2.18	1.50	92240	97.2
11551	3.60	3.67	1.0	59349	2.30	2.34	0.03	1886	2.06	2.19	1.52	90014	98.3
12271	3.60	3.68	1.0	61240	2.31	2.34	0.03	1682	2.06	2.19	1.52	93122	98.5
12994	3.61	3.67	1.0	59203	2.30	2.34	0.03	1599	2.06	2.19	1.54	91272	99.9
13713	3.61	3.67	1.0	58872	2.31	2.34	0.02	1206	2.06	2.18	1.54	90880	100
14436	3.60	3.67	1.0	62023	2.31	2.34	0.02	1274	2.06	2.18	1.54	95498	99.8
15156	3.59	3.67	1.0	61072	2.31	2.34	0.02	1201	2.06	2.18	1.54	94104	99.8
15878	3.59	3.67	1.0	58961	2.31	2.33	0.02	953	2.06	2.18	1.54	90832	99.8
16598	3.61	3.67	1.0	59686	2.31	2.34	0.02	979	2.07	2.18	1.55	92315	100
17322	3.59	3.67	1.0	62618	2.32	2.33	0.01	768	2.07	2.18	1.53	96056	99.4
18039	3.60	3.67	1.0	55570	2.31	2.34	0.02	936	2.06	2.18	1.55	85993	100
18768	3.60	3.67	1.0	62464	2.31	2.33	0.01	733	2.06	2.18	1.56	97216	100
19481	3.60	3.67	1.0	56072	2.31	2.34	0.01	735	2.07	2.18	1.55	87096	100
20202	3.60	3.67	1.0	57235	2.31	2.34	0.01	645	2.07	2.18	1.56	89095	100

4.5 References

[1] C. E. Müller, P. R. Schreiner, *Angew. Chem. Int. Ed.* **2011**, *50*, 6012–6042.

[2] S. Xu, I. Held, B. Kempf, H. Mayr, W. Steglich, H. Zipse, *Chem. Eur. J.* **2005**, *11*, 4751–4757.

[3] I. Held, E. Larionov, C. Bozler, F. Wagner, H. Zipse, *Synthesis* **2009**, *2009*, 2267–2277.

[4] R. Tandon, T. Unzner, T. A. Nigst, N. De Rycke, P. Mayer, B. Wendt, O. R. P. David, H. Zipse, *Chem. Eur. J.* **2013**, *19*, 6435–6442.

[5] N. A. Richard, G. D. Charlton, C. A. Dyker, *Org. Biomol. Chem.* **2021**, *19*, 9167–9171.

[6] T. Furuta, T. Kawabata, in *Lewis Base and Acid Catalysis* (Ed.: B. List), Georg Thieme Verlag KG, Stuttgart, **2012**, p. 497–546.

[7] G. Höfle, W. Steglich, H. Vorbrüggen, *Angew. Chem.* **1978**, *90*, 602–615.

[8] E. Guibe-Jampel, G. Le Corre, M. Wakselman, *Tetrahedron Lett.* **1979**, *20*, 1157–1160.

[9] A. C. Spivey, S. Arseniyadis, *Angew. Chem. Int. Ed.* **2004**, *43*, 5436–5441.

[10] V. Lutz, J. Glatthaar, C. Würtele, M. Serafin, H. Hausmann, P. R. Schreiner, *Chem. Eur. J.* **2009**, *15*, 8548–8557.

[11] E. Vedejs, S. E. Denmark, *Lewis Base Catalysis in Organic Synthesis, 3 Vol. Set*, Wiley-VCH, Weinheim, **2016**.

[12] G. Höfle, W. Steglich, H. Vorbrüggen, *Angew. Chem. Int. Ed.* **1978**, *17*, 569–583.

[13] F. A. Carey, R. J. Sundberg, *Advanced Organic Chemistry: Part A: Structure and Mechanisms*, Springer Science & Business Media, New York, **2007**.

[14] S. Mayr, H. Zipse, *Eur. J. Org. Chem.* **2022**, *2022*, e202101521.

[15] I. Held, S. Xu, H. Zipse, *Synthesis* **2007**, *2007*, 1185–1196.

[16] A. Hassner, V. Alexanian, *Tetrahedron Lett.* **1978**, *19*, 4475–4478.

[17] A. Sakakura, K. Kawajiri, T. Ohkubo, Y. Kosugi, K. Ishihara, *J. Am. Chem. Soc.* **2007**, *129*, 14775–14779.

[18] D. R. Lide, *CRC Handbook of Chemistry and Physics, 85th Edition*, CRC Press, Washington DC, **2004**.

[19] C. Reichardt, *Chem. Rev.* **1994**, *94*, 2319–2358.

[20] C. Reichardt, G. Schäfer, *Liebigs Ann.* **1995**, *1995*, 1579–1582.

[21] C. Reichardt, *Green Chem.* **2005**, *7*, 339–351.

[22] V. G. Machado, R. I. Stock, C. Reichardt, *Chem. Rev.* **2014**, *114*, 10429–10475.

[23] V. Gutmann, *Electrochimica Acta* **1976**, *21*, 661–670.

[24] C. Reichardt, T. Welton, *Solvents and Solvent Effects in Organic Chemistry: Fourth Edition*, Wiley-VCH, Weinheim, **2011**.

[25] T. Tsutsumi, A. Saitoh, T. Kasai, M. Chu, S. Karanjit, A. Nakayama, K. Namba, *Tetrahedron Lett.* **2020**, *61*, 152047.

[26] J. Helberg, T. Ampßler, H. Zipse, *J. Org. Chem.* **2020**, *85*, 5390–5402.

[27] R. K. Harris, E. D. Becker, S. M. C. de Menezes, R. Goodfellow, P. Granger, *Pure Appl. Chem.* **2001**, *73*, 1795–1818.

[28] S. Hoops, S. Sahle, R. Gauges, C. Lee, J. Pahle, N. Simus, M. Singhal, L. Xu, P. Mendes, U. Kummer, *Bioinformatics* **2006**, *22*, 3067–3074.

Chapter 5. Reactivity Enhancement of Chiral Lewis Base Catalysts through Ion Pair Formation

Veronika Burger, Stella-Marie Bauer and Hendrik Zipse

Unpublished results.

Autor contributions: Veronika Burger (V.B.) and Hendrik Zipse (H.Z.) conceived the study. Synthetic procedures were performed by V.B. and Stella-Marie Bauer (S.B.). Kinetic and mechanistic studies were performed by S.B. in her master project under the supervision of V.B. Computational studies were performed by V.B.

Additional information: Experimental procedures and kinetic studies of S.B. are omitted here and can be found in "Acylation with 2,2,2-Trichloro-*tert*-butyl chloroformate – Kinetic and Mechanistic Studies", Master thesis, LMU München (Munich), **2022**.

5.1 Introduction

Pyridine-based organocatalysts represent a large class of Lewis Base catalysts for several organocatalytic transformation reaction.[1,2] DMAP (**1**) is the best-known catalyst of this class, and its scaffold was widely used as a basic framework for the development of multiple chiral derivatives for stereoselective reactions.[3–6] These chiral variations of **1** can be divided into three subgroups based on their overall topology (see Chart 5.1).

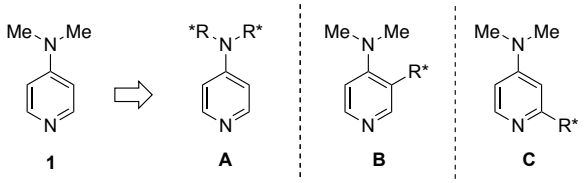

Chart 5.1. Pyridine-based Lewis base catalysts sorted by topology.

Group **A** positions the chiral element within one of the donor groups of the dialkylamino substituents attached to the C4 position of the pyridine ring. Given the distance between these substituents and the catalytically active pyridine-nitrogen, this approach requires a rather large substituent. Group **B** features a chiral side chain, or an axially chiral ligand attached to the C3 position of the pyridine ring. This brings the chiral information closer the Lewis basic reaction center but may also cause conformational changes in the C4 substituent, potentially leading to a reduced absolute catalytic reactivity. Group **C** attaches the chiral substituent to the C2 position, placing it in close proximity of the catalytic center. However, exactly this closeness is known to significantly reduce the nucleophilic activity pyridines.[5,6] The main reason for the reduced reactivity lies in the structure of the *N*-acylpyridinium ion **26**, which is formed in the first addition step in the acylation mechanism for pyridine-based catalysts as shown in Figure 5.1.[2] Ideally it would occupy a planar conformation to maximize the conjugation between the electron donor and the acyl group. C2-Substitutents, however, force the acyl group out of plane due to steric interactions, which ultimately destabilizes the acylated intermediate **27**, resulting in a lower reaction by increased activation energy.[7]

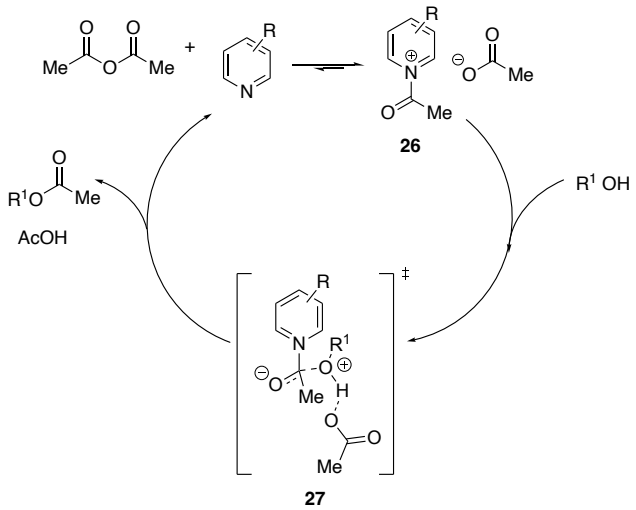

Figure 5.1. Mechanism for acylation of alcohols catalyzed by pyridine-based catalysts, adapted from Denmark *et al*.[2]

In 1996, Vedejs *et al.* published one of the first chiral DMAP derivatives in organocatalysis with a C2-substituent (Vedejs Cat, **28**).[8] The catalytic efficiency of **28** is, however, strongly reduced due to the C2-substitution such that a classical stereoselective catalytic process was not observed. Nevertheless, the pyridinium acyl salt of **28** was successfully employed in the stereoselective acylation of secondary alcohol

29 using 2,2,2-trichloro-1,1-dimethylethyl chloroformate (**30**) as acylation reagent to form 1-phenylethyl-2,2,2-trichloro-1,1-dimethylethyl carbonate **31** as product, as shown in Scheme 5.1.

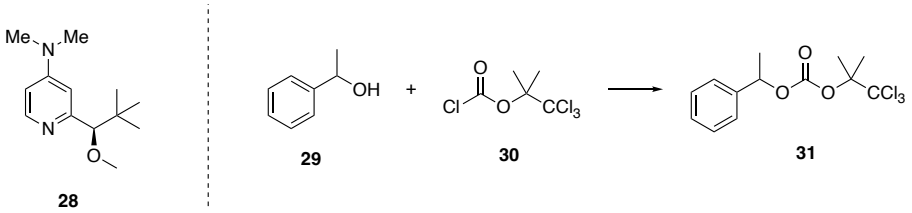

Scheme 5.1. Vedejs' chiral DMAP derivative **28** and its original benchmark reaction.

We already demonstrated that the nucleophilic reactivity of catalysts can be increased by introducing ionic moieties into the scaffold. Therefore, the aim of this study was to investigate the potential enhancement of catalytic activity of chiral Lewis base catalysts with previously low reactivity by transforming them into anionic compounds. For this reason, the Vedejs' catalyst **28** was chosen as scaffold, whereas the *N*-dimethylamino group was to be replaced with a sulfonamide group (see Scheme 5.2).

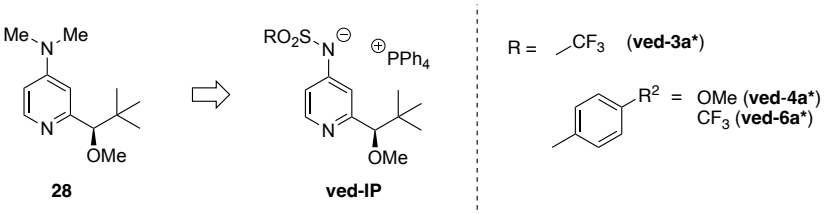

Scheme 5.2. Proposed chiral pyridinamide ion pairs based on Vedejs' catalyst (**28**).

To achieve this goal, several synthetic strategies were explored to develop a viable procedure for the synthesis of a chiral pyridinamide ion pair (**ved-IP**). The synthesis of chiral DMAP **28** was used as a reference point. However, the first acylation step proved to be challenging. Various methods were employed to introduce the substituent at the C2 position, including direct metalation with organometallic reagents and a milder approach *via* lithium-bromide exchange. When these strategies proved unsuccessful, a radical approach was attempted. Despite these efforts, we have so far had only limited success in developing a viable procedure for the synthesis of a chiral pyridinamide. This chapter provides a detailed account of the attempts conducted and could serve as a foundation for future studies.

5.2 Results and Discussion

5.2.1 Synthesis of Chiral Pyridinamide Derivatives

The original synthesis of Vedejs'[8] catalyst **28** started with the protection of DMAP using BF_3 etherate, followed by the metalation at the C2-position using lithium tetramethylpiperidine (LiTMP) and subsequent acylation by pivaloyl chloride (PivCl) to synthesize ketone **32** in step **A**. In step **B**, an enantioselective reduction was performed with (-)-diisopinocampheyl chloroborane, yielding (*R*)-alcohol **33**, which was then methylated by using potassium hydride in presence of 18-crown-6 and methyl iodide to obtain Vedejs' catalyst **28** as final product in step **C**, as it is shown in Scheme 5.3.

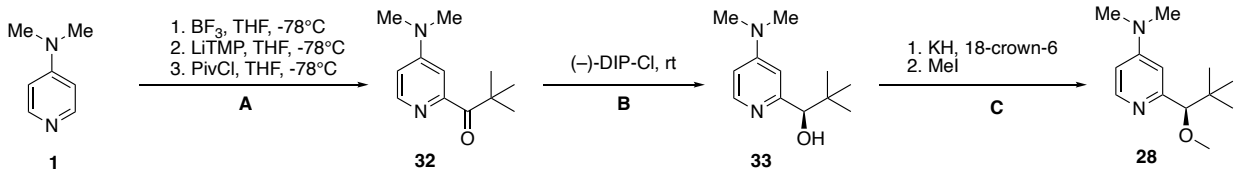

Scheme 5.3. Vedejs' original three step synthesis.[8]

Based on this procedure, an initial synthesis plan for the formation of chiral sulfonamide derivatives **ved-IP** was developed, keeping the synthesis steps as close to the original synthesis as possible. The first consideration was the selection of a starting compound that would allow the easy introduction of the sulfonamide group after synthesizing the chiral side arm.

In a first attempt, 4-aminopyridine (**34**) was double protected using sodium hydride and benzyl bromide. The protected product **35** was then subjected to step **A** of Vedejs' original synthesis as depicted in Scheme 5.4. After purification *via* column chromatography, instead of the desired C2-ketone **36**, the starting material was reisolated. A potential reason for the failed metalation might have been residual ethyl acetate (EtOAc) in compound **35**. Substrate **35** was dried in high vacuum over two days. However, the NMR spectra still showed a high content of EtOAc in the sample.

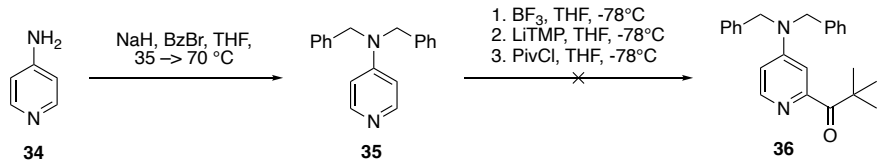

Scheme 5.4. Metalation of 4-dibenzylaminopyridine with tetramethyl piperidine lithium (LiTMP) and subsequent acylation with pivaloyl chloride according to Vedejs[8]; not successful.

Next, we employed 2-bromo-4-nitropyridine (**37**) as starting compound for the synthesis of ketone **38** (see Scheme 5.5). Instead of direct metalation, a lithium-bromide exchange with *n*-BuLi at -78 °C was attempted, followed by acylation with pivaloyl chloride at -78 °C. The NMR of the crude product showed promising signals. However, only starting material was isolated after column chromatography. Thereafter, a modified procedure from Bolm *et al.*,[9] consisting of a lithium-bromide exchange with *n*-BuLi at -78 °C, followed by the addition of pivalonitrile and subsequent hydrolysis with dilute sulfuric acid, was attempted. Again, no desired product **38** could be isolated after column chromatography. The high-resolution mass spectrometry (HRMS) analysis of the isolated compound, still showed bromine in the sample, indicating that the lithium-bromide exchange did not occur. This would subsequently have prohibited the acylation.

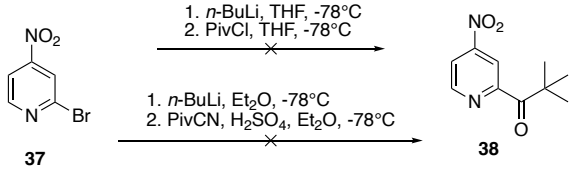

Scheme 5.5. Metalation of 4-nitropyridine with *n*-butyl lithium, followed by acylation with different reagents; not successful.

Another potential reason why these procedures failed might be the absence of a protected pyridine nitrogen, which could have led to side reactions. To avoid this issue, 4-nitropyridine-*N*-oxide (**39**) was used as the next starting compound (see Scheme 5.6). First, a direct metalation on the C2 position of 4-nitropyridine-*N*-oxide according to Vedejs' original synthesis was attempted, followed by acylation with pivaloyl chloride. The crude NMR of this reaction only showed the signals of the starting material instead of product **40**. Next, 4-nitro-2-bromo-pyridine-*N*-oxide (**41**) was used to undergo a lithium-bromide exchange, followed by acylation with pivaloyl chloride in THF at -78 °C. Here, the crude NMR did not show any aromatic signals, indicating compete degradation of the starting material.

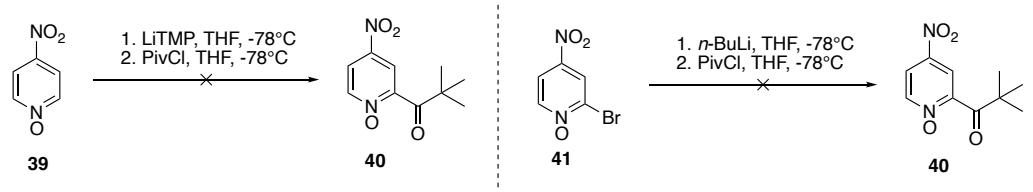

Scheme 5.6. Different metalation conditions for 4-nitropyridine-*N*-oxides **39** and **41**, followed by acylation with pivaloyl chloride; not successful.

Afterwards, Grignard reagents were used instead of lithium reagents, as depicted in Scheme 5.7. 2-Bromo-4-nitropyridine (**37**) was used as the starting material. First, *iso*-propylmagnesium chloride lithium chloride complex (*i*-PrMgCl x LiCl) was utilized for the metal-halogen exchange, followed by transmetalation with copper cyanide di(lithium chloride) complex (CuCN x 2 LiCl) in THF at -40 °C. The subsequent acylation was performed with pivaloyl chloride. In the first attempt, the acylation reagent was directly added to the Grignard solution at -40 °C. In the second attempt, the Grignard solution was added dropwise to a solution of pivaloyl chloride in THF at -40 °C. In both cases, no aromatic signals were detected in the crude NMR, indicating degradation of the pyridine ring during the reaction.

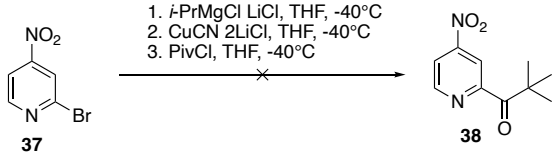

Scheme 5.7. Magnesium-bromide exchange with 2-bromo-4-nitropyridine, followed by transmetalation with copper cyanide and subsequent acylation with pivaloyl chloride; not successful.

The nitro group is a strongly deactivating group, which could explain the lack of product formation under the tested reaction conditions for synthesizing the new derivative C2-ketone **32**. Additionally, instead of focusing on synthesizing the ketone, we attempted to synthesize a derivative of alcohol **33** directly, aiming for an enantioselective separation rather than a stereoselective reduction. Therefore, the next starting compound, 2-bromo-4-chloropyridine (**42**), was used. A modified procedure based on Bolm *et al*.[9] was performed, using lithium-bromide-exchange and pivalaldehyde for the alcohol formation (see Scheme 5.8). However, the crude NMR did not show any aromatic signals, again indicating the degradation of the pyridine ring.

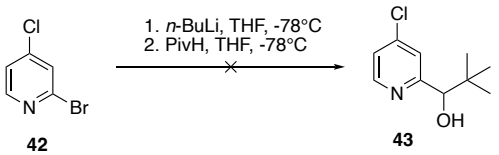

Scheme 5.8. Metalation of 2-bromo-4-chloropyridine with *n*-BuLi, followed by reaction with pivalaldehyde; not successful.

Next, the procedure by Chopping *et al*.[10] was given a try. As shown in Scheme 5.9, dimethylamino ethanol (DMAE) was used to form a lithiation reagent *in situ* with *n*-BuLi at -5.0 °C. The mixture was then cooled down to -78 °C before pivalaldehyde was added slowly. Once again, the crude NMR did not show any aromatic signals, indicating degradation of the pyridine ring.

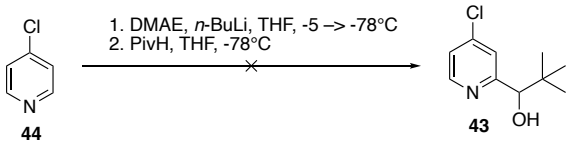

Scheme 5.9. Metalation of 4-chloropyridine with dimethylamino ethanoate/*n*-BuLi and acylation with pivaloyl chloride; not successful.

As an alternative to metalation procedures, the carbonyl group was attempted to be introduced via a Weinreb amide. As depicted in Scheme 5.10, methyl-4-chloropicolinate (**45**) was first hydrolyzed under alkaline conditions. The resulting carboxylic acid **46** was converted into the Weinreb amide **47** using *N,O*-dimethyl hydroxylamine, HATU, and Hünig's base. Subsequently, attempts were made to convert Weinreb **47** into the C2-ketone derivative **48**. However, the desired product **48** was not isolated after column chromatography. Instead, the NMR spectra showed another alkylated product, that was not further characterized.

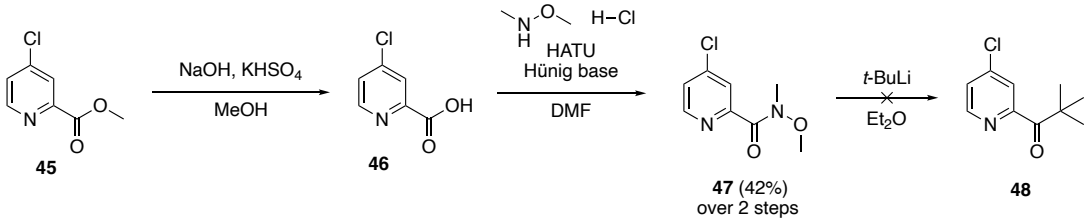

Scheme 5.10. Weinreb amide synthesis starting with methyl-4-chloropicolinat (**45**), followed by reaction with *tert*-butyl lithium yielding C2-ketone derivative **48**; not successful.

Potentially, chloride might be still too deactivating for a successful synthesis of either a derivative of ketone **32** or a non-chiral derivative of alcohol **33**. Therefore, another starting compound, 4-methoxypyridine (**49**), was tested, as shown in Scheme 5.11. Compound **49** was first subjected to the reaction conditions of the original Vedejs' catalyst synthesis. However, the crude NMR did not show aromatic signals, indicating the degradation of the pyridine ring.

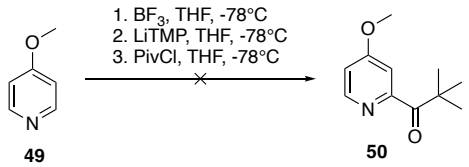

Scheme 5.11. Metalation of 4-methoxypyridine (**49**) with LiTMP and subsequent acylation with pivaloyl chloride according to Vedejs[8]; not successful

Next, 4-methoxypyridine (**49**) was brominated using the procedure of Bori and Comins,[11] involving a direct metalation with BuLi-LiDMAE[12] (see Scheme 5.12). This was followed by bromination with 1,2-dibromo tetrachloroethane to form compound **51**, which was then used in the synthesis of ketone **50**. The bromination was successful, yielding 35 % of brominated product **51**. Subsequently, the procedure of Bolm *et al.*[9] was followed for the synthesis of ketone **50**, which yielded 12 %. While the reaction needs to be optimized, the formation of the ketone **50** was successful for the first time using another starting compound than DMAP (**1**).

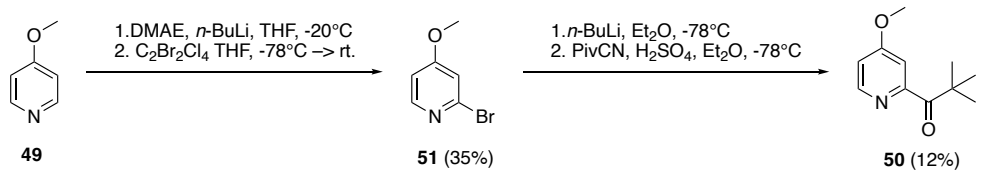

Scheme 5.12. Bromination of 4-methoxypyridine (**49**), followed by lithium-bromide exchange and acylation with pivalonitrile.

However, simultaneously performed test reactions on 4-methoxypyridine **49** to transform the 4-methoxy substituent into a group, that could be converted into the sulfonamide group of the final ionic catalyst were unsuccessful (see Chapter 5.4 for details). Consequently, this synthesis pathway was set aside.

Instead of focusing on acylation *via* organometallic methods, a radical approach using the Minisci reaction type was tested next with 4-cyanopyridine (**52**) as starting material, as shown in Scheme 5.13.[13,14]

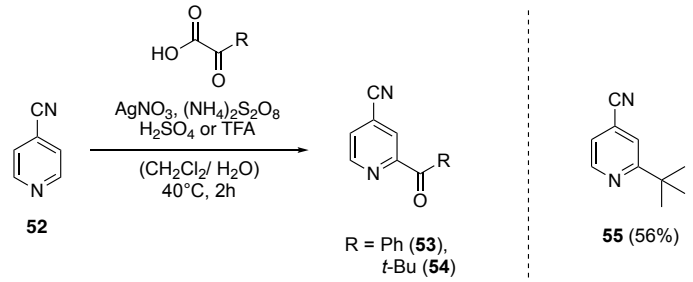

Scheme 5.13. Radical acylation of 4-cyanopyridine.

The Minisci reaction works well for the acylation with phenyl glyoxylic acid, yielding 98 % of product **53**. However, with 3,3-dimethyl-2-oxobutanoic acid, instead of the desired acylation, an alkylation occurred due to the better stabilization of the *tert*-butyl radical compared to the acyl radical. Thus, instead of acylation product **54**, the alkylated product **55** was formed. Nevertheless, this approach could be an alternative for the investigation of future chiral side chain in the Vedejs' catalyst.

The synthesis was continued with the reduction of compound **53**, as shown in Scheme 5.14. First, we attempted the stereoselective reduction using (-)-DIP-Cl, according to Vedejs' original synthesis. After five days, instead of (*R*)-**56**, only the starting material **53** was recovered after column chromatography. Next, a classical reduction with sodium borohydride was performed, yielding 65 % of racemic alcohol rac-**56**. The next step would be a diastereomeric separation of the racemic alcohol by reacting rac-**56** with e.g. (1*S*)-camphanoyl chloride to facilitate a chromatographic separation of the resulting diastereomers.[9]

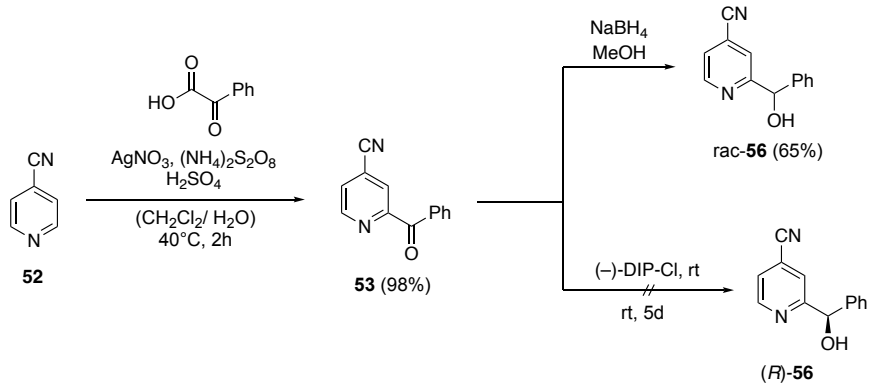

Scheme 5.14. Radical acylation of 4-cyanopyridine (**52**), followed by reduction of ketone **53**. Stereoselective reduction with (-)-DIP-Cl was not successful.

Furthermore, the conversion of the nitrile group into, for example, a free amino group has to be tested to confirm the validity of this synthetic plan for the synthesis of an ionic Vedejs' catalyst derivative. Scheme 5.15 shows a potential route.[15]

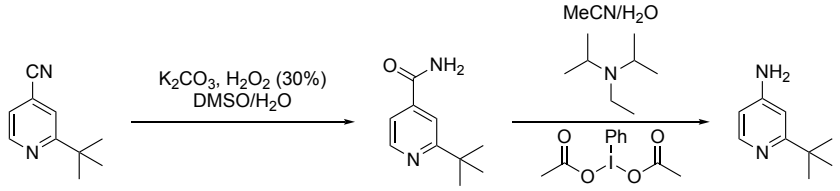

Scheme 5.15. Proposed synthesis rout to convert 2-(*tert*-butyl)isonicotinonitrile into 2-(*tert*-butyl)pyridin-4-amine.

So far, the task of finding a successful synthesis plan for the preparation of an ionic Vedejs catalyst has not been solved. However, to determine what potential result can be expected, computational studies were performed to: a) identify the most promising sulfonamide substituent to enhance the reactivity of

the chiral pyridinamide ion pair, and b) to assess what reactivity and enantioselectivity can be expected from the ionic Vedejs derivative compared to the original neutral compound **28**.

5.2.2 Computational Study

To examine which chiral pyridinamide derivative should be the focus of our synthetic endeavors, preliminary computational studies regarding their reactivity and stereoinductive potential were performed at the SMD($CHCl_3$)/B3LYP-D3/6-31+G(d) level of theory. The strategy of the conformational search is detailed in Chapter 5.4, however, it should be noted that additional studies regarding the procedure should be undertaken to minimize computational costs and effort. Relative affinity values, such as acyl cation affinities (ΔACA) and methyl cation affinities (ΔMCA), have been shown to correlate well with experimentally obtained rate constants.[16–18] As shown in Scheme 5.16, acyl cation affinities (ΔACA) were calculated as reaction enthalpies at 298.15 K of an isodesmic group transfer reaction with pyridine as reference system.

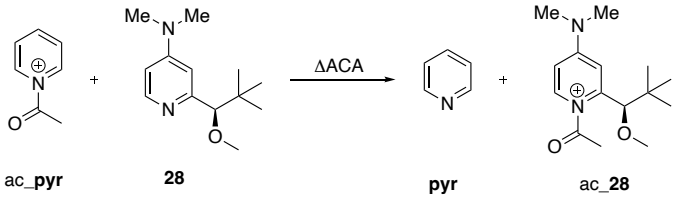

Scheme 5.16. Isodesmic acyl transfer reaction for acyl cation affinity (ACA) calculation between reference pyridine and Vedejs' catalyst **28**.

The Lewis basicity of **28** was lower than that of neutral non-chiral reference organocatalyst DMAP (**1**) due to the deactivating effect of the C2-substituent. Chiral pyridinamide anions **ved-3***, **ved-4***, and **ved-6*** showed a much larger Lewis basicity despite carrying the same C2-substituent. However, looking at the respective chiral ion pair **ved-3a*** the Lewis basicity was reduced by a factor of two. Applying this factor to pyridinamide anion **ved-4*** and **ved-6***, the Lewis basicity of their respective ion pair can be expected to be located in the region around -50 to -60 kJ mol^{-1}. Even so, **ved-3a*** surpassed **28** in terms of relative Lewis basicity towards the acyl group. Therefore, a higher reactivity can be expected, which would fulfill the first aim of this study: the enhancement of chiral Lewis base catalysts through ion formation.

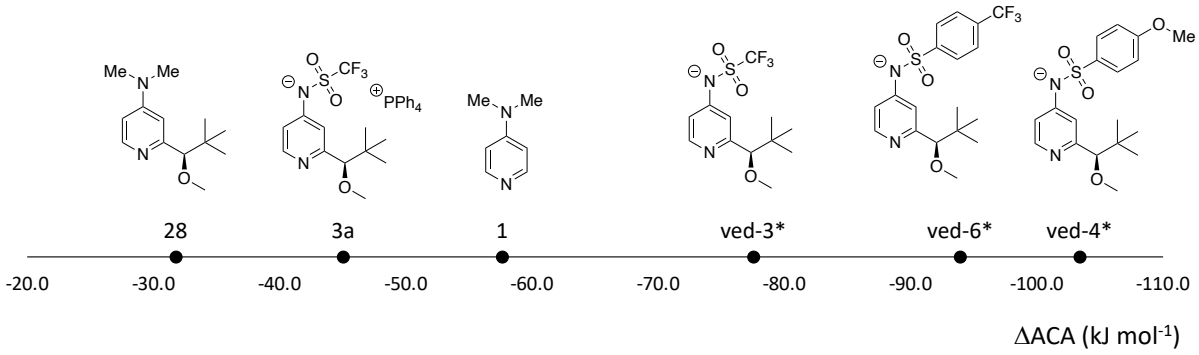

Figure 5.2. Acyl cation affinity values (ΔACA) of DMAP (**1**), Vedejs catalyst (**28**), chiral pyridinamide ion pair **3a***, and chiral pyridinamide anion **ved-3***, **ved-4***, and **ved-6***.

The enhancement of reactivity is only useful if the selectivity of the new chiral pyridinamide catalyst remains the same or improves. To predict the stereo-inductive potential of chiral pyridinamide ion pair derivatives, a modified version of Mosher's cation approach, first introduced as a chirality prediction tool by Zipse *et al.*[19] in 2008, was used. Previously, the Mosher's cation fragment **57** was attached directly to the catalytic center of the chiral compound, once in (*R*)-configuration and once in (*S*)-configuration. In

this work, the carbonyl group of Mosher's acid was included in the chiral fragment **58** and the chiral adducts to maintain a closer representation of the experimental conditions (see Scheme 5.17A).

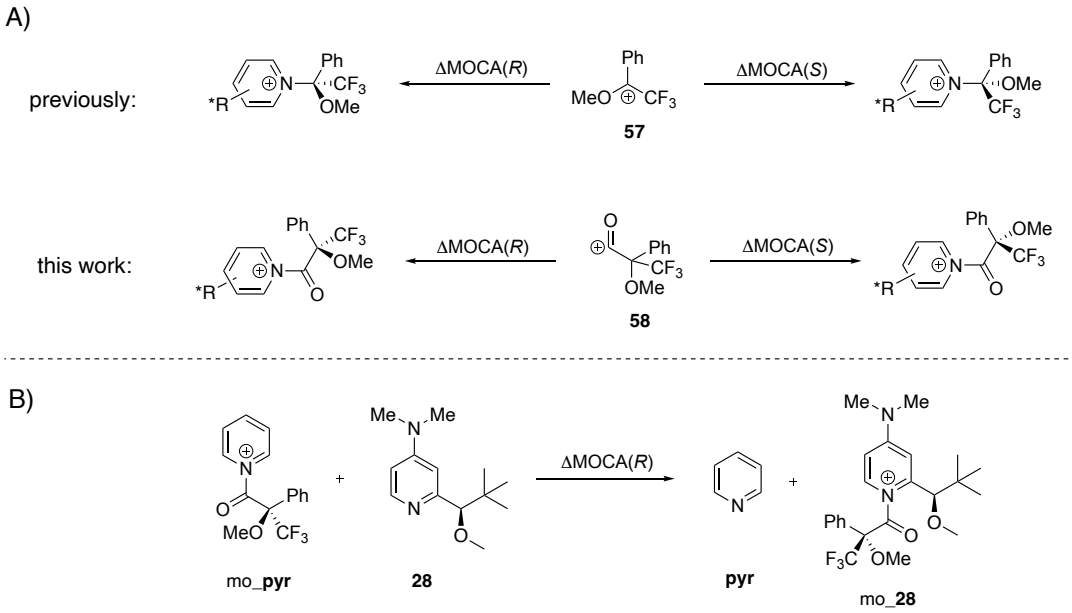

Scheme 5.17. A) Simplified model reaction of Mosher's cation affinity (MOCA) calculation. B) Exemplary isodesmic Mosher's cation transfer reaction for calculation of Mosher's cation affinity values (ΔMOCA).

The Mosher's cation affinity was then calculated as the reaction enthalpy of an isodesmic group transfer reaction with pyridine as reference compound as shown in Scheme 5.17B. Subtracting the resulting affinity values ΔMOCA(*R*-*S*) supposedly indicates which enantiomer will be preferred.

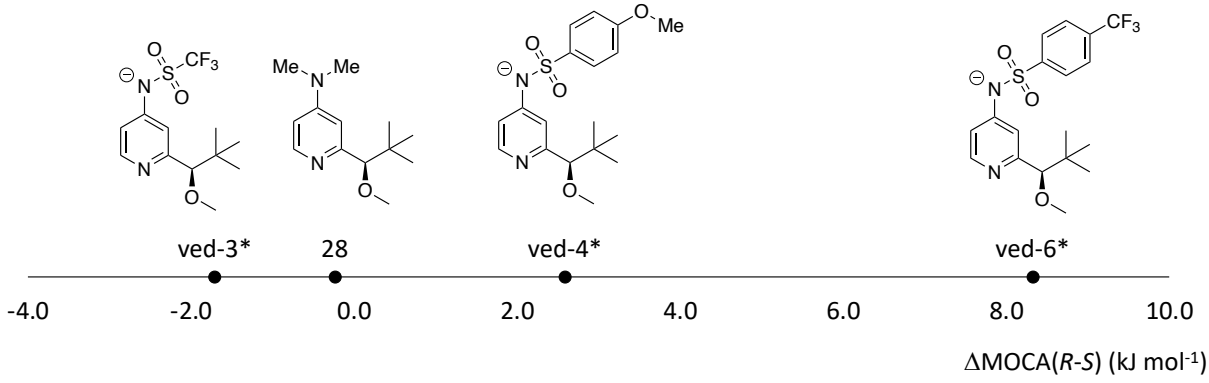

Figure 5.3. Mosher's cation affinity values (ΔMOCA(*R*-*S*)) of Vedejs' catalyst (**28**) and chiral pyridinamide anion **3***, **4***, and **6***.

The preliminary results for the ΔMOCA of the chiral pyridinamide anions indicated a preference for the *S*-configuration for chiral anion **ved-3***, whereas chiral anions **ved-4*** and **ved-6*** clearly favor the *R*-configuration. Vedejs *et al.* reported the enantiomeric purity of the *S*-enantiomer of the ester product to be greater than 90 % at conversions in the 20-40 % range.[8] Thus, even with a strongly reduced reactivity, the loaded pyridinium salt of the catalyst displayed a high stereoselectivity. This clear preference for the *S*-configuration of the ester product was not evident in the ΔMOCA(*R*-*S*) of the Vedejs' catalyst. These findings tell us that this ΔMOCA approach to quantify the stereo-inductive potential of catalysts does not provide reliable results as it stands.

5.3 Conclusion & Outlook

The synthesis of chiral pyridinamide derivatives posed significant challenges, especially when adapting Vedejs' original synthesis for various 2-substituted pyridine derivatives. Metalation and subsequent acylation, particularly with strongly deactivating groups, such as nitro group and chloro group at the C4 position, repeatedly failed. Despite various attempts, including alternative approaches, such as lithium-bromide exchange and Grignard reagents, the successful synthesis of derivatives of ketone **32** or alcohol **33** was only achieved in the low-yield synthesis of 1-(4-methoxypyridin-2-yl)-2,2-dimethylpropan-1-one (**50**) starting from 4-methoxypyridine (**49**). The exploration of the Minisci reaction for radical acylation proved to be a potential alternative, although the stereoselective reductions have not been successful, so far. Classical reduction methods, however, showed promising results and, in combination with diastereomeric separation of enantiomers, could lead to potential future ionic Vedejs' catalyst derivatives.

Computational studies aimed at predicting the reactivity and stereoselectivity of chiral pyridinamide derivatives yielded mixed results, indicating the need for refined methods to improve their predictive accuracy.

Future efforts in this area should focus on finding a synthetic route for chiral ionic Vedejs derivatives. The Minisci reaction might be a viable alternative for the acylation step if a phenyl group instead of a *tert*-butyl group is an acceptable alternative. However, the transformation of the nitrile group might still prove to be problematic. Particular attention should be paid to the protection of the pyridine nitrogen in future reactions as this may be a reason for the repeated failures. Suitable protection strategies would be the use of *N*-oxide derivatives as starting materials or to protect the pyridine *N* with BF_3, as done by Vedejs, or BH_3, as done by other researchers.[8,20]

An alternative strategy could be the synthesis of 2-cyano-4-chloropyridine, followed by conversion of the cyano group to the pivaloyl group with an organometallic reagent, such as *t*-BuLi or *t*-butylmagnesium bromide, which could be hydrolyzed to the corresponding acyl group.[21,22] Subsequent stereoselective reduction and methylation would be done according to Vedejs' procedure. The transformation of the 4-chloro substituent could be done with a Buchwald-Hartwig reaction, followed by the final ion pair synthesis.

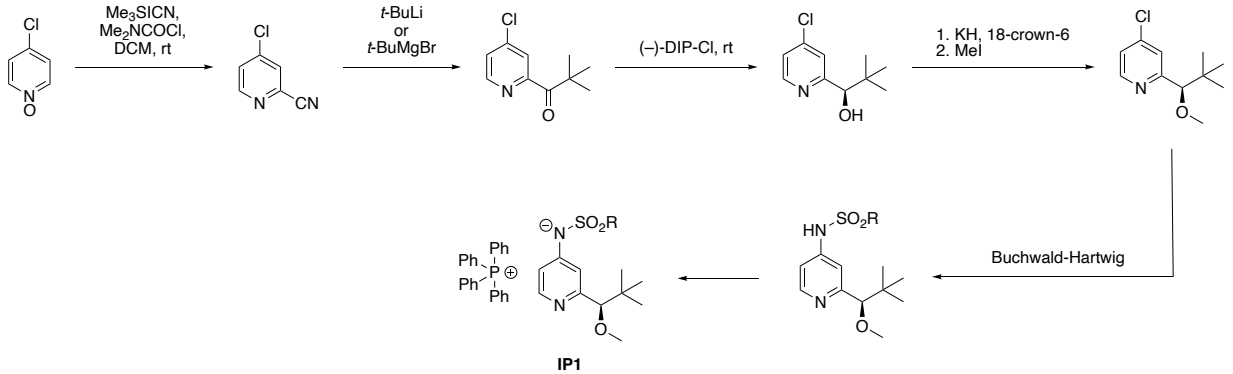

5.4 Supporting Information

5.4.1 Experimental Data

5.4.1.1 General

All reactions sensitive to air and moisture were performed in dried glassware under nitrogen atmosphere, if not stated otherwise. All reagents were purchased from Sigma Aldrich, TCI or Acros and used without further purification, unless otherwise noted. All air and water sensitive reagents were stored under nitrogen. Solvents were obtained from Acros Organics, Sigma Aldrich, or Merck and purified by simple distillation in a rotary evaporator, unless otherwise specified.

Silica gel for column chromatography was purchased from Acros Organics (mesh 35-70). Thin-layer chromatography was performed by using TLC plates purchased from Merck (silica gel 60 F254, thickness 0.2 mm).

Nuclear magnetic resonance (NMR) spectra were recorded on Bruker 400 MHz or an INOVA 400 and 600 MHz machines. The following abbreviations were used in the analysis of NMR spectra: s = singlet, d = doublet, t = triplet, q = quartet, m = multiplet, br s = broad singlet. NMR signals were assigned based on 2D spectra (COSY, HSQC, HMBC, NOESY) experiment analysis. Chemical shifts were given in ppm. The internal reference was set to the residual solvent signals ($CDCl_3$). The ^{13}C NMR spectra (101 or 151 MHz) were recorded under broadband proton-decoupling. The spectra were imported and processed in the program MestreNova (version 14.1.1 and 14.3.2).

5.4.1.2 Synthetic Procedures

N,*N*-dibenzylpyridin-4-amine (**35**)

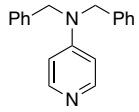

A solution of 4-aminopyridine (500 mg, 1.0 eq) in THF (10.0 mL) at 35 °C was treated with NaH (2.2 eq) in small portions and stirred for 1.5 h. Thereafter, benzylbromide (2.2 eq) was added and the mixture was heated to 70 °C for 4 h. The mixture was hydrolyzed with saturated aqueous solution of NH_4Cl (8.0 mL). The volatile solvent was evaporated, and the residue was extracted with EtOAc (2 x 20 mL). The organic layer was washed with water (1 x 20 mL) and brine (1 x 20 mL). Then, the organic layer was dried with $MgSO_4$, filtered and the solvent was evaporated. After purification by column chromatography (EtOAc + 1% NEt_3) product **35** (195 mg, 15 %) was isolated as yellowish oil.

^1H NMR (400 MHz, $CDCl_3$): δ [ppm] = 8.22 – 8.15 (m, 2 H), 7.39 – 7.28 (m, 6 H), 7.20 (dd, *J* = 6.9, 1.8 Hz, 4 H), 6.61 – 6.52 (m, 2 H), 4.66 (s, 4 H).

1-(4-(dibenzylamino)pyridin-2-yl)-2,2-dimethylpropan-1-one (**36**) (not successful)

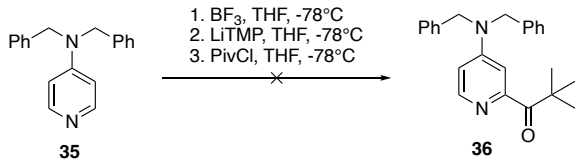

35 **36**

Following Vedejs' synthetic procedure[8], *N*,*N*-dibenzylpyridin-4-amine (195 mg, 1.0 eq) was dissolved in dry THF (3.0 mL) and cooled to 0 °C before BF_3 etherate (1.06 eq) was added. The mixture was stirred at 0 °C for 30 min. In a second flask, 2,2,2,2-tetramethyl piperidine (TMP, 110 mg, 1.0 eq) in dry THF (2.0 mL) at -78 °C was treated with *n*-BuLi (1.10 eq) before the solution was warmed to rt. The protected *N*,*N*-dibenzylpyridin-4-amine solution was cooled to -78 °C before the LiTMP solution was added via syringe. The resulting orange solution was stirred at -78 °C for 30 min. In a third flask, pivaloyl chloride (2.0 eq) in dry THF (3.0 mL) was cooled to -78 °C before the previously prepared solution was added dropwise. The combined mixture was stirred at -78 °C for 5 h before being allowed for warm up to rt. Water (2.0 mL), MeOH (2.0 mL), and 6 N HCl (2.0 mL) were added sequentially, and the mixture was stirred at 38 °C overnight. The volatile solvents were removed, the residue was brought to pH = 9 with 2 N NaOH and extracted with diethyl ether (1 x 15 mL) and EtOAc (2 x 20 mL). The organic phase was washed with

brine (1 x 20 mL) and dried over $MgSO_4$ before evaporation. Purification was attempted with column chromatography (EtOAc + 1% NEt_3), only starting material was isolated.

2,2-dimethyl-1-(4-nitropyridin-2-yl)propan-1-one (**38**) (not successful)

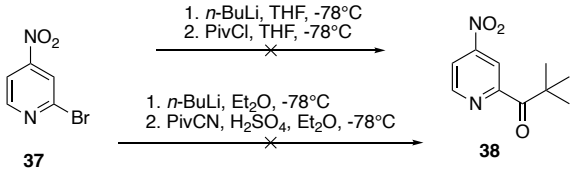

2-Bromo-4-nitropyridine (315 mg, 1.0 eq) was treated with *n*-BuLi (1.1 eq) in dry THF (6.0 mL) at -78 °C and stirred for 1 h. Pivaloyl chloride (2.0 eq) was added dropwise at -78 °C. The reaction mixture was stirred at -78 °C for 5 h before it was allowed to warm to rt. 6 N HCl (2 mL) and water (4.0 mL) were added, stirred for 30 min, and the two phases were separated. The aqueous phase was brought to pH = 9 with 2 M NaOH and extracted with Et_2O (3 x 15 mL), dried over $MgSO_4$ before evaporating the solvent. Purification was attempted with column chromatography (*n*-Hex/EtOAc = 5/1, + 5% NEt_3), however only starting material was reisolated.

In a second attempt, 2-bromo-4-nitropyridine (321 mg, 1.0 eq) was treated with *n*-BuLi (1.1 eq) in dry THF (3.0 mL) at -78 °C and stirred for 1.5 h. In a second flask, pivaloyl chloride (1.3 eq) in dry THF (3.0 mL) was cooled to 78 °C and the mixture of flask 1 was added dropwise over 30 min. The combined reaction solution was stirred at 78 °C for 5 h before being allowed to reach rt. Water (2.0 mL), MeOH (1.0 mL), and 6 N HCl (2.0 mL) were added sequentially at 0 °C and stirred for 30 min. After phase separation, the aqueous solution was extracted with Et_2O (3 x 15 mL) and THF (1 x 15 mL), dried over $MgSO_4$ and evaporated. Purification was attempted with column chromatography (*n*-Hex/EtOAc = 8/1 –> 7/1 –> 5/1 –> 1/2 –> 0/1 + 1% NEt_3), however only starting material was obtained.

Following a procedure adapted from Bolm *et al.*[9], 2-bromo-4-nitropyridine (305 mg, 1.0 eq) was treated with *n*-BuLi (1.1 eq) in dry Et_2O (6.0 mL) at -78 °C and stirred for 30 min. Pivalonitrile was added dropwise and stirred for 1.5 h at -78 °C before the mixture was allowed to reach rt. Then, 2 N H_2SO_4 (5.1 mL) was added, the mixture was refluxed for 2 h, and then stirred at 30 °C overnight. After cooling down to rt. Et_2O was added and the aqueous layer was brought to pH = 9 with 2 N NaOH and extracted with Et_2O (3 x 15 mL), dried with $MgSO_4$ and evaporated. Purification was attempted with column chromatography (*n*-Hex/EtOAc = 2/1), no desired product was isolated.

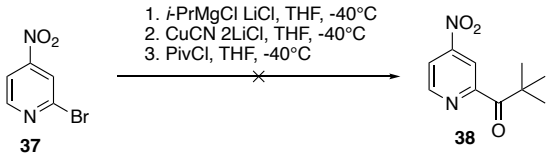

2-Bromo-4-nitropyridine (225 mg, 1.0 eq) in dry THF (5.5 mL) at -40 °C was treated with *i*-PrMgCl x LiCl (1.1 eq) at stirred for 1.5 h. CuCN x 2 LiCl (1.1 eq) was added and resulting mixture was stirred for another 30 min at -40 °C before pivaloyl chloride (1.1 eq) was added. The mixture was stirred at -40 °C for 30 min before being allowed to warm to rt. Subsequently, it was stirred at rt. overnight before adding aqueous ammonium chloride solution (4.0 mL) and 2 N NH_3 (1.0 mL). After phase separation, the aqueous layer was extracted with Et_2O (3 x 15 mL). The combined organic phases were dried over $MgSO_4$, filtered and the solvent was evaporated. Purification was attempted with column chromatography (*n*-Hex/EtOAc = 5/1 + 5% NEt_3 –> 1/1), no desired product was isolated.[23]

The reaction was repeated with 2-bromo-4-nitropyridine (201 mg, 1.0 eq) in dry THF (5.0 mL) at -40 °C. The mixture was treated with *i*-PrMgCl x LiCl (1.1 eq) and stirred for 15 min. Subsequently, CuCN x 2 LiCl (1.1 eq) was added, and the resulting mixture was stirred for an additional 45 min at -40 °C. Thereafter, mixture was added to a solution of pivaloyl chloride (1.0 eq) in dry THF (2.0 mL) at -40 °C. The mixture was stirred at -40 °C for 3 h before being allowed to slowly warm to rt overnight. Then, aqueous ammonium chloride solution (4.0 mL) and 2 N NH_3 (1.0 mL) was added. Following phase separation, the aqueous layer was extracted with Et_2O (3 x 15 mL). The combined organic phases were dried over $MgSO_4$, filtered, and the solvent was evaporated. The crude NMR exhibited no aromatic signals, indicating the degradation of the pyridine ring.

4-nitro-2-pivaloylpyridine 1-oxide (**40**) (not successful)

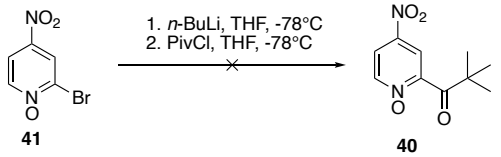

41 **40**

2-Bromo-4-nitropyridine-1-oxide (306 mg, 1.0 eq) in dry THF (5.0 mL) was treated with *n*-BuLi (1.1 eq) at -78 °C and stirred for 40 min. In a second flask, pivaloyl chloride (1.8 eq) in dry THF (5.0 mL) was cooled to -78 °C and the mixture of flask 1 was added dropwise over a period of 30 min. The combined reaction solution was stirred at 78 °C for 4 h, after which it was allowed to warm to rt. and stirred further overnight. Next, 2 M HCl (2.0 mL) and water (2.0 mL) was added at 0 °C. Following phase separation, the aqueous phase was adjusted to pH = 9 with 2 M NaOH and extracted with Et_2O (3 x 15 mL). The combined organic layer was then dried over $MgSO_4$, filtered and the solvent was evaporated. The crude NMR showed only weak shifts of the starting material.

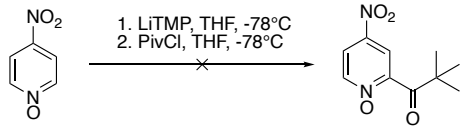

39 **40**

In a second attempt, TMP (1.1 eq) in dry THF (3.0 mL) at -78 °C was treated with *n*-BuLi (1.1 eq) and stirred for 30 min before it was allowed to warm to rt. A solution of 4-nitropyridine-1-oxide (401 mg, 1.0 eq) in dry THF (3 mL) at -78 °C was treated with the LiTMP solution and stirred for 30 min. In a third flask, pivaloyl chloride (1.3 eq) in dry THF (5.0 mL) at -78 °C was treated with the previously prepared reaction mixture. The final reaction mixture was stirred at -78 °C for 4 h before it was warmed to rt. Thereafter, 2 M HCl (2.0 mL), water (2.0 mL), and MeOH (2.0 mL) was added at 0 °C and stirred for 30 min. After addition of water, the phases were separated, and the aqueous layer was adjusted to pH = 9 with 2 M NaOH. Subsequently, it was extracted with Et_2O (1 x 15 mL) and EtOAc (2 x 20 mL). The organic layer was dried over $MgSO_4$, filtered and the solvent was evaporated. The crude NMR showed only shifts of the starting material.

1-(4-chloropyridin-2-yl)-2,2-dimethylpropan-1-ol (**43**) (not successful)

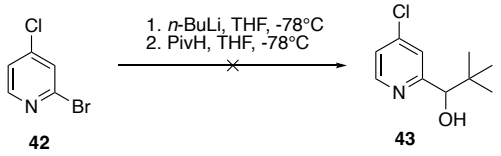

42 **43**

An adapted procedure of Bolm's et al.[9] was followed. Therefore, 2-bromo-4-chloropyridine (393 mg, 1.0 eq) in dry THF (10.0 mL) at -78 °C was treated with n-BuLi (1.1 eq) and stirred for 1 h. Pivalaldehyde (1.5 eq) was added at -78 °C and the solution was stirred for 1.5 h before it was allowed to warm to rt. After stirring for 1 h, the mixture was cooled to 0 °C and treated with water (10.0 mL). After phase separation, the aqueous layer was extracted with DCM (3 x 15 mL). The combined organic layers were dried over $MgSO_4$, filtered and the solvent was evaporated. The crude NMR did not show aromatic signals, indicating the degradation of the pyridine ring.

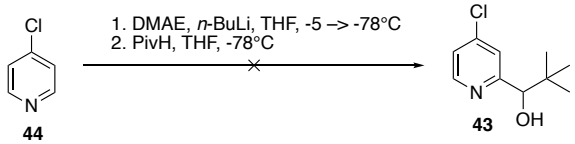

44 **43**

The starting material was gained by dissolving 4-chloropyridine hydrochloride (510 mg) in water (pH = 2) and adjusting the pH to pH = 9 with aqueous K_2CO_3 solution at 0 °C. DCM was added and stirred for 30 min. After phase separation, the aqueous layer was extracted with DCM (3 x 10 mL). The organic layer was dried over $MgSO_4$, filtered and the solvent was evaporated at rt. using a rotary evaporator, yielding 4-chloropyridine (265 mg, 69%).

Next, a procedure by Choppin *et al.*[10] was followed. 2-Dimethylaminoethanol (DMAE, 4.0 eq) in dry *n*-hexane (5.0 mL) at -4 °C was treated with *n*-BuLi (8.0 eq) and stirred for 30 min. After cooling to -78 °C, a solution of neutralized 4-chloropyridine (250 mg, 1.0 eq) in *n*-hexane (5.0 mL) was added dropwise. After stirring for 1 h, the solution was treated with a solution of pivalaldehyde in *n*-hexane (20 mL) at-78 °C. The reaction mixture was then allowed to warm slowly to rt. and was then hydrolyzed with water (20 mL) at 0 °C. The aqueous layer was extracted with DCM (3 x 15 mL). The organic layer was dried over $MgSO_4$, filtered and the solvent was evaporated. The crude NMR did not show aromatic signals, indicating the degradation of the pyridine ring.

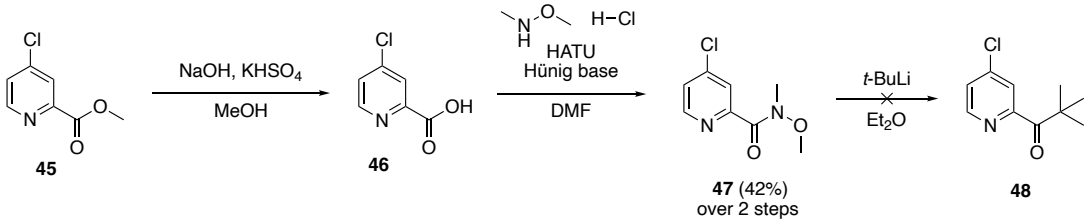

Methyl 4-chloropicolinate (**45**) (502 mg, 1.0 eq) in THF/MeOH (1:1; 28 mL) was treated with 2M NaOH (1.1 eq) and stirred at rt. overnight. Thereafter, 1 M potassium bisulfat ($KHSO_4$, 1.0 eq) was added. The mixture was extracted with EtOAc (3 x 50 mL). The organic layer was washed with brine (1 x 50 mL), dried over $MgSO_4$, and filtered. Evaporation of the solvent yielded 4-chloropicolinic acid **46** (355 mg, 77%) as off-white solid.

^{1}H NMR (400 MHz, DMSO-d_6): δ [ppm] = 13.57 (s, 1 H), 8.68 (d, *J* = 5.3 Hz, 1 H), 8.06 (d, *J* = 2.2 Hz, 1 H), 7.80 (dd, *J* = 5.3, 2.1 Hz, 1 H).

A solution of 4-chloropicolinic acid (**46**) (355 mg, 1.0 eq) in DMF (3.5 mL) was treated with HATU (1.5 eq), amin (1.5 eq) and Hünig base (3.0 eq) at rt and stirred overnight. After addition of aqueous $NaHCO_3$ (25.0 mL), the mixture was extracted with EtOAc (3 x 25 mL). The combined organic layers were washed with water (3 x 50 mL) and brine (1 x 40 mL) and dried over $MgSO_4$. The solvent was evaporated, and the crude product was purified with column chromatography (Hex/EtOAc = 1:1) yielding 4-chloro-*N*-methoxy-*N*-methylpicolinamide **47** (246 mg, 55%) as off-white solid.[24]

^{1}H NMR (400 MHz, $CDCl_3$): δ [ppm] = 8.52 (d, *J* = 5.3 Hz, 1 H), 7.66 (s, 1 H), 7.37 (dd, *J* = 5.3, 2.1 Hz, 1 H), 3.75 (s, 3 H), 3.40 (s, 3 H).

A solution of 4-chloro-*N*-methoxy-*N*-methylpicolinamide (**47**) (245 mg, 1.0 eq) in Et_2O (6.0 mL) at -78 °C was treated slowly with *t*-BuLi (1.1 eq). After 1 h, the mixture was allowed to warm to rt. and aqueous NH_4Cl (5.0 mL) was added. The aqueous layer was extracted with Et_2O (3 x 10 mL). The organic layer was dried over $MgSO_4$, filtered and the solvent was evaporated. Purification was attempted with column chromatography (*n*-Hex/EtOAc = 5/1 –> 3/1 –> 1/1), product **48** could not be isolated.

<u>1-(4-methoxypyridin-2-yl)-2,2-dimethylpropan-1-one (**50**)</u> (not successful)

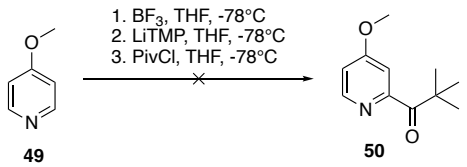

Following a modified procedure from Vedejs *et al.*, 4-methoxypyridine (300 mg, 1.0 eq) in THF (1.0 mL) at 0 °C was treated with BF_3 etherate (1.06 eq) and stirred for 30 min. A solution of TMP (1.06 eq) in dry THF (4.0 mL) at -78 °C was treated with *n*-BuLi (1.1 eq) before the solution was slowly warmed to rt. The protected 4-methoxypyridine solution was treated with the LiTMP solution at -78 °C and stirred for 30 min. In a third flask, pivaloyl chloride (2.0 eq) in dry THF (3.0 mL) was cooled to -78 °C and treated with the previously prepared reaction mixture. The combined solution was stirred at -78 °C for 4 h before being allowed for warm up to rt. Water (2.0 mL), MeOH (2.0 mL), and 6 N HCl (2.0 mL) were added sequentially, and the mixture was stirred overnight. The volatile solvents

were removed (rotary evaporator), the residue was brought to pH = 9 with 2 N NaOH and extracted with diethyl ether (1 x 15 mL) and EtOAc (2 x 20 mL). The organic phase was washed with brine (1 x 20 mL) and dried over $MgSO_4$ before evaporation. The crude NMR did not show aromatic signals, indicating the degradation of the pyridine ring.

1-(4-methoxypyridin-2-yl)-2,2-dimethylpropan-1-one (**50**) (successful)

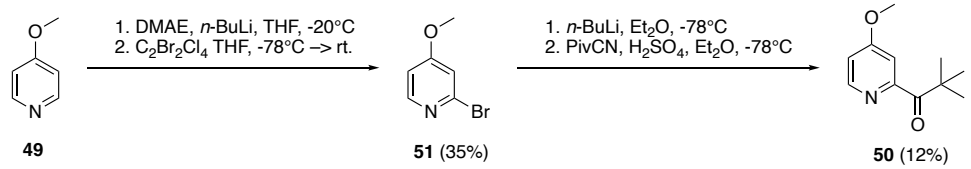

A solution of DMAE (2.0 eq) in dry THF (2.6 mL) at -20 °C was treated with *n*-BuLi (4.0 eq) and stirred for 30 min. 4-Methoxypyridine (200 mg, 1.0 eq) was added and the solution was cooled to -78 °C. A solution of 1,2-dibromo-1,1,2,2-tetrachloroethane (2.4 eq) in dry THF (2.3 mL) was added and mixture was stirred in the cooling bath to slowly warm up overnight. Thereafter, the solution was hydrolyzed with water (6.0 mL) at 0 °C. The aqueous layer was extracted with Et_2O (3 x 15 mL) and DCM (1 x 10 mL). The organic layer was dried over $MgSO_4$, filtered and the solvent was evaporated yielding 2-bromo-4-methoxypyridine **51** (124 mg, 35 %).[11]

^{1}H NMR (400 MHz, $CDCl_3$): δ [ppm] = 8.18 (dd, *J* = 8.8, 5.8 Hz, 1H), 6.92 (dd, *J* = 65.3, 2.3 Hz, 1H), 6.77 (ddd, *J* = 11.2, 5.8, 2.3 Hz, 1H), 3.85 (s, 2H).

Following a procedure adapted from Bolm *et al.*[9], 2-bromo-4-methoxypyridine (94.0 mg, 1.0 eq) in dry THF (2.0 mL) at -78 °C was treated with *n*-BuLi (1.1 eq) and stirred for 45 min. Pivalonitrile was added dropwise and stirred at -78 °C for 1 h, before the mixture was allowed to reach rt. After addition of 2 N H_2SO_4 (1.4 mL), the mixture was refluxed for 2 h (60 °C oil bath). After cooling down to rt. Et_2O was added and the aqueous layer was extracted with Et_2O (3 x 15 mL). The organic layer was dried over $MgSO_4$, filtered and the solvent was evaporated. Purification was performed with column chromatography (*n*-Hex/EtOAc = 6/1), yielding 1-(4-methoxypyridin-2-yl)-2,2-dimethylpropan-1-one **50** (11.7 mg, 12 %).

^{1}H NMR (400 MHz, $CDCl_3$): δ [ppm] = 8.42 (d, *J* = 5.6 Hz, 1 H), 7.40 (d, *J* = 2.6 Hz, 1 H), 6.88 (dd, *J* = 5.6, 2.6 Hz, 1H), 3.87 (s, 3 H), 1.44 (s, 9 H).

^{13}C NMR (101 MHz, $CDCl_3$): δ [ppm] = 207.1, 166.4, 156.8, 149.2, 112.6, 109.0, 55.4, 44.4, 27.6.

N,*N*-dibenzylpyridin-4-amine (**35**) (not successful)

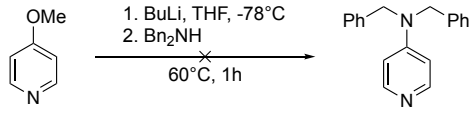

Following a procedure from Wang *et al.*, *N*,*N*-dibenzylamine (1.6 eq) in dry THF (1.0 mL) at -78 °C was treated with *n*-BuLi (1.76 eq). The mixture was stirred for 10 min at rt. 4-Methoxypyridine (54.5 mg, 1.0 eq) was added and the mixture was stirred at 60 °C for 1 h. Thereafter, the mixture was cooled down to rt., hydrolyzed with water (6.0 mL), and then extracted with DCM (3 x 10 mL). The organic layer was dried with $MgSO_4$, filtered and the solvent was evaporated. Purification was attempted with column chromatography (EtOAc + 1 % NEt_3), however, no product was found.

General acylation procedure for 4-cyanopyridine (adapted from Fontanta *et al.*[14])

4-Cyanopyridine (1.0 eq) with the respective α-keto acid (3.0 eq), $AgNO_3$ (0.1 eq), $NH_4S_2O_8$ (3.0 eq), and H_2SO_4 or trifluoroacetic acid (TFA) was added to a DCM/water mix (25 mL each) and stirred at 40 °C for 2 h. After cooling down to rt., the aqueous layer was extracted with DCM (3 x 20 mL). The organic layer was dried with $MgSO_4$, filtered

over celite and the solvent was evaporated. The crude product was purified with column chromatography (hex/EtOAc = 5/1).

2-Benzoylisonicotinonitrile (**53**)

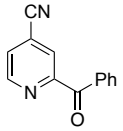

4-Cyanopyridine (1.00 g, 1.0 eq), 2-oxo-2-phenylacetic acid (3.0 eq), $AgNO_3$ (0.1 eq), $NH_4S_2O_8$ (3.0 eq), and H_2SO_4 (1.0 eq) were reacted accoriding to the general acylation procedure. After purification by column chromatography (hex/EtOAc = 5/1), **53** (1.94 g, 97 %) was obtained as an off-white solid.

^{1}H NMR (400 MHz, $CDCl_3$): δ [ppm] = 8.91 (dd, *J* = 5.0, 0.9 Hz, 1 H), 8.28 (dd, *J* = 1.6, 0.9 Hz, 1 H), 8.11 – 8.05 (m, 2 H), 7.72 (dd, *J* = 5.0, 1.6 Hz, 1 H), 7.68 – 7.62 (m, 1 H), 7.55 – 7.46 (m, 2 H).

^{13}C NMR (101 MHz, $CDCl_3$): δ [ppm] = 191.77, 156.27, 149.59, 135.29, 133.78, 131.18, 128.53, 127.40, 126.53, 122.05, 116.01.

2-Pivaloylisonicotinonitrile (**55**)

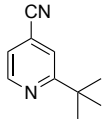

4-Cyanopyridine (300 mg, 1.0 eq), 3,3-dimethyl-2-oxobutanoic acid (3.0 eq), $AgNO_3$ (0.1 eq), $NH_4S_2O_8$ (3.0 eq), and TFA (1.0 eq) were reacted according to the general acylation procedure. After purification by column chromatography (hex/EtOAc = 5/1), instead of the wanted acylation product 2-pivaloylisonicotinonitrile, the alkylation product 2-(*t*-butyl)isonicotinonitrile (302 mg, 56 %) was isolated as an off-white solid.

^{1}H NMR (400 MHz, $CDCl_3$): δ [ppm] = 8.73 (d, *J* = 5.0 Hz, 1 H), 7.55 (s, 1 H), 7.32 (dd, *J* = 4.9, 1.6 Hz, 1 H), 1.37 (s, 9 H).

^{13}C NMR (101 MHz, $CDCl_3$): δ [ppm] = 171.2, 149.8, 122.2, 121.2, 120.60 117.3, 38.1, 30.0.

(*R*)-2-(hydroxy(phenyl)methyl)isonicotinonitrile (*R*-**56**) (not successful)

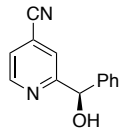

To a solution of (-)-DIP chloride (1.5 eq) in dry THF (5.0 mL) at rt. 2-benzoylisonicotinonitrile (500 mg, 1.0 eq) was added and stirred vigorously for 5 d. Thereafter, diethanolyamin (1.0 mL), MeOH (2.0 mL), water (2.5 mL), and conc HCl (1.0 mL) was added, and the mixture was heated to 40 °C for 4 h. EtOAc was added and the phases were separated. The organic layer was washed with 2 N HCl (2 x 20 mL). The combined aqueous layer was adjusted to pH = 9 with 2 N NaOH and extracted with EtOAc (2 x 20 mL). The combined organic layer was dried with $MgSO_4$, filtered and the solvent was removed. After purification by column chromatography (hex/EtOAc = 5/1) the starting material (90 %) was recovered.

2-(hydroxy(phenyl)methyl)isonicotinonitrile (rac-**56**)

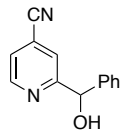

2-benzoylisonicotinonitrile (498 mg, 1.0 eq) was dissolved in ample dry MeOH and EtOH (approx. 25.0 mL). After addition of sodium borohyride ($NaBH_4$, 0.3 eq), the mixture was stirred at rt. for 4 h. Water (10.0 mL) and DCM (10.0 mL) were added at 0 °C. The volatile solvents were removed, and the residue was extracted with DCM (3 x 15 mL). The organic layer was dried with $MgSO_4$, filtered and the solvent was evaporated. After purification by column chromatography (hex/EtOAc = 1/1) product rac-**56** (327 mg, 65 %) was isolated as yellowish oil.

^{1}H NMR (400 MHz, $CDCl_3$): δ [ppm] = 8.74 (d, *J* = 5.1 Hz, 1 H), 7.49 (s, 1 H), 7.43 (d, *J* = 5.0 Hz, 1 H), 7.40 – 7.30 (m, 5 H), 5.83 (s, 1 H), 4.49 (s, 1 H).

^{13}C NMR (101 MHz, $CDCl_3$): δ [ppm] = 171.3, 163.2, 149.3, 141.9, 129.1, 128.6, 127.1, 124.0, 123.2, 121.4, 116.5, 75.4.

5.3.1.3 NMR Spectra

N,*N*-dibenzylpyridin-4-amine (**35**)

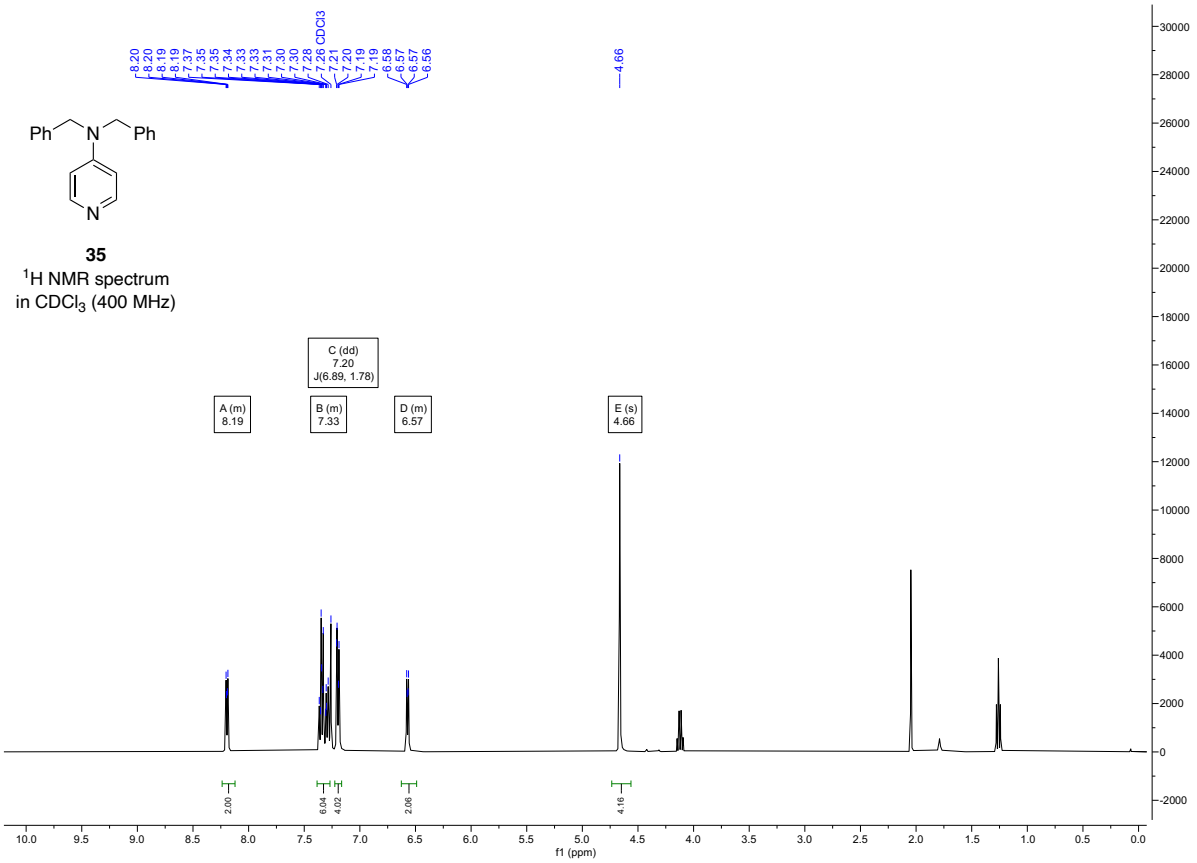

4-Chloropicolinic acid (**46**)

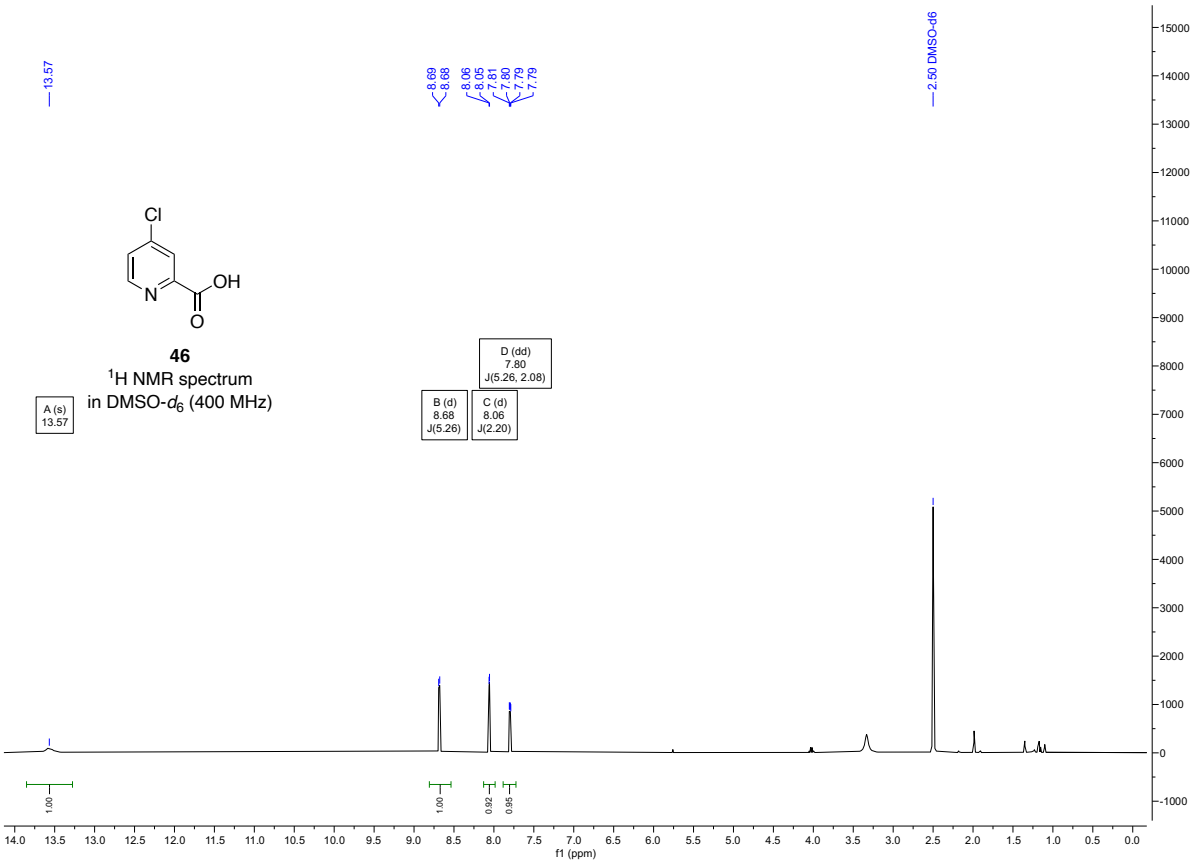

4-Chloro-*N*-methoxy-*N*-methylpicolinamide (**47**)

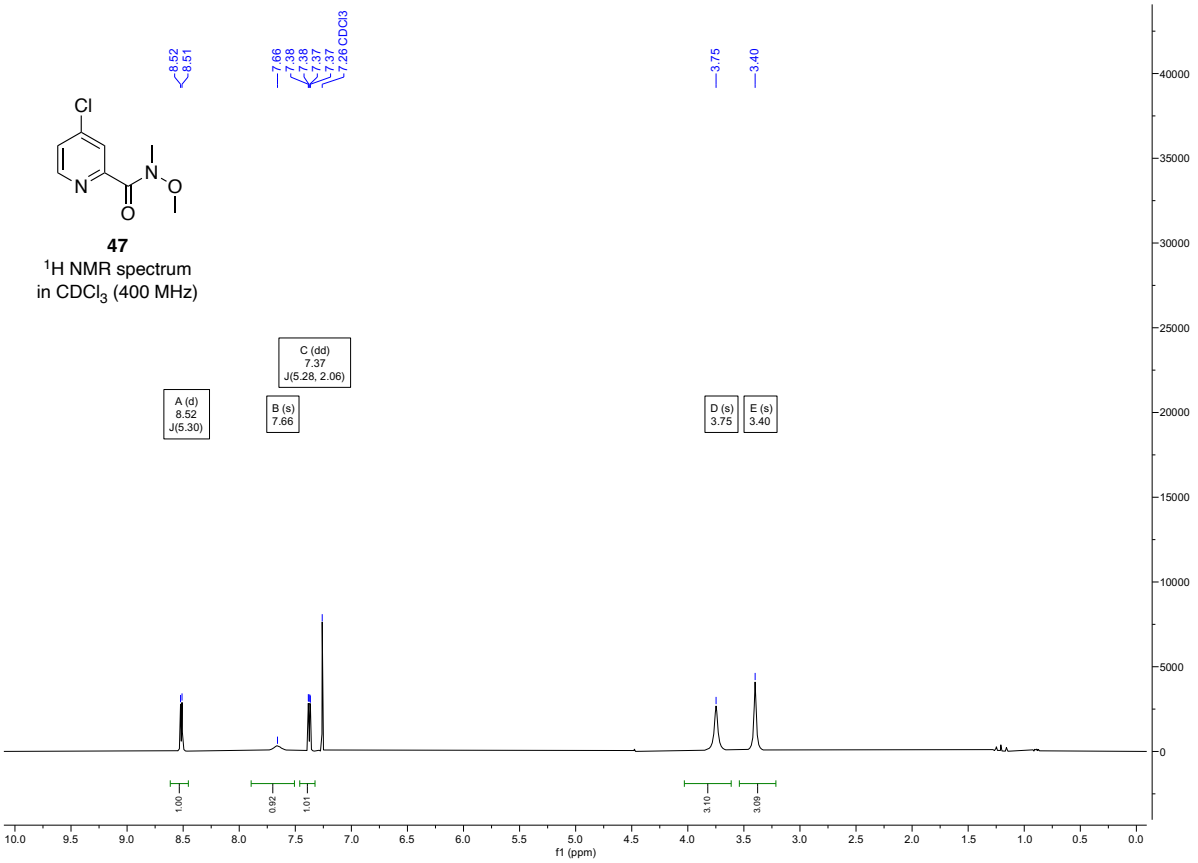

2-Bromo-4-methoxypyridine (**51**)

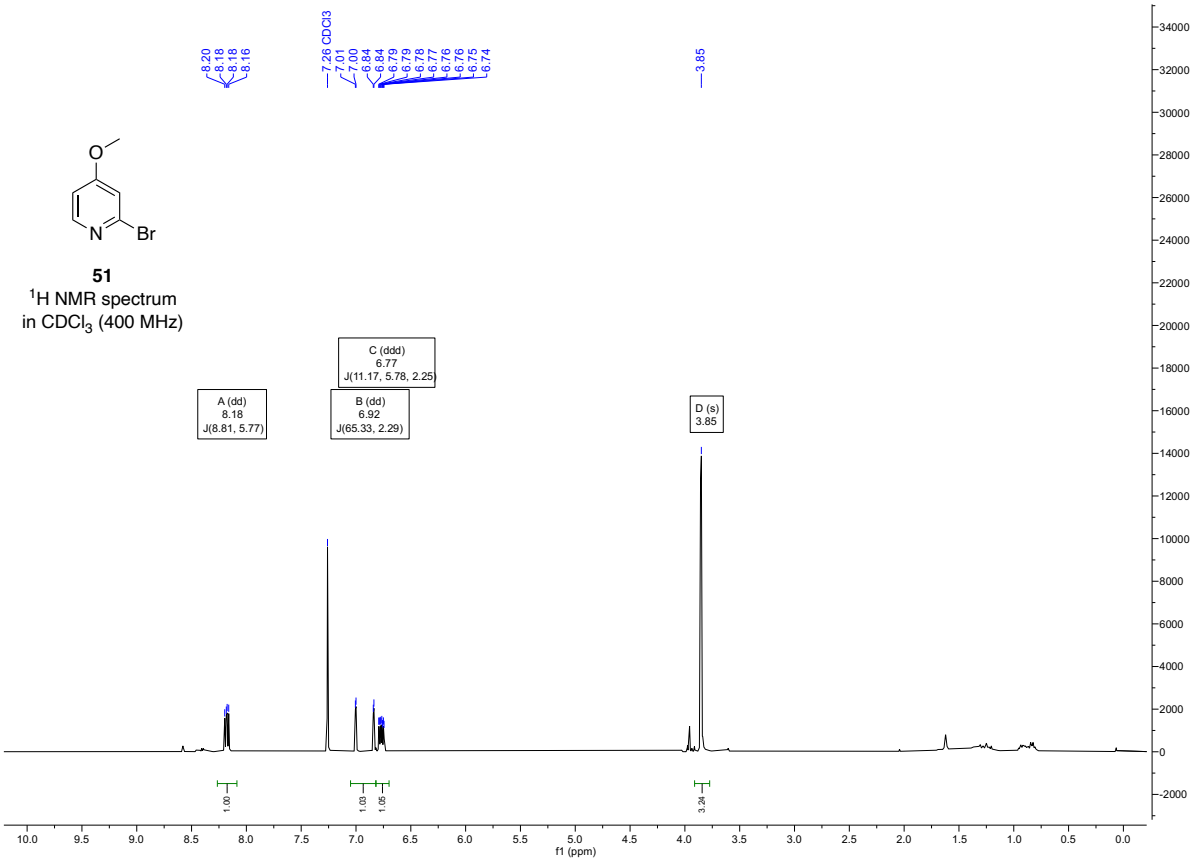

1-(4-Methoxypyridin-2-yl)-2,2-dimethylpropan-1-one (**50**)

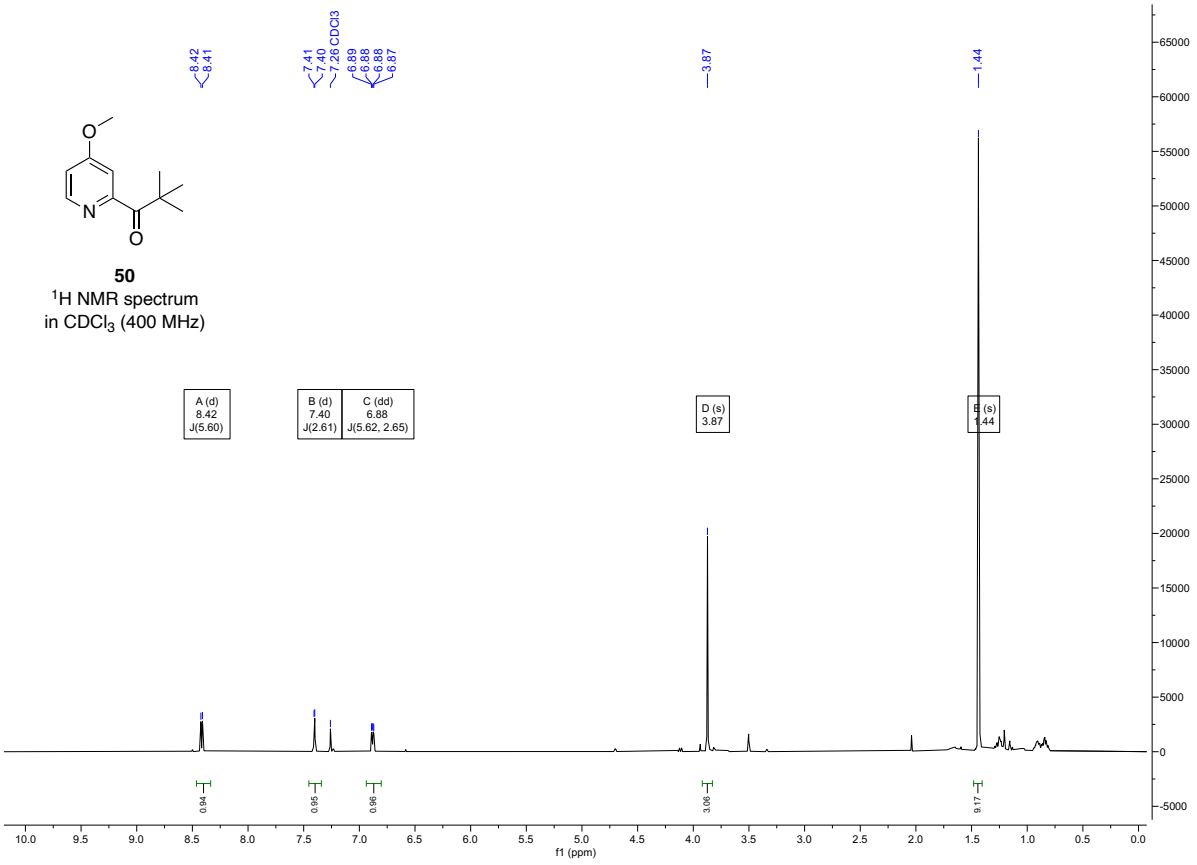

50
^{1}H NMR spectrum
in $CDCl_3$ (400 MHz)

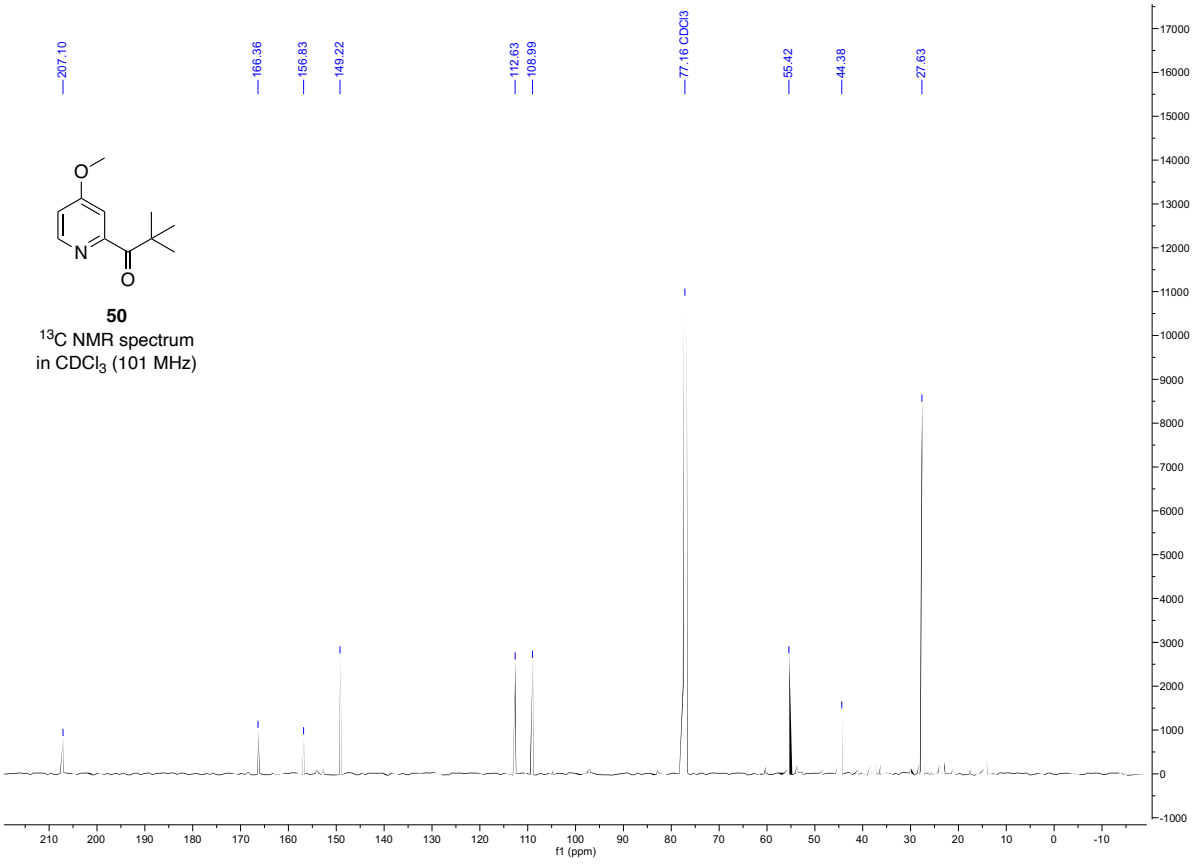

50
^{13}C NMR spectrum
in $CDCl_3$ (101 MHz)

2-Benzoylisonicotinonitrile (**53**)

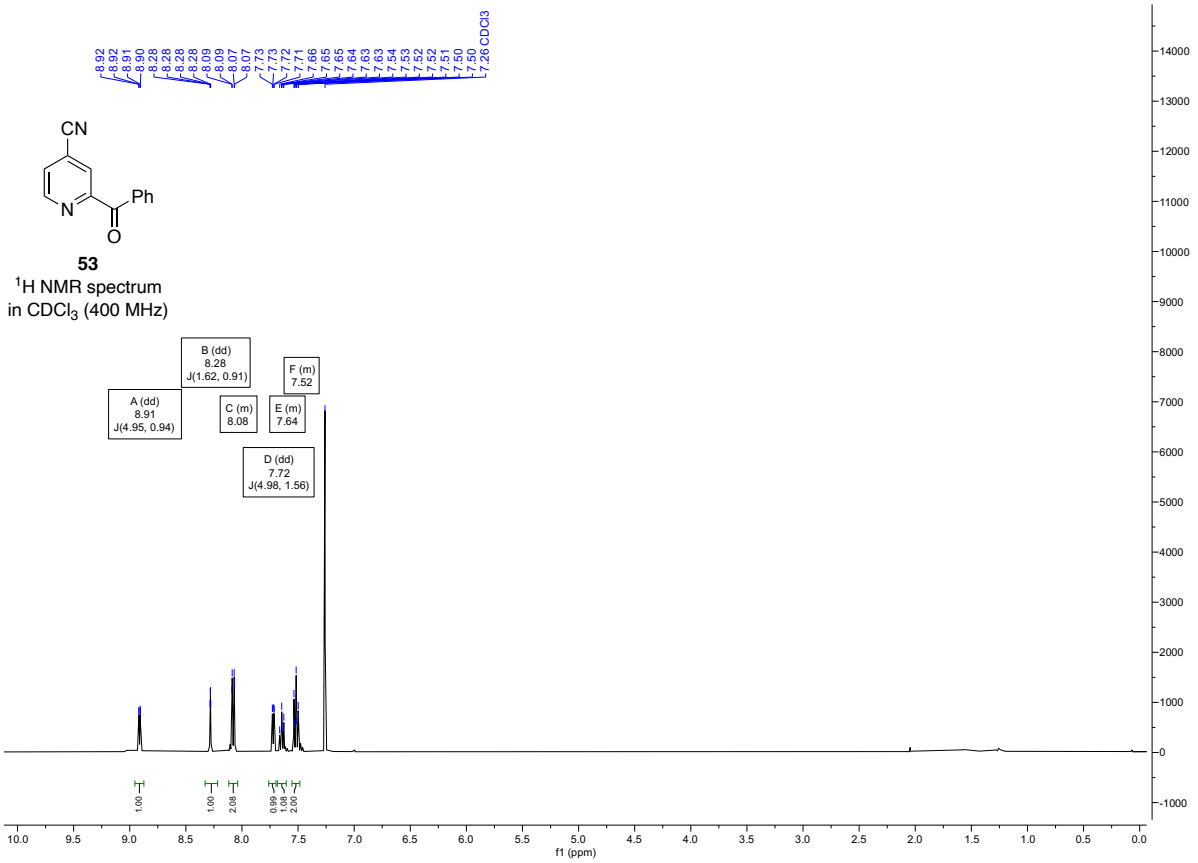

53
^{1}H NMR spectrum
in $CDCl_3$ (400 MHz)

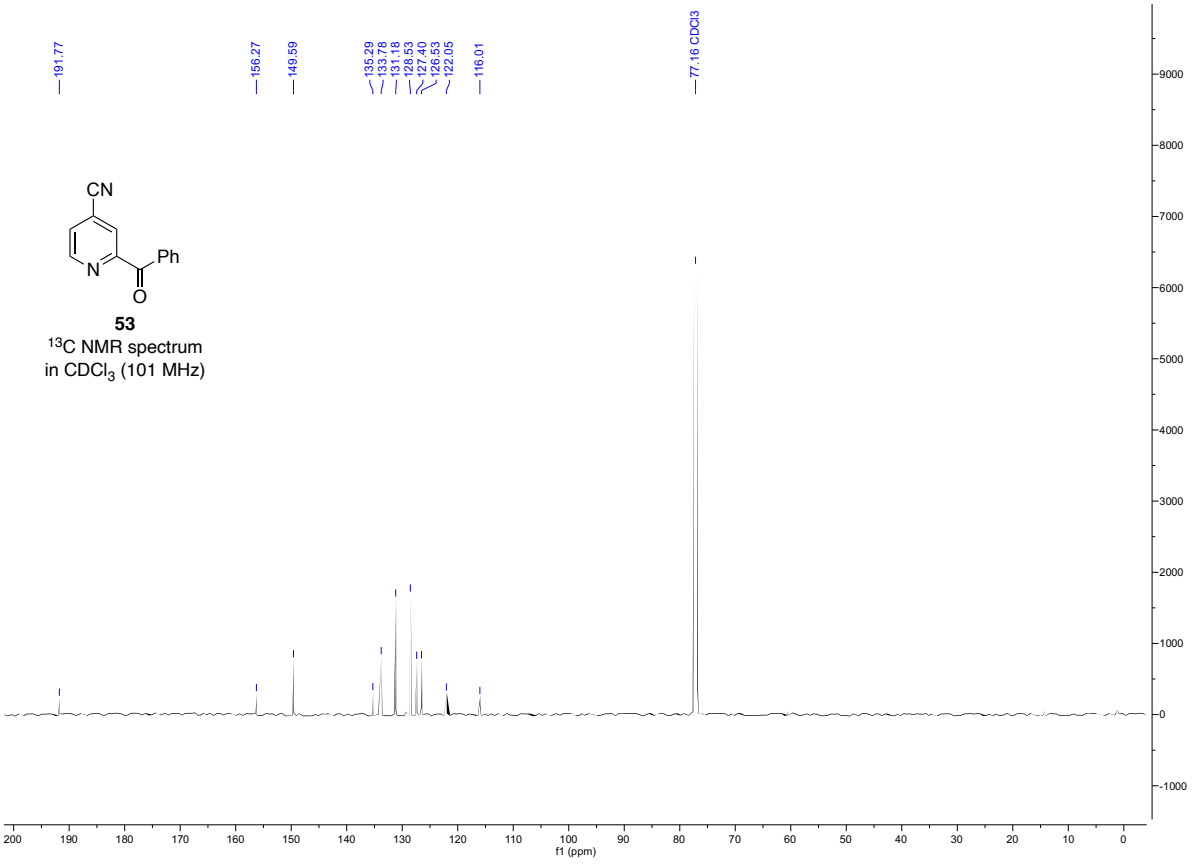

53
^{13}C NMR spectrum
in $CDCl_3$ (101 MHz)

2-(Hydroxy(phenyl)methyl)isonicotinonitrile (rac-**56**)

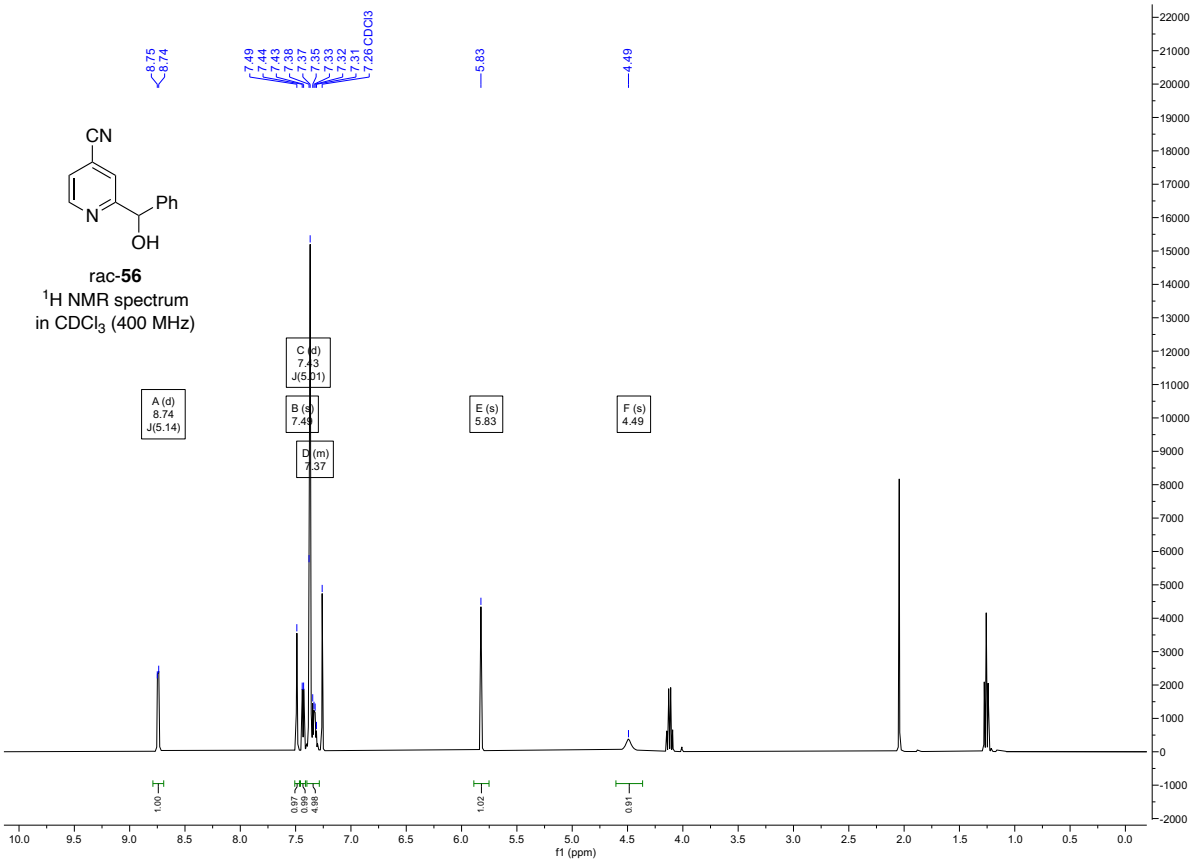

rac-**56**
^{1}H NMR spectrum
in $CDCl_3$ (400 MHz)

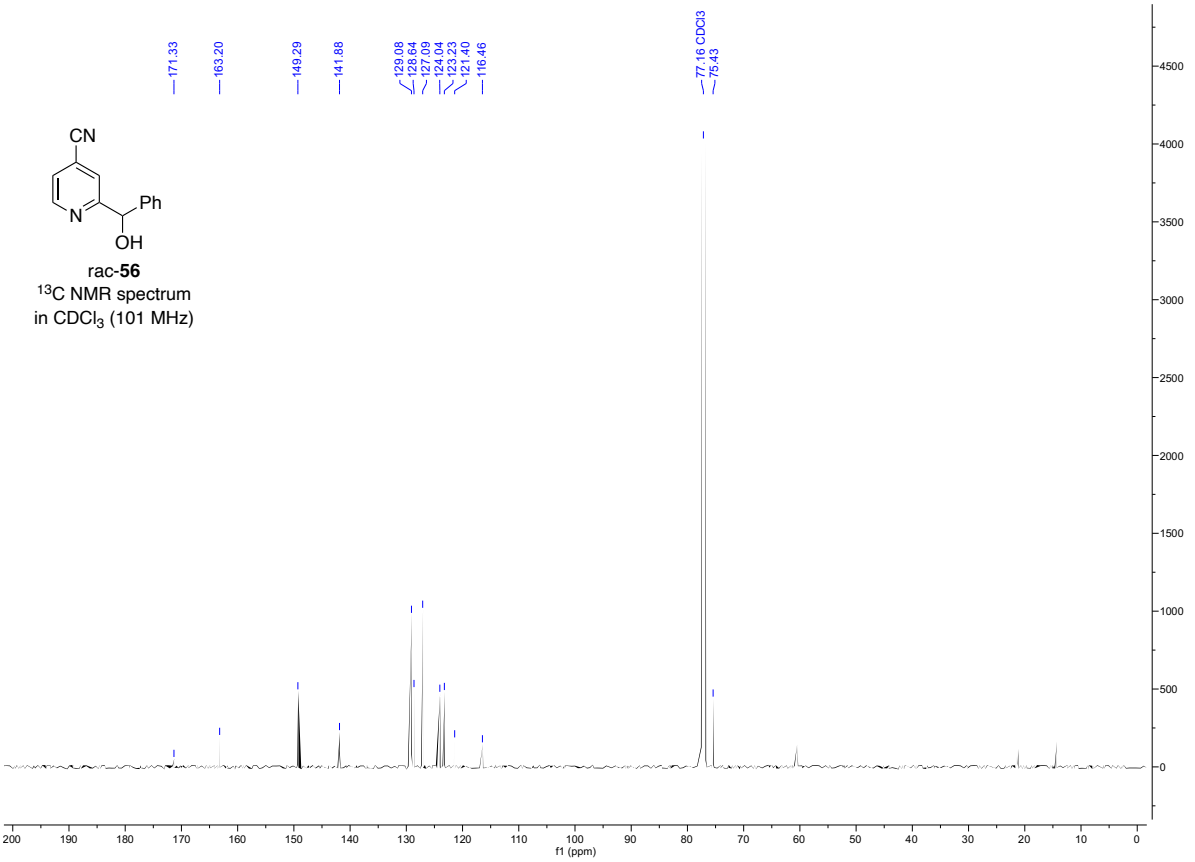

rac-**56**
^{13}C NMR spectrum
in $CDCl_3$ (101 MHz)

2-Pivaloylisonicotinonitrile (**55**)

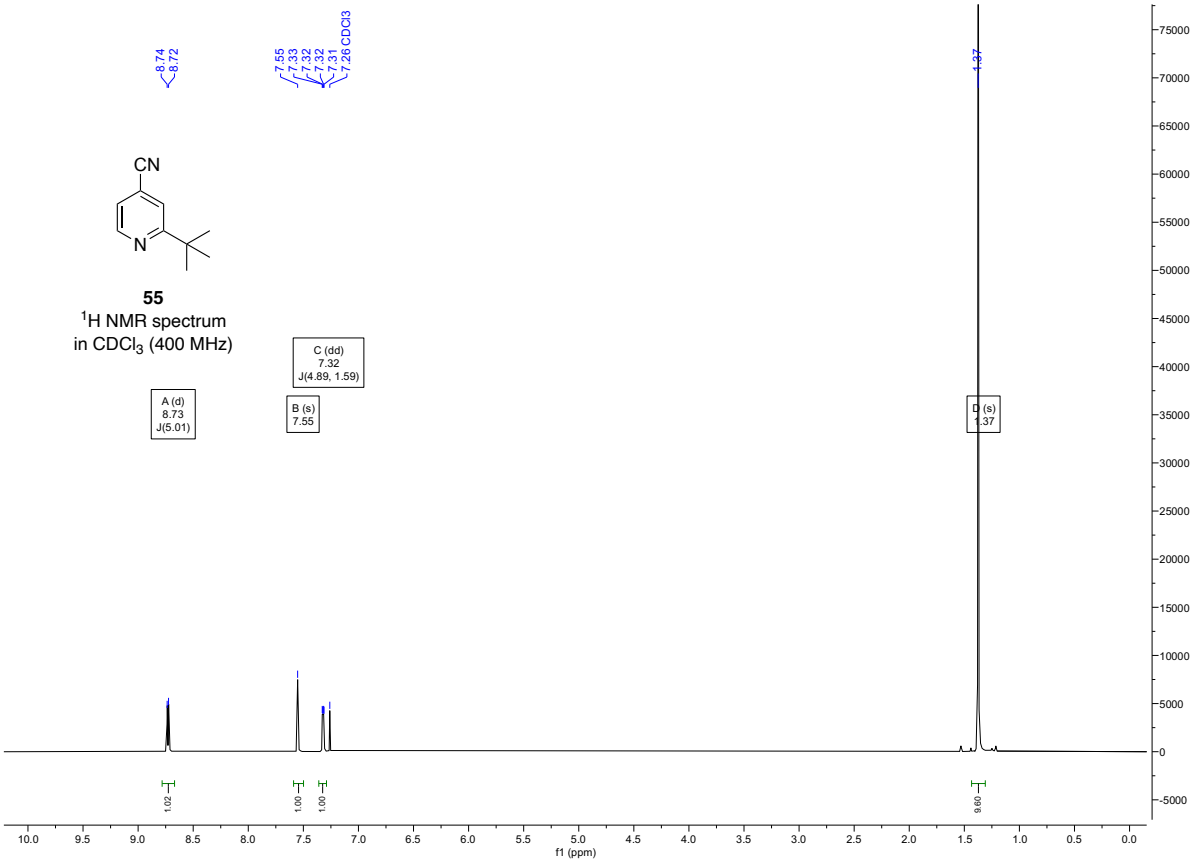

55
^{1}H NMR spectrum
in $CDCl_3$ (400 MHz)

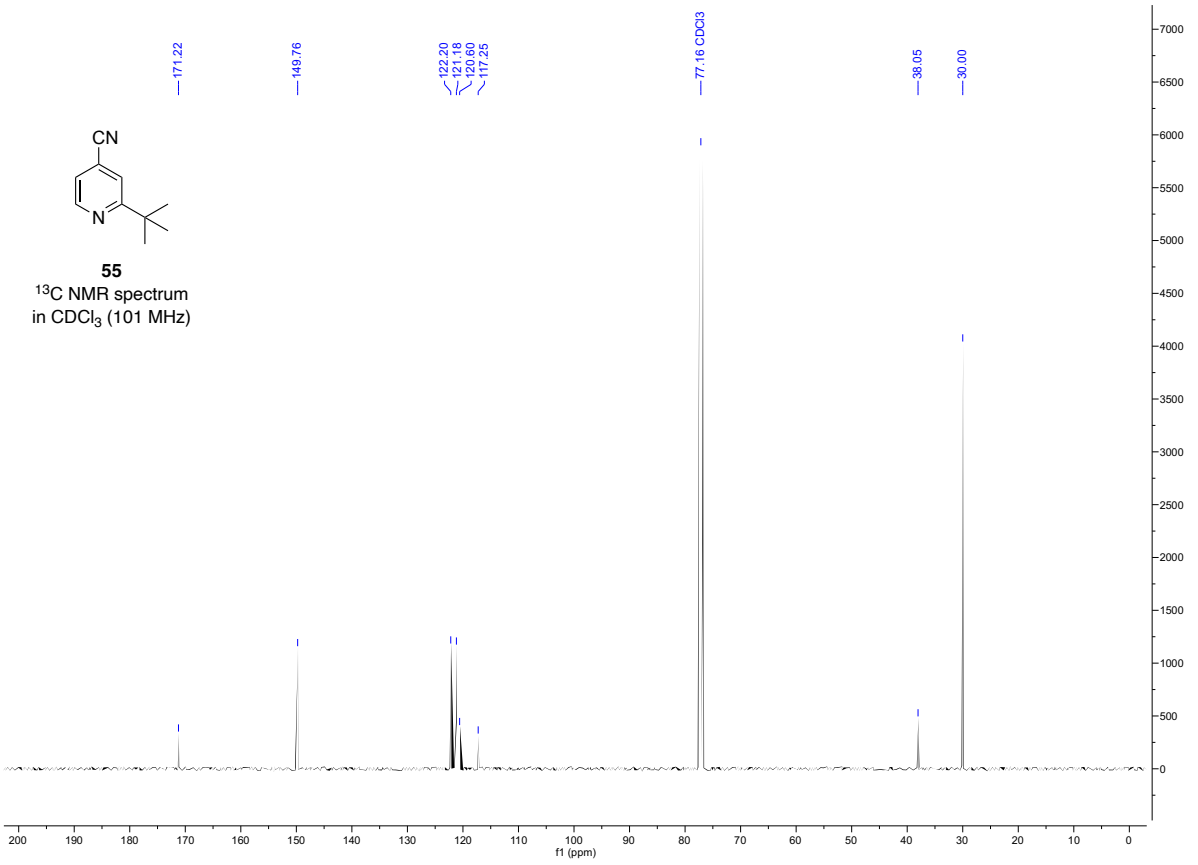

55
^{13}C NMR spectrum
in $CDCl_3$ (101 MHz)

5.4.2 Computational Data

Calculation Method. Geometry optimization and vibrational frequency calculations were performed using the B3LYP-D3 hybrid function[25–27] in combination with the 6-31+G(d) basis set.[28] Chloroform solvation effects were allowed for with the SMD continuum solvation model.[29] This combination has been found to perform well for the description of charge-separated intermediates.[30,31] Thermochemical corrections to 298.15 K have been calculated for all minima from unscaled vibrational frequencies obtained at this same level. All calculations have been performed using Gaussian 09.[32]

Conformer generation. For the ion pair catalysts, the conformers of the single tetraphenylphosphonium cations were obtained from a former group member. Conformers for single anion **1** were generated with Maestro[33] using a 30 to 50 kJ/mol energy window to obtain a good conformational coverage. For the final ion pair the six best anion conformers (15kJ/mol energy window) were taken und combined with the best cation conformer by using the stochastic kick procedure invented by Saunders[34] and further developed by Sakic[35] to generate 20 new conformers per starting point. This resulted in 120 new ion pair conformers for which geometry optimization and vibrational frequency calculations were performed.

Conformer generation for acylated catalyst adducts. For each of the obtained neutral catalysts was manually generated two acetyl adducts in the plane of the pyridine ring in Gauss View and geometry optimization and vibrational frequency calculations were performed. For the ion pair derivatives, the 10 best conformers were manually acylated to generate two acetyl adducts, whereas the acetyl group was drawn in a 90° and 180°, respectively, towards the pyridine ring in Gauss View. Subsequently, geometry optimization and vibrational frequency calculations were performed.

Conformer generation for Mosher's acid cation catalyst adducts. For the Vedejs-based ion pair derivatives the conformers of the anions were generated with Maestro[33] using a 50 kJ/mol energy window. For each generated conformer, however, a two-step optimization (MaxCycles=2) at the SMD ($CHCl_3$)/B3LYP-D3/6-31+G(d) level of theory was performed. The conformers were sorted according to their energies and the best conformers in a 40 kJ/mol window were selected for a full geometry optimization and vibrational frequency calculations. No conformer had to be excluded before the 40 kJ/mol window was established.

Following the geometry optimization and frequency calculation, acyl cation affinities were calculated as Lewis basicity parameter relative to pyridine as reference system. The relative Lewis basicity towards the acyl-cation was calculated as the reaction enthalpy at 298.15 K in the isodesmic group transfer reaction shown in Scheme 5.18.

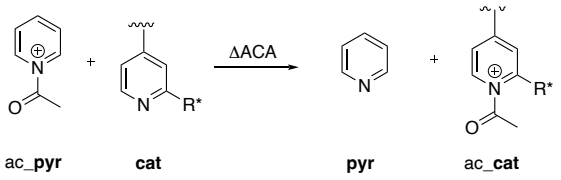

Scheme 5.18. Acyl Cation Affinity (ACA) model between reference pyridine and the calculated Vedejs catalysts derivatives with R* being the chiral substituent.

Another descriptor that was investigated is the "Mosher's cation affinities" (MOCA) to descript chirality of the catalyst. In theory, the reaction of "Mosher's cation" (MOC, Scheme 5.19a) with a chiral compound can occur from either the *re* or the *si* side of the cation, yielding to diastereomeric adducts with two different affinity values: MOCA(*R*) and MOCA(*S*). The originally proposed procedure for MOCA calculations was slightly modified.[19] Instead of calculating the reaction of the catalyst with the chiral Mosher's acid fragment, the chirality descriptor was calculated as the reaction enthalpy at 298.15 K in the isodesmic group transfer reaction shown in Scheme 5.19. Pyridine was chosen as reference compound and the Mosher's acid was added as chiral acyl group.

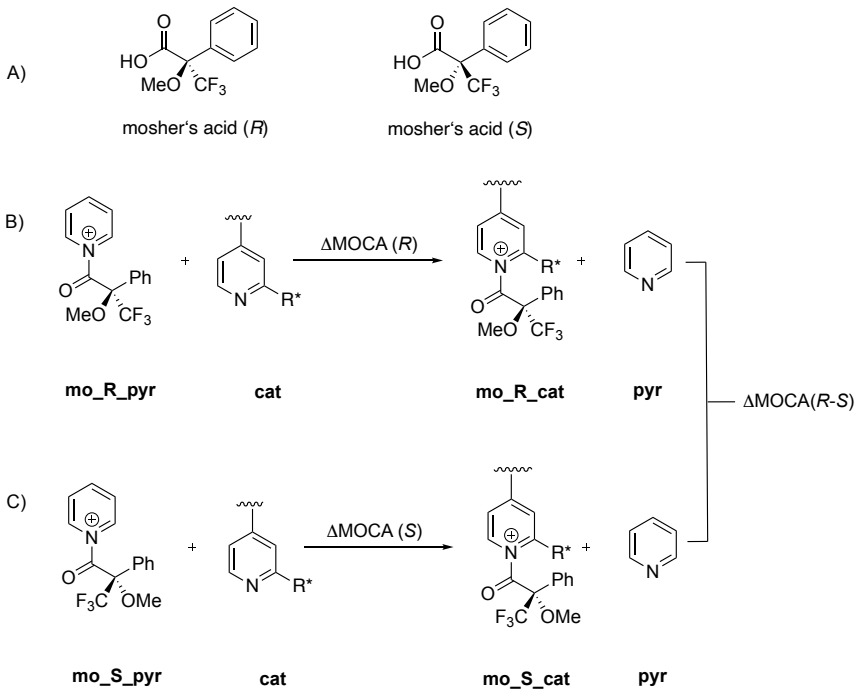

Scheme 5.19. A) Mosher's acid with (*R*) and (*S*) stereochemistry. B) Mosher's acid cation affinity (MOCA) model for pyridine-derived catalysts with a (*R*) stereochemistry for the Mosher's adduct and C) with a (*S*) stereochemistry, calculated at the SMD($CHCl_3$)/B3LYP-D3/6-31+G(d) level of theory**.**

The resulting affinity values are summarized in Table 5.1.

Table 5.1. Summary of acyl cation affinities and Mosher's cation affinities of

catalyst	ΔACA	ΔMOCA(*R*)	ΔMOCA(*S*)	ΔMOCA(*R*)-ΔMOCA(*S*)
1	-57.6	–	–	–
28	-31.7	-39.6	-38.4	-1.3
ved-an3	-77.5	-88.5	-85.8	-2.7
ved-an4	-103.4	-102.2	-104.4	+2.2
ved-an6	-93.9	-94.8	-102.4	+7.6
3a*	-45.0	–	–	–
1	-57.6	–	–	–
28	-30.6	-38.1	-37.9	-0.2
ved-an3	-76.7	-86.8	-85.1	-1.7
ved-an4	-102.3	-101.7	-104.3	+2.6
ved-an6	-93.2	-93.8	-102.1	+8.3
3a*	-45.0	–	–	–

The calculated total energies, enthalpies and free energies of all computed system are listed below. The blue marked cells show the Boltzmann-averaged values.

5.4.2.1 Neutral compounds

Table 5.2. Energies for the reference system pyridine.

pyr

catalyst	Filename	E_{tot} SMD/B3LYP-D3/6-31+G(d)	H_{298} SMD/B3LYP-D3/6-31+G(d)	G_{298} SMD/B3LYP-D3/6-31+G(d)	Rel. ΔH_{298} (kJ/mol)	
Pyridine	**pyr_opt_fr**	**-248.3105322**	**-248.2163592**	**-248.2489942**	**0.0**	
						ΔACA
Ac_py	**pyr_ac_opt_fr**	**-401.3988258**	**-401.2504828**	**-401.2913438**	**0.0**	**0.0**
						ΔMOCA
Mo_R_py	**mo_pyr_001_ofr**	**-1084.0397841**	**-1083.7624221**	**-1083.8273451**	**0.0**	**0.0**
	mo_pyr_002_ofr	-1084.0343962	-1083.7572172	-1083.8216642	13.7	
	mo_pyr_008_ofr	-1084.0331981	-1083.7565711	-1083.8238331	15.4	
	mo_pyr_007_ofr	-1084.0335037	-1083.7565277	-1083.8215977	15.5	
	mo_pyr_003_ofr	-1084.0329560	-1083.7559500	-1083.8217280	17.0	
	mo_pyr_005_ofr	-1084.0328936	-1083.7556256	-1083.8203486	17.8	
	mo_pyr_006_ofr	-1084.0325849	-1083.7555229	-1083.8193599	18.1	
	mo_pyr_004_ofr	-1084.0320803	-1083.7549923	-1083.8193713	19.5	

Table 5.3. Energies for the neutral organocatalyst DMAP (**1**).

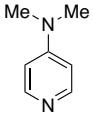

1

catalyst	Filename	E_{tot} SMD/B3LYP-D3/6-31+G(d)	H_{298} SMD/B3LYP-D3/6-31+G(d)	G_{298} SMD/B3LYP-D3/6-31+G(d)	Rel. ΔH_{298} (kJ/mol)	
DMAP	**dmap_opt_fr**	**-382.2995489**	**-382.1274099**	**-382.1701299**	**0.0**	
						ΔACA
Ac_DMAP	**dmap_ac_opt_fr**	**-535.4106505**	**-535.1834785**	**-535.2331145**	**0.0**	**-57.6**

Table 5.4. Energies for the Vedejs catalyst and the Vedejs-MOCA (R) and (S) adducts (best 15 conformers for each).

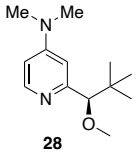

28

catalyst	Filename	E_{tot} SMD/B3LYP-D3/6-31+G(d)	H_{298} SMD/B3LYP-D3/6-31+G(d)	G_{298} SMD/B3LYP-D3/6-31+G(d)	Rel. ΔH_{298} (kJ/mol)	
28	**vedejs_015_ofr**	**-693.4265956**	**-693.0714526**	**-693.1352836**	**0.0**	
	vedejs_016_ofr	-693.4229512	-693.0680942	-693.1321762	8.8	
	vedejs_004a_ofr	-693.4162524	-693.0610664	-693.1244734	27.3	
	vedejs_024_ofr	-693.4163034	-693.0609624	-693.1245174	27.5	
	vedejs_018_ofr	-693.4145737	-693.0591807	-693.1230897	32.2	
	vedejs_027_ofr	-693.4135417	-693.0585407	-693.1220887	33.9	
	vedejs_006_ofr	-693.4137902	-693.0583832	-693.1223552	34.3	
	vedejs_014_ofr	-693.4134844	-693.0583804	-693.1221574	34.3	
	vedejs_026_ofr	-693.4138569	-693.0583349	-693.1221399	34.4	
		-693.4265199	**-693.0713591**	**-693.1351718**		
						ΔACA
Ac_Vedejs	**ac_ved_015_A_ofr**	**-846.5278713**	**-846.1176653**	**-846.1878033**	**0.0**	**-31.7**
	ac_ved_015_Bma_ofr	-846.5259924	-846.1158674	-846.1856694	4.7	

	ac_ved_018_A_ofr	-846.5254517	-846.1156287	-846.1843787	5.3	
	ac_ved_016_B_ofr	-846.5252400	-846.1153180	-846.1848880	6.2	
	ac_ved_006_B_ofr	-846.5144376	-846.1040876	-846.1737936	35.6	
	ac_ved_026_B_ofr	-846.5144532	-846.1038202	-846.1730632	36.4	
	ac_ved_027_A_ofr	-846.5138803	-846.1031583	-846.1730513	38.1	
	ac_ved_006_A_ofr	-846.5114906	-846.1006976	-846.1712566	44.5	
	ac_ved_014_A_ofr	-846.5110951	-846.1004811	-846.1708821	45.1	
	ac_ved_004a_B_ofr	-846.4995694	-846.0890024	-846.1585014	75.3	
	ac_ved_018_Ba_ofr	-846.4994825	-846.0888275	-846.1583695	75.7	
	ac_ved_004a_A_ofr	-846.4987130	-846.0877200	-846.1566640	78.6	
		-846.5273965	**-846.1171469**	**-846.1874236**		**-30.6**
						ΔMOCA (*R*)
Mo_R_vedejs	**mo_R_ved_090_ofr**	**-1529.1721004**	**-1528.6326144**	**-1528.7247534**	**0.0**	**-39.6**
	mo_R_ved_016_ofr	-1529.1695718	-1528.6302328	-1528.7226628	6.3	
	mo_R_ved_049_ofr	-1529.1686569	-1528.6298219	-1528.7230979	7.3	
	mo_R_ved_047_ofr	-1529.1687042	-1528.6295482	-1528.7220152	8.1	
	mo_R_ved_086_ofr	-1529.1688377	-1528.6294087	-1528.7198117	8.4	
	mo_R_ved_085_ofr	-1529.1688274	-1528.6293964	-1528.7191454	8.4	
	mo_R_ved_063_ofr	-1529.1682738	-1528.6290458	-1528.7224938	9.4	
	mo_R_ved_073_ofr	-1529.1685084	-1528.6287614	-1528.7207454	10.1	
	mo_R_ved_012_ofr	-1529.1678734	-1528.6284934	-1528.7221074	10.8	
	mo_R_ved_046_ofr	-1529.1676731	-1528.6282231	-1528.7222051	11.5	
	mo_R_ved_036_ofr	-1529.1666960	-1528.6274060	-1528.7199560	13.7	
	mo_R_ved_029_ofr	-1529.1649723	-1528.6257903	-1528.7185143	17.9	
	mo_R_ved_011_ofr	-1529.1641206	-1528.6250026	-1528.7184306	20.0	
	mo_R_ved_010_ofr	-1529.1643341	-1528.6249511	-1528.7174341	20.1	
	mo_R_ved_024_ofr	-1529.1643131	-1528.6249201	-1528.7180661	28.6	
		-1529.1714351	**-1528.6318851**	**-1528.7238844**		**-38.1**
						ΔMOCA (*S*)
Mo_S_vedejs	**mo_S_ved_027_ofr**	**-1529.1709714**	**-1528.6321344**	**-1528.7245744**	**0.0**	**-38.4**
	mo_S_ved_028_ofr	-1529.1709757	-1528.6320997	-1528.7243557	0.1	
	mo_S_ved_051_ofr	-1529.1704679	-1528.6311109	-1528.7253849	2.7	
	mo_S_ved_011_ofr	-1529.1681211	-1528.6290581	-1528.7221771	8.1	
	mo_S_ved_009_ofr	-1529.1681714	-1528.6289304	-1528.7221184	8.4	
	mo_S_ved_015_ofr	-1529.1680953	-1528.6286893	-1528.7228133	9.0	
	mo_S_ved_106_ofr	-1529.1678936	-1528.6285346	-1528.7198056	9.5	
	mo_S_ved_113_ofr	-1529.1655048	-1528.6262708	-1528.7168418	15.4	
	mo_S_ved_033_ofr	-1529.1651172	-1528.6261402	-1528.7198762	15.7	
	mo_S_ved_034_ofr	-1529.1651342	-1528.6255522	-1528.7179712	17.3	
	mo_S_ved_068_ofr	-1529.1638534	-1528.6247664	-1528.7176894	19.3	
	mo_S_ved_004_ofr	-1529.1635312	-1528.6246522	-1528.7162252	19.6	
	mo_S_ved_010_ofr	-1529.1636618	-1528.6242668	-1528.7162238	20.7	
	mo_S_ved_024_ofr	-1529.1639932	-1528.6242462	-1528.7159752	20.7	
	mo_S_ved_050_ofr	-1529.1634998	-1528.6240568	-1528.7165048	21.2	
		-1529.1706476	**-1528.6317943**	**-1528.7247910**		**-37.9**
						ΔMOCA (R-*S*) -1.3
						-0.2

5.4.2.2 Chiral pyridinamide anion systems

Table 5.5. Energies for the chiral anion ved-an3 catalyst and the ved-an3-MOCA (R) and (S) adducts (best 15 conformers for each).

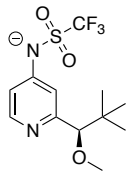

ved-an3

catalyst	Filename	E_{tot} SMD/B3LYP-D3/6-31+G(d)	H_{298} SMD/B3LYP-D3/6-31+G(d)	G_{298} SMD/B3LYP-D3/6-31+G(d)	Rel. ΔH_{298} (kJ/mol)	
ved_an3	**ved_an3_007_ofr**	-1499.9575769	**-1499.6547349**	**-1499.7282609**	**0.0**	
	ved_an3_008_ofr	**-1499.9576101**	-1499.6545651	-1499.7277861	0.4	
	ved_an3_003_ofr	-1499.9551162	-1499.6523592	-1499.7257502	6.2	
	ved_an3_004_ofr	-1499.9547631	-1499.6517791	-1499.7247651	7.8	
	ved_an3_005_ofr	-1499.9543872	-1499.6516612	-1499.7259782	8.1	
	ved_an3_002_ofr	-1499.9518687	-1499.6493407	-1499.7235427	14.2	
	ved_an3_012_ofr	-1499.9473628	-1499.6444618	-1499.7182158	27.0	
	ved_an3_013_ofr	-1499.9473558	-1499.6440658	-1499.7174448	28.0	
	ved_an3_014c_ofr	-1499.9468339	-1499.6436109	-1499.7169449	29.2	
	ved_an3_016_ofr	-1499.9470884	-1499.6434454	-1499.7155234	29.6	
	ved_an3_009_ofr	-1499.9444175	-1499.6416805	-1499.7163905	34.3	
	ved_an3_011_ofr	-1499.9435239	-1499.6402039	-1499.7144849	38.2	
		-1499.9573888	**-1499.6544353**	**-1499.7278237**		
						ΔACA
Ac_ved_an3	**ac_ved_an3_007_Apa_ofr**	-1653.0757718	**-1652.7183888**	-1652.7990638	**0.0**	**-77.5**
	ac_ved_an3_008_A_ofr	**-1653.0758490**	-1652.7183810	-1652.7990980	0.0	
	ac_ved_an3_005_Aa_ofr	-1653.0754979	-1652.7181879	**-1652.8003409**	0.5	
	ac_ved_an3_003_A_ofr	-1653.0743424	-1652.7171314	-1652.7974294	3.3	
	ac_ved_an3_007_B_ofr	-1653.0742935	-1652.7167655	-1652.7968715	4.3	
	ac_ved_an3_004_A_ofr	-1653.0740713	-1652.7167083	-1652.7966493	4.4	
	ac_ved_an3_003_B_ofr	-1653.0737459	-1652.7166419	-1652.7974869	4.6	
	ac_ved_an3_005_Ba_ofr	-1653.0737230	-1652.7166150	-1652.7988170	4.7	
	ac_ved_an3_004_B_ofr	-1653.0735322	-1652.7165262	-1652.7982912	4.9	
	ac_ved_an3_008_B_ofr	-1653.0738840	-1652.7164710	-1652.7965960	5.0	
	ac_ved_an3_002_A_ofr	-1653.0733680	-1652.7162560	-1652.7976370	5.6	
	ac_ved_an3_002_B_ofr	-1653.0728842	-1652.7156312	-1652.7967082	7.2	
	ac_ved_an3_014c_B_ofr	-1653.0646841	-1652.7074711	-1652.7891721	28.7	
	ac_ved_an3_016_B_ofr	-1653.0646277	-1652.7073127	-1652.7881947	29.1	
	ac_ved_an3_014c_A_ofr	-1653.0615719	-1652.7041069	-1652.7860369	37.5	
		-1653.0752023	**-1652.7177854**	**-1652.7994080**		**-76.7**
						ΔMOCA (*R*)
Mo_R_ved_an3	**mo_R_ved_an3_173_ofr**	**-2335.7209087**	**-2335.2344897**	**-2335.3379557**	**0.0**	**-88.5**
	mo_R_ved_an3_157_ofr	-2335.7200464	-2335.2338314	-2335.3361604	1.7	
	mo_R_ved_an3_164_ofr	-2335.7176649	-2335.2314429	-2335.3349559	8.0	
	mo_R_ved_an3_122_ofr	-2335.7171227	-2335.2310877	-2335.3353977	8.9	
	mo_R_ved_an3_034_ofr	-2335.7166133	-2335.2309023	-2335.3366813	9.4	
	mo_R_ved_an3_123_ofr	-2335.7175137	-2335.2308467	-2335.3332037	9.6	
	mo_R_ved_an3_105_ofr	-2335.7172738	-2335.2308188	-2335.3333608	9.6	
	mo_R_ved_an3_210_ofr	-2335.7168736	-2335.2304866	-2335.3323566	10.5	
	mo_R_ved_an3_224_ofr	-2335.7171725	-2335.2304525	-2335.3341635	10.6	
	mo_R_ved_an3_117_ofr	-2335.7168266	-2335.2303896	-2335.3349476	10.8	
	mo_R_ved_an3_231_ofr	-2335.7168850	-2335.2303010	-2335.3349670	11.0	
	mo_R_ved_an3_153_ofr	-2335.7167495	-2335.2302635	-2335.3362305	11.1	
	mo_R_ved_an3_226_ofr	-2335.7164919	-2335.2302079	-2335.3358289	11.2	
	mo_R_ved_an3_163_ofr	-2335.7164359	-2335.2299649	-2335.3324419	11.9	
	mo_R_ved_an3_181_ofr	-2335.7164164	-2335.2298614	-2335.3313754	12.2	
		-2335.7199157	**-2335.2335141**	**-2335.3365808**		**-86.7**
						ΔMOCA (*S*)
Mo_S_ved_an3	**mo_S_ved_an3_090_ofr**	-2335.7193757	**-2335.2334757**	-2335.3369247	**0.0**	**-85.8**
	mo_S_ved_an3_161_ofr	-2335.7194180	-2335.2334450	-2335.3375500	0.1	
	mo_S_ved_an3_093_ofr	**-2335.7194785**	-2335.2333745	**-2335.3388185**	0.3	
	mo_S_ved_an3_102_ofr	-2335.7193439	-2335.2331179	-2335.3362509	0.9	
	mo_S_ved_an3_191_ofr	-2335.7191036	-2335.2327186	-2335.3367086	2.0	
	mo_S_ved_an3_127_ofr	-2335.7187672	-2335.2326712	-2335.3371592	2.1	
	mo_S_ved_an3_103_ofr	-2335.7186688	-2335.2325738	-2335.3368628	2.4	
	mo_S_ved_an3_105_ofr	-2335.7185367	-2335.2324927	-2335.3364437	2.6	
	mo_S_ved_an3_176_ofr	-2335.7188820	-2335.2324470	-2335.3355400	2.7	
	mo_S_ved_an3_107_ofr	-2335.7184753	-2335.2323013	-2335.3355643	3.1	
	mo_S_ved_an3_189_ofr	-2335.7184753	-2335.2322993	-2335.3363033	3.1	
	mo_S_ved_an3_109_ofr	-2335.7184320	-2335.2322310	-2335.3357010	3.3	
	mo_S_ved_an3_139_ofr	-2335.7171754	-2335.2304644	-2335.3319764	7.9	
	mo_S_ved_an3_128_ofr	-2335.7166543	-2335.2301473	-2335.3318333	8.7	

	mo_S_ved_an3_073_ofr	-2335.7159452	-2335.2295182	-2335.3335042	10.4	
		-2335.7189227	**-2335.2328631**	**-2335.3377208**		**-85.1**
						ΔMOCA (R-*S*) -2.7
						-1.7

Table 5.6 Energies for the chiral anion ved-an4 catalyst and the ved-an4-MOCA (R) and (S) adducts (best 15 conformers for each).

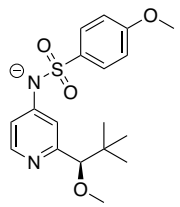

ved-an4

catalyst	Filename	E_{tot} SMD/B3LYP-D3/6-31+G(d)	H_{298} SMD/B3LYP-D3/6-31+G(d)	G_{298} SMD/B3LYP-D3/6-31+G(d)	Rel. ΔH_{298} (kJ/mol)	
ved_an4	**ved_an4_016a_ofr**	-1508.5172545	**-1508.1011645**	-1508.1813035	**0.0**	
	ved_an4_014_ofr	**-1508.5174251**	-1508.1011271	-1508.1798461	0.1	
	ved_an4_015_ofr	-1508.5170096	-1508.1009066	-1508.1809096	0.7	
	ved_an4_017_ofr	-1508.5168370	-1508.1008680	**-1508.1816430**	0.8	
	ved_an4_031_ofr	-1508.5142857	-1508.0985147	-1508.1801927	7.0	
	ved_an4_030_ofr	-1508.5142430	-1508.0982550	-1508.1788700	7.6	
	ved_an4_033_ofr	-1508.5126921	-1508.0966641	-1508.1772981	11.8	
	ved_an4_032_ofr	-1508.5127061	-1508.0966391	-1508.1774911	11.9	
	ved_an4_019_ofr	-1508.5118802	-1508.0961152	-1508.1786352	13.3	
	ved_an4_018_ofr	-1508.5118693	-1508.0960093	-1508.1777493	13.5	
	ved_an4_002_ofr	-1508.5096239	-1508.0938249	-1508.1759749	19.3	
	ved_an4_012_ofr	-1508.5069857	-1508.0906337	-1508.1701447	27.6	
	ved_an4_028_ofr	-1508.5069580	-1508.0904810	-1508.1704530	28.0	
	ved_an4_007_ofr	-1508.5065601	-1508.0901091	-1508.1690821	29.0	
	ved_an4_024_ofr	-1508.5061505	-1508.0900855	-1508.1706925	29.1	
		-1508.5170885	**-1508.1009224**	**-1508.1810417**		
						ΔACA
Ac_ved_an4	**ac_ved_an4_014_A_ofr**	**-1661.6452911**	**-1661.1746611**	-1661.2628971	**0.0**	**-103.4**
	ac_ved_an4_015_A_ofr	-1661.6448949	-1661.1743989	**-1661.2635339**	0.7	
	ac_ved_an4_016a_A_ofr	-1661.6448634	-1661.1743314	-1661.2622464	0.9	
	ac_ved_an4_017_Aa_ofr	-1661.6447716	-1661.1740616	-1661.2619366	1.6	
	ac_ved_an4_014_B_ofr	-1661.6434054	-1661.1727524	-1661.2605224	5.0	
	ac_ved_an4_016a_B_ofr	-1661.6430747	-1661.1724947	-1661.2597627	5.7	
	ac_ved_an4_019_A_ofr	-1661.6426892	-1661.1722452	-1661.2624322	6.3	
	ac_ved_an4_018_A_ofr	-1661.6427061	-1661.1721061	-1661.2615501	6.7	
	ac_ved_an4_015_B_ofr	-1661.6426880	-1661.1719270	-1661.2594260	7.2	
	ac_ved_an4_017_B_ofr	-1661.6425492	-1661.1717772	-1661.2594232	7.6	
	ac_ved_an4_031_A_ofr	-1661.6413858	-1661.1713298	-1661.2592208	8.7	
	ac_ved_an4_030_A_ofr	-1661.6414641	-1661.1712271	-1661.2588941	9.0	
	ac_ved_an4_019_B_ofr	-1661.6407727	-1661.1703537	-1661.2602487	11.3	
	ac_ved_an4_018_B_ofr	-1661.6408620	-1661.1703270	-1661.2599150	11.4	
	ac_ved_an4_031_B_ofr	-1661.6404023	-1661.1700883	-1661.2573603	12.0	
		-1661.6446309	**-1661.1740273**	**-1661.2626871**		**-102.3**
						ΔMOCA (*R*)
Mo_R_ved_an4	**mo_R_ved_an4_043_ofr**	**-2344.2857546**	**-2343.6861686**	-2343.7971196	**0.0**	**-102.2**
	mo_R_ved_an4_082_ofr	-2344.2851700	-2343.6858660	-2343.7969540	0.8	
	mo_R_ved_an4_286_ofr	-2344.2852366	-2343.6857246	**-2343.7971526**	1.2	
	mo_R_ved_an4_226_ofr	-2344.2849565	-2343.6853455	-2343.7959095	2.2	
	mo_R_ved_an4_036_ofr	-2344.2844291	-2343.6851691	-2343.7935861	2.6	
	mo_R_ved_an4_051_ofr	-2344.2836635	-2343.6843195	-2343.7940495	4.9	
	mo_R_ved_an4_285_ofr	-2344.2824193	-2343.6831983	-2343.7957993	7.8	
	mo_R_ved_an4_017_ofr	-2344.2810004	-2343.6815434	-2343.7900894	12.1	
	mo_R_ved_an4_208_ofr	-2344.2800861	-2343.6808011	-2343.7907741	14.1	
	mo_R_ved_an4_020_ofr	-2344.2791620	-2343.6801890	-2343.7901080	15.7	

	mo_R_ved_an4_068_ofr	-2344.2796028	-2343.6800298	-2343.7911198	16.1	
	mo_R_ved_an4_031_ofr	-2344.2794331	-2343.6800261	-2343.7928811	16.1	
	mo_R_ved_an4_301_ofr	-2344.2795703	-2343.6796093	-2343.7858103	17.2	
	mo_R_ved_an4_041_ofr	-2344.2787136	-2343.6793126	-2343.7890946	18.0	
	mo_R_ved_an4_009_ofr	-2344.2786052	-2343.6790902	-2343.7890512	18.6	
		-2344.2851796	**-2343.6856640**	**-2343.7968186**		**-101.7**
						ΔMOCA (*S*)
Mo_S_ved_an4	**mo_S_ved_an4_329_ofr**	**-2344.2868593**	**-2343.6869973**	-2343.7936793	**0.0**	**-104.4**
	mo_S_ved_an4_226_ofr	-2344.2850278	-2343.6857128	-2343.7953668	3.4	
	mo_S_ved_an4_141_ofr	-2344.2828353	-2343.6834523	**-2343.7962003**	9.3	
	mo_S_ved_an4_318_ofr	-2344.2804666	-2343.6808316	-2343.7933856	16.2	
	mo_S_ved_an4_304_ofr	-2344.2802655	-2343.6806985	-2343.7907755	16.5	
	mo_S_ved_an4_279_ofr	-2344.2801290	-2343.6805220	-2343.7907940	17.0	
	mo_S_ved_an4_389_ofr	-2344.2789255	-2343.6795475	-2343.7907815	19.6	
	mo_S_ved_an4_190_ofr	-2344.2787325	-2343.6792985	-2343.7877545	20.2	
	mo_S_ved_an4_257_ofr	-2344.2784657	-2343.6791617	-2343.7904907	20.6	
	mo_S_ved_an4_340_ofr	-2344.2790773	-2343.6791603	-2343.7912473	20.6	
	mo_S_ved_an4_031_ofr	-2344.2781114	-2343.6786304	-2343.7887404	22.0	
	mo_S_ved_an4_206_ofr	-2344.2773832	-2343.6779812	-2343.7899622	23.7	
	mo_S_ved_an4_036_ofr	-2344.2766798	-2343.6776618	-2343.7861118	24.5	
	mo_S_ved_an4_045_ofr	-2344.2750722	-2343.6760312	-2343.7870612	28.8	
	mo_S_ved_an4_010_ofr	-2344.2743567	-2343.6748567	-2343.7850217	31.9	
		-2344.2865607	**-2343.6866489**	**-2343.7957055**		**-104.3**
						ΔMOCA (R-*S*) +2.2
						+2.6

Table 5.7. Energies for the chiral anion ved-an6 catalyst and the ved-an6-MOCA (R) and (S) adducts (best 15 conformers for each).

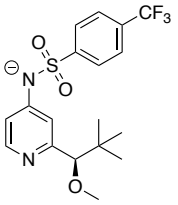

ved-an6

catalyst	Filename	E_{tot} SMD/B3LYP-D3/6-31+G(d)	H_{298} SMD/B3LYP-D3/6-31+G(d)	G_{298} SMD/B3LYP-D3/6-31+G(d)	Rel. ΔH_{298} (kJ/mol)	
ved_an6	**ved_an6_009a_ofr**	**-1731.0506373**	**-1730.6620123**	**-1730.7463083**	**0.0**	
	ved_an6_010_ofr	-1731.0505531	-1730.6619211	-1730.7458711	0.2	
	ved_an6_011_ofr	-1731.0503790	-1730.6617530	-1730.7459980	0.7	
	ved_an6_005_ofr	-1731.0472174	-1730.6589604	-1730.7432684	8.0	
	ved_an6_004_ofr	-1731.0472425	-1730.6588245	-1730.7441205	8.4	
	ved_an6_008_ofr	-1731.0457326	-1730.6573496	-1730.7423366	12.2	
	ved_an6_007_ofr	-1731.0457128	-1730.6572688	-1730.7424048	12.5	
	ved_an6_006_ofr	-1731.0454741	-1730.6572381	-1730.7439901	12.5	
	ved_an6_013_ofr	-1731.0450208	-1730.6566788	-1730.7430468	14.0	
	ved_an6_012_ofr	-1731.0450048	-1730.6566558	-1730.7420388	14.1	
	ved_an6_001_ofr	-1731.0449067	-1730.6566477	-1730.7429747	14.1	
	ved_an6_002_ofr	-1731.0427118	-1730.6542688	-1730.7397318	20.3	
	ved_an6_023_ofr	-1731.0396953	-1730.6507643	-1730.7339813	29.5	
	ved_an6_031_ofr	-1731.0394990	-1730.6506490	-1730.7347630	29.8	
	ved_an6_028_ofr	-1731.0394219	-1730.6505499	-1730.7352719	30.1	
		-1731.0504271	**-1730.6617734**	**-1730.7457816**		
						ΔACA
Ac_ved_an6	**ac_ved_an6_009_A_ofr**	**-1884.1749580**	**-1883.7319080**	**-1883.8248990**	**0.0**	**-93.9**
	ac_ved_an6_011_A_ofr	-1884.1748039	-1883.7318239	-1883.8239199	0.2	
	ac_ved_an6_010_A_ofr	-1884.1748677	-1883.7318217	-1883.8247057	0.2	
	ac_ved_an6_010_B_ofr	-1884.1730517	-1883.7299657	-1883.8219957	5.1	
	ac_ved_an6_009_B_ofr	-1884.1731436	-1883.7299396	-1883.8205456	5.2	

	ac_ved_an6_011_B_ofr	-1884.1727894	-1883.7296894	-1883.8207854	5.8	
	ac_ved_an6_012_A_ofr	-1884.1723041	-1883.7293191	-1883.8232331	6.8	
	ac_ved_an6_013_A_ofr	-1884.1724722	-1883.7292922	-1883.8227382	6.9	
	ac_ved_an6_004_A_ofr	-1884.1716668	-1883.7289858	-1883.8208318	7.7	
	ac_ved_an6_005_A_ofr	-1884.1716744	-1883.7289784	-1883.8205714	7.7	
	ac_ved_an6_005_B_ofr	-1884.1710292	-1883.7281392	-1883.8186092	9.9	
	ac_ved_an6_004_B_ofr	-1884.1710292	-1883.7281392	-1883.8186102	9.9	
	ac_ved_an6_013_B_ofr	-1884.1706193	-1883.7276413	-1883.8205953	11.2	
	ac_ved_an6_012_B_ofr	-1884.1705158	-1883.7276068	-1883.8213708	11.3	
	ac_ved_an6_007_A_ofr	-1884.1696428	-1883.7267738	-1883.8191678	13.5	
		-1884.1744283	**-1883.7313893**	**-1883.8243007**		**-93.2**
						ΔMOCA (*R*)
Mo_R_ved_an6	**mo_R_ved_an6_044_ofr**	**-2566.8160734**	**-2566.2441934**	**-2566.3584554**	**0.0**	**-94.8**
	mo_R_ved_an6_186_ofr	-2566.8144794	-2566.2420544	-2566.3570464	5.6	
	mo_R_ved_an6_036_ofr	-2566.8139475	-2566.2419075	-2566.3537645	6.0	
	mo_R_ved_an6_066_ofr	-2566.8134776	-2566.2411826	-2566.3523526	7.9	
	mo_R_ved_an6_168_ofr	-2566.8132498	-2566.2405228	-2566.3521618	9.6	
	mo_R_ved_an6_052_ofr	-2566.8125499	-2566.2403109	-2566.3548809	10.2	
	mo_R_ved_an6_069_ofr	-2566.8121009	-2566.2402869	-2566.3561099	10.3	
	mo_R_ved_an6_014_ofr	-2566.8122774	-2566.2402174	-2566.3545564	10.4	
	mo_R_ved_an6_109_ofr	-2566.8117051	-2566.2394551	-2566.3529771	12.4	
	mo_R_ved_an6_227_ofr	-2566.8116807	-2566.2393267	-2566.3520857	12.8	
	mo_R_ved_an6_148_ofr	-2566.8112775	-2566.2390195	-2566.3526455	13.6	
	mo_R_ved_an6_117_ofr	-2566.8109142	-2566.2389302	-2566.3536642	13.8	
	mo_R_ved_an6_106_ofr	-2566.8095743	-2566.2373443	-2566.3503723	18.0	
	mo_R_ved_an6_115_ofr	-2566.8094897	-2566.2372977	-2566.3496037	18.1	
	mo_R_ved_an6_039_ofr	-2566.8090289	-2566.2371669	-2566.3530889	18.4	
		-2566.8152709	**-2566.2434905**	**-2566.3578670**		**-93.8**
						ΔMOCA (*S*)
Mo_S_ved_an6	**mo_S_ved_an6_306_ofr**	**-2566.8195514**	**-2566.2470814**	**-2566.3615534**	**0.0**	**-102.4**
	mo_S_ved_an6_175_ofr	-2566.8184239	-2566.2464469	-2566.3608319	1.7	
	mo_S_ved_an6_081_ofr	-2566.8183646	-2566.2463376	-2566.3608066	2.0	
	mo_S_ved_an6_131_ofr	-2566.8153952	-2566.2432652	-2566.3575802	10.0	
	mo_S_ved_an6_223_ofr	-2566.8149295	-2566.2430275	-2566.3579445	10.6	
	mo_S_ved_an6_165_ofr	-2566.8148591	-2566.2428881	-2566.3583441	11.0	
	mo_S_ved_an6_150_ofr	-2566.8125228	-2566.2402338	-2566.3541308	18.0	
	mo_S_ved_an6_257_ofr	-2566.8115396	-2566.2398006	-2566.3520246	19.1	
	mo_S_ved_an6_083_ofr	-2566.8112596	-2566.2390496	-2566.3530006	21.1	
	mo_S_ved_an6_147_ofr	-2566.8112892	-2566.2386812	-2566.3533902	22.1	
	mo_S_ved_an6_017_ofr	-2566.8093461	-2566.2375121	-2566.3527751	25.1	
	mo_S_ved_an6_208_ofr	-2566.8091140	-2566.2369830	-2566.3518830	26.5	
	mo_S_ved_an6_033_ofr	-2566.8086433	-2566.2368193	-2566.3516173	26.9	
	mo_S_ved_an6_099_ofr	-2566.8083353	-2566.2364203	-2566.3507053	28.0	
	mo_S_ved_an6_314_ofr	-2566.8077994	-2566.2361594	-2566.3537804	28.7	
		-2566.8190520	**-2566.2466602**	**-2566.3610862**		**-102.1**
						ΔMOCA (R-*S*) +7.6
						+8.3

5.4.2.3 Chiral ion pair systems

Table 5.8. Energies for the chiral ion pair catalyst **ved-3a*** (best 15 conformers for each).

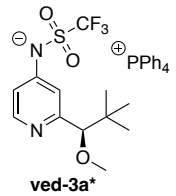

ved-3a*

catalyst	Filename	E_{tot}	H_{298}	G_{298}	Rel. ΔH_{298}	

		SMD/B3LYP-D3/6-31+G(d)	SMD/B3LYP-D3/6-31+G(d)	SMD/B3LYP-D3/6-31+G(d)	(kJ/mol)	
ved_1b	**ved_1b_028a_o_fr**	-2767.8933169	**-2767.1984779**	-2767.3243129	**0.0**	
	ved_1b_096a_o_fr	**-2767.8935127**	-2767.1983547	**-2767.3286367**	0.3	
	ved_1b_007_o_fr	-2767.8926956	-2767.1982156	-2767.3254226	0.7	
	ved_1b_015a_o_fr	-2767.8922879	-2767.1975549	-2767.3235099	2.4	
	ved_1b_036a_o_fr	-2767.8923836	-2767.1974486	-2767.3233676	2.7	
	ved_1b_024a_o_fr	-2767.8920486	-2767.1971136	-2767.3228806	3.6	
	ved_1b_097a_o_fr	-2767.8919265	-2767.1969665	-2767.3218185	4.0	
	ved_1b_011a_o_fr	-2767.8914256	-2767.1964336	-2767.3229906	5.4	
	ved_1b_022a_o_fr	-2767.8910156	-2767.1963576	-2767.3231356	5.6	
	ved_1b_084a_o_fr	-2767.8911410	-2767.1962050	-2767.3231480	6.0	
	ved_1b_026a_o_fr	-2767.8913345	-2767.1961495	-2767.3212685	6.1	
	ved_1b_003a_o_fr	-2767.8914731	-2767.1960711	-2767.3215741	6.3	
	ved_1b_099a_o_fr	-2767.8905898	-2767.1960388	-2767.3251028	6.4	
	ved_1b_067a_o_fr	-2767.8903527	-2767.1959167	-2767.3219327	6.7	
	ved_1b_037a_o_fr	-2767.8906400	-2767.1958650	-2767.3238320	6.9	
		-2767.8924032	**-2767.1975061**	**-2767.3282319**		
						ΔACA
Ac_ved_1b	**ac_ved_1b_028_A_ofr**	**-2920.9994979**	**-2920.2497519**	**-2920.3827449**	**0.0**	**-45.0**
	ac_ved_1b_097_A_ofr	-2920.9987369	-2920.2490189	-2920.3826459	1.9	
	ac_ved_1b_036_A_ofr	-2920.9984647	-2920.2489877	-2920.3823317	2.0	
	ac_ved_1b_096_Aa_ofr	-2920.9983239	-2920.2484879	-2920.3796869	3.3	
	ac_ved_1b_024_A_ofr	-2920.9974338	-2920.2478038	-2920.3818678	5.1	
	ac_ved_1b_097_Ba_ofr	-2920.9974541	-2920.2477201	-2920.3797241	5.3	
	ac_ved_1b_007_B_ofr	-2920.9966865	-2920.2469395	-2920.3797225	7.4	
	ac_ved_1b_028_B_ofr	-2920.9968992	-2920.2469372	-2920.3780582	7.4	
	ac_ved_1b_015_Aa_ofr	-2920.9964361	-2920.2465921	-2920.3800011	8.3	
	ac_ved_1b_015_B_ofr	-2920.9960199	-2920.2459869	-2920.3786499	9.9	
	ac_ved_1b_011_A_ofr	-2920.9957490	-2920.2457110	-2920.3775720	10.6	
	ac_ved_1b_024_B_ofr	-2920.9954758	-2920.2456458	-2920.3791918	10.8	
	ac_ved_1b_096_Ba_ofr	-2920.9954443	-2920.2452823	-2920.3762523	11.7	
	ac_ved_1b_011_B_ofr	-2920.9946501	-2920.2446571	-2920.3760041	13.4	
	ac_ved_1b_022_A_ofr	-2920.9941410	-2920.2440050	-2920.3748340	15.1	
		-2920.9986044	**-2920.2489224**	**-2920.3822915**		**-45.0**

5.5 References

[1] R. P. Wurz, *Chem. Rev.* **2007**, *107*, 5570–5595.

[2] S. E. Denmark, G. L. Beutner, *Angew. Chem. Int. Ed.* **2008**, *47*, 1560–1638.

[3] W. Steglich, G. Höfle, *Angew. Chem. Int. Ed.* **1969**, *8*, 981–981.

[4] G. Höfle, W. Steglich, *Synthesis* **1972**, *11*, 619–621.

[5] G. Höfle, W. Steglich, H. Vorbrüggen, *Angew. Chem. Int. Ed.* **1978**, *17*, 569–583.

[6] E. F. V. Scriven, *Chem. Soc. Rev.* **1983**, *12*, 129–161.

[7] S. Xu, I. Held, B. Kempf, H. Mayr, W. Steglich, H. Zipse, *Chem. Eur. J.* **2005**, *11*, 4751–4757.

[8] E. Vedejs, X. Chen, *J. Am. Chem. Soc.* **1996**, *118*, 1809–1810.

[9] C. Bolm, M. Ewald, M. Felder, G. Schlingloff, *Chem. Ber.* **1992**, *125*, 1169–1190.

[10] S. Choppin, P. Gros, Y. Fort, *Eur. J. Org. Chem.* **2001**, *2001*, 603–606.

[11] I. D. Bori, D. L. Comins, *Arkivoc* **2021**, *2021*, 57–72.

[12] D. Cuperly, P. Gros, Y. Fort, *J. Org. Chem.* **2002**, *67*, 238–241.

[13] F. Minisci, R. Bernardi, F. Bertini, R. Galli, M. Perchinummo, *Tetrahedron* **1971**, *27*, 3575–3579.

[14] F. Fontana, F. Minisci, M. C. Nogueira Barbosa, E. Vismara, *J. Org. Chem.* **1991**, *56*, 2866–2869.

[15] G. Gavory, M. Ghandi, A. Chicas, M. Warmuth, *Treatment of MYC-Driven Cancers with GSP1 Degraders*, **2022**, WO2022152822A1.

[16] P. Patschinski, C. Zhang, H. Zipse, *J. Org. Chem.* **2014**, *79*, 8348–8357.

[17] J. Helberg, T. Ampßler, H. Zipse, *J. Org. Chem.* **2020**, *85*, 5390–5402.

[18] S. Mayr, H. Zipse, *Eur. J. Org. Chem.* **2022**, *2022*, e202101521.

[19] Y. Wei, G. N. Sastry, H. Zipse, *Org. Lett.* **2008**, *10*, 5413–5416.

[20] M. A. Zajac, *J. Org. Chem.* **2008**, *73*, 6899–6901.

[21] A. S. Felts, A. L. Rodriguez, A. L. Blobaum, R. D. Morrison, B. S. Bates, A. Thompson Gray, J. M. Rook, M. N. Tantawy, F. W. Byers, S. Chang, D. F. Venable, V. B. Luscombe, G. D. Tamagnan, C. M. Niswender, J. S. Daniels, C. K. Jones, P. J. Conn, C. W. Lindsley, K. A. Emmitte, *J. Med. Chem.* **2017**, *60*, 5072–5085.

[22] H. Benjamin, M. A. Fox, A. S. Batsanov, H. A. Al-Attar, C. Li, Z. Ren, A. P. Monkman, M. R. Bryce, *Dalton Trans.* **2017**, *46*, 10996–11007.

[23] P. Knochel, N. M. Barl, V. Werner, C. Sämann, *HETEROCYCLES* **2014**, *88*, 827.

[24] M. D. Andrews, S. K. Bagal, D. G. Brown, K. R. Gibson, K. Omoto, T. Ryckmans, Y. Sabnis, S. E. Skerratt, P. A. Stupple, *Preparation of Pyrrolopyrimidine Derivatives for Use as Tropomyosin-Related Kinase Inhibitors*, **2014**, WO2013-IB58890.

[25] C. Lee, W. Yang, R. G. Parr, *Phys. Rev. B* **1988**, *37*, 785–789.

[26] J. Antony, S. Grimme, *Phys. Chem. Chem. Phys.* **2006**, *8*, 5287–5293.

[27] S. Grimme, *J. Chem. Phys.* **2006**, *124*, 034108

[28] G. W. Spitznagel, T. Clark, J. Chandrasekhar, P. V. R. Schleyer, *J. Comput. Chem.* **1982**, *3*, 363–371.

[29] A. V. Marenich, C. J. Cramer, D. G. Truhlar, *J. Phys. Chem. B* **2009**, *113*, 6378–6396.

[30] M. Marin-Luna, B. Pölloth, F. Zott, H. Zipse, *Chem. Sci.* **2018**, *9*, 6509–6515.

[31] M. Marin-Luna, P. Patschinski, H. Zipse, *Chem. Eur. J.* **2018**, *24*, 15052–15058.

[32] Gaussian 09, Revision D.01, M. J. Frisch, G. W. Trucks, H. B. Schlegel, G. E. Scuseria, M. A. Robb, J. R. Cheeseman, G. Scalmani, V. Barone, G. A. Petersson, H. Nakatsuji, X. Li, M. Caricato, A. V. Marenich, J. Bloino, B. G. Janesko, R. Gomperts, B. Mennucci, H. P. Hratchian, J. V. Ortiz, A. F. Izmaylov, J. L. Sonnenberg, D. Williams-Young, F. Ding, F. Lipparini, F. Egidi, J. Goings, B. Peng, A. Petrone, T. Henderson, D. Ranasinghe, V. G. Zakrzewski, J. Gao, N. Rega, G. Zheng, W. Liang, M. Hada, M. Ehara, K. Toyota, R. Fukuda, J. Hasegawa, M. Ishida, T. Nakajima, Y. Honda, O. Kitao, H. Nakai, T. Vreven, K. Throssell, J. A. Jr. Montgomery, J. E. Peralta, F. Ogliaro, M. J. Bearpark, J. J. Heyd, E. N. Brothers, K. N. Kudin, V. N. Staroverov, T. A. Keith, R. Kobayashi, J. Normand, K. Raghavachari, A. P. Rendell, J. C. Burant, S. S. Iyengar, J. Tomasi, M. Cossi, J. M. Millam, M. Klene, C. Adamo, R. Cammi, J. W. Ochterski, R. L. Martin, K. Morokuma, O. Farkas, J. B. Foresman, D. J. Fox, **2010**, p Gaussian, Inc, Wallingford CT.

[33] Maestro, rev 12.2.012. Schrödinger, New York, **2019**.

[34] M. Saunders, *J. Comput. Chem.* **2004**, *25*, 621–626.

[35] D. Šakić, M. Hanževački, D. M. Smith, V. Vrček, *Org. Biomol. Chem.* **2015**, *13*, 11740–11752.

Chapter 6. Conclusion and Outlook

Pyridine-based Lewis base catalysts represent a large and extensively studied group of organocatalysts.[1,2] The first significant discovery in this field was the synthesis of dimethylamino pyridine (DMAP) in 1967.[3,4] Subsequent developments were the introduction of 4-pyrrolidine (PPY)[5] and 9-azajulolidine (TCAP),[6] pushing the boundaries of catalytic activity. Since then, based on the success of TCAP, numerous donor-substituted organocatalysts have been developed with the aim to further enhance the catalytic activity. Recently, Helberg and Zipse[7] presented an overlooked strategy to increase the electron density of the pyridine ring by employing stabilized 4-pyridinamide anions. These pyridinamide ion pairs display an enhanced reactivity in the urethane reaction of isocyanates with 1-butanol and in *aza*-Morita-Baylis Hillman reactions. However, studying ionic substrates requires a new methodological approach to gain insights into their unique reactivity.

In this study, an analytical protocol was developed to facilitate insights into the concentration of specific ions, their association patterns, and the nucleophilicity of the anions involved. A combination of conductivity, diffusion-ordered (DOSY) NMR, and kinetic measurements was employed to study the complex association behavior of pyridinamide ion pairs in organic solvents of low polarity and its impact on catalytic performance. With the combination of conductivity and DOSY measurements, an asymmetric association pattern of cationic and anionic triple sandwich complexes with the corresponding free counterion in organic solvents of low polarity such as dichloromethane (DCM), was deciphered. Without this combination of conductivity and DOSY measurements, this result would have been impossible, as conductivity alone does not reveal insights on the type of charged species being measured. The association pattern is strongly influenced by the size and structure of the cation, which affects the balance between cationic and anionic sandwich association. The association constants of pyridinamide salts derived from conductivity data revealed a lower degree of association in ion pairs with larger aryl substituted cations, which also correlates with their catalytic activity. Meanwhile, DOSY NMR results, which support this theory, showed a predominant cationic sandwich association in smaller anion–larger cation volume pairs. This is essential for maintaining a higher concentration of free nucleophilic anions in solution. The insights gathered in this study provide valuable guidelines for the future design of pyridinamide ion pair catalysts. Specifically, adjusting the size disparity between anion and cation within the ion pair could optimize the interplay between the degree of association and catalytic efficiency. This asymmetric association could open pathways for utilizing highly reactive free anions to activate substrates, that have previously been inaccessible to catalytic transformations.

The reactivity of the highly nucleophilic anions was quantified with the newly developed ionic strength-controlled benzhydrylium ion method. This method facilitates the comparison of pyridinamide salts with neutral nucleophilic catalysts, such as DMAP and TCAP. Pyridinamide ion pairs exceed the nucleophilic reactivity of the highly reactive neutral Lewis base TCAP by up to two orders of magnitude in DCM. Comparing the second-order rate constant k_2 values for pyridinamide anions reacting with cationic reference electrophiles at constant ionic strength I = 1.0 mM revealed the most nucleophilic anion **4** to be 90 times more reactive than TCAP. This newly developed methodology now allows for the investigation of pyridinamide anion reactivity toward a broader range of electrophiles, such as quinone methides[8] or benzylidene malononitriles[9], which were previously difficult to study due to the narrow concentration window needed to prevent ion association from influencing the nucleophilic activity of pyridinamide anions. With the newly gained control over the ion association through the regulation of ionic strength, it is now possible to access a broader range of electrophiles, including those requiring higher concentration due to lower absorbance. This advancement facilitates a more comprehensive study of the nucleophilicity of pyridinamide anions in low-polarity organic solvents.

The Brønsted basicity of pyridinamide salts has been quantified as pK_a values in water and water/organic solvent mixtures. The Lewis basicity of pyridinamide salts was quantum chemically calculated as methyl cation affinities (MCA). Therefore, the relative Lewis basicity towards Me^+ was calculated as the free reaction energy of an isodesmic transfer reaction with pyridine as reference system.

The superior reactivity of pyridinamide anions was demonstrated in the urethane benchmark reaction, where **4a** catalyzes the reaction seven times more efficiently than TCAP. Despite its high nucleophilicity and basicity, pyridinamide salt **4a** displayed only moderate catalytic activity in the Steglich acylation reaction. To investigate the cause of this reduced activity, the possibility of deactivation via protonation was explored. However, this hypothesis was ruled out through experiments with various auxiliary bases. Quantum chemical calculations focusing on the stabilization of the acylated pyridinium intermediate **12** might provide an explanation for the reduced catalytic activity of this strong Lewis base catalyst.[10,11] To fully exploit their catalytic potential, it is recommended to employ pyridinamide salts primarily in addition reactions or rearrangement reactions, where acidic byproducts would not interfere with their catalytic effectiveness.

Given their enhanced reactivity, pyridinamide salts are excellent candidates for expanding their catalytic scope towards asymmetric catalysis. However, initial attempts to synthesize a chiral pyridinamide derivative posed significant challenges, particularly when adapting Vedejs' original synthesis for various 2-substituted pyridine derivatives. Computational studies offer a promising pathway to predict the reactivity and stereoselectivity of these derivatives, though further refinement of these methods is needed to enhance predictive accuracy.

In conclusion, we have established a solid analytical protocol for pyridinamide ion pairs in organic solvents of low polarity. The gained insights provide valuable guidelines for designing future ion pair catalysts with tailored association behaviors to enhance their reactivity. While the synthesis of chiral pyridinamide derivatives remains challenging, the potential of these catalysts in asymmetric catalysis warrants further investigation.

References

[1] S. E. Denmark, G. L. Beutner, *Angew. Chem. Int. Ed.* **2008**, *47*, 1560–1638.

[2] E. Vedejs, S. E. Denmark, *Lewis Base Catalysis in Organic Synthesis, 3 Vol. Set*, Wiley-VCH, Weinheim, **2016**.

[3] L. M. Litvinenko, A. I. Kirichenko, *Dokl. Akad. Nauk SSSR Ser. Khim.,* **1967**, *176*, 97–100.

[4] W. Steglich, G. Höfle, *Angew. Chem. Int. Ed.* **1969**, *8*, 981–981.

[5] W. Steglich, G. Höfle, *Tetrahedron Lett.* **1970**, *11*, 4727–4730.

[6] M. R. Heinrich, H. S. Klisa, H. Mayr, W. Steglich, H. Zipse, *Angew. Chem. Int. Ed.* **2003**, *42*, 4826–4828.

[7] J. Helberg, T. Ampßler, H. Zipse, *J. Org. Chem.* **2020**, *85*, 5390–5402.

[8] R. Lucius, R. Loos, H. Mayr, *Angew. Chem. Int. Ed.* **2002**, *41*, 91–95.

[9] T. Lemek, H. Mayr, *J. Org. Chem.* **2003**, *68*, 6880–6886.

[10] F. A. Carey, R. J. Sundberg, *Advanced Organic Chemistry: Part A: Structure and Mechanisms*, Springer Science & Business Media, New York, **2007**.

[11] S. Mayr, H. Zipse, *Eur. J. Org. Chem.* **2022**, *2022*, e202101521.

List of Abbreviations

κ	Conductivity (μS cm^{-1})
λ_i	Limited (molar) ionic conductivity (S cm^2 mol^{-1})
δ_i	Scaling factor for converting Λ_m into the respective λ_i
Λ_m	Specific molar conductivity (S cm^2 mol^{-1})
B3LYP	Hybrid DFT method with Becke's three parameter exchange functional and Lee-Yang-Parr's correlation functional
calc.	calculated
CCDC	Cambridge Crystallographic data Centre
DMAP	Dimethylamino pyridine
DMSO	Dimethyl sulfoxide
DOSY	Diffusion-ordered spectroscopy
EI	Electron ionization
ESI	Electrospray Ionization
EtOAc	Ethyl acetate
EtOH	Ethanol
GC	Gas chromatography
h	Hour
H_2O	Water
HMPN	1,8-Bis(hexamethyltriaminophosphazenyl)naphthalene
HPLC	High-performance liquid chromatography
HRMS	High resolution mass spectrometry
IR	Infrared
K_{ACA}	Anionic sandwich association constant (M^{-2})
K_{CAC}	Cationic sandwich association constant (M^{-2})
K_{IP}	1:1 Ion association constant (M^{-2})
LiTMP	Lithium tetramethylpiperidine
m.p.	Melting point
MCA	Methyl cation affinity
Me	Methyl
MeCN	Acetonitrile
MeOH	Methanol
MTBE	Methyl-*t*-butyl ether
NCI	Non-covalent interaction
NEt_3	Triethylamine
NMR	Nuclear magnetic resonance spectroscopy
OMe	Methoxy
Ph	Phenyl
PPh_4BF_4	Tetraphenylphosphonium tetrafluoroborate
PPY	4-pyrrolidinopyridine
PTC	Phase-transfer catalysis
R	Rest
RMSE	Root-mean-square-error
rt.	Room temperature
RTG	Research training group
TCAP	9-Azajulolidine
THF	Tetrahydrofuran
TMAJ	1,1,7,7-tetramethyl-9-azajulolidine
UV	Ultraviolet light
UV/Vis	Ultraviolet /visible light
vol_{an}	Anion volume
vol_{cat}	Cation volume

Curriculum Vitae

Personal Details

Name: Veronika Burger

ORCID: 0009-0003-5482-9025

Academic Career and Education

2019/11 – 2024/12 *Ludwig-Maximilians-Universität München*

Ph.D. student with Prof. Dr. Hendrik Zipse on „Highly Reactive Pyridinamide Anions in Lewis Base Catalysis"

2023/04 – 2023/07 *Durham University, United Kingdom*

Research Stay aboard in the group of Prof. AnnMarie C. O'Donoghue

2021/04 – 2024/03 *Universität Regensburg*

Ph.D. student in the Research Training Group (RTG 2620) „Ion Pair Effects in Molecular Reactivity."

2016/10 – 2019/03 *Technische University München*

Master of Science in Chemistry (M.Sc.), Thesis with Prof. Dr. Tanja Gulder

2013/10 – 2016/08 *Technische University München*

Bachelor of Science in Chemistry (B.Sc.), Thesis with Prof. Dr. Hubert A Gasteiger.

2005/09 – 2013/07 *Gymnasium Seligenthal, Landshut*

Allgemeine Hochschulreife (Abitur)